Fatigue and Fracture Testing of WELDMENTS

McHenry/Potter
editors

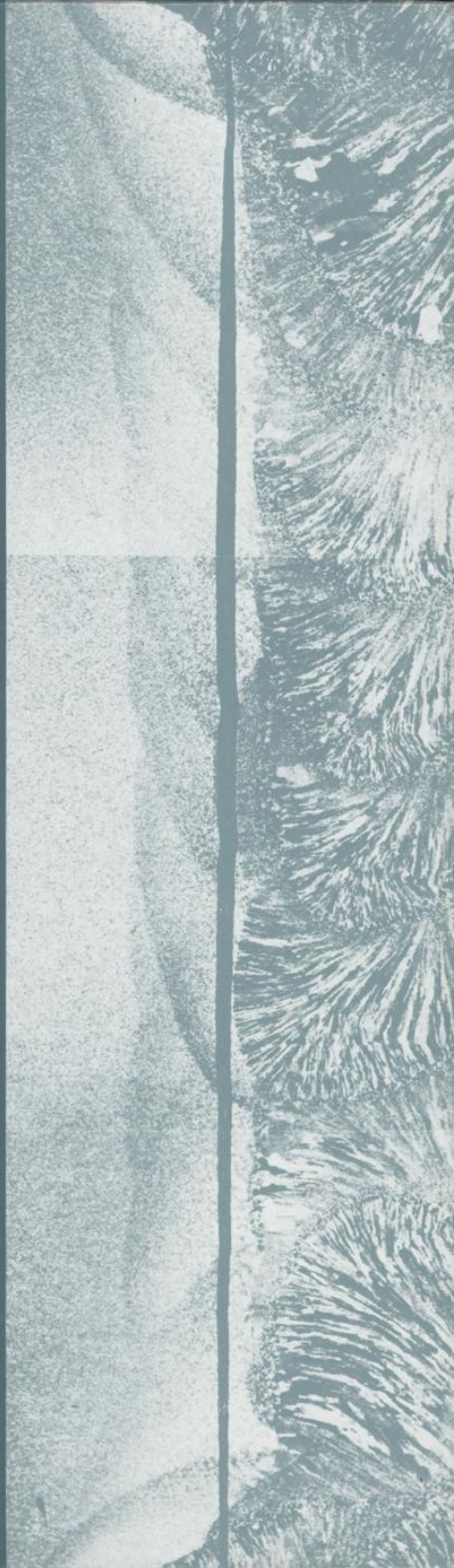

ASTM

STP 1058

STP 1058

Fatigue and Fracture Testing of Weldments

McHenry/Potter, editors

ASTM
1916 Race Street
Philadelphia, PA 19103

Library of Congress Cataloging-in-Publication Data

Fatigue and fracture testing of weldments / McHenry/Potter, editors.
(STP; 1058)
Papers from a symposium held 25 April 1988, Sparks, Nev.; sponsored by ASTM Committees E-9 on Fatigue and E-24 on Fracture Testing.
"ASTM publications code number (PCN) 04-010580-30"—T.p. verso.
Includes bibliographical references.
ISBN 0-8031-1277-7
1. Welded joints—Fatigue—Congresses. 2. Welded joints—Testing—Congresses. 3. Welded joints—Cracking—Congresses. I. McHenry, Harry I. II. Potter, John M., 1943-. III. ASTM Committee E-9 on Fatigue. IV. ASTM Committee E-24 on Fracture Testing. V. Series: ASTM special technical publication; 1058.
TA492.W4F37 1990
671.5'20422—dc20 90-251
CIP

NOTE

The Society is not responsible, as a body, for the statements and opinions advanced in this publication.

Peer Review Policy

Each paper published in this volume was evaluated by three peer reviewers. The authors addressed all of the reviewers' comments to the satisfaction of both the technical editor(s) and the ASTM Committee on Publications.

The quality of the papers in this publication reflects not only the obvious efforts of the authors and the technical editor(s), but also the work of these peer reviewers. The ASTM Committee on Publications acknowledges with appreciation their dedication and contribution of time and effort on behalf of ASTM.

Printed in Baltimore, MD
June 1990

Foreword

The symposium on Fatigue and Fracture Testing of Weldments was held on 25 April 1988 in Sparks, Nevada. The event was sponsored by ASTM Committees E-9 on Fatigue and E-24 on Fracture Testing. The symposium chairmen were John M. Potter, U.S. Air Force, and Harry I. McHenry, National Institute of Standards and Technology, both of whom also served as editors of this publication.

Contents

INDEXES

Overview

The symposium on Fatigue and Fracture Testing of Weldments was organized to define the state of the art in weldments and welded structures and to give direction to future standards activities associated with weldments.

Weldments and welded joints are used in a great variety of critical structures, including buildings, machinery, power plants, automobiles, and airframes. Very often, weldments are chosen for joining massive structures, such as offshore oil drilling platforms or oil pipelines, which themselves can be subject to adverse weathering and loading conditions. The weldment and the welded joint together are a major component that is often blamed for causing a structure to be heavier than desired or for being the point at which fatigue or fracture problems initiate and propagate. The study of fatigue and fracture at welded joints, then, is of significance in determining the durability and damage tolerance of the resultant structure.

This volume contains state-of-the-art information on the mechanical performance of weldments. Its usefulness is enhanced by the range of papers presented herein, since they run the gamut from basic research to very applied research. Details of interest within this volume include basic material studies associated with relating the metallurgy and heat treatment condition of the weld material to the growth behavior in a weld-affected area, often including the effects of corrosive media. Also addressed are the residual stress and structural load distributions within the weldment and their effects upon the flaw growth behavior. At the application end of the spectrum are papers concerning the flaw growth behavior within weldments where the sizes of the sub-scale test elements are measured in feet or metres. The broad range of the topics covered in this Special Technical Publication makes it an excellent resource for designers, analysts, students, and users of weldments and welded structures.

This volume is also meant to serve as a means of setting the directions for future efforts in standards development associated with fatigue and fracture testing of weldments. The authors were charged with defining the "holes" or deficiencies in standards associated with fatigue and fracture testing. As such, this volume will be of significance to the standards definition communities within ASTM's Committees E-9 on Fatigue and E-24 on Fracture Testing, as well as to other relevant industry standards development organizations.

Weldments provide efficient means of ensuring structural integrity in many applications; this type of joining is often used where there is no other competitive, in terms of cost or mechanical strength, approach to getting the job accomplished. The subject of weldments deserves significant attention in both the technical and the standards communities because of the importance of the structures that are welded and the consequences associated with their failure.

John M. Potter
Wright Research and Development Center, Wright-Patterson Air Force Base, OH 45433-6523; symposium cochairman and editor.

Harry I. McHenry
National Institute of Standards and Technology, Boulder, CO 80303-3328; symposium cochairman and editor.

Fatigue

G. S. Booth[1] *and J. G. Wylde*[2]

Procedural Considerations Relating to the Fatigue Testing of Steel Weldments

REFERENCE: Booth, G. S. and Wylde, J. G., **"Procedural Considerations Relating to the Fatigue Testing of Steel Weldments,"** *Fatigue and Fracture Testing of Weldments, ASTM STP 1058,* H. I. McHenry and J. M. Potter, Eds., American Society for Testing and Materials, Philadelphia, 1990, pp. 3–15.

ABSTRACT: Although fatigue design rules for welded steel joints are well developed, many cyclically loaded structures and components contain details that are not covered by these rules. It is often necessary, therefore, to generate fatigue data so that service performance may be rigorously assessed. However, for fatigue data to be of value, it is essential to identify and control many factors associated with the fatigue test itself.

The present paper summarizes the main parameters to be controlled when performing weldment fatigue tests. Four distinct areas are discussed—specimen design and fabrication, specimen preparation, testing, and, finally, reporting. Based on experience, recommendations are given regarding suitable practices in each of these areas.

KEY WORDS: weldments, steel, welded joints, fatigue

Fatigue failures remain a depressingly common occurrence, despite the century or so of research effort that has been directed to this area since the first fatigue failures in mine hoists and railway axles were documented [*1*]. Many structures and components that are subjected to cyclic loading are now fabricated by welding, and recent experience has shown that a high proportion of fatigue failures are associated with weldments [*2*].

The importance of designing welded structures against fatigue failure has been recognized for some time, and current standards and codes of practice include fatigue design rules for welded joints [*3*,*4*]. Despite the continuing occurrence of fatigue failures, there does not seem to be any evidence of an inadequacy in current design rules. In some fatigue failures the possibility of this failure mode was never considered, although the incidence of this category of fatigue failure is steadily decreasing. In others, fatigue design was not carried out sufficiently thoroughly, the main deficiencies being incorrect estimates of the stress range, unexpected cyclic loading, and the presence of significant weld flaws arising from poor welding and inspection practices.

Conventional fatigue design of welded joints is based on *S-N* curves provided in design rules for various joint geometries. The designer, however, is often faced with assessing the fatigue strength of a joint under circumstances that are not expressly covered in the design rules. For example, this may be because the specific joint geometry is not included or because the structure will be operating in an environment other than air at room temperature. In these cases, there is often a need to generate fatigue data upon which to base the design.

For fatigue testing to be of value it is vital to ensure that the data obtained are relevant

[1] Edison Welding Institute, Columbus, OH 43212.
[2] The Welding Institute, Cambridge, United Kingdom CB1 6AL.

to the final application. In essence, this means that the laboratory fatigue tests must mirror as closely as possible the anticipated service conditions. It is important, therefore, to identify and control a large number of factors associated with the fatigue testing of weldments to ensure the validity and applicability of the data thus obtained.

The present paper summarizes the major parameters to be controlled when performing fatigue tests on weldments. Its scope is restricted to steel weldments and tests to obtain *S-N* curve data—fatigue crack growth rate testing applied to weldments is not considered.

Specimen Design and Fabrication

Material

For as-welded joints loaded in air, fatigue strength is independent of the steel specification [2]. Figure 1 shows that, over the range of 300 to 800 N/mm^2, ultimate tensile strength does not influence weldment fatigue strength, whereas increasing tensile strength results in an increase in fatigue strength for unwelded components. For joints loaded in corrosive environments and for joints that are postweld treated to improve fatigue strength, the steel type is more important in determining fatigue behavior. It is therefore considered sound practice to manufacture laboratory specimens from steel similar to that used in the structure or component.

Specimen Geometry

Detailed joint geometry is by far the most important factor in determining fatigue performance, and accurate representation of the structural detail is therefore essential. In its simplest form, this implies that the specimen geometry reflects the detail under consideration, for example, a transverse butt weld or longitudinal stiffener. Under these circumstances a simple planar specimen may model the joint sufficiently accurately. In an increasing number of cases, however, it is not possible to model the joint by a simple geometry and some form of full-scale test is necessary. This is particularly important for tubular joints and large beams

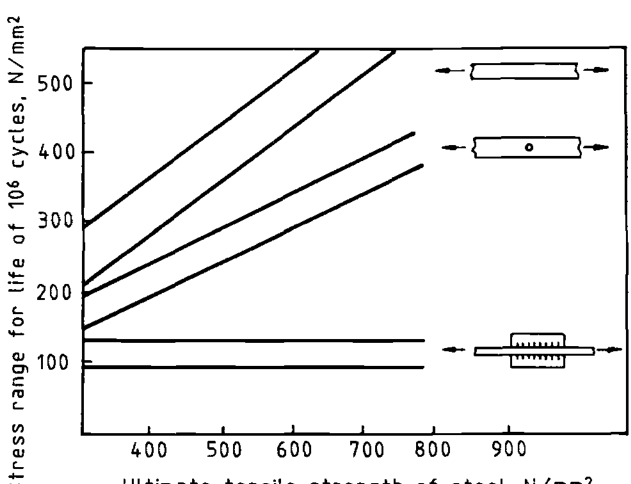

FIG. 1—*The influence of tensile strength on the fatigue strength of plain, notched, and welded steel.*

where the geometry precludes simple modeling. The remarks in this paper apply to both simple joints and full-scale joints.

In many joint geometries, failure may occur from more than one crack initiation site. For example, in trough-to-deck fatigue tests used to model steel bridge decks, fatigue cracking may initiate at three locations—the toe of the weld in the deck, the toe of the weld in the trough, and through the weld throat. Clearly data relating to one failure location are not relevant to others, and care must be taken to ensure that the failure location in the laboratory specimen is the same as that of concern in the structure.

Specimen Size

Specimen size is important for two reasons that are easily confused. First, the specimen must be sufficiently large to be able to contain realistic residual stress levels. Second, assuming that the specimen meets the first criterion, there is a significant effect of specimen size and, in particular, plate thickness on fatigue behavior.

Residual Stress Levels

Residual stresses are those stresses that exist in a body in the absence of any external load. They are always self-balancing and may be divided into two types, "residual welding stresses" and "reaction" stresses. Residual welding stresses are formed during welding primarily as a result of local heating and cooling (and hence expansion and contraction) in the vicinity of the weldment. In an as-welded structure, residual welding stresses are usually of yield tensile magnitude in the vicinity of the weld. Reaction stresses are due to long-range interaction effects, such as those introduced when fabricating a large frame structure. Reaction stresses may be either tensile or compressive in the vicinity of a weld.

For design purposes it is usually assumed that the residual stresses in the vicinity of the weldment are tensile and of yield magnitude. During fatigue loading, the stresses near the weld cycle from yield stress downwards, irrespective of the applied mean stress [*5*]. Hence, nominally compressive applied stresses become tensile near the weld and the whole of the stress range is damaging. This is illustrated in Fig. 2, which demonstrates that fatigue behavior is independent of the stress ratio (i.e., the mean stress) for as-welded longitudinal fillet welded joints [*6*]. Should a laboratory specimen not contain yield tensile residual stresses, then under partly compressive cycling a fraction of the stress cycle may become compressive near the weld and hence less damaging. This would lead to a lifetime of the laboratory specimen in excess of that of the structure.

Relatively large specimens are required to ensure that yield magnitude residual stresses are created. In general, the specimen width must be greater than approximately 100 mm and the stiffener or attachment length must be of similar dimensions. To confirm residual stress levels, nondestructive techniques such as hole drilling can be used. If there is a concern that the specimen may not provide sufficient restraint to allow yield level residual stresses to form during welding, then a technique involving spot heating can be used to introduce local residual stresses of yield tensile magnitude.

Effect of Thickness

The fatigue strength of welded joints is to some extent dependent on the absolute joint dimensions [*7*]. For geometrically similar joints loaded axially, fatigue strength decreases with increasing plate thickness. Although, in reality, geometric similarity is not maintained as plate thickness increases, one code of practice [*8*] requires that the fatigue strength of

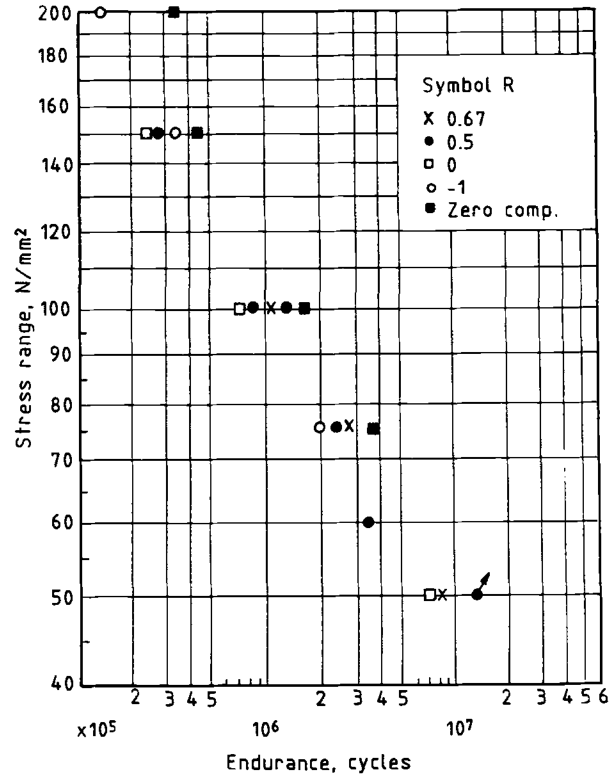

FIG. 2—*Fatigue results for as-welded longitudinal fillet welded joints tested at various applied stress ratios.*

planar joints be reduced in proportion to (plate thickness)$^{-0.25}$ for thicknesses greater than 22 mm. The experimental data supporting this expression are summarized in Fig. 3.

There is not yet a complete understanding of the role of thickness in fatigue strength, nor is there agreement on how to incorporate thickness effects in fatigue design codes. Nevertheless, the implications for weldment fatigue testing are clear—the dimensions of the laboratory specimens must be as close as possible to those of the structure and particular attention must be paid to plate thickness.

Welding Procedure

For fillet welded joints there is conflicting evidence regarding the influence of the welding procedure on fatigue strength. The effect, if any, is relatively small and fatigue design rules do not distinguish on the basis of welding procedure or process. In contrast, as shown in Fig. 4, the behavior of butt welded joints is strongly dependent on the reinforcement shape [*2*] and this, in turn, is dependent on the welding procedure. In particular, positional and site welds are downgraded [*3*] because of the difficulty of controlling the weld shape.

In view of this, it is important to fabricate the laboratory specimens using a welding process and procedure similar to those to be used in practice. Furthermore, some investigations have specifically compared the fatigue behavior of joints made by a range of welding processes—for example, shielded metal arc, submerged arc, friction, laser, and electron beam processes.

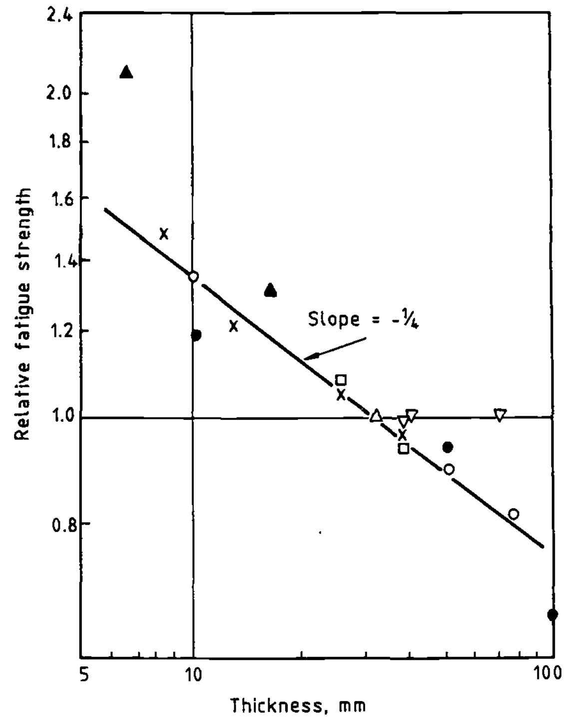

FIG. 3—*Influence of plate thickness on fatigue strength (normalized to a thickness of 32 mm).*

Postweld treatments may also conveniently be considered as forming part of the total welding procedure. As discussed earlier, residual stress levels play an important role in determining fatigue strength, and hence postweld heat treatment or stress relief by mechanical vibration may significantly affect fatigue behavior. Many investigations have studied methods of improving fatigue strength, such as toe grinding, hammer peening, and shot peening [*9*]. Adequate control of these operations is essential for consistent fatigue data.

Specimen Preparation

Strain Gages

It is obviously important when performing fatigue tests on welded joints to have information regarding the load on the specimen. This can be determined either directly from the machine, provided it has been adequately calibrated, or from strain gages located on the specimen. One of the advantages of using strain gages is that they can be used to detect any secondary bending stresses in the specimen. However, when strain gages are used, considerable care is required with regard to their location [*10*] and to the surface preparation.

Strain gages should be set back from the weld toe for two reasons:

1. They should not be so close to the weld that they pick up the local stress concentration associated with the weld itself. This is sometimes referred to as the "notch effect."

2. The preparation of the surface of the specimen to accommodate the strain gage must not encroach on the weld toe.

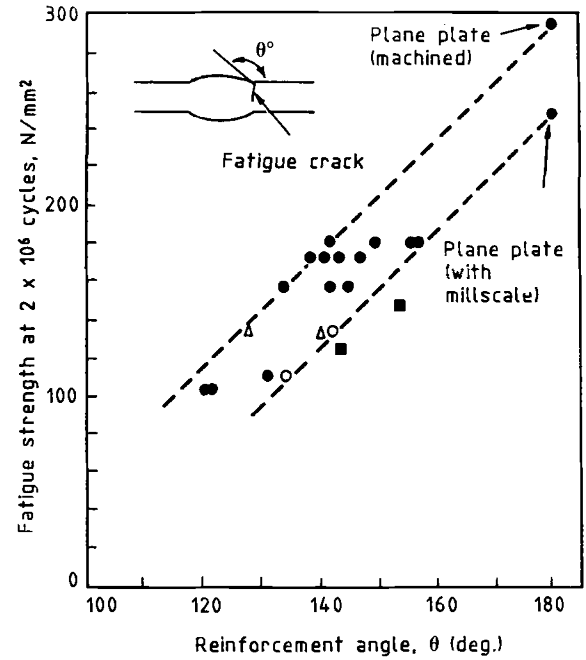

FIG. 4—*The relationship between the reinforcement angle and fatigue strength of transverse butt welds.*

It is conventional to express fatigue results for welded joints in terms of the nominal stress remote from the weld. This approach is sensible because the very local stress adjacent to the weld toe will be influenced by the local geometry and shape of the weld. This is a feature over which the designer can have no control. By expressing the stress as a nominal value, any variations in the local stress at the weld toe can be accounted for as scatter in the test data. Thus, by adopting a lower bound to the experimental data, the designer is effectively taking account of normal variations in the geometric shape of the weld. It has been found that the notch effect associated with a weld toe decays to the nominal value in the plate within about 0.2 of the plate thickness. Thus, it is recommended that strain gages be at least 0.4 of the plate thickness away from the weld toe.

If an attempt is made to locate a strain gage so close to the weld that the local effect of the weld toe is recorded by the gage, it is inevitable that the weld toe itself will be ground when preparing the surface for the strain gage. This is extremely important, as it is likely to lead to an artificially high fatigue endurance for the specimen. In essence, this is the same as the weld toe grinding technique, which is used to improve fatigue strength.

When using strain gages it is conventional to locate a pair of strain gages on each side of the specimen. The advantage of this is that the gages will record any secondary bending stresses in the specimen due to misalignment or nonaxiality of applied loading. If the specimen does have any geometric irregularities, the secondary bending stresses can be very high and the strain gage results will be essential in the interpretation of the fatigue results.

Specimen Straightness and Alignment

Under axial loading, bowing and misalignment give rise to local bending stresses, which may be considerably greater than the nominal axial stress [*11*]. This results in a false measurement of specimen endurance, which is much smaller than would have been obtained from straight or aligned specimens. Both butt welded and fillet welded joints are susceptible to bowing, but the situation can be remedied by using plastic deformation to straighten the joint. However, plastic deformation of the weld itself is equivalent to a tensile overload and hence affects fatigue endurance. It is usual to straighten specimens in a four-point bending device, thus ensuring that the plastic deformation is remote from the weldment.

A major problem with transverse butt welds is axial misalignment. The stress concentration factor (K_t) is given by

$$K_t = 1 + \frac{3e}{t}$$

where

e = eccentricity, and
t = thickness.

Examination of this equation shows that a small misalignment gives rise to a relatively large stress concentration factor, and a much greater effect on endurance. There is little that can be done to correct misalignment—adequate control of the welding procedure is required. The importance of minimizing misalignment is shown in Fig. 5 [12], which illustrates that even relatively small degrees of misalignment significantly reduce fatigue strength.

The most useful method of assessing the effects of bowing or misalignment is to install

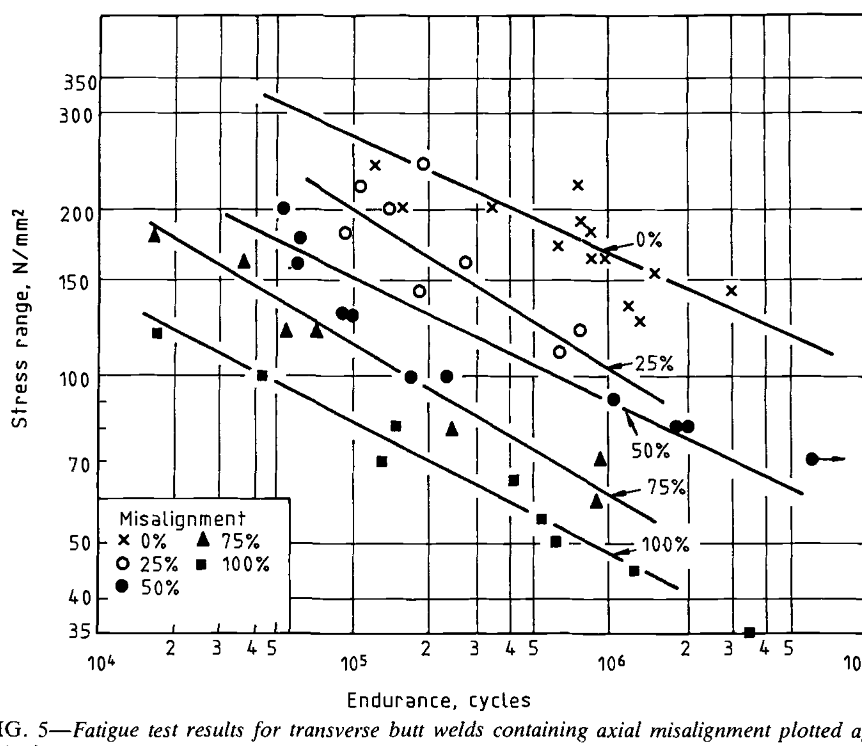

FIG. 5—*Fatigue test results for transverse butt welds containing axial misalignment plotted against nominal stress.*

strain gages on both sides of the specimen. In this way, the local bending stress can be identified and the specimen can be straightened or rejected, as appropriate.

When testing under bending loading, bowing or misalignment do not introduce very large stress raisers and hence are not as important.

Edge Grinding

Specimen edges provide alternative fatigue crack initiation sites that may give rise to premature failure. To avoid this, it is usual to grind the specimen edges, obtaining a smooth profile corresponding to a radius of approximately 2 mm.

Fatigue Testing

Calibration

Although standards exist for the calibration of testing machines under static loading [e.g. ASTM Practices for Load Verification of Testing Machines (E 4-83a)], calibration under dynamic loading has received relatively little attention. It has frequently been assumed that, if a machine satisfies static calibration criteria, it will also perform satisfactorily under dynamic loading. This, of course, does not necessarily follow, and the stress range experienced by a specimen may be significantly different from that indicated by the machine. In the United Kingdom, a standard is in preparation concerned with dynamic calibration of testing machines, but dynamic calibration standards have not gained widespread acceptance, despite the existence of the ASTM Recommended Practice for Verification of Constant Amplitude Dynamic Loads in an Axial Load Fatigue Testing Machine [E 467-76(1982)].

The use of strain gages to determine the actual strain and stress ranges is clearly desirable. This in turn leads to the observation that all electrical equipment associated with the strain gages requires periodic calibration.

Loading Conditions

For axially loaded joints, the results are usually expressed in terms of the stress based on load divided by the cross-sectional area; for joints loaded in bending, the stress range is usually the extreme fiber stress range. When expressed in these terms, the fatigue strength of joints loaded in bending is greater than that of joints loaded axially. Selection of the correct loading mode that most closely resembles the service conditions is therefore essential.

Applied mean stress does not influence the fatigue performance of as-welded joints because of the presence of high tensile residual stresses in the vicinity of the weld: i.e., the weld always experiences a high tensile mean stress. In contrast, for stress-relieved joints and for joints that have been dressed to improve fatigue strength, an increase in applied mean stress results in a decrease in fatigue strength. Applied mean stress should always be controlled and the conventional method of doing this is by defining the stress ratio (R = minimum stress/maximum stress). The most common stress ratios employed are $R = 0$ (zero to tension loading) and $R = -1$ (alternating loading).

For joints loaded in air, the number of cycles to failure is independent of the test frequency. It is usual, therefore, to carry out fatigue tests at the highest frequency attainable by the test machine to reduce the testing times and, hence, costs.

Number of Tests

When an overall assessment of joint performance is required, it is customary to test a series of specimens over an interval of stress ranges to produce endurances ranging from 10^5 to 2×10^6 cycles. Obviously, *S-N* curve definition increases as more specimens are tested, but for most practical circumstances, six to eight specimens are usually sufficient.

In contrast, when the service stress range is known and the best estimate of endurance at that stress is required, then it is inappropriate to determine a full *S-N* curve. Under these circumstances, it is preferable to test all specimens at the stress range of interest. Once again, six to eight specimens are normally sufficient to obtain reasonable estimates of the mean and lower bound behavior.

Environment

The comments in this paper have been principally concerned with joints loaded in air. However, there is an increasing demand for welded fabrications to operate in hostile environments, e.g., offshore structures and nuclear power plants. Corrosive environments may significantly affect fatigue behavior and there is an increasing need for corrosion fatigue testing of weldments. Figure 6 shows the effect of seawater on fatigue behavior, for conditions simulating an offshore structure [*13*]. In corrosive environments, it is first necessary to characterize the environment accurately, in terms of its chemical composition, temperature, and other essential factors, and then to reproduce and maintain the environment in the laboratory.

Furthermore, other parameters, which are not normally important for testing in air, assume much greater significance. In particular, an increase in testing frequency results in a decrease in the number of cycles to failure, because of the reduced time available per cycle for corrosive attack. The test frequency must therefore be the same as that to be encountered in service. For applications where the service loading frequency is low—for example, offshore structures loaded by wave action at a frequency of approximately 0.1 Hz—very long testing times may result. To obtain data in realistic time scales, it has often been necessary to build multiple testing stations so that many joints can be tested simultaneously.

Monitoring

To ensure adequate control of the test, periodic monitoring of the load range and strain gage output (where appropriate) is required. Valuable additional information about joint behavior may be obtained by monitoring crack initiation and growth. Initiation is usually detected visually, often with the aid of soap solution, or it may be detected by a fall in output from a strain gage located close to the initiation site. Crack growth may be monitored visually, or by conventional nondestructive inspection techniques. The most commonly used technique is the electrical resistance potential drop, with direct-current techniques employed for relatively small, planar specimens and alternating-current techniques used for larger, complex geometries. Ultrasonic methods (including time-of-flight techniques) have been used in certain circumstance, but the resolution tends to be less than that of electrical resistance techniques.

In some cases, compliance changes during crack extension are of interest and measurements of actuator displacement are of value.

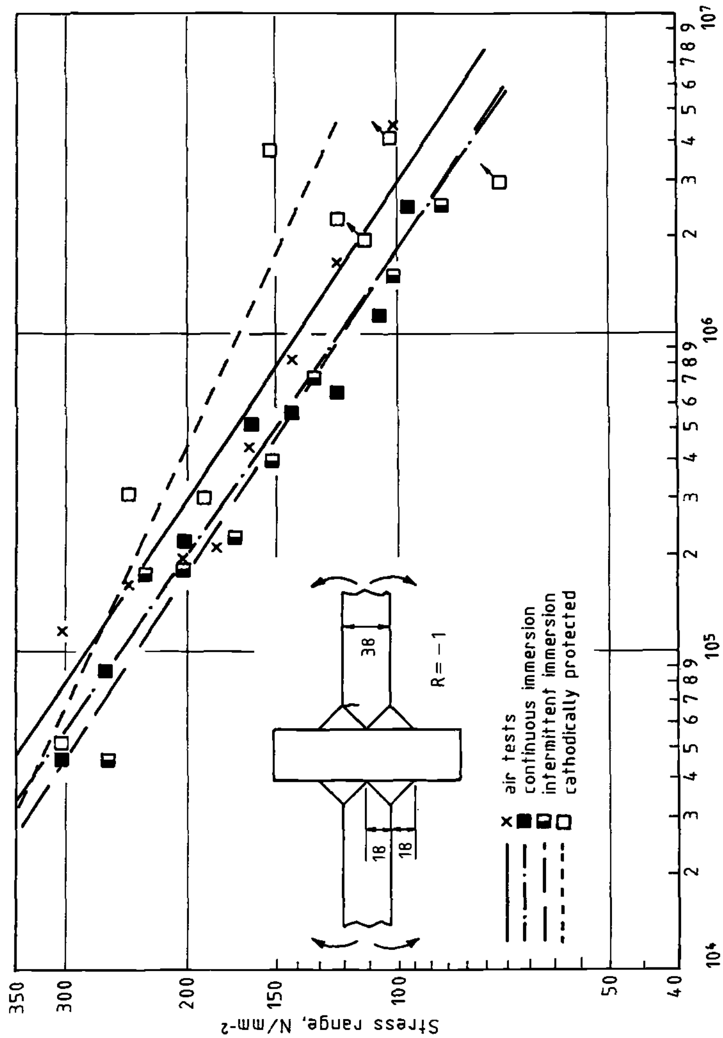

FIG. 6—*Results for transverse joints tested in seawater (stress ratio = −1).*

Failure Criterion

The most common and usually the most appropriate failure criterion is complete specimen separation. For joints loaded in bending, however, specimen compliance increases very rapidly with crack growth, and achievement of a through-thickness crack is unrealistic. In these cases, the end of the test is normally defined as when the actuator reaches its stroke limit; i.e., failure corresponds to a specific displacement. This normally occurs when the crack has grown through about half the plate thickness—the rate of crack growth is then so large that the number of cycles remaining to complete separation is negligible.

In structural testing other failure definitions are sometimes more appropriate. For example, in tests on tubular joints [*14*], failure is sometimes declared when the fatigue crack has grown a specified distance from the joint. Compliance changes (i.e., actuator stroke limitations) are also often used to define failure in tubular joints. A typical relationship [*14*] between actuator displacement and crack size is illustrated in Fig. 7.

Reporting Data

Information Required

A full report should include complete information on the work. This paper has described the main factors to be considered—these should all be addressed in a report. Experience shows that many reports fail to include the definition of the stress range used, the failure criterion, or the failure location.

Presentation of Results

The conventional method of presenting fatigue results is on stress-range/number-of-cycles-to-failure graphs (*S-N* plots) using logarithmic axes. This form of presentation is extremely valuable as it provides a direct visual method of assessing the influence of specific parameters on fatigue behavior. One limitation, however, is that it can be very difficult for other workers to use the data for comparison because the scale of the *S-N* plots usually employed precludes

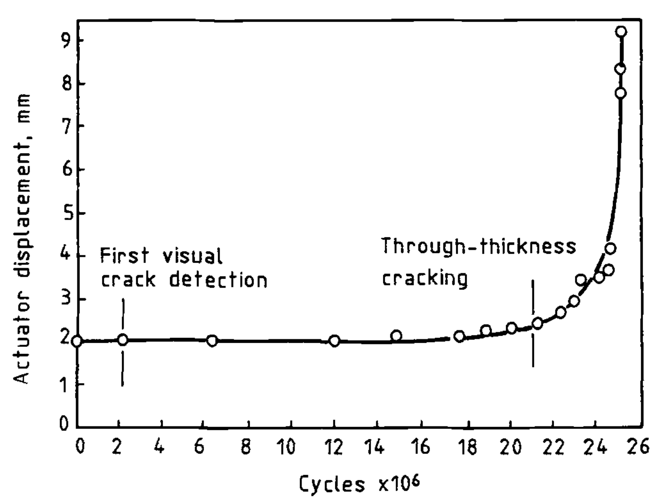

FIG. 7—*Actuator displacement on a 914-mm-diameter T-joint subjected to in-plane bending.*

accurate determination of each data point. For this reason, tabular presentation of data, in addition to graphical display, is greatly encouraged.

Concluding Remarks

Welding is used to fabricate a great number of structures and components that are subjected to cyclic loading. Although many instances are covered by existing fatigue design rules, there are many cases which are outside the scope of current standards. There is a need for fatigue data to enable welded joints to be used safely in these latter applications. Furthermore, it is anticipated that demand for fatigue data for welded joints in a range of materials will continue in the future. It is obvious that great care will be needed in the generation of those data to ensure their validity and applicability.

This paper has highlighted the main procedural considerations relating to the fatigue testing of weldments. Unfortunately, incorrect procedure often, although not always, gives rise to optimistic estimates of fatigue endurance. In view of this, it is perhaps surprising that national standards for the fatigue testing of weldments are not well developed in any country. It is time to review the position and debate whether there are advantages to be gained from having a formal statement, in the form of a national standard, relating to procedures for fatigue testing of weldments.

Acknowledgments

The authors wish to thank their colleagues at The Welding Institute for passing on their experiences with fatigue testing of welded joints.

References

[*1*] Wohler, A., "Tests to Determine the Forces Acting on Railway Carriage Axles and the Capacity of Resistance of the Axles," abstract in *Engineering,* Vol. 11, 1871, p. 199.
[*2*] Gurney, T. R., *Fatigue of Welded Structures.* 2nd ed., Cambridge University Press, Cambridge, England, 1979.
[*3*] "Steel, Concrete and Composite Bridges: Code of Practice for Fatigue," BS5400: Part 10, British Standards Institution, London, England, 1980.
[*4*] Structural Welding Code D1.1, American Welding Society, New York, 1988.
[*5*] Wylde, J. G., "The Influence of Residual Stresses on the Fatigue Design of Welded Steel Structures," *Proceedings,* Conference on Residual Stress in Design, Process and Materials Selection, Cincinnati, OH, April 1987.
[*6*] Maddox, S. J., "Influence of Tensile Residual Stresses on the Fatigue Behavior of Welded Joints in Steel," *Residual Stress Effects in Fatigue, ASTM STP 776,* American Society for Testing and Materials, Philadelphia, 1982.
[*7*] Maddox, S. J., "The Effect of Plate Thickness on the Fatigue Strength of Fillet Welded Joints," The Welding Institute, Cambridge, England, 1987.
[*8*] U.K. Department of Energy, *Offshore Installations: Guidance on Design and Construction,* Her Majesty's Stationery Office, London, 1984.
[*9*] Booth, G. S., "Improving the Fatigue Performance of Welded Joints," The Welding Institute, Cambridge, England, 1983.
[*10*] Wylde, J. G., "The Application of Fatigue Design Rules to Complex Fabrications," *Proceedings,* Society of Automotive Engineers, Conference, Peoria, IL., 1985.
[*11*] Burke, J. D. and Lawrence, F. V., "Influence of Bending Stress on Fatigue Crack Propagation Life in Butt Joint Welds," *Welding Journal,* Vol. 56, No. 1, February 1977, p. 61.
[*12*] Wylde, J. G. and Maddox, S. J., "Effect of Misalignment on Fatigue Strength of Transverse Butt Welded Joints," *Proceedings,* Conference on Significance of Deviations from Design Shapes, Institution of Mechanical Engineers, London, 1979.

[13] Booth, G. S., "The Influence of Simulated North Sea Environmental Conditions on the Constant Amplitude Fatigue Strength of Welded Joints," Paper 3420, *Proceedings,* Offshore Technology Conference, Houston, TX, 1979.
[14] Wylde, J. G. and McDonald, A., "Modes of Fatigue Crack Development and Stiffness Measurements in Welded Tubular Joints," *Fatigue in Offshore Structural Steels,* Institution of Civil Engineers, London, 1981.

Linda R. Link[1]

Fatigue Crack Growth of Weldments

REFERENCE: Link, L. R., "**Fatigue Crack Growth of Weldments,**" *Fatigue and Fracture Testing of Weldments, ASTM STP 1058,* H. I. McHenry and J. M. Potter, Eds., American Society for Testing and Materials, Philadelphia, 1990, pp. 16–33.

ABSTRACT: Fatigue crack growth rate experiments were performed on compact tension specimens of base plate and weldments of 5456-H116 aluminum and of base plate and the heat-affected zone (HAZ) of ASTM A710 Grade A steel. Stress ratios for the tests were 0.1 for both materials, with the aluminum weld also being tested at $R = 0.5$. Crack opening levels were determined for both the weld and the base plate in the aluminum material and for the A710 material in the as-welded and stress-relieved conditions. The fatigue crack growth rates of the welds and HAZ, when the total applied load was used, were significantly less than those of plate for both materials. Using the effective stress intensity, which accounts for crack closure and thus represents the actual stress intensity at the crack tip, results in a shift of the da/dN versus ΔK curves to a faster growth rate. Comparison of the curves shows that the fatigue crack growth rates of the aluminum weld material fall in the same scatter band of data as those for base plate and that, for the A710 material, the HAZ shifts to faster growth rates than the base plate does. This shift of data leads to more accurate estimates on fatigue life, based on the intrinsic properties of the material.

KEY WORDS: weldments, fatigue crack growth rates, crack closure, effective stress-intensity range, aluminum, steel

Since discontinuities leading to fatigue cracks generally occur in welds, it is important to understand and characterize the particular features of welds that affect fatigue properties. For example, when the fatigue life is characterized by stress versus cycles to failure, the specimen size and the weld reinforcement geometry are major parameters. In fatigue crack growth rate testing, where specimens have carefully controlled geometries, additional factors can significantly affect the observed properties. Factors such as residual stresses, corrosion debris, surface roughness, and crack-tip plasticity can influence the crack growth rate observed during fatigue testing by altering the effective stress intensity of the crack tip. Little is known about how residual stress fields are affected by crack growth and how these altered stress fields affect crack growth. For instance, residual stresses at surface stress concentrations may be released by local yielding due to service loads, but the reequilibrated distribution in depth may still have a significant influence on subsequent fatigue crack growth [*1*].

In the past, fatigue crack growth rates of welded materials have been reported to be slower than those for base plate [*2–5*]. Davis and Czyryca also reported that the weld residual stress effects were more significant than environmental effects on the crack growth behavior [*2,3*]. This slower growth rate behavior has raised several questions, because conventional fatigue (*S-N*) behavior indicates a lower fatigue limit for weldments than for base plate. A recent explanation for this includes the presence of tensile residual stresses from welding [*6*]. Residual stresses are produced in welded structures by thermal expansion, plastic deformation, and shrinkage during cooling. The amount of constraint determines the amount

[1] Materials engineer, David Taylor Research Center, Annapolis, MD 21402.

of residual stress. Some researchers have measured tensile residual stresses from welding on the order of 60 to 75% of the material's tensile yield strength. Others estimate that welding produces yield-strength-level residual stresses. Bucci reported that the residual stress distribution was largely responsible for the different propagation rates observed when crack starter notches were located in different regions of identically fabricated extruded rods [7]. Since the effect of tensile residual stresses on a real structure is dependent on their magnitude, the conservative design assumption must be that yield-level residual stresses exist.

Preparing a specimen notch by removing metal that is under residual weld tensile stresses can induce compressive residual stresses at the notch tip in welded materials (Fig. 1). These stresses act to oppose the applied testing loads and keep the crack tip closed even under an applied tensile load. This phenomenon is known as crack closure and can occur at loads significantly above the minimum applied test load. Elber [8] first reported closure to be a result of plasticity in the wake of the growing crack. Elber described the concept of an effective stress-intensity range, ΔK_{eff}, which assumes that crack propagation is controlled by the stress intensity only if the crack tip is opened [8]. When the closure load, P_{cl}, is greater than the minimum applied load, the stress intensity calculated using applied loads will be greater than that actually present at the crack tip. Thus, the effects of the crack tip

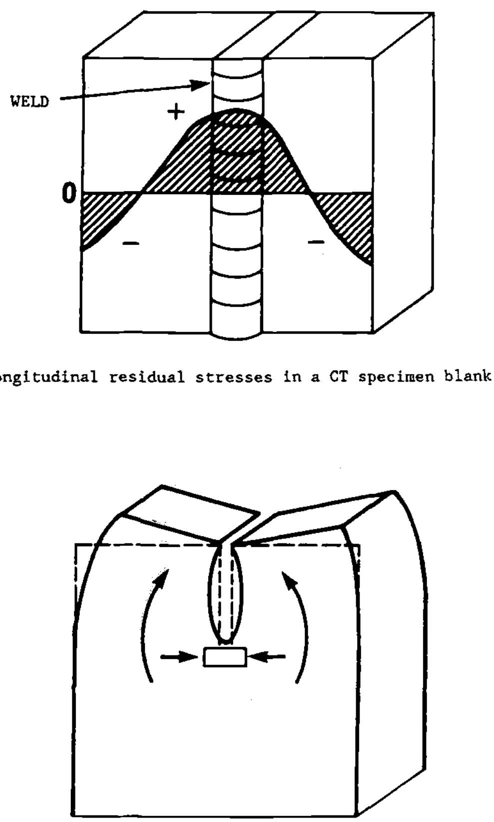

FIG. 1—*Schematic illustration of crack closure produced in a compact tension specimen by longitudinal residual welding stresses.*

closure must be considered to achieve a more accurate estimate of crack growth response to the stress-intensity range.

Crack tip closure can be readily detected by monitoring the trace of the load, P, versus crack opening displacement (COD) on an oscilloscope. Figure 2*a* shows the P-COD response of an ideal specimen loaded elastically, where the slope of the curve is related to the specimen compliance; Fig. 2*b* shows the P-COD behavior with closure. The lower slope is the response of the specimen to the load necessary to overcome any residual stress and open the crack. The upper slope corresponds to the compliance of the specimen with the crack open and is similar to that of the ideal specimen of Fig. 2*a*. The closure load has been measured by several methods, including the lowest tangent point of the upper slope, the intersection of the tangents of the two slopes [*9,10*], a compliance differential method [*11–13*], and a point of predefined deviation from the upper slope [*14*].

This study has compared the fatigue crack growth rate of an aluminum 5456-H116, an aluminum 5086, and an ASTM A710 steel in the as-welded condition with their respective base-plate growth rates. A load ratio effect was determined for the aluminum weld, and

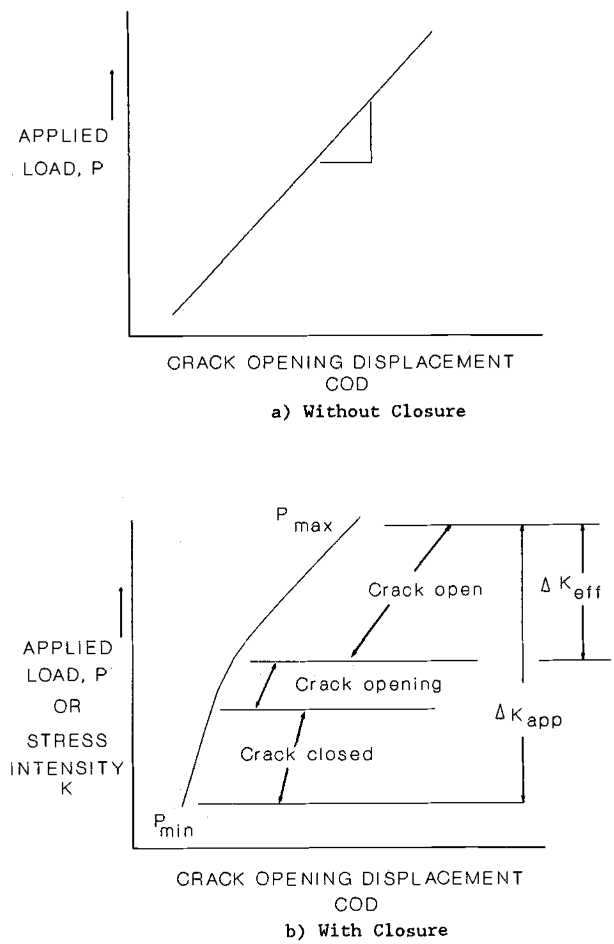

FIG. 2—*Load versus crack opening displacement behavior:* (a) *without closure and* (b) *with closure.*

the effects of stress relief of the steel was examined with respect to applied and effective stress intensities.

Materials and Experimental Procedure

The materials used for this study included 9.4-mm (3/8-in.)[2]-thick 5456-H116 aluminum base plate and weld, 25.4 mm (1-in.)-thick 5086 aluminum, and a 15.9-mm (5/8-in.)-thick ASTM A710 Grade A steel base plate and heat-affected zone (HAZ). The welding conditions for each material are shown in Table 1. Aluminum butt welds were fabricated in the flat position using the automatic gas-metal-arc weld (GMAW) spray transfer process. The weld joints were prepared by machining a 60° included angle double-V joint, using a 5556 aluminum electrode for both thicknesses. The welding techniques—including scraping the machined joint surface, wire brushing and acetone wiping prior to welding each pass, and inclining the welding torch 10° in the direction of travel—were employed to eliminate porosity and lack of fusion defects. One weld pass was deposited from each side to fill the joint. The root of the first pass was removed using a pneumatic chipping hammer with a 3.2-mm (1/8-in.)-radius chisel.

ASTM A710 welds were fabricated in the flat position using the submerged-arc welding (SAW) process with a MIL-100S-1 electrode. Weld joints were prepared with a single bevel (35° included angle) in order to form a straight-sided joint for HAZ testing. Base plate specimens were notched parallel to the plate rolling direction (T-L). The aluminum weld and A710 HAZ specimens were etched and scribed prior to notch preparation and were notched parallel to the welding direction through the weld metal deposit for the aluminum and in the straight-sided HAZ for the steel. Figure 3 shows the specimen dimensions and

TABLE 1—*Welding conditions used in this study.*

CONDITION	5456 ALUMINUM (9.4mm)	5086 ALUMINUM (25.4mm)	ASTM A710 (15.9mm)
Electrode	Alloy 5556	Alloy 5556	Mil-100S-1
Weld Process	GMAW	GMAW	SAW
Electrode Diameter (mm)	1.2	1.6	1.6
Voltage (V)	25	29	34
Current (amp)	210	290	400
Travel Speed (mm/min)	533	686	277
Heat Input (J/mm)	591	787	2953

[2] The original measurements were made in English units and appear in parentheses.

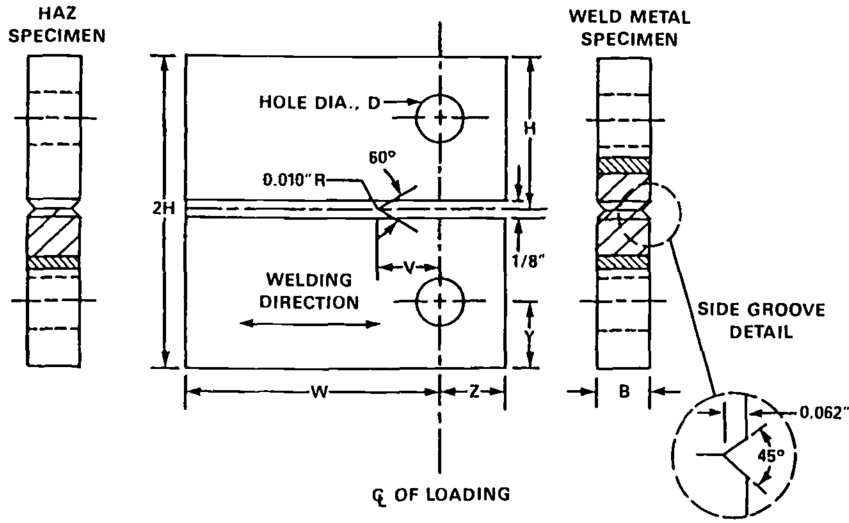

SPECIMEN	W	B	H	D	V	Y	Z
ALUMINUM	3.3(83.8)	0.375(9.5)	2(50.8)	0.5 (12.7)	0.75(19)	1.1(28)	0.95 (24.1)
ASTM A710	4(101.6)	0.625(15.9)	2-7/16 (61.9)	1(25.4)	1(25.4)	1(25.4)	1(25.4)

NOTE: ALL DIMENSIONS IN INCHES (mm)

FIG. 3—*Specimen dimensions and notch locations for aluminum weld and ASTM A710 steel HAZ specimens.*

notch locations for the weld and HAZ specimens. The nominal compositions and typical mechanical properties of both materials are listed in Tables 2 and 3. The specimens were tested using the constant-load-amplitude method, as outlined in the ASTM Test for Measurement of Fatigue Crack Growth Rates (E 647-86a). Fatigue crack growth tests were performed in air using compact tension (CT) specimens under sinusoidal loading at a test frequency of 40 and 10 Hz for the aluminum and 5 Hz for the steel. The steel specimens were side grooved 10% of the specimen thickness on each side to help establish a straight crack front (see Fig. 2). Applied load ratios of 0.1 and 0.5 were used for the aluminum and 0.1 for the steel. Crack length, a, was estimated from specimen compliance using the expression for an edge line compact tension specimen [*15*]

$$a = W(1.001 - 4.6695u + 18.46u^2 - 236.82u^3 + 1214.9u^4 - 2143.6u^5)$$

where

$$u = \frac{1}{\sqrt{\frac{EvB_e}{P}} + 1}$$

TABLE 2—*Chemical composition, in weight percent, and mechanical properties of the aluminum alloys used.*

MATERIAL	Yield Strength (ksi)	Ultimate Strength (ksi)	%EL	RA	Mg	Mn	Cr	Fe	Si	Zn	Ti	Cu
Plate 5086	29.4	45.4	26.6	38.5	4.00	0.04	0.14	0.31	0.08	0.06	0.00	0.09
Plate 5456	42.0	56.0	13.0	11.0	4.90	0.68	0.10	0.30	0.05	0.12	0.03	0.14
Weld Filler 5556	-	45.5	-	-	4.80	0.62	0.07	0.28	0.07	0.12	0.05	0.07

TABLE 3—*Chemical composition, in weight percent, and mechanical properties of the ASTM A710, Grade A steel used.*

MATERIAL	Yield Strength (ksi)	Ultimate Strength (ksi)	%EL	RA	C	Mn	Si	P	S	Ni	Mo	Cr	Cb	Cu
HSLA-80	97.2	108	37	73	0.05	0.69	--	0.01	0.004	0.92	0.19	0.83	0.04	1.20
Weld Filler	92.2	102	22	62	0.08	1.50	--	0.01	0.01	1.75	0.4	0.3	-	-

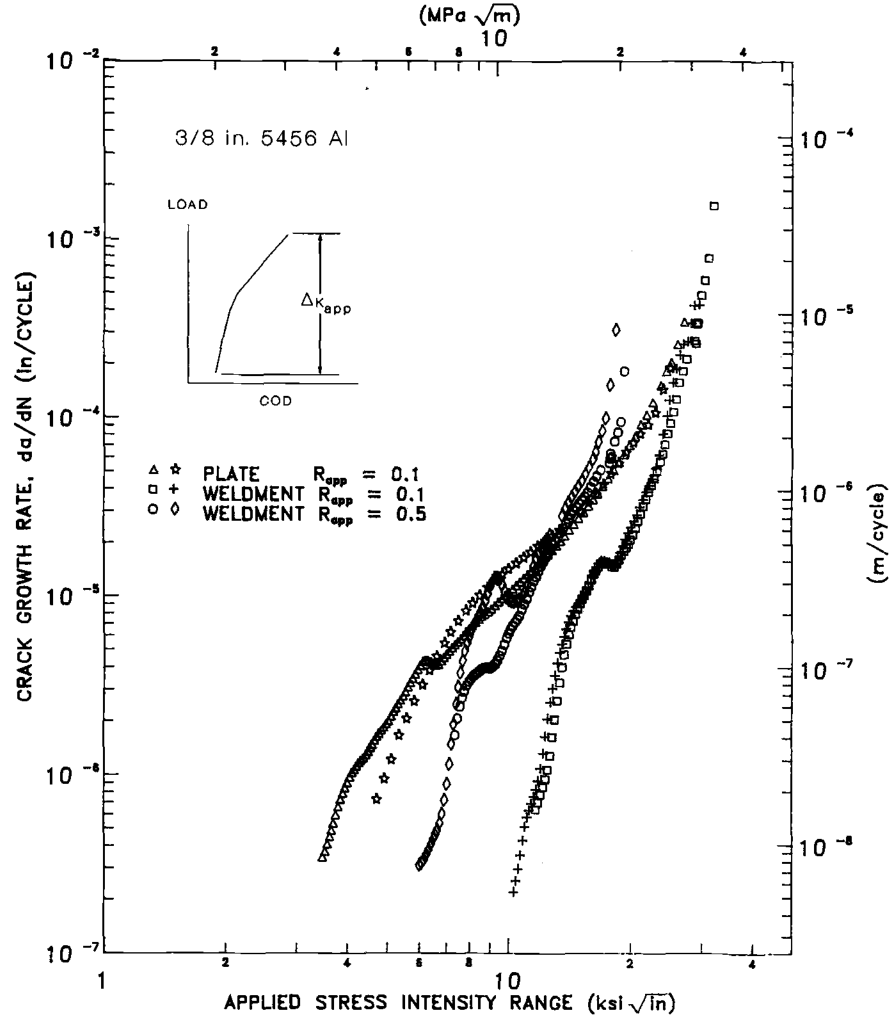

FIG. 4—*Fatigue crack growth rate versus applied stress-intensity range for aluminum alloy 5456-H116 base plate at* R = *0.1 and weldment at* R = *0.1 and 0.5.*

and

P = load, N;
v = crack opening displacement, mm,
E = modulus of elasticity, N/mm^2;
B_e = effective specimen thickness, mm, $B_{max} - [(B_{max} - B_{min})^2/B_{max}]$; and
W = specimen width, mm.

Compliance measurements were based on the upper linear portion of the P-COD traces and were stored, with the cycle count, at crack length intervals of 0.508 mm (0.02 in.). Visual crack length measurements were taken after the test to compare and correct, if

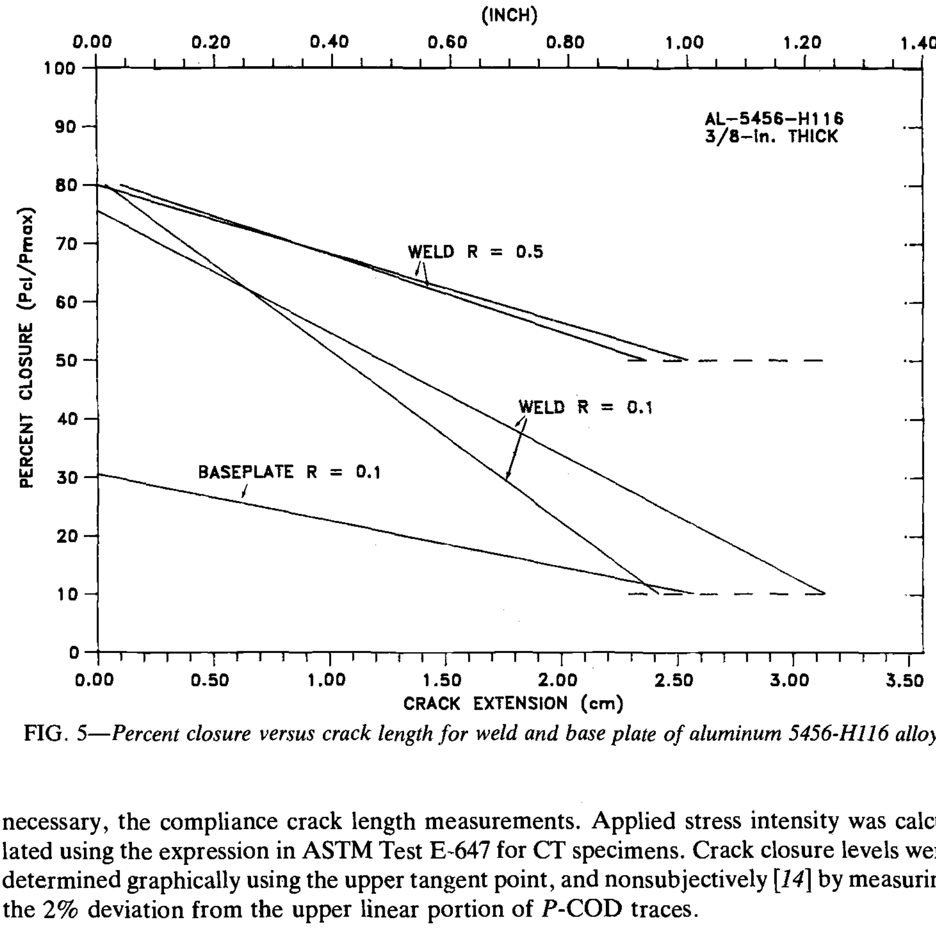

FIG. 5—*Percent closure versus crack length for weld and base plate of aluminum 5456-H116 alloy.*

necessary, the compliance crack length measurements. Applied stress intensity was calculated using the expression in ASTM Test E-647 for CT specimens. Crack closure levels were determined graphically using the upper tangent point, and nonsubjectively [*14*] by measuring the 2% deviation from the upper linear portion of *P*-COD traces.

Results

Aluminum

Figure 4 shows the fatigue crack growth rates of the aluminum alloy for base plate and weld at a stress ratio of $R = 0.1$ and for weld at $R = 0.5$. The stress-intensity factor range, plotted on the abscissa, is calculated using the applied load. The figure shows that, based on the applied stress-intensity range, cracks appear to propagate more slowly in welds than in plate at the same load ratio. Also the crack growth rates of weldments appear to increase with increasing R. This finding is consistent with those of other reports [*4,16,17*].

Results of the crack closure measurements made on the specimens are plotted using least squares regression of the percentage of closure versus crack extension in Fig. 5. It can be seen that near the beginning of the test (zero crack extension) the closure loads are maximum, and they decrease as the crack grows. Initial closure loads for the welds are near 80% of maximum applied load, P_{max}, and for plate they are about 30% of P_{max}. The initial closure values are nearly uniform within each group. These findings are consistent with the explanation that crack closure in welds results from the redistribution of weldment residual stresses

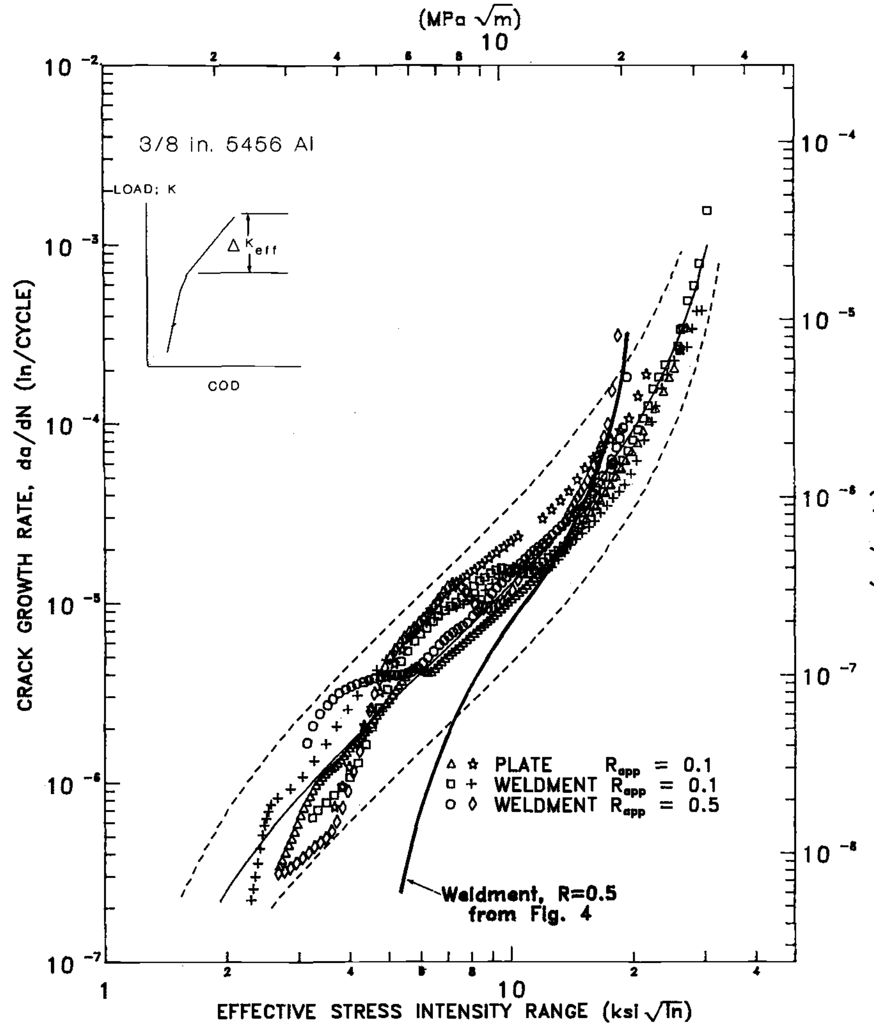

FIG. 6—*Fatigue crack growth rate versus effective stress-intensity range for aluminum alloy 5456 base plate and weldment.*

due to machining of the specimen notch, and also through crack propagation [*3,18,19*], that is, stress relief with crack extension. Although residual stresses in welds are typically very high (approaching yield strength), those in plate usually are considered insignificant. However, the H116 temper of the alloy tested does incorporate a strain-hardening operation that induces a significant residual stress (although not as high as that from welding).

Taking crack closure into account results in the fatigue crack growth rate curves for the three test conditions plotted in Fig. 6. In this figure ΔK_{app} is replaced by ΔK_{eff} as the independent variable. Because the closure load rather than the minimum load is considered, ΔK_{eff} represents the fatigue response to the actual stress state at the crack tip. The most visible effect of using ΔK_{eff} is the extreme shift of the weld data to the left (to higher growth rates) at lower ΔK. As the crack grows, the amount of crack closure decreases (release of residual stress); thus, ΔK_{eff} approaches ΔK_{app}. Compare the weld data at R = 0.5. When

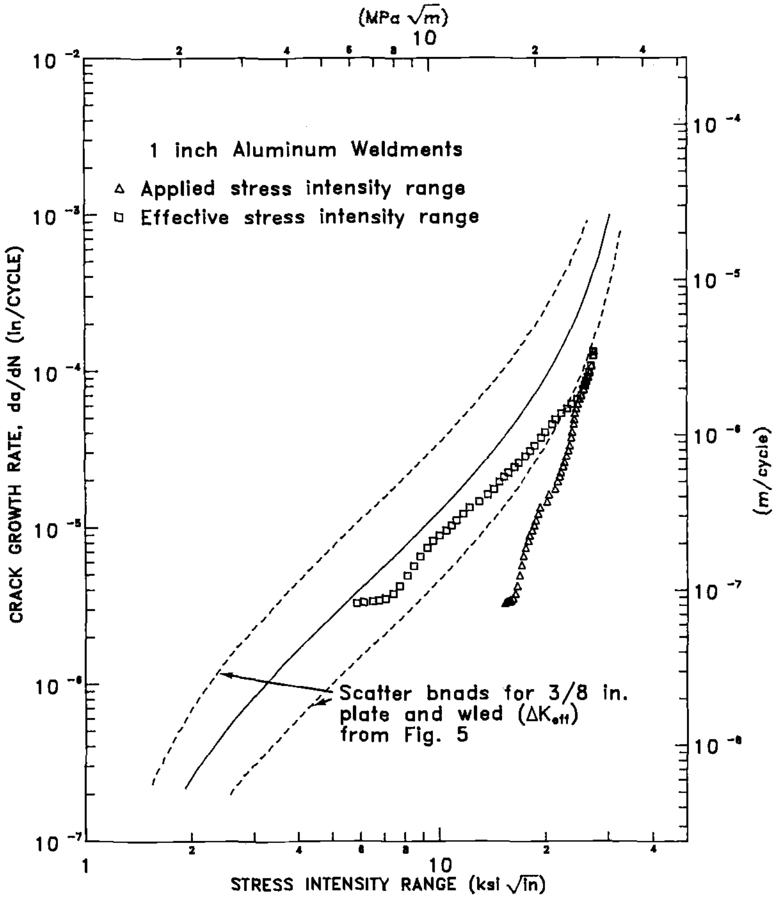

FIG. 7—*Comparison of fatigue crack growth rates of 9.4-mm (3/8-in.) and 25.4-mm (1-in.)-thick aluminum weldments,* R = *0.1.*

data from all conditions are superimposed, the close grouping indicates that ΔK_{eff} accounts for the differences in crack growth rate observed for plate, weld, and load ratio.

A comparison of the results for a 25.4-mm (1-in.)-thick weld specimen with those of the 9.5-mm (3/8-in.)-thick specimen are shown in Fig. 7. The 25.4-mm (1-in.) specimen crack growth rates are shown as two curves, one plotted against ΔK_{app} and the other against ΔK_{eff}. Examination of Fig. 7 highlights the earlier observation of crack closure—namely, that the maximum effect is at lower ΔK (and lower growth rates), which corresponds to shorter crack lengths. In addition, the ΔK_{eff}-based curve for the thick weld lies on the lower side of the scatter band of the thin specimen results. These results show that, at least in this case, crack closure effects were similar for the thick and the thin welded specimens.

A710 Steel

Figure 8 shows the crack growth rates of the ASTM A710 material notched in the base plate and the heat-affected zone (HAZ) with respect to the applied stress-intensity factor

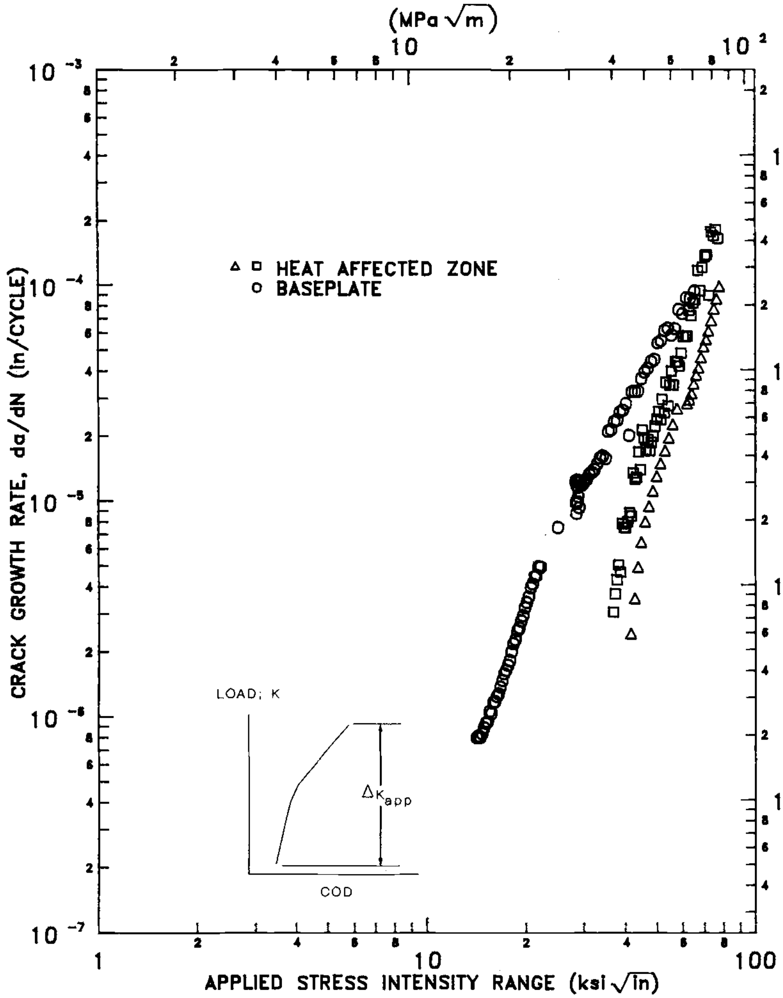

FIG. 8—*Fatigue crack growth rate versus applied stress-intensity range for ASTM A710 steel base plate and HAZ.*

range, ΔK_{app}. As is true for the aluminum weld, the growth rates for the HAZ are slower than those for the base plate. The measured closure levels are shown in Fig. 9 on several *P*-COD traces. As is shown, the closure level, initially 80% of the maximum applied load, decreases as the crack extends into the specimen to a level of about 40% of P_{max}. Further crack extension resulted in additional reduction in the measured closure level to as low as the minimum applied load. Taking into account these closure measurements, the crack growth rates were determined using ΔK_{eff} and are shown in Fig. 10. Now, the growth rate has shifted to the left of the base plate data, that is, to faster growth rates.

To determine the extent that the residual stress influenced the crack growth rates, two specimens were stress relieved at 685°C (1200°F) for 1 h prior to testing. Figure 11 shows the results based on ΔK_{app}. Assuming that the base plate would be unaffected by a similar heat treatment, stress relieving of the weld resulted in the attainment of properties similar

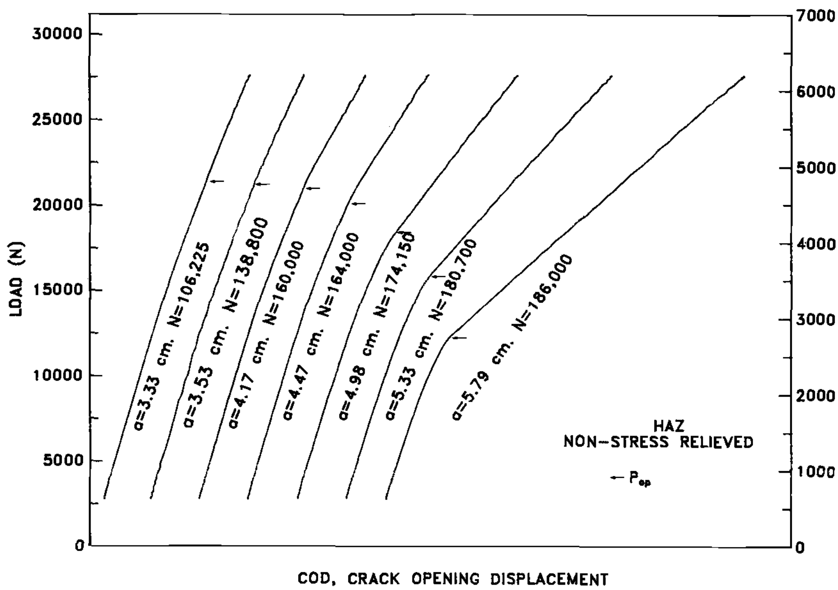

FIG. 9—P-*COD traces showing closure levels (measured visually) of non-stress-relieved ASTM A710 steel HAZ.*

to those of the base plate. However, closure levels were still detected, though not to as significant levels as in the non-stress-relieved specimens (Fig. 12). Initial closure levels were measured at 45% of the maximum load. Also, the maximum load necessary to obtain similar ranges in applied stress intensities was significantly lower than that for the non-stress-relieved specimens, 9.3 kN (2100 lb) versus 27.6 kN (6200 lb). So, taking into account these closure levels, the growth rates were reevaluated based on ΔK_{eff}. The combined results of the base plate, stress-relieved HAZ, and non-stress-relieved HAZ tests are shown in Fig. 13. Using ΔK_{eff} for all cases reveals that the stress-relieved data now fall into the same scatter band as the non-stress-relieved data, which correspond to faster crack growth rates than the base plate rates. Table 4 shows the Paris law constants for base plate, non-stress-relieved HAZ, and stress-relieved HAZ based on both the applied and the effective stress-intensity range. The slope, n, values of the HAZ applied are significantly higher than either the base-plate or stress-relieved HAZ values, especially the average effective HAZ value.

Discussion

Accurate measurement of fatigue crack growth and fracture properties requires caution so that the determined properties are not artifacts of residual stresses remaining in the test coupon. The problem develops in that stress-intensity factors are generally reproduced in fracture mechanics specimens with relatively small applied stresses and large cracks. In an engineering structure, however, the same stress-intensity factor is often produced by large stresses and small cracks [7]. Therefore, residual stresses perceived to be small in the engineering sense can affect the growth rate measurement when the ratio of residual stress to applied stress in the test coupon is significant. Under this premise, fatigue crack growth rates at low ΔK levels represent the fracture mechanics property likely to be most seriously

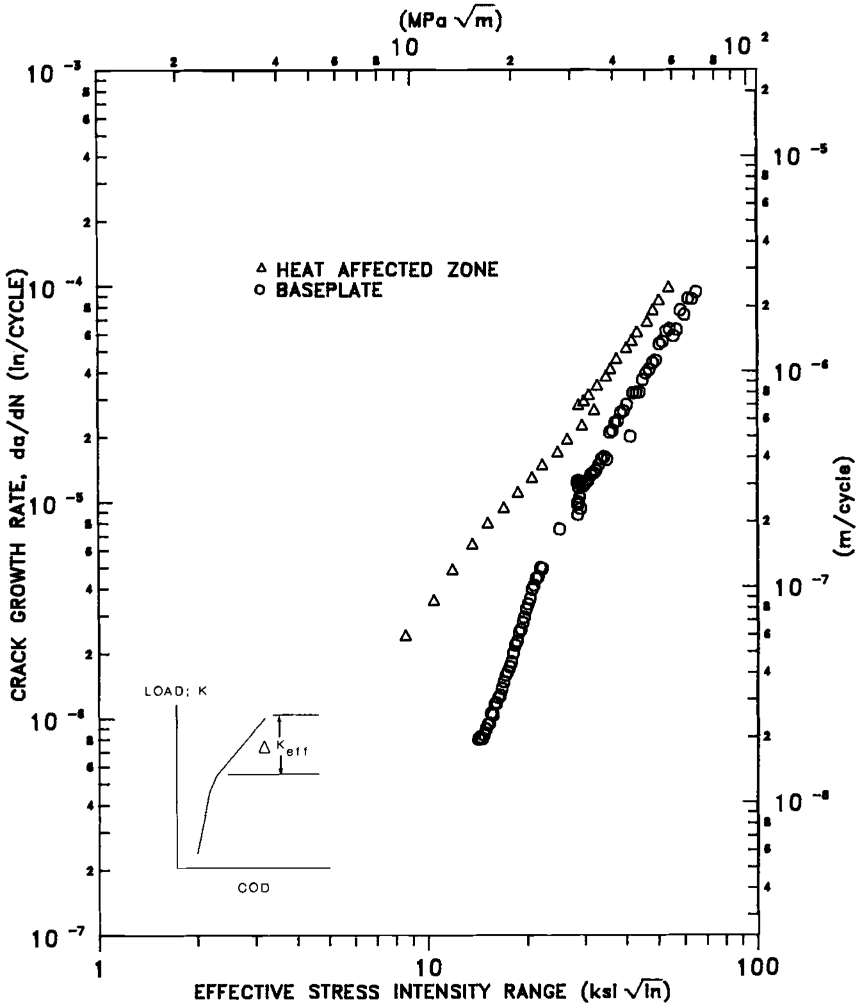

FIG. 10—*Fatigue crack growth rate versus effective stress-intensity range for ASTM A710 steel HAZ.*

affected by residual stress influences. And, as is shown in Figs. 6, 7, and 13, the greatest shift in the growth rate curves occurs at the lower growth rates.

Raising the load ratio has the effect of reducing the effective stress intensity because the minimum applied load becomes closer to the actual minimum load at which the crack is opening. If the stress ratio is sufficiently raised, to above the crack closure level, then no difference in crack growth should be detected. For the case of the aluminum, closure levels were measured as high as 80% of the maximum load, so that the stress ratio applied (R = 0.5) was not enough to overcome the actual stress at the crack tip until the crack had been extended significantly (Fig. 5).

At relatively short crack lengths, the large initial closure level measured for the steel HAZ explains why the non-stress-relieved specimens required a much higher maximum load than the stress-relieved specimens to propagate a crack at equivalent growth rates early in the test. In non-stress-relieved specimens, the closure level decreased with stress relief during

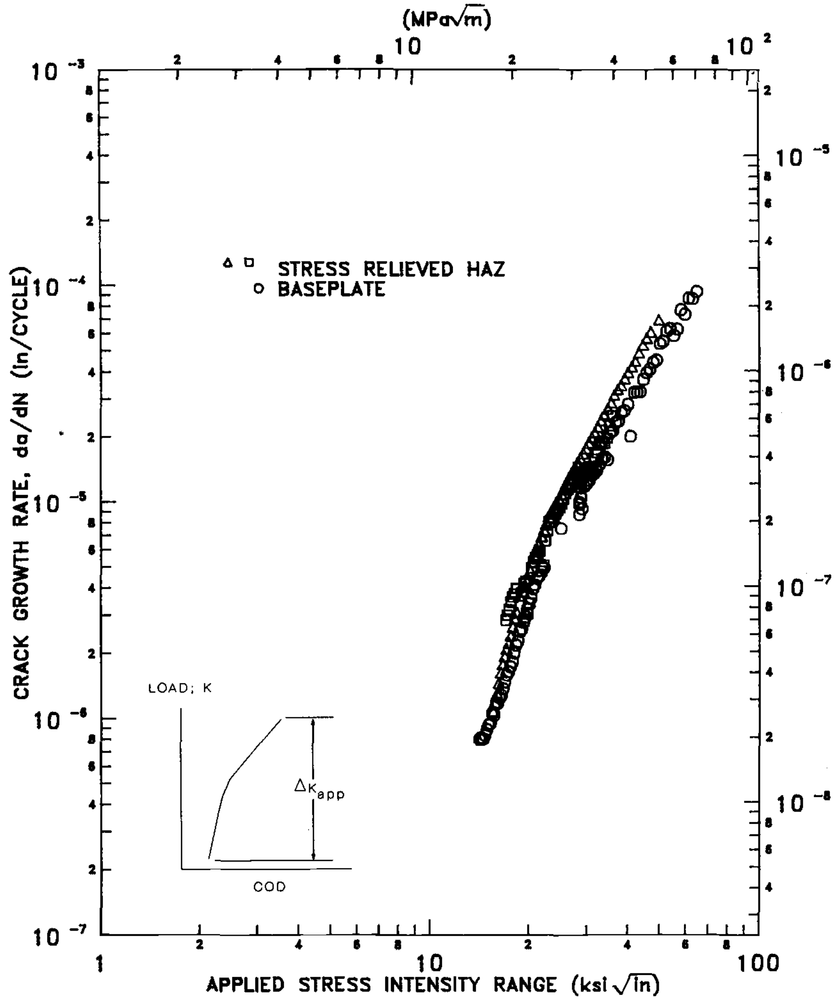

FIG. 11—*Fatigue crack growth rate versus applied stress-intensity range for stress-relieved ASTM A710 steel HAZ.*

crack extension. This explains the near equivalence of da/dN versus ΔK in both stress-relieved and non-stress-relieved specimens at high ΔK levels (long crack lengths) [*19*]. The closure levels observed in the stress-relieved specimen indicate that the heat treatment applied to the specimens did not completely relieve the residual weld stresses.

Some precautions need to be addressed when testing weldments. The initial fatigue pre-crack can sometimes be difficult to initiate and may require high initial ΔK values with subsequent load shedding before fatigue crack growth testing can begin. Once a precrack has initiated, some difficulty may arise in developing a straight crack path. The residual stresses that are present can cause the crack to initiate, and then propagate, from only one side of the blunt notch. Procedures that can eliminate this phenomenon include specimen side grooving, applying an initial compressive load, and using chevron notches to aid in crack initiation. However, even with specimen side grooving the steel specimens in this study still had significant difficulty in establishing straight crack fronts. Side grooving can

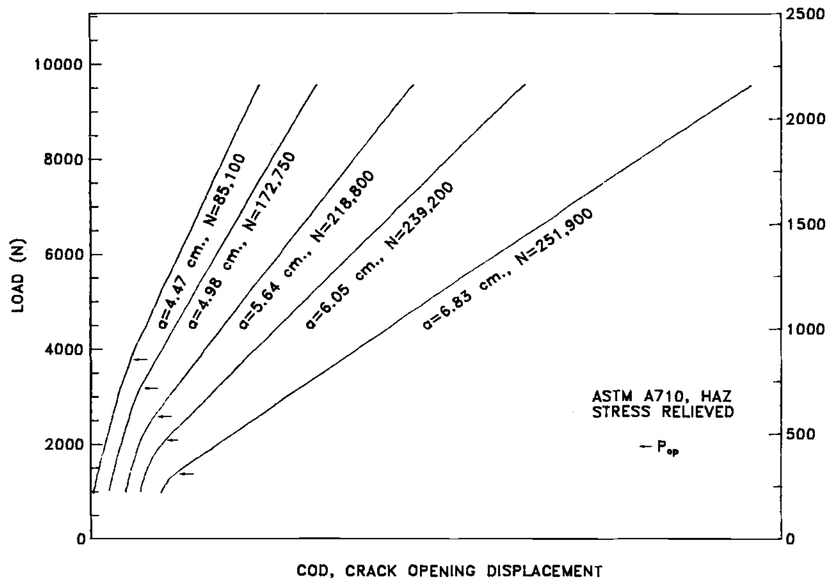

FIG. 12—P-*COD traces showing closure levels (measured visually) of stress-relieved ASTM A710 steel HAZ.*

also aid in planar crack propagation, that is, crack propagation perpendicular to the applied load [*20*]. Seeley et al. [*20*] reported a tendency for cracks to deviate from the midplane of the specimen, perpendicular to the axis of load application. They also reported that those specimens in which the cracks deviated from midplane resulted in higher crack growth rates. Because initial closure levels can be significant (greater than 80% of maximum load) when testing welds, it is important to ensure that only the portion of the *P*-COD trace where the crack is totally open, that is, the upper linear region, is used for compliance measurements for crack length determinations.

The effects of crack tip closure must be considered to achieve a more accurate estimate of crack growth response to the stress intensity range. The opening load is required to offset compression at the crack tip caused by the superposition of clamping forces attributed to residual stress in the bulk material and forces caused by the wedging action of residual deformation left in the wake of the propagating crack [*7*]. ASTM Test E-647 assumes the internal stresses to be zero, and uses external loads only to compute the stress intensity. Hence, although growth rates from weldments are completely accurate and valid according to ASTM practice, the data should not be considered representative of the true behavior of the material. The means of taking into account crack closure include increasing the *R* ratio, so that crack closure does not occur, or stress relief of the material to eliminate the effect of the internal stresses. Caution should be advised when stress relieving, to ensure that no metallurgical changes take place that might affect the intrinsic fatigue crack growth response of the material.

Conclusions

The crack growth rates of welded material can be significantly reduced in the presence of welding residual stresses due to the effects of crack closure. Closure loads of up to 80%

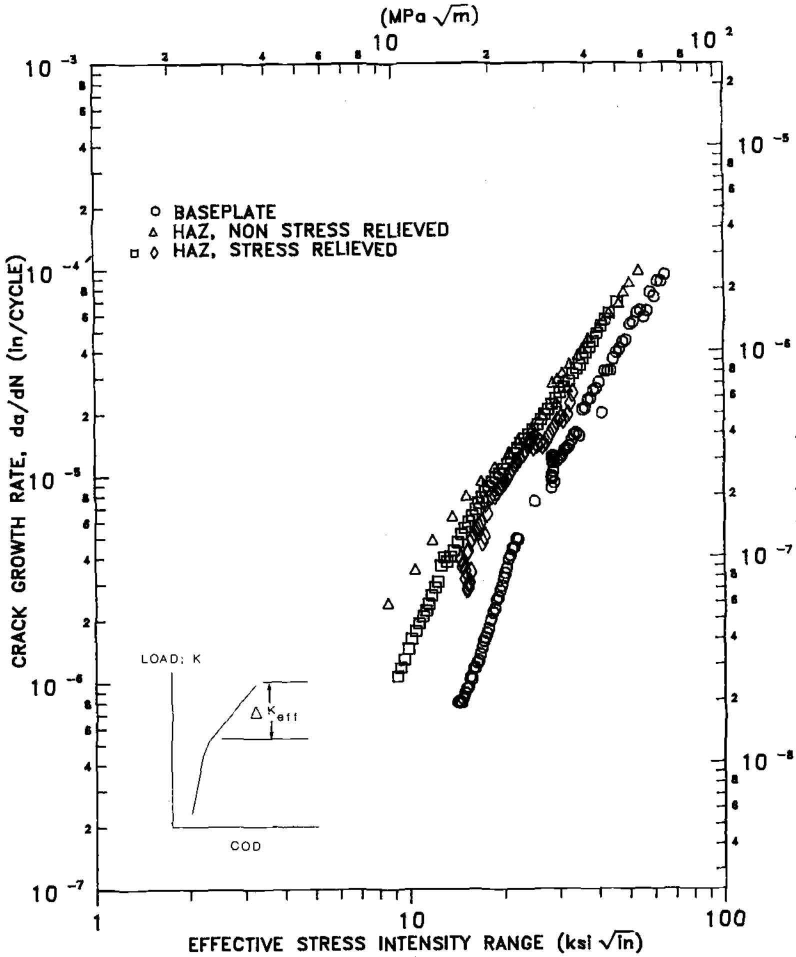

FIG. 13—*Fatigue crack growth rate versus effective stress-intensity range for ASTM A710 steel base plate, non-stress-relieved HAZ, and stress-relieved HAZ.*

of the maximum load have been measured in fatigue crack growth weldment specimens of both aluminum and steel alloys. These closure levels are predominantly an effect of the presence of weld residual stress. Increasing the applied stress ratio can reduce the closure effects in weldments by raising the minimum applied load closer to or above the opening load at the crack tip. Stress relieving ASTM A710 weldments shifted the fatigue crack growth rates to rates equivalent to those of base plate; however, closure levels up to 40% of maximum load still remained because of incomplete stress relief. The fatigue crack growth rate data, when using the effective stress-intensity range, is shifted to faster growth rates in welds, resulting in more accurate estimates of fatigue life, based on the intrinsic properties of the material.

TABLE 4—*Paris law constants for ASTM A710 steel base plate and HAZ.*

	C mm/cycle (in/cycle)	n
AS-RECEIVED HAZ (ΔK_{app})	2.18×10^{-15} (8.57×10^{-14})	4.96
	1.05×10^{-15} (4.15×10^{-14})	4.95
BASEPLATE	5.16×10^{-12} (2.03×10^{-10})	3.19
STRESS RELIEVED HAZ (ΔK_{app})	2.21×10^{-11} (8.71×10^{-10})	2.86
	4.04×10^{-12} (1.59×10^{-10})	3.40
HAZ (ΔK_{eff}) (COMBINED)	8.59×10^{-10} (3.38×10^{-8})	1.99

References

[1] Nelson, D. V., "Effects of Residual Stress on Fatigue Crack Propagation," *Residual Stress Effects in Fatigue, ASTM STP 776,* American Society for Testing and Materials, Philadelphia, 1982, pp. 172–194.

[2] Davis, D. A. and Czyryca, E. J., "Corrosion Fatigue Crack-Growth Behavior of HY-130 Steel and Weldments," *Transactions of the ASME,* Vol. 103, November 1981, pp. 314–321.

[3] Davis, D. A. and Czyryca, E. J., "Corrosion-Fatigue Crack Growth Characteristics of Several HY-100 Steel Weldments with Cathodic Protection," *Corrosion Fatigue: Mechanics, Metallurgy, Electrochemistry, and Engineering, ASTM STP 801,* T. W. Crooker and B. N. Leis, Eds., American Society for Testing and Materials, Philadelphia, 1983, pp. 175–196.

[4] Benoit, D., Lieurade, H.-P., and Truchon, M., "A Study of the Propagation of Fatigue Cracks in the Heat-Affected Zones of Welded Joints in E-36 Steel," *European Offshore Steels Research Seminar,* Cambridge, United Kingdom, November 1978, pp. VI/P13-1-7.

[5] Kaufman, J. G. and Kelsey, R. A., "Fracture Toughness and Fatigue Properties of 5083-0 and 5183 Plate for Liquefied Natural Gas Applications," *Properties of Material for Liquefied Natural Gas Tankage, ASTM STP 579,* American Society for Testing and Materials, Philadelphia, 1975, pp. 464–482.

[6] Baird, J. E. M. and Knott, J. F., "Fatigue Crack Propagation in the Vicinity of Weld Deposits in High-Strength, Structural Steel," Fifth International Conference on Fracture, D. Francois, Ed., Vol. 5, 1982, pp. 2061–2069.

[7] Bucci, R. J., "Effect of Residual Stress on Fatigue Crack Growth Rate Measurement," *Fracture Mechanics: Thirteenth Conference, ASTM STP 743,* Richard Roberts, Ed., American Society for Testing and Materials, Philadelphia, Pa. 1981, pp. 28–47.

[8] Elber, W. "The Significance of Fatigue Crack Closure," *Damage Tolerance in Aircraft Structures, ASTM STP 486,* American Society for Testing and Materials, Philadelphia, 1971, pp. 230–242.

[9] Deans, W. F. and Richards, C. E., *Journal of Testing and Evaluation,* Vol. 7, 1979, pp. 147–154.

[10] Allison, J. E. and Williams, J. C. in *Titanium, Science and Technology,* Vol. 4, G. Leutjering, U. Zwicker, and W. Bunk, Eds., DGM Publishers, Oberusel, 1985, pp. 2243–2250.

[11] Paris, P. C. and Herman, L. in *Fatigue Thresholds,* J. Backlund, A. Blom, and C. J. Beevers, Eds., EMAS Publications Ltd., Warley, United Kingdom, 1981, pp. 3–32.

[12] Liaw, P. K., Hudak, S. J., Jr., and Donald, J. K., *Metallurgical Transactions A,* Vol. 13A, 1982, pp. 1633–1645.

[13] Fleck, N. A., "An Investigation of Fatigue Crack Closure," Ph.D. thesis, Cambridge University, Cambridge, England, 1984.

[14] Donald, J. K., "A Procedure for Standardizing Crack Closure Levels," *Mechanics of Fatigue Crack Closure, ASTM STP 982,* J. C. Newman and W. Elber, Eds., American Society for Testing and Materials, Philadelphia, 1988, pp. 222–229.

[15] Saxena, A. and Hudak, S. J., "Review and Extension of Compliance Information for Common Crack Growth Specimens," *Journal of Testing and Evaluation,* Vol. 8, No. 1, 1980, pp. 19–24.

[16] Katcher, M. and Kaplan, M., "Effects of R-Factor and Crack Closure on Fatigue Crack Growth for Aluminum and Titanium Alloys," *Fracture Toughness and Slow-Stable Cracking, ASTM STP 559,* American Society for Testing and Materials, Philadelphia, 1974, pp. 264–282.

[17] Vazquez, J. A., Morrone, A., and Ernst, H., "Experimental Results on Fatigue Crack Closure for Two Aluminum Alloys," *Engineering Fracture Mechanics,* Vol. 12, 1979, pp. 231–240.

[18] Nordmark, G. E., Mueller, L. N., and Kelsey, R. A., "Effect of Residual Stresses on Fatigue Crack Growth Rates in Weldments of Aluminum Alloy 5456 Plate," *Residual Stress Effects in Fatigue, ASTM STP 776,* American Society for Testing and Materials, Philadelphia, 1982, pp. 44–62.

[19] Underwood, J. H., Pook, L. P., and Sharples, J. K., "Fatigue-Crack Propagation Through a Measured Residual Stress Field in Alloy Steel," *Flaw Growth and Fracture, ASTM STP 631,* American Society for Testing and Materials, Philadelphia, 1977, pp. 402–415.

[20] Seeley, R. R., Katz, L., and Smith, J. R. M., "Fatigue Crack Growth in Low Alloy Steel Submerged Arc Weld Metals," *Fatigue Testing of Weldments, ASTM STP 648,* D. W. Hoeppner, Ed., American Society for Testing and Materials, Philadelphia, 1978, pp. 261–284.

D. Erickson[1] *and D. Kosteas*[1]

Assessing Transverse Fillet Weld Fatigue Behavior in Aluminum from Full-Size and Small-Specimen Data

REFERENCE: Erickson, D. and Kosteas, D., "**Assessing Transverse Fillet Weld Fatigue Behavior in Aluminum from Full-Size and Small-Specimen Data,**" *Fatigue and Fracture Testing of Weldments, ASTM STP 1058*, H. I. McHenry and J. M. Potter, Eds., American Society for Testing and Materials, Philadelphia, 1990, pp. 34–46.

ABSTRACT: Differences between full-size and small specimens in the fatigue performance of transverse welded aluminum joints are investigated. Residual stresses and their possible effect on fatigue strength are also discussed. In addition, comparative methods of evaluating and presenting test data are introduced.

KEY WORDS: weldments, aluminum, welding, fatigue, residual stresses, component testing, data evaluation

For many years, small-specimen test data have served as the major source of information upon which fatigue design specifications have been based. Many of the data from small-specimen testing have now been gathered and are stored on computer as part of the Aluminum Data Bank [*1*]. Small-specimen testing carries with it several advantages—i.e., it is less costly, the weld detail is well defined, and there is greater control over the manufacturing and testing of the specimen. However, small-specimen testing cannot always be expected to offer a true representation of the actual detail in service—thus the need for full-size testing.

Extensive full-size (or component) testing, on the other hand, has only recently been accomplished [*2*]. Full-size testing can more closely represent actual service conditions as well as examine such load facets as residual stress effects, crack initiation and propagation, and weld imperfection effects. The testing of full-size and small specimens should serve to complement one another. It is the purpose of this paper to examine and explain differences found between full-size and small-specimen data in transverse fillet weld fatigue behavior.

Background

Between 1982 and 1985 an extensive test program was undertaken at the Technical University of Munich, Munich, West Germany, to examine the fatigue behavior of full-size components of the 5083 and 7020 series aluminum alloys. The 5000 and 7000 series aluminum alloys are to be found in use in transportation vehicles, ship structures, and other structural engineering applications where aluminum serves as the primary load-bearing component. Fatigue testing was performed on 52 aluminum beams, as shown in Fig. 1. Forty beams were subjected to constant-amplitude loading with R-ratios of -1.0 and 0.1. In addition, residual stresses were measured on several beams using the hole drilling method. Typical

[1] Technical University of Munich, 8000 Munich 2, West Germany.

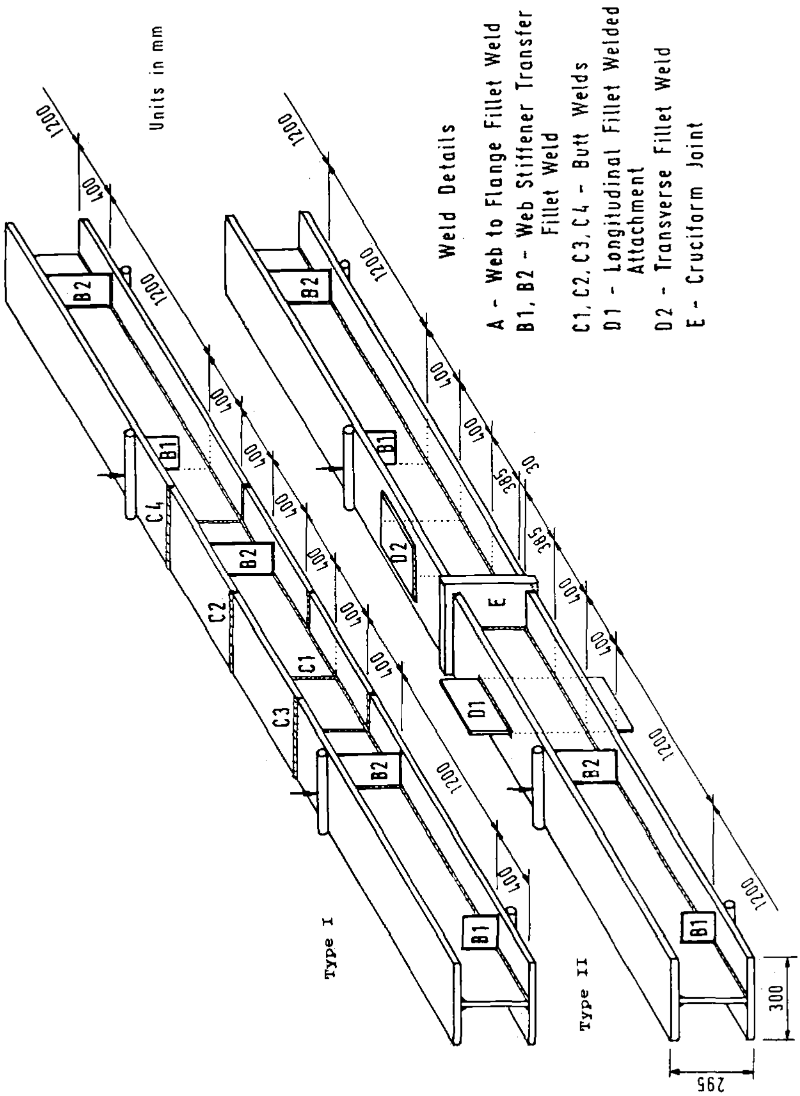

FIG. 1—Welded beam fatigue testing specimens.

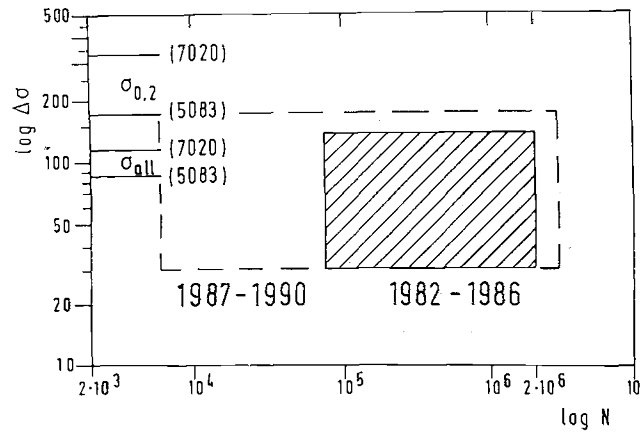

FIG. 2—*Stress-life region of the beam tests.*

weld details are indicated by weld Details A through E in Fig. 1. The particular weld details that will be examined in this paper are the transverse fillet welds on the cover plate (Detail D2) and on the cruciform joint (Detail E). The stress-life region of the tests is shown in Fig. 2. Figures 3 through 6 are the resulting *S-N* diagrams. The figures are divided according to joint type and *R*-ratio. Test results have not yet shown a significant difference in fatigue strength between the two alloys.

Having identified those weld attachments utilizing tranverse fillet welds on full-size specimens, it now became necessary to identify corresponding small-specimen data from the Aluminum Data Bank. For that purpose, two joint types from small-specimen data were chosen. These were the cruciform joint and the transverse welded non-load-carrying at-

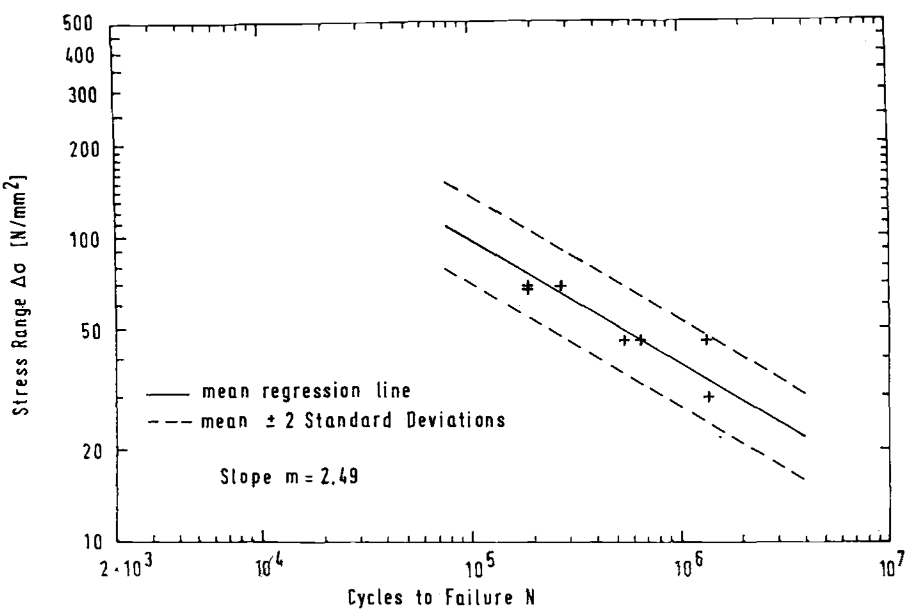

FIG. 3—S-N *diagram of full-size test results/Alloys 7020 and 5083/*R = *+0.1/cruciform joint.*

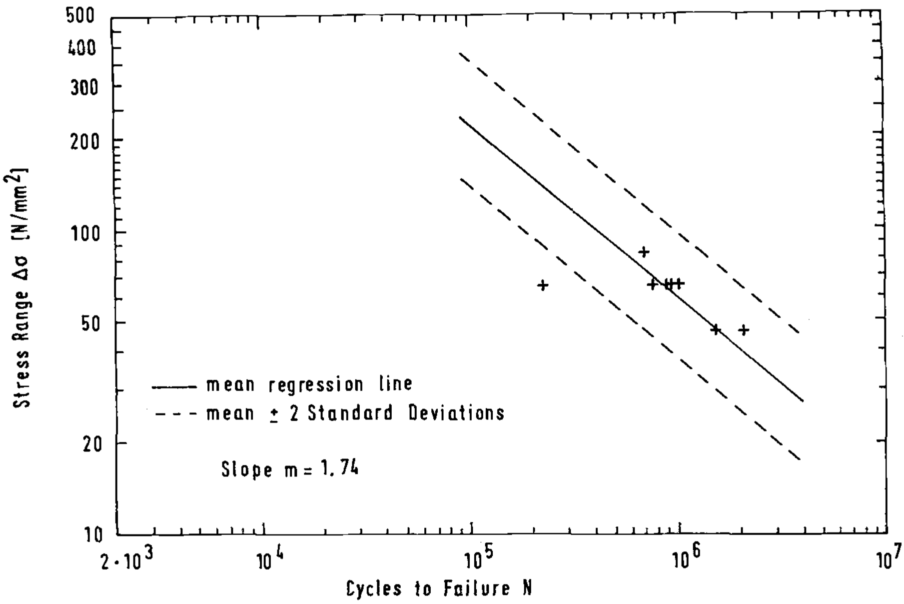

FIG. 4—S-N *diagram of full-size test results/Alloys 7020 and 5083/*R = *−1.0/cruciform joint.*

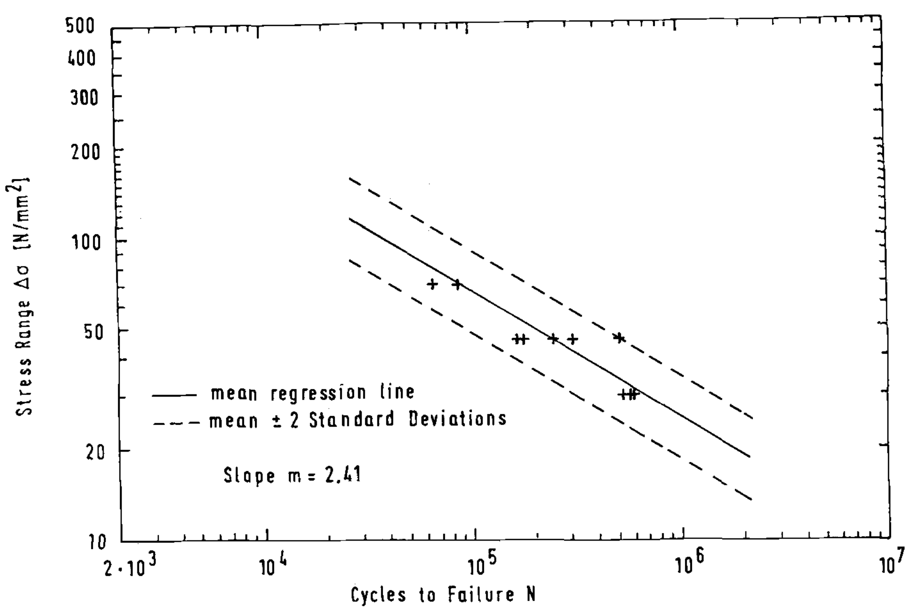

FIG. 5—S-N *diagram of full-size test res.lts/Alloys 7020 and 5083/*R = *+0.1/cover plate detail.*

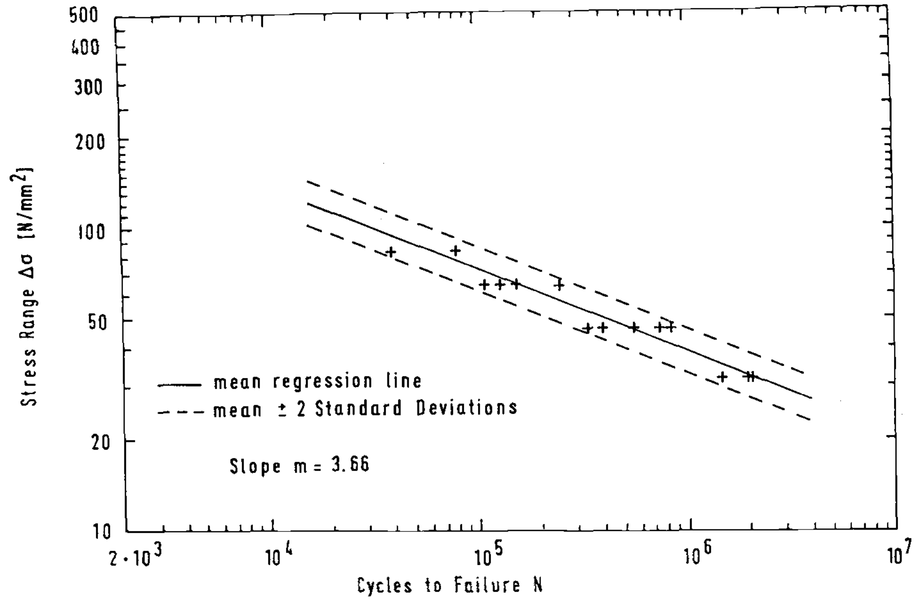

FIG. 6—S-N *diagram of full-size test results/Alloys 7020 and 5083/*R = *−1.0/cover plate detail.*

tachment (Fig. 7). Both joint types are axially loaded. The small-specimen cruciform joint construction is very similar to that of the beam specimens. Finding small-specimen data to compare with the beam cover plate data was slightly more difficult. The beam cover plates do obviously carry some load. However, the cover plates are relatively short and were not specifically designed as load-carrying members. Therefore, the transverse-welded non-load-carrying attachment small-specimen data were analyzed and were compared with full-size cover plate data. A more precise determination of beam cover plate behavior is part of the current beam testing program being carried out at the Technical University of Munich.

For the cruciform joint, 30 data sets and 616 data points were identified from small-specimen test data [*3,4*]. Twenty data sets and 347 data points were identified for the non-load-carrying attachment. A data set is defined as a group of fatigue data having the same following individual characteristics: a source or laboratory or researcher, alloy, geometry, joint type, welding parameters, and loading conditions. Three methods of analyzing the small-specimen data were undertaken. The first method was individual analysis of each data set based on a stress-level statistical analysis and a corresponding linear regressional analysis for development of *S-N* curves. The resulting *S-N* curve was then plotted over the specific life of the test (i.e., no run-outs were allowed). The results are shown in Figs. 8 through 15. The second analysis method used the total data field for each data set to estimate the mean regression curve and corresponding scatter parameters. Again, these curves were plotted over the specific life of the test and are included where necessary in Figs. 8 through 15. Shown in each of the figures are the data points resulting from beam testing and where feasible, the outermost 90% confidence bands (the two that are farthest from the mean curves) resulting from Analysis Method 1. Analysis Method 3 was a linear regressional analysis of the combined data sets for a specific alloy, joint type, and *R*-ratio. The important results of Analysis Methods 1, 2, and 3 are summarized in Tables 1 and 2.

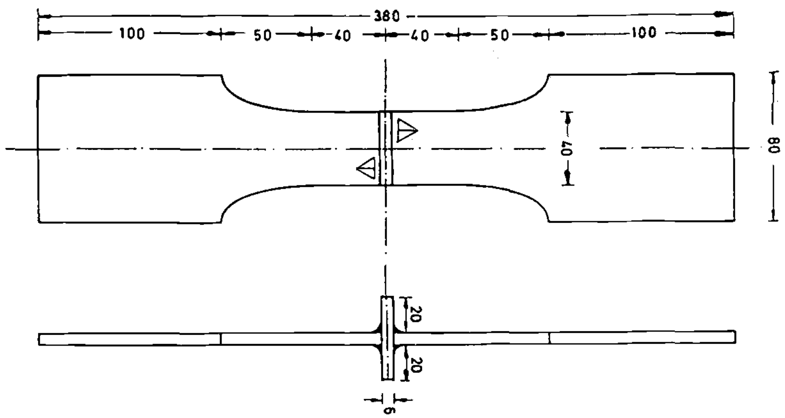

a. Small Specimen Cruciform Joint

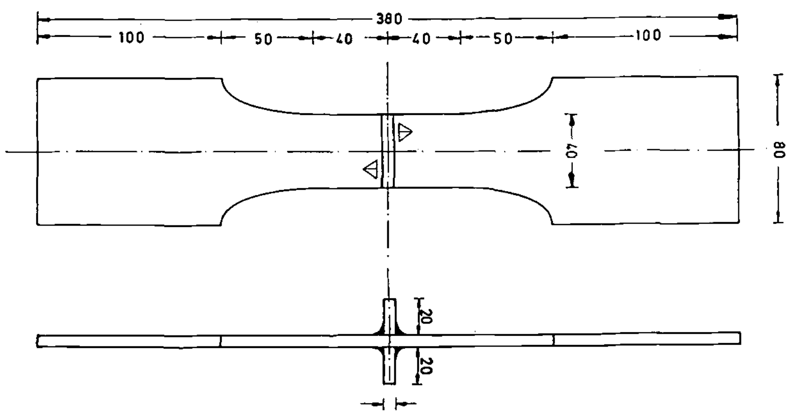

b. Small Specimen Non-Load Carrying Attachment

FIG. 7—*Typical small-specimen joint types.*

Observations

As can be seen from Figs. 8 through 11, most of the cruciform joint full-size specimen data points lie slightly below the small-specimen *S-N* curves. This would indicate a reduction in the fatigue strength of cruciform joints between full-size and small specimens. In small specimens the load is applied directly to the joint and is therefore the effective stress. On the other hand, the stresses for the full-size specimens are the nominal bending stresses calculated at the outermost fiber. This difference in defined stresses is one possible reason for this reduction in strength. However, a far more likely reason for the decrease in strength is the presence of much higher residual stresses in the full-size specimens [5]. The beams

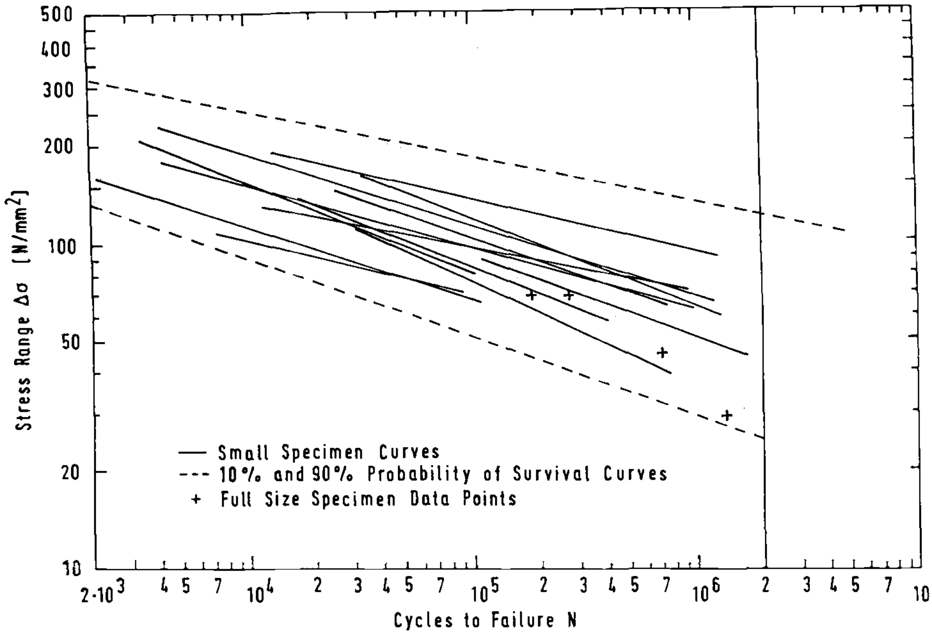

FIG. 8—S-N *diagrams of small-specimen data/7000 series alloys/*R = *0.0/cruciform joint.*

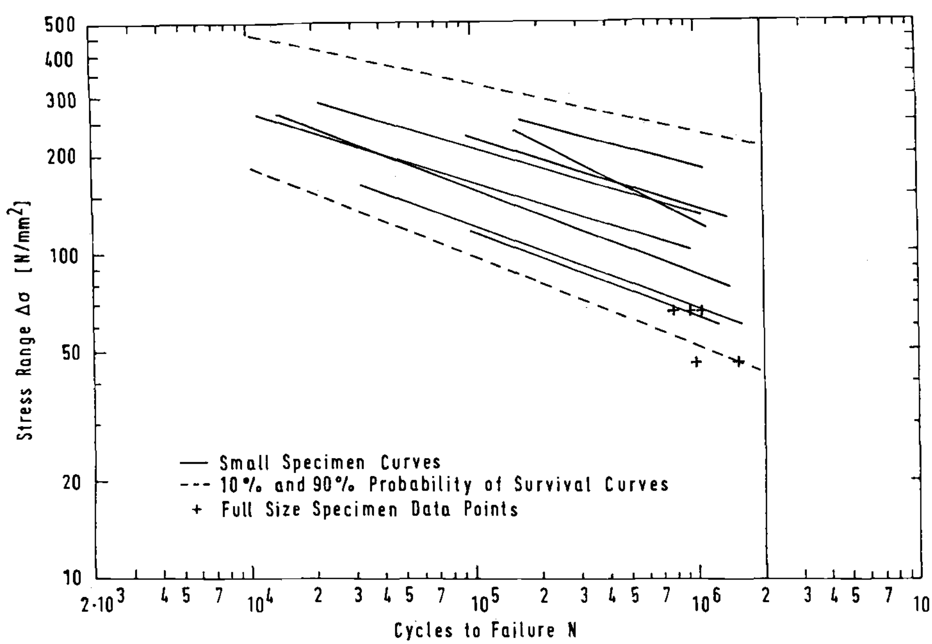

FIG. 9—S-N *diagrams of small-specimen data/7000 series alloys/*R = *−1.0/cruciform joint.*

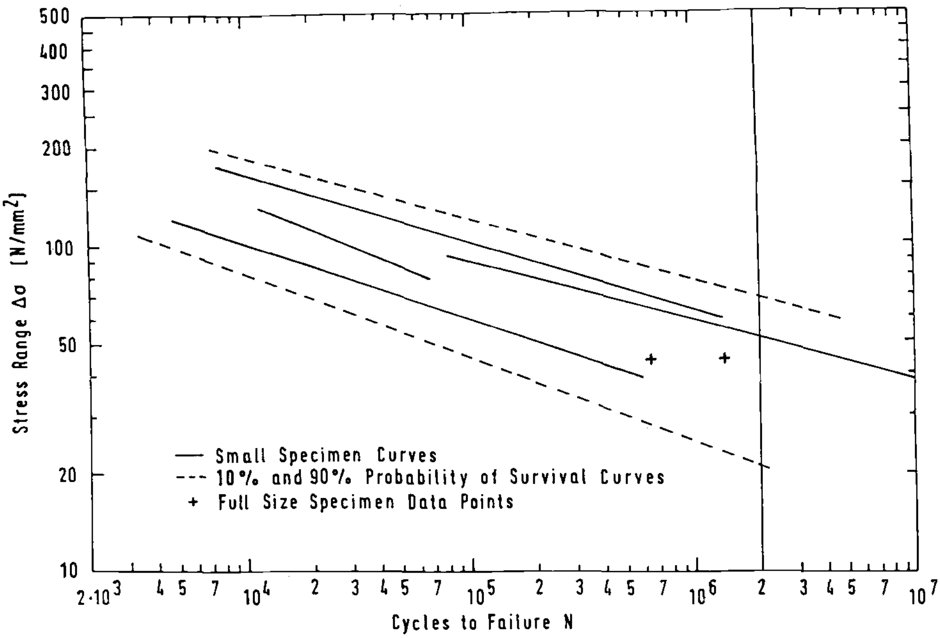

FIG. 10—S-N *diagrams of small-specimen data/5000 series alloys/*R = *0.0/cruciform joint.*

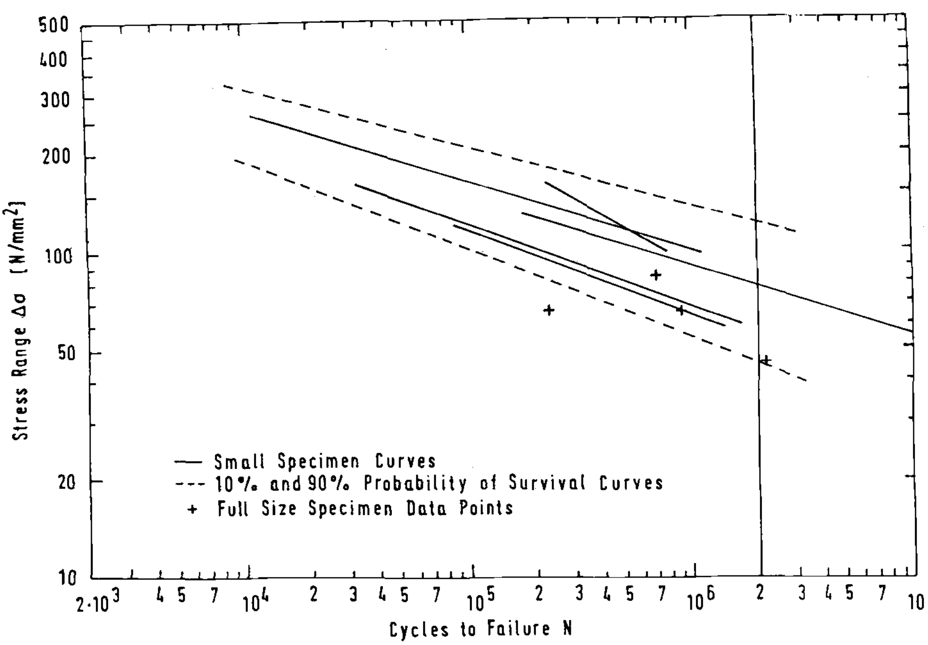

FIG. 11—S-N *diagrams of small-specimen data/5000 series alloys/*R = *−1.0/cruciform joint.*

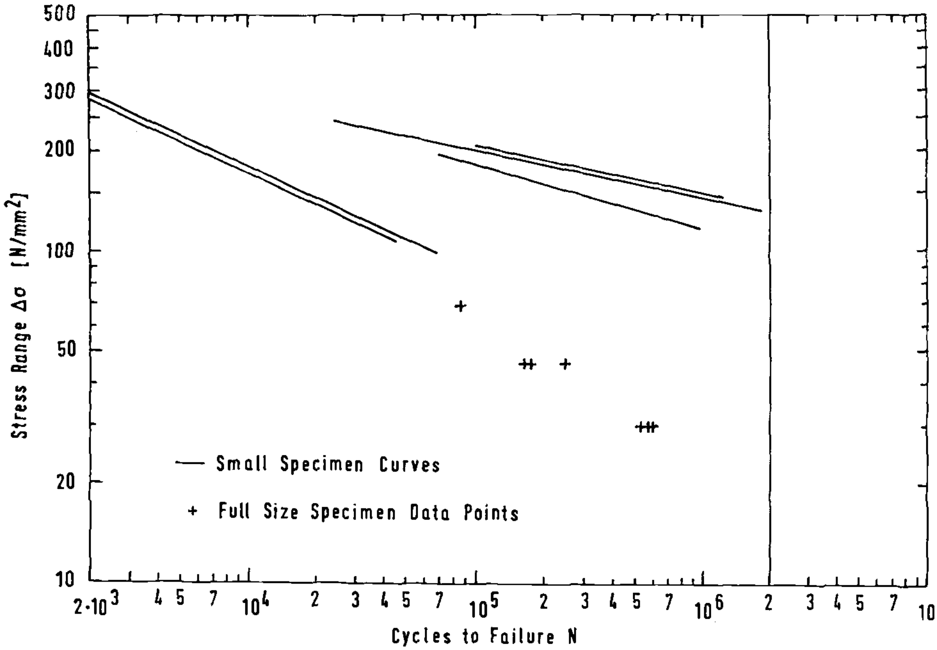

FIG. 12—S-N *diagrams of small-specimen data/7000 series alloys*/R = *0.0/non-load-carrying attachments.*

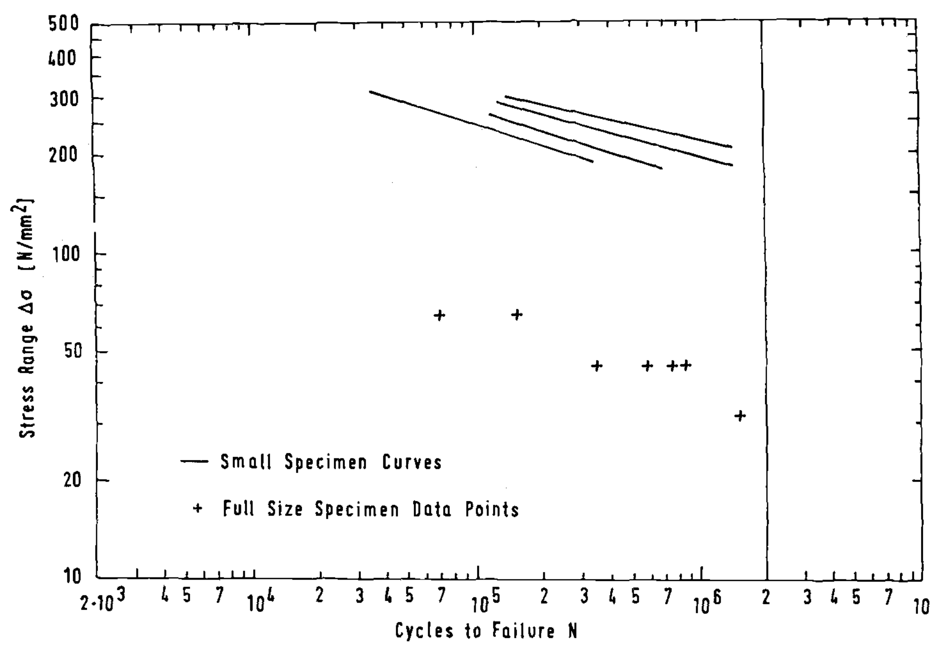

FIG. 13—S-N *diagrams of small-specimen data/7000 series alloys*/R = *−1.0/non-load-carrying attachments.*

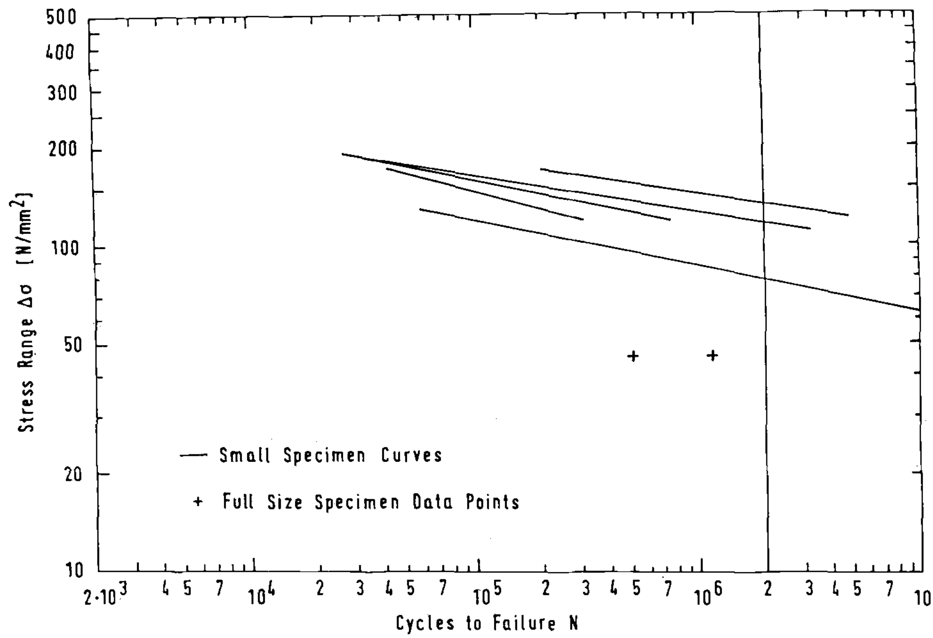

FIG. 14—S-N *diagrams of small-specimen data/5000 series alloys/*R = *0.0/non-load-carrying attachments.*

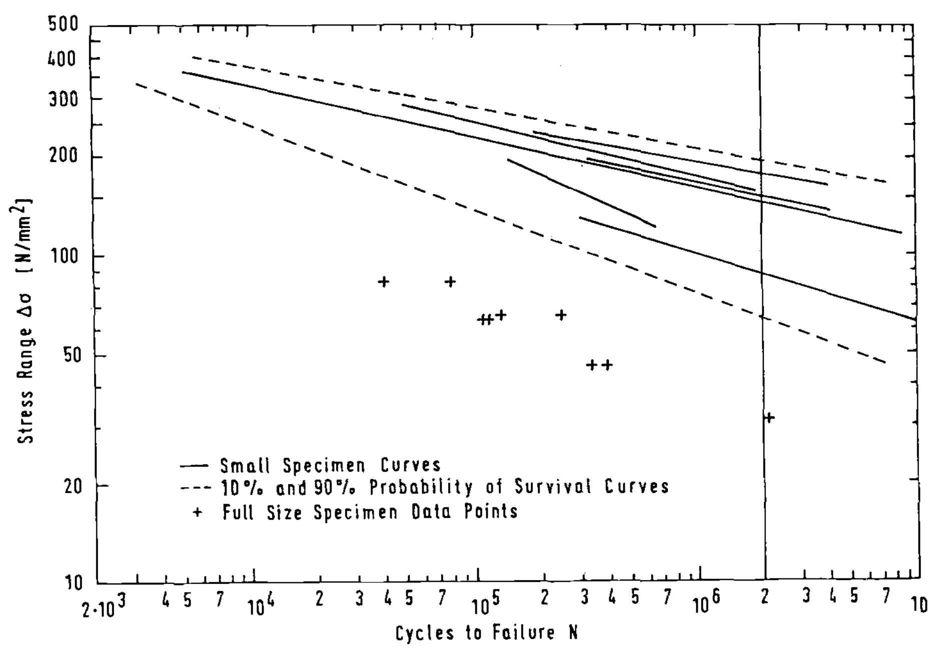

FIG. 15—S-N *diagrams of small-specimen data/5000 series alloys/*R = *−1.0/non-load-carrying attachments.*

TABLE 1—*Comparison of slope* m *for small-specimen data.*

Joint Type and Alloy	R-Ratio	Median Slope of Individual Data Sets	Slope of Combined Data Sets
Cruciform			
7000 Series	0	4.56	3.69
	−1	4.20	2.72
5000 Series	0	4.54	4.65
	−1	4.03	3.76
Non-load-carrying attachment			
7000 Series	0	5.30	4.97
	−1	5.47	5.05
5000 Series	0	7.63	5.39
	−1	6.10	3.86

were constructed of plate elements and are therefore welded together between the flange and web. For the cruciform joint, residual stresses measured before testing were particularly high in the area where the web and flange are joined together (Fig. 16). Small specimens, on the other hand, do not normally achieve such high residual stresses during manufacture because of their relatively narrow width [*6*]. Such high residual stresses may therefore have been present during the entire load cycle and would have contributed to the reduction in strength.

Figures 12 through 15 show a rather sharp difference between the fatigue strength of the full-size cover plates and the non-load-carrying attachment small-specimen data. As mentioned previously, the beam cover plates are likely to carry some load. Therefore, they do not behave as true non-load-carrying attachments. However, the possible contributing role of residual stresses is much more obvious here. Initial failure (e.g., initial cracking) took place each time in the weld toe of the flange directly above the web-to-flange weld. As can be seen from Fig. 16, this is also the area where the largest residual stresses were measured prior to testing.

TABLE 2—*Comparison of standard deviations of log* N.

Joint Type and Alloy	R-Ratio	Median Stress Level $s_{\log N}$	Median $s_{\log N}$ of Individual Data Sets	$s_{\log N}$ of Combined Data Sets
Cruciform				
7000 Series	0	0.175	0.670	0.787
	−1	0.190	0.650	0.731
5000 Series	0	0.288	0.910	1.164
	−1	0.197	0.715	0.851
Non-load-carrying attachment				
7000 Series	0	0.126	0.683	0.925
	−1	0.171	0.530	0.635
5000 Series	0	0.267	0.735	0.954
	−1	0.274	0.750	0.916

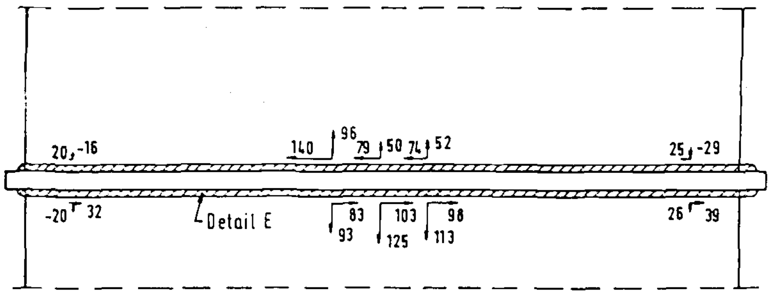

a. Full Size Cruciform Joint

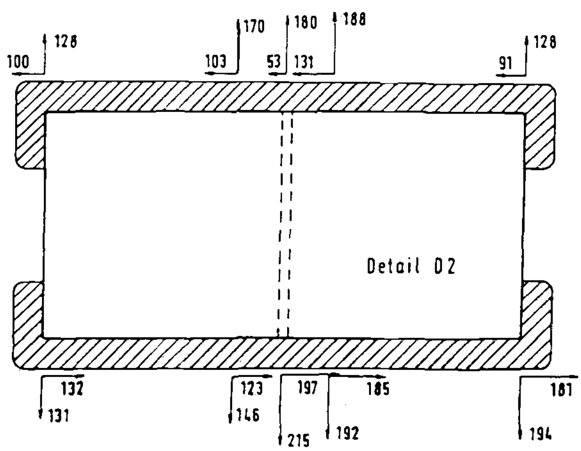

b. Full Size Cover Plate

FIG. 16—*Residual stresses measured prior to testing.*

Several things can be determined upon inspection of only the small-specimen data. For the cruciform joint, no apparent differences in slope appear to be due to the different alloys. Differences in slope do arise that are due to the R-ratio, with slightly higher slopes due an R-ratio of zero. For non-load-carrying attachments, small-specimen data differences do arise due to the alloy. Differences are also apparent due to R-ratio for the 5000 series alloy, with slightly higher slope values for $R = -1.0$. Based on the standard deviation results of Table 2, it can be seen that the stress level scatter is relatively small compared with that of the total and combined analysis methods. Better results might have been achieved if a multi-parametric, rather than a linear regressional analysis method had been employed [7].

Conclusions

Differences between full-size and small-specimen data in the fatigue strength of transverse fillet welds were examined. The following conclusions can be drawn:

1. For cruciform joints, a reduction in fatigue strength exists between full-size and small specimens. The most likely cause for this decrease is the high residual stresses to be found in the joint after welding.
2. In many cases it is difficult to draw upon small-specimen data to explain the behavior shown by full-size specimens. Therefore, there is a continued need for full-size testing.
3. Based on the cruciform joint small-specimen data, differences in slope m due to the alloy were generally not present. The R-ratio tends to contribute more to differences found in the slope.
4. Differences in slope m are present due to the different alloys for non-load-carrying attachment small-specimen data.

References

[1] Sanders, W. W., Jr., and Day, R. H., "Fatigue Behavior of Aluminum Alloy Weldments," Welding Research Council Bulletin 286, Welding Research Council, New York, NY, August 1983.

[2] Kosteas, D. and Weldl, F., "Aluminium Beam Test Programme: Assessing the Results," *Proceedings,* International Conference on Fatigue of Welded Constructions, Brighton, England, 7–9 April 1987.

[3] Kosteas D., Kirou, I., and Sanders, W. W., Jr., "A Report with Data from the Committee on Aluminum Fatigue Data Exchange and Evaluation (CAFDEE)," Vols. 1–4, Iowa State University, Ames, IA, August 1986.

[4] Centre International de Développement de L'Aluminium, Final Report, "Fatigue Behavior of Aluminum Alloys," Zürich, Switzerland, January 1974.

[5] Kosteas, D., "Estimating Residual Stresses and Their Effect in Welded Aluminum Components in Fatigue," *Analytical and Experimental Methods for Residual Stress Effects in Fatigue, ASTM STP 1004,* American Society for Testing and Materials, Philadelphia, 1988, pp. 122–130.

[6] Gurney, T. R., *Fatigue of Welded Structures,* 2nd ed., Cambridge University Press, Cambridge, England, 1979.

[7] Steinhardt, O. and Kosteas, D., "Die Schwingfestigkeit geschweißter Aluminiumverbindungen," Berichte der Versuchsanwalt für Stahl, Holz und Stein, Karlsruhe University, Karlsruhe, West Germany, 1971.

J. C. McMahon,[1] *G. A. Smith,*[2] *and F. V. Lawrence*[3]

Fatigue Crack Initiation and Growth in Tensile-Shear Spot Weldments

REFERENCE: McMahon, J. C., Smith, G. A., and Lawrence, F. V., **"Fatigue Crack Initiation and Growth in Tensile-Shear Spot Weldments,"** *Fatigue and Fracture Testing of Weldments, ASTM STP 1058*, H. I. McHenry and J. M. Potter, Eds., American Society for Testing and Materials, Philadelphia, 1990, pp. 47–77.

ABSTRACT: Fatigue crack initiation and growth in SAE 960X steel tensile-shear spot welds were studied by sectioning companion specimens and by replicating the exposed site of crack initiation in a presectioned weldment. Constant-amplitude $R = 0$ and $R = -1$ tests, as well as variable-load history tests were performed on as-welded weldments and weldments peened ("coined") after welding.

Approximately 50% of the total fatigue life was devoted to developing a 0.25-mm-depth crack under constant-amplitude loading in the life range 10^4 to 10^6 cycles. At lives greater than 10^6 cycles, this percentage appeared to increase. Similar results were found under a variable load history, although, in this case, only 40% of the life was devoted to developing a 0.25-mm-depth crack. Postweld coining increased the fatigue life by over an order of magnitude. Several analytical models for predicting the fatigue life of the tensile-shear spot weldments studied were compared.

KEY WORDS: weldments, tensile-shear spot welds, fatigue, fatigue crack initiation, fatigue crack propagation, fatigue life prediction models, high-strength, low alloy (HSLA) spot welds

Nomenclature

- a Crack depth measured in the plane of the crack
- a' Depth of largest possible undetected crack
- a_f Final crack size
- a_m Measured crack depth on the plane of polish
- a_o Initial crack depth
- a_{pz} Reversed plastic zone size
- a_{th} Threshold crack length
- b Fatigue strength exponent
- c Ellipse minor semi-axis
- C Fatigue crack growth constant
- d Distance between the successive planes of polish or the depth of polish
- D Nugget diameter
- D Distance between the plane of sectioning and the position of the maximum crack depth
- D_p Diameter of the coining indenter

[1] Engineer, Advanced Cardiovascular Systems, Temecula, CA 92390.
[2] Engineer, General Electric Corp., Cincinnati, OH 45215.
[3] Professor of civil engineering and metallurgy, University of Illinois at Urbana, Urbana, IL 61801.

HSLA High-strength, low-alloy
K Stress-intensity factor
K_f Peterson's fatigue notch factor
$K_{f\max}$ Maximum value of the fatigue notch factor for a given notch
K_o Initial value of the stress-intensity factor for a tensile-shear spot weldment (TSSW) (after Pook)
K_t Elastic stress concentration factor
n Fatigue crack growth exponent
N_a Number of cycles to develop a crack of length a
N_{I} Number of cycles to the end of Stage I, i.e., a crack depth of 0.25 mm
N_{II} Number of cycles to the end of Stage II, i.e., a crack depth of 1.40 mm
N_{III} Number of cycles to the end of Stage III, i.e., the onset of plastic instability
N_P Fatigue crack propagation life during Stage II
N_{P1} Calculated fatigue crack propagation life, assuming $a_o = a_{th}$
N_{P2} Calculated fatigue crack propagation life, assuming $a_o = 0.25$ mm
P Load
q Beta function parameter
R Load or stress ratio
R Aspect ratio of elliptical cracks
r Beta function parameter
SAE Society of Automotive Engineers
S_u Ultimate tensile strength
t Sheet thickness
TSIP Three-stage initiation-propagation model for tensile-shear weldments
TSSW Tensile-shear spot weldment
W Specimen width
Y Geometry factor
ΔK Range of stress-intensity factor
ΔK_{th} Threshold range of stress intensity
ΔP Load range
ΔS Stress range
ϕ Angle between the surface of the sheets and the plane of crack growth
θ Angle between the center line of the specimen and a given position around the periphery of the nugget
σ_f' Fatigue strength coefficient
σ_m Local mean stress

Background

The Spot Weld

The tensile-shear weld geometry is one of the most convenient and effective geometries for utilizing the electrical resistance spot weld in joining sheet steel, despite the fact that this configuration induces considerable bending and attendant joint rotation. Most models proposed for predicting the fatigue life of tensile-shear spot welds assume that the junction between the two sheets is virtually a crack and that crack propagation begins with the first application of load (see Fig. 1). Models based solely on crack propagation have been suggested by Davidson [*1*], Davidson and Imhof [*2*], Cooper and Smith [*3,4*], Smith and Cooper [*5*], and more recently, Wang and Ewing [*6*].

Wang et al. [*7*] proposed a model for the fatigue life of tensile-shear spot welds based on

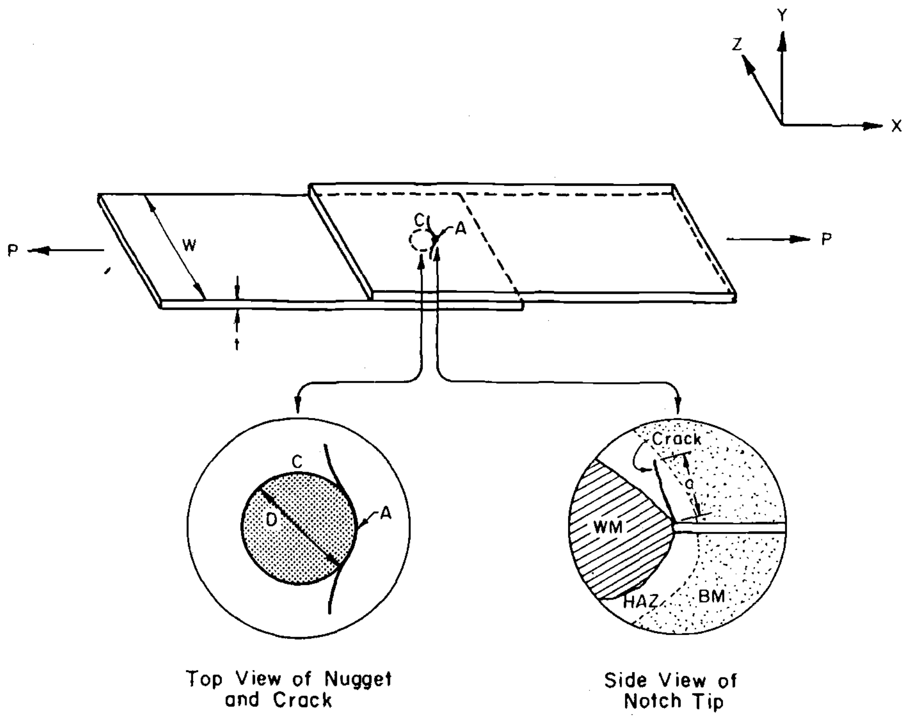

FIG. 1—*Patterns of crack initiation and propagation in TSSW. The right inset shows the location of initiation in Stage I and crack propagation in Stage II. The left inset shows the pattern of fatigue crack propagation during Stage III. A indicates the location of initiation. D is the nugget diameter.*

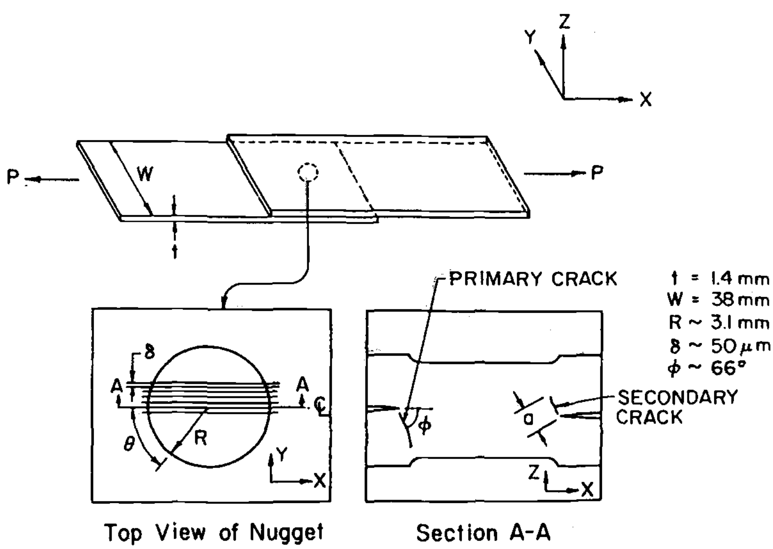

FIG. 2—*Companion specimen method of monitoring fatigue cracks. The weldments were sectioned on planes A-A. Primary and secondary fatigue cracks were usually observed, particularly at shorter lives.*

fatigue crack initiation and early crack growth, as well as fatigue crack propagation [the three-stage initiation-propagation (TSIP) model]. Fatigue crack initiation and early growth life predictions of this model are based on the strain-controlled fatigue behavior of laboratory smooth specimens and on the concept of the fatigue notch factor (K_f) [*8,9,10*]. The TSIP model predicts that fatigue crack initiation and early growth become increasingly dominant at long lives. Recent papers by Socie [*11*] and Nowak and Marissen [*12*] also show the increasing importance of fatigue crack initiation at long lives, as do experimental results presented in this work in which the development of fatigue cracks in tensile-shear spot welds was directly observed.

Fatigue Failure in Tensile-Shear Spot Weldments

Discussion of the fatigue life of a tensile-shear spot weldment (TSSW) is complicated by the lack of uniform definitions of fatigue crack initiation, the stages of fatigue crack propagation, and fatigue failure. Wang et al. [*7*] divided the fatigue life of a TSSW into three stages.

Stage I—Crack initiation and early crack growth. At the end of Stage I, a detectable crack or a crack of some agreed-upon (small) size is present at the periphery of the weld nugget (see Figs. 1 and 2). In this study, the end of Stage I is defined as a crack length of 0.25 mm, and the life at which this crack length is observed is termed N_I.

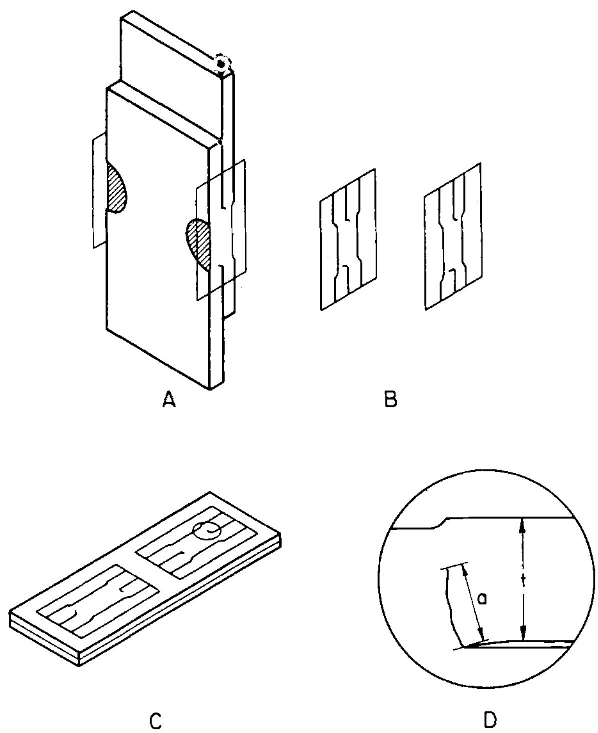

FIG. 3—*Presectioned method of monitoring fatigue cracks:* (a) *replicas made of exposed surfaces with the specimen under load;* (b) *replicas stripped;* (c) *replicas mounted between glass slides;* (d) *observation of crack depth using transmitted light microscopy.*

TABLE 1—*Chemical composition of galvanized SAE 960X sheet steel, in weight percent.*[a]

C	Mn	P	S	Si	Nb	Al	Ce
0.06	0.43	0.11	0.02	0.03	0.029	0.03	<0.008

[a] Data supplied by manufacturer (Inland Steel Hi-Form 60)

Stage II—Crack propagation from the periphery of the nugget through the thickness of the sheet to its external surface. Early growth proceeds initially at an angle ϕ of 66°, but ultimately the growth during this period is nearly perpendicular to the sheet, so that the sheet thickness (1.4 mm) is roughly equal to the crack length at the end of Stage II. The life at the end of Stage II is termed N_{II} in this study. At the end of Stage II, a crack becomes visible at the external surface of the weldment.

Stage III—Crack propagation laterally across the specimen width until failure occurs through plastic instability (tearing or rupture). At the end of Stage III, virtual separation of the two sheets comprising the tensile-shear weldment has occurred. The life at the end of Stage III is termed N_{III} in this study.

Davidson [*1*] and Davidson and Imhof [*2*] terminated fatigue tests after the nugget failed in shear or after the development of a "thumb-nail" crack observable on the exterior of the specimen (the end of Stage II or the beginning of Stage III). Orts [*13*] and Wilson and Fine [*14*] defined failure as a certain displacement which usually corresponds to the end of Stage III (N_{III}). Cooper and Smith [*3*] defined failure as the end of Stage III (N_{III}) but noted the cycles to the end of Stage II (N_{II}). A practical definition of TSSW fatigue failure is the cycles to the end of Stage II (N_{II}) since most manufacturers prefer this conservative definition.

This paper summarizes the results of two studies. In the first study, Smith and Lawrence [*15*] directly observed the development of fatigue cracks in TSSW by sectioning companion specimens cycled for various fractions of life devoted to Stages I and II (see Fig. 2). To

TABLE 2—*Mechanical properties of galvanized SAE 960X sheet steel.*[a]

Property	Symbol	Value	Units
Yield Strength	Sy	424	MPa
Ultimate Tensile Strength	Su	476	MPa
Reduction in Area	RA	69	%
True Fracture Ductility	ε_f	1.17	
Fatigue Strength Coefficient	σ'_f	553	MPa
Fatigue Strength Exponent	b	-0.054	

[a] Data supplied by manufacturer (Inland Steel Hi-Form 60)

TABLE 3—*Typical welding schedule for galvanized SAE 960X steel.*

Electrode Force kN	Hold Time Cycles[b]	Weld Time Cycles	Weld Current kA	Nugget Dia. mm
3.6	30	20	12.1	6.1

[a] Current was monitored and adjusted to maintain constant nugget diameter.

[b] 60 cycles = 1 sec.

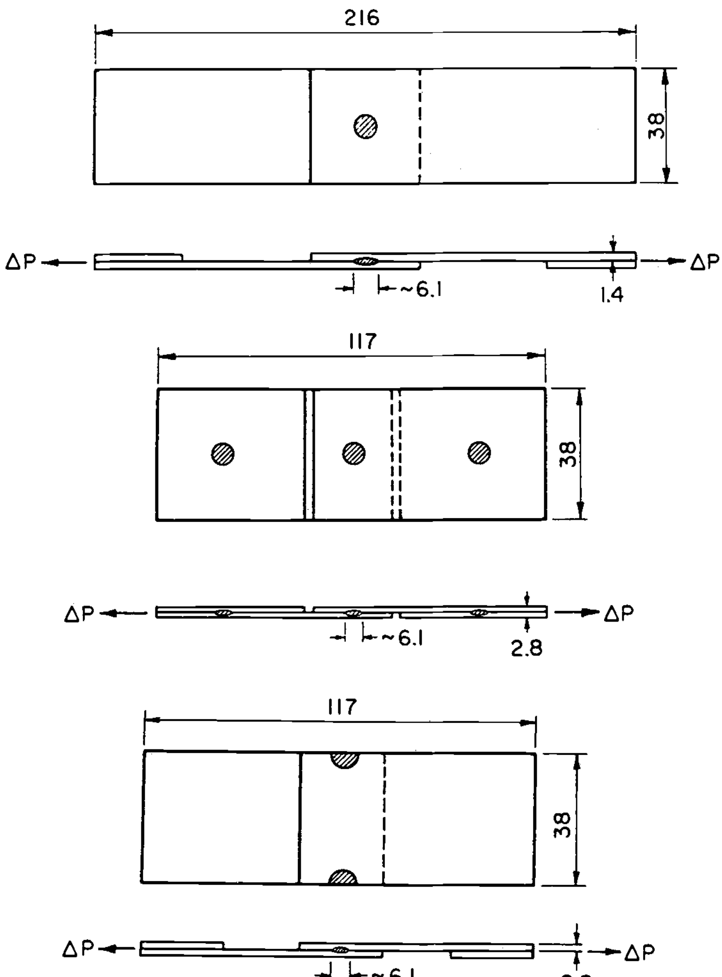

FIG. 4—*Tensile-shear spot-weld test-piece geometry (dimensions in mm)*: (top) *companion specimen design used for* R = *0 tests;* (middle) *companion specimen design used for* R = *−1 and variable-load history tests;* (bottom) *presectioned specimen design.*

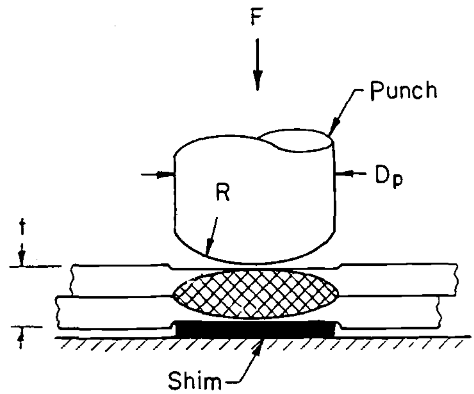

FIG. 5—*Schematic diagram of a "coining" procedure in which the spot weld nugget was indented with a hemispherical indenter. The shim prevented bending of the spot weld.*

reduce the considerable time and effort required in the companion specimen technique, a specimen was developed by McMahon and Lawrence [*16*] and Lawrence et al. [*17*] in which a TSSW with two weld nuggets was machined and polished to produce a symmetrical test piece containing two half spot welds with their midsections exposed at either edge to permit continuous observation of crack development during Stages I and II (see Fig. 3).

Experimental Observations of TSSW Fatigue Crack Development

Materials, Weld Fabrication, and Mechanical Testing

A hot-rolled, G-90 galvanized high-strength low-alloy (HSLA) steel of 1.4-mm sheet thickness was used. The material was similar to SAE 960X steel, and its chemical composition and mechanical properties are given in Tables 1 and 2.

TSSW test pieces were fabricated using a Sciaky single-phase microprocessor-controlled A-C electrical resistance spot welder. Peel tests were performed and the welding parameters were readjusted until the desired nugget diameters were obtained. Peel tests were repeated after the welding of every eight to ten specimens to guarantee the production of similar welds having a constant nugget diameter of desired size. The welding conditions are listed in Table 3. Three test-piece geometries were fabricated, as shown in Fig. 4.

Following fabrication, all the specimens were radiographed in order to reject those which had undersized nuggets, excessive expulsion, or irregular nugget outlines. One specimen series was "coined" prior to testing by indenting the nugget on one side with a spherical indenter. This procedure is shown schematically in Fig. 5; otherwise, all the specimens considered here were tested in the as-welded condition.

Fatigue tests were performed in a 3-kip-capacity MTS test system under ambient laboratory conditions at test frequencies of 10 to 20 Hz. Baseline fatigue information was collected for $R = 0$ and $R = -1$ constant-amplitude load histories.

Variable-load history tests were performed using an automotive load history donated by the Ford Motor Co. [*18*] (see Figs. 6 and 7). This history was collected on an automotive spot weld during test track trials, which included rough road, maneuvering and special events, and chuck hole trials. The histogram of the unedited Ford history resembles a Beta function, as can be seen in Fig. 6. The unedited Ford history originally had over 18 844 reversals but was edited to 5320 by the removal of the many small cycles having stress ranges of less than

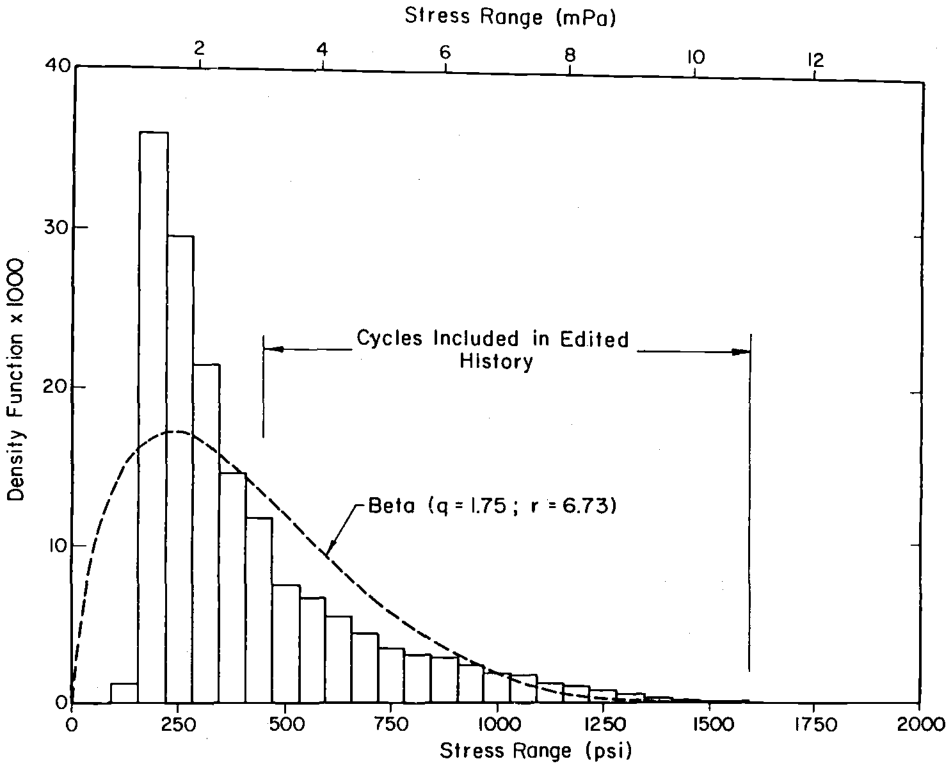

FIG. 6—*Histogram of the Ford Co. variable-load history* [18], *having 18 844 reversals. The histogram can be represented by a beta function probability distribution. Stress ranges less than 3.0 MPa were edited.*

3.0 MPa. Both the edited and unedited histories had no net mean stress and contained many large (damaging) events. The edited history gave longer fatigue lives by a factor of 1.8 [*17*].

Observation of Crack Development Using Companion Specimens

Essentially identical specimens were fatigue tested for a predetermined number of cycles corresponding to various percentages of the anticipated total life at the load level of the test. The tests were terminated at 10% intervals of the expected total lives, and as a consequence, ten companion specimens were generally tested at a given load level. Several test series were carried out at load levels producing short, intermediate, and long total lifes for both $R = 0$ and $R = -1$ constant-amplitude load cycles. Table 4 summarizes the companion-specimen test program.

Following fatigue testing, each companion specimen was sectioned at distances of 1.3 mm from the weld center line using a low-speed diamond wafering blade (see Fig. 2). The distance of the initial section from the weld center line ensured that the location of crack initiation would be encountered as the mounted section was successively polished and examined (see Figs. 8 and 9). Each section was mechanically polished to a 0.05 to 0.13-mm depth and lightly chemically milled (to remove any mechanical polishing artifacts), and the length of any observed fatigue crack was measured using standard metallographic techniques.

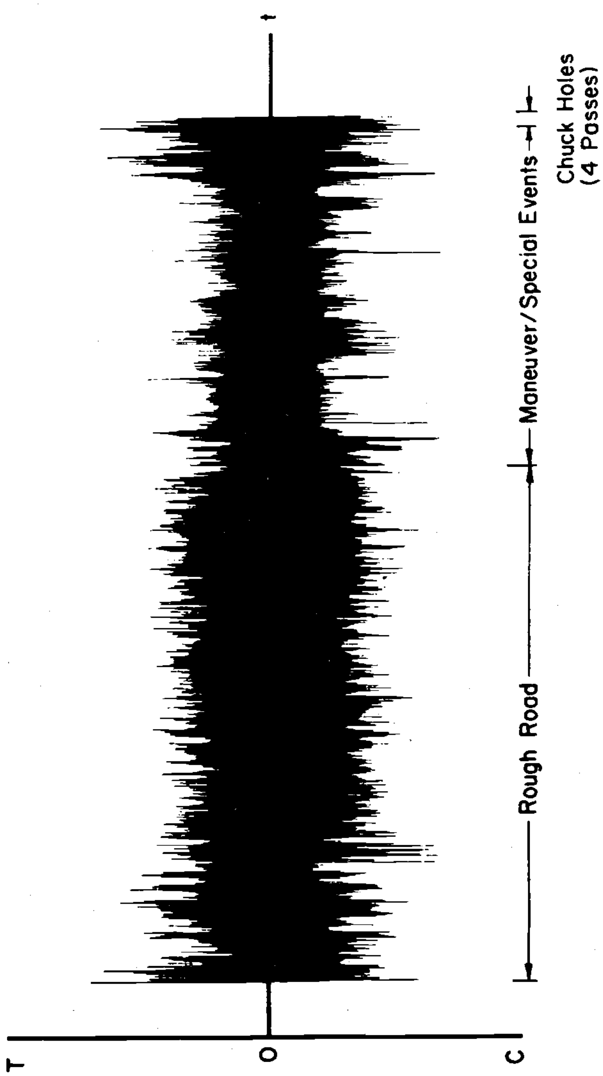

FIG. 7—*Edited Ford Co. variable-load history (5320 reversals).*

TABLE 4—*Summary of tests using the companion specimen method.*

Series	R Ratio	Condition	Load Range kN	Number of Tests	N_{III} Cycles
E	-1	As welded	6.2	12	20,000
F	-1	As welded	4.0	11	151,000
G	-1	As welded	2.2	10	1,200,000
H	-1	Coined	5	5	500,000
A	0	As welded	3.6	10	54,000
B	0	As welded	2.2	9	431,000
C	0	As welded	1.8	7	1,200,000
D	0	As welded	1.6	4	3,650,000
I	≈-1[a]	As welded	5	5	143 blocks

[a] Variable load history tests having zero mean stress.

The polished sections were generally not etched to avoid obscuring small cracks with microstructural details. The lengths of fatigue cracks at both the primary and secondary crack growth sites were measured (see Figs. 2 and 8). Cracks as small as 10 μm could be detected by this technique.

Figure 8 shows the results of carefully sectioning one fatigued TSSW. The depth of the many initiated cracks observed around the periphery of the weld nugget were plotted as a function of the angle θ for both the primary and secondary cracks. Lines have been drawn connecting the depths of individual cracks on each section. The maximum crack depth was roughly 0.3 mm, so that this figure represents conditions at the end of Stage I. It can be seen that Stage I in this instance is characterized by crack initiation at many sites around the periphery of the nugget at both the primary and secondary sites. Figure 9 shows the observed positions of crack initiation sites in the companion specimen test program as a function of angle θ. Initiation at the center line ($\theta = 0$) is most probable, but sites as far off the center line as $\theta = 10°$ were also observed.

Typical results with the companion specimen technique are given in Fig. 10. For N_{III} of less than 2×10^6 cycles, cracks generally initiated at opposite sites of the weld nugget. Figure 10 shows the development of cracks at both the primary and secondary sites in ten nearly identical companion specimens, each cycled for different fractions of the anticipated total life (N_{III}) and sectioned. The primary crack was defined as the crack which ultimately became dominant and caused the final failure of the specimen. In Fig. 10, the development of a secondary crack occurred almost simultaneous with the development of the primary crack, but the secondary crack ceased to propagate at a depth of about 0.5 mm. The average value of $N_{III} = 151\,000$ for the test Series *F* is indicated in Fig. 10 by an arrow. The N_{II} is approximately 100 000 cycles, as defined by cycles at which the curve best fit to the primary crack data exceeds the sheet thickness of 1.40 mm. The first observable crack was about 18 μm in length and was first seen at 18 000 cycles.

Observation of Crack Development in Presectioned Specimens

To reduce the time and effort required by the companion specimen technique, a specimen was developed [*16*] in which a TSSW with two weld nuggets was machined and polished to

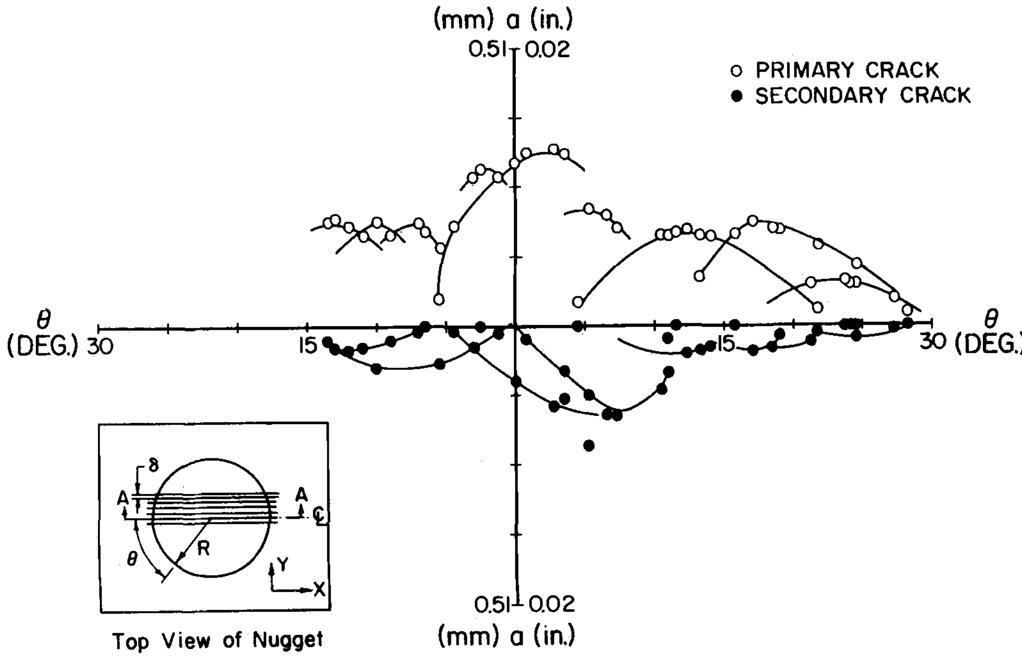

FIG. 8—*Distribution and size of primary and secondary fatigue cracks as a function of the angle around the nugget* (θ). *The specimen was cycled 300 000 cycles at a 2.2-kN-load constant-amplitude loading,* R = *0. The lines connect the depths of individual cracks on each section.*

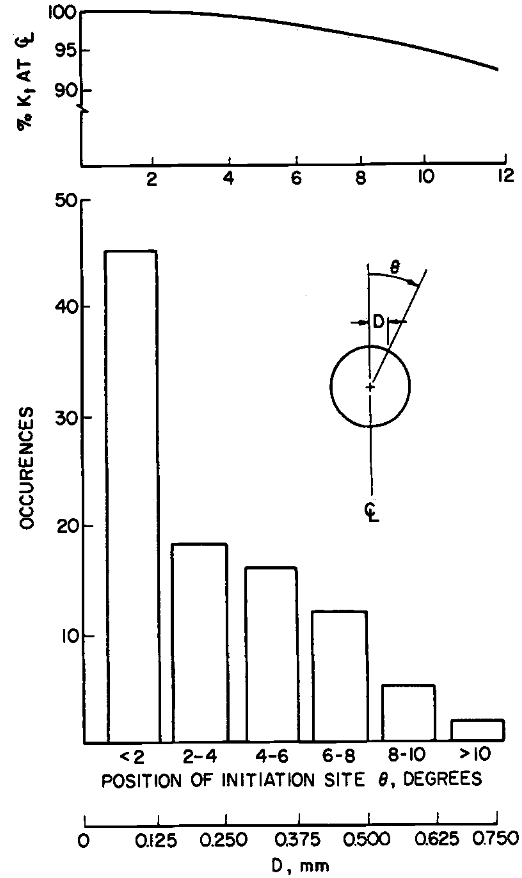

FIG. 9—*Distribution of initiation sites in companion specimens:* (top) *variation of the elastic stress concentration factor* (K_t) *with angle* (θ) *around the nugget;* (bottom) *distribution of observed crack initiation sites in companion specimens.*

produce a symmetrical test piece containing two half spot welds with their midsections exposed for observation (see Fig. 3). The stress-intensity factor for the half spot welds was found by finite-element analysis [*16*] to be greater than that for the companion specimen geometry by a factor of 1.074, because of the free surface. Thus, the loads applied to the presectioned specimens were reduced by a factor of 1.07 to produce the same notch root stresses and, therefore, to permit comparison of crack development in the two different specimen geometries.

Crack initiation and growth was monitored at each of the four exposed notch roots by interrupting the fatigue test and taking a surface replica of the two exposed sectioned weld nuggets (see Fig. 3).

Tests were run using $R = 0$ and $R = -1$ constant-amplitude and variable-load history loadings. Tests on coined presectioned specimens were performed. Table 5 summarizes the presectioned specimen test program.

Typical test results using presectioned specimens are given in Fig. 11. As shown in Fig. 11, cracks generally initiated at all four possible initiation sites at lives of fewer than 2 ×

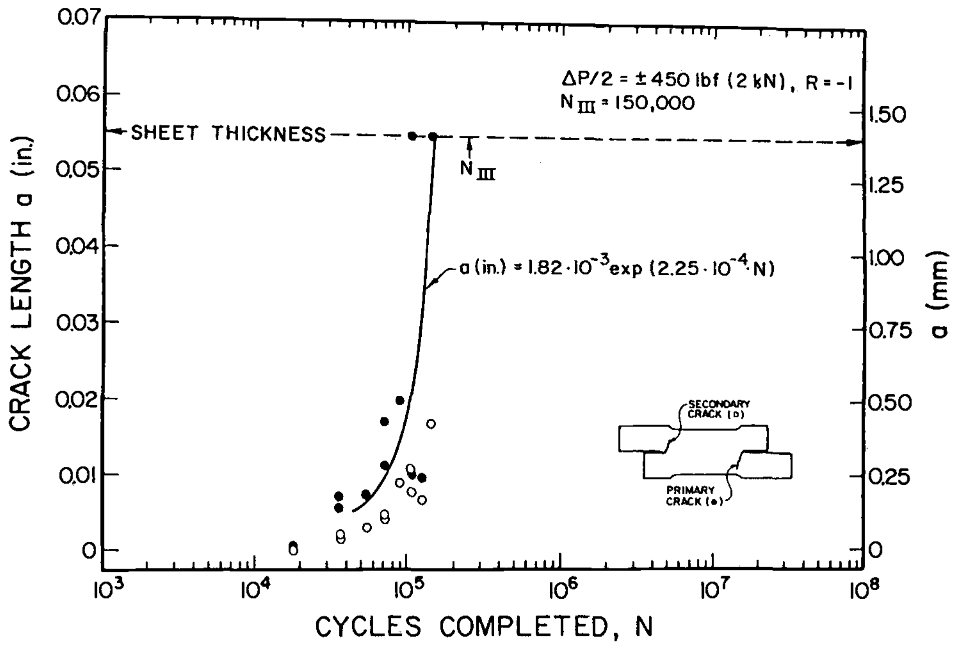

FIG. 10—*Observed fatigue crack growth in companion specimen test Series F. The primary crack is denoted by solid symbols; secondary cracks are denoted by open symbols. Load range = 4 kN;* R = *−1;* N_{III} ≈ *151 000 cycles.*

TABLE 5—*Summary of tests using the presectioned specimen method.*

Specimen No.	R Ratio	Condition	Load Range kN	N_{III} cycles or blocks (B)
216	0	As welded	4.5	25,000
219	0	As welded	2.67	320,000
224	0	As welded	1.8	1,600,000
209	-1	As welded	4.45	150,000
201	-1	As welded	4.00	180,000
218	-1	As welded	3.11	600,000
203	-1	As welded	2.66	1,200,000
222	-1	As welded	2.22	1,857,000
225	-1	As welded	2.22	3,500,000
220	-1	As welded	2.2	>10,000,000
221	-1	As welded	2.2	>8,000,000
210	-1	As welded	2.0	>7,000,000
215	-1	Coined	5.34	370,000
217	-∞	As welded	4.45	400,000
208	≈-1[a]	As welded	3.55 max	181 (B)
204	≈-1[a]	As welded	2.66 max	180 (B)
207	≈-1[a]	As welded	2.66 max	750 (B)

[a] Variable load history tests having zero mean stress.

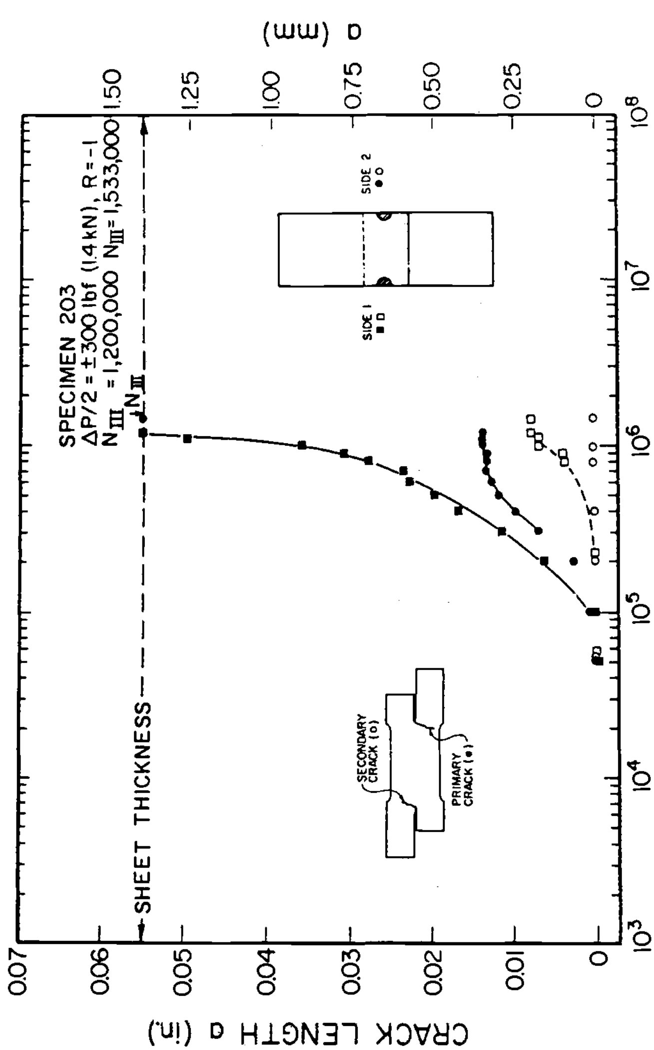

FIG. 11—*Observed fatigue crack growth presectioned Specimen 203. The primary and secondary cracks of the half-nugget causing failure are denoted by solid symbols; secondary cracks of the other side are denoted by open symbols. Load range* = 2.8 *kN; R* = −1; $N_{III} \approx 1\ 533\ 000$ *cycles.*

10^6 cycles, but only one of these became dominant and caused failure of the specimen and was thus termed the primary crack. In Fig. 11, the primary crack was first observed at a length of 15 μm after 100 000 cycles. The end of Stage II occurred at 1 200 000 cycles, and the end of Stage III occurred at 1 533 000 cycles.

At lower load levels and longer lives, generally only one of the two half-nuggets would initiate a fatigue crack. The fatigue lives and observed crack development of the presectioned specimens were similar to those of the companion specimens at the same applied load levels when allowance was made for the slight difference in notch-root stress conditions discussed above. Following testing, all presectioned specimens were sectioned to observe the depth of the plane of crack initiation relative to the plane of polish (see Table 6).

Results and Discussion

Observed TSSW Fatigue Crack Development

The combined constant-amplitude test results for the companion specimen and presectioned specimen tests on as-welded TSSW are shown in Fig. 12. The results for the companion specimens are identified in this figure by horizontal brackets under their data points so that they can be distinguished from the results for the presectioned specimens.

The presectioned specimens gave slightly shorter N_I and longer N_{II} than did the companion specimens at comparable stresses. The agreement is reasonably good, considering the difference between the two specimen types. The longer N_I in the presectioned specimens may be due to initiation of fatigue cracks slightly below the sectioned surfaces of these specimens. The shorter N_{II} may be caused by the difference in stress state described earlier and corrected for by the factor 1.07, as well as by the fact there are two load paths in the presectioned specimen.

TABLE 6—*Observed distances between the section plane and the crack initiation site for presectioned specimens.*

Specimen No.	R Ratio	Load Range kN	N_{III} cycles or blocks (B)	D Distance between a_{max} and plane of section	
				Primary Crack	Secondary Crack
219	0	2.66	320,000	0.25	<0.127
209	-1	4.45	150,000	0.25	0.127
201	-1	4.00	180,000	0.5	0.25
218	-1	3.11	600,000	0.25	<0.127
203	-1	2.66	1,200,000	0.38	-
222	-1	2.22	1,857,000	0.25	<0.127
225	-1	2.22	3,500,000	0.25	<0.127
215	-1 (coined)	5.34	370,000	0.25	0.25
217	-∞	4.45	400,000	0.25	0.127
208	≈-1[a]	3.55 max	181 (B)	0.127	0.127
204	≈-1[a]	2.66 max	180 (B)	0.25	-
207	≈-1[a]	2.66 max	750 (B)	0.25	-

[a] Variable load history tests having zero mean stress.

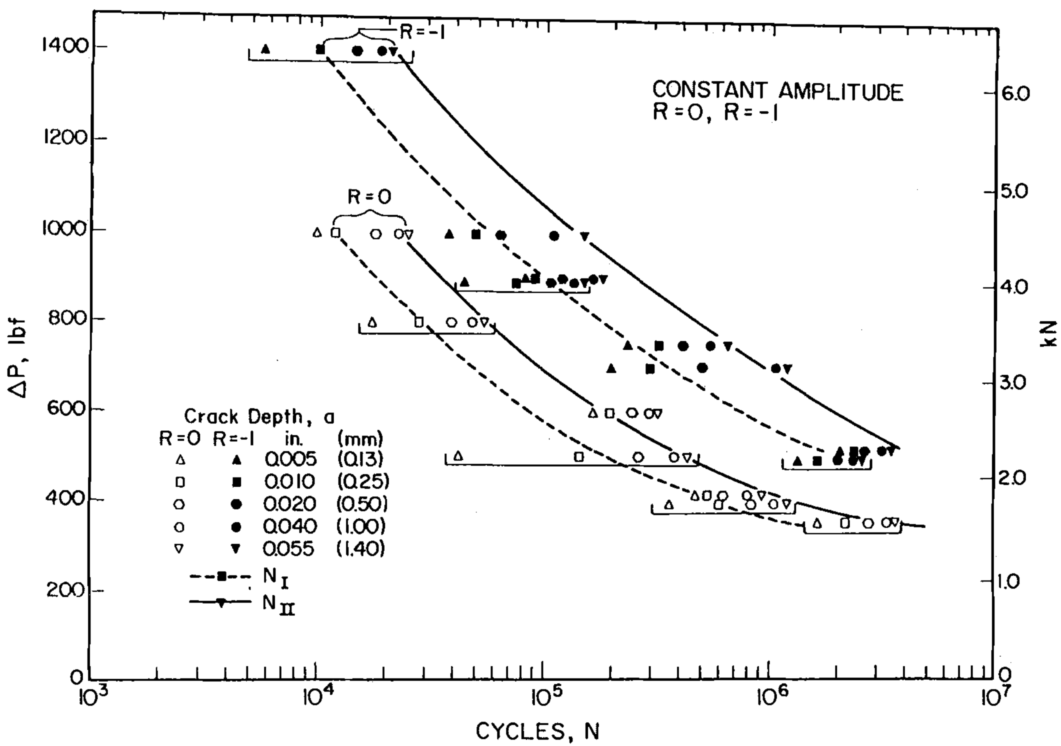

FIG. 12—*Summary of results for both companion specimens and presectioned specimens for constant-amplitude loading,* R = *−0 and −1. The dashed lines are* S-N_I *curves. The solid lines are* S-N_{II} *curves. Horizontal brackets have been drawn under the data for the companion specimen test series.*

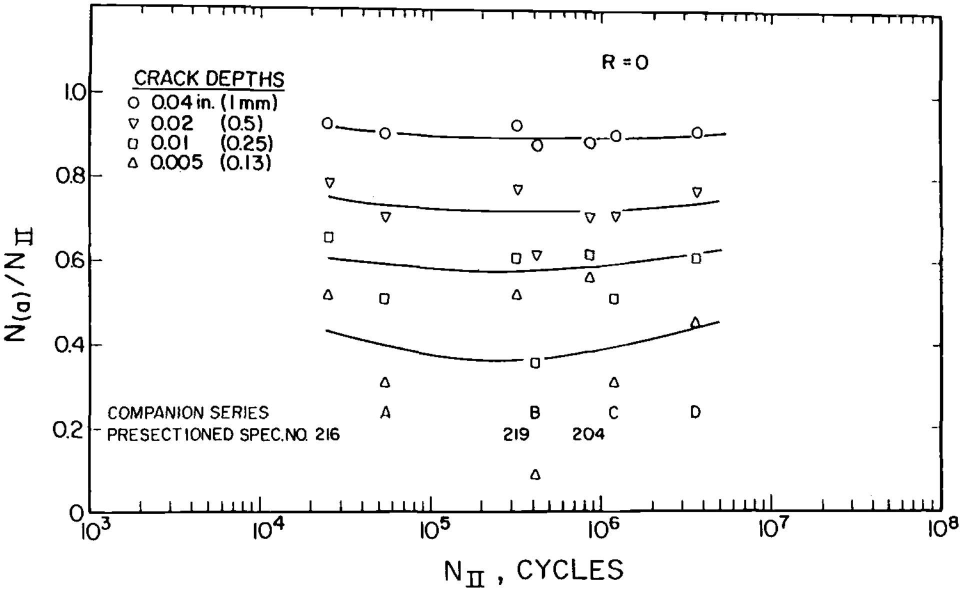

FIG. 13—*Fraction of* N_{II} *required to develop fatigue cracks of a given depth as a function of the total life* (N_a/N_{II})*. Results are given for both companion and presectioned specimen tests, constant amplitude loading,* R = *0.*

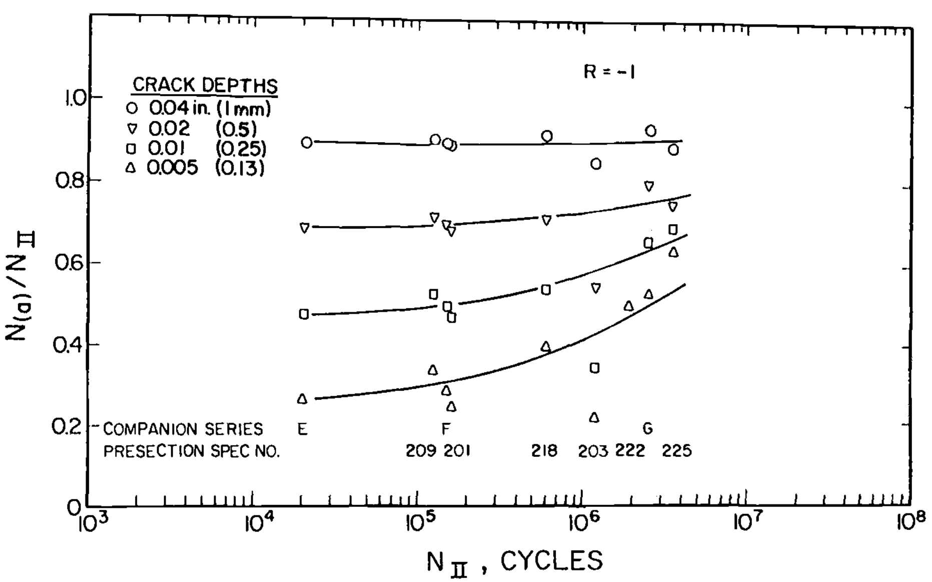

FIG. 14—*Fraction of* N_{II} *required to develop fatigue cracks of a given depth as a function of the total life* (N_a/N_{II})*. Results are given for both companion and presectioned specimen tests, constant amplitude loading,* R = *−1.*

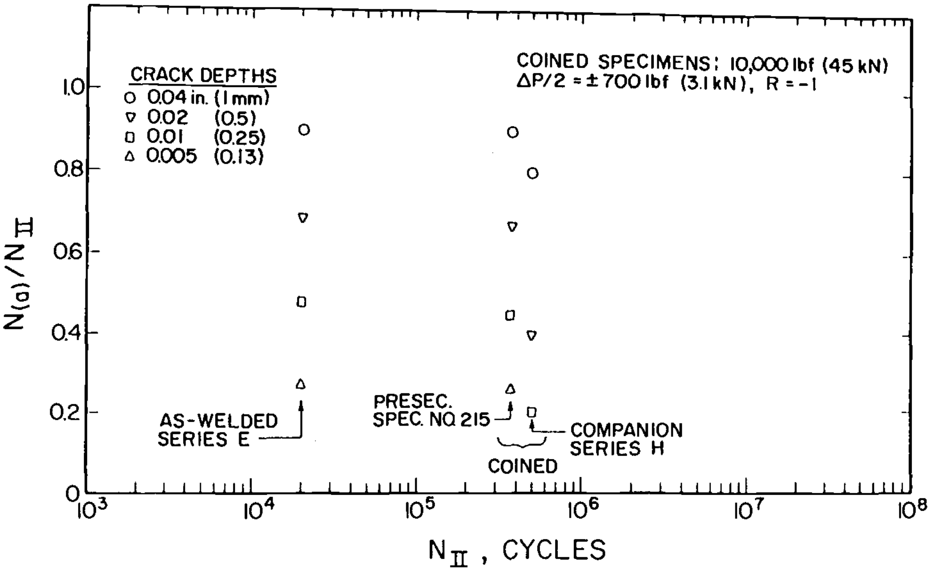

FIG. 15—*Fraction of* N_{II} *required to develop fatigue cracks of a given depth as a function of the total life for coined specimens* (N_a/N_{II}). *Results are given for both companion and presectioned specimen tests, constant amplitude loading,* $R = 0$.

The dashed lines in Fig. 12 describe a load range-life curve for the development of 0.25-mm-length cracks (N_I). Solid lines describe a load range-life curve for the development of 1.40-mm-length cracks (N_{II}). A substantial difference is behavior for the $R = -1$ and $R = 0$ load cycles is evident.

The test results are also presented in Figs. 13 and 14, in which the fraction of N_{II} required to develop the dominant or primary fatigue crack to a given length (N_a) is plotted as a function of N_{II}. Both the companion specimen and presectioned specimen tests showed the same trends, although there is some disagreement between the results of the two techniques for the small crack lengths (0.13 mm).

For lives of fewer than 10^6 cycles, approximately 50% of the total fatigue life was devoted to developing a 0.25-mm dominant fatigue crack, and for lives of more than 10^6 cycles, there is an apparent tendency for this percentage to increase. This increase is most pronounced for the $R = -1$ load cycle. While there are only limited data available in this life regime, the test results appear to confirm the increasing importance of fatigue crack initiation and early growth predicted by the TSIP model and reported by Socie [*11*] and Nowak and Marissen [*12*].

Figure 15 presents the results for coined specimen fatigue under constant-amplitude loading using both the companion specimen and the presectioned specimen techniques. Coining apparently increased N_{II} about an order of magnitude by uniformly increasing both Stages I and II. The large effect of coining is attributed to the induction of compressive notch-root residual stresses. Producing compressive notch-root residual stresses by overstressing TSSWs in tension prior to fatigue testing provides similar life improvements [*17*]. The fatigue crack initiation site after coining is frequently located on the surface of the sheet as far as 1 mm away from the notch root [*17*].

The test results for the edited Ford Co. variable-load history show trends similar to the constant-amplitude test results (see Figs. 16 and 17). Stage I occupied a smaller percentage

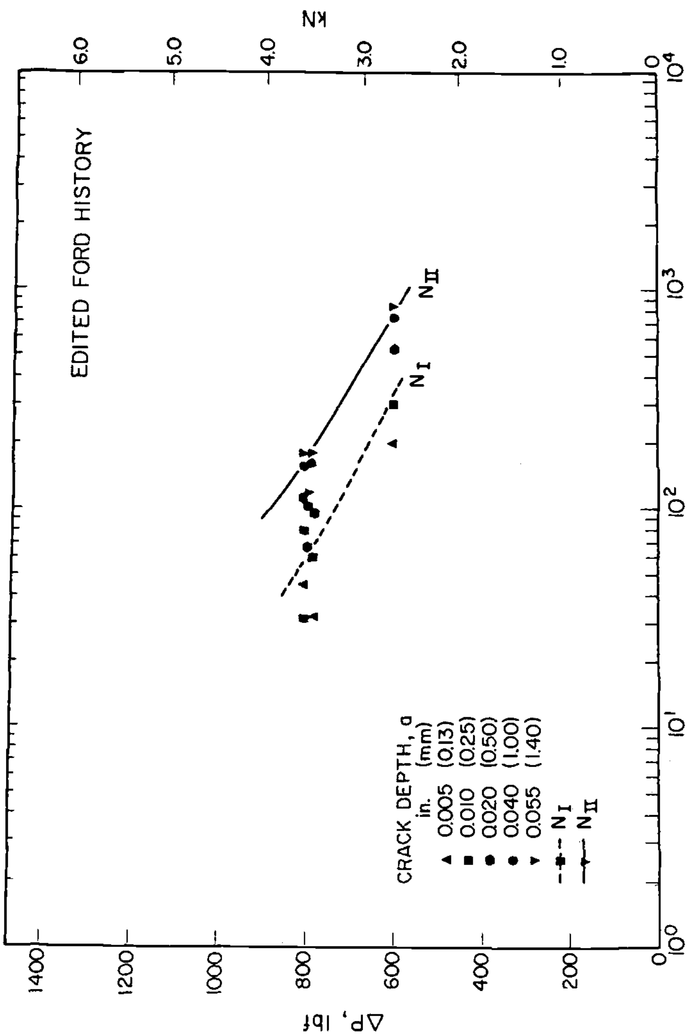

FIG. 16—*Summary of results for both companion specimens and presectioned specimens for the edited Ford history. The dashed lines are* S-N_I *curves. The solid lines are* S-N_{II} *curves.*

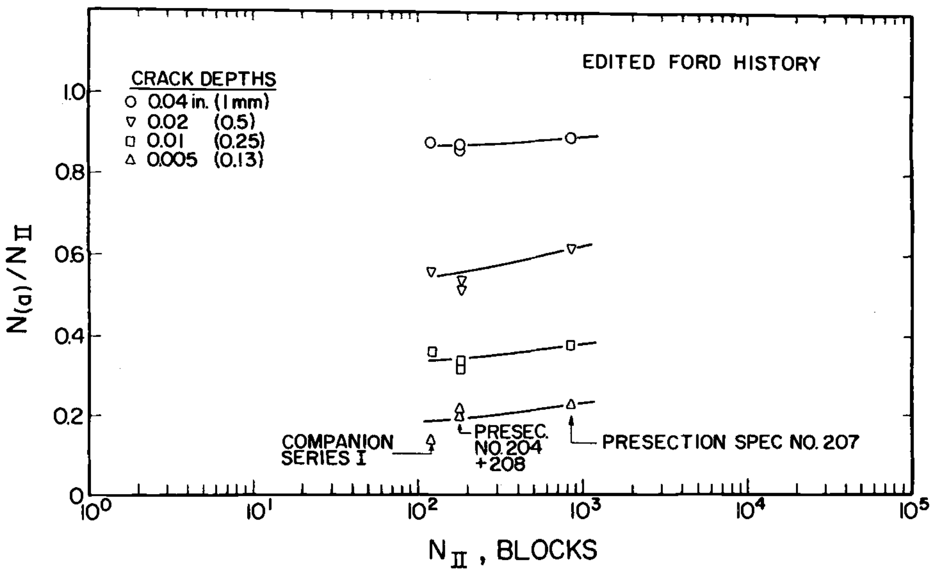

FIG. 17—*Fraction of* N_{II} *(blocks) required to develop fatigue cracks of a given depth as a function of the total life* (N_a/N_{II}). *Results are given for both companion and presectioned specimen variable-load history tests using the edited Ford Co. history.*

of the life for this variable-load history than was observed under constant-load amplitude: developing a fatigue crack of 0.25 mm required only 40% rather than 60% of the total life at 10^3 blocks ($\approx 5 \times 10^6$ cycles). There is a tendency for this percentage to increase with life (blocks), which suggests that Stage I becomes increasingly important at long lives under variable as well as constant-amplitude loading.

Measurement Accuracy

Both the companion specimen and the presectioned specimen methods measured crack depths on a section perpendicular to the plane of the crack and near the plane of the crack's maximum depth. In the case of the companion specimen method, a small crack could have been entirely missed if the planes of polish had been widely spaced. Typical depths of the polish (δ) separating successive observations were between 0.125 and 0.25 mm. Assuming a presumed worst case, a semicircular crack shape and a maximum polish plane separation (δ) of 0.25 mm, the largest possible crack that could be missed would have had a depth (a) of 0.125 mm.

In the case of the presectioned specimen, measurement error would occur if the plane of the maximum crack depth was not at the outer surface of the specimen (see Fig. 18). Assuming an elliptical crack profile, the maximum crack depth which could have been missed could be no larger than 0.17 mm and was probably no larger than 0.08 mm, based on the observed positions of crack initiation in these specimens (see Table 6 and Figs. 18 and 19). For both specimen types, the absolute possible measurement error diminishes with increasing maximum crack depth (see Fig. 19).

Comparison of Measured and Predicted Fatigue Lives

The TSIP model of Wang et al. [7] was modified and used by Lawrence et al. [*17*] to predict N_I and N_{II} of the HSLA TSSW tested in this study. Stage III was not considered in

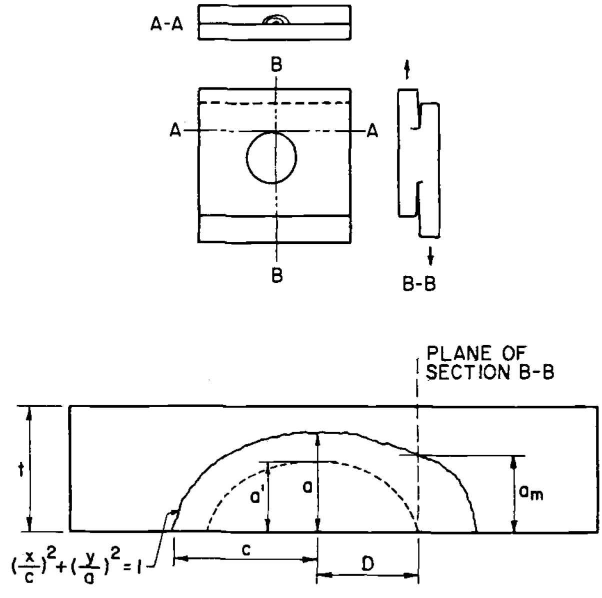

t: SHEET THICKNESS
c: MJR. ELLIPSE AXIS
a: MAX. CRACK DEPTH
a_m: MEASURED CRACK DEPTH AT B-B
a': MAX. UNDETECTED CRACK FOR D AND c/a
D: DISTANCE BTWN. MAX a AND PLANE B-B

FIG. 18—*Error analysis of fatigue crack measurements for both companion and presectioned specimens. The crack shown has an actual depth of* a *but its measured depth at the plane of polish B-B is* a_m. *The dashed line defines the depth* a' *of the largest crack which would not be detected on Section B-B.*

the experiments reported here. The average fatigue lives of the as-welded companion specimen and the presectioned specimen constant-amplitude tests are given in Tables 4 and 5.

N_I was estimated using the Basquin-Morrow [*19*] expression (Eq 1) and estimates of $K_{f\max}$, the maximum value of the fatigue notch factor (Eq 2). The expression of $K_{f\max}$ of TSSW was derived from Pook's [*20*] expression for the TSSW initial stress-intensity factor (K_o) (Eq 3). A full discussion of the initiation-propagation model and the estimation of Stage I is given in Refs *7, 8, 16,* and *17.*

$$\frac{\Delta S}{2} K_{f\max} = (\sigma_f' - \sigma_m)(2N_I)^b \tag{1}$$

$$K_{f\max} = 1 + \left(\frac{0.002\,41 W S_u t^{1/2}}{D}\right)\left[1.61\left(\frac{D}{t}\right)^{0.397} + 0.593 + 0.34\left(\frac{D}{t}\right)^{0.710}\right] \tag{2}$$

$$K_o = \frac{P}{D^{3/2}}\left(1.61\left(\frac{D}{t}\right)^{0.397} + 0.593 + 0.34\left(\frac{D}{t}\right)^{0.710}\right) \tag{3}$$

where W is the specimen width or the spacing between nuggets, D is the nugget diameter,

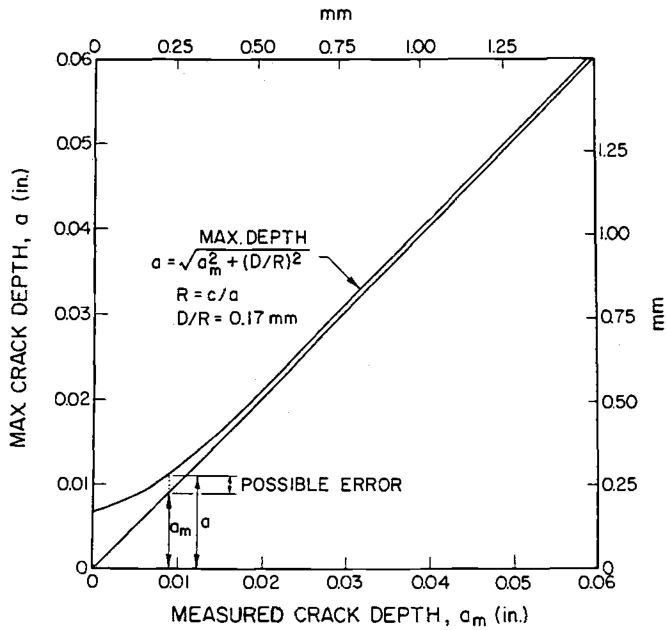

FIG. 19—*Possible error in the measured crack depths as a function of the actual crack depth. The error depends upon the aspect ratio* (R) *and the distance between the location of the plane of maximum crack depth relative to the plane of polish* (D). *The largest errors are possible at the smallest crack depths.*

TABLE 7—*Observed and predicted*[a] N_I *and* N_{II} *using the modified TSIP Model.*

Specimen or Test Series	Calc. a_{th} mm	Observed Fatigue Lives N_{ath} kcycles	Observed Fatigue Lives N_I kcycles	Observed Fatigue Lives N_{II} kcycles	Predicted Fatigue Lives N_I kcycles	Predicted Fatigue Lives N_I+N_{P1} kcycles	Predicted Fatigue Lives N_I+N_{P2} kcycles
E	6.22	2	10	20	4	37	9
F	4.00	40	75	151	31	145	80
G	2.22	1670	1670	2510	475	1396	1396
A	3.6	10	28	54	53	108	68
B	2.22	100	154	432	265	516	419
D	1.56	2200	220	3650	7500	7500	8300
C	1.78	500	606	1190	2000	2564	2471
216	4.45	5	12	25	12	43	17
219	2.67	1356	195	320	180	314	242
224	1.78	500	530	940	2070	2634	2541
209	4.45	35	50	150	15	97	45
201	4.00	60	90	180	31	145	80
218	3.11	230	320	650	159	429	330
203	2.67	300	300	1200	288	758	658
225	2.22	2400	2400	1100	474	921	1396

[a] N_{P1} is the propagation life calculated assuming $a_0 = a_{th}$. N_{P2} is the propagation life calculated assuming $a_0 = 0.25$ mm

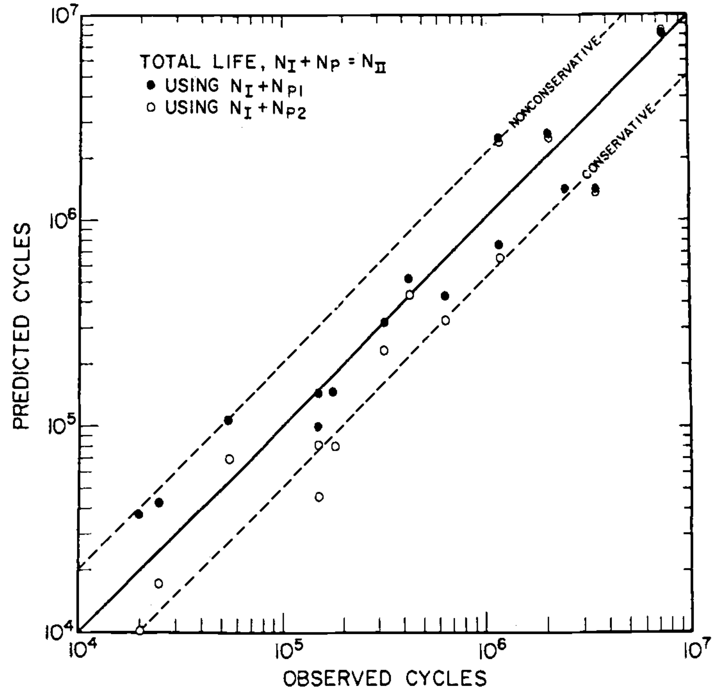

FIG. 20—*Comparison of observed and predicted* N_{II} *using the modified TSIP model (Model 7).*

t is the sheet thickness, and S_u is the ultimate tensile strength of the notch root material (see Fig. 1). As suggested by Reemsnyder [*21*], McMahon used the elastic stress concentration factor (K_t) rather than Peterson's fatigue notch factor (K_f) in the set-up-cycle analysis and found good agreement between the calculated fatigue crack initiation life (N_I) and the observed life at which the fatigue cracks exceeded the calculated threshold crack length (a_{th}), calculated in Eq 4 (see Table 7). The threshold crack length was calculated using Barsom's [*22*] expression for threshold stress-intensity factor (Eq 5) and an empirical expression for the geometry factor (Y) found by fitting a cubic equation to the observed crack growth behavior of the companion and presectioned test pieces (Eq 6).

$$a_{th} = \frac{\Delta K_{th}^2}{\pi(Y\Delta S)^2} \tag{4}$$

$$\Delta K_{th} = 6.4(1 - 0.85R) \qquad \text{for } R < 0.1 \qquad (\text{MPa}\sqrt{\text{m}}) \tag{5}$$

$$Y = 14.39 - 19.54\left(\frac{a}{t}\right) + 20.24\left(\frac{a}{t}\right)^2 - 8.2\left(\frac{a}{t}\right)^3 \tag{6}$$

The length of Stage II or life devoted to through-thickness fatigue crack propagation (N_P) was calculated using the Paris power law and the expression for Y above (Eq 6).

$$\frac{da}{dN} = C(\Delta K)^n \tag{7}$$

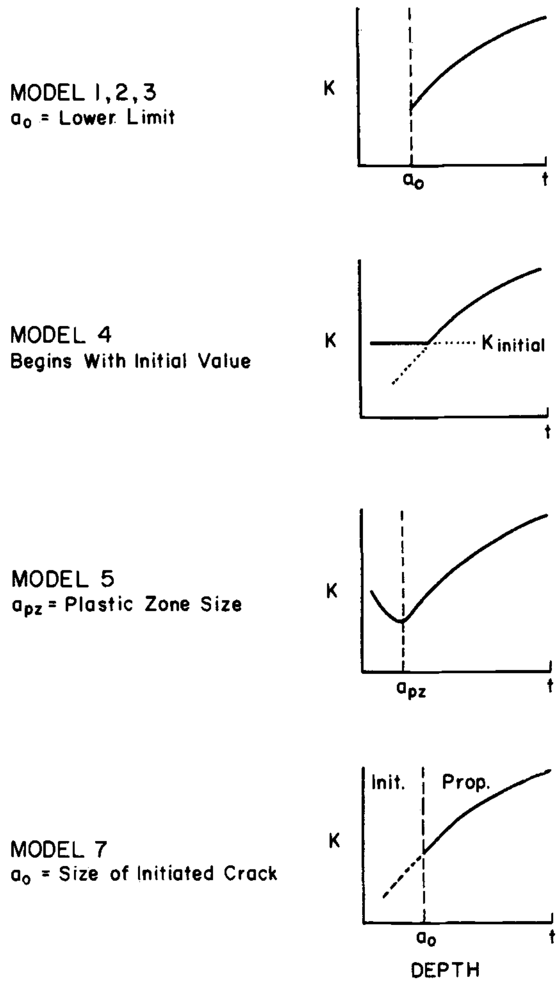

FIG. 21—*Variation of stress-intensity factor* (K) *with crack depth used in the various prediction models.*

$$N_P = \frac{1}{C}\int_{a_o}^{a_f} \Delta K^{-n} da \tag{8}$$

where $\Delta K = Y\Delta S(\pi a)^{1/2}$. In the present study, the calculated value of a_{th} was used as the lower limit of integration in Eq 8, rather than the fixed (arbitrary) value of 0.25 mm used by Wang et al. [7]. In Table 7, estimates of N_P made using these two assumptions for initial flaw size (a_o) are labeled N_{P1} and N_{P2}, respectively. The values of the constants (C and n) in the Paris power law appropriate for the heat-affected zone (HAZ) of the SAE 960X TSSW were estimated as $C = 10^{-13}$ MPa $\sqrt{\text{m}}$, and $n = 5.0$ [7]. Thus the total life to the end of Stage II is the sum of the results of Eqs 1 and 8.

$$N_{\text{II}} = N_{\text{I}} + N_P \tag{9}$$

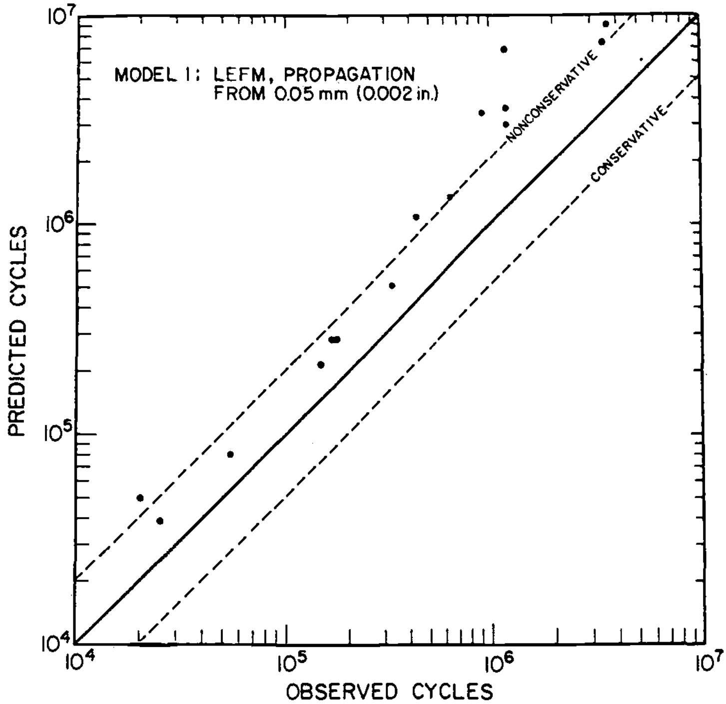

FIG. 22—*Comparison of observed and predicted* N_{II} *using the Model 1, propagation only,* $a_o = 0.05$ *mm.*

A comparison of experimental and estimated N_{II} using the modified TSIP model is given in Table 7 and Fig. 20. While it is evident from Fig. 20 that the modified TSIP model gives reasonably good estimates of the fatigue life (N_{II}) of TSSW, the authors also estimated N_{II} for the weldments studied here using the alternative models described below and shown in Fig. 21.

Model	Logic	Definition of Initiated Crack Length, a_o
Model 1	$N_{II} \approx N_{P2}$	0.05 mm
Model 2	$N_{II} \approx N_{P2}$	0.25 mm
Model 3	$N_{II} \approx N_{P2}$	a_{th}
Model 4	$N_{II} \approx N_{P2}$	0 using constant initial ΔK (Pook [*20*])
Model 5	$N_{II} \approx N_{P2}$	0 closure modeled to a_{pz} (Verreman [*23*])
Model 6	$N_{II} \approx N_I$	...
Model 7	$N_{II} \approx N_I + N_{P1 \text{ or } 2}$	a_{th} or 0.25 mm (modified TSIP model)

Models 1 and 2 gave estimates of N_{II} based on calculations of N_P using two definitions of a_o (0.05 mm and 0.25 mm). As shown in Figs. 22 and 23, Model 1 generally overestimated and Model 2 generally underestimated N_{II}; moreover, the slope of estimates based on a fixed initial crack size leads to inaccuracies in either the short or long life regions, depending upon the choice of a_o. The use of a_{th} as the value of the initiated crack length (Model 3) gave good predictions at short lives but increasingly conservative (under) estimates at long lives (see Fig. 24).

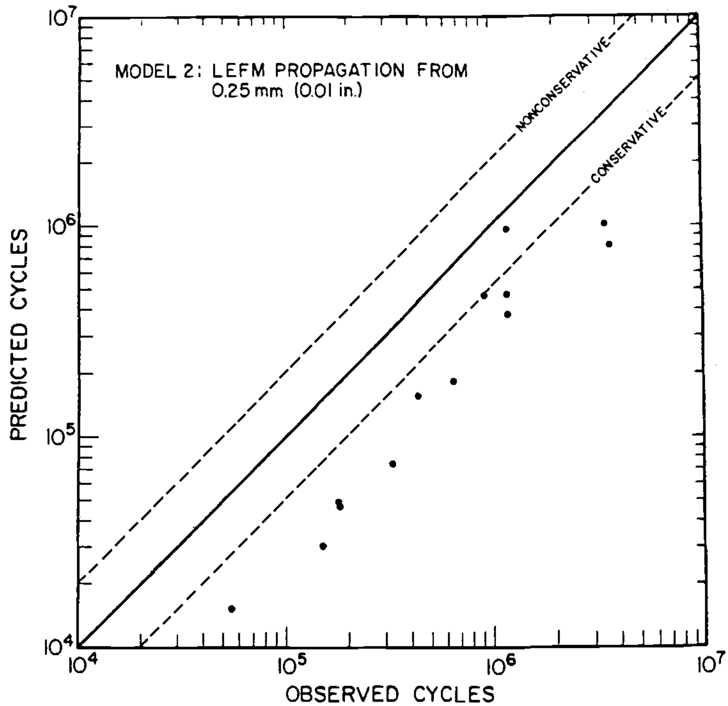

FIG. 23—*Comparison of observed and predicted* N_{II} *using the Model 2, propagation only,* a_o = *0.01 mm.*

Model 4 gave estimates of N_{II} based on calculation of N_P, assuming Pook's [*20*] initial value of the stress-intensity factor (K_o) (Eq 3). The Paris power law was integrated from a crack size of zero to the sheet thickness, assuming a constant and then increasing relationship between ΔK and crack depth (see Fig. 21). Model 4 gave very good predictions in the life range of 10^4 to 10^6 cycles but overestimated the life beyond 10^6 cycles, as shown in Fig. 25. Model 5 gave estimates of the total life based on calculation of N_P, assuming Pook's initial value of the stress-intensity factor but modeling crack closure in the manner of Verreman et al. [*23*] to a crack depth of the calculated plastic zone size (a_{pz}). The results for this model are shown in Fig. 26.

Model 6 gave estimates of total life based on calculation of N_I only. As shown in Fig. 27, this model gave overly conservative life estimates at short lives but good estimates at lives beyond 10^6 cycles. Model 7 (the TSIP model) gave estimates of total life, based on calculation of both Stages I and II, which were generally within a factor of two of the observed lives (see Fig. 20).

Conclusions

1. Approximately 50% of the total life of the SAE 960X tensile-shear spot welds studied was devoted to developing a 0.25-mm-depth crack under constant-amplitude loading in the life range of 10^4 to 10^6 cycles. At lives greater than 10^6 cycles, this fraction begins to increase,

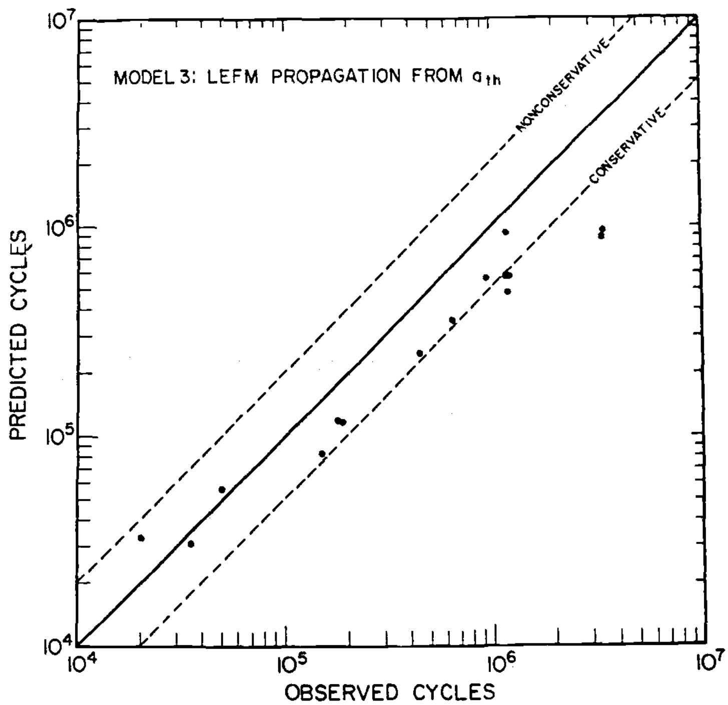

FIG. 24—*Comparison of observed and predicted* N_{II} *using the Model 3, propagation only,* $a_o = a_{th}$.

particularly for the $R = -1$ load cycle. Similar results were found for an automotive variable-load history containing several large overload events; however, in this case only 40% of life was devoted to developing the same crack depth.

2. Postweld coining increased the fatigue life by a factor of five, presumably through the induction of compressive notch-root residual stresses.

3. Several propagation and initiation-propagation models for predicting the fatigue life of the specimens studied were compared. Best results were obtained with a propagation model that used Pook's stress-intensity factor as an initial value of stress-intensity factor and with the initiation-propagation model proposed.

Acknowledgments

This study was supported in part by the Committee of Sheet Steel Producers of the American Iron and Steel Institute under Grant 1201-448 and in part by the University of Illinois Fracture Control Program. The authors wish to thank K. Ewing and her associates at the General Motors Technical Center for supplying the materials and assistance in the fabrication of specimens. R. Langraf of Ford Motors kindly supplied the variable-load history used in this study. All mechanical testing was carried out in the Materials Engineering Research Laboratory at the University of Illinois at Urbana—Champaign.

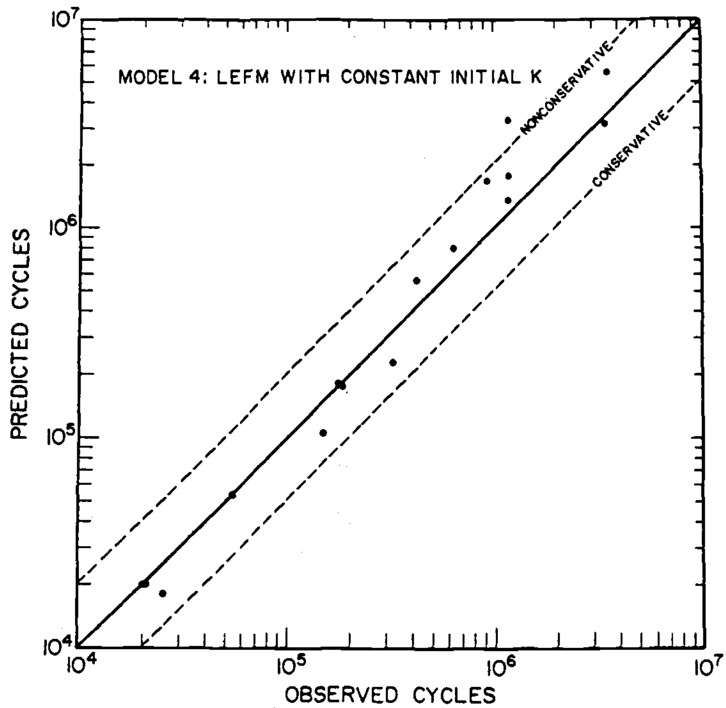

FIG. 25—*Comparison of observed and predicted* N_{II} *using the Model 4, propagation only, constant initial stress-intensity factor after Pook* [20], *until exceeded by measured values,* $a_o = 0$.

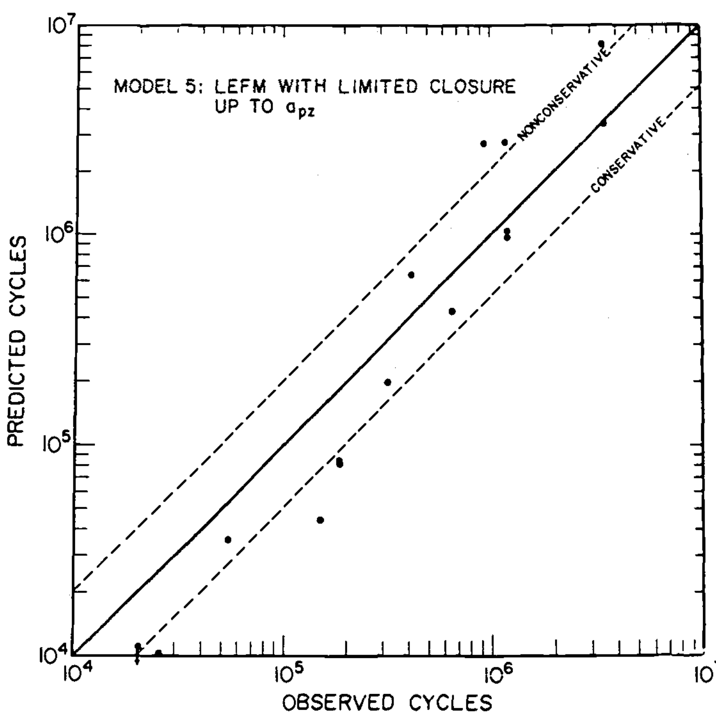

FIG. 26—*Comparison of observed and predicted* N_{ll} *using the Model 5, propagation only, constant initial stress-intensity factor after Pook* [20], *with effects of crack closure modeled after Verreman et al.* [23] *until* $a = a_{pz}$, $a_o = 0$.

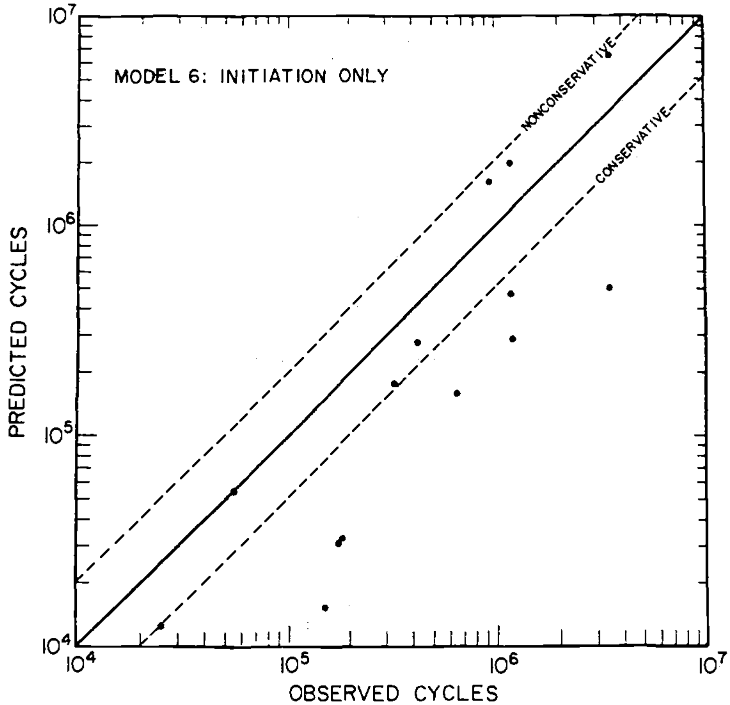

FIG. 27—*Comparison of observed and predicted* N_{tt} *using the Model 6, initiation only.*

References

[1] Davidson, J. A., "A Review of Fatigue Properties of Welded Sheet Steel," SAE Technical Paper 84110, Society of Automotive Engineers, Warrendale, PA, 1984.

[2] Davidson, J. A. and Imhof, E. J., "The Effect of Tensile Strength on the Fatigue Life of Spot-Welded Sheet Steels," SAE Technical Paper 84110, Society of Automotive Engineers, Warrendale, PA, 1984.

[3] Cooper, J. F. and Smith, R. A., "The Measurement of Fatigue Cracks at Spot Welds," *International Journal of Fatigue,* Vol. 7, No. 3, 1985, pp. 137–140.

[4] Cooper, J. F. and Smith, R. A., "Fatigue Crack Propagation at Spot Welds," *Metal Construction,* Vol. 18, No. 6, 1986, pp. 383R–386R.

[5] Smith, R. A. and Cooper, J. F., "Theoretical Predictions of the Fatigue Life of Shear Spot Welds," International Conference on Fatigue of Welded Constructions, S. J. Maddox, Ed., Brighton, England, 1987.

[6] Wang, P. C. and Ewing, K. W., "A *J*-integral Approach to Fatigue Resistance of T-3 Spot Welds," SAE Technical Paper 880373, Society of Automotive Engineers, Warrendale, PA, 1988.

[7] Wang, P. C., Corten, H. T., and Lawrence, F. V., "A Fatigue Life Prediction Method for Tensile-Shear Spot Welds," SAE Technical Paper 850370, Society of Automotive Engineers, Warrendale, PA, 1985.

[8] Lawrence, F. V., Ho, N. J., and Mazumdar, P. K., "Predicting the Fatigue Resistance of Welds," *Annual Review of Materials Science,* 1981, pp. 401–425.

[9] Ho, N. J. and Lawrence, F. V., Jr., "Constant Amplitude and Variable Load History Fatigue Test Results and Predictions for Cruciform and Lap Welds," *Theoretical and Applied Fracture Mechanics,* Vol. 1, No. 1, 1984, pp. 3–21.

[10] Lawrence, F. V. and Yung, J. Y., "Estimating the Effects of Residual Stress of the Fatigue Life of Notched Components," *Advances in Surface Treatments,* A. Niku-Lari, Ed., *Residual Stress,* Vol. 4, Pergamon Press, New York, 1987, pp. 483–509.

[11] Socie, D. F., "Fatigue Damage Maps," *Proceedings*, Vol. II, Third International Conference on Fatigue and Fatigue Thresholds, Charlottesville, VA, 1987, pp. 599–616.
[12] Nowack, H. and Marissen, R., "Fatigue Crack Propagation of Short and Long Cracks: Physical Basis, Prediction Methods, and Engineering Significance," *Proceedings*, Vol. II, Third International Conference on Fatigue and Fatigue Thresholds, Charlottesville, VA, 1987, pp. 599–616.
[13] Orts, D. H., "Fatigue Strength of Spot Welded Joints in HSLA Steel," SAE Technical Paper 810355. Society of Automotive Engineers, Warrendale, PA, 1981.
[14] Wilson, R. B. and Fine, T. E., "Fatigue Behavior of Spot Welded High-Strength Steel Joints," SAE Technical Paper 810354, Society of Automotive Engineers, Warrendale, PA, 1981.
[15] Smith, G. A. and Lawrence, F. V., "Fatigue Crack Development in Tensile-Shear Spot Weldments," Fracture Control Program Report No. 108, University of Illinois, Urbana, IL, 1984.
[16] McMahon, J. C. and Lawrence, F. V., "Fatigue Crack Initiation and Early Growth in Tensile-Shear Spot Weldments," Fracture Control Program Report No. 131, University of Illinois, Urbana, IL, 1985.
[17] Lawrence, F. V., Jr., Corten, H. T., and McMahon, J. C., "Improvement of Steel Spot Weld Fatigue Resistance," Report to the American Iron and Steel Institute, Urbana, IL, April 1985.
[18] Landgraf, R. W., Ford Motor Co., personal communication, 1984.
[19] Landgraf, R. W., "Effect of Means Stress on the Fatigue Behavior of a Hard Steel," M.S. thesis, University of Illinois at Urbana-Champaign, Urbana, IL, 1966.
[20] Pook, L. P., "Approximate Stress Intensity Factor for Spot Welds and Similar Welds," Report No. 588, National Engineering Laboratory, United Kingdom, April 1975.
[21] Reemsnyder, H. S., "Evaluating the Effect of Residual Stresses on Notched Fatigue Resistance," *Materials, Experimentation and Design in Fatigue*, Westbury Press, Guilford, England, 1981.
[22] Barsom, J. M., "Fatigue Behavior of Pressure-Vessel Steels," *WRC Bulletin*, No. 194, May 1974, pp. 1–22.
[23] Verreman, Y., Baïlon, J. P., and Masounave, J. "Closure and Propagation Behavior of Short Fatigue Cracks," *Proceedings*, Vol. I, Third International Conference on Fatigue and Fatigue Thresholds, Charlottesville, VA, 1987, pp. 371–380.

Anil K. Sablok[1] *and William H. Hartt*[1]

Fatigue of Welded Structural and High-Strength Steel Plate Specimens in Seawater

REFERENCE: Sablok, A. K. and Hartt, W. H., "**Fatigue of Welded Structural and High-Strength Steel Plate Specimens in Seawater,**" *Fatigue and Fracture Testing of Weldments, ASTM STP 1058,* H. I. McHenry and J. M. Potter, Eds., American Society for Testing and Materials, Philadelphia, 1990, pp. 78–95.

ABSTRACT: Corrosion fatigue data for three series of experiments involving a butt-welded structural and nine higher strength steels (yield stress, 370 to 750 MPa)—with the latter representing relatively new strengthening technologies such as microalloying, control rolling, thermomechanical control processing, and precipitation hardening—have been evaluated comparatively. Variables in the tests included: (1) the *R* ratio, (2) the as-welded versus ground and postweld heat-treated conditions, and (3) freely corroding versus cathodically protected conditions, although the nature and duration of the experiments was not conducive to a systematic treatment of these factors. Fatigue life data for the freely corroding specimen experiments reflected an influence of the weld toe geometry and the associated stress-concentration factor for as-welded specimens and of the *R* ratio for postweld heat-treated ones. On the other hand, no effect of the material strength was apparent. Limited data for the cathodically polarized specimens indicated improvement in fatigue life over that for the freely corroding specimens and for higher strength steels over structural steels.

KEY WORDS: weldments, structural steels, high-strength steels, welded steels, fatigue, residual stress, stress concentration, seawater, cathodic protection, postweld heat treatment, stress ratio

Fatigue failure of welded connections in offshore service is an important consideration for long-term structural integrity [*1–3*]. The situation is complicated by the fact that as many as 10^7 to 10^8 stress cycles may occur during the design life of a structure, with most of the damage accumulation occurring at relatively low stress amplitudes [*3*]. Also, this corrosion fatigue process involves numerous variables. These may be divided into four general categories: (1) mechanical, (2) material, (3) environmental, and (4) electrochemical variables. Figure 1 [*4*] illustrates these, along with examples of each. The complexity of fatigue property evaluation develops because these factors may be mutually interactive, and a change in one may modify the influence of others. Also, because the corrosion fatigue process is frequency dependent, an accelerated experimental study will not necessarily yield relevant information.

In the past, relatively low-strength steels have been employed to fabricate offshore structures, and only limited consideration has been given to using higher strength alternatives. The corrosion fatigue research that has been performed upon such welded steels in seawater has focused largely upon conventional high-strength low-alloy (HSLA) materials, such as the high-yield (HY) type [*5*]. However, recent developments in steelmaking have resulted in materials with mechanical properties comparable to these (HY series) but with a low

[1] Center for Marine Materials, Department of Ocean Engineering, Florida Atlantic University, Boca Raton, FL 33431.

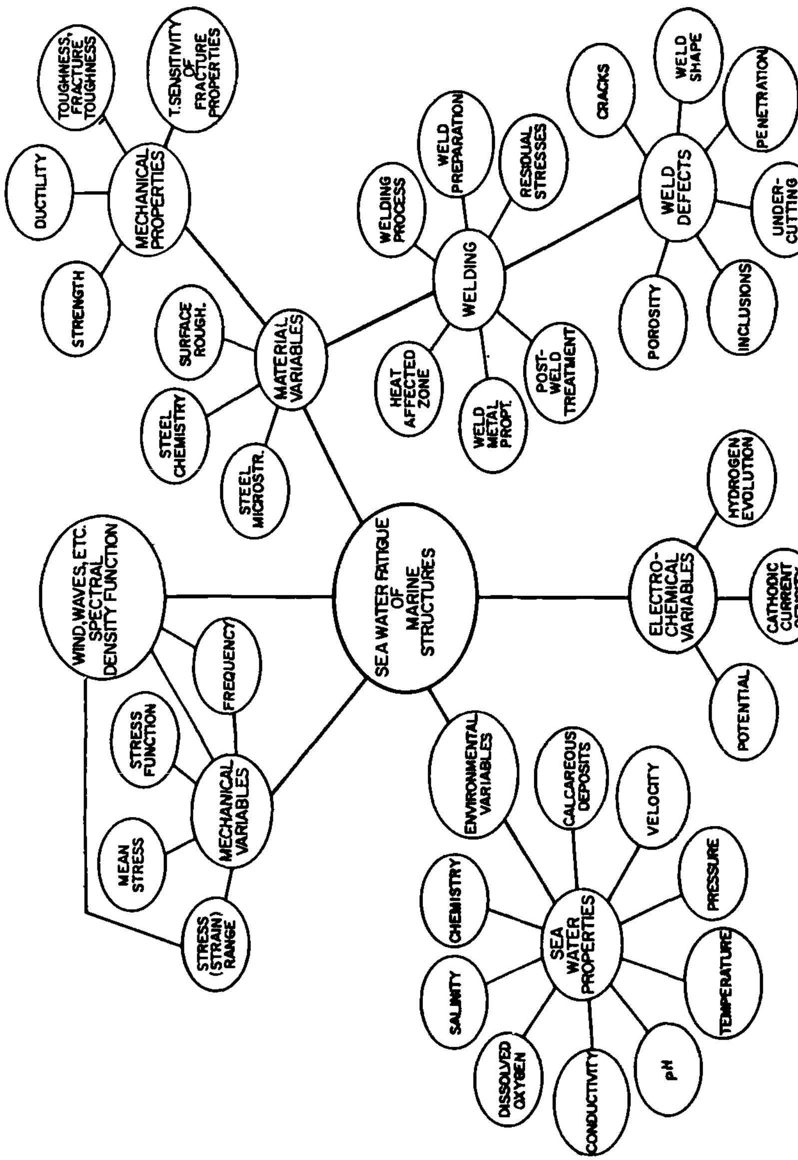

FIG. 1—*Variables that influence fatigue of welded steel connections in seawater.*

carbon equivalent and enhanced weldability. Some of these alloys are strengthened by processes or mechanisms other than martensitic phase development [6], such as precipitation hardening, control rolling, and thermomechanical control processing (TMCP) [7].

The high-cycle fatigue life of steel in air typically increases with increasing strength. However, there is little or no benefit from this fatigue strength enhancement in applications where there is concurrent aqueous corrosion [8,9]. Some benefit from the greater material strength can be retained during fatigue loading in hostile environments if corrosion mitigation techniques such as cathodic polarization are employed. However, this may result in embrittlement due to hydrogen, as has been observed even for structural steel [10]. Because the brittle cracking tendency typically increases with strength level, it is important that any fatigue-critical corrosion application of these steels be preceded by a comprehensive evaluation of environmentally assisted cracking effects.

Residual stresses due to welding can play an important role with regard to the effect of the stress ratio on corrosion fatigue strength (CFS) [11,12]. Thus, the stress ratio is apparently not significant for high-cycle CFS of as-welded specimens [11–15]. On the other hand, stress-relieved specimens typically show a decrease in CFS with increasing stress ratio [12].

In the course of the past several years, the authors' laboratory has been involved in three experimentally similar, but parametrically distinct, projects that investigated the high-cycle fatigue properties of welded structural and higher strength steels in seawater. The purpose of the present paper is to evaluate comparatively the results of these projects and to rationalize, based upon this, the influence of critical factors.

Experimental Procedure

These experiments have been broadly categorized in three test series, listed in Table 1. Series I experiments employed as-welded, ABS-DH32 steel, whereas Series II experiments involved ground and postweld heat-treated (PWHT) specimens fabricated from several low-alloy, quenched and tempered alternatives. Series III tests, on the other hand, were based upon relatively new, higher strength, low-carbon-equivalent, as-welded steels.

The material properties and welding procedures for the steels employed in the Series I and II experiments have been presented previously [16,17] and are summarized here in Tables 2 through 5. A total of six steels were employed in Series III and are listed in Table 6, along with the strengthening mechanism or processing procedure for each. It was intended that these represent the best available low-carbon-equivalent steelmaking technology for the strength range in question, as affected by the various manufacturing processes. Tables 7 and 8 give the chemical compositions and mechanical properties for these Series III steels. The welding of these materials was by the submerged-arc process in the flat position, employing the best available yard technology. A detailing of this procedure and the welding parameters have been described elsewhere [18]. Although the weld profile varied among the materials, in all cases the reinforcement height was minimal and the filler metal merged smoothly with the parent plate. The Series III specimens were tested in the as-welded condition.

All the specimens were machined from 25.4-mm plate subsequent to welding. Figure 2

TABLE 1—*Test specimens and conditions for each series.*

Series 1	reverse-bend fatigue tests on as-welded structural steel specimens
Series 2	bending fatigue tests on conventional quenched and tempered high-strength steel specimens
Series 3	reverse-bend fatigue tests on new high-strength steel specimens

TABLE 2—*Mechanical properties of Series I structural steel specimens (ABS-DH32).*

Yield Strength, MPa (ksi)	Tensile Strength, MPa (ksi)	Elongation, % in 20.3 cm	Transverse Charpy Value
390 (56.6)	536 (77.7)	38	42 J at −10°C.

TABLE 3—*Mechanical properties of Series II high-strength steels.*

Material	Supplier	Yield Stress (MPa)	Tensile Stress (MPa)	Elongation %	Charpy Impact Energy Joules at -20 °C
2 1/4 Cr-Mo	JSW	636	821	20	
U-80 Plate (Pipeline X)	NKK	625	688	25	305
HY-80	Lukens	622	742	22	
2 1/4 Cr-Mo	Kawasaki	607	751	22	260
U-80 Plate (Pipeline Y)	Kawasaki	606	699	27	

TABLE 4—*Specimen designations for Series II tests.*

Specimen Designation	Base Materials
HY	HY-80 (Lukens) welded to HY-80 (Lukens)
X	2 1/4 Cr-1Mo (JSW) welded to Pipeline X (NKK)
Y	2 1/4 Cr-1Mo (Kawasaki) welded to Pipeline Y (Kawasaki)

TABLE 5—*Welding procedures for Series II test specimens.*

Specimen Type	Welding Process	Joint Design	Preheat (Min) C	Interpass (max) C	Heat Input	PWHT
HY	SMAW-Root SAW-Fill	Double Bevel	93 93	150 150	12 KJ/cm 8.5 KJ/cm	607 C/1Hr 607 C/1Hr
X	SMAW-Root SAW-Fill	Double Bevel	177 177	370 370	13 KJ/cm 14 KJ/cm	620 C/Hr
Y	SAW	Double Bevel	149	205	14 KJ/cm	650 C/Hr

TABLE 6—*Listing of Series III steels.*

STEEL	TYPE
ASTM A 710	PrecipitationHardened
QT 80 QT 108	Quenched and Tempered
EH 36 (ABS)	Control Rolled
ASTM A 537 Direct Quench ASTM A 537 Accelerated Cool	Thermomechanically Control Processed (TMCP)

TABLE 7—*Chemical compositions of Series III steels.*

STEEL ELEMENT	A 710	QT-80	QT-108	EH-36	A 537 (d.q)	A 537 (a.c)
C	0.04	0.08	0.11	0.13	0.12	0.07
Si	0.30	0.23	0.23	0.37	0.41	0.26
Mn	0.45	1.40	0.86	1.42	1.30	1.35
P	0.004	0.01	0.004	0.018	0.014	0.011
S	0.002	0.002	0.003	0.002	0.003	0.003
Cu	1.14	0.01	0.24	0.01	0.01	0.14
Ni	0.82	0.43	0.98	0.01	0.03	0.14
Cr	0.67	0.09	0.43	0.02	0.04	0.01
Mo	0.18	0.06	0.44	0.01	0.05	0.02
Nb	0.037	0.002	_.__	0.025	_.__	0.017
V	0.004	0.04	0.027	0.003	0.044	_.__
B	0.0001	0.0001	0.0009	_.__	_.__	_.__
Ti	0.002	0.005	_.__	0.022	_.__	_.__
N	0.0047	0.0026	_.__	0.0038	_.__	_.__
Sol. Al	0.034	0.051	_.__	0.046	_.__	_.__
O	_.__	_.__	_.__	_.__	_.__	_.__
Carbon Equivalent	0.7108*	0.4165£	0.3807£	0.4853*	0.3890*	0.3781*

* Ceq = C + Mn/6 + Si/24 + Ni/40 + Cr/5 + Mo/4 + V/14

£ Ceq = C + Mn/6 + Cu/15 + Ni/15 + Cr/5 + Mo/5 + V/5

TABLE 8—*Mechanical properties of Series III steels.*

Steel	Yield Stress, MPa (Ksi)	Tensile Stress MPa (Ksi)	Elongation %	Charpy Impact Energy at -40°C, Joules
A 710	563 (81.7)	622 (90.3)	31.8	378
QT 80	537 (77.9)	613 (88.9)	27.9	333
QT 108	745 (108)	824 (119)	24.0	216
EH 36	416 (60.4)	536 (77.7)	34.0	216
A 537 d.q.	500 (72.5)	598 (86.7)	28.0	122
A 537 a.c.	452 (65.9)	551 (80.3)	30.0	-

presents a schematic view of the specimen geometry and weld configuration employed for the Series II and III experiments, although a modification of this was employed for Series I [*16*]. Thus, a constant-stress, tapered cantilever-type specimen was employed with the weld oriented transverse to the stressing direction. Some Series II specimens contained a central, longitudinal weld also. The specimens were fatigued by a bending procedure with a seawater bath mounted about the central region of the specimen. Details of the fatigue machines, test procedure, electrolyte properties, and technique for cathodic polarization have been described in detail elsewhere [*16,17*]. Table 9 summarizes the testing parameters employed in each series.

Results and Discussion

Data for freely corroding specimens for each series of the program have been presented separately elsewhere [*16,17,19*] but are reproduced here in Figs. 3 through 5. With regard to Series I, the relatively close agreement between data for ambient temperature at 3 Hz and data for 4°C at 0.5 Hz suggests either that the frequency and temperature variations in the range considered had little or no effect upon the fatigue life or that the effect of each

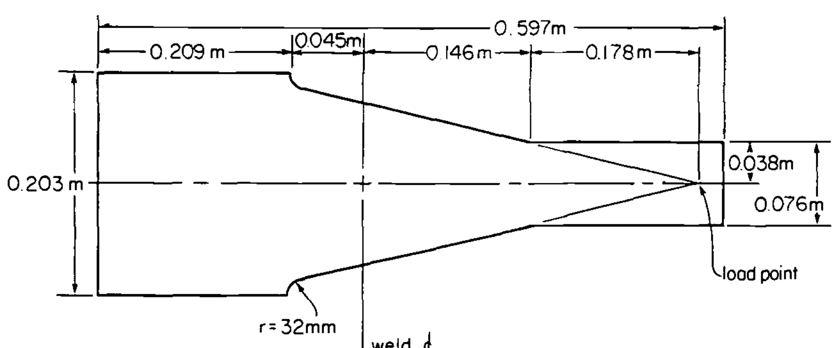

FIG. 2—*Geometry and dimensions of the Series II and III test specimens.*

TABLE 9—*Testing parameters for each series.*

	Series 1	Series 2	Series 3
Material	ABS-DH32 Structural Steel	Conventional Quenched & Tempered Steels	New High Strength Steels
Weld	As-welded	Ground & PWHT	As-welded
Mean Stress	0	145 MPa	0
Stress Ratio	-1	0.02 to 0.8	-1
Frequency	0.5 Hz or 3 Hz	0.3 Hz	0.3 Hz
Temperature	Ambient or 4 C	Ambient	Ambient
C.P. tests	-0.78V or -0.93V (SCE)	-0.900V (SCE)	-0.8V, -1.0V or -1.1V (SCE)

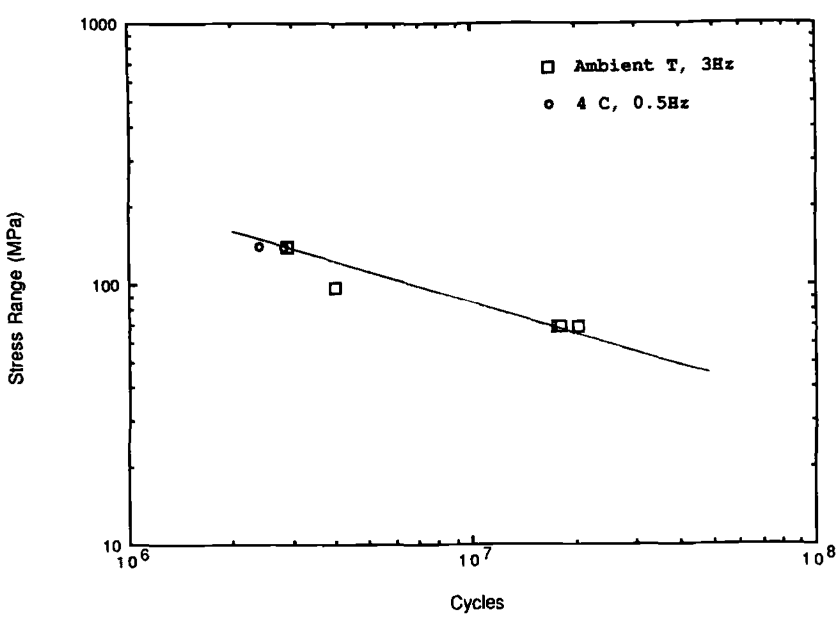

FIG. 3—*Series I test results for freely corroding specimens.*

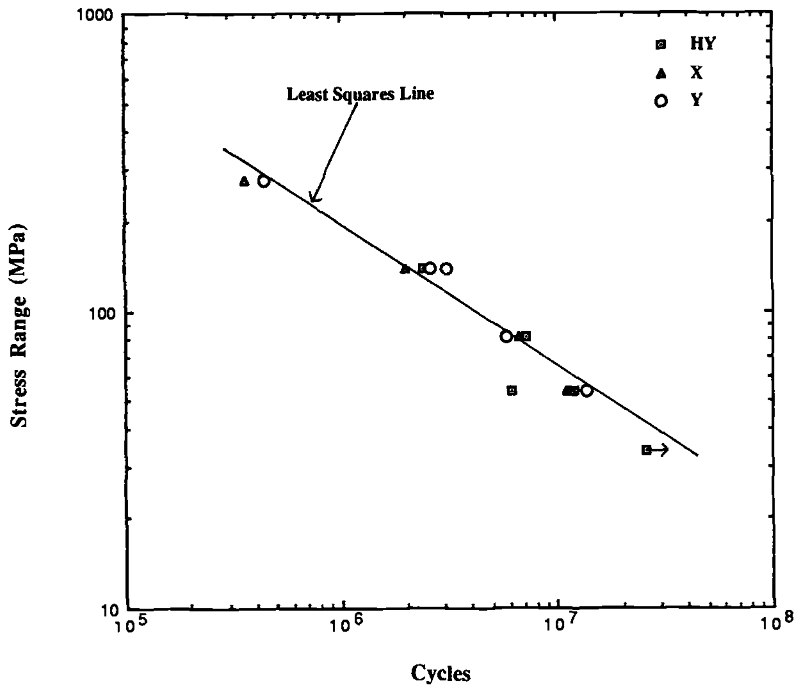

FIG. 4—*Series II test results for freely corroding specimens.*

factor was offset. The latter possibility is the most realistic, since previous investigators [*18,20–23*] have reported that fatigue strength increases with increasing frequency and with decreasing temperature.

In contrast to Series I and II results, the data from Series III exhibit relatively large scatter (Fig. 5). It has been shown, however, that the greater fatigue life of Steels EH36 and A537AC may be reconciled with that for the other steels when the weld toe stress-concentration factor is taken into account and the local stress range is considered [*19*]. Thus, in Fig. 6 the data for Steels EH36, A537AC, and A537DQ (the latter representing behavior typical of the other steels, see Fig. 5) have been replotted on a local stress basis (the weld toe stress-concentration factor multiplied by the nominal stress range), and it is apparent that data for all three may be represented by a single curve.

In Fig. 7, the least squares *S-N* curves for the three data sets have been superimposed. While as much as 50% difference in fatigue strength is apparent at the life extremes investigated, at the same time, the distinctions between the three may lie within the normal scatter range. This, however, could be fortuitous in view of the different test conditions employed in the program. To investigate this latter point, the 3-Hz Series I data were corrected to a frequency of 0.3 Hz, based on the variable frequency data developed in the previous program [*4*] and according to the expression

$$N = 1.4 \log f + 2.23$$

where

N = cycles to failure in million, and
f = frequency of loading.

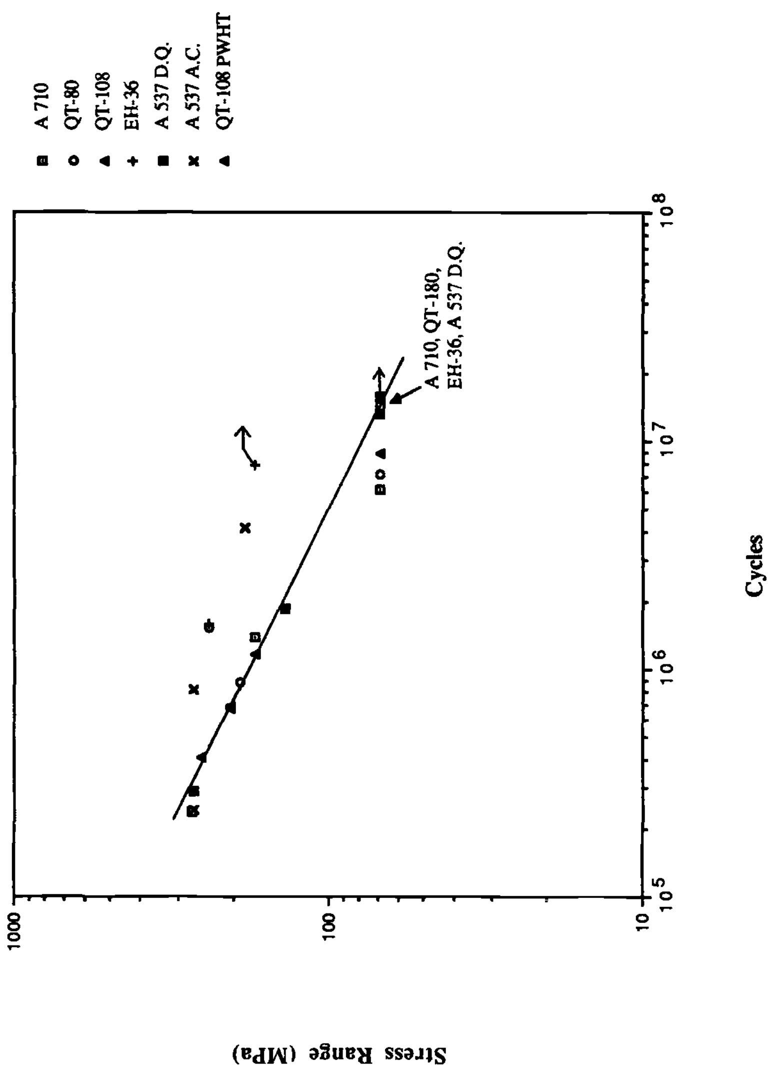

FIG. 5—*Series III test results for freely corroding specimens.*

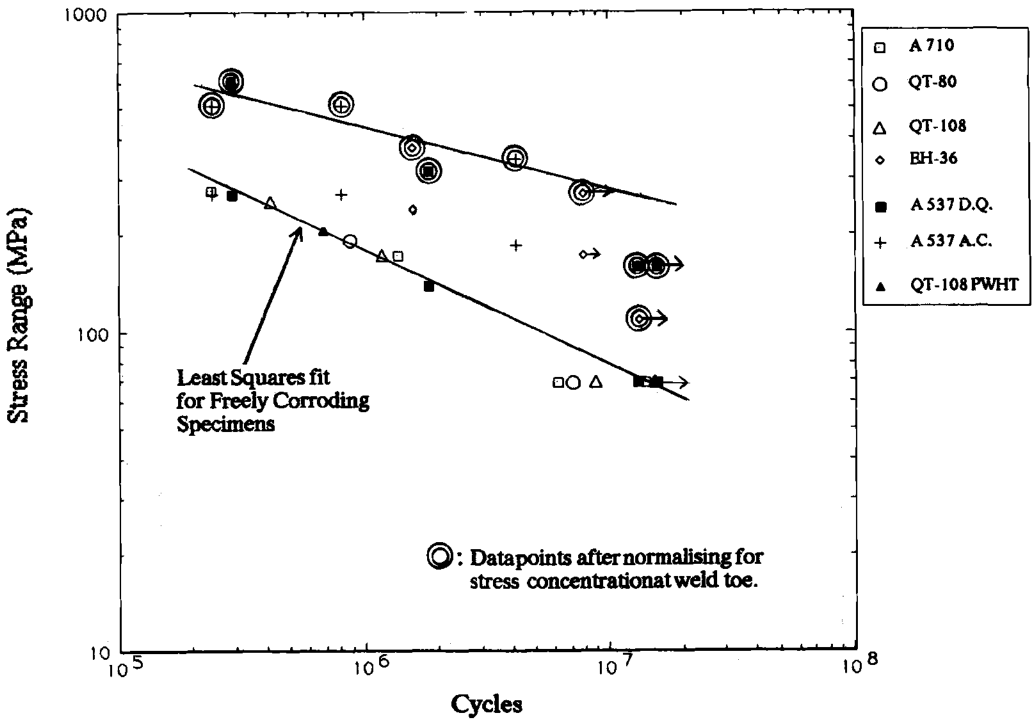

FIG. 6—*Comparison of Series III fatigue data for freely corroding specimens on a nominal and local stress basis.*

Figure 8 presents the frequency-corrected Series I least squares *S-N* curve in relation to the Series II and III results. This reduction in life for the Series I data does not alter the above conclusion, however, that the three curves may superimpose within the limits of experimental variations.

While the mean stress is not generally considered to influence the fatigue life of as-welded connections, because of the relatively high residual tensile stresses preexisting near the weld toe, this is not the case for PWHT material, for which the fatigue life decreases with increasing *R* ratio [*12*]. While both Series I and III experiments involved a constant *R* value of -1, for the PWHT specimens (Series II) the mean stress varied so that *R* increased as the stress range decreased. This, in fact, may account for the steeper slope to these data compared with the slopes for Series I and III (see Fig. 7). Correspondingly, Fig. 9 compares again the three least squares *S-N* curves but with the PWHT data corrected to $R = -1$, according to the results of Vaessen and de Back [*12*]. On this basis, the Series II *S-N* curve is displaced to a higher stress range and rotated counterclockwise. Interestingly, this line now corresponds closely to the local (concentrated) stress-range/cycles-to-failure curve for Series III data, which is presented in Fig. 6. This suggests that residual stresses, which are expected to be present in as-welded material, did not influence fatigue life in the present specimens.

The results of cathodically polarized fatigue experiments for the three series have also been presented previously [*16–17,19*] and are summarized here as Figs. *10–12*. A compounding factor in comparing these is that potential was different for the three series, and at the same time, fatigue life is a function of potential [*10,19*]. In the case of Series I and III, however, the distinction was only 0.02 V. While the difference could be important at stress ranges near the endurance limit, it is probably not significant at higher values. Figure 13 presents an *S-N* curve for the Series I, -0.78 V experiments, which has been developed

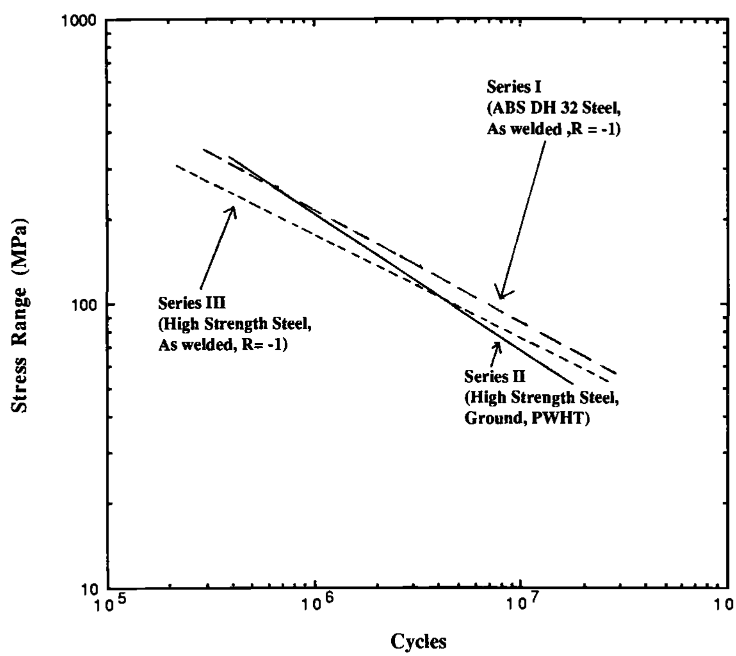

FIG. 7—*Least squares* S-N *curves for freely corroding specimens in the three series.*

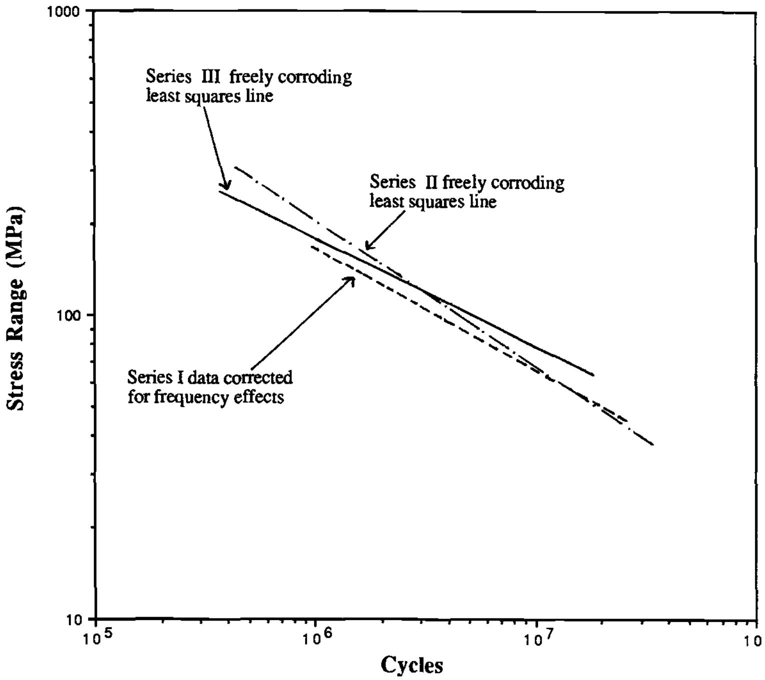

FIG. 8—*Frequency-corrected least squares* S-N *curve for Series I freely corroding specimens compared with Series II and III curves.*

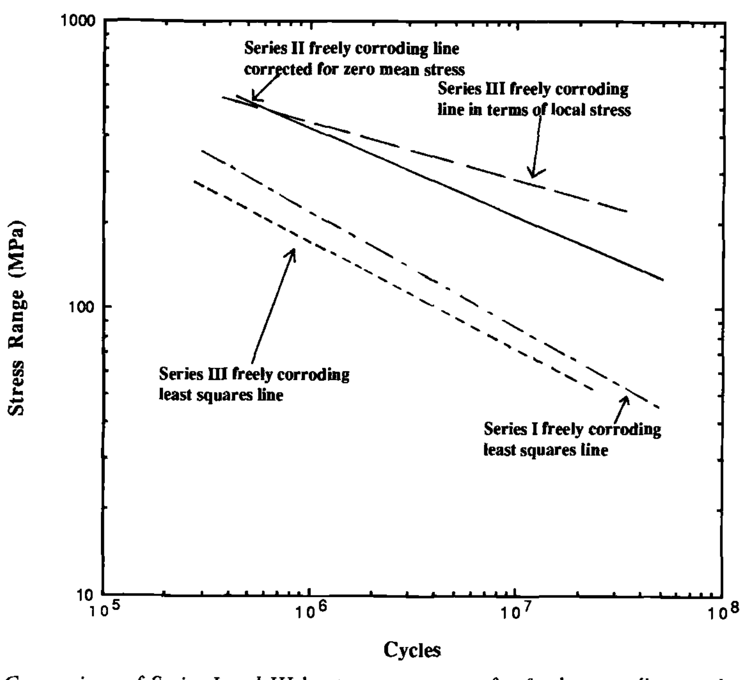

FIG. 9—*Comparison of Series I and III least squares curves for freely corroding specimens and the Series II* S-N *curve, corrected for mean stress.*

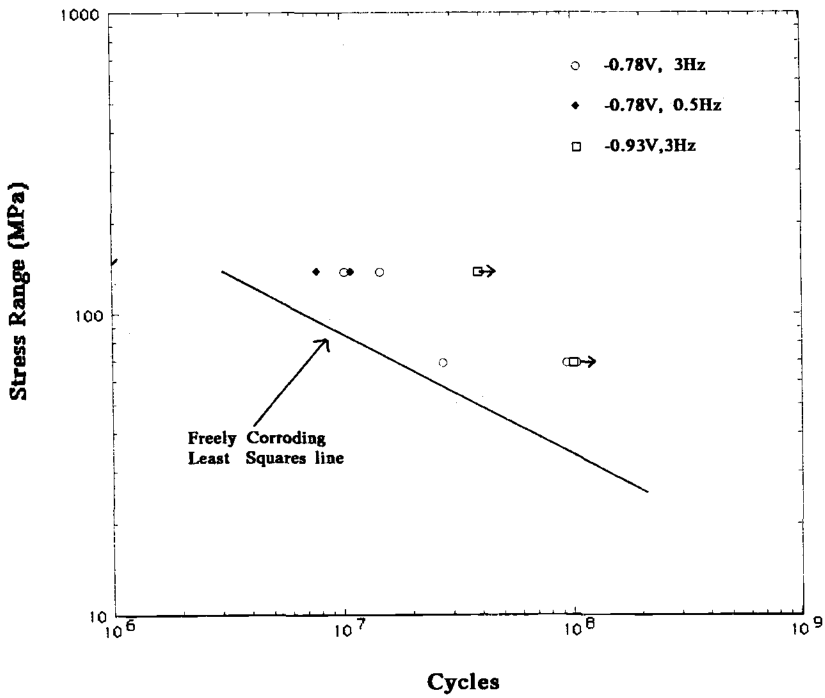

FIG. 10—*Cathodically polarized data for the Series I tests.*

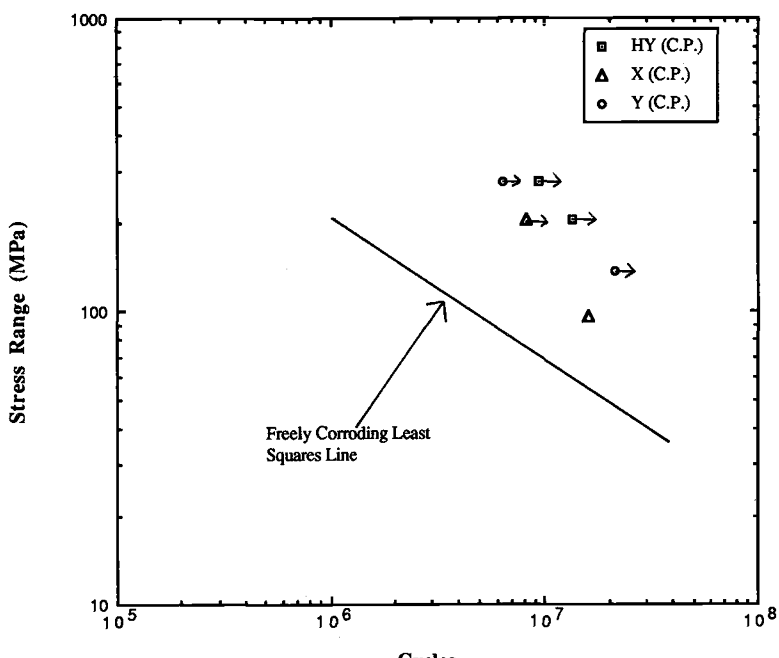

FIG. 11—*Cathodically polarized data for the Series II tests.*

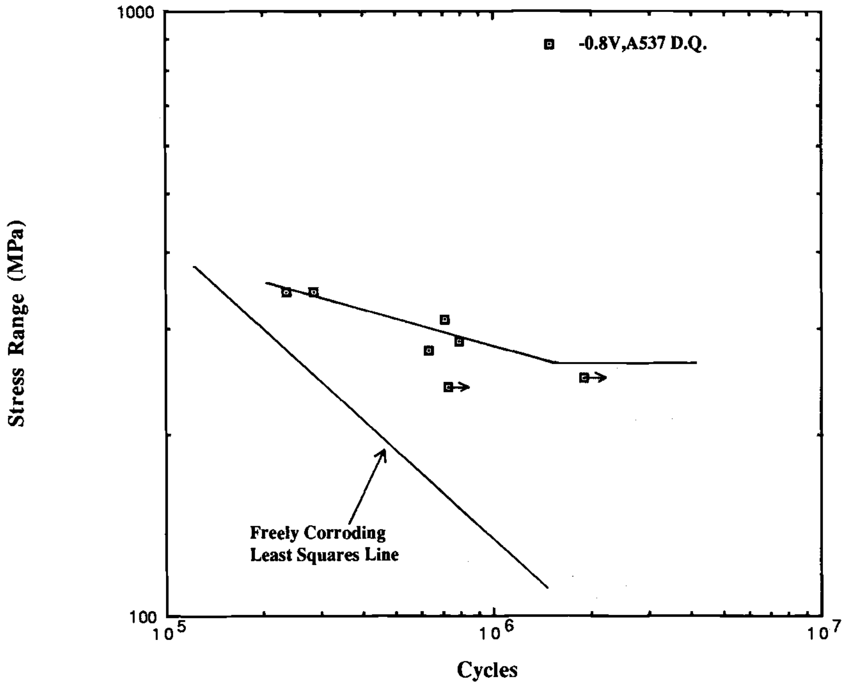

FIG. 12—*Cathodically polarized data for the Series III (A537DQ) tests.*

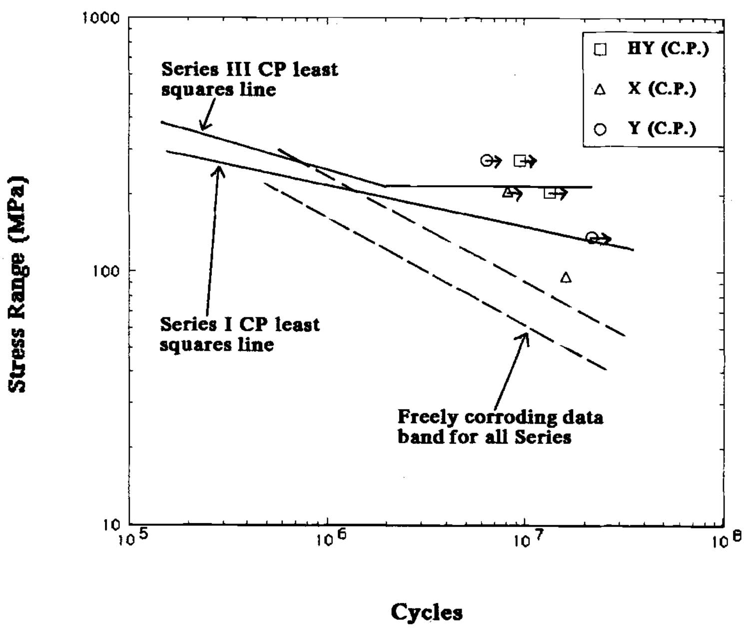

FIG. 13—*Comparison of Series I and III cathodically polarized least squares* S-N *curves with Series II data.*

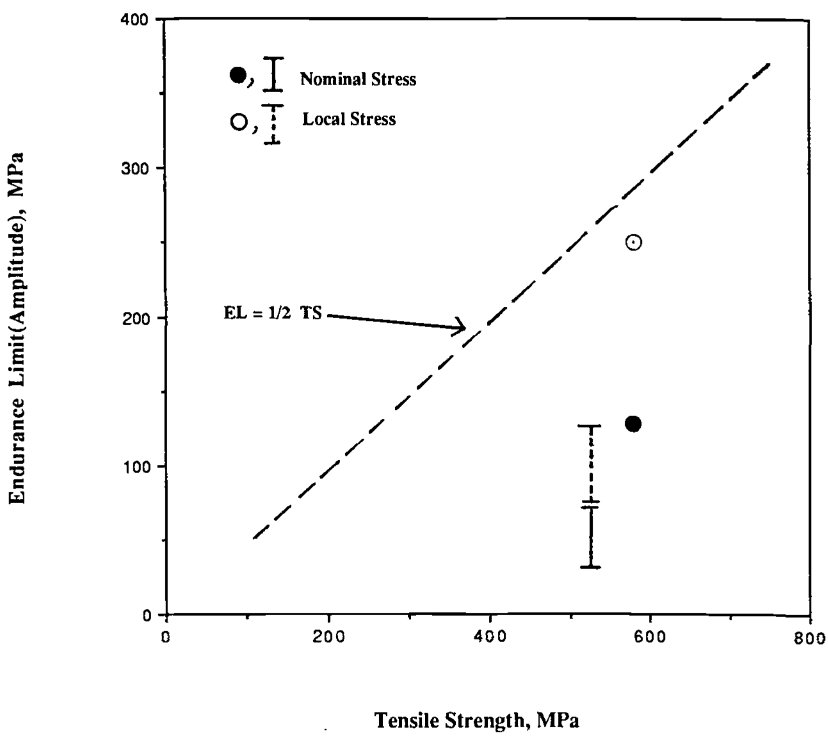

FIG. 14—*Comparison of endurance limit and tensile strength for Series I and III steels.*

[*16*] based upon the data in Fig. 10 and Ref *24*, and this curve is compared with the *S-N* curve from Fig. 12 for as-welded A537DQ steel and with the Series II data. The latter are not conducive to comparison, however, because most specimens were runouts. Figure 13 reveals that the higher material strength of A537DQ in comparison with ABS-DH32 has increased the fatigue strength and endurance limit at the potential considered by as much as a factor of two. This is shown also in Fig. 14, which compares the endurance limits of the two steels on both a nominal and a local stress basis. In the latter case, the stress-concentration factor for A537DQ (K_t = 2.29) was obtained from Ref *19* and that for ABS-DH32 (K_t = 2.18) from Ref *25*. Because cathodic polarization to the range −0.78 to −0.80 V does not correspond to optimum endurance limit restoration conditions for these steels in seawater [*10,16,26*], it is not surprising that the data fall below the classical trend of one-half tensile strength, even on a local stress basis. On the other hand the difference between the endurance limit and tensile strength is relatively large, and this may indicate a compounding effect of hydrogen embrittlement.

Conclusions

1. The variations in freely corroding specimen *S-N* data for as-welded, high-strength steel specimens in seawater could be explained by differences in the weld geometry and the associated stress-concentration factor.
2. Representation of as-welded data in terms of local (concentrated) weld toe stress indicated that the fatigue life is the same as for ground and postweld heat-treated

specimens if an R ratio correction is applied to the latter. This suggests that residual stresses for the former (as-welded) specimens did not affect fatigue life.

3. The fatigue life of freely corroding specimens was independent of the material tensile strength.
4. The fatigue strength and endurance limit of cathodically polarized specimens ($\phi = -0.78$ to -0.80 V, SCE) were greater than those for the freely corroding ones. For the higher strength steels investigated under this test condition, the endurance limit was greater than that for the structural steel, indicating the beneficial effect of enhanced material strength.

Acknowledgment

This research was sponsored by the American Petroleum Institute, Chevron Oil Co., and a consortium of companies including Chevron, Conoco, Exxon, Kawasaki, Marathon, MMS, NKK, Pont-a-Mousson, Shell, Sohio, and Sumitomo, to whom the authors are most grateful.

References

[*1*] Hicks, J. G., "Materials and Structural Problems in Offshore Installations," *Proceedings,* Vol I, International Conference on Welding in Offshore Construction, Newcastle-upon-Tyne, England, 1974, p. 1.

[*2*] Wintermack, H., "Materials and Welding in Offshore Constructions," 1975 Portevin Lecture, International Institute of Welding, London, England, 1975.

[*3*] Marshall, P. W., "Problems in Long-Life Fatigue Assessment for Fixed Offshore Structures," *Proceedings,* ASCE National Water Resources and Ocean Engineering Conference, San Diego, CA, April 1976.

[*4*] Hartt, W. H., "Fatigue of Welded Structural Steel in Sea Water," *Proceedings,* Second International Conference on Environmental Degradation of Engineering Materials, Blacksburg, VA, 1981.

[*5*] Heller, S. R., Fioriti, H., and Vasta, J., *Naval Engineers Journal,* February 1965, p. 29.

[*6*] Watanabe, I., "Applications of New Steel Material Produced by TMCP," *Journal of the Japan Welding Society,* Vol. 55, No. 1, January 1984, pp. 49–55.

[*7*] Peterson, M. L., "TMCP Steels for Offshore Structures," Paper No. 5552, *Proceedings,* Offshore Technology Conference, Houston, TX, 1987.

[*8*] Kitagawa, H., "A Fracture Mechanics Approach to Ordinary Corrosion Fatigue of Unnotched Steel Specimens," *Corrosion Fatigue: Chemistry, Mechanics, and Microstructure,* NACE-2, National Association of Corrosion Engineers, Houston, TX, 1972, pp. 521–528.

[*9*] Ishiguro, T., "Corrosion Fatigue Strength of Steels for Marine Structures," *Nippon Steel Technical Report,* No. 9, April 1977, pp. 27–36.

[*10*] Solli, O., "Corrosion Fatigue of Welded Joints in Structural Steel and the Effect of Cathodic Protection," Paper No. 10, Select Seminar on European Offshore Steels Research, Cambridge, England, 27–29 Nov. 1978.

[*11*] Wildschut, H., De Back, J., Portland, W., and Van Leeuwen, O. L., "Fatigue Behavior of Welded Joints in Air and Seawater," *Proceedings,* Offshore Steels Conference, The Welding Institute, Cambridge, England, November 1978, pp. 112–155.

[*12*] Vaessen, H. H. G. and de Back, J., "Fatigue Behavior of Welded Steel Joints in Air and Seawater," *Proceedings,* Vol. 1, Eleventh Annual Offshore Technology Conference, Houston, TX, 30 April–3 May 1979, pp. 555–562.

[*13*] Booth, G. S., "Constant Amplitude Fatigue Tests on Welded Steel Joints Performed in Seawater," *Proceedings,* Offshore Steels Conference, The Welding Institute, Cambridge, England, November 1978, pp. 227–252.

[*14*] Booth, G. S., "The Influence of Simulated North Sea Environmental Conditions on the Constant Amplitude Fatigue Strength of Welded Joints," *Proceedings,* Vol. 1, Eleventh Offshore Technology Conference, Houston, TX, 30 April–3 May 1979, pp. 547–554.

[*15*] Holmes, R., "Fatigue and Corrosion Fatigue of Welded Joints Under Random Loading Conditions," *Proceedings,* Offshore Steels Conference, The Welding Institute, Cambridge, England, November 1978, pp. 288–335.

[16] Hartt, W. H., "Fatigue of Welded Structural Steel in Sea Water," *Proceedings*, 13th Annual Offshore Technology Conference, Houston, TX, 1981, pp. 87–94.
[17] Sablok, A. K. and Hartt, W. H., "Fatigue of High Strength Steels in Sea Water," *Proceedings*, Seventh International Conference on Offshore Mechanics and Arctic Engineering, Houston, TX, 1988.
[18] Jaske, C. E., Broek, D., Slater, J. E., Utah, D. A., and Martin, C. J., "Corrosion Fatigue of Cathodically Protected Welded Carbon Steel in Cold Sea Water," Final Report submitted to the American Petroleum Institute by Battelle Columbus Laboratories, Columbus, OH, 11 Feb. 1977.
[19] Rengan, K., Sablok, A. K., and Hartt, W. H., "Fatigue Properties of Exemplary High Strength Steels in Sea Water," Paper No. 5663, *Proceedings*, 20th Annual Offshore Technology Conference, Houston, TX, 1988.
[20] Endo, K. and Komai, K., "Influence of Secondary Stress Fluctuations of Small Amplitude on Low-Cycle Corrosion Fatigue," *Corrosion-Fatigue Technology, ASTM STP 642*, American Society for Testing and Materials, Philadelphia, 1978, pp. 74–97.
[21] Gould, A. J., "The Influence of Temperature on the Severity of Corrosion Fatigue," *Engineering*, 8 May 1936, pp. 495–496.
[22] Dugdale, D. S., "Corrosion Fatigue of Sharply Notched Steel Specimens," *Metallurgica*, January 1972, pp. 27–28.
[23] Watanabe, M. and Mukai, Y., "Corrosion Fatigue Properties of Structural Steel and Its Welded Joints in Sea Water—Properties Under High Amplitude and Slow Rate of Cyclic Stressing," *Proceedings*, Vol. 1, International Conference on Welding in Offshore Constructions, Newcastle-upon-Tyne, England, published by The Welding Institute, Cambridge, England, 1974, pp. 46–53.
[24] Jaske, C. E., Slate, J. E., Broek, D., Leis, B. N., Anderson, W. E., Turn, J. C., and Omar, T., "Corrosion Fatigue of Welded Carbon Steel for Application to Offshore Structures," Interpretative Report submitted to the American Petroleum Institute by Battelle Columbus Laboratories, Columbus, OH, 1 Feb. 1977.
[25] Nerolich, S. M., Martin, P. E., and Hartt, W. H., "Influence of Weld Profile on Fatigue of Welded Structural Steel in Sea Water," *Corrosion Fatigue: Mechanics, Metallurgy, Electrochemistry and Engineering, ASTM STP 801*, American Society for Testing and Materials, Philadelphia, 1983, pp. 491–507.
[26] Rajpathak, S. S. and Hartt, W. H., "Keyhole Compact Tension Specimen Fatigue of Selected High Strength Steels in Sea Water," *Environmental Assisted Cracking, ASTM STP 1049*, American Society for Testing and Materials, Philadelphia, in press.

S. Dharmavasan,[1] J. C. P. Kam,[1] and W. D. Dover[1]

Corrosion Fatigue Testing of Welded Tubular Joints Under Realistic Service Stress Histories

REFERENCE: Dharmavasan, S., Kam, J. C. P., and Dover, W. D., "**Corrosion Fatigue Testing of Welded Tubular Joints Under Realistic Service Stress Histories,**" *Fatigue and Fracture Testing of Weldments, ASTM STP 1058,* H. I. McHenry and J. M. Potter, Eds., American Society for Testing and Materials, Philadelphia, 1990, pp. 96–114.

ABSTRACT: Because of the large number of stress cycles experienced by offshore structures in the North Sea, fatigue has become a major design consideration for such structures. Extensive research and testing has therefore been carried out to study the fatigue behavior of offshore structural components, particularly the welded tubular joints.

The laboratory technology for fatigue testing of tubular joints has now progressed to the point where realistic in-service stress history can be used. Crack growth results have been obtained with the use of more realistic load histories, coupled with the effects of the environment.

This paper summarizes some of the progress in the design and simulation philosophy for fatigue testing load histories. The latest crack growth data for welded tubular joints tested under realistic fatigue stress histories, in air and in a corrosive environment, are also presented. In most cases, the crack growth can be predicted reasonably accurately with standard fracture mechanics methodology. However, some unexpected crack growth retardation behavior was also observed, and there is currently no established calculation procedure to predict this phenomenon. Therefore, further studies are required to explain this unusual crack growth feature.

KEY WORDS: weldments, offshore tubular joints, corrosion fatigue, fracture mechanics modeling, fatigue crack growth, wave action standard history (WASH), realistic service history, automated fatigue testing

Nomenclature

a	Crack depth
da/dN	Crack growth rate
f	Frequency
h_x	Filter function of random process X
k	Number of linear segments representing the corrosion crack growth (da/dN versus ΔK) curve
m, m_i	Paris crack growth constant and the constant for segment i in

$$\frac{da}{dN} = C_i(\Delta K)^{m_i}$$

[1] NDE Centre, Department of Mechanical Engineering, University College London, London, England WC1E 7JE.

$p(\Delta S)$ Probability density function for ΔS
t Time
B Sub-block duration
C, C_i Paris crack growth constant and the constant for segment i in

$$\frac{da}{dN} = C_i(\Delta K)^{m_i}$$

F_i Fraction of time of sea state i
$H_x(w)$ Transfer function of random process X in the angular frequency domain
N Number of fatigue stress cycles
S_h Equivalent stress range or weighted average stress range, as defined in Eq 6
S_i Average duration of sea state i
T Transition matrix of sea states
T_{ij} or $T(i,j)$ Transition probability from sea state i to sea state j
Y Stress-intensity modification factor, as defined in Eq 7
$\epsilon(t)$ Time history of a white noise (uniform spectral heights)
$\eta_x(t)$ Time history of a random process X
ω Angular frequency
ΔK Stress-intensity factor range
ΔS Individual stress factor range
ΔS_{j-1}, ΔS Lower and the upper bounds of the stress range, to which the corresponding stress-intensity ranges are the respective lower and upper bounds of a crack growth segment j in a da/dN versus ΔK curve
$\Phi_x(\omega)$ Power spectrum of random process X in the angular frequency domain
$\Phi_\epsilon(\omega)$ Power spectrum of a white noise (uniform spectral heights)
$\Pi(n)$ Matrix containing the sea state distribution after n transitions

Because of the completion of several major research programs [*1,2*], a large amount of data has been gathered concerning the fatigue behavior of welded offshore structural components, mainly the tubular joints. However, the majority of these data are stress-life (S-N) information. Crack growth data, on the other hand, are limited. Most of the crack growth data were obtained from testing of materials and joints under constant-amplitude loading. Consequently, the understanding of crack growth behavior is adequate only for fatigue in air and in a corrosive environment (seawater) under constant-amplitude loading. It has therefore become necessary to start testing joints under a realistic load history in order to correlate realistic behavior with that observed from simpler load histories (such as constant-amplitude sine wave loading).

The realistic history is formulated from information extracted from some extensive in-service load history monitoring projects [*3*]. Obviously, the monitored results will be unique to the location, platform dimensions, configuration, payload, foundation behavior, and other factors. It is unlikely that the load history experienced by one structure will be repeated exactly on another. Therefore, it is necessary to extract from these lengthy records the most salient features relevant to fatigue. At the same time, as many characteristics of the load history as possible should be incorporated to avoid omitting any hidden factors related to fatigue, which may not be evident from current knowledge.

The in-service load history was found to behave like a random sequence of short sea states, and therefore the long-term root mean square (zero mean) of stress/strain varies continuously (Fig. 1). The short sea states were found to be generally stationary and their frequency content can be described by broad-band, double-peak power spectra (Fig. 2). In

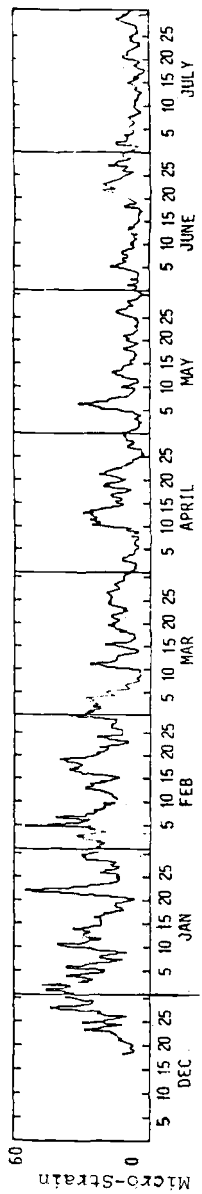

FIG. 1—*Typical root mean square (rms) strain history.*

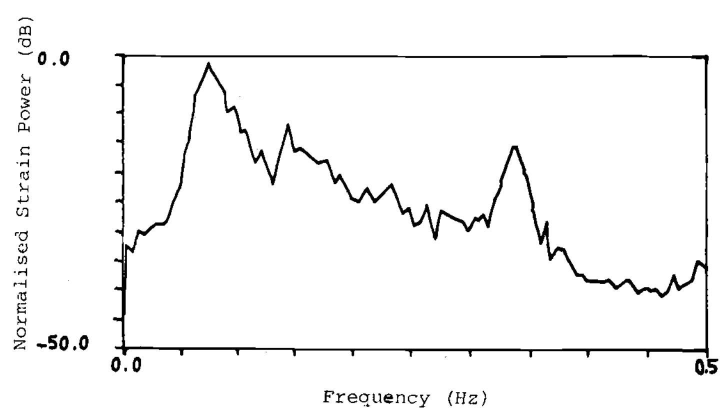

FIG. 2—*Typical strain power spectrum.*

the majority of cases, the random load history can be approximated as a Gaussian process. The most noticeable exception is the loading on small-diameter secondary members near the mean sea level. The non-Gaussian effect is principally caused by the nonlinear drag response of the structural members.

Wirsching proposed a series of eleven sea states for fatigue reliability analysis of offshore structures [*4*]. This series makes use of an equation combining the Bretschneider wave spectra with a nominal response peak to describe the sea state structural response spectra. Based on the same idea, Hartt and Lin [*5*] developed a six sea state (Fig. 3) sequence suitable for fatigue testing. The random sea state sequence is dependent on the long-term occurrence statistics (fractions of time) and is generated by a Markov chain technique.

An international committee was set up to carry out a detailed study of all the recent North

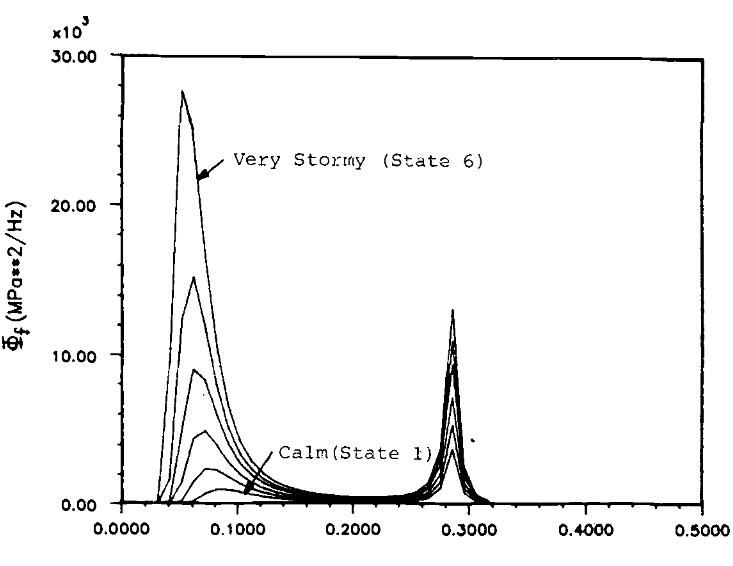

FIG. 3—*Power spectra corresponding to different sea states.*

Sea monitoring results with the objective of producing a realistic wave loading history. The proposed standard, known as the wave action standard history (WASH), followed up the sequence developed by Hartt and has produced a series of twelve sea states [6] (Table 1).

In the recommended WASH standard history, the two highest sea states have been combined with the third highest state because of the very small occurrence probability of the former. Moreover, in order to compress the lengthy history into a reasonable size suitable for laboratory testing, the lowest two states are omitted, and the probability of occurrence of the third lowest state has been reduced to 4.7%. Therefore, the WASH standard load history comprises the "most relevant" 20% of a year-round history. Further development to incorporate the non-Gaussian/nonlinear effect is still continuing. A prototype method replicating the data obtained from an existing platform has also been developed [7]. It is important to note that each sea state contains both small and large cycles. The compression of the time history is achieved by omitting entire sea states, thereby still maintaining the damaging nature of the entire load history.

The following describes the techniques involved in generating the above load histories for fatigue testing and outlines the framework adopted for the WASH load history.

Simulation Procedure

Markov Chain for Sea State Sequence

The random sea state sequence is controlled by the long-term distribution of the states (fraction of time) and other state duration parameters. However, the occurrence of any one state in a sequence does not affect the overall distribution. Moreover, the state after a current state must be the one above, below, or the same as the current one. This chain

TABLE 1—*Sea state data for WASH.*

Sea State Number	Significant Wave Height (m)	Dominant Period (s)	Fraction of Time (%)
0	1.75	7.17	38.5
1	2.55	7.92	28.5
2	3.40	8.70	17.5
3	4.15	9.35	7.18
4	4.80	10.01	3.40
5	5.45	10.53	2.16
6	6.15	11.23	1.31
7	6.90	11.77	0.678
8	7.80	12.52	0.334
9	8.80	13.29	0.154
10	10.35	14.70	0.0797
11	13.60	17.56	0.0043

behavior can be shown in Fig. 4. The Markov chain process can be described by the following equation.

$$\mathbf{\Pi}(n + 1) = \mathbf{T}'\mathbf{\Pi}(n) = (\mathbf{T}')^n\mathbf{\Pi}(0) \tag{1}$$

where

$\mathbf{\Pi}(n)$ = the sea state distribution after n transitions, and
$\mathbf{T}'$ = the transpose of the transition matrix; because of the chain behavior, each row of $\mathbf{T}$ has at most only three nonzero elements, $T_{i,i-1}$, $T_{i,i}$, and $T_{i,i+1}$.

The elements in $\mathbf{T}$ can be evaluated as

$$\begin{gathered} T_{ii} = 1 - \frac{B}{S_i} \\ \frac{F_i}{S_i} = \frac{F_{i-1}}{S_{i-1}} \cdot \frac{T_{i-1,i}}{(1 - T_{i-1,i-1})} + \frac{F_{i+1}}{S_{i+1}} \cdot \frac{T_{i+1,i}}{(1 - T_{i+1,i+1})} \\ T(i_{\min} - 1, i_{\min}) = T(i_{\max}, i_{\max} + 1) = 0 \end{gathered} \tag{2}$$

where

T_{ij} = the probability of transition from sea state i to sea state j,
B = the (sub) block duration,
S_i = the average duration of sea state i, and
F_i = the fraction of time spent in sea state i.

A special property of the Markov chain process is that as $n \rightarrow \infty$

$$\begin{gathered} \mathbf{\Pi}(n + 1) = \mathbf{\Pi}(n) = \mathbf{\Pi}(\infty) = \text{long-term sea state distribution} \\ \mathbf{\Pi}(\infty) = \mathbf{T}'\mathbf{\Pi}(\infty) \end{gathered} \tag{3}$$

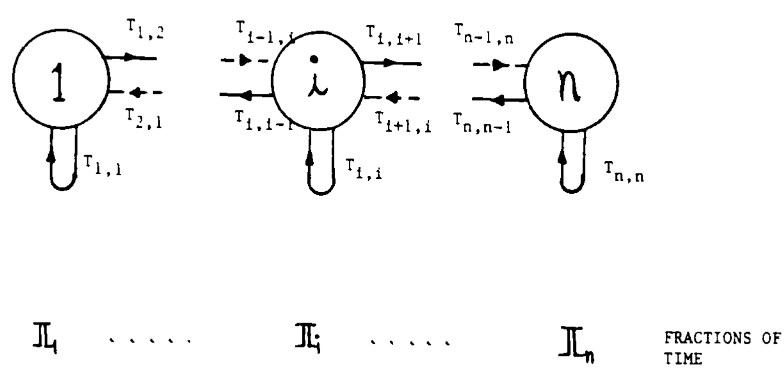

FIG. 4—*Figure showing the Markov chain simulation of sea states.*

Therefore, the occurrence of any sea state does not affect the long-term distribution statistics, and this agrees with the observed phenomena.

The transition of state is modeled by a random number generator, which generates uniformly distributed random numbers. The cumulative probabilities are compared with the random number, and then the necessary transition is found (Fig. 5). The WASH sequence specifies a machine-independent random number generator [*8*], and exactly the same sea state sequence can be generated in any computer/load actuator system.

Random Load History Within a Sea State

For each characteristic power spectrum, $\Phi_x(\omega)$, a digital filter, $h_x(\tau)$, can be found. This filter is the discrete inverse Fourier transform of $H_x(\omega)$, the transfer function of $\Phi_x(\omega)$. Therefore

$$\Phi_x(\omega) = |H_x(\omega)|^2\Phi_\epsilon(\omega) \tag{4}$$

where $\Phi_\epsilon(\omega)$ is the power spectrum of a white noise (uniform spectrum). Function $h_x(\tau)$ effectively amplifies all the desired frequencies so that unwanted frequencies remain but only as an insignificant part of the time history. The desired time history is therefore given by

$$\eta_x(t) = \int_0^\infty h_x(\tau)\epsilon(t - \tau)d\tau \tag{5}$$

The white noise sources, $\epsilon(t)$, are generated by the pseudo-random binary shift (PRBS) register technique. This technique makes use of a register containing a series of digits 0 and 1. At every clock pulse (signal output time) all the digits are shifted one place to the right. The last digit is abandoned and the first is formed from either a two-way or a four-way programmable feedback loop (Fig. 6). The advantage of this technique is the excellent frequency control. Figure 7 shows the input and the generated spectra for Hartt state 5 [5]

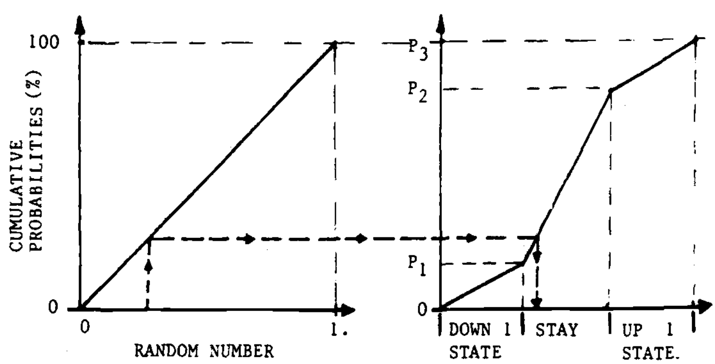

$P_1 = T_{i,i-1}$
$P_2 = P_1 + T_{i,i}$
$P_3 = P_2 + T_{i,i+1} = 100\ \%$

FIG. 5—*Figure showing the sea state transition by Monte Carlo method for state* i.

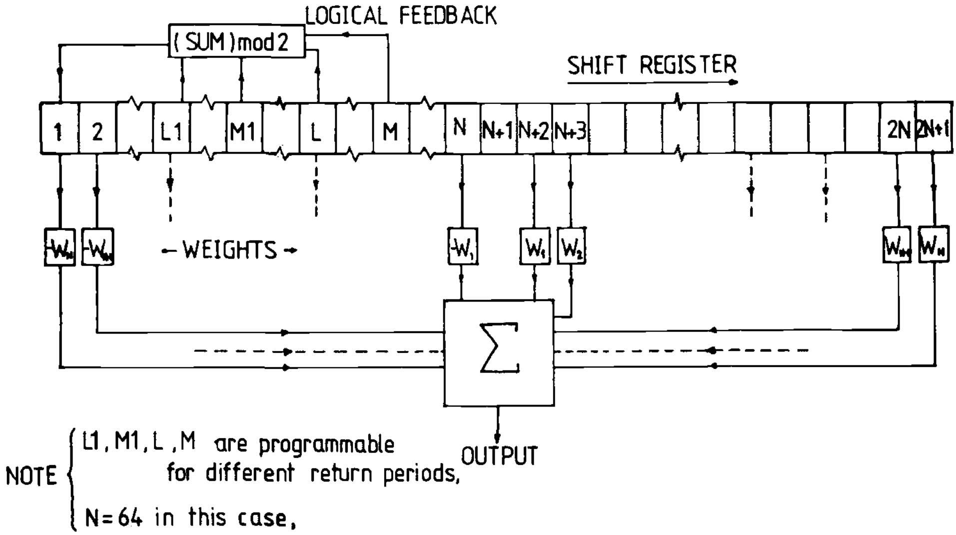

FIG. 6—*Schematic diagram of pseudo-random signal generation.*

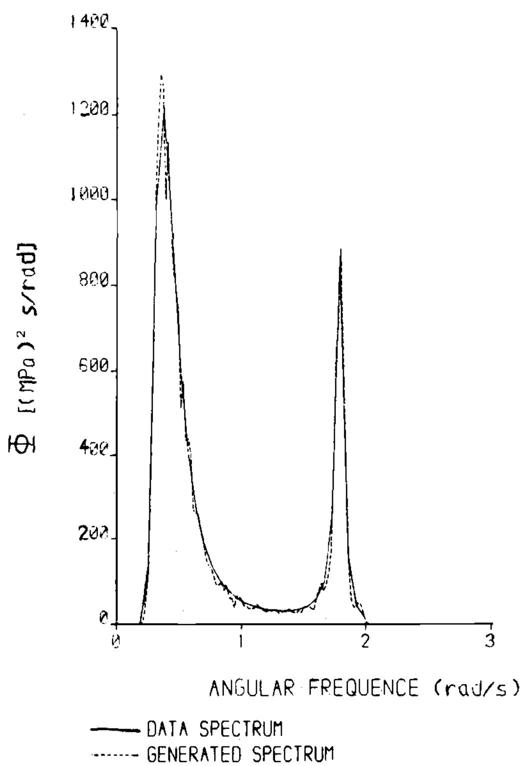

FIG. 7—*Required and generated sea state 5 (Hartt proposal).*

The frequency content is considered one of the more important factors in corrosion fatigue, and therefore the PRBS method is considered necessary.

The random history within a sea state can be non-Gaussian for some cases. This behavior can be simply modeled by raising the generated time history to a specified power. More sophisticated methods using windowing techniques are also available [*9*]. However, these techniques require more information concerning the load history than just the power spectra. This extra information, at the moment, is still very limited, and therefore this extension to the work has not yet been implemented.

Automated Fatigue Testing

A series of fatigue tests on large tubular joints was carried out. These joints were subjected to realistic random load histories. During the course of the test the crack shape evolution was monitored using a high-frequency alternating-current field measurement (ACFM) technique [*10*] with multiple fixed probes.

An integrated general purpose computer program has been developed for automating fatigue tests. This program, FLAPS [*11*], provides facilities for both waveform generation and data acquisition, including collection of crack growth data. Other facilities include conditional branching based on collected data. A database facility is an integral part of the program and allows different types of information to be stored in a user-defined format.

The general structure of the program is shown in Fig. 8. The different phases of the program are described below.

System Setup

The system setup phase is used to select system-dependent information, such as the type of controller being used and the type of crack measurement system, in addition to setting up the various parameters necessary before running a test, such as calibration, engineering

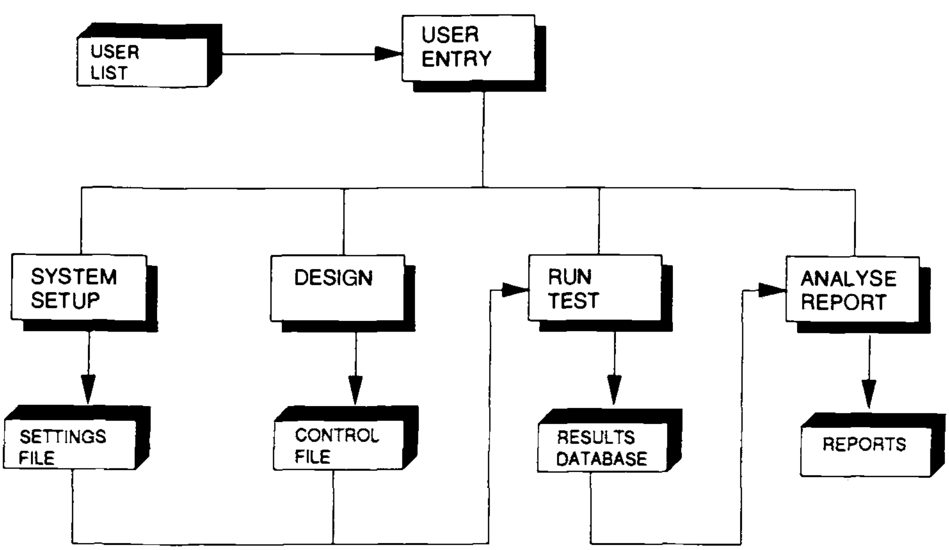

FIG. 8—*Program structure for FLAPS.*

TABLE 2—*Summary of variable amplitude tests on tubular joints.*[a]

Joint Code	Shape of Joint	Chord Wall Thickness	Variable Amplitude Loading	Mode of Loading	S_b (MPa)	Fatigue Life (x 10^6 cycles)	Environment
YIPB2	Y	16 mm	Single (UCL)	IPB	168	1.95	air
UCX4	X	25 mm	Single (UCL)	Axial	220	0.32	air
UCX5	X	20 mm	Single (UCL)	Axial	170	0.83	air
KOPB1B	K	16 mm	Multiple (Hartt 3-6)	OPB	146	2.90	air
KOPB2A	K	16 mm	Multiple (Hartt 3-6)	OPB	146	1.88+[1]	*
KOPB2B	K	16 mm	Single (Hartt 6)	OPB	220	0.46	*

[a] Key to abbreviations:
1 = a runout test.
* = corrosive environment (seawater), catholic protection = −850 mV.
UCL = University College London double-peak spectrum, clipping ratio = 4.
Hartt = Hartt multiple sea state proposal [5].
IPB = in plane bending.
OPB = out of plane bending.

units, and other parameters. This information is used during the Run phase to control the test in the most appropriate manner.

Design

The design phase allows the setting up of templates known as control files to run specific applications. The various waveform generation, data collection, and program control options are chosen and the sequence of operation defined. This process is carried out prior to testing and provides a library of test routines.

Run Test

The Run phase uses the data stored in the control file, in conjunction with the calibration and units information from the settings file, to control a test on Instron equipment. This module makes extensive use of the local intelligence capabilities of the Instron controllers to off-load processing from the computer.

Analysis/Report

This module has capabilities for further analysis and report generation, including presentation-quality graphics. The analysis part is performed with commercially available spread sheets as there are facilities to transfer the data from the FLAPS database structure to the commercial spread-sheet packages.

Crack Growth Data in Air and Seawater

The general information concerning the series of fatigue tests mentioned above, is summarized in Table 2. The air tests were used to establish the "basic" behavior, with which the corrosion data can be compared. An empirical model, the two-phase model (TPM), coupled with the equivalent stress (S_h) approach, was found to be adequate [*12*] in predicting the fatigue behavior in air. The equivalent stress range of a random load history can be calculated as

$$S_h = \left\{ \int_0^\infty \Delta S^m \, p(\Delta S) d(\Delta S) \right\}^{1/m} \tag{6}$$

where

ΔS = an individual stress range,
$p(\Delta S)$ = the probability density of ΔS, which describes the stress range distribution in a random loading history, and
m = the Paris crack growth constant.

There are three usual ways of comparing the predicted and experimental fatigue crack growth in air. The first is the comparison of the stress-intensity modification (Y) factor.

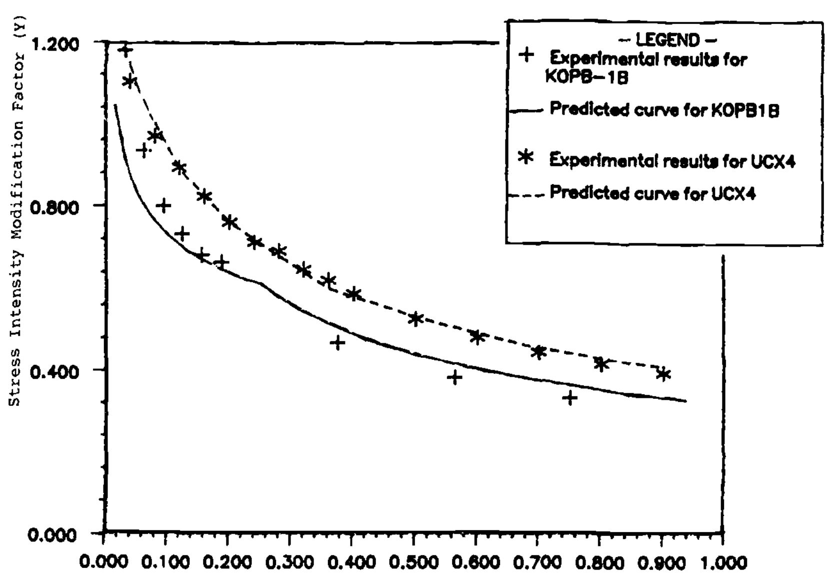

FIG. 9—*Comparison of the experimental and predicted* Y *distribution for Tests KOPB-1B and UCX-4.*

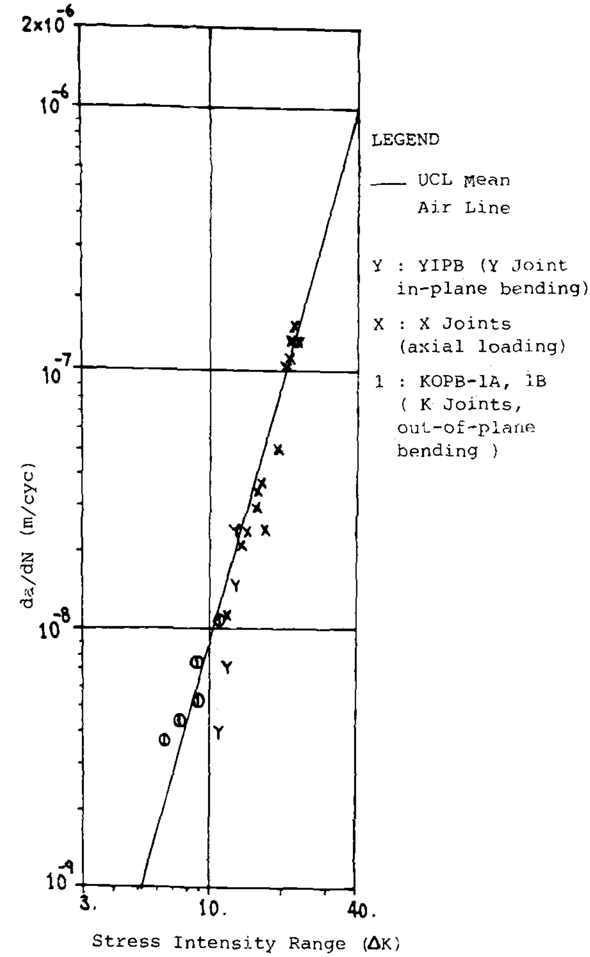

FIG. 10—*Experimental* da/dN *versus predicted* ΔK *for crack growth in air.*

The stress-intensity range (ΔK) is calculated by the following equation

$$(\Delta K) = YS_h\sqrt{\pi a} \tag{7}$$

where a is the instantaneous crack depth. The Y factor includes the effects of stress distribution, crack geometry, and factors specific to the structure in which the crack is found. The crack growth rate is related to the stress-intensity range through, for example, the Paris law

$$\frac{da}{dN} = C(\Delta K)^m \tag{8}$$

where da/dN is the instantaneous crack growth rate, and C, m are the Paris material constants.

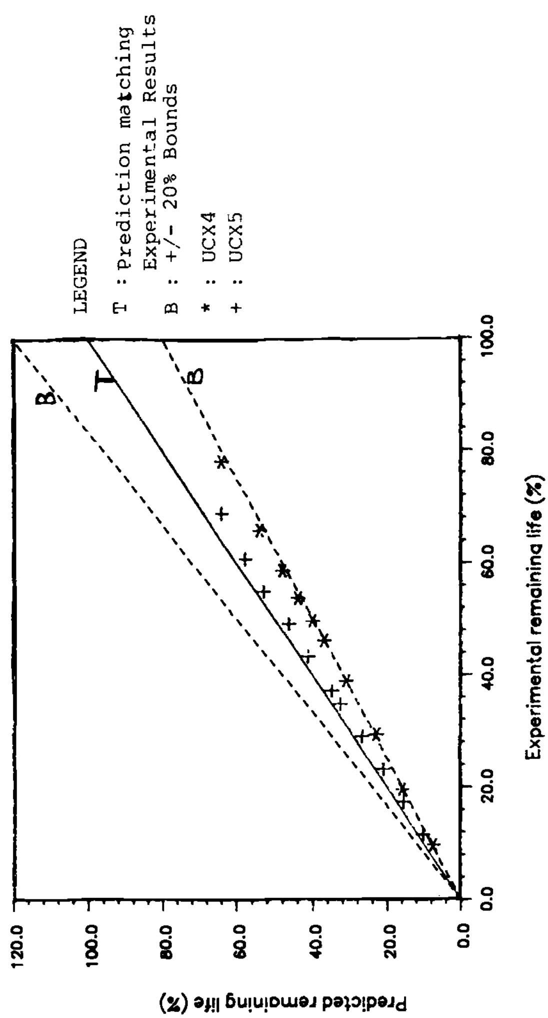

FIG. 11—*Comparison of the experimental and predicted remaining fatigue life for Tests UCX-4 and UCX-5.*

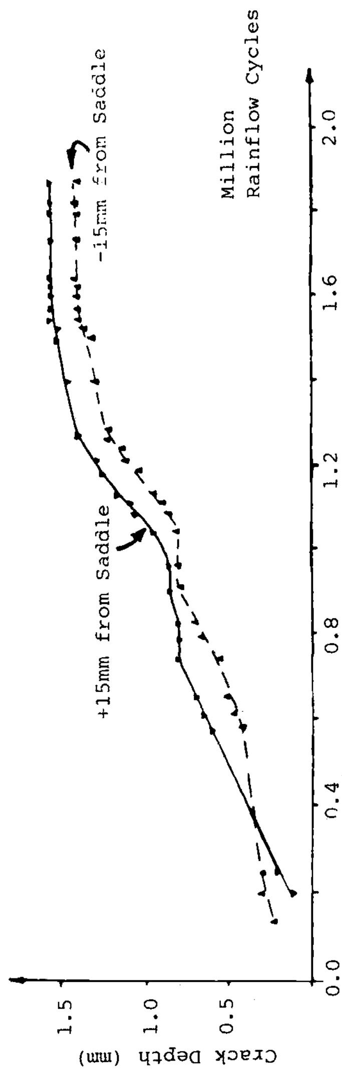

FIG. 12—*Leading crack depth growth in Test KOPB-2A.*

Therefore, once the Y function is found, the crack growth pattern is defined. Hence, it is useful first of all to compare the predicted Y values and the experimental Y values (deduced from measured crack sizes and crack growth rates backward through Eq 8 and Eq 7). Figure 9 shows good agreement in this comparison.

The second comparison is the da/dN versus ΔK behavior. Using the predicted ΔK and the measured crack growth rate (da/dN), experimental points can be plotted and compared with the mean materials line. Again, the agreement is shown to be good in Fig. 10.

Finally, in practical cases, crack growth prediction is used to calculate the remaining life of a joint when a crack is found in service. Figure 11 compares the prediction calculation and the experimental remaining lives. The center line (T) shows the percentage of life remaining, which was deduced backward from the experimental failure point. The predictions lie within 20% of the test results.

The last of the air tests, Test KOPB-1B, was carried out with the top four states (states 3 through 6) in the Hartt series. The crack growth was predicted with reasonable accuracy. However, when the same load history was applied in a corrosion test (Test KOPB-2A), the crack experienced serious retardation (Fig. 12). There the crack effectively stopped growing and an infinite life is implied. Although slow growth has been observed previously in some constant-amplitude corrosion tests [*13*], this retardation is much more serious than any slow growth observed before. The test was, therefore, terminated after more than 1.88 million cycles had been exerted (that is, at the end of 16 weeks of continuous testing) and counted as a runout.

A single stormy sea state (state 6 of the Hartt series) was then used to continue testing the same joint in Test KOPB-2B. The serious retardation seems to have disappeared and "normal" growth was regained. Later analysis showed that this "normal growth" was still relatively slower than the growth normally expected for cases under the same equivalent stress ranges in air (Fig. 13).

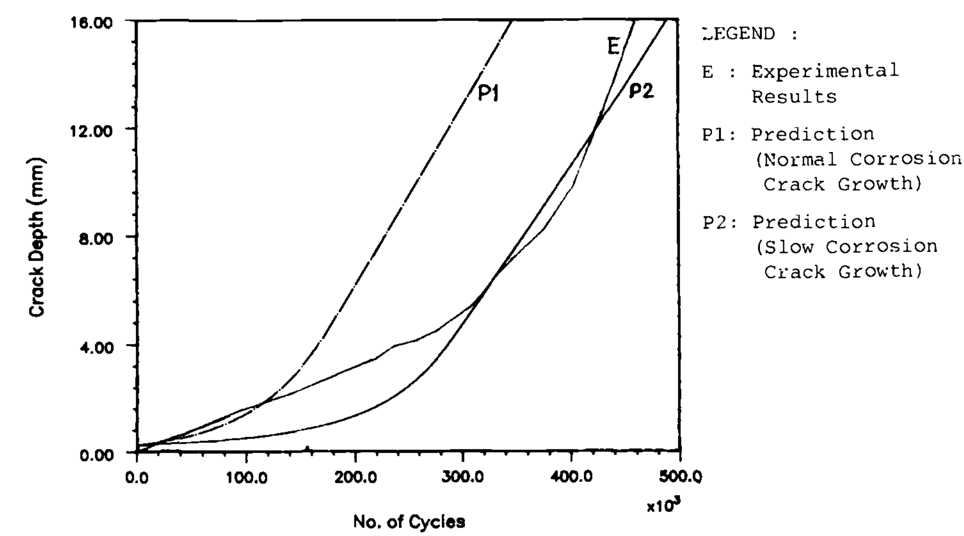

FIG. 13—*Comparison between experimental and predicted corrosion crack growth for Test KOPB-2B.*

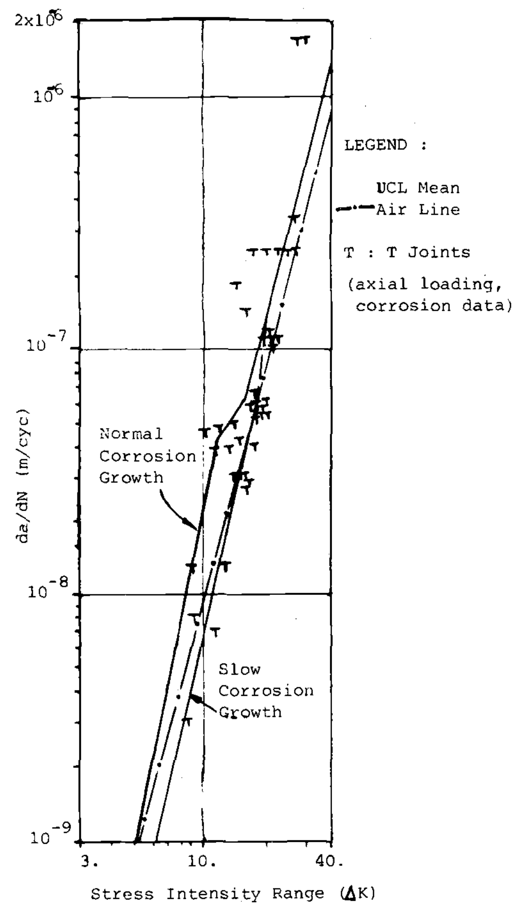

FIG. 14—*Experimental* da/dN *versus predicted* ΔK *for corrosion fatigue crack growth.*

Analysis and Discussion

Previous corrosion tests [*13*] carried out under constant-amplitude loading (0.17 Hz) yielded some useful corrosion *da/dN* versus ΔK data (Fig. 14). In the previous tests, a slow growth phenomenon was observed and it appeared to affect mainly joints tested under small load ranges (compare Figs. 15 and 16). Using TPM, this behavior can be reasonably modeled. When the same prediction methodology is applied to Test KOPB-2B, it becomes apparent that the observed growth is nearer to the slow growth prediction (Fig. 13). This could have been the result of the serious retardation in the previous test (Test 2A).

The cause and mechanism of the serious retardation is still not fully understood. One hypothesis is that the retardation was caused by crack closure due to calcareous deposits [*14*]. This phenomenon could be further influenced by the nature of the crack shape under corrosion fatigue (a tendency to shorter, deeper cracks in comparison with air data). However, further studies are required to establish the true nature of the causes.

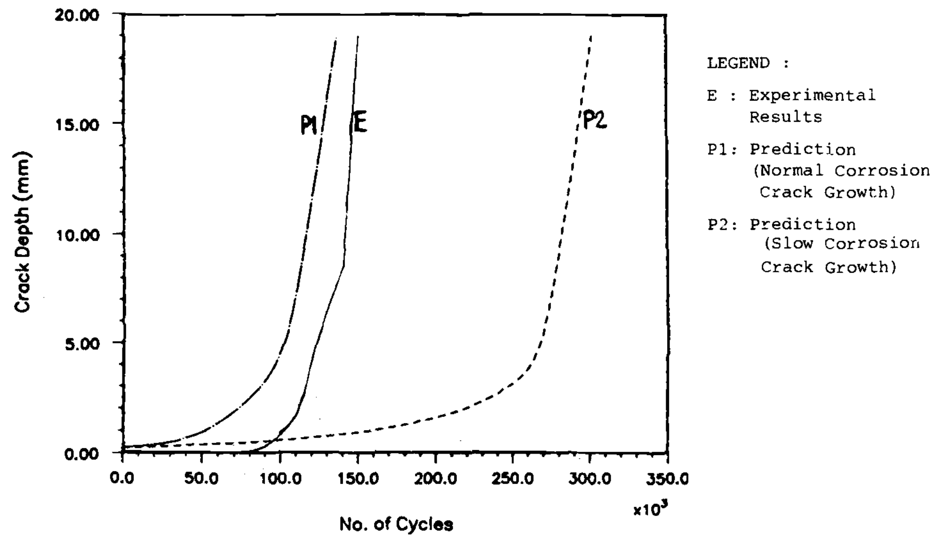

FIG. 15—*Comparison between experimental and predicted corrosion crack growth for TWJ1 (250 MPa).*

The slow growth in the single-state test (Test 2B) is quite unexpected at that level of equivalent stress range (220 MPa) in air. Another problem with random load testing in a corrosive environment is that the equivalent stress range, S_h, is not a constant value. It is because there is more than one m value in the corrosion da/dN versus ΔK curve (Fig. 14) that the S_h will change according to the crack depth (because of different Y values).

The prediction reported in this paper calculates crack growth by summing statistically the

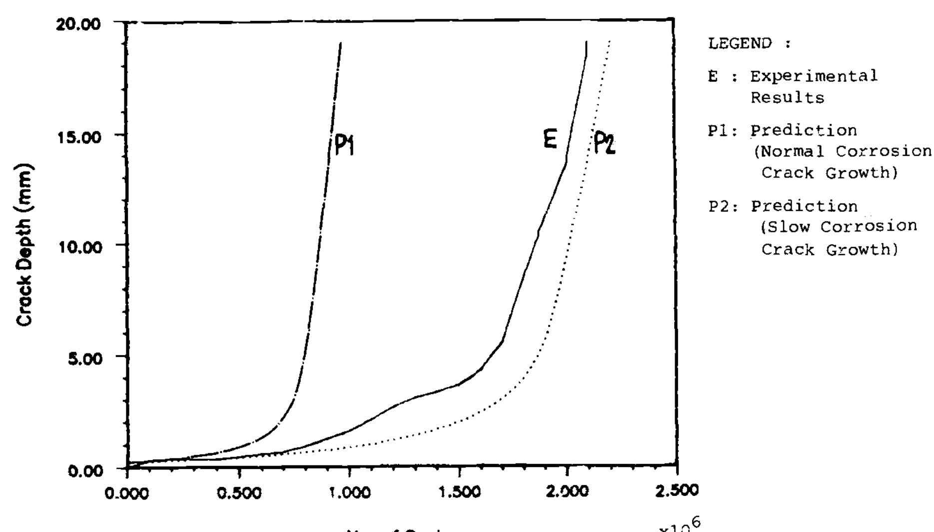

FIG. 16—*Comparison between experimental and predicted corrosion crack growth for TWJ2 (140 MPa).*

TABLE 3—*Paris constants for multiple-segment crack growth curves.*

(A) Normal Corrosion Crack Growth

$C_1 = 7.05 \times 10^{-13}$	$m_1 = 4.51$
$C_2 = 1.23 \times 10^{-9}$	$m_2 = 1.45$
$C_3 = 9.88 \times 10^{-17}$	$m_3 = 3.23$
$C_4 = 4.50 \times 10^{-12}$	$m_4 = 3.3$ (air segment)

(B) Slow Corrosion Crack Growth

$C_1 = 1.17 \times 10^{-12}$	$m_1 = 3.77$
$C_2 = 3.23 \times 10^{-17}$	$m_2 = 7.43$
$C_3 = 9.88 \times 10^{-12}$	$m_3 = 3.23$
$C_4 = 4.50 \times 10^{-12}$	$m_4 = 3.3$ (air segment)

All values for ΔK in $MPa\sqrt{m}$

and $\frac{da}{dN}$ in m/cyc

crack growth rates due to individual stress ranges, over each of the k segments of the corrosion crack growth (da/dN versus ΔK) curve. The details of this calculation can be found in Ref *14*

$$\frac{da}{dN} = \sum_{j=1}^{k} \left\{ C_j(Y\sqrt{\pi a})^{m_j} \int_{\Delta S_{j-1}}^{\Delta S_j} (\Delta S)^{m_j} p(\Delta S) d(\Delta S) \right\} \tag{9}$$

where C_j, m, are Paris crack growth constants for each growth segment and ΔS_j is the transitional load range ($\Delta S_0 = 0$; $\Delta S_k = \infty$). The C and m values for the corrosion crack growth curves used in all the predictions are given in Table 3. With this calculation procedure, the complete stress range distribution can be taken into account and all the predictions appear to be reasonably accurate.

Concluding Remarks

Tests have been carried out on tubular welded joints using complex random load histories that reproduce the main characteristics of the service loading experienced offshore.

The crack growth data under realistic random loading in a corrosive environment have highlighted some retardation effects which are not evident under narrow-band random or constant-amplitude loading. Studies are currently under way on large-scale tubular joints to explain some of these retardation effects and to produce appropriate crack growth models to predict these effects.

References

[*1*] Dover, W. D., Ed., "Cohesive Program of Research and Development into the Fatigue of Offshore Structures 1983–85, Final Report," Department of Energy, Science and Engineering Research Council, Marine Technology Directorate, Ltd. United Kingdom, 1986.

[*2*] Webster, S. E., "Review of ECSC Funded Research in Marine Technology 1981–1987," *Proceedings*, Conference on Steel in Marine Structures, Amsterdam, The Netherlands, 1987.

[*3*] Kenley, R. M., "Measurement of Fatigue Performance of Forties Bravo," Paper OTC 4402, *Proceedings*, Offshore Technology Conference, Houston, TX, 1982.

[*4*] Wirsching, P. H., "Preliminary Dynamic Assessment of Deep-Water Platforms," *Journal of the Structural Division of ASCE*, Vol. ST7, July 1976, pp. 1447–1462.

[*5*] Hartt, W. H. and Lin, N. K., "A Proposed Stress History for Fatigue Testing Applicable to Offshore Structures," University of Florida, Gainesville, FL, 1985.

[*6*] Olagnon, M., "Characterization of Sea States for Fatigue Testing Purposes," *Proceedings*, Conference on Offshore Mechanics and Artic Engineering, American Society of Mechanical Engineers, Houston, TX, 1988.

[*7*] Klatschke, H. and Sonsino, C. M., "Proposal for the Generation of a Standard Load Sequence for Medium Platforms," Fraunhofer-Institut für Betriebsfestigkeit, Report to the WASH Committee, Darmstadt, West Germany, January 1988.

[*8*] Kam, J. C. P. and Dover, W. D., "The Procedure to Generate the Wave Action Standard History (WASH): The Manual," Draft 1.1, University College London, Report to the WASH Committee, London, England, January 1988.

[*9*] Rabiner, L. R. and Gold, B., *Theory and Application of Digital Signal Processing*, Prentice-Hall, New York, 1975.

[*10*] Inspectorate Unit Inspection Ltd., Swansea, United Kingdom.

[*11*] Instron Corp., Canton, MA.

[*12*] Kam, J. C. P. and Dover, W. D., "Structural Integrity of Welded Tubular Joints in Random Load Fatigue Combined with Size Effect," *Proceedings*, Third International Conference on the Integrity of Offshore Structures, Glasgow, Scotland, 1987.

[*13*] Dover, W. D. and Wilson, T. J., "Corrosion Fatigue of Tubular Welded Joints," *Proceedings*, International Conference on Fatigue and Crack Growth in Offshore Structures, Institution of Mechanical Engineers, London, England, April 1986.

[*14*] Kam, J. C. P. and Dover, W. D., "Fatigue Crack Growth in Offshore Welded Tubular Joints Under Real Life Variable Amplitude Loading," *Proceedings*, International Conference on Fatigue Crack Growth Under Variable Amplitude Loading, French Metallurgical Society, Paris, June 1988.

Fracture

D. P. Fairchild[1]

Fracture Toughness Testing of Weld Heat-Affected Zones in Structural Steel

REFERENCE: Fairchild, D. P., "**Fracture Toughness Testing of Weld Heat-Affected Zones in Structural Steel,**" *Fatigue and Fracture Testing of Weldments, ASTM STP 1058,* H. I. McHenry and J. M. Potter, Eds., American Society for Testing and Materials, Philadelphia, 1990, pp. 117–141.

ABSTRACT: Multipass weld HAZs in structural steel exhibit a high level of heterogeneity. High-toughness and low-toughness microstructures can exist within 1 or 2 mm of each other. Low-HAZ crack-tip opening displacement (CTOD) results in some structural steels have been attributed to local brittle zones (LBZs), which exist in the coarse-grain heat-affected zone (HAZ) region (CGHAZ). Fracture initiation in an LBZ occurs by a weak-link process, which is described in this paper. If a particular weld contains LBZs, before a low CTOD result will occur, the precrack must be located close enough to the weak link that the crack-tip process zone can initiate fracture. HAZ CTOD precrack placement for welds containing LBZs is discussed, and the importance of posttest sectioning techniques is also explained. The line fraction of CGHAZ that was sampled by the crack tip was calculated for 485 HAZ CTOD tests (22 structural steels). These data are statistically analyzed to show that for welds containing LBZs, a low CTOD result becomes more probable if the crack samples more CGHAZ.

KEY WORDS: weldments, structural steels, heat-affected zone, fracture toughness, crack-tip opening displacement, local brittle zones, microstructure, weak link

When a structural steel is welded, the multiple thermal cycles that create the heat-affected zone (HAZ) are responsible for various precipitate reactions and phase changes. As a result, the metallurgical heterogeneity that exists in the HAZ is extremely large. Certain physical properties, such as fracture resistance, are sensitive to the heterogeneity of the HAZ, and this sensitivity manifests itself as data scatter. Complications in HAZ testing and data interpretation have discouraged users and researchers from addressing the subject of HAZ fracture toughness. This paper, however, will concentrate on the subject of HAZ fracture phenomena.

The micromechanisms of cleavage initiation in the HAZ will be described first to provide a basis for understanding the fracture data. Because of the metallurgical variations in the HAZ, it is also necessary to explain certain toughness testing techniques that are specific to HAZs. Statistical methods are used to quantify trends typically hidden by data scatter. These trends help develop testing philosophies for detecting low HAZ toughness.

Background

During the early 1980s, the North Sea offshore industry noted a change in the HAZ toughness results reported for some low-carbon, microalloyed platform steels. The frequency

[1] Senior research engineer, Exxon Production Research Co., Houston, TX 77001.

of low HAZ crack-tip opening displacement (CTOD) results escalated to a higher-than-normal level. Upon further investigation, it was found that these low results were caused by small areas of limited cleavage resistance within the coarse-grain HAZ; these areas are called local brittle zones (LBZs) [*1*]. Since research on LBZs began, LBZs have been found to cause low fracture-toughness results in specimens ranging from Charpy-size bars to wide plates [*2*]. Paradoxically, LBZs are not reported as a significant cause of structural failure in offshore platforms. While LBZ-related platform failures have not occurred, it should be noted that low HAZ toughness can be a cause of failure under certain circumstances [*3*]. In this light, it is disturbing to encounter linear elastic fracture results (even at a low frequency) when testing weldments in an otherwise ductile structural steel. Because the structural significance of LBZs has not yet been determined, some users have elected to evaluate HAZ toughness of candidate steels prior to purchase of the steel [*4*].

When testing a steel with LBZs by HAZ CTOD, there is some probability of sampling the critical microstructure and obtaining a low result. This sampling concept has been incorporated in two recently published industry standards, American Petroleum Institute standard API RP 2Z [*5*] and Engineering Equipment and Materials Users' Association standard EEMUA 150 [*6*]. Both standards contain, in some form, a requirement that certain HAZ CTOD specimens must sample 15% of the coarse-grain HAZ microstructure (described later). In the study covered by this paper, approximately 500 HAZ CTOD tests are analyzed with respect to coarse-grain HAZ sampling, and statistical calculations are given to show the usefulness of the 15% criterion.

Much of the technology presented in this paper was generated by studying offshore structure steels, but the basic concepts are applicable to pipeline steels, ship steels, pressure-vessel steels, bridge steels, and others. For various steel structures, however, key differences will occur in such areas as the distribution of LBZs, the manner in which LBZs are loaded, the steel thickness, the structural redundancy, the inspection frequency, the overall risk of failure, and the consequences of failure. Each industry will need to treat the significance of LBZs on its own.

Definition of a Local Brittle Zone

The formation and metallurgical structure of local brittle zones have been described previously [*1,7–10*], and it will suffice here to review them briefly. The various HAZ regions of a multipass weld in structural steel are defined in Fig. 1. The complicated metallurgy is a direct result of the overlapping thermal profiles. Although Fig. 1 shows a multipass weld, only single and double thermal-cycle areas are depicted. While this is sufficient for the purpose of this paper, it should be noted that triple-cycle microstructures are significant and have been studied in relation to LBZs [*10*]. On an actual polished and etched weld cross section, the coarse-grain, fine-grain, and intercritical areas (and their reheated derivatives) will etch. The etched HAZ does not include the unaltered subcritical HAZ (SCHAZ).

For medium-strength structural steels—with 310 to 520 MPa (45 to 75 ksi) yield strength—past experience has shown that three general HAZ areas may suffer toughness degradation: the subcritical HAZ (SCHAZ), the intercritical HAZ (ICHAZ), and the coarse-grain (CG) regions. While it may be prudent to test the ICHAZ/SCHAZ area for low toughness during material qualification [*4,5,6*], this paper will address only fracture phenomena occurring in the CG regions.

The CG regions consist of the unaltered CGHAZ, the intercritically reheated CGHAZ (IRCG), and the subcritically reheated CGHAZ (SRCG) (see Fig. 1). It has been found during in-house research and elsewhere [*11*] that LBZ-related fracture initiation occurs in the coarsest areas of the CGHAZ. Therefore, the CG regions shown in Fig. 1 are defined

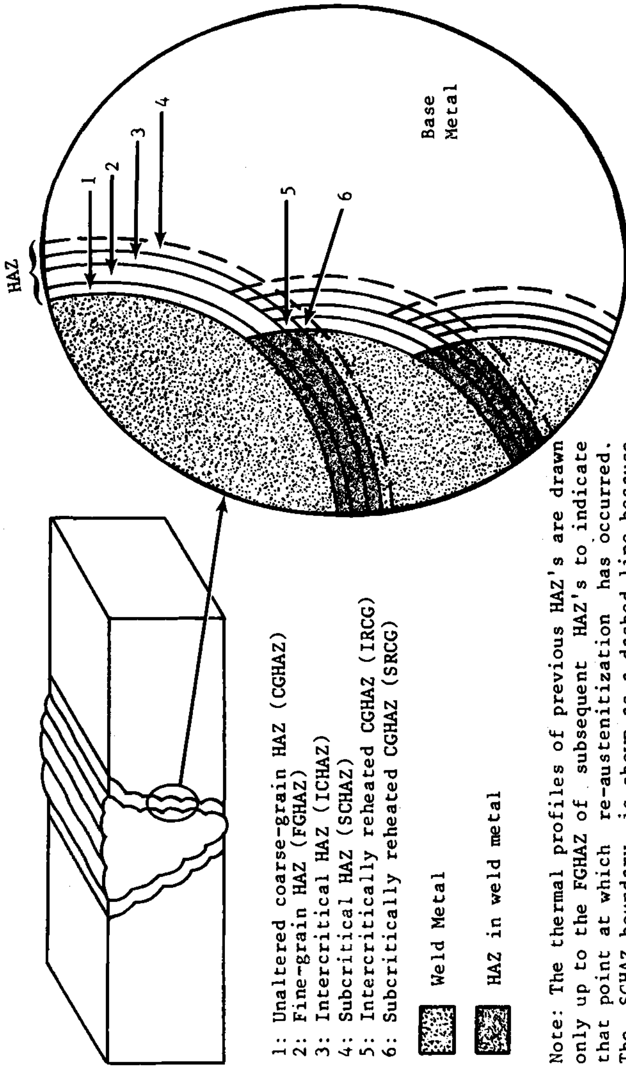

Note: The thermal profiles of previous HAZ's are drawn only up to the FGHAZ of subsequent HAZ's to indicate that point at which re-austenitization has occurred. The SCHAZ boundary is shown as a dashed line because the SCHAZ in the base metal does not etch.

FIG. 1—*Various HAZ regions in a multipass weld.*

as coarser than about 70 to 80 μm. It must be realized that the CG regions do not account for all of the traditional CGHAZ, but comprise only the coarsest portion.

Local brittle zones are low-toughness [CTOD <0.10 mm (0.004 in.)] CG regions. Not all CG regions exhibit low toughness; thus, the terms LBZ and CG regions are not synonymous.

The main metallurgical contributors to the low toughness of LBZs are the following [*1*]:

1. Matrix microstructure of upper bainite.
2. Microalloy precipitation.
3. Large prior austenite grain size.
4. Martensite islands (most notably, at prior austenite grain boundaries in the IRCG).

The size and shape of individual CG regions depend mainly on the heat input, weld-bead placement, and weld-bead shape. It is possible to eliminate LBZs from a weld completely by using techniques that create a large degree of HAZ overlap. Unfortunately, it is difficul to control HAZ overlap to the extent that LBZ elimination can be guaranteed throughou a large construction.

Fracture in the LBZ

Figures 2*a* and 2*b* are schematics showing how LBZs are sampled by the fatigue crack in both through-thickness (TT) and surface-notched (SN) CTOD specimens. In-house testing, single-sponsor work at The Welding Institute and other published research [*11*] have shown that when LBZs are present, the lower-bound CTOD magnitude is the same for TT and SN specimens. It is usually easier to sample LBZs using the TT geometry [*4*], and the offshore industry employs this method most frequently. In this section of this report, however, fracture initiation is described for the SN geometry simply to make the illustrations clearer. The initiation process is not expected to be different for the two-notch orientations when a brittle event occurs.

The author takes note of previously proposed low-toughness mechanisms [*12,13*] and offers the following explanation for weak-link fracture initiation in an LBZ. A fatigue crack intersects an LBZ, as shown schematically in Fig. 3*a*, and the crack tip is located in the IRCG. Figure 3*b* shows the crack tip and several low-toughness metallurgical features at higher magnification. When a load is applied, a process zone (region of high stress) develops at the fatigue-crack tip. At loads slightly less than that necessary to cause fracture, small microcracks develop near the martensite islands within the process zone but do not propagate (Fig. 3*c*). Some microcracks may occur because of decohesion at the ferrite-martensite boundary [*12*]. Some microcracks may develop as brittle "pops" in the ferrite between two or more martensite islands. This second mechanism (the brittle pop) deserves further explanation.

Figure 3*d* shows two martensite islands within a ferrite matrix. There is a small area of ferrite with dimensions $A \times B$ between the islands. Transmission electron microscopy has revealed that the islands are primarily plate martensite with a twinned substructure, and this morphology is indicative of a high carbon content [*7*] (~0.5 weight percent). The high-carbon martensite islands are stiff compared with the adjacent ferrite. When subjected to the triaxial stresses of the process zone, the islands shown in Fig. 3*d* resist deformation and force the surrounding matrix (including area $A \times B$) to accommodate the strain. If the ferrite area between the islands is small compared with the islands themselves, then the ferrite will be constrained and unable to accommodate deformation. Finally, the ferrite in area $A \times B$ fails by cleavage. At loads slightly less than that which causes complete fracture, the cleavage crack within area $A \times B$ does not propagate beyond this area.

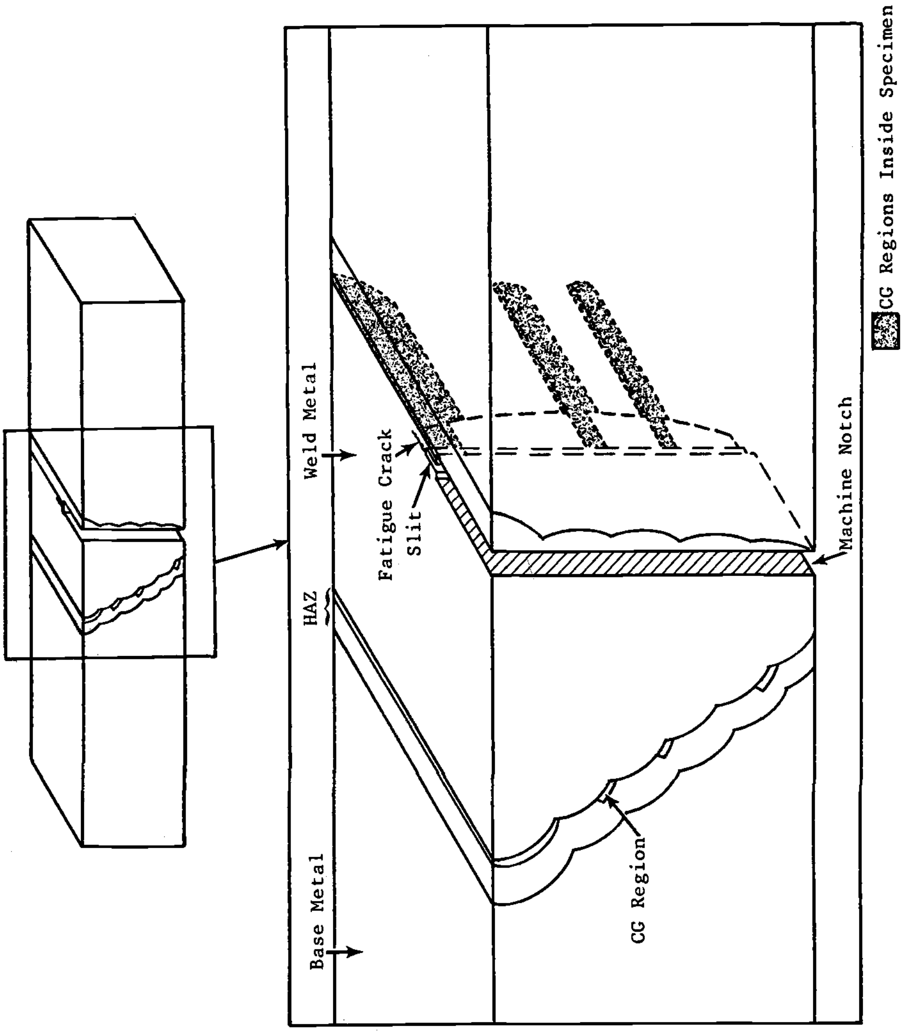

FIG. 2a—*Sampling CG regions (LBZs) in a through-thickness, notched CTOD specimen.*

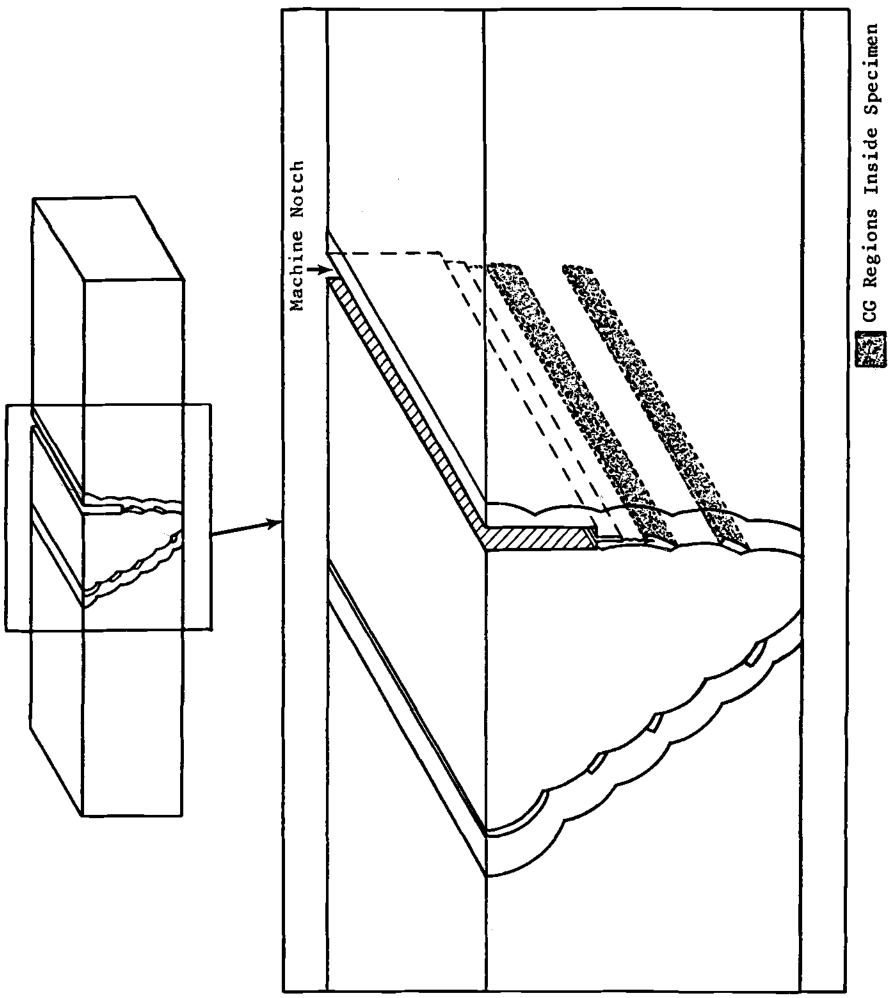

FIG. 2b—*Sampling CG regions (LBZs) in a surface-notched CTOD specimen.*

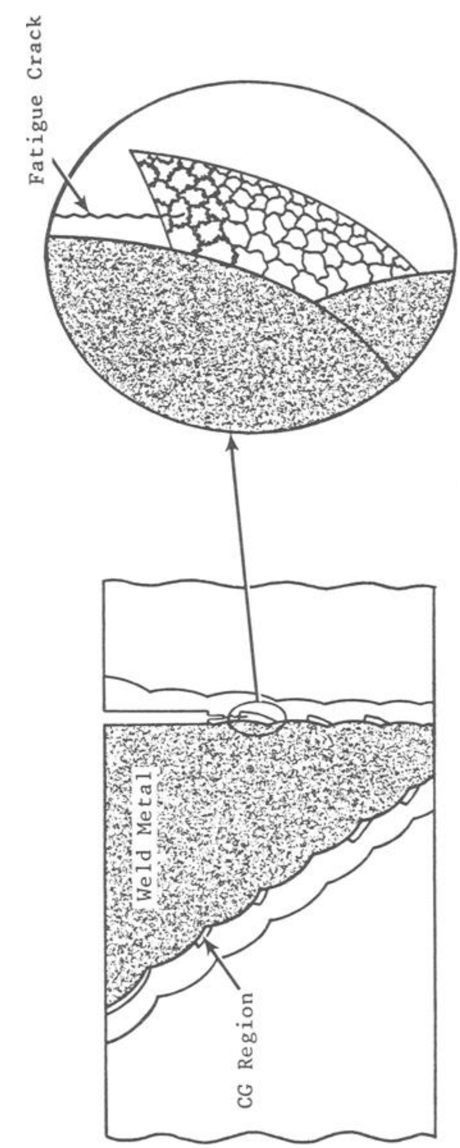

FIG. 3*a*—*Fatigue crack intersecting an LBZ.*

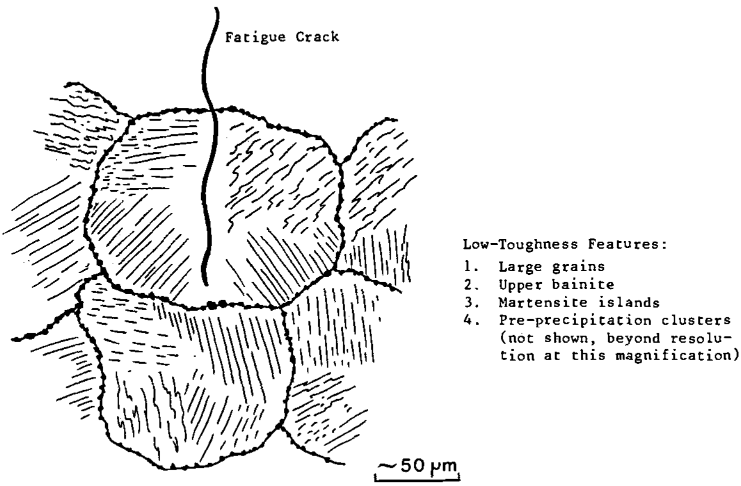

FIG. 3*b*—*Fatigue crack shown relative to several low-toughness metallurgical features.*

When the load finally reaches a certain level, a critical event occurs. One of the brittle pops between martensite islands contains sufficient dynamic energy to allow it to propagate outside area $A \times B$. This is the event that defines the critical CTOD. In one direction, this crack connects with the fatigue-crack tip; in the other direction, it propagates through the IRCG (Fig. 3*e*). The crack continues through the other CG regions, as the upper bainitic packets offer little resistance to cleavage [*14*]. When the crack reaches the end of the CG

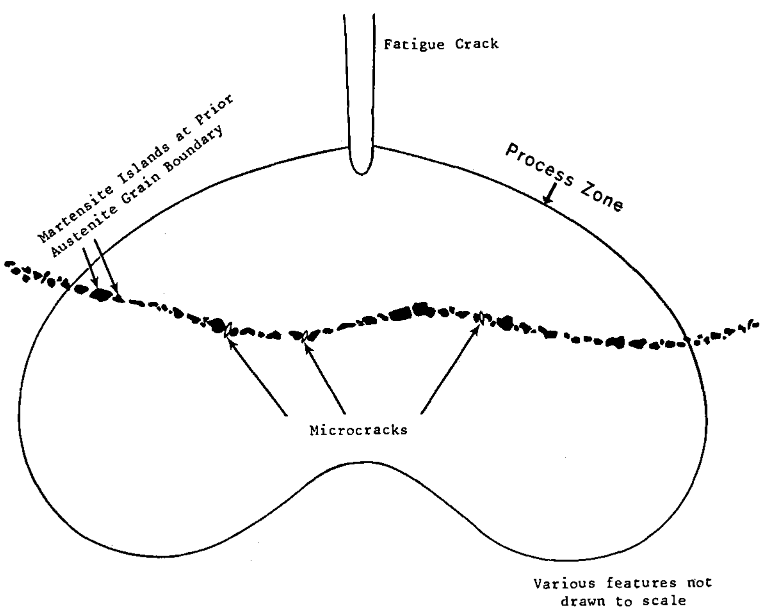

FIG. 3*c*—*Microcracks developing in the crack-tip process zone.*

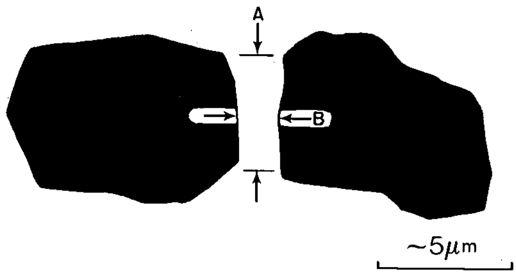

FIG. 3d—*Martensite islands in a ferrite matrix.*

regions (i.e., the LBZ has now cleaved), it will encounter a tougher, finer-grained microstructure (Fig. 3*f*). Depending upon the dynamic energy/driving force available for this running crack, it may arrest at the fine-grain material or continue to run and sever the entire specimen. If arrest occurs, a pop-in may be recorded on the load-displacement curve.

In the case described above, the martensite islands that were responsible for the critical cleavage crack acted as the weak link within the overall metallurgical system. Under a different set of welding conditions or heat-treatment conditions or in a different steel, the weak link could be other than martensite islands. For example, in the post-weld heat-treated (PWHT) condition, martensite islands will be decomposed and will not act as the weak link. LBZs have been found to exist in the PWHT condition, so it can be reasoned that some other metallurgical subfeature, such as precipitate clusters, caused initiation.

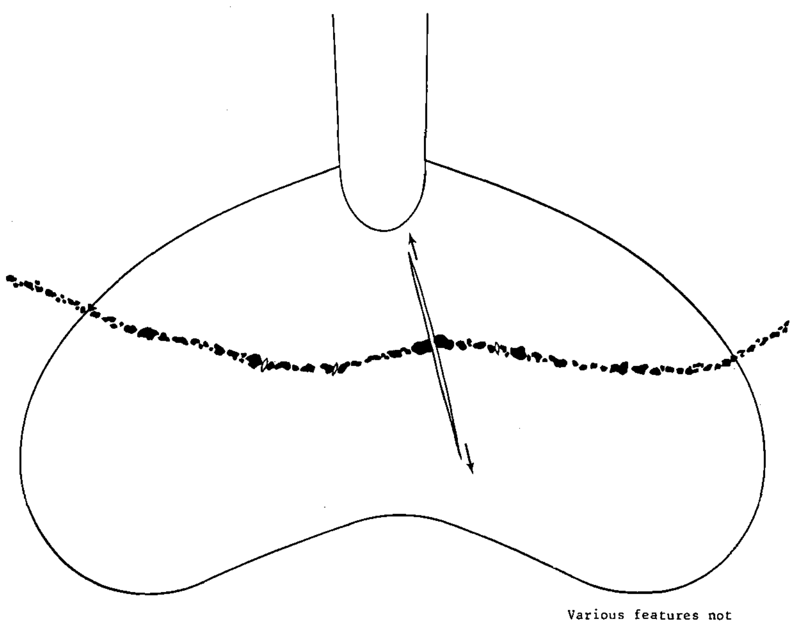

FIG. 3e—*The critical cleavage initiation event.*

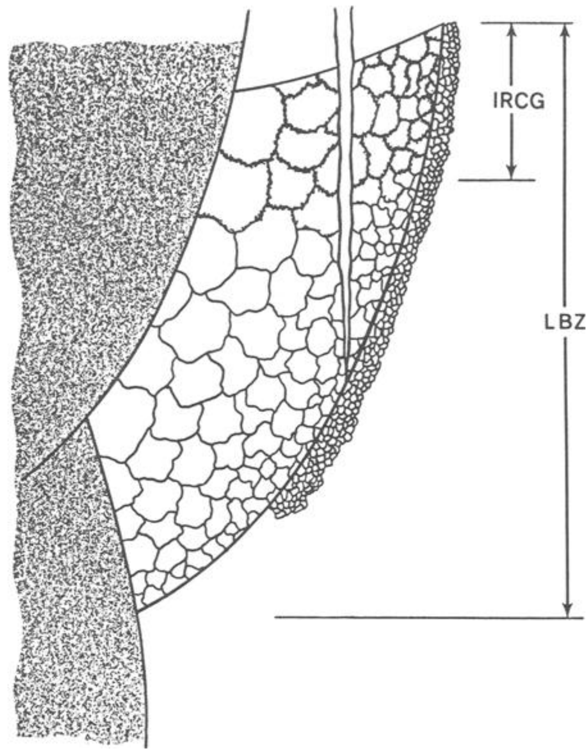

FIG. 3*f*—*Propagating cleavage crack at the moment it exits the CG region.*

The important realization is that initiation occurs from some critical subfeature within the LBZ (i.e., within the CG regions). Before a low-toughness event will occur, the crack tip must be located close enough to the weak link that the process zone can instigate the critical event. Not only is the distance between the fatigue-crack tip and the weak link important, but the orientation of the weak link also plays a role. The weak link should be favorably oriented with respect to the fatigue-crack tip, the process-zone stresses, and the cleavage plane of the adjacent microstructure.

When conducting a HAZ CTOD test on a weldment with LBZs, merely sampling a CG region does not guarantee a low toughness result. While the CG regions have a low-toughness-matrix microstructure, they do not have zero toughness. The CG regions can support some level of stress without fracturing. Herein lies the cause of data scatter when testing the fracture toughness of the HAZ, even when it is believed that the correct microstructure has been sampled. Sometimes, when the crack tip samples the LBZ, the critical metallurgical features will be so positioned that they cause a low-toughness result; however, sometimes the positioning will not be critical, and the toughness will be higher.

Because of the nature of weak-link fracture initiation, HAZ fracture will obey complex statistical laws. HAZ fracture data must be viewed with this in mind, or they will be incorrectly interpreted. At this point in time, the statistical interpretation of HAZ fracture data (particularly when LBZs are present) is in its infancy.

Fatigue-Crack Sampling

When testing a steel for LBZ behavior (i.e., low HAZ toughness), it is the intent of the test program to detect low toughness if it exists. During such a program, it is imperative that the broken fracture specimens be sectioned and metallurgically examined to verify that the CG regions have been sampled by the fatigue crack. If this verification is avoided and CG-region sampling is not checked, then a steel with LBZs can escape detection by one or a combination of the following two scenarios:

- A high-HAZ-overlap welding procedure is used for the test welds, and the CG regions (LBZs) are eliminated. High toughness values result because the fatigue cracks sample high-toughness material.
- The welding procedure is such that LBZs are present, but the fatigue cracks wander away from the fusion-line area and sample a high-toughness material (weld metal, fine-grain HAZ (FGHAZ), or other material). The results show high toughness values.

The volume of weldments in a large construction is tremendous, and HAZ overlap (weld-bead placement) is difficult to control. Therefore, when a steel that escapes LBZ detection is used for construction, it is likely that the structure will contain LBZs. For this particular structure, the risk of LBZ-related brittle fracture (i.e., fracture due to low HAZ toughness) is not accurately represented by the test program.

In the absence of fatigue-crack sampling (FCS) information, HAZ toughness data may be misleading. Prior to realization of the LBZ phenomenon (about 1982), detailed FCS documentation was not generated for HAZ toughness studies. Because FCS information was not available before about 1982, HAZ toughness studies of structural steels prior to that time are difficult, if not impossible, to interpret. Considering what is now understood about multipass weld HAZ geometry, metallurgy, and fracture initiation, it is no longer sufficient to state simply that "the crack was aimed at the coarse-grain HAZ."

Three methods of documenting FCS information for TT-notched CTOD specimens have recently been published [*1,15,16*]. The method used in generating data for the subsequent parts of this paper (described in Refs *1* and *4* through *6*) is specific to CG-region sampling. With this technique, cross sections are taken to reveal FCS information close to the tip of the fatigue crack (Fig. 4). From enlarged photographs (enlarged 3 to 6 times), the line fraction of CG regions sampled by the fatigue crack is calculated. This line fraction is termed the "%CG regions" that were sampled. Since it is known that the CG regions potentially contain the weak-link subfeature, this FCS sectioning technique relates to the probability of sampling the weak link and, thus, to the chances of brittle fracture when the steel is susceptible to LBZs.

Figure 5 shows an FCS photograph of an actual HAZ CTOD test. The original montage photograph provided a ×5-magnification picture of the specimen. In work with enlarged photographs (as opposed to observation under a microscope), the quality of the polish, etch, and photograph is very important. If the various HAZ regions cannot be distinguished, then the %CG regions calculation will be inaccurate.

The purpose of the FCS sectioning technique shown in Fig. 5 is to determine how much of the potential low-toughness microstructure (which contains the weak link) was sampled by the front portion of the fatigue crack. Alternatively, it is possible to use this technique to investigate the microstructures sampled when initiation occurs. In this case, the saw cut into the fracture face should be positioned at the initiation site [*1,15,16*] (instead of exposing the front portion of the fatigue crack). Revealing FCS information relative to an initiation

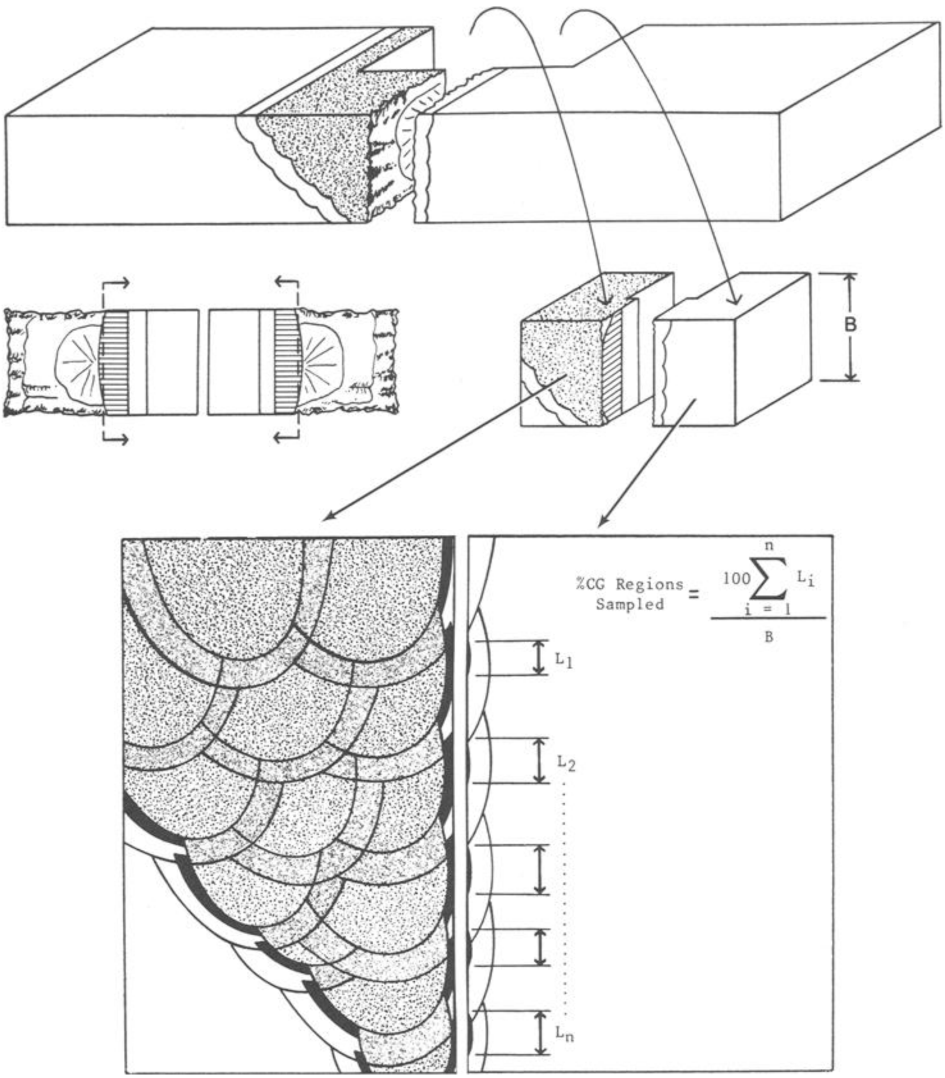

FIG. 4—*Sectioning a broken CTOD specimen and calculating the %CG regions sampled.*

site is important in researching the causes of fracture in a specific material. If, however, a toughness testing program is conducted to accept or reject a steel or to compare the performance of two or more steels, then it is not necessary to focus on initiation sites. In these situations, it is sufficient to monitor FCS at the fatigue-crack front.

Experimental Program

As explained in the previous sections, when LBZ fracture initiation occurs, the weak-link subfeature is contained within the CG regions. Therefore, when conducting HAZ CTOD tests, the probability that a low toughness result will occur should increase as the fatigue

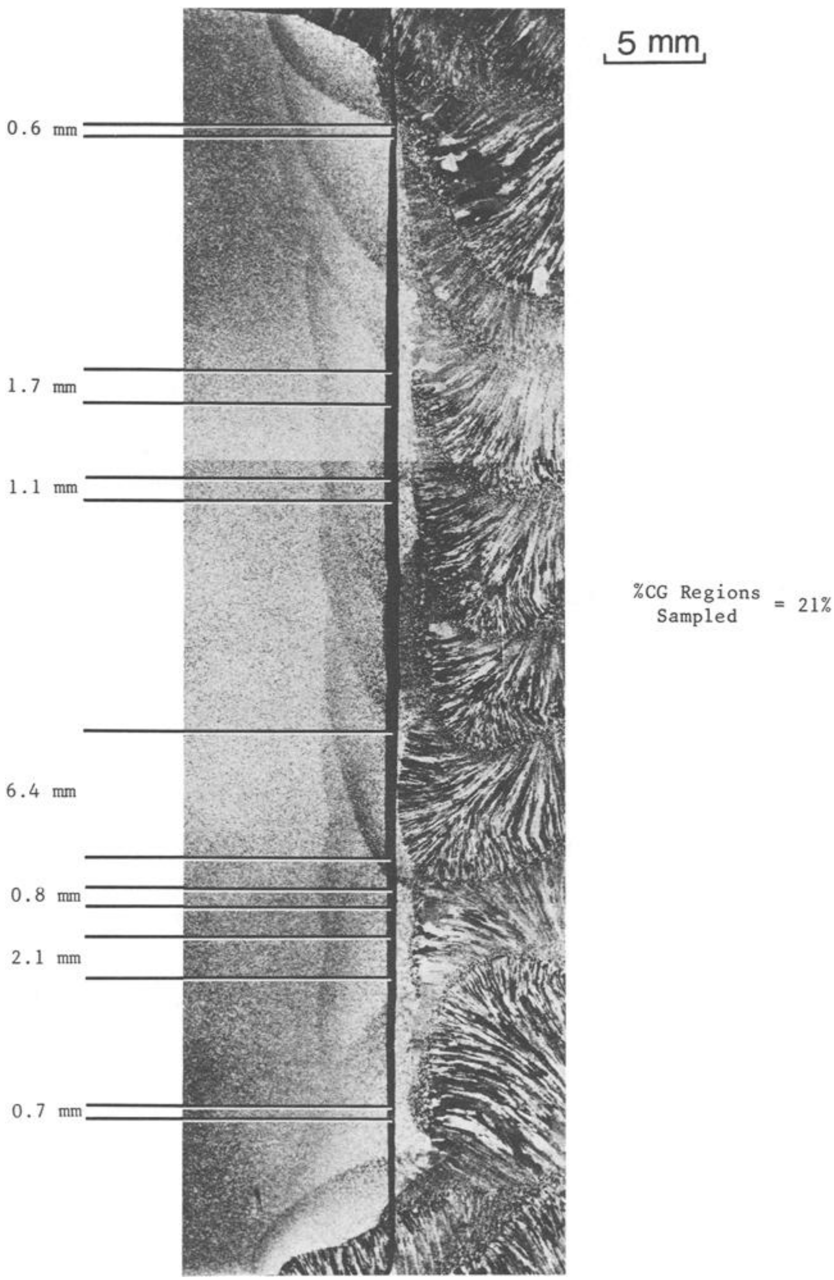

FIG. 5—*Fatigue crack sampling in an actual HAZ CTOD specimen.*

precrack samples more (or larger) CG regions. The following experimental data were analyzed to test this hypothesis.

Fatigue-Crack Sampling Data

Fatigue-crack sampling data (i.e., the %CG regions) were generated using the method shown in Fig. 4 for 485 HAZ CTOD tests. The steels included 13 normalized and 9 thermomechanically controlled process (TMCP) offshore platform materials. The thicknesses ranged from 50 to 88 mm (2.0 to 3.5 in.). It was not the purpose of this investigation to study the effects of steel composition; however, a general guide to the chemistries is given in Tables 1*a* through 1*c*. Table 1*d* also gives strength ranges. The CTOD specimens included both $B \times B$ and $B \times 2B$ geometries, and the crack depth was $a/w \sim 0.5$. All CTOD tests were conducted at −10°C (14°F). The specimens were tested in both the as-welded and post-weld heat-treated condition.

All welding was conducted using the submerged-arc (SAW) technique, and both the K-bevel and half-K-bevel (single-bevel) preparations were employed. Two heat inputs were used, approximately 3 and 5 kJ/mm. Lower heat inputs (<2 kJ/mm) were not studied because LBZ problems have not been apparent in this range. With respect to bevel design, bead

TABLE 1*a*—*Steel composition, average for all steels, in weight percent.*

C	Mn	P	S	Si	Al	Mo	N
0.11	1.45	0.009	0.004	0.32	0.032	no addition	0.0050

TABLE 1*b*—*Alloying schemes tested.*

Normalized	TMCP
C-Mn-Nb C-MN-Nb-V C-Mn-Nb-Ti C-Mn-Ni-Cu-Nb C-Mn-Ni-Cu-V C-Mn-Ni-Nb-V C-Mn-Ni-Cu-Cr-V C-Mn-Ni-Cu-Nb-V-Ti	C-Mn-Nb-Ti C-Mn-Ni-Cu-Nb-Ti

TABLE 1*c*—*Average alloying additions, when added, in weight percent.*

Ni	Cu	Cr	Nb	V	Ti
0.32	0.22	0.38	0.02	0.05	0.009

TABLE 1*d*—*Steel strength ranges.*

Yield Strength		Tensile Strength	
MPa	ksi	MPa	ksi
303 to 434	44 to 63	497 to 559	72 to 81

placement, and HAZ overlap, the welding procedures used in this study were not necessarily intended to represent fabrication welding practice. The welding procedures and subsequent HAZ CTOD tests were conducted to assess LBZ resistance (i.e., material performance). A genuine attempt was made to produce sufficient CG regions and to sample them with a fatigue precrack.

Figure 6*a* shows a graph of CTOD versus %CG regions for all 485 tests. While considerable scatter is apparent, at least one observation can be made if the window through which the data are viewed is reduced. Figure 6*b* shows the reduced window. An upper CTOD limit is drawn at 3 mm (0.12 in.) because no data lie above this value. An upper limit for %CG regions is drawn at approximately 34% because few test results occur above this value (three tests). Within the reduced window, it is apparent that an area in the lower left-hand corner of the graph is relatively void of data (see Fig. 6*b*). This area corresponds to the simultaneous occurrence of low CTOD and low %CG regions. The fact that data points do not exist here indicates that, if the fatigue crack samples a small amount of the CG regions, then a low CTOD is unlikely. This is, of course, related to the hypothesis stated above (it was stated above that, if the crack samples much CG, a low CTOD is more likely).

Concerning Fig. 6*b*, there are several areas void of data at approximately 30% CG regions. However, these areas have few data points because only a few CTOD specimens gave FCSs of about 30%. In fact, only 13 results out of 485 exist above 25%. With more test results in the vicinity of 30%, it is anticipated that data points would fill these areas. On the other hand, the area in the lower, left-hand corner of the graph in Fig. 6*b* is not caused by a lack of data. Well over 100 test results exist below 10% CG regions. It is believed, therefore, that this area represents a real phenomenon.

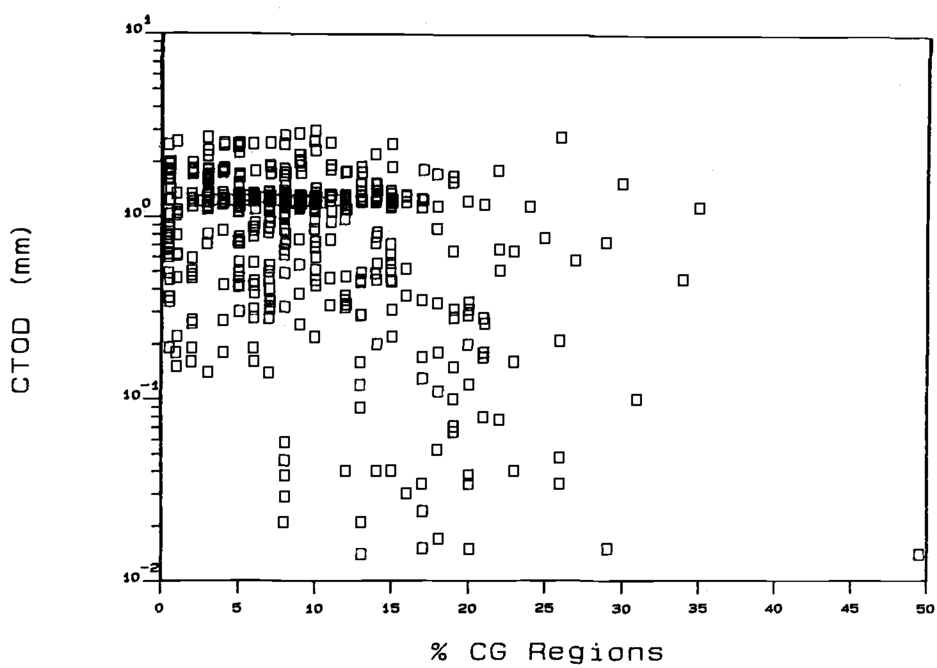

FIG. 6*a*—*CTOD versus %CG regions for all steels (485 tests).*

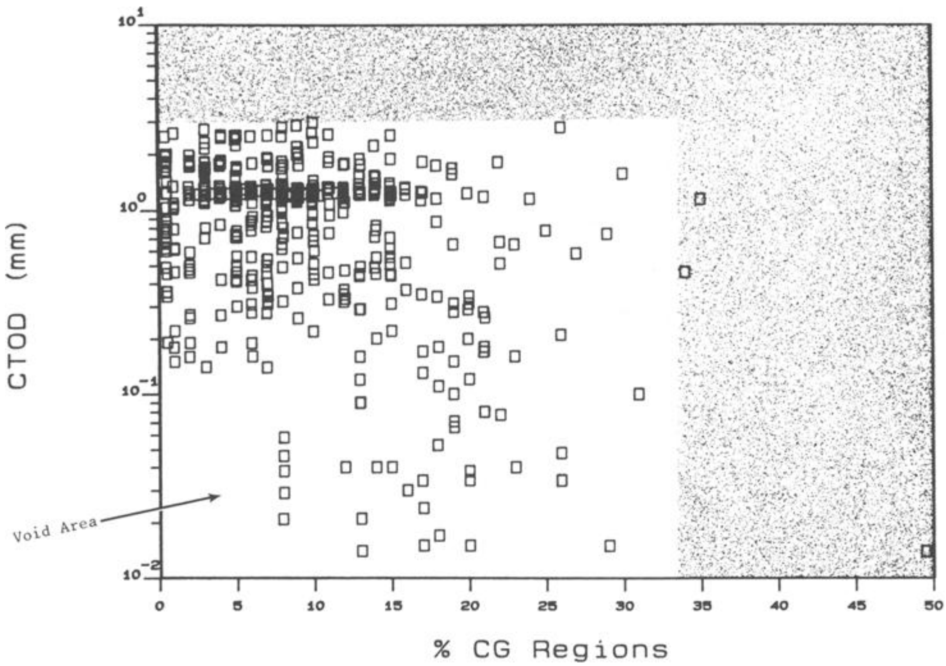

FIG. 6b—*CTOD versus %CG regions for all steels, showing the reduced window.*

Upon detailed review of the CTOD data, it became apparent that some materials were more resistant than others to LBZ formation; i.e., the microstructure in the CG regions of some steels was tougher than that in others. Figure 7 shows data for steels that gave no CTOD values below 0.10 mm (0.004 in.). Both normalized and TMCP steels are represented in Fig. 7.

The FCS data for steels that displayed some tendency toward LBZ formation are shown in Fig. 8 (Figs. 7 and 8 superimpose to give Fig. 6). In Fig. 8, a downward trend of CTOD is observed as the %CG regions increases. This trend supports the hypothesis stated earlier.

Statistical Analysis of FCS Data

Statistical calculations are presented here to help quantify the trend shown in Fig. 8. The aim is to calculate the probability that a low CTOD (<0.10 mm) will occur with respect to various ranges of %CG regions.

The following definitions are necessary:

i = lower bound of the %CG region range,
n = upper bound of the %CG region range,
L_i = number of low CTODs for %CG regions = i,
T_i = total number of CTODs that give %CG regions = i,
P = probability of incurring a low CTOD when all tests in the range $i \leq$ %CG $\leq n$ are considered.

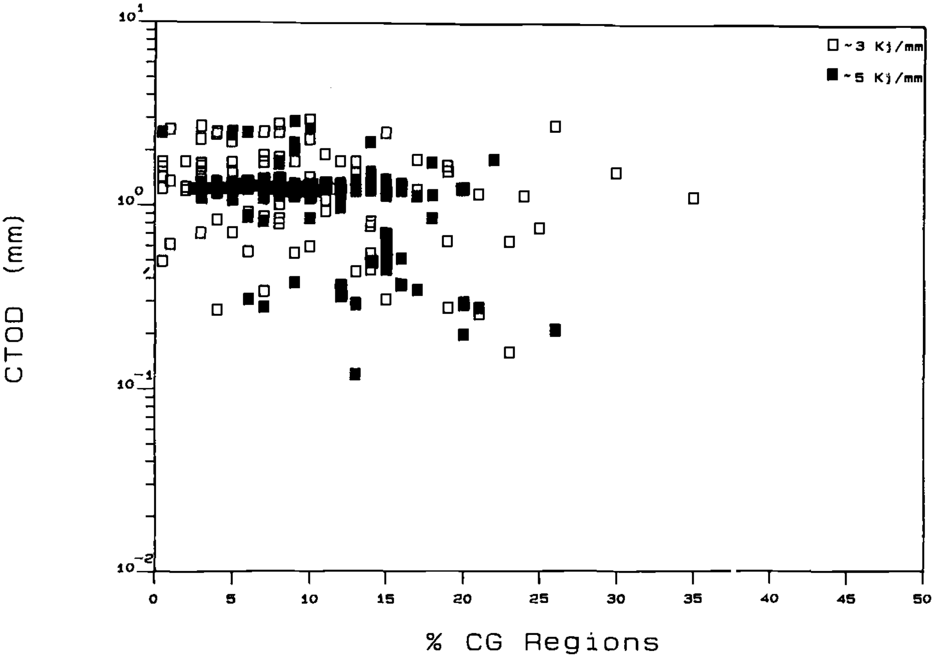

FIG. 7—*CTOD versus %CG regions for steels showing some resistance to LBZs (no values < 0.10 mm).*

$$P = \frac{\text{number of low CTODs within the range}}{\text{total number of CTODs within the range}} = \frac{\sum_{j=i}^{n} L_j}{\sum_{j=i}^{n} T_j} \tag{1}$$

For the first calculation of P, n will be held constant at 50%, and i will be varied. Each value of P will, therefore, represent all data above %CG regions = i. Values of i, L_i, T_i, and P for the data in Fig. 8 are given in Table 2. The probability (P) that a low CTOD will occur is shown versus the %CG regions (i) in Fig. 9. A Bezier polynomial curve fit is used. On the upper x-axis, the total number of CTOD tests used to calculate P is periodically shown directly above the %CG region to which it corresponds. In other words, the numbers on the upper x-axis are values of the denominator for calculations of P (e.g., at 0% CG regions, all 196 test results shown in Fig. 8 are used to calculate P). Values of P are calculated only up to i = 31 because too few data (<3 tests) exist above 31% CG regions.

In Fig. 9, from 0% CG regions to 26% CG regions, the probability that a low CTOD will occur increases as the lower bound of the range of %CG regions (i) increases. This supports the hypothesis stated earlier. Above 27% CG regions, there appears to be a downward trend; however, it is believed that this trend is an artifact caused by too few test results. As shown on the upper x-axis of Fig. 9, the number of CTOD test results above

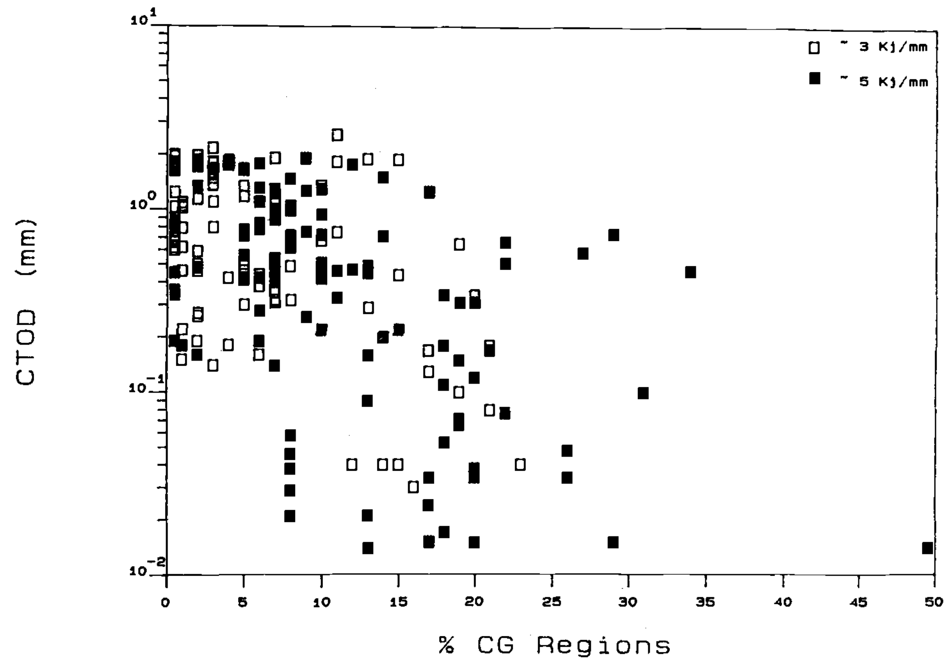

FIG. 8—*CTOD versus %CG regions for steels showing some LBZ behavior.*

about 27% CG regions is small. Because the trend above 27% is believed to be inaccurate, the curve is not drawn in this area. It is anticipated that if more test results were generated at higher %CG regions, the curve in Fig. 9 would show a general upward trend as the %CG regions increased above 27%.

It is important to interpret Fig. 9 correctly. For the data point at 0% CG regions, the *y*-axis reads 16% probability. This does not mean that when the fatigue crack samples 0% CG regions, the probability of a low value is 16%. Figure 8 clearly shows that no low values occurred at 0% CG regions. *P* is calculated using a *range* of data. Correctly interpreted, the data point in Fig. 9 at 0% CG regions means that when *all* the CTOD results are considered ($0 \leq \%CG \leq 50$), the probability that a low value will occur is 16%. Similarly, when only the data above, for example, 15% CG regions, are considered ($15 \leq \%CG \leq 50$), the probability that a low value will occur is 48%.

A second calculation of *P* was generated to examine the probability that a low CTOD would occur within smaller, individual ranges of %CG regions. The definitions of i, n, L_i, T_i, and *P* remain as stated above, but in this case, n will vary. The probability that a low CTOD will occur is calculated for each of eight ranges of i to n: 0 to 4, 5 to 8, 9 to 12, . . . 25 to 28, 29 to 32. These data are given in Table 3 and plotted in Fig. 10. Again, higher ranges are not used to calculate *P* because too few data points exist.

Figure 10 shows (as does Fig. 9) an increasing probability that a low CTOD will occur as higher ranges of %CG regions are considered. Figure 10 also shows that when small amounts of %CG are sampled by the fatigue crack, the probability that a CTOD of <0.10 mm will occur is low. In fact, when <5% CG regions are sampled, the probability is zero. Figures 9 and 10 both help quantify and support the hypothesis being tested. Therefore, these statistical data are also consistent with the weak-link mechanism explained earlier.

TABLE 2—*Statistical data for steels with LBZs* (n = *50*).

%CG Regions, i	Total Number of Tests, T_i	CTODs <0.10 mm, L_i	$\sum_{j=i}^{50} T_j$	$\sum_{j=i}^{50} L_j$	P[a]
0[b]	22	0	196	32	16
1	9	0	174	32	18
2	14	0	165	32	19
3	13	0	151	32	21
4	7	0	138	32	23
5	14	0	131	32	24
6	11	0	117	32	27
7	15	0	106	32	30
8	13	5	91	32	35
9	4	0	78	27	35
10	9	0	74	27	35
11	5	0	65	27	42
12	3	1	60	27	45
13	9	4	57	26	46
14	4	1	48	22	46
15	4	1	44	21	48
16	2	2	40	20	50
17	6	3	38	18	47
18	5	2	32	15	47
19	5	2	27	13	48
20	6	3	22	11	50
21	4	2	16	8	50
22	3	1	12	6	50
23	1	1	9	5	56
24	0	0	8	4	50
25	0	0	8	4	50
26	2	2	8	4	50
27	1	0	6	2	33
28	0	0	5	2	40
29	2	1	5	2	40
30	0	0	3	1	33
31	1	0	3	1	33
32	1	0	2	1	...
33 to 48	0	0	1	1	...
49	1	1	1	1	...
50	0	0	0	0	...

[a] See Eq 1.
[b] Tests with %CG regions = 0 are shown on Figs. 6 through 8 as %CG regions = 0.5. This is to improve visual clarity of the y-axis tick marks.

Discussion

Because LBZs have been shown to cause low results in a fracture mechanics test, it seems reasonable that they will increase the risk of fracture in a real structure. To determine exactly how much risk is caused by LBZs, a probabilistic analysis must be conducted. Such an analysis has not yet been developed; thus, the risk of LBZ-related fracture cannot be quantified at this time. This leaves the engineering community in somewhat of a dilemma; i.e., what should be done concerning LBZs if their significance is not well understood?

Many factors that control the integrity of a large structure are difficult to quantify; thus, the structural significance of LBZs cannot be based solely on service performance. The

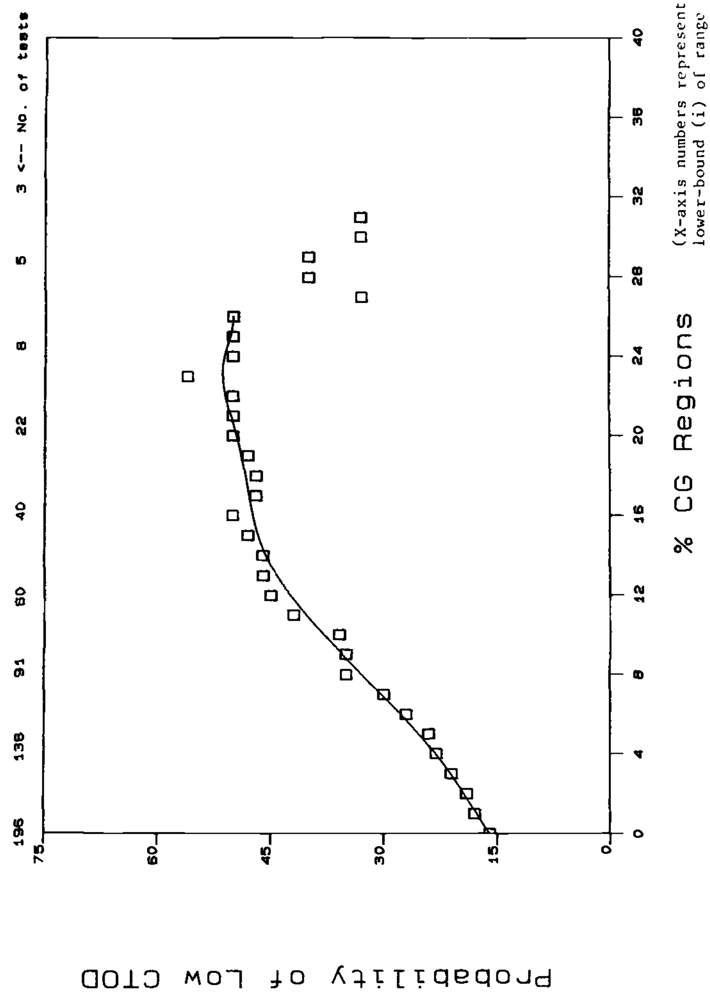

FIG. 9—*Probability of a low CTOD versus different ranges of %CG regions derived for the data shown in Fig. 8. In this case, the upper bound of the %CG regions range is fixed at 50%.*

TABLE 3—*Statistical data for steels with LBZs* (n = *varied*).

%CG Regions, i to n	$\sum_{j=i}^{n} T_j$	$\sum_{j=i}^{n} L_j$	P[a]
0 to 4	65	0	0
5 to 8	53	5	9
9 to 12	21	1	5
13 to 16	23	8	35
17 to 20	22	10	45
21 to 24	8	4	50
25 to 28	3	2	67
29 to 32	3	2	67

[a] See Eq 1.

absence of LBZ-related failures may be due to unquantified "protectors" such as overdesign or non-occurrence of the design load. If LBZs are ignored as a result of good service records, then future changes that eliminate protective factors (colder service temperatures, design changes, new welding practices) may cause LBZs to emerge as critical. In light of LBZ-related low toughness results, it seems prudent to pursue the LBZ issue until its structural significance is resolved.

LBZs can be controlled by implementing one or both of the following two strategies:

- Favor the use of steels that are resistant to LBZs, i.e., steels in which the CG regions have acceptable toughness.
- Use welding techniques that eliminate or at least reduce the amount of LBZs, ie., high HAZ overlap welding procedures or restricted heat inputs, or both.

The pros and cons of each approach will not be discussed, but it should be recognized that both strategies (and, in fact, any strategy regarding LBZ control) will require the use of a fracture-toughness testing philosophy capable of detecting LBZs if they are present. Obviously, if a particular testing program cannot distinguish between a weld with LBZs and one without LBZs, then neither of the two strategies listed above can be pursued with any degree of confidence.

HAZ CTOD tests on thick (>50-mm) structural steel are relatively expensive. As a result, when testing a particular steel (or welding technique) for the presence of LBZs, the investigation will be limited in size and scope. The question becomes how to ensure the detection of LBZs if only a few tests are conducted. The statistical data presented earlier indicate that if certain restrictions are placed on fatigue-crack sampling, then a limited program can be successful.

When a HAZ toughness testing program is conducted to detect LBZs, at least one low result must be generated to understand that LBZs are present. Therefore, it can be said that a successful program must generate at least one low result. To increase the probability of success, it is desirable to increase the probability of generating low results. Figure 9 shows that when LBZs are present, the probability of a low result increases as higher ranges of %CG regions are considered. When conducting a HAZ toughness test program, the probability of success is increased when only those specimens meeting a minimum %CG region sampling requirement are considered.

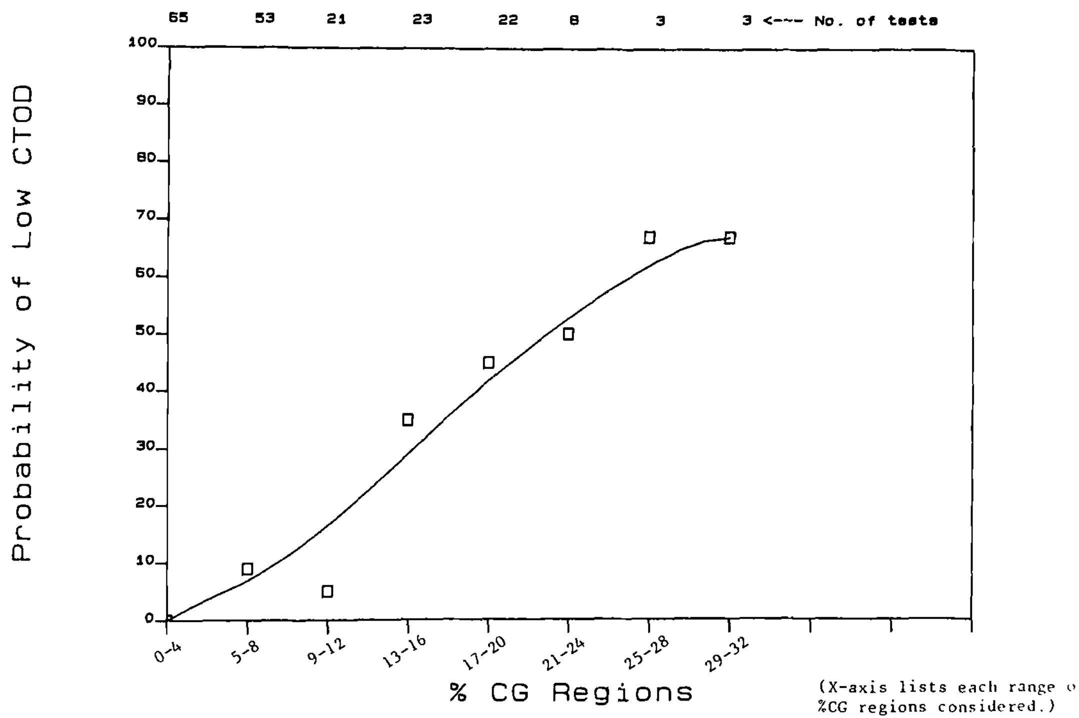

FIG. 10—*Probability of a low CTOD versus different ranges of %CG regions derived from the data shown in Fig. 8. In this case, the upper bound of the range varies.*

The usefulness of fatigue-crack sampling criteria can be further quantified as follows:

success = generating at least one low result when LBZs are present,
i = %CG region sampling criteria (i.e., the lower bound of the %CG range),
N = number of tests conducted giving %CG regions $\geq i$,
P = probability that one test result is low (from Eq 1), and
$(1 - P)$ = probability that one test result is not low (i.e., this single result is misleading).

If N tests are conducted that give %CG regions $\geq i$, the probability that none of these results is low (i.e., all the tests are misleading) can be written

$$(1 - P_1)(1 - P_2)(1 - P_3) \ldots (1 - P_N)$$

$$\prod_{j=1}^{N} (1 - P_N) \tag{2}$$

where each P_N is the probability (that one test result is low) associated with the %CG regions given by the specimen N. Because all N tests gave %CG regions $\geq i$ and because of the positive slope in Fig. 9, it can be said that

$$P_i \leq P_1 \leq P_2 \leq P_3 \ldots \leq P_N$$

Therefore, a lower-bound number can be calculated for Eq 2 by assuming $P_N = P_i$.

$$\prod_{j=1}^{N} (1 - P_N) = (1 - P_i)^N \tag{3}$$

Equation 3 gives the probability that no low results occur (i.e., LBZs are not detected) when considering only those specimens that give %CG regions $\geq i$. The "probability of success" is defined as that situation in which Eq 3 is not the case.

$$\text{Probability of success} = 1 - (1 - P_i)^N \tag{4}$$

Consider a test program in which three specimens ($N = 3$) must meet a fatigue-crack sampling criterion of %CG regions $\geq i$. Using Eq 4, the probability of success for this program can be calculated for various values of i. Figure 11 shows a graph of the probability of success versus the %CG-region sampling criterion for the case $N = 3$. It is shown that when a limited program is conducted, there is an advantage in imposing a fatigue-crack sampling criterion. This advantage is optimized at approximately 15% CG regions.

Just as for Fig. 9, it is important not to misinterpret Fig. 11. If an FCS criterion of %CG regions ≥ 0 is used, Fig. 11 indicates a 40% chance of success. However, this assumes that all the test specimens are welded in a manner consistent with the entire population of data in Fig. 8. It was stated previously that the data in Fig. 8 were produced using welds that intentionally had some CG regions available for sampling. Typically, these welds had 10 to 30% CG regions available. Because it is almost impossible to sample all the CG regions available, if a weld containing %CG regions ≤ 10 is tested, then 0 to 8% CG regions will probably be sampled. Figure 10 shows that for this case, the probability of detecting LBZs

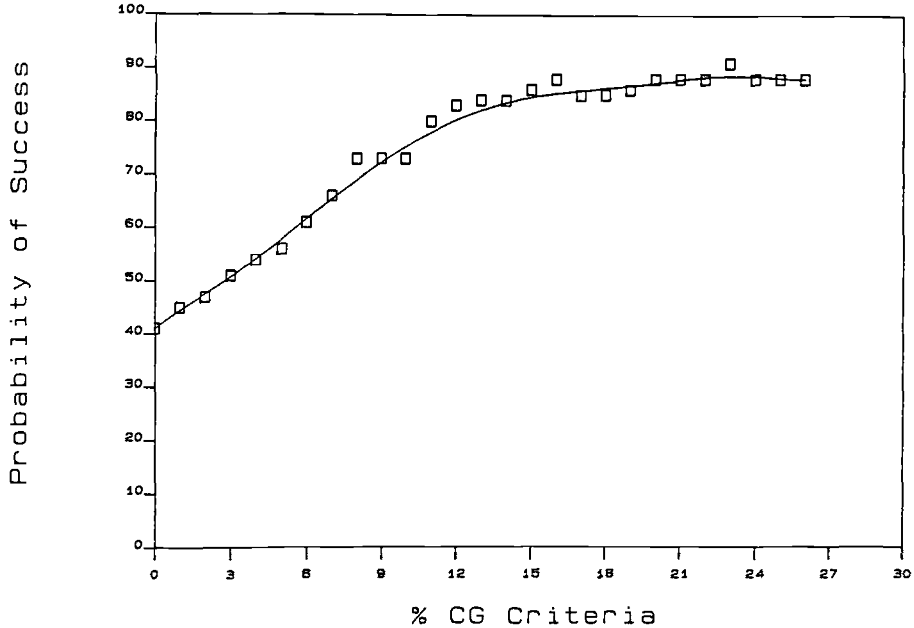

FIG. 11—*Probability of at least one low CTOD occurring when three tests are conducted on a weld with LBZs.*

is quite low. The information in Fig. 11 cannot be used for welds that contain a small volume of CG regions.

Future Research

Many fracture-mechanics principles are developed on paper (mathematical) and then substantiated experimentally in the laboratory using base metals. It should be recognized, however, that in real structures, the vast majority of cracks, defects, and other stress concentrations exist in or near welds. Therefore, it seems logical that sound engineering philosophies concerning fracture behavior are needed more for weld metals and HAZs than for base metals. Fracture-control philosophies for welded structures should be developed with an understanding of at least the following two areas:

- The metallurgical heterogeneity that exists in weld metals and HAZs.
- The statistical nature (data scatter) of weld metal and HAZ fracture toughness data.

Future research is necessary to further understand fracture behavior in heterogeneous materials. Probabilistic strategies also need to be developed to account for statistical data scatter.

Conclusions

1. LBZs are low-toughness CG regions. The CG regions consist of the unaltered CGHAZ and the intercritically and subcritically reheated CGHAZ (IRCG and SRCG). The CG regions have a grain size larger than 70 to 80 μm. Low toughness is defined for the purpose of this paper as CTOD < 0.10 mm.

2. LBZ-related fracture initiates at some critical metallurgical subfeature within the LBZ (i.e., a weak-link phenomenon). The CG regions contain the weak link.
3. In order to fully understand HAZ fracture-toughness data, broken specimens must be sectioned and metallurgically examined to determine what microstructures were sampled by the fatigue crack.
4. When testing a weld that contains LBZs, the probability of a low CTOD result increases as the fatigue crack samples more CG regions.
5. If a limited HAZ toughness testing program is conducted to determine if a particular weld contains LBZs, then imposing a fatigue-crack sampling criterion can improve the chances of success.

Acknowledgments

The author is grateful to the following individuals for their helpful discussions: Drs. C. P. Royer, J. Y. Koo, N. V. Bangaru, Y. S. Wang, and H. Banon.

References

[*1*] Fairchild, D. P., "Local Brittle Zones in Structural Welds," *Welding Metallurgy of Structural Steels,* The Metallurgical Society, Warrendale, PA, 1987.
[*2*] Webster, S. E. and Walker, E. F., "The Significance of Local Brittle Zones to the Integrity of Large Welded Structures," Paper OMAE-88-919, Seventh International Conference on Offshore Mechanics and Arctic Engineering, Houston, TX, February 1988.
[*3*] Harrison, J. D., "Why Does Low Toughness in the HAZ Matter?" The Welding Institute Seminar, Coventry, England, June 1983.
[*4*] Fairchild, D. P., Theisen, J. D., and Royer, C. P., "Philosophy and Technique for Assessing HAZ Toughness of Structural Steels Prior to Steel Production," Paper OMAE-88-910, Seventh International Conference on Offshore Mechanics and Arctic Engineering, Houston, TX, February 1988.
[*5*] "API Specification for Preproduction Qualification for Steel Plates for Offshore Structures," API RP2Z, American Petroleum Institute, Dallas, TX, March 1987.
[*6*] "Steel Specification for Fixed Offshore Structures," EEMUA Publication No. 150, Engineering Equipment and Materials User's Association, London, England, 1987.
[*7*] Koo, J. Y. and Ozekcin, A., "Local Brittle Zone Microstructure and Toughness in Structural Steel Weldments," *Welding Metallurgy of Structural Steels,* The Metallurgical Society, Warrendale, PA, 1987.
[*8*] Amano, K., Itakura, N., Shiga, C., and Enami, T., "Metallurgical Factors Controlling Local Brittle Zone in Weld HAZ," Iron & Steel Research Laboratories, Kawasaki Steel Corp., Chiba, Japan, 1985.
[*9*] Haze, T. and Aihara, S., "Metallurgical Factors Controlling HAZ Toughness in HT50 Steels," IIW Document IX-1423-86, International Institute of Welding, Tokyo, Japan, May 1986.
[*10*] Haze, T. and Aihara, S., "Influence of Toughness and Size of Local Brittle Zone on HAZ Toughness of HSLA Steels," Seventh International Conference on Offshore Mechanics and Arctic Engineering, Houston, TX, February 1988.
[*11*] Bateson, P. H., Webster, S. E., and Walker, E. F., "Assessment of HAZ Toughness Using Small Scale Tests," Seventh International Conference on Offshore Mechanics and Arctic Engineering, Houston, TX, February 1988.
[*12*] Aihara, S. and Haze, T., "Influence of High Carbon Martensitic Islands on Crack-Tip Opening Displacement Value of Weld Heat-Affected Zone in HSLA Steels," The Metallurgical Society, Annual Meeting, Phoenix, AZ, January 1988.
[*13*] Chen, J. H., "Micro-Fracture Behavior Induced by M-A Constituent in Simulated Welding Heat Affected Zone of HT80 High Strength Low Alloyed Steel," *Acta Metall.*, 32 (10), 1986, pp. 1770–1788.
[*14*] Pickering, F. B., "The Structure and Properties of Bainite in Steels," Climax-Molybdenum Symposium, Transformation and Hardenability in Steels, February 1967.
[*15*] Pisarski, H. G., "Measurement of HAZ Fracture Toughness," Steel in Marine Structures, Amsterdam, 1987.
[*16*] Mackay, K., "CTOD Testing and Validation—State of the Art for Recent North Sea Projects," Seventh International OMAE Conference, Houston, TX, February 1988.

Susumu Machida,[1] Takashi Miyata,[2] Masahiro Toyosada,[3] and Yukito Hagiwara[4]

Study of Methods for CTOD Testing of Weldments

REFERENCE: Machida, S., Miyata, T., Toyosada, M., and Hagiwara, Y., "**Study of Methods for CTOD Testing of Weldments,**" *Fatigue and Fracture Testing of Weldments, ASTM STP 1058,* H. I. McHenry and J. M. Potter, Eds., American Society for Testing and Materials, Philadelphia, 1990, pp. 142–156.

ABSTRACT: Several precracking methods for crack-tip opening displacement (CTOD) testing of weldments were studied, including as local precompression, reverse bending, and high *R*-ratio fatigue. The precracking procedure could influence the validity of the precrack shape. However, it was found that an irregular precrack front had little effect on CTOD values of the heat-affected zone (HAZ). Results indicate that the current limitations on the fatigue precrack shape can be relaxed.

CTOD values comparable to those of the standard $B \times 2B$ specimen were obtained from the subsidiary $B \times B$ specimen with a through-thickness notch of a length-to-specimen-width ratio of 0.5. Hence, it can be possible to use $B \times B$ specimens instead of $B \times 2B$ specimens in the standard CTOD testing of weldments.

The CTOD test results for weld HAZ were strongly affected by the notch positioning in the welded joint. By analyzing the weld thermal history, HAZ microstructures were classified. Then, it was revealed that CTOD values were closely related to the maximum size of the local brittle zone (LBZ) at the crack tip.

KEY WORDS: weldments, crack-tip opening displacement, fracture toughness, welded joint, weld heat-affected zone, residual stress, testing standards, local brittle zone, fracture testing

As the integrity of a structure (defect significance and material selection) is assessed based on fracture mechanics, crack-tip opening displacement (CTOD) testing of weldments is often required for steel qualification or welding procedure qualification. The standard procedure of CTOD testing has been prescribed for a parent material [*1*]. However, there are several difficulties in the CTOD testing of welded joints. The CTOD testing of weldments is influenced by many mechanical and metallurgical factors, such as welding residual stress and toughness variation in the heat-affected zone (HAZ), which should be taken into account to establish the standard procedure for CTOD test of weldments [*2,3*].

Welding residual stress exists in the welded joint. The distribution of welding residual stress through the thickness affects the fatigue crack propagation rate, and the compressive residual stress restrains the formation and growth of a fatigue crack. Hence, the residual

[1] Professor, Department of Naval Architecture and Ocean Engineering, University of Tokyo, Tokyo, 113 Japan.

[2] Associate professor, Department of Iron and Steel Engineering, Nagoya University, Nagoya 464 Japan.

[3] Associate professor, Department of Naval Architecture, Kyushu University, Fukuoka, 812 Japan.

[4] Senior research engineer, R & D Laboratories, Nippon Steel Corp., Sagamihara, 229 Japan.

stress distribution results in an irregular fatigue precrack front. In order to reduce the residual stress and to get a uniform shape of the fatigue precrack, normally, the local precompression procedure [4] is applied in the CTOD test of weldments.

To keep the procedure effective, the diameter of a platen should be larger in proportion to the specimen thickness so that the plastic strain due to precompression will reach the mid-thickness portion of a multiple-pass welded joint, where the compressive welding residual stress usually exists. The required precompression load becomes very large for a thick specimen. Therefore, it is important to study the possible alternative methods [5] to get a uniform precrack in a CTOD test specimen.

Moreover, the standard rectangular $B \times 2B$ specimen becomes larger as the thickness increases because the full thickness is required for CTOD testing [1]. The square $B \times B$ specimen with a notch-depth-to-specimen-width ratio of 0.5 is considered to be an alternative. The weight of the $B \times B$ specimen is one fourth that of the standard $B \times 2B$ specimen, and the load required for CTOD testing of the $B \times B$ specimen is a half that of the $B \times 2B$ specimen. So, it would be very convenient for testing if the $B \times B$ CTOD test gave a result comparable to that of the $B \times 2B$ CTOD test.

Concerning the metallurgical factors, the critical CTOD is very sensitive to the toughness of microstructures at the crack tip. As is well known, many different microstructures are generated in HAZ, depending on the thermal cycles, as a result of welding and the chemical composition of the steel. Consequently, the CTOD test results for HAZ have a wide scatter due to the variation of the crack position in the welded joint.

A low CTOD value is often observed if the precrack tip samples a local brittle zone (LBZ) [6–8]. It has been demonstrated [7,8] that the critical CTOD is closely related to the maximum size of the LBZ as well as its toughness. Then, it is very important in CTOD testing of HAZ to clarify whether the precrack intersects LBZ or not by examining the cross section at the precrack after testing.

In the present paper, precracking procedures such as local precompression, reverse bending [9], and high R-ratio (minimum load/maximum load) fatigue [10] were investigated. The effect of unevenness of the precrack front on CTOD was examined. The effect of the specimen geometry was also studied using a square specimen. After CTOD testing, sectioning and observation of the precrack position were conducted. The distributions of the peak temperatures caused by the welding beads were analyzed as a function of a distance from the weld fusion line. The LBZ was identified by taking into account the thermal cycles, and the effect of the size of the LBZ on CTOD was discussed.

Experimental Procedure

Material and Welded Joints

Normalized steel of 50-mm-thick BS4360-50E grade was used in the experiments. This type of steel has been widely applied in offshore structures. The chemical composition and the mechanical properties are shown in Tables 1 and 2, respectively. The steel contained 0.12% carbon and small amount of vanadium (0.041%) and niobium (0.026%). The carbon equivalent was 0.39%.

The welded joints were made by means of submerged-arc welding. The edge preparation was a double V (X shape), as shown in Fig. 1. In this figure, the pass sequences of the multiple-pass weld are also shown. The welding conditions are summarized in Table 3. The heat input was 47 to 59 kJ/cm, which is a little higher than that used in normal welding practice in offshore structure manufacturing yards.

TABLE 1—*Chemical composition of the steel used.*

Steel Grade	Thickness, mm	Chemical Composition, weight %									
		Carbon	Silicon	Manganese	Phosphorus	Sulfur	Copper	Nickel	Vanadium	Niobium	Carbon Equivalent
BS4360-50E	50	0.12	0.41	1.40	0.016	0.003	0.20	0.19	0.041	0.026	0.39

TABLE 2—*Mechanical properties of the steel used.*

Yield Strength, N/mm^2	Tensile Strength, N/mm^2	Elongation, %
421	539	32

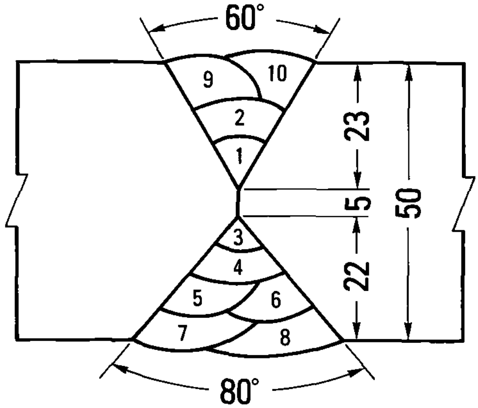

FIG. 1—*Double V weld preparation and pass sequences of submerged-arc welding (SAW).*

Precracking Methods for CTOD Testing of Weldments

Four types of precracking methods were applied to the standard $B \times 2B$ specimens extracted from the welded joints: local precompression, reverse bending, and high R-ratio fatigue, in addition to fatigue precracking alone, without taking into account crack front irregularity (conventional method).

In these CTOD tests, the notch was placed so as to intersect the weld fusion line at a location with around 50% weld metal and 50% HAZ/base metal.

Precompression was applied with a platen 60 mm in diameter before a notch was machined. The precompression load was 2.27 MN, and the plastic strain of precompression was 1.0 to 1.2% of the specimen thickness.

Reverse bending was carried out for a notched CTOD specimen. This method was proposed because the tensile yield stress at the crack tip caused by unloading of the reverse bending can cancel or reduce the compressive welding residual stress. One of the possible criteria for reverse bending is that the fatigue crack length, Δa_f, is greater than the plastic zone size formed at the prebending stage.

The plastic zone size produced by reverse bending is expressed by the following equation under the small-scale yielding condition.

$$\omega_{rb} = \frac{\pi}{8}\left(\frac{K_{rb}}{L_{\sigma_Y}}\right)^2 \tag{1}$$

where

K_{rb} = stress-intensity factor due to reverse bending,
ω_{rb} = plastic zone size due to reverse bending,
σ_Y = yield stress, and
L = plastic constraint factor.

In the present study, $\Delta a_f/\omega_{rb} = 2$ is used. Then

$$K_{rb} = 2\sqrt{\frac{\Delta a_f}{\pi}}\, L_{\sigma_Y} \tag{2}$$

TABLE 3—*Welding condition.*

Welding Method	Current, A	Voltage, V	Speed, cm/min	Heat Input, kJ/cm
Submerged arc welding	850 to ~900	30 to ~33	30 to ~36	47 to ~59

The prebending load was determined by substituting $\Delta a_f = 2.5$ mm and $L = 2.3$ into Eq 2. This load is about 1.2 times higher than the fatigue load for precracking. However, the fatigue precrack has penetrated through the compressive yield zone caused by the reverse bending, so that the effect of it on CTOD is thought to be small.

In the case of the high R-ratio method, fatigue precracking was performed with $R = 0.5$ and the same maximum fatigue load used for normal fatigue precracking. Therefore, it takes a longer time for precracking because of the reduced stress range. In comparison, a CTOD test with just fatigue precracking (conventional method) was also carried out. In all cases, the maximum fatigue stress-intensity factor was set to be $K_f = 1400\ \mathrm{N{\cdot}mm^{-3/2}}$, which is lower than the specified value in British Standard (BS) 5762.

CTOD Testing of Subsidiary Specimens

The possibility of using a subsidiary square ($B \times B$) specimen as a standard CTOD test specimen was investigated, although the $B \times 2B$ specimen is recommended in BS 5762. Usually, a $B \times B$ specimen has been employed for surface notch CTOD testing with a precrack-length-to-specimen-width ratio, a/W, of 0.3. However, in the present study, a through-thickness precrack of $a/W = 0.5$ was employed, because the constraint at the crack tip in the $B \times B$ specimen was intended to be comparable to that of the $B \times 2B$ specimen.

CTOD Testing

Standard CTOD tests using specimens precracked by the precompression method were carried out at various low temperatures in order to obtain the CTOD transition curve. From this experimental result, a particular test temperature was chosen at which the average critical CTOD value is around 0.1 mm in the transition range, and about ten specimens were tested for each condition to investigate the scatter in CTOD values for weldments in relation to the microstructures at the notch location.

Sectioning and Examination of the Notch Location

It has been widely recognized that CTOD values of HAZ vary according to the microstructures at the fatigue precrack tip. Hence, it has become common to section near the fatigue precrack front and examine the cross section to identify the position in terms of HAZ microstructures. In this experiment, sectioning was conducted for all standard specimens, as shown in Fig. 2, and the notch tip position was investigated by analyzing the peak temperature distribution.

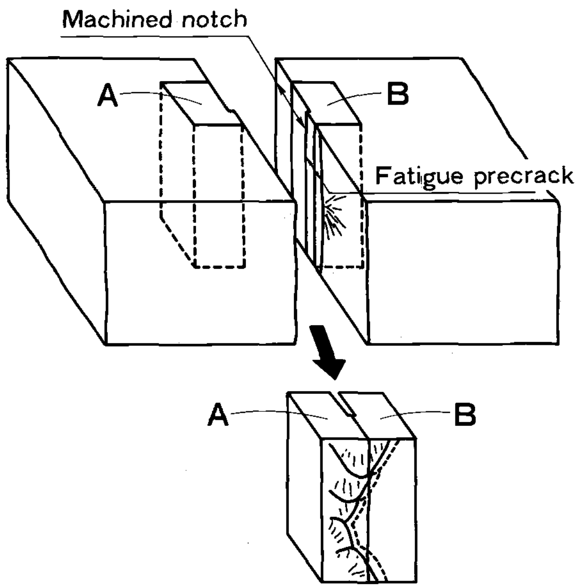

FIG. 2—*Sectioning technique of a CTOD specimen of a weldment.*

Results

Effect of Precracking Methods on CTOD

Several precracking methods to reduce the effect of residual stress were examined, and the effect of the precracking procedure on the shape of the fatigue precrack and the CTOD value was investigated.

Figure 3 shows the CTOD transition curve obtained for HAZ of the specimens' welded joints. The critical CTOD value of about 0.1 mm was obtained at −30°C. Ten specimens for each precracking method were tested at this temperature. Following the British Standards Institution (BSI) standard for CTOD testing [*1*], a fatigue crack length was measured at the positions of the maximum and minimum length and at three points—Δa_{f1}, Δa_{f2}, and Δa_{f3}, which were 25, 50, and 75% of B, respectively. The standard prescribes the following conditions for the fatigue crack length:

(*a*) the difference in Δa_{f1}, Δa_{f2}, and $\Delta a_{f3} \leqq 5\%\ W$ (W is the specimen width),
(*b*) $\Delta a_{f\,\max} - \Delta a_{f\,\min} \leqq 10\%\ W$, and
(*c*) $\Delta a_{f\,\min} \geqq 2.5\%\ W$ or 1.25 mm.

The CTOD values at −30°C for differently precracked specimens are shown in Fig. 4. The open circles indicate data from specimens having an invalid precrack shape because of the above requirements. Specimens precracked by the conventional method without any specific consideration produced 90% of the invalid data. Eighty percent of the specimens for the reverse bending method and 60% of those for the high R-ratio method were also judged to be invalid. Prescription (*c*) on the minimum precrack length could not be satisfied in those specimens, although $\Delta a_{\min}$ is not zero. In contrast, the precracked specimens after local precompression met all requirements. Consequently, with respect to the precrack shape, precompression might be the most preferable method.

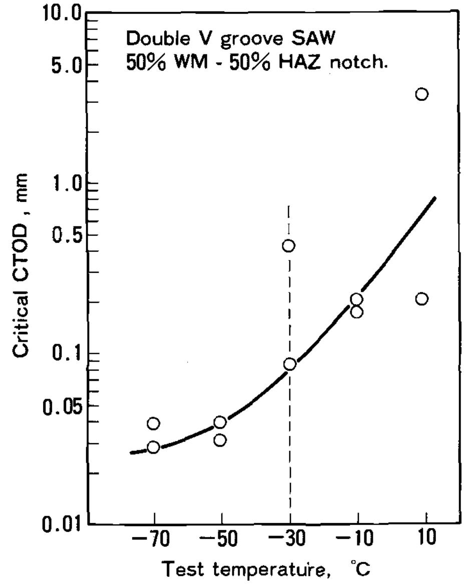

FIG. 3—*CTOD transition curve obtained from* B × 2B *standard testing for a SAW joint.*

The CTOD values in Fig. 4 were calculated in accordance with the plastic hinge equation in BS 5762, regardless of whether the precrack shape was valid or not, because Prescriptions (*a*) and (*b*) were satisfied for all specimens.

As is shown in Fig. 4, some differences in CTOD values can be observed between the various precracking methods; for example, the lowest CTOD value for the precompression specimens seems to be smaller than those for the other specimens. However, from obser-

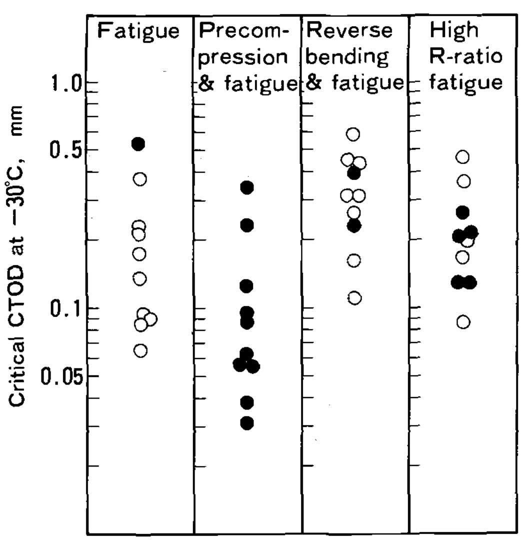

FIG. 4—*Effect of the precracking method and unevenness of the crack front shape on CTOD values at −30°C. The open circles indicate data invalid because of the precrack shape, according to BS 5762.*

vation of fracture surfaces and the macro-etched section, it has been confirmed that, in any specimens with a CTOD lower than 0.1 mm, there was LBZ at the precrack front. Hence, the above-mentioned differences seem to be attributable to the crack tip location in relation to microstructures rather than to the irregularity of the crack front shape, which depends on the precracking methods. In other words, it is also shown in Fig. 4 that whether the precrack shape is valid or invalid seems to have little influence on CTOD values.

As is discussed later, low values of CTOD can be clearly related to the size of the LBZ along the precrack front, irrespective of the precracking methods or precrack validity. In other words, different precracking methods, including precompression and an irregular crack front shape, have relatively little effect on CTOD for weldments, especially for HAZ. The restrictions on the fatigue precrack shape can be relaxed. It may be unnecessary to require the minimum crack length to be proportional to the specimen width.

Effect of Specimen Geometry on CTOD

Twelve square $B \times B$ subsidiary specimens with a fatigue precrack produced by the precompression method were tested at −30°C. Figure 5 shows the CTOD values obtained for subsidiary and standard specimens. A significant difference between the CTOD values of both specimens cannot be observed, since lower CTOD values in standard specimens occasionally reflect the LBZ at the crack tip, as was previously mentioned.

Consequently, it can be said that CTOD values in weldments, especially in HAZ, which has a heterogeneity in toughness, are strongly influenced by the presence of LBZ at the crack tip, and the effects of the precracking method, the unevenness of the precrack front, and the specimen geometry are relatively small.

Discussion

Analysis of the Thermal History of HAZ

Variation in the CTOD values of HAZ is caused by the different microstructures produced by the thermal cycles of multiple-pass welding, and it has been shown that a low CTOD

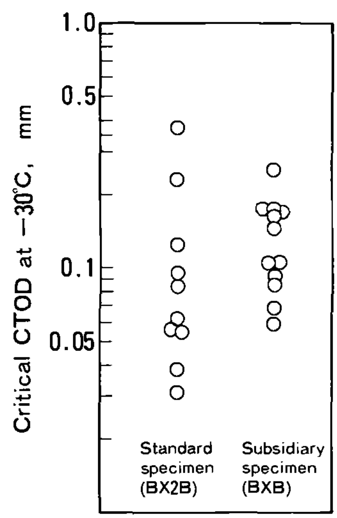

FIG. 5—*Effect of specimen geometry on CTOD values at −30°C.*

value is observed if the LBZ is located at the precrack front of the specimen. From a metallurgical point of view, the factors controlling the CTOD values of HAZ have been extensively investigated by means of CTOD tests for simulated HAZ as well as for the welded joint [6]. Typical microstructures in the HAZ of muliple-pass welds can be classified as follows [3]:

CGHAZ = coarse-grained HAZ
FGHAZ = fine-grained HAZ
ICHAZ = intercritically heated HAZ
SCHAZ = subcritically heated HAZ
SCFGHAZ = supercritically reheated fine-grained HAZ
ICCGHAZ = intercritically reheated coarse-grained HAZ
SCCGHAZ = subcritically reheated coarse-grained HAZ

In these microstructures, ICCGHAZ is the most embrittled region for offshore structural steels, such as those used in the present study, because it has unfavorable coarse precipitation of high-carbon martensite islands (M*) in the coarse-grained HAZ [6]. In addition, CGHAZ and SCCGHAZ are also considered to be a possible LBZ, and the total length of CGHAZ, ICCGHAZ, and SCCGHAZ along the precrack front through the thickness direction is prescribed by the American Petroleum Institute (API) [3]. Moreover, ICHAZ has relatively low toughness because of the formation of M* in the carbon-rich areas of the base metal. In the tempering thermal cycle, some fraction of M* is decomposed and the toughness of ICCGHAZ and ICHAZ recovers, although the amount of decomposition is influenced by the chemical composition [6].

By taking into account these possible LBZ areas, the thermal cycle analysis was carried out to classify the microstructures as mentioned above. All the broken CTOD specimens were sectioned near the precrack tip and the cross section was polished and etched to reveal the microstructures, as shown in Fig. 2. An example of a macrograph is shown in Fig. 6.

In the case of two-dimensional heat flow, the peak temperature is given by the following expression [11].

$$\frac{1}{T_p - T_o} = \frac{4.13c\rho y}{\frac{q}{v}} + \frac{1}{T_m - T_o} \tag{3}$$

where

T_p = peak temperature,
T_m = molten temperature of the material,
T_o = initial temperature of the plate,
c = specific heat,
ρ = density,
v = welding velocity,
q = heat input per unit thickness, and
y = distance from the fusion line.

A formula similar to Eq 3 was proposed for three-dimensional heat flow [12]. If we put

$$A = \frac{4.13c\rho}{\frac{q}{v}} \tag{4}$$

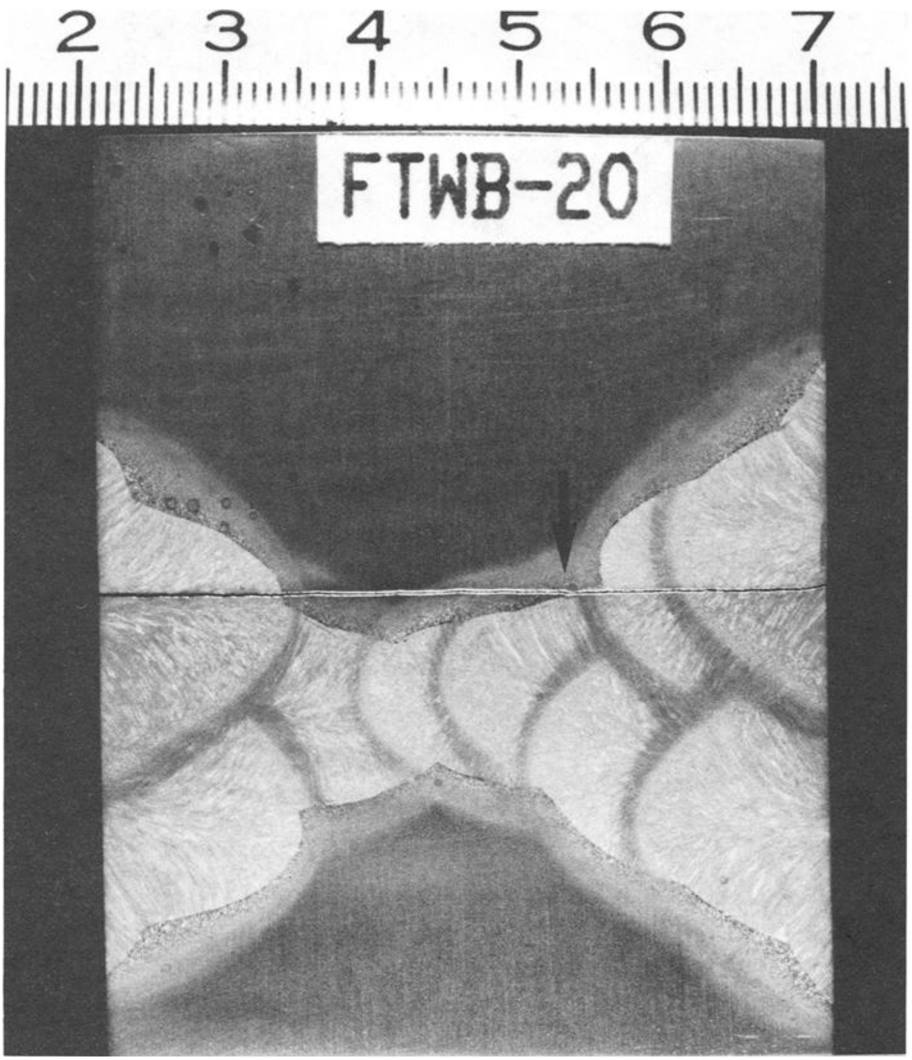

FIG. 6—*Example of a macrograph of a cross section near the precrack tip of a CTOD specimen. The arrow indicates the fracture initiation point.*

Eq 3 is rewritten as follows.

$$\frac{1}{T_p - T_o} = Ay + \frac{1}{T_m - T_o} \quad (5)$$

The peak temperature of HAZ boundary observed on the macrographs of the welded joint is assumed to be 900°C, because it nearly corresponds to the $Ac3$ line. By measuring the width of HAZ from the fusion line and substituting it into Eq 5, the factor of A is determined and the isothermal lines corresponding to various peak temperatures are obtained. Figure 7 shows an illustration of a macrograph of a bead-on-plate weld by submerged-

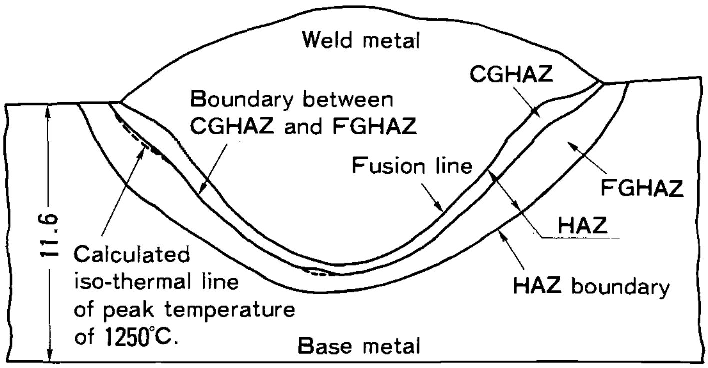

FIG. 7—*Comparison of the observed and estimated boundaries of CGHAZ and FGHAZ from Eq 5 for a SAW bead-on-plate welded joint.*

arc welding. The boundary between CGHAZ and FGHAZ was determined by observation on the magnifying projector. The isothermal line of the peak temperature of 1250°C, which is thought to be the temperature between CGHAZ and FGHAZ, is estimated based on the measured HAZ width and Eq 5 and is shown as a dotted line in Fig. 7. It is apparent that the estimation agrees with the measurements.

The analysis of isothermal lines corresponding to various peak temperatures was carried out on macrographs, and the microstructures of HAZ along the precrack front were decided for all specimens tested. The various peak temperatures corresponding to typical HAZ microstructures were assumed to be as follows:

Above 1250°C = CGHAZ
850°C to 1250°C = FGHAZ
750°C to 850°C = ICHAZ
450°C to 750°C = tempering temperature range

Examples of the results of thermal cycle analysis are shown in Figs. 8 and 9. In the diagrams, the location of the fatigue precrack and the fracture initiation point or points observed on the fracture surface are indicated. The specimen shown in Fig. 8 has several regions with ICCGHAZ microstructure and one of them is intersected by the fatigue precrack, which just corresponds to the fracture initiation point. In this case, the very low CTOD value of 0.031 mm was observed.

For the specimen in Fig. 9 (CTOD = 0.206 mm), the fatigue precrack does not sample an ICCGHAZ itself, but it was tempered by the thermal cycle of the subsequent weld pass (dotted area). It is recognized in this specimen that brittle fracture occurred macroscopically from two points, but these were not in untempered ICCGHAZ. One of the fracture initiation points corresponds to ICHAZ and the CTOD value is much higher than that of the previous specimen. It is confirmed from these observations that CTOD values are strongly dependent on the kinds of microstructures in the fatigue precrack samples.

Effect of LBZ on CTOD

The most embrittled LBZ can be ICCGHAZ, so the relationship between the size of ICCGHAZ intersected by the fatigue precrack and the CTOD value was studied, as shown in Fig. 10. The symbols with a superscript *T* indicate that the microstructures were tempered

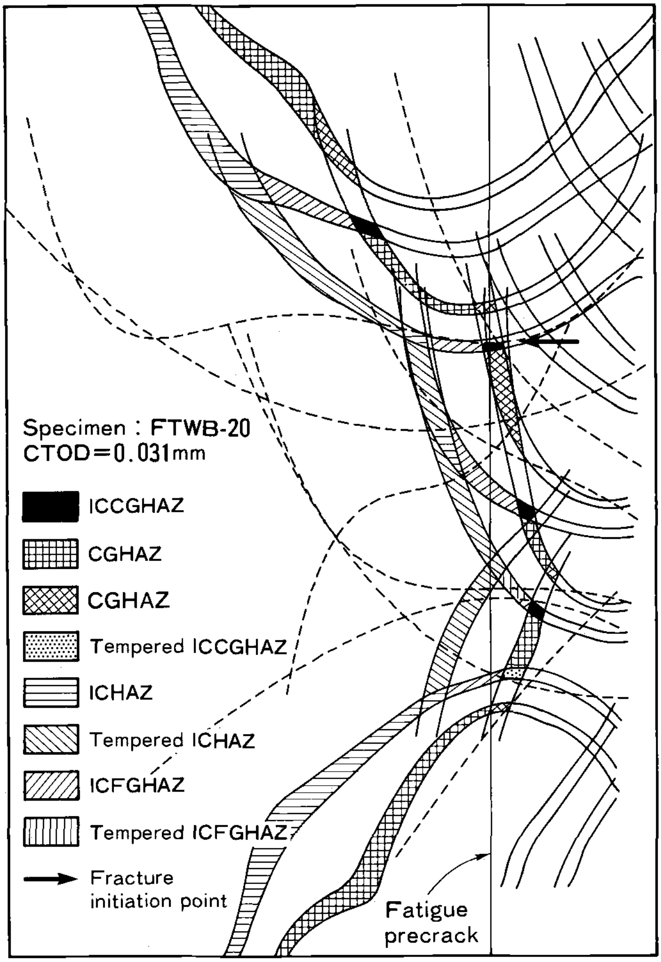

FIG. 8—*Microstructures of HAZ estimated by thermal cycle analysis, fatigue precrack location, and brittle fracture initiation point for Specimen FTWB-20 (CTOD = 0.031 mm).*

by the subsequent thermal cycle. The solid line in Fig. 10 indicates the relationship between the CTOD and the LBZ size of untempered ICCGHAZ (B_o), except for the data of B_o = 0 and symbols with a superscript of T. It is apparent that the CTOD value decreases as the size of ICCGHAZ at the precrack front increases. It is also revealed from Fig. 10 that the specimens with invalid precrack geometry according to BS 5762 show CTOD values comparable to those of specimens with valid precrack shape.

Concerning the specimens of B_o = 0 in Fig. 10, the relationship between CTOD values and other possible LBZ of CGHAZ (including SCCGHAZ) and ICHAZ was studied. The results are shown in Fig. 11. It is apparent that even though ICCGHAZ is not sampled at the precrack, the CTOD value decreases when the size of another LBZ becomes large at the precrack front. Figure 11 shows that CTOD values decrease as the size of LBZ of CGHAZ increases, but ICCGHAZ gives lower CTOD values than CGHAZ when the size of LBZ is the same.

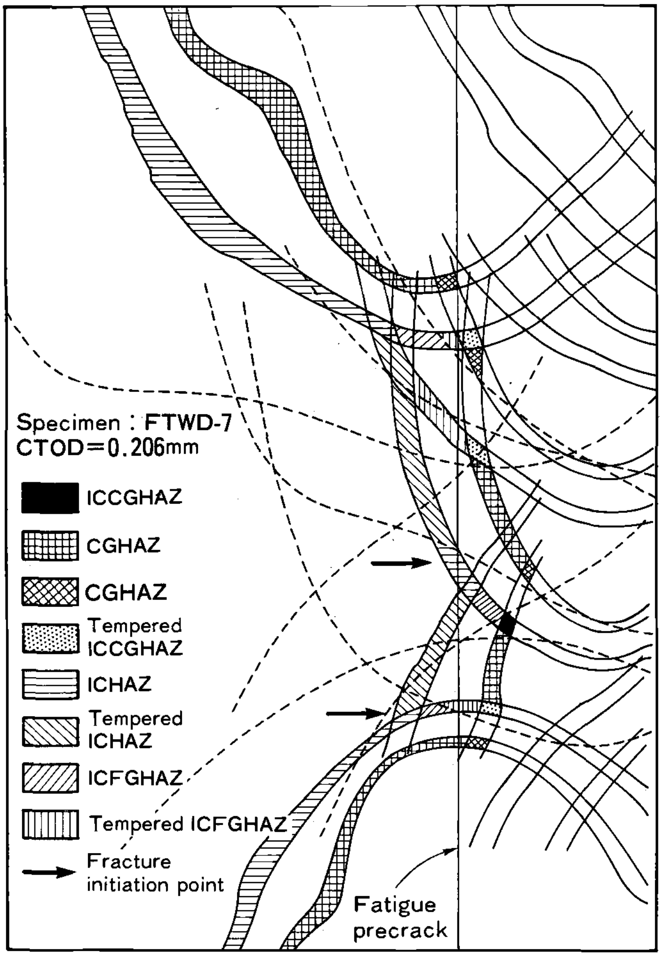

FIG. 9—*Microstructures of HAZ estimated by thermal cycle analysis, fatigue precrack location, and brittle fracture initiation points for Specimen FTWD-7 (CTOD = 0.206 mm).*

The present study revealed that the critical CTOD value was closely correlated with the maximum size of LBZ. Results [*8*] have been obtained, showing that the total size of the LBZ along the precrack has poor correlation with the CTOD values; however, this should be investigated in more detail by changing the LBZ size at the precrack tip, e.g., by using K- and X-groove welded joints with the same welding condition.

Furthermore, the significance of LBZ should be considered from the engineering point of view. The possible crack direction should be taken into account, because a fatigue crack initiated at the toe of a fillet weld of a tubular joint normally propagates in a direction perpendicular to the surface and, consequently, does not reach to the LBZ. Therefore, probabilistic and reliability analyses should be utilized to estimate the fracture probability of a structural member with LBZ present.

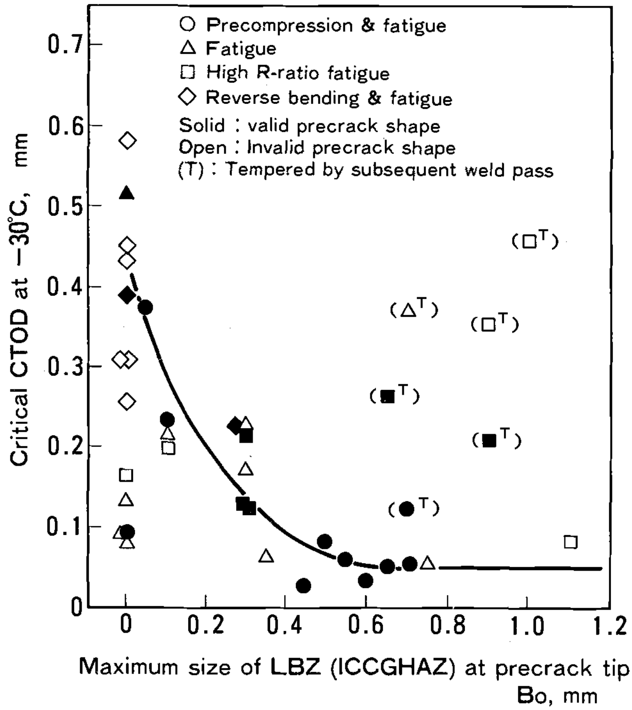

FIG. 10—*Relationship between CTOD and the maximum size of LBZ (ICCGHAZ) at the precrack tip.*

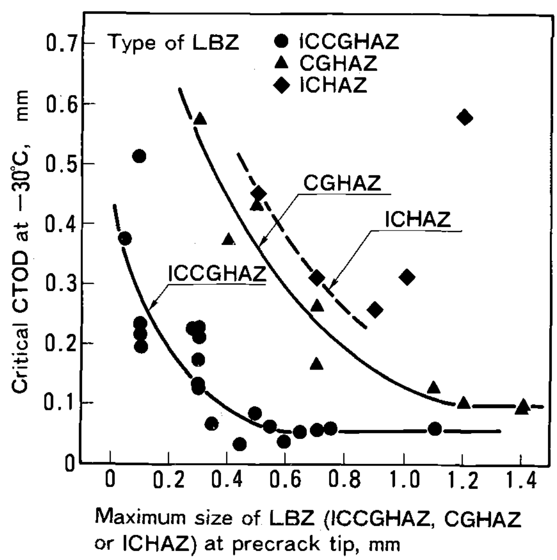

FIG. 11—*Relationship between CTOD and the maximum size of various kinds of LBZ (ICCGHAZ, CGHAZ, and ICHAZ) at the precrack tip.*

Conclusions

1. Precracking methods, such as the usual local precompression, reverse bending, and high R-ratio fatigue, can affect the validity of the precrack shape, although it depends on their precise conditions. However, the precracking method and an irregular precrack front shape have relatively little effect on the CTOD values of HAZ.
2. Subsidiary square specimens with a through-thickness notch of a crack-length-to-specimen-width ratio of 0.5 give CTOD values comparable to those of the standard $B \times 2B$ specimen. The possibility of the use of the square specimen instead of the $B \times 2B$ specimen was confirmed.
3. The CTOD value is strongly affected by the presence of LBZ at the precrack tip, depending on the size of the LBZ and the kinds of microstructures in it. The toughness is lowest in ICCGHAZ, followed by CGHAZ for the steel in the present study. The CTOD value decreases as the maximum size of the LBZ increases.

Acknowledgment

The authors would like to express their thanks to the members of the FTW committee of the Japan Welding Engineering Society for their cooperation on this work. This work has been supported by the Japan Welding Engineering Society and Scientific Research Grants No. 6255-0322 and 6130-2050 from the Japan Ministry of Education.

References

[*1*] "Method for Crack Opening Displacement (COD) Testing," BS 5762, British Standards Institution, London, England, 1979.
[*2*] Squirrell, S. J., Pisarski, H. G., and Dawes, M. G., "Recommended Procedures for the Crack Tip Opening Displacement (CTOD) Testing of Weldments," Research Report 311/1986, The Welding Institute, Cambridge, England, August 1986.
[*3*] "API Recommended Practice for Preproduction Qualification for Steel Plates for Offshore Structures," RP 2Z, American Petroleum Institute, Dallas, TX, 1986.
[*4*] Dawes, M. G., "Fatigue Pre-cracking Weldment Fracture Mechanics Specimen," *Metal Construction and British Welding Journal,* Vol. 3, No. 2, 1971, pp. 61–65.
[*5*] Towers, O. L. and Dawes, M. G., "Welding Institute Research on the Fatigue Precracking of Fracture Toughness Specimens," *Elastic-Plastic Fracture Test Methods: The User's Experience, ASTM STP 856,* American Society for Testing and Materials, Philadelphia, 1985, pp. 23–46.
[*6*] Haze, T. and Aihara, S., "Metallurgical Factors Controlling HAZ Toughness in HT50 Steels," IIW Document IX-1423-86, The International Institute of Welding, Tokyo, Japan, 1986.
[*7*] Toyosada, M., Nohara, K., Otsuka, T., and Hagiwara, Y., "Effect of Specimen Thickness and Local Brittle Zone on CTOD at HAZ of Weld Joint," IIW Document X-1104-86, The International Institute of Welding, Tokyo, Japan, 1986.
[*8*] Haze, T. and Aihara, S., "Influence of Toughness and Size of Local Brittle Zone on HAZ Toughness of HSLA Steels," *Proceedings,* Seventh International Conference on Offshore Mechanics and Arctic Engineering, Houston, TX, February 1988.
[*9*] Sakano, K., "Precompression Cracking Method for Fracture Toughness Test—2nd Report," *Journal of the Society of Naval Architects of Japan,* Vol. 144, December 1988, pp. 352–361.
[*10*] Towers, O. L., "The Use of High R-Ratio for Growing Fatigue Cracks in Fracture Toughness Specimens," Paper 25, *Proceedings,* International Conference on Fracture Toughness Testing, The Welding Institute, Cambridge, England, 1982.
[*11*] Adams, C. M., "Cooling Rates and Peak Temperatures in Fusion Welding," *Welding Journal,* Vol. 37, No. 5, 1958, pp. 210s–215s.
[*12*] Paley, Z., Lynch, J. N., and Adams, C. M., "Heat Flow in Welding Heavy Steel Plate," *Welding Journal,* Vol. 43, No. 2, 1964, pp. 71s–79s.

Rudi M. Denys[1]

Wide-Plate Testing of Weldments: Introduction

REFERENCE: Denys, R. M., **"Wide-Plate Testing of Weldments: Introduction,"** *Fatigue and Fracture Testing of Weldments, ASTM STP 1058,* H. I. McHenry and J. M. Potter, Eds., American Society for Testing and Materials, Philadelphia, 1990, 157–159.

ABSTRACT: No one single source currently exists which gives an overall picture of the meaning and usefulness of wide-plate test data. The intent of this series of papers is to provide a summary of the status of available knowledge—attained by the author as the result of almost 20 years of experience and study of the literature in the field of wide-plate testing—relating to the prevention of (brittle) fracture initiation.

In terms of organization, this series of papers begins with a short general introduction to show why the papers were written. The wide-plate test is then reviewed from various viewpoints. As the reader will see, the subject is presented in three self-contained papers, bearing the following titles:

Part I—Wide-Plate Testing in Perspective
Part II—Wide-Plate Evaluation of Notch Toughness
Part III—Heat-Affected-Zone Wide-Plate Studies

Part I is concerned with a brief review of the historical development of wide-plate testing in relation to the major achievements of wide-plate/small-scale test correlations. From these considerations, the future role of wide-plate tests in fracture performance evaluations and design practice are discussed. Part II presents the various wide-plate and defect designs for evaluating the overall stress/strain behavior of plain and welded plates. Furthermore, the performance requirements in relation to the purpose of the test are critically reviewed. Part III considers the present state of the art in heat-affected-zone wide-plate testing procedures. The presentation provides a step-by-step analysis of the actual testing requirements. Particularly, emphasis is given to detailed metallographic posttest validation requirements for the crack tip location.

KEY WORDS: weldments, wide-plate testing, crack-tip opening displacement, (CTOD), Charpy V-notch impact test, brittle fracture, residual stress, defects, cracks, notches, toughness requirements, high-strength steels

Before discussing the subject of wide-plate testing in detail, it is important to emphasize first that, because of the size of its specimens, the wide-plate test does not have the same purpose as the small-scale test, which is mainly used for material quality control. The main purpose of wide-plate testing is to simulate as closely as conceivable the service performance of base metals and their welded configurations.

The wide-plate test specimen was developed during the time period 1944 through 1962. The main incentive for its development was the need for a laboratory test specimen that would provide "full-scale" data on a material's fracture behavior. Past experience has shown that this development was successful and that wide-plate testing is an effective means of

[1] Professor and research manager, Laboratorium Soete Rijksuniversiteit Gent, B 9000 Gent, Belgium.

providing information on the fracture initiation and propagation toughness levels of steel plates and weldments [1–6] (see the reference list in Part I, the following paper).

Upon examination of the earlier wide-plate results one finds that most studies were concerned with low-stress brittle fracture caused by strain aging embrittlement in the sub-critical heat-affected zone (HAZ) and the presence of yield-magnitude residual stresses. To simulate these conditions, longitudinally welded wide-plate test specimens with single or crossed welds and with the notch perpendicular to the longitudinal weld have been tested.

Since wide-plate tests are rather expensive to be used as a means of evaluating a material's resistance to brittle fracture, a variety of small-scale and fracture mechanics tests have been devised as alternative means of determining the notch and fracture toughness properties. In many instances, relatively good empirical correlations were obtained between results of the small-scale Charpy V-notch impact or the crack-tip opening displacement (CTOD) fracture mechanics test and wide-plate test performance. These correlations were used for setting minimum Charpy V-notch toughness requirements in material selection standards [7] or to validate the degree of conservatism implied by a specific fracture mechanics defect assessment procedure (such as the CTOD design curve approach) [8–9].

With the appearance of low-carbon, low-alloy, high-yield-strength (350 MPa) steels in the early 1980s, however, the validity of those correlations has been put into question. The concerns are mainly related to the finding of low (less than 0.1 mm) CTOD values, which are triggered by small areas of poor toughness within the coarse-grain HAZ of low-carbon steel weldments [10–15]. Because of the ongoing debate on the engineering significance of those low CTOD values, interest has revived recently in application of wide-plate tests as a empirical means of evaluating this specific low-toughness problem. Since the region of lowest toughness is no longer associated with the transformed HAZ, emphasis is now placed on fatigue-precracked, surface-notched, welded wide-plate specimens in which the weld is arranged transverse to the applied load. The change in specimen design has also necessitated a change in wide-plate testing procedures. Since the performance characteristics of this test configuration depend essentially on the HAZ/weld metal structures sampled, it is nowadays required that the crack be located in the most brittle region (i.e., either the HAZ or the weld metal) of the weldment. The requirements include the use of specific notch placement techniques and a metallurgical evaluation of the crack tip location after testing [16].

Similar low-toughness problems in specially designed low-carbon microalloyed, high-yield-strength (450 to 500 MPa) steel grades intended for use in heavy-duty structures are expected. In addition, the alloy design and the strain hardening properties of these steel differ considerably from those in the 350-MPa high-yield-strength steels. That is, the performance characteristics of the 450 to 500-MPa-yield-strength steels have still to be established. Therefore, it is also believed that more wide-plate test data will be needed to provide or revise material selection criteria.

Long-standing experience in wide-plate testing offers numerous reasons why wide-plate testing provides further scope in fundamental and applied fracture research. In fact, one of the most important factors that makes the wide-plate test so important in fracture testing is connected with its overall dimensions. Because of the future importance of wide-plate test data in fracture evaluations, knowledge of the many aspects of the test is a prerequisite for appreciation of the physical significance of its test results. In the author's experience, most fracture mechanics experts are not very familiar with the wide-plate test. This is partly due to the fact that only a few laboratories possess the required testing equipment. Moreover, the basic aspects of wide-plate testing are rather poorly documented. In particular, no one single source of information currently exists that gives an overall picture of the meaning and usefulness of wide-plate test data. Therefore, it is the intent of this series of papers to provide a summary of the status of available knowledge.

The information contained in these papers is based on almost 20 years of the author's testing experience and study of the literature in the field of wide-plate testing. During review of the various aspects of wide-plate testing, some outstanding problems will be shown to illustrate that a great deal of wide-plate testing work remains to be done, particularly with respect to the fracture assessment of weldments.

In terms of organization, the subject is broken down into three main parts and presented in three papers bearing the following titles:

Part I—Wide-Plate Testing in Perspective
Part II—Wide-Plate Evaluation of Notch Toughness
Part III—Heat-Affected-Zone Wide-Plate Studies

As will become evident, each part is self-contained. The first two parts summarize the background development and describe the role of the various wide-plate test specimen designs, as well as the use of wide-plate test data in fracture research. Part III deals with the current testing requirements related to HAZ testing.

References

[*1*] "Weldment Evaluation Methods," DMIC Report 244, Washington, DC, August 1968.

[*2*] Tipper, C. F., *The Brittle Fracture Story*, Cambridge University Press, Cambridge, England, 1962.

[*3*] Burdekin, F. M., "The Practical Application of Fracture Tests to Prevent Service Failures," *Welding Research Supplement*, March 1968, pp. 129–139.

[*4*] Dawes, M. G., Dolby, R. E., Egan. G. R., Harrison, J. D., and Saunders, G. G., "An Assessment of Brittle Testing Techniques," *TWI Report*, November 1969.

[*5*] Masubuchi, K., *Analysis of Welded Structures, International Series on Material Science and Technology*, Vol. 33, Pergamon Press, New York, 1980.

[*6*] Dawes, M. G. and Denys, R. M., "BS 5500 Appendix D: An Assessment Based on Wide Plate Brittle Fracture Test Data," *International Journal of Pressure Vessels and Piping*, Vol. 15, 1984, pp. 161–192; and "BS 5500 Appendix D: Fusion Welded Pressure Vessels for Use in Chemical, Petroleum and Allied Industries: Part 1—Carbon and Ferritic Alloys Steels, Recommended Practice For Vessels Required to Operate at Low Temperature," British Standards Institution, London, England.

[*7*] Burdekin, F. M. and Stone, D. E., "The Crack Opening Displacement Approach to Fracture in Yielding Materials," *Journal of Strain Analysis*, Vol. 1.2, 1966, pp. 145–153.

[*8*] Kamath, M. S., "The COD Design Curve: An Assessment of Validity Using Wide-Plate Tests," Research Report 71/1978/E, The Welding Institute, September 1978; and "The COD Design Curve: An Assessment of Validity Using Wide-Plate Tests," *International Journal of Pressure Vessels and Piping*, Vol. 9, No. 2, 1982, pp. 79–105.

[*9*] Fairchild, D. P., "Local Brittle Zones in Structural Welds," *Proceedings*, Conference on Welding Metallurgy of Structural Steels, The Metallurgical Society, Denver, CO, October 1987.

[*10*] Royer, C., "A User's Perspective on Heat-Affected Zone Toughness," *Proceedings*, TMS Conference, Denver, CO, February 1987.

[*11*] Walker, F. E., "Steel Quality, Weldability, and Toughness," *Steel in Marine Structures*, Elsevier Science Publishers, Amsterdam, The Netherlands, 1987.

[*12*] Walker, E. F., "Fracture Toughness Testing—Present Status of Charpy V-Notch Impact and CTOD Testing," *Proceedings*, Symposium on the State of the Art in Materials Testing, Koninklijke Vlaamse Ingenieurs Vereniging, Antwerp, Belgium, November 1986.

[*13*] Pisarski, H. G., "Measurement of Heat-Affected Zone Fracture Toughness," *Proceedings*, Third International ECSC Offshore Conference on Steel in Marine Structures (SIMS '87), Delft, The Netherlands, 15–18 June 1987.

[*14*] Webster, S. E., "The Structural Significance of Low Toughness HAZ Regions in a Modern Low Carbon Structural Steel," *The Fracture Mechanics of Welds*, EGF Publication No. 2, Mechanical Engineering Publications, London, England, 1987, pp. 59–75.

[*15*] Hall, W. J., Kihara, H., Soete, W., and Wells, A. A., "Brittle Fracture of Welded Plate," *International Series in Theoretical and Applied Mechanics*, Prentice Hall, Englewood Cliffs, NJ, 1967, pp. 11–125.

[*16*] Denys, R. M., "Wide Plate Fracture Toughness Evaluation of the Weld HAZ of Low Carbon Micro-alloyed Structural Steel Weldments," *Proceedings*, CIM/CSFM Symposium, Winnipeg, Canada, August 1987.

Rudi M. Denys[1]

Wide-Plate Testing of Weldments: Part I—Wide-Plate Testing in Perspective

REFERENCE: Denys, R. M., **"Wide-Plate Testing of Weldments: Part I—Wide-Plate Testing in Perspective,"** *Fatigue and Fracture Testing of Weldments, ASTM STP 1058,* H. I. McHenry and J. M. Potter, Eds., American Society for Testing and Materials, Philadelphia, 1990, pp. 160–174.

ABSTRACT: Depending on the ultimate purpose of the test, many wide-plate test specimen designs have been developed to provide a quantitative framework for evaluating both the fracture initiation and the fracture propagation or arrest conditions. This paper focuses on historical developments in wide-plate testing with respect to fracture initiation behavior problems only. This paper also addresses the role, as well as the limitations, of wide-plate testing in fracture research.

KEY WORDS: weldments, wide-plate testing, crack-tip opening displacement (CTOD), Charpy V-notch impact test, brittle fracture, residual stress, defects, cracks, notches, toughness requirements, test requirements

Interest in wide-plate testing was stimulated greatly by the increased number of brittle fractures in welded ships and oil storage tanks in the late 1940s and the early 1950s. A characteristic of these fractures was that the actual failures usually occurred at stress levels well below the base metal yield strength for loading conditions which were completely static. Coupled with this knowledge was the fact that the brittle fractures often originated at discontinuities or weld flaws in the structure and that a normal tension test specimen did not break in the same brittle manner at the temperature of the casualty. Hence, a notch was regarded as essential in simulating service behavior. Also, the effects of low temperature and the specimen size on the occurrence of brittle fracture became so manifest that a number of investigators in the United States, Britain, Japan, and Belgium showed interest in the development of large-scale testing facilities for the purpose of matching and studying, under controlled conditions in the laboratory, the casualty behavior of both base metals and their weldments.

Before going into details of the historical development of wide-plate testing, it might be useful to note that throughout this paper the term brittle fracture is tied to the macroscopic observation of "low-stress" fracture initiation. Thus, fracture accompanied by local yielding at the crack tip is defined as brittle fracture when the degree of prefracture strain is less than the amount of strain expected in service. In light of this definition, it is clear that fracture with a mixed-fracture appearance (i.e., a combination of a flat fracture surface—cleavage—with stable tearing and ductile shear lips) may still be brittle.

[1] Professor and research manager, Laboratorium Soete Rijksuniversiteit Gent, B 9000 Gent, Belgium.

Historical Aspects of Wide-Plate Testing

The application of wide-plate testing to fracture problems involves interrelated developments in tests for both notched base metal and welded and notched wide-plate specimens [*1–9*]. In view of the importance of these developments to the current use of wide-plate test data, this section includes a brief review of the historical aspects of wide-plate testing.

Wide-Plate Studies on Base Metal

In 1944–45, Roop [*10*] performed the first wide-plate tension tests. He performed these tests to study the effects of (*a*) the notch tip acuity, (*b*) the temperature, and (*c*) the material properties at the notch tip on the brittle fracture characteristics of mild steel plates by means of statically (uniaxially) loaded tension tests on 300-mm (12-in.)-wide center-notched specimens of base metal.

These base metal wide-plate tests were followed by further wide-plate test studies at the Universities of California (1947–48) and Illinois (1948–51) [*11–17*]. These studies involved various plate widths [the maximum width was up to 2700 mm (108 in.)]; that is, these investigations were primarily studies for explaining the effects of, along with the variables just described, (*a*) the section size (plate thickness and plate width) and (*b*) the mode of fracture on the brittle fracture strength and ductility at various temperatures (transition temperature) [*18*].

The studies cited [*10–18*] were part of investigations into the World War II ship fracture problem. These investigations were aimed at determining the possible causes of brittle fracture that occurred in welded ships by exploring the idea that the capacity for elongation (notch ductility) of the base metal was more important than its strength. In this connection, it should be noted that a tension test was preferred for the simple reason that elongations could easily be measured. One of the major conclusions of the studies reported in Refs *10* through *18* was that a 300-mm (12-in.) wide-plate test specimen would provide a reliable index to the ductility transition behavior of large ship plates. Therefore, the 300-mm-wide notch tension specimen was accepted as a standard of reference for wide-plate tests for evaluating the notch ductility of (ship) steel.

The next major development in base metal testing took place in Japan. In 1964, Akita and Ikeda [*19*] proposed the use of a deep-notched wide-plate specimen to investigate the fracture initiation properties of high-strength steels at low temperatures. Their studies led to a standard deep-notched specimen, which is normally 400 mm wide and contains two edge notches, either 80 or 120 mm long. By using this specimen design, it was possible to produce brittle fracture in notched base metal plates at low stress levels.

Curiously enough, the investigators in previous studies gave little [*18*] or no consideration [*10–17*] to the effects of defect size on the specimen's wide-plate test performance. As the aim of testing was to determine the transition temperatures so that steels might be ranked on the basis of their wide-plate tension test performances, notch lengths of about one fourth or more of the width of the plate were considered satisfactory for that purpose [*13*].

In recognition of this shortcoming, Soete and Denys investigated in 1970–76 the effects of defect size on transition behavior in assessing the crack initiation properties of base metal steel plates [*20*]. They identified, depending on the spread of plasticity and the testing temperature, four different deformation regimes that a notched plate can experience (Fig. 1). These regimes are (*a*) linear elastic behavior with a limited amount of yielding at the crack tip; (*b*) elastic-plastic behavior or contained yielding, for which a macroscopic yield zone develops ahead of the crack tip; (*c*) net section yielding (NSY), or uncontained ligament

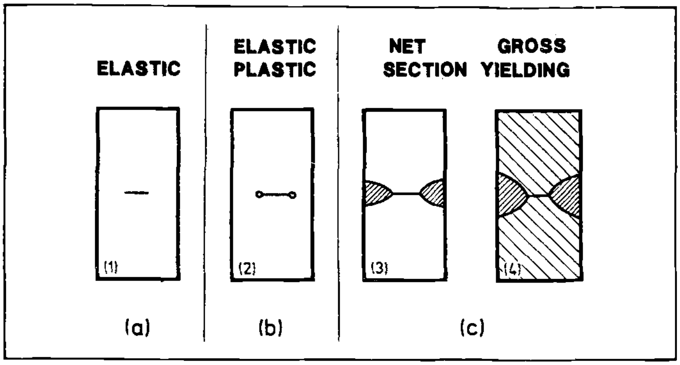

FIG. 1—*Schematic representation of deformation patterns in tension-loaded cracked wide-plate specimens. (The hatched areas represent plastically deformed material).*

yielding; and (*d*) gross section yielding (GSY). These observations (see Part II, the next paper) led also to the adoption of the gross section yielding concept for defect acceptance [*20*].

Welded and Notched Wide-Plate Tests

The first major development in wide-plate testing of welded panels occurred because of interest in the effect of residual stresses upon the fracture initiation properties of strain-aged embrittled subcritical heat-affected zone (HAZ). For that purpose, Wilson and Hao conducted wide-plate *tension* tests in 1946 on 600-mm (40-in.)-wide longitudinally welded test panels which were *free* from defects [*21*]. These tests were not so successful (although some effects of residual stresses could be demonstrated) because appreciable differences in fracture stress could not be found nor could low-stress brittle fracture be produced.

In 1945, Kennedy [*22*] investigated the role of residual stresses on the resistance of brittle fracture initiation in transversely (surface) notched and longitudinally welded plates by *bending* 300-mm (12-in.)-wide specimens through stretching the surface along the weld. Kennedy's work was succeeded by that of Greene [*23*]. In 1949, Greene conducted bend tests on 915-m-square (3-ft-square) longitudinally welded panels containing an artificial defect (Fig. 2). This defect consisted of a pair of fine coplanar surface saw cuts in the edges (tensile surface) prepared for welding (a slightly modified version of this defect design was later adopted by many other investigators). Although Kennedy had observed low fracture stresses in many of his tests, Greene's tests clearly demonstrated for the first time that initiation of brittle fracture at stresses far below the yield strength level could be obtained consistently under controlled laboratory conditions with rather simple large-scale test specimens. Another achievement of these wide-plate bend test studies was that, were brittle fracture was observed prior to thermal stress relief, a thermal stress-relieving treatment of the steels was effective in preventing brittle fractures at low stress levels.

Thanks to the vision of Wells [*24*], it became possible in 1956 to produce brittle fractures at stresses well below the yield stress of the material in static *tension*. Wells used a 915-mm-square (3-ft-square) longitudinally welded specimen with symmetrical through-thickness coplanar V notches prepared before welding (Fig. 3). For this purpose, Wells designed also a large-scale tension rig which served as a prototype for many wide-plate testing machines [*24*]. Wells's carefully controlled wide-plate tests illustrated for the first time that a gross

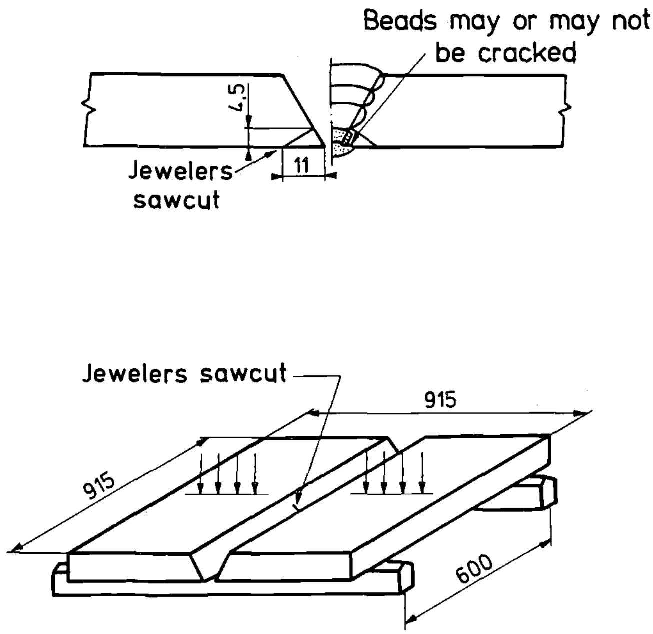

FIG. 2—*The Greene specimen, a longitudinally welded wide-plate bend test specimen with saw-cut defect.*

elongation (or strength) transition temperature existed, above which brittle fracture, even when the residual stress was superposed on the notched specimen, could not initiate [*25*].

After the work done by Wells and his collaborators at the British Welding Institute, extensive research on the brittle fracture behavior of weldments was conducted in 1959 by Masubuchi [*1*] and Kihara and Masubuchi [*26*], in 1961 by Iida [*27*], and in 1962–65 by Hall et al. [*28*]. All these studies involved longitudinally welded and notched "Wells type" wide-plate steel specimens in which different types of notches were investigated. As illustrated in Fig. 4, V-shaped notches in which the weld was essentially intact, V-shaped notches

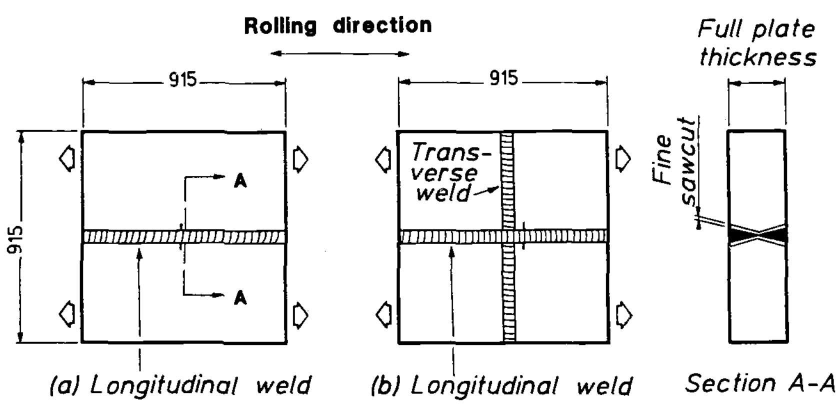

FIG. 3—*The Wells specimen, a longitudinally welded wide-plate tension test specimen with notch perpendicular to the weld.*

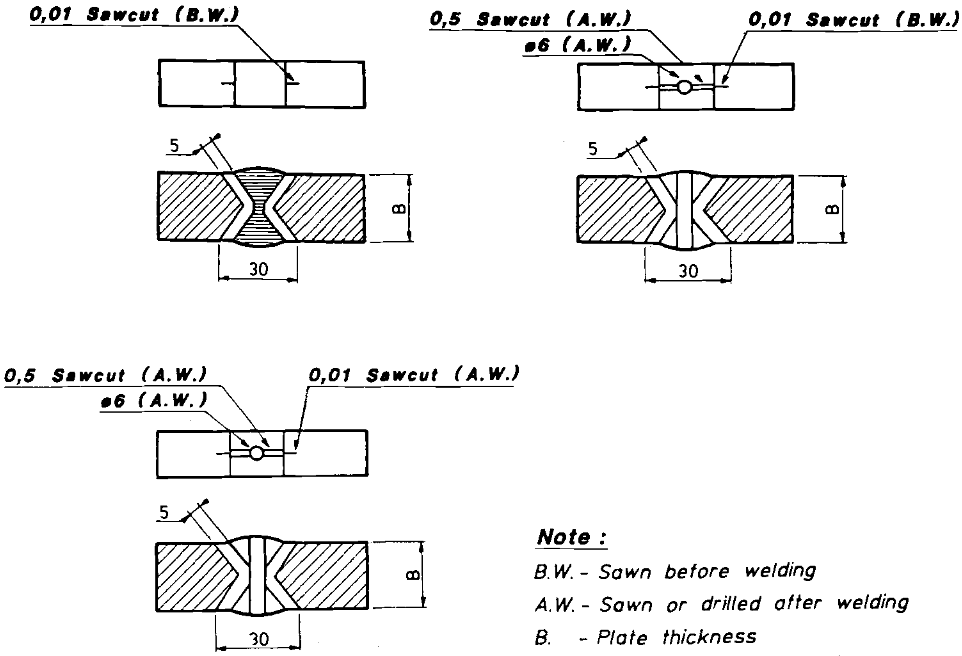

FIG. 4—*Details of typical saw-cut notches used in a longitudinally welded wide-plate tension test specimen.*

in which the weld was cut through, and V-shaped notches made before and after welding were studied. It was found from these studies that low-stress fracture could be initiated both from notches made after the completion of welding and from notches present during the welding process.

In 1959, Kihara and Masubuchi [26] investigated the brittle fracture properties of the weld metal and the transformed (visible) heat-affected zone using 1000-mm-square transversely loaded, cross-welded, and notched wide-plate tension test specimens (Fig. 5). This and other

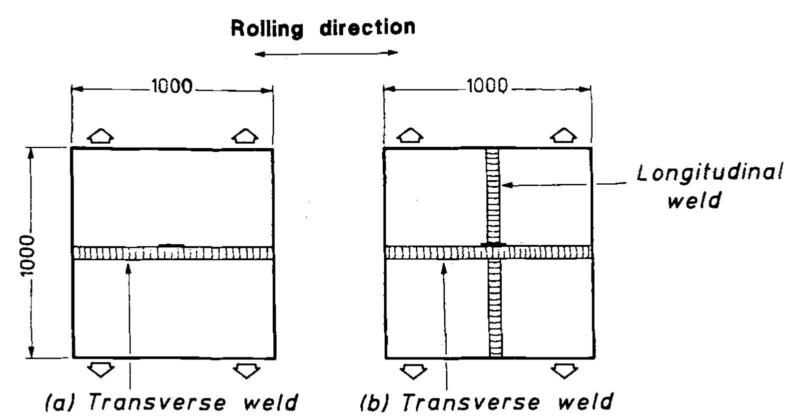

FIG. 5—*The transversely welded wide-plate tension test specimen with notch parallel to the weld.*

configurations (see Part II, the next paper) made it possible to use notches sited in various regions of the welded joint [26]. To investigate the fracture toughness of these regions, a change in notching procedure was needed, and the notch design or shape was no longer restricted to a V-shape. Through-thickness notches, surface notches, and edge notches became available for use. Also, the philosophy adopted in the deep-notched wide-plate testing of base metal was continued in 1967 when both the longitudinally (for maximum effect of the residual stresses) and the transversely *welded* deep-notched wide-plate test were used [29].

In the 1970s, far fewer wide-plate tests were performed. At that time it was assumed that the available wide-plate test data provided sufficient information to avoid the low-toughness problems associated with strain-aging embrittlement in the subcritical HAZ. For this reason, wide-plate test results were correlated with small-scale test results to establish material selection requirements, based on Charpy V-notch impact testing. The backgrounds of these developments are discussed in the next section of this paper.

The use of higher strength steels and the improved steel-making technology in the early 1980s (which, in fact, provided the means for solving the strain-aging problem) created a new series of incentives for conducting wide-plate tests. With the use of low-alloyed carbon-manganese (C-Mn) steels, welding shifted the region of low toughness to the transformed HAZ [30,31]. Since 1986, this problem has amplified the need for wide-plate testing in order to clarify certain issues which could not be resolved on the basis of small-scale fracture mechanics testing alone [6,32–35].

Wide-Plate Testing and Small-Scale Testing Requirements

Insofar as the conditions for initiation of fracture from a defect associated with welding are adequately modeled, it is generally accepted that the wide-plate test will provide a reliable method of estimating service performance. For this reason, throughout its development the wide-plate test has always been, as illustrated below, and still is considered a well-adapted means of verifying the structural significance of small-scale test results and their performance requirements.

Charpy V-Notch Impact Testing Requirements

In 1964, the Oil Companies Materials Association (OCMA) in the United Kingdom used the results of 60 tests on notched and longitudinally welded wide-plate specimens to devise Charpy V-notch impact test requirements as a basis for steel selection for pressure vessels [1,2,36] and storage tanks [37–39] to be used at temperatures below 0°C.

These Charpy testing temperature requirements [defined as material reference temperatures (MRTs)] were derived from correlations between the temperature at which (*a*) the wide-plate test resisted four times the yield strain of the plate metal before fracture initiation [the minimum design temperature (MDT)] and (*b*) the base plate showed a Charpy energy absorption of 27 J [36]. It should be emphasized that the results of these correlations apply only to carbon and C-Mn steels and that they assume fabrication and inspection in accord with normal code requirements. In other words, the results of these correlations should not be extrapolated to different materials without experience. This also explains why, in 1986, a comparable MRT/MDT analysis of the results of about 350 base metal and HAZ notched wide-plate tests was performed. The purpose of this analysis was to validate and obtain the Charpy V-notch impact test requirements for base metal steel plate and the HAZ region in the offshore steel plate specification required by the United Kingdom Department of Energy [40,41].

CTOD Design Curve

Wide-plate tests are time-consuming and are thus not suitable for examining small variations in welding procedure or in material specifications. For this reason, attempts have been made to use fracture mechanics principles to obtain the same information from the cheaper crack-tip opening displacement (CTOD) test as is gained from wide-plate tests. The basis for a successful but conservative correlation between wide-plate and CTOD test results was provided in 1966. The theoretical and experimental work undertaken by Burdekin and Stone [*3*] validated the concept of a critical CTOD for fracture initiation by correlating the results of 50-mm-thick notched (CTOD) bend and 17 through-thickness notched tensile loaded base-metal wide-plate specimen tests. A point to be noted is that the yielding pattern close to the crack tip was equivalent in both the wide-plate and CTOD test specimens. Thus, the conditions for fracture initiation at the crack tip in both test geometries were quite similar.

These correlations encouraged Harrison, Burdekin, and Young in 1968 [*42*] to propose the CTOD test for evaluation of the fracture toughness and prediction of allowable defect sizes for steels and weldments by introducing the CTOD design curve. When more wide-plate specimens became available, Burdekin and Dawes modified the experimental part of the design curve in 1971 [*43*], while Dawes in 1974 [*44*] used wide-plate tests produced by Egan in 1972 [*45*] to modify the semi-experimental portion of the design curve into its present form.

Finally, Kamath started in 1978 a detailed analysis of 73 (flat, plate metal, and welded) wide-plate tension test specimens containing known defects to estimate the degree of conservatism inherent in the CTOD design curve approach for e/e_Y ratios larger than 0.5 [*4*]. This analysis showed that, on average, the design curve has a built-in factor of safety of approximately 2.5. The assessment also showed that, when residual stresses were present, there were no significant differences in the average factors of safety for through-thickness and surface cracks. However, in the absence of residual stresses, the factors of safety were higher for surface cracks.

Limitations and Future Needs

The above examples show that wide-plate test results can be successfully used to establish toughness performance requirements for small-scale tests. With this background, the results of the MRT/MDT analysis cited and the design curve (CTOD) concept are in widespread use for purposes of both material selection and defect assessment. However, it is worth emphasizing that those correlations were established for "old type" low-strength C-Mn steels and that almost all of the early work on MRT/MDT and CTOD made use of wide-plate specimens with machined notches [*4,46,47*]. In other words, material selection based upon a minimum service temperature (MRT/MDT) approach involves many parameters which as yet are not adequately documented for use in specifications for modern structural steels.

The difficulties can be appreciated when it is realized that wide-plate test performance and, thus, its correlation with small-scale test behavior may be influenced by (*a*) the plate thickness; (*b*) the plate heat-treatment condition (i.e., as-welded versus stress-relieved); (*c*) the type, size (the depth of the crack is of particular importance), and location of the defect; (*d*) the microstructures sampled by the tip of the crack; (*e*) the base metal yield strength properties; and finally, (*f*) the performance requirements set.

Comparable observations can be made with regard to the limitations inherent in the design curve concept. While the fracture problems of base metals may be caused by the inherent crack-tip toughness characteristics, much remains to be understood concerning the role of

HAZ/weld-metal fracture toughness as a factor in the performance of weldments. For instance, quantitative treatment of the effects of weld-metal yield-strength matching on the CTOD requirements is an area which has been badly neglected [*48*]. The solutions obtained for the base steel problem point to similar approaches to questions of HAZ/weld metal fracture toughness.

Previous observations can be extrapolated when it is realized that many changes have taken place (*a*) in the base metal properties (i.e., as a result of alloy design, manufacturing thermal treatment, plate thickness, and other factors) and (*b*) in the type of service (e.g., offshore constructions) that is required of the weldments. In particular, empirical justification of the toughness requirements for modern fine-grained higher strength steels is a major issue. Further, it is also important to recognize that elastic-plastic low-constraint fracture problems make it necessary to obtain a second parameter, which characterizes the degree of constraint.

Unfortunately, it should be noted that there is a paucity of wide-plate test data for solving these problems in a quantitative way. Past experience has shown that Charpy impact/CTOD correlations alone do not provide the information needed [*49*]. Also, the CTOD test cannot be considered a substitute for the wide-plate test in establishing small-scale testing requirements.

From the point of view of immediate application, there is apparently no alternative but to use relatively large test specimens for the prediction of fracture initiation behavior in regions of poorly defined or changing elastic-plastic and plastic strain fields. Therefore, it is the author's belief that a generalized picture of the importance of the problems cited may be obtained only by consideration of wide-plate test data as well as information obtained from tests of the actual components.

Role of Wide-Plate Testing in Fracture Toughness Assessments

Long-standing experience in wide-plate testing has demonstrated that a wide variety of test variables and combinations of them can be found in wide-plate test specimens. In particular, the dimensional effects, which influence the interpretation of any particular small-scale test, and the material property effects associated with the base metal and weldment can be adequately duplicated.

Wide-Plate Test Specimen Design

The main factors that can be controlled in choosing the wide-plate specimen design are related to the specimen size and defect design, while the performance of the test can be affected by such factors as the degree of constraint, the loading mode, and the test temperature. These factors are briefly discussed here:

1. The wide-plate test is the only known realistic laboratory test which can provide a rational basis for the establishment/validation of base-plate and weldment fracture toughness requirements and quality levels necessary for small-scale testing.
2. The wide-plate test permits reproduction of the service situations more readily than small-scale tests. In particular, the wide-plate test specimen can be designed to be directly representative of an important number of structures, such as pressure vessels, pipe line, storage tanks, and other structures. Further, it is quite simple to simulate any specific defect configuration when the notch acuity has been defined and quantified, while the effects of full plate thickness, weld joint design (the shape of the weld bevel), weld arrangement (single versus crossing welds), angular distortion, misalignment, and

some other types of geometrical stress/strain concentrations, such as fillet weld attachments, can be directly accounted for.

3. Fracture under conditions of low constraint presents considerable analytical difficulty at the present time. In such cases, both the crack tip geometry and the testing geometry make it necessary for the effect of strain hardening to be taken into account, since strain hardening is a precondition for fracture. In such cases, the use of the assumed equivalence of the linear elastic stress-intensity factor, K, for shallow surface/buried and through-thickness cracks contributes to conservative defect size estimates. In other words, wide-plate testing in the case of elastic-plastic material behavior may be more economical for evaluation of surface and buried cracks.
4. Wide-plate testing is very effective in the study of the effects of residual stresses on weld joint performance, since the overall specimen dimensions make it possible for residual welding stresses to be retained in the specimen (the extraction of small test specimens from a large welded panel reduces the residual stress level). This fact, particularly when the effect of a post-weld heat treatment (stress relieving) on weld joint performance is being studied, is one of the most attractive reasons for serious consideration of wide-plate testing in fracture testing.
5. The brittle-to-ductile *transition temperature* range of wide-plate specimen test performance is different from that observed in small-scale Charpy V-notch impact/CTOD testing; i.e., the loading mode (bending versus tension) and the overall specimen dimensions are deciding factors in the test performance. It is therefore not surprising that the results of Charpy V-notch impact/CTOD tests often point to poor (brittle) material behavior, while a notched wide-plate specimen fails in a ductile manner. Thus, a reduction in constraint may lead to a significant change in the fracture mode with a large consequent increase in toughness. In addition, the interpretation of correlations between the results obtained with various notched specimens has proved to be very controversial and has thereby raised many questions concerning the general applicability of the small-scale test as a means of predicting fracture behavior. For an important number of applications (storage tanks, pipelines, and others) there is no evident direct transposition of fracture toughness data, as measured in a bend loading mode, to prediction of the fracture behavior of welded structures in which a tension loading mode dominates.

Material-Related Property Effects

The material-related property effects that influence wide-plate performance involve the effects of the base metal properties and the effects of welding. The effects of both are also interrelated.

1. The wide-plate test provides useful information on the effects of the base metal mechanical properties (i.e., the yield point strain and strain hardening rate) and the base metal processing variables (or the thermal treatment in plate manufacturing) on weldment behavior [*50*]. As the strain hardening properties of the plate material are often the overriding factor in weldment performance and since a simple analytical modeling of these effects is beset with numerous difficulties, experimental study of the role of strain hardening on weldment performance could benefit from testing large-size specimens.
2. The wide-plate test specimen is the most suitable specimen for testing the interaction between the crack size, plate material, HAZ, and weld metal properties. Owing to the composite nature of weldments, the distribution of the (remote) applied strain

between the weld metal, HAZ, and base metal depends on the mechanical properties of each of these. Provided the weld metal more than matches the base metal in strength, wide-plate testing produces experimental evidence that transversely loaded welds will suffer proportionally less deformation than the softer base metal. Under these circumstances, the weld metal may have toughness properties inferior to those of the base metal without hampering the satisfactory overall behavior of a structure [*48,54*].

Use of Wide-Plate Test Results

When the loading mode and the test specimen are carefully designed to be structurally representative, wide-plate test data can be used as follows:

(*a*) To assess the degree of conservatism implied in fracture-mechanics-based assessments. This can be achieved through a direct comparison of the allowable crack sizes predicted by, for instance, the design curve and the critical crack sizes in wide-plate tests (see also Part II, the next paper). The fact that the currently used design curve is based on wide-plate test data for different conditions in different materials and, in the case of HAZs, the fact that dissimilar regions are sampled in the $B \times 2B$ bend and wide-plate tests illustrate that a fracture assessment on the basis of small-scale fracture test results alone is not simple and that a great deal of engineering judgment is required [*4,55,56*]. Also, the evaluation of ductile material behavior in terms of CTOD is difficult and is sometimes a matter of debate. In this context, the wide-plate test would be more extensively used for assessment/development of existing plastic collapse criteria in defect assessment procedures. The plastic collapse assessment methods currently in use are indeed a source of confusion [*51–53*]. For instance, when ligament yielding ahead of a part wall defect occurs, this part wall defect is "degraded" into a through-thickness defect in brittle fracture assessment procedures. This is rather an unrealistic assessment of material behavior, since a further increase in load is required to cause plastic collapse of the whole cracked ligament.

(*b*) To provide a direct and quantifiable measure of weldment ductility. Fracture initiation is controlled by local conditions at the crack tip, but in wide-plate tests it is difficult to measure this local strain. It is usual to measure the mean strain over a considerable gage length and, therefore, performance is conveniently evaluated in terms of elongation; the measured value of elongation is often persuasive, so that a further analysis is not required.

Situations for Which Wide-Plate Testing Merits Consideration

Past experience has shown that there is no direct reason to challenge the future use of the 25-year-old and well-established methods of analysis for (*a*) validating small-scale toughness performance requirements and (*b*) developing weld procedure and defect assessment methods for predicting structural integrity for modern steels and their weldments. However, some rationalization in the decision-making process for wide-plate testing is possible. In this context, it is worthwhile mentioning the situations for which wide-plate tests could be considered:

1. When the fracture toughness requirements for the normal range of material thicknesses (expressed in terms of the Charpy V-notch impact or CTOD test) are satisfied, there are (unless there are also defect geometries larger than the postulated sizes) no reasons to consider wide-plate testing in weldment performance evaluation.

2. In qualification testing, and especially when incidental small-scale production tests fail to meet the specified requirements, it could be convenient to use wide-plate tests in place of repeat testing in an endeavor to achieve the specified Charpy V-notch or CTOD properties. The viewpoint that must be adopted to evaluate the situation is that wide-plate testing may be more economical than retesting small-scale specimens. The final decision for conducting a wide-plate investigation depends on the balance of the following costs:

   (*a*) costs caused by production delays,
   (*b*) costs incurred in preparing new test plates, and
   (*c*) costs involved in conducting (small-scale) retesting until satisfactory results are obtained. The importance of these costs should not be underestimated. In cases where free-issue materials are to be used, the expense of a less cost-effective welding procedure or process may be quite high.

3. When new steel grades or new alloy designs are used or in situations in which material thicknesses are involved for which no former tests of that type are available, wide-plate test results would help to substantiate the application limits of the materials or designs during their evaluation phase.
4. Wide plates would be mandatory to demonstrate the necessity for stress relieving thicker sections. The 40 to 50-mm thickness limit which is currently specified for the pressure vessel and offshore industry is considered to be conservative for most modern steel weldments. Although a post-weld heat treatment is commonly practiced to reduce the level of residual stresses, it should be realized that, depending on the alloy design for the transformed HAZ structures of low-alloy C-Mn steels, a heat treatment in some cases can improve the toughness properties while, in other cases, the properties may become degraded.

Finally, to keep the number of wide-plate tests low, it could be argued further that a worst-case approach could be followed in which a decision would be made to combine a representative set of variables (such as, edge preparation, heat input, defect size, and so forth). Guidance from design engineers would also be sought.

Limitations of Wide-Plate Testing

Despite the many achievements of the wide-plate test, objection is often made to its use on the grounds that wide-plate tests are expensive to use as a means of evaluating a weldment's resistance to brittle fracture. However, this argument is not always valid when small-scale test requirements result in safety factors that are unnecessarily generous and when high-performance steel structures are to be evaluated. On the other hand, wide-plate tests are too expensive, time-consuming, and not suitable for examining small variations in welding procedure or in material specifications. (The cost ratio between a HAZ fatigue precracked wide-plate test and a HAZ fatigue precracked CTOD test, fully documented with a complete metallographic record of the crack tip location after testing, is about 6:1.)

Apart from this, it is not always possible to model a defective structural detail in the most appropriate way. For example, it is very difficult to model welded connections, changes in sections, and complex load paths [*30*]. The more complex weld details thus require some kind of simulation because of the practical limitations associated with testing equipment. In these instances and where possible, recourse has to be made to a simplified testing geometry, and the performance criteria need to be modified to provide a more reliable measure of the available toughness (these possibilities are described in Part II, the next paper). In other cases, the test geometry proposed will not necessarily measure the service toughness. However, it is safe to state here that more attention should be given to the correlation between small- and large-scale weldment tests and that better evaluation methods should be developed to assess complex situations. This last suggestion takes on even more meaning when one contemplates the host of higher strength steels, larger plate thicknesses, and so forth, already in existence.

Concluding Remarks

The information contained in this paper has shown that the wide-plate test can provide a quantitative framework for evaluating the fracture initiation condition of base metals and weldments. The following conclusions can be made:

1. Continued use of wide-plate tests will be needed if fracture control methods that are not overconservative are to be based on fracture mechanics concepts. In other words, research activities directed toward the development of fracture-mechanics-based toughness requirements should be accompanied by a more meaningful large-scale type of test. This information can then be used to validate the developed toughness criteria and to examine the extent to which the specified requirements provide adequate and non-overconservative design and quality control fracture toughness requirements.
2. In particular, in the case of ductile material behavior, service behavior cannot always be realistically predicted from the information produced by one of the many (inexpensive) small-scale fracture tests. Reliance on small-scale-test-based target values often produces inappropriate and overconservative information when no reference is made to the crack size, the geometry of the structural detail, and the stress level. Provided that the structural detail is adequately modeled, wide-plate test data can play a useful role in identifying the limitations inherent in standard tests. The very fact that the Charpy V-notch impact and CTOD test requirements generate considerable controversy shows the need to reestablish the fundamentals underlying fracture and notch toughness requirements. A substantially enlarged wide-plate test database representative of potential ductile material behavior would certainly be in order.
3. The wide-plate test can, in many instances, provide most of the information required for arriving at an improved understanding of fracture behavior. The results of this test in many applications may be closer to those of practice than the results and analyses of small-scale tests. In this context, however, it cannot be ignored that the application of flat wide-plate tests also has certain limitations.
4. It is important to reemphasize here that the wide-plate test will never reach the status of a routine test and would therefore only be conducted to evaluate critical situations or be used in a material's development phase. Unless the small-scale test target values cannot be satisfied during qualification and production testing of the material, one should not consider wide-plate tests as a replacement material or weldment characterization test for the material or weldment in these instances.
5. When a wide-plate test is used, it must be carefully designed since many test variables can influence the performance level of the test. The next paper will deal with these aspects of the test, as well as with the interpretation of the test results obtained.

References

[1] Masubuchi, K., *Analysis of Welded Structures, International Series on Material Science and Technology*, Vol. 33, Pergamon Press, New York, 1980.
[2] Dawes, M. G. and Denys, R. M., "BS 5500 Appendix D: An Assessment Based on Wide Plate Brittle Fracture Test Data," *International Journal of Pressure Vessels and Piping*, Vol. 15, 1984.

pp. 161–192; and "BS 5500 Appendix D: Fusion Welded Pressure Vessels for Use in Chemical, Petroleum and Allied Industries: Part 1—Carbon and Ferritic Alloy Steels, Recommended Practice for Vessels Required to Operate at Low Temperatures," British Standards Institution, London, England, 1987.

[3] Burdekin, F. M. and Stone, D. E., "The Crack-Opening Displacement Approach to Fracture in Yielding Materials," *Journal of Strain Analysis,* Vol. 1.2, 1966, pp. 145–153.

[4] Kamath, M. S., "The COD Design Curve: An Assessment of Validity Using Wide Plate Tests," Research Report 71/1978/E, The Welding Institute, Cambridge, England, September 1978; and "The COD Design Curve: An Assessment of Validity Using Wide Plate Tests," *International Journal of Pressure Vessels and Piping,* Vol. 9, No. 2, 1982, pp. 79–105.

[5] Hall, W. J., Kihara, H., Soete, W., and Wells, A. A., *Brittle Fracture of Welded Plate, International Series in Theoretical and Applied Mechanics,* Prentice Hall, Englewood Cliffs, NJ, 1967, pp. 11–125.

[6] Denys, R. M., "Wide Plate Fracture Toughness Evaluation of the Weld HAZ of Low Carbon Micro-Alloyed Structural Steel Weldments," *Proceedings,* CIM/CSFM Symposium, Winnipeg, Canada, August 1987.

[7] Denys, R. M., Dhooge, A., and Lefevre, A. A., "HAZ Fatigue Precracking of Welded Wide Plate Specimens," *Proceedings,* Symposium on the State of the Art in Materials Testing, Antwerp, Belgium, November 1986.

[8] Watanabe, I., Kagawa, H., and Matsuda, Y., "Evaluation of Coarse-Grained HAZ Toughness by Wide Plate Testing," *Proceedings,* Seventh International Conference on Offshore Mechanics and Arctic Engineering, February 1988, pp. 387–394.

[9] Webster, S. E. and Walker, E. F., "The Significance of Local Brittle Zones to the Integrity of Large Welded Structures," *Proceedings,* Seventh International Conference on Offshore Mechanics and Arctic Engineering, February 1988, pp. 395–404.

[10] Roop, W. P., "Notes on the Conditions of Brittle Rupture of Ship Plates of Medium Steel," TMB Report R-276, U.S. Navy, Washington, DC, July 1944.

[11] Windenburg, D. F. and Roop, W. P., "Notes on the Conditions of Fracture of Medium Steel Ship Plates," *Welding Journal, Research Supplement,* November 1945, pp. 580–587.

[12] Boodberg, A., Davis, H. E., Parker, E. R., and Troxell, G. E., "Causes of Cleavage Fracture in Ship Plate—Tests of Wide Notched Plates," *Welding Journal,* April 1948, p. 186.

[13] Wilson, W. M., Hechtman, R. A., and Bruckner, W. H., "Cleavage Fracture of Ship Plates as Influenced by Size Effects," *Welding Journal, Research Supplement,* April 1948, p. 200.

[14] Hall, W. J., "Wide Plate Studies in the United States," IIW Doc. X-304-62, International Institute of Welding, London, England, 1962.

[15] Windenburg, D. F. and Thomas, H. R., "A Study of Slotted Tensile Specimens for Evaluating the Toughness of Structural Steel," *Welding Journal, Research Supplement,* April 1948, p. 209.

[16] MacCutcheon, E. M., Pittigloi, C. L., and Raring, R. H., "Transition Temperature of Ship Plate in Notched Tensile Tests," *Welding Journal, Research Supplement,* April 1950, p. 184.

[17] Carpenter, S. T. and Roop, W. P., "Tensile Tests of Internally Notched Plate Specimens," *Welding Journal, Research Supplement,* April 1950, p. 161.

[18] Hoeltje, W. C. and Newmark, N. M., "Brittle Strength and Transition Temperature of Structural Steel," *Welding Journal, Research Supplement,* November 1952, p. 515.

[19] Akita, Y. and Ikeda, K., "On Brittle Fracture Initiation: First Report—Deep Notch Test," *Journal of the Society of Naval Architects of Japan,* Vol. 116, December 1964.

[20] Soete, W. and Denys, R., "Fracture Toughness Testing of Welds," *Proceedings,* Conference on Welding of HSLA (Microalloyed) Structural Steels, American Society for Metals, Rome, Italy, November 1976, pp. 63–84.

[21] Wilson, W. M. and Hao, C.-C., "Residual Stresses in Welded Structures," *University of Illinois Engineering Experiment Station Bulletin,* No. 361, 1946.

[22] Kennedy, H. E., "Some Causes of Brittle Failures in Welded Mild Steel Structures," *Welding Journal, Research Supplement,* November 1945, pp. 588–598.

[23] Greene, T. W., "Evaluation of Effect of Residual Stresses," *Welding Journal, Research Supplement,* May 1949, pp. 193–204.

[24] Wells, A. A., "The 600-Ton Test Rig for Brittle Fracture Research," *Transactions of the Royal Institution of Naval Architects,* Vol. 98, 1956, p. 156.

[25] Burdekin, F. M., "Investigations in the UK into the Effects of Residual Stresses on Brittle Fracture," IIW Doc. X-309-62, International Institute of Welding, London, England, 1962.

[26] Kihara, H. and Masubuchi, K., "Effect of Residual Stress on Brittle Fracture," *Welding Journal, Research Supplement,* April 1959, p. 159.

[27] Iida, K., "Effect of Welding Residual Stresses and/or Structural Discontinuities on Low Stress Brittle Fracture, "doctoral dissertation, University of Osaka, Osaka, Japan, 1961; and Kihara,

H., "Recent Studies in Japan on Brittle Fracture of Welded Steel Structures Under Low Stress Levels," IIW Doc. X-291-62, International Institute of Welding, London, England, 1962.

[28] Hall, W. J., Nordell, W. J., and Munse, W. H., "Studies of Welding Procedures—Parts I and II," *Welding Journal, Research Supplement,* November 1962, p. 505, and *Research Supplement,* April 1965, p. 183.

[29] Ikeda, K., Akita, Y., and Kihara, H., "The Deep Notch Test and Brittle Fracture Initiation," *Welding Journal, Research Supplement,* March 1967, pp. 133–143.

[30] Pisarski, H., "Philosophy of Welded Wide Plate Testing for Brittle Fracture Assessment," *The Fracture Mechanics of Welds,* EGF Publication No. 2, Mechanical Engineering Publications, London, 1987, pp. 191–208.

[31] Walker, F. E., "Steel Quality, Weldability and Toughness," *Steel in Marine Structures,* Elsevier Science Publishers, Amsterdam, The Netherlands, 1987, pp. 49–70.

[32] Royer, C., "A User's Perspective on Heat-Affected Zone Toughness," *Proceedings,* TMS Conference on Welding Metallurgy of Structural Steels, J. Koo, Ed., Denver, CO, February 1987, pp. 255–262.

[33] Denys, R. and McHenry, H. I., "Local Brittle Zones in Steel Weldments: An Assessment of Test Methods," *Proceedings,* Seventh International Conference on Offshore Mechanics and Arctic Engineering, February 1988, pp. 379–386.

[34] Denys, R., "The Effect of Defect Size on Wide Plate Test Performance of Multipass Welds with Local Brittle Zones," *Proceedings,* TMS Conference on Welding Metallurgy of Structural Steels, J. Koo, Ed., Denver, CO, February 1987, pp. 319–334.

[35] Webster, S. E., "The Structural Significance of Low Toughness HAZ Regions in a Modern Low Carbon Structural Steel," *The Fracture Mechanics of Welds,* EGF Publication No. 2, Mechanical Engineering Publications, London, 1987, pp. 59–75.

[36] Woodley, C. C., Burdekin, F. M., and Wells, A. A., "Mild Steel for Pressure Equipment at Sub-Zero Temperatures," *British Welding Journal,* Vol. 11, No. 3, 1964, pp. 123–136.

[37] "Vertical Steel Welded Storage Tanks with Butt Welded Shells for the Petroleum Industry," BS 2654, and "Vertical Cylindrical Welded Steel Storage Tanks for Low Temperature Service: Single Wall Tanks for Temperatures down to −50°C," BS 4751, British Standards Institution, London, England, 1987.

[38] Huppertz, P. H. and Retter, A., "Selection of Materials for Pressure Vessels and Chemical Plants," *Zeitschrift for Werkstofftechnik,* Vol. 11, 1980, pp. 124–133.

[39] Harrison, J. D., "Fracture Prevention in Petro-Chemical Systems," *Proceedings,* Conference on Fracture Prevention in Energy and Transport Systems, Rio de Janeiro, Brazil, November 1983.

[40] Pisarski, H. G., "Basis for the Charpy V Requirements for Parent Plate, HAZ and Weld Metal in the Proposed Revisions to the 1977 Edition of the Department of Energy Guidance Notes," Report for the Department of Energy 3866/2/85, London, United Kingdom, February 1985, pp. 11–40.

[41] Pisarski, H. G. and Harrison, J. D., "Fracture Toughness Considerations for Offshore Structures in UK Waters," *Proceedings,* Conference on Welding for Challenging Environments, Toronto, Canada, October 1985.

[42] Harrison, J. D., Burdekin, F. M., and Young, J. G., "A Proposed Acceptance Standard for Weld Defects Based upon Suitability for Service," *Proceedings,* Second Conference on the Significance of Defects in Welds, London, May 1967.

[43] Burdekin, F. M. and Dawes, M. G., "Practical Use of Linear Elastic and Yielding Fracture Mechanics with Particular Reference to Pressure Vessels," *Proceedings,* Conference on Practical Application of Fracture Mechanics to Pressure Vessel Technology, I. Mech.E. Paper C5/71, Institution of Mechanical Engineers, London, England, May 1971.

[44] Dawes, M. G., "Fracture Control in High Yield Strength Weldments," *Welding Journal Research Supplement,* Vol. 53, No. 9, September 1974, pp. 369–379.

[45] Egan, G. R., "Application of Yielding Fracture Mechanics to the Design of Welded Structures," London University, London, 1972, and "The Application of Fracture Toughness Data to the Assessment of Pressure Vessel Integrity," Paper II.74, *Proceedings,* International Conference on Pressure Vessel Technology, San Antonio, TX, October 1973, p. 1037.

[46] Baker, R. G., Barr, R. R., Gulvin, T. F., and Terry, P., "The Use of Wide Plate Test Data for Design Against Brittle Fracture," Paper II.75, *Proceedings,* International Pressure Vessel Technology Conference, San Antonio, TX, 1–4 Oct. 1973, p. 1049.

[47] Gulvin, T. F., "Brittle Fracture Resistance of Welded Joints of Some High Strength Steels of Medium Thickness," *Proceedings,* International Symposium on the Production and Use of Heavy Plate, Commission of the European Communities, Luxembourg, Belgium, February 1979, pp. 413–466.

[48] Denys, R. M., "Toughness Requirements in Transversely Load Welded Joints—An Evaluation

Based on Wide Plate Testing," *The Fracture Mechanics of Welds*, EGF Publication No. 2, J. G. Blauel and K.-H. Schwalbe, Eds., Mechanical Engineering Publications, London, 1987, pp. 155–189.

[49] Dolby, R. E., "Charpy V and COD—Correlations Between Test Data for Ferritic Weld Metals," *Metal Construction*, Vol. 13, No. 1, January 1981, pp. 20–26.

[50] Denys, R. M., "Wide Plate Fracture Toughness Evaluation of the Weld HAZ of Low Carbon Micro-Alloyed Structural Steel Weldments," *Proceedings*, CIM/CSFM Symposium, Winnipeg, Canada, August 1987.

[51] Willoughby, A. A., "A Survey of Plastic Collapse Solutions Used in the Failure Assessment of Part Wall Defects," Research Report 191/1982, The Welding Institute, Abington Hall, Cambridge, England, September 1982.

[52] Willoughby, A. A., "Recategorisation of Defects in PD 6493," *The Welding Institute Research Bulletin*, July 1982.

[53] Carne, N., Towers, O., and Willoughby, A. A., "The Defect Recategorisation Procedures of PD 6493," *The Welding Institute Research Bulletin*, September 1982.

[54] Musgen, B. and Denys, R., "Auswirkungen fertigungstechnischer Einflussgrossen auf das Verformungs- und Bruchverhalten der Baustahle wahrend der verarbeitung und Anwendung: Report for Forschungsbericht der Studiengesellschaft fur Anwendungstechnik von Stahl und Eisen," Dusseldorf, West Germany, April 1982, pp. 1–210.

[55] Dawes, M. G., "The CTOD Design Curve Approach: Limitations, Finite Size and Application," Research Report 278/1985, The Welding Institute, Cambridge, England, July 1985.

[56] Harrison, J. D., "The "State of the Art" in Crack-Tip Opening Displacement (CTOD) Testing and Analysis," W.I., 7302.10/80/210.2, The Welding Institute, Cambridge, England, 1980.

Rudi M. Denys[1]

Wide-Plate Testing of Weldments: Part II—Wide-Plate Evaluation of Notch Toughness

REFERENCE: Denys, R. M., **"Wide-Plate Testing of Weldments: Part II—Wide-Plate Evaluation of Notch Toughness,"** *Fatigue and Fracture Testing of Weldments, ASTM STP 1058,* H. I. McHenry and J. M. Potter, Eds., American Society for Testing and Materials, Philadelphia, 1990, pp. 175–203.

ABSTRACT: This paper, which is Part II of this series on wide-plate testing of weldments, reviews various wide-plate test specimen designs in relation to their intended uses. In addition, some specimen designs are discussed which are recommended for particular structural details that cannot be modeled by means of a flat uniaxial wide-plate test. Further, the preparation and testing of wide-plate specimens are reviewed. Finally, consideration is given to certain aspects of the weldment test procedure and to the interpretation and significance of wide-plate test results.

KEY WORDS: weldments, wide-plate testing, crack-tip opening displacement (CTOD), Charpy V-notch impact test, brittle fracture, residual stress, defects, cracks, notches, toughness requirements, high-strength steels

Nomenclature

a	Length of a through-thickness crack
a_{gy}	Maximum length of a through-thickness crack producing gross section yielding in a wide-plate test specimen
CTOD	Crack-tip opening displacement, as measured in a conventional bend test
COD	Crack-mouth opening displacement, as measured in tension on a small gage length
CY	Contained yielding
E	Young's modulus
e	Overall strain
GSY	Gross section yielding
l	Length of a surface-breaking crack
NSY	Net section yielding
P	Applied load
SCF	Stress concentration factor
t	Defect depth
y	Gage length
W	Plate width
σ_n	Average net section stress at fracture

[1] Professor and manager, Laboratorium Soete Rijksuniversiteit Gent, B 9000 Gent, Belgium.

σ_N Gross section stress (load/gross section)
σ_y Yield strength (subscripts pl = plate, w = weld).

The fracture resistance of base metals and weldments to brittle/low-strain fracture cannot be studied without the presence of a preexisting crack, unless the testing temperature is very low. Indeed, it is only when a mechanical-notched or a fatigue-precracked specimen is tested that fracture with reduced ductility may be obtained. The reason for the difference between cracked and uncracked specimens in test performance is associated, first with the concentration of stresses at the tip of the crack and, second, with the development of a triaxial stress system at this same point.

The majority of the proposed small-scale test specimen designs, developed to provide criteria for material selection and defect assessment, do not, because of their size, reproduce the relevant factors of service performance.

The cracked wide-plate test specimen is the only laboratory test specimen which can model many structural details of interest. However, the performance level of a cracked wide-plate test specimen depends mainly on the crack size, the test temperature, and the notch and fracture toughness properties of the material sampled. Furthermore, the fracture initiation characteristics of the test specimen depend also on the combined effects of (*a*) the plate section thickness, (*b*) the crack acuity, (*c*) crack shape, (*d*) crack orientation, (*e*) crack position, (*f*) the presence of geometric stress concentrations, (*g*) the degree of tension or bending, and (*h*) the property interaction of the materials present in a weldment. These observations illustrate quite clearly that a meaningful specimen configuration must be selected to duplicate as closely as possible the structural detail under consideration. In other words, in order to obtain structure-specific test data, the test specimen geometry, the arrangement of the test weld with respect to the loading direction, the design of the crack, and the type of loading must bear a relationship to service conditions. In this context, consideration must also be given to the inherent spread in the yield and tensile strength properties of the parts composing the weldment. This problem, however, shall not be pursued here.

In the following sections, the most commonly used "flat" specimen designs suitable for examining the effects on wide-plate performance of "uniaxial" tensile stresses are reviewed. In some situations, however, flat wide-plate specimens are unsuitable for simulating a particular structural detail. Consequently, the flat specimen design must be modified to suit the structure-specific requirements. For these cases, guidance is given for optimizing wide-plate specimen design. In addition, the preparation and testing of wide-plate specimens are reviewed. Since the testing method has altered considerably in recent years, certain aspects of the weldment test procedure and of the interpretation and significance of wide-plate test results are addressed toward the end of this paper.

Wide-Plate Test Specimen Designs

It must be apparent that there is no single wide-plate test specimen design. A wide variety of specimen designs is available for evaluating base metal and specific weldment geometries. The choice of a structurally representative specimen design depends on the design of the structural detail, the intended service condition, and the type of information required.

Wide-Plate Test Specimens Dimensions

No standard plate widths have as yet been adopted for wide-plate test specimens. In most instances, the nominal specimen dimensions are determined by the design of the testing equipment, its load capacity, the test plate tensile properties, and the crack size. In Europe, specimen widths between 300 and 1000 mm are commonly used, while, in Japan, 400 to 500-mm-wide specimens are considered standard. It is also true that in Japan much wider (up to 2000-mm) plates are tested.

After reviewing the development of the wide-plate specimen, one can see that there is no adequate basis available for establishing the minimum specimen width. In particular, difficulties arise with extensive yielding. In these instances, the high intrinsic material ductility present produces conditions in which the strain hardening strongly affects the type of yield zone development (contained versus net or gross section yielding). Because the crack dimensions determine the extent to which strain hardening occurs, there is little doubt that a quantitative answer to this problem is difficult to obtain.

Despite the complexity of the plate width issue, some experts [*1*] recommend that the crack length to plate width (a/W) ratio should be smaller than 0.1 in order to produce wide-plate toughness data representative of full-scale behavior. No attempt is made in this review to report in detail the experiments which have led to this limiting value, but some comments are in order. When applied to higher strength steels having a low strain-hardening capacity, the mentioned limiting value may be inadequate (too optimistic) and may thus produce incorrect wide-plate test performance levels because of the occurrence of undesirable plate edge effects [*2*]. On the other hand, it is also possible that the width in practical ($W > 1000$ mm) wide-plate specimens may be insufficient for low-strength materials with sufficient inherent ductility. In other words, a specimen size sufficient to simulate the practical constraint at a given temperature will be more than sufficient at a much lower temperature and insufficient at a much higher temperature. From an applications viewpoint, it is clear from the information reviewed above that vigilance must be exercised to guarantee that the specimen dimensions are truly representative of the service condition of interest.

In the author's opinion, some other definition of minimum specimen width is required. First, and whenever possible, the plate width in welded specimens should be maximized in order to incorporate correctly the effects of residual stress on wide-plate specimen performance. Second, instead of limiting the a/W ratio, the yielding pattern at fracture should be used as the governing criterion to demonstrate that the test results are not affected by the specimen dimensions. Wide-plate tests giving rise to contained (net section fracture stress $\sigma_n < \sigma_y$) or gross section yielding (gross section fracture stress $\sigma_N > \sigma_y$) at fracture are considered to satisfy the above requirement, as it is believed that the plate edge effects on wide-plate test performance are negligible in these instances (Fig. 1). After testing, it should thus be verified that the plate edges remained parallel during the test; i.e., in order to produce realistic wide-plate test data, a minimum plate width should be tested so that the proximity of the plate edges does not influence the deformation behavior during testing. This criterion implies also that brittle material behavior (i.e., when fracture is associated with contained yielding) may be studied by means of narrow plates, while ductile material behavior requires testing of wide plates.

The information contained in Ref *3* suggests, in the case of ductile material behavior, that the lower the material's yield strength, the wider the specimen width should be. This requirement reflects the fact that the yield zone development (and thus relaxation of constraint) depends on the combined effects of yield point elongation, the strain hardenings rate, the plate thickness, the testing temperature, and the crack dimensions. Moreover, the spread of yielding in a direction about 45° to the tension axis or in planes forming an angle of some 45° to the plate surface, or both, further affects the sequence of relaxation of crack-tip constraint and thus the choice of the plate width.

Finally, it should be emphasized that the constraint to crack-tip deformation is more readily relieved in a narrow specimen than in a wide-plate specimen. The results of narrow-

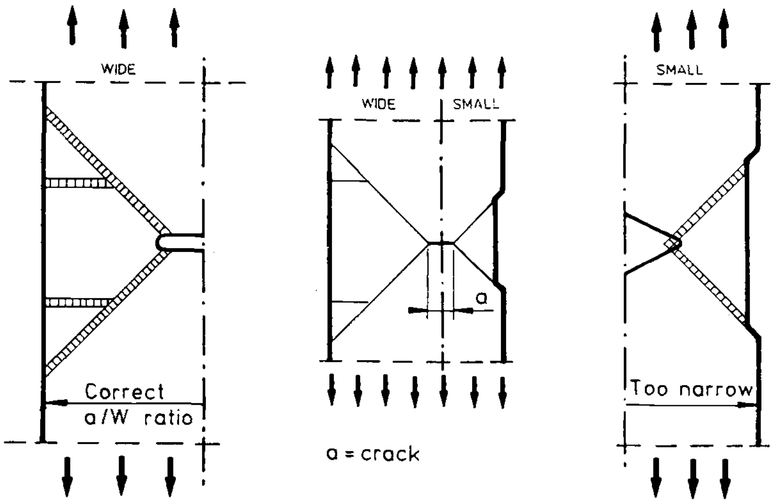

FIG. 1—*Schematic showing the effect of plate width on wide-plate specimen deformation behavior. The hatched bands represent plastically deformed material.*

plate tests may therefore differ from the test results for wider specimens. This implies that care is required in interpreting the results of narrow "wide-plate specimens" since (*a*) the measured gross strain will be too large, (*b*) the measured gross stress will be too small, and (*c*) the measured COD will be too large [*3*].

Flat Wide-Plate Test Specimen Designs

A "flat" wide-plate test specimen is a specimen designed so that its fracture behavior during testing is not affected by stress gradients produced by geometric discontinuities, such as angular distortion, misalignment, and so forth. Flat wide-plate specimens fall into two basic groups: unwelded (base metal) specimens and welded specimens. For the latter, a further distinction is made between (*a*) single-welded and (*b*) multiple- or cross-welded wide-plate specimens. Each of these may be loaded (*a*) in tension, (*b*) by bending, or (*c*) with a combination of tension and bending. In what follows, emphasis will be laid on tension-loaded specimens [*3–11*].

Base Metal Wide-Plate Specimens

Center-cracked or edge-cracked wide-plate specimens are suitable specimen designs for studying the fracture initiation characteristics of the base metal (Fig. 2). More particularly, since the dimensions of the crack, its acuity, and its shape in relation to the test specimen as a whole affect the deformation pattern at fracture, the base metal wide-plate test is also capable of assessing the base metal's resistance to brittle fracture, along with the conditions for plastic collapse. Various crack configurations can be tested. There is a choice between through-thickness (center or edge) and surface-machined notches or fatigue cracks. For surface cracks, the effects of various length/depth aspect ratios can be studied.

In Japan, the deep-notched wide-plate specimen [*4*] is often used in a base metal characterization test. This specimen is normally 500 mm wide and contains two edge-machined notches either 80 or 120 mm long. Because of the notch length, this specimen design induces

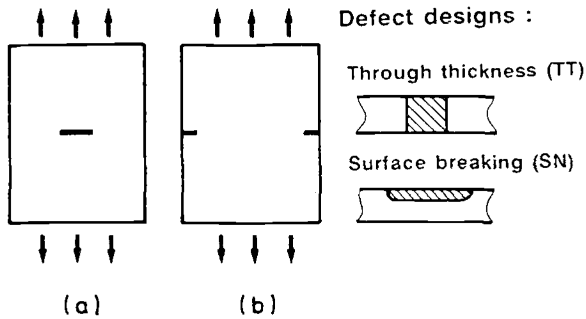

FIG. 2—*Notched base metal wide-plate specimen designs:* (a) *center notched;* (b) *double-edge deep notched (TT = through thickness; SN = surface notched).*

a high degree of triaxial constraint, which causes the spread of plastic deformation to be confined always to the notched section. As a result, deep-notch wide-plate data will always produce lower bound fracture toughness estimates.

The results of base metal wide-plate tests have been and are being used to validate fracture mechanics data based defect assessment procedures. The test results are also used to preclude the use of the base metal as its lower shelf ductility range (transition temperature approach). For this reason, the base metal wide-plate test is mainly conducted by steel manufacturers with the aim of exploring the toughness limits of newly developed structural steels in relation to temperature. For that purpose, Japanese researchers invariably use the deep-notched specimen, while the central-notched specimen is most widely used in Europe.

Welded Wide-Plate Specimen Designs

As can be seen in Fig. 3, a distinction is made between longitudinally and transversely loaded welded wide-plate specimens. These specimens are notched or fatigue precracked so that the plane of the crack is perpendicular to the direction of the applied stresses. In the longitudinal weld test, the notch tips are located in the heat-affected zone (HAZ) of the longitudinal weld, while in the transverse test, it is possible to locate the notch in the base metal, the HAZ, or the weld metal. Note that it is normal practice to arrange the plate rolling direction parallel to the plane of the crack.

From a metallurgical point of view, the choice between a longitudinally or a transversely loaded test specimen depends upon the type of HAZ embrittlement to be assessed. The visible or transformed grain coarsened HAZ regions (which include the unrefined metal heated to a temperature in excess of 1200°C and both the intercritical and subcritical reheated grain coarsened regions) adjacent to the fusion boundary normally have a lower toughness than the other parts of the HAZ. These regions are also called local brittle zones (LBZ) (see the next paper). The degree of embrittlement and the size and location of these fabrication-induced coarse-grained HAZ regions depend primarily on the steel chemistry, the heat input (cooling rate/thermal cycle), the angle of attack between the electrode and the preparation edge, and the degree of weld bead overlap [5]. The other HAZ regions that may give rise to a loss of toughness are associated with the intercritical (heated to 720 to 900°C) and the subcritical HAZ (heated to less than 720°C). Subcritical HAZ embrittlement may be significant if the welding is performed in the presence of a strain concentrator sited in the base metal microstructure, because the material at the tip of a preexisting crack, which is not melted out, is also strained during the welding process. This form of embrit-

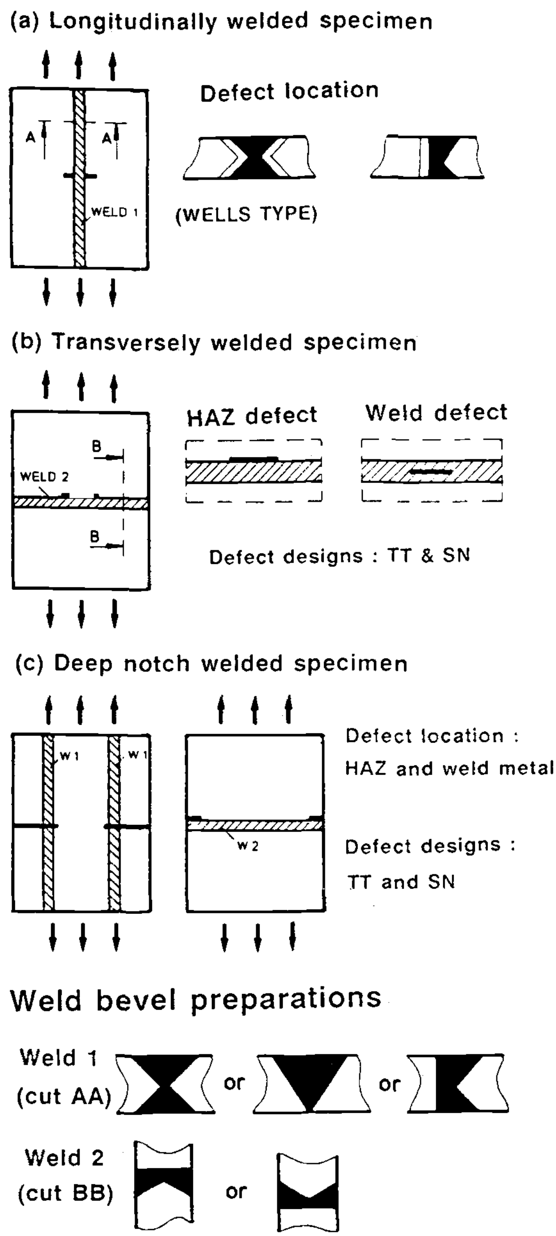

FIG. 3—*Single-weld and notched wide-plate specimen designs* (*TT* = *through thickness; SN* = *surface notched*).

tlement, however, is less marked in microalloyed steels, where, in general, the transformed coarse-grained HAZ shows the greatest embrittlement.

As cracks formed during or subsequent to welding may be sited with their tips at any point in the HAZ, it is necessary in addition, to account for this effect in HAZ testing. Crack orientation (parallel versus transverse to the fusion boundary) may theoretically result in different measured toughnesses when the tips of the crack sample the same microstructure. However, the chance that a transverse crack will sample a larger portion of coarse-grained material than a crack lying parallel to the fusion boundary is rather small (Fig. 4).

A further complicating feature in the choice of a longitudinally or a transversely loaded welded wide-plate specimen is related to the effect of the relative strength of the weld metal and surrounding base metal on deformation behavior. The practical effect of this difference is directly related to the direction of the applied (remote) strain and depends upon whether the weld metal is constrained to deform in the same manner as the adjacent base metal or whether it is free to behave as a separate unit (Fig. 5). Provided the applied stress is parallel to the weld, the former situation can be modeled by a wide-plate specimen containing a longitudinal weld, while the latter situation can be modeled by a transversely welded wide-plate specimen.

In light of the previous observations, it is obvious that the effects of the various types of embrittlement, crack orientation, and weld matching can be assessed in various ways. These effects can be evaluated separately, by means of single weld, or together, by means of multiple-weld wide-plate test specimen configurations.

Single-Weld Wide-Plate Specimen Designs

Longitudinally Welded Test Specimen—The longitudinal weld specimen is strained parallel to the weld. In this specimen configuration, the weld, heat-affected zone, and base metal are strained equally and simultaneously. The weld metal, regardless of strength, will be forced to strain with the base metal (Fig. 5*a*). This implies that weld metal overmatching will not be beneficial in test performance.

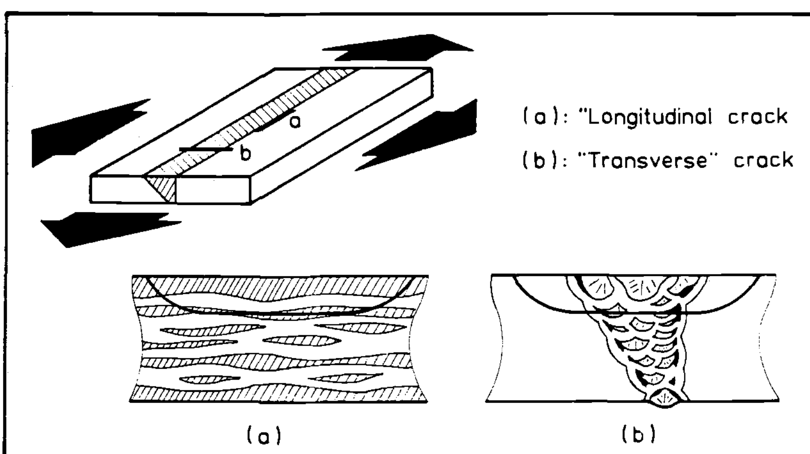

FIG. 4—*Effect of defect orientation on the probability of sampling coarse-grained HAZ (CGHAZ) regions. The CGHAZ regions are hatched* (a) *or fully black* (b); *the open regions are grain-refined material.*

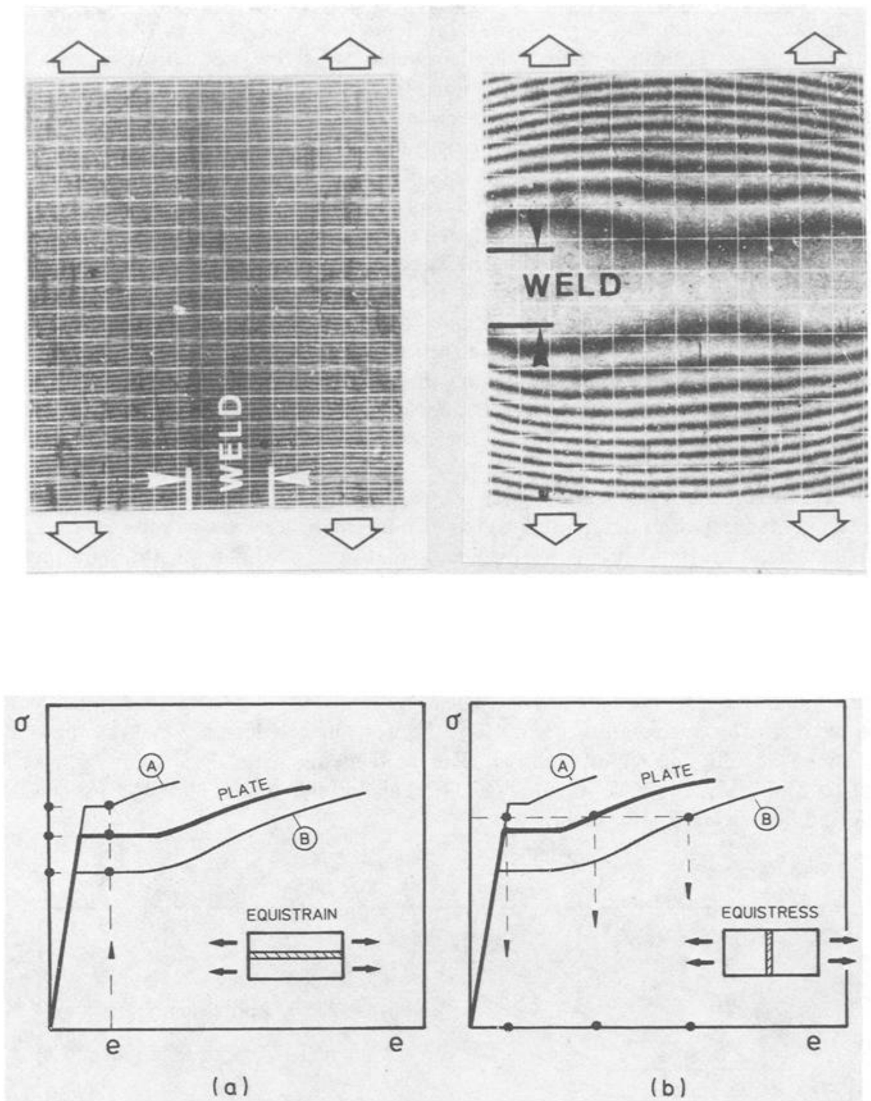

FIG. 5—*Effect of weld metal yield strength overmatching/undermatching on the weldment deformation performance (the line grid density is 10 lines/mm): Curve A, overmatching weld metal; Curve B; undermatching weld metal;* (a) *longitudinally loaded weldment;* (b) *transversely loaded weldment.*

The interest in the longitudinally welded specimen lies in the ease with which the effects of longitudinal tensile residual stresses can be studied. Provided the plate width is sufficiently large, the tensile residual stresses can reach their maximal amplitude of yield point level. It should be noted that, because of the nature of longitudinal residual stresses, their effect is confined to regions close to the weld zone. Therefore, it is important to note that the effect of residual stresses on test performance depends on the crack size.

The longitudinally welded test specimen can be used to assess the degree of strain-aging damage experienced by preexisting defects in a weldment. In a more general context, one should note that the material toughness/fracture resistance at the crack tip also plays an important role in test performance. The effect of residual stresses on fracture performance is more important where the failure may occur under elastic conditions, whereas in elastic-plastic conditions some of the residual stresses will be relaxed by plastic deformation.

In cases where strain-aging damage is a matter of concern, the longitudinally welded (Wells-type) [*6*] wide-plate specimen is mechanically notched *before* being welded (Fig. 3*a*). In the Wells-type test, the length of the crack is bound to the subcritical HAZ and is thus dependent on heat input [*7,8*]. Thus, the notch tips have to follow the weld preparation. When the weld bevel preparation is a double V, the notches take the form of chevrons; straight fronted notches can also be tested by using a K-weld preparation. When the notch is introduced *after* welding, the specimen configuration is less severe because of the absence of strain-aging effects. Finally, the longitudinally welded specimen is also adequate for evaluating cases where weld-metal hydrogen-induced chevron cracks are present.

Transversely Welded Test Specimen—The effect of a crack, sited parallel to the fusion boundary in the plate material, in the coarse-grained HAZ region, or in the weld metal deposit, on weldment performance can be evaluated with a wide-plate specimen in which the weld is arranged transverse to the applied load (Fig. 3*b*) [*8–10*]. This specimen design allows testing of any crack shape, i.e., through-thickness, surface-breaking, or buried. By varying the crack dimensions, a sensitivity study of their significance to fracture resistance can easily be performed. More particularly, this design is perfectly fit for assessing the beneficial effect of weld metal overmatching. As shown in Fig. 3*c*, the deep notch test has also been proposed for testing the transformed HAZ or weld metal regions [*11*].

When assessing the result of a transversely loaded wide-plate specimen it should be borne in mind that, although the nominal stresses across all regions of the test weld are the same, the nominal strains in these regions may be different (Fig. 5*b*). The other important point about the transversely loaded weldments is that when the weld metal yield strength overmatches that of the plate, nearly all of the plastic strain occurs outside the weld, while the load-extension behavior of the whole specimen is controlled by that of the base metal (Fig. 6). For undermatching weld metal, the plastic strain and fracture will be confined to the weld metal region, while the load-elongation behavior of the weldment will coincide with that of the weld metal [*13*]. The practical implication is that undermatching weld metals require vastly increased toughness in the presence of weld cracks.

When the weld metal yield strength significantly exceeds that of the plate, extensive yielding and strain hardening of the plate is needed to reach the weld metal yield strength. Provided that the size of the weld crack is such that all regions of the weldment are not constrained to deform simultaneously, the overmatching weld metal will be protected from straining plastically for stress levels of plate yield magnitude (Fig. 7, Curves A and B). This protection will not be effective when the weld metal toughness is so poor that it leads to failure under elastic conditions. Alternatively, if the crack dimensions are such that all regions of the weldment are forced to deform simultaneously, the use of overmatching weld metal will provide very little or no protection from the overmatching yield strength (Fig. 7*b*, Curve D). Another conclusion which follows from the preceding finding is that crack size largely determines weldment performance [*2,3,12–14*].

Multiple-Weld Wide-Plate Specimen Designs

As noted previously, the single longitudinal weld test specimen is not very practical in that transverse service cracks sampling the whole subcritical HAZ are very rare. On the other hand, no advantage can be taken of the single-weld transverse test specimen for

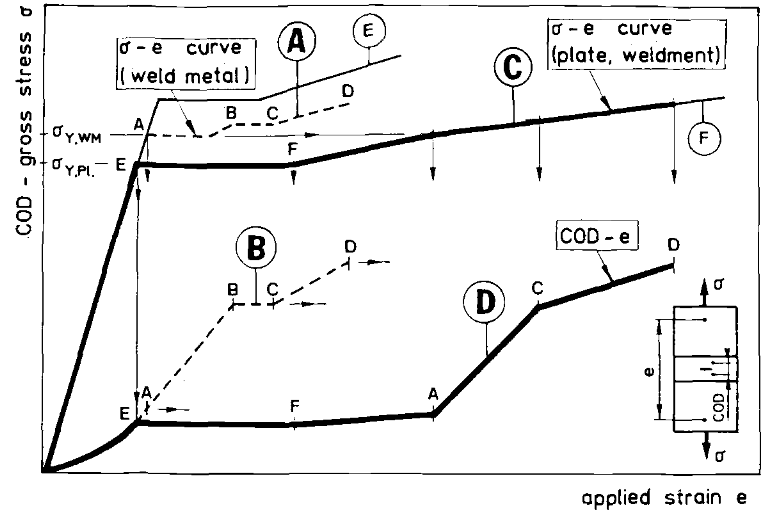

FIG. 6—*Schematic diagram illustrating the correspondence between the applied gross stress-strain* (σ-e) *and the crack-mouth opening displacement/strain* (*COD*-e) *curves for* (a) *notched weld metal only* (*Curves A and B, dashed lines*) *and* (b) *transversely loaded weldments* (*Curves C and D*), *where* E = *the weld metal stress-strain curve and* F = *the base material stress-strain curve. Note that the circled letters in the figure identify the curves, while the noncircled letters identify the interaction between the COD and gross stress with increasing strain.*

studying the effects of yield-amplitude tensile residual stresses. In order to take account of the combined effects of the stresses, multiple-weld wide-plate specimens containing a longitudinal and a transverse weld are worthy of consideration [*15–18*]. It should be noted here that the weld metal yield strength of the transverse weld may become a key factor in wide-plate test performance: overmatching weld metal yield strength properties may be beneficial, while undermatching could produce poor test results. The test, therefore, should be designed to reflect the behavior of the actual weldment in the structure.

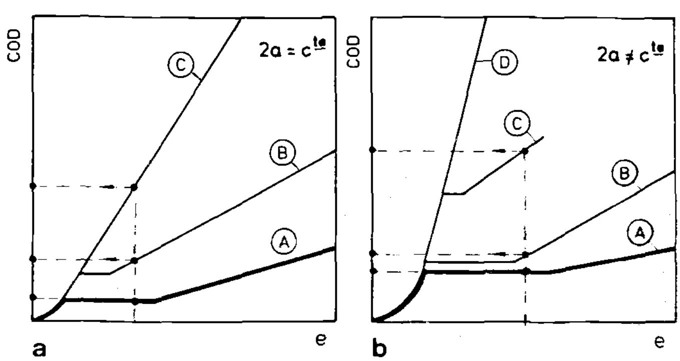

FIG. 7—*Schematic illustrating the dependence of the crack-mouth opening displacement* (*COD*) *on applied strain in a transversely loaded weldment with overmatching weld metal yield strength:* (a) *the effect of weld metal yield strength overmatching for a fixed crack length* (*A, highly overmatched; B, overmatched; and C, undermatched*); (b) *the effect of crack length* ($a < a_1 < a_2 < a_3$) [*A; highly overmatched with* $a = a_1$; *B, C, D, overmatched with* $a = a_1$ (*B*), $a_2 > a_1$ (*C*), *and* $a_3 > a_2$ (*D*)].

The influence of transverse cracks in multiple welds at intersecting butt joints where a crack longitudinal to one weld is transverse to the other is representative of a number of practical situations. In such cases, the crack tip might be sited in the transformed grain coarsened HAZ, where thermal straining may reduce the toughness locally at the crack tip. This situation can be modeled and evaluated by means of a wide-plate specimen containing crossing welds. The variations shown in (Fig. 8) allow various possibilities to be studied.

In the straight cross-welded specimen (Fig. 8*a*), the tip of a crack is subjected to an additional deformation cycle when the crack is located in the grain coarsened HAZ regions of the transverse weld before the final longitudinal weld is made. The weld edge preparation, a chevron-shaped or a straight-fronted notch, can be tested by using a double-V- or K-weld preparation, respectively [*8,10*]. If the concern is related to the effect of the longitudinal residual stresses on a transverse crack sited in the transformed HAZ or the weld metal

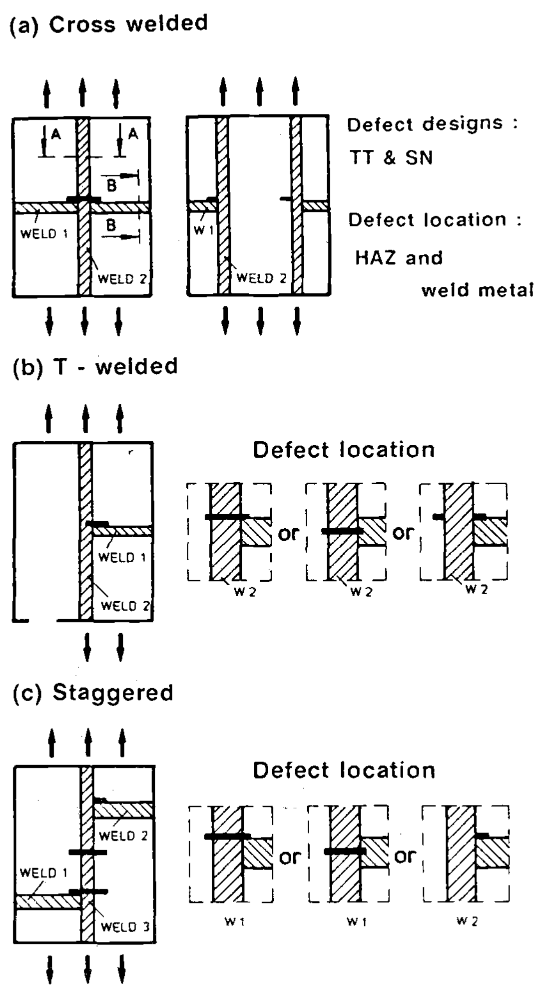

FIG. 8—*Typical notched and welded multiple wide-plate specimen designs. Note that the defect location can be varied to sample the region of interest (TT = through thickness; SN = surface notched).*

deposit of the transverse weld, it is not necessary to make the notch before welding is initiated (Fig. 9) [*19–23*]. In the latter case, the notch length can be freely chosen.

Another and perhaps more suitable specimen design for evaluating the effect of yield magnitude residual stresses on cracks located in the transformed HAZ consists of testing a T-welded wide-plate specimen. The transverse weld could be made with the "weld consumable to be tested," whereas the longitudinal weld is made by a consumable with high notch toughness (Fig. 8*b*). To find out whether fracture initiation is more likely to occur in the transformed HAZ or the subcritical HAZ, the tips could be located in the grain coarsened HAZ of the transverse weld, while the other notch tip would be located in the subcritical HAZ of the base metal side of the T-weld.

The poorest region of the weld can be identified by testing the wide-plate specimen design shown in Fig. 8*c*. The use of notches in various positions along the specimen length should not be encouraged because the yielding pattern belonging to each of the parallel notches will affect the other notches if the spacing (in the direction of the applied load) between them is smaller than the plate width [*14*]. However, this restriction is not applicable if fracture is expected to occur in the elastic (contained yielding) condition or where the specimen is designed to test multiple parallel cracks close together (as could be the case from chevron cracks).

Wide-Plate Tests on Structural Details

The effects of an in-service stress/strain gradient in the form of a geometric discontinuity or the like can be evaluated either by means of a tension-loaded flat wide-plate specimen test, in combination with an appropriate toughness requirement (discussed further on in this paper), or by considering a tension-loaded wide-plate test specimen design in which the stress gradient is directly incorporated. The viewpoint that must be adopted is that, although "modified" wide-plate tests may provide useful information, they cannot always be used as a substitute for tests on structural details. Therefore, where possible, one should always attempt to model stress gradient effects truly if the required testing equipment is available.

Wide Plate Tests in Bending

Instead of testing a tension-loaded specimen, consideration could also be given to the use of a flat wide-plate test specimen tested in three-point or four-point (pure) free bending,

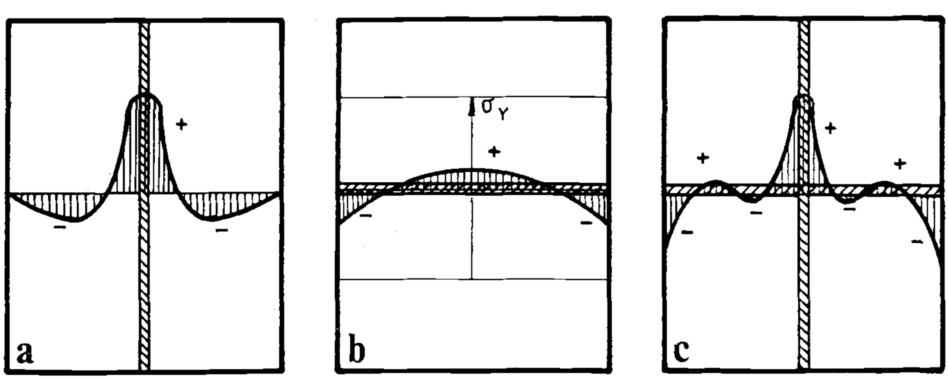

FIG. 9—*Residual stress patterns in butt welded joints:* (a) *longitudinal joint,* (b) *transverse joint, and* (c) *cross joint. For cases* (a) *and* (c), *the residual stresses can be as high as the yield point magnitude. For case* (b), *the residual stresses are much less, a typical value is 20% of the base metal yield strength.*

the former loading condition being more severe than the latter [24–25]. For specimens loaded in (free) bending, the span length to specimen thickness ratio for three-point bending is important, since this ratio determines whether the test is conducted in either shear or bending stress control. Pure bending or four-point symmetrical loading eliminates the effect of shear between the central loading points so that fiber elongations are proportional to the distance from the neutral axis of the specimen in the elastic loading range and approximately so in the plastic region. Four-point loading is advantageous for testing transverse welded specimens because the weld, HAZ, and base metal are stressed simultaneously in the constant-moment central section of the test specimen. In this instance, bend ductility performance can readily be evaluated by measuring the elongation of the outer fibers. The three-point bend test configuration, however, is less convenient for measuring elongation over a large gage length. Particularly for deep cracks, the deformation preceding specimen failure will be concentrated in the plane of the crack (in contrast to the spread of yielding in a CTOD test). In the case of ductile behavior, the applied deformation will cause bending of the specimen, and this may result in specimen shorting when the elongation is measured over a large gage length.

There is a similarity in results between the three-point bend wide-plate test with an infinite long crack and the CTOD test. In other words, the wide-plate bend test represents an "extra" wide CTOD specimen. The deformation behavior of the CTOD test specimen (which contains a continuous crack across the specimen thickness) and that of a wide-plate bend specimen can be made different by obstruction of free bending through limiting the crack length in the wide-plate bend specimen.

The performance characteristics of a wide-plate bend test specimen depend very much on the crack size. This effect will complicate evaluation of the test result. The yielding pattern in the wide-plate bend specimen containing an infinite *long* and *deep surface* crack will consist of a plastic hinge (curved slip lines) (Fig. 10*a*). When the same crack depth is tested in a tension-loaded wide-plate specimen (Fig. 10*b*), the yielding pattern will spread along planes inclined at approximately 45° to the loading direction (45° through-thickness yielding, straight slip lines). The differences in yield spread will also affect the relaxation of triaxial constraint at the crack tip. The relief of constraint in a tension-loaded specimen will happen at an earlier stage than that in a bend-loaded specimen. For this reason, other things being constant, wide-plate bend specimens will fail at lower stress/elongation levels than tension-loaded specimens. For the situations in which relief of crack tip constraint is

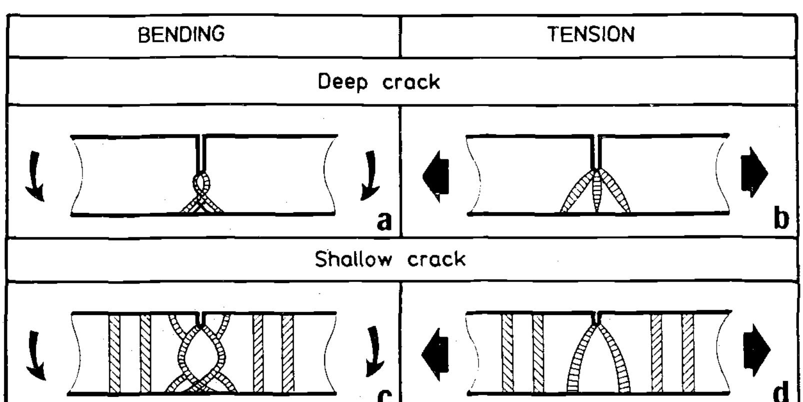

FIG. 10—*Schematic representation of yield deformation patterns ahead of the crack tip:* (a), (b) *for deeply notched and* (c), (d) *for shallow single-edge notch bending and tension specimens.*

possible, the effect of the differences between yield spread mechanisms on wide-plate test performance will disappear gradually as soon as the plane of the crack is plastically deformed. When this occurs, the wide-plate bend test specimen permits accommodation of both a plastic hinge and 45° through-thickness plastic deformation.

When smaller but sizeable cracks in strain-hardening materials are tested, the difference in the spread of yielding between a bend- and a tension-loaded specimen will hardly differ in the plane of the crack. At higher loads, strain hardening may cause yielding in the remote uncracked specimen section, so that the two loading modes will produce quite similar plastic deformation patterns before specimen failure ensues (Fig. 10, *c* and *d*).

In a bend test it is also desirable to locate the crack tip as near as possible to the surface on the tension side of the plate, where the imposed bending stresses are highest. However, the use of a shallow crack conflicts with the desired achievement of triaxial restraint in the direction of plate thickness. Thus, since the deformation mode [compare the in-plane and 45° through-thickness yielding (Fig. 10, *a* and *b*)] developed prior to fracture initiation is the deciding factor in wide-plate test performance, it could well be that neither the pure tension-loaded nor the pure bend-loaded wide-plate specimen provides the required information.

Direct Modeling of Structural Details

The next step in the testing of stress gradients consists of reproducing the actual stress/strain gradient present in the structure. In some cases, this problem can conveniently be solved by choosing a specimen design that models the combined effects of tension/bending-related stress gradients. The transversely loaded butt-welded specimen in which effects of angular distortion and misalignment (Fig. 11) are directly incorporated is a suitable specimen configuration for achieving this aim. Angular distortion/misalignment causes a local increase in stress on one surface in the region of the weld so that the acting stress equals the remote applied stress and the bending stress because of angular distortion/misalignment. The actual bending stress level in this form of specimen depends on the degree of angular distortion/misalignment and the acting restraint to weld rotation. When the restraint to rotation cannot be maintained during the test, insignificant test results can be produced.

A further alternative specimen design consists of a wide-plate tension specimen containing a local stiffener or stiffeners. This test configuration is suitable for testing the combined effects of tension and bending. Again, various designs can be proposed. As an example, Fig. 12 shows that a distinction can be made between load-carrying and non-load-carrying joints.

A quite new specimen configuration is currently being used to test the girth and longitudinal welds in line pipes. As shown in Fig. 13, either the full pipe or part of it can be tested [*26*]. In the case of full section pipe testing, the maximum pipe dimensions (diameter by wall thickness) are determined by the loading capacity of the test equipment [approximately 10 kN (1000 tons), at Gent University, Belgium]. For large-diameter pipes, recourse must be made to the more versatile "curved wide-plate test." With this specimen configuration, the pipe curvature is retained. This is achieved by welding the curved test specimen onto special transition pieces so that the centroid of the prismatic test section coincides with that of the machine lugs. This design has, in comparison with flattened specimens, the advantage that the detrimental effects of cold deformation, induced during the flattening of a curved pipe segment, are completely eliminated. Because of the specimen design, the arc length in the prismatic cross section is limited to about 300 to 400 mm.

The preceding review illustrates that relatively simple joints and structural details can be readily modeled by means of a flat wide-plate specimen. However, more complex details

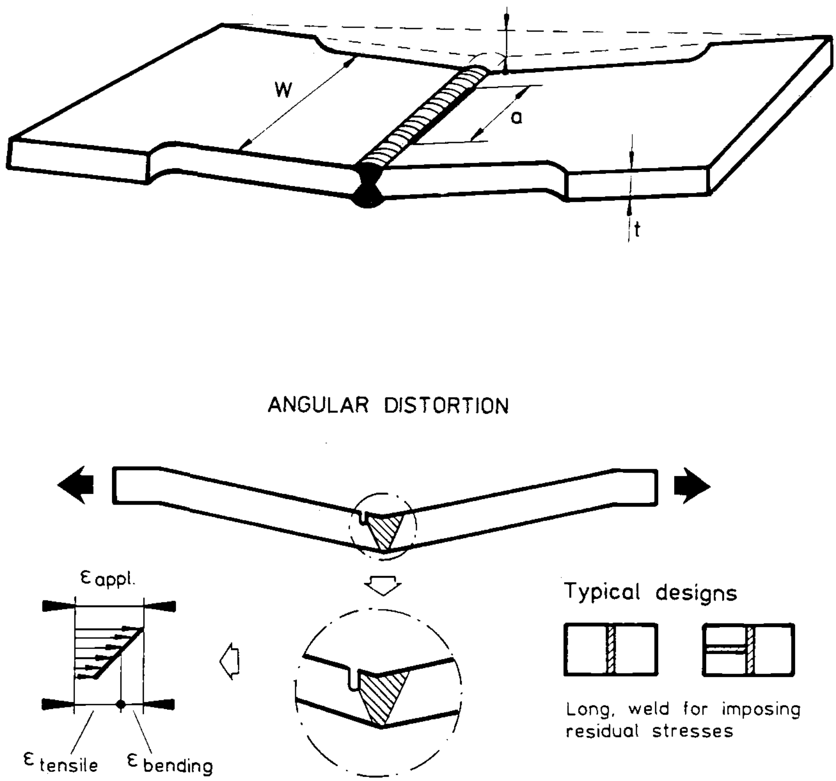

FIG. 11—*Schematic of a notched and welded wide-plate specimen with incorporated angular distortion.*

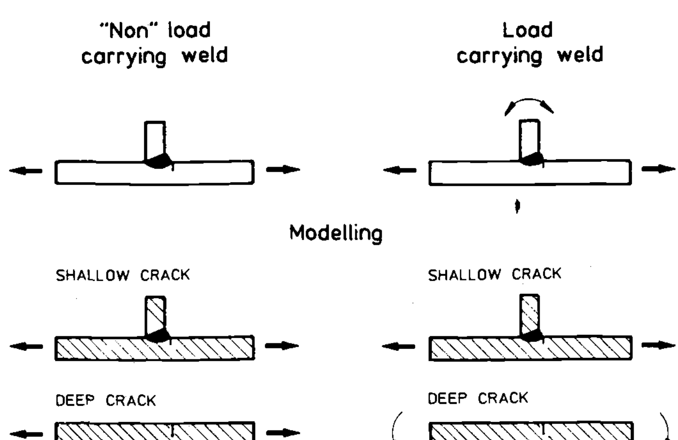

FIG. 12—*Wide-plate configurations for modeling of structural details.*

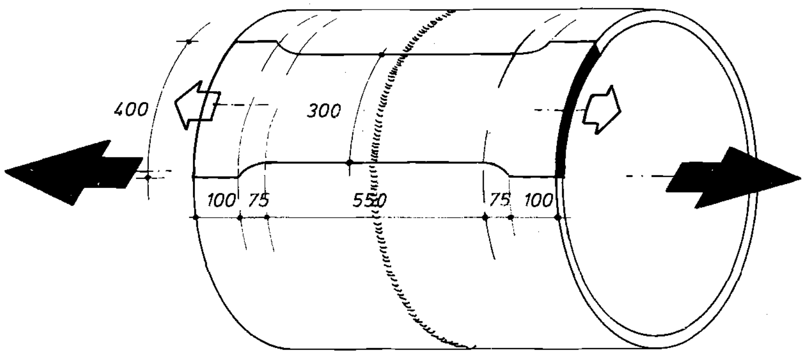

FIG. 13—*Full-size pipe tension and curved wide-plate specimen configurations.*

cannot always be modeled for testing on a laboratory scale because of the constraints imposed by the available testing equipment.

Crack Preparation

As stated earlier, crack size has a quite important effect on wide-plate test performance. In addition, a crack of a particular size and shape may vary in its significance according to its position in the weldment, the nature of the service required from the weldment, and the structure within which the weld is contained. Although, a detailed discussion of this subject is beyond the scope of this paper, it is important to be aware of the significant variables involved in the choice of the crack shape and size [*3,14*]. This choice depends upon such factors as the specimen geometry, testing temperature, properties of the base and weld metal, weld joint design, specimen thickness, loading mode, residual stresses, the kind of information needed, and other factors. On the other hand, it would also be reasonable to choose the crack configuration that resembles the type of flaw likely to occur in service. For example, lack of penetration might be best modeled by lack of penetration.

Crack Shape

Apart from testing natural defects, there are two crack geometries, i.e., the through-thickness and the surface crack, which are often used in wide-plate testing. The through-thickness crack was commonly employed in the early days of wide-plate testing [*8*]. This crack geometry was most effective in its ability to produce low-strain fractures, although those tests were not designed to measure specific crack size effects, but only to find the temperature limit below which a large reduction in ductility, in the presence of a notch sampling brittle material, occurred.

In support of the desire for evaluating crack geometries other than through-thickness cracks, surface cracks are now frequently used to account for crack shape effects and, above all, to enable a particular microstructure to be sampled. It is evident that, for the elastic-plastic case where yielding can no longer be treated as small, testing surface cracks may help to estimate the conservatism inherent in the use of the linear elastic fracture mechanics based crack conversion method. Note that the degree of conservatism will vary with the crack length/depth ratio, the size of the uncracked ligament in the back face direction of the test specimen, and the yield strength properties of the material.

When the simulation of a leak-before-break type of crack is not required, it is obvious that testing a through-thickness crack is not as structurally relevant. On the other hand, it is extremely difficult, if not impossible, to sample significant amounts of low-toughness HAZ regions by the use of a through-thickness crack (see also the next paper of this series). For these reasons, and since the large majority of service imperfections are nearly always surface breaking, it is now usual practice to employ surface cracks. In this connection, the type, location, shape, and size of a surface-breaking crack can be easily adapted to simulate the effect of natural cracks and service fatigue crack growth on weld joint performance. Finally, it is obvious that the crack dimensions should be chosen so that they are conservative and also incorporate service fatigue crack growth.

Crack Tip Acuity

Crack tip acuity is a critical feature in fracture testing, particularly when brittle material behavior is due to occur. In order to obtain a realistic indication of the material's resistance to fracture initiation, fatigue-sharpened cracks should be tested. Whenever possible, testing of machined defects should be avoided.

To facilitate dimensional control and to assure a correct placement of the crack tip in the desired sampling position, a machined crack starter notch is needed. Fatigue-sharpened surface cracks are easy to produce in either three- or four-point bending fatigue. Various types of mechanical starter notches (see the next paper) can be used provided that they have a sufficient degree of sharpness to produce fatigue cracks in a reasonable number of cycles. A blunt mechanical starter notch is normally resistant to initiation around its entire periphery; therefore, it is normal practice to use a high initiation load, which is subsequently lowered when initial fatigue crack growth is observed. In any case, care should be taken that the notch preparation technique does not change the local material conditions near the crack tip, so that the fracture behavior of the wide-plate specimen is not affected by the fatigue precracking process.

Wide-Plate Test

Instrumentation

The maximum or fracture load is not the only quantity to be recorded during the test. Monitoring the overall and local deformation of the specimen is just as important. During the test, the output signals of a load-sensing transducer, the displacement [linear variable displacement transducer (LVDT)] outputs, the COD (i.e., the crack-mouth opening displacement), and the strain gage readings should be recorded by means of a computer data logger (Fig. 14).

Deformation Measurements

To distinguish both the contained and net section yielding from the gross section yielding, two measures of deformation (or strain) can be considered: the gage length strain and the remote strain [*26–32*]. The gage length or overall strain is defined as the change in the gage length divided by the original gage length. The remote strain is the strain which occurs in the uncracked specimen section. This strain can conveniently be measured by strain gages that are located away from the plane of the crack. It should be noted that the difference between the gage length or overall strain and the remote or gross section strain is a measure of the strain concentration introduced by the crack [*29–32*].

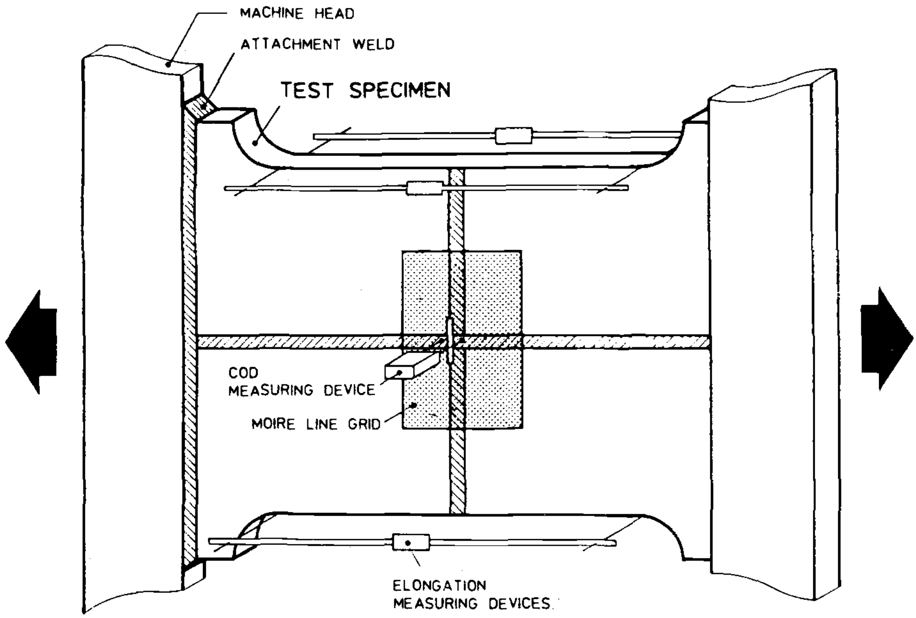

FIG. 14—*Instrumentation of the wide-plate tension test.*

Overall (Gage Length) Deformation Measurements—The overall elongation is measured on a gage length at least equal to the plate width in order to include definitely all plastic deformation, including the Luders slip deformation, emanating from the notch tips. The overall elongation can be measured by means of extensometers fixed either on both plate edges or on both plate surfaces [*33*]. The former method measures the in-plane bending; the latter method is able to measure the out-of-plane bending. The gage points may be spot welded or screwed onto the specimen. The output signals of the extensometers should be recorded individually or combined.

In some instances, and especially in cases where the moiré technique [*34*] cannot be applied (discussed further on in this paper) or when more information about the deformation behavior of the remote regions of the wide-plate specimen is required, a load-versus-elongation diagram of these areas can be recorded [*2,29–32*].

Measurement of the Local Deformation--The local deformation can be monitored by means of one or a combination of the following methods: (*a*) crack-mouth opening displacement measurements at the plate surface (COD or CMOD), (*b*) the moiré method, and (*c*) strain gage measurements [*33–35*].

The crack-mouth opening displacement at the plate surface can be monitored by measuring the displacement of the notch flanks at the very notch tip for through thickness or at the midlength for surface cracks. The gage length for the COD measurements should be as small as possible. The method of attaching the clip-on device to the specimen should not alter the material properties. An autographic plot of the COD versus the overall elongation is normally used to monitor both the crack-mouth opening displacement and the deformation behavior during the test. Note that a plot of the load against the COD provides less information on the specimen's yielding behavior during the test.

Valuable information about the distribution of the plastic deformations on larger areas can be obtained from the application of the moiré technique [34]. The moiré method may assist in the visualization and determination of the strain distribution over large plastically strained areas. Alternatively, electrical resistance strain gages (single or rosette) can be used. Detailed measurements must be performed when the extent of Luders deformation is small. In this instance, a high number of strain gages will be needed to monitor all plastic deformation occurring within the prismatic test section. Single-element strain gages can be placed on two parallel vertical lines so that they overlap each other's gage length. Postyield rosette gages should be used to monitor the strain developed near the crack ends. For tests on welded specimens, additional single-element strain gages can be placed at a distance from the crack in the weld metal in order to evaluate the difference between strain occurring in the base plate and that in the weld metal.

Propagation of a surface crack entirely through the specimen thickness (breakthrough) under monotonic load is often an event of interest. If the test is conducted at room temperature, visual observation under oblique light is sometimes sufficient. For tests carried out at low temperature, remote reading instruments are necessary [35]. One approach is to bond a frangible wire to the back face of the specimen immediately behind the crack and connect it to a simple continuity circuit. Another method is to clamp a pressure or vacuum chamber to the back face; when breakthrough occurs, pressure or vacuum is lost, causing a sensitive pressure switch to be actuated.

Testing Procedure

The testing procedure is similar to that of conventional tension testing practice [33]. Testing is normally performed in the displacement or strain-controlled condition (testing in the load-controlled condition is not feasible when large plastic deformation occurs). Load or crosshead rates should customarily be chosen so that failure occurs within 15 to 30 min after the start of loading. In the case of ductile material behavior, the test can be discontinued at an overall strain of about 3%. Further straining up to specimen failure may be considered to facilitate crack profile measurements after testing.

Measurements During the Conduct of the Test—At a minimum, the instrumentation must provide autographic plots of the applied load against the overall elongation (stress-strain curve) and the overall elongation against the COD (or CMOD) (COD-strain curve) during the test.

Measurements After Testing—The plots of (*a*) the applied load against the overall elongation (stress-strain curve), (*b*) the overall elongation against the crack-mouth opening displacement (COD), or (*c*) the applied load against the strain gage readings are the simplest and most useful ways to display the wide-plate test performance in terms of plastic deformation behavior at failure (or at the end of testing). From such plots the following data can be obtained:

(*a*) the pseudo yield stress of a cracked test plate;
(*b*) the gross section stress at specimen failure (or at the end of testing);
(*c*) the net section stress at specimen failure (or at the end of testing);
(*d*) the overall strain at specimen failure (or at the end of testing);
(*e*) the crack-mouth opening displacement at specific loading stages, notably, at specimen failure; and
(*f*) the yield pattern at specimen failure. This information can be obtained by comparing the yield strength, σ_Y, of the material remote from the crack with the gross stress,

σ_N, at specimen failure and by comparing the yield strength of the defective or cracked section with the net section stress, σ_n, at specimen failure. The former comparison will help to identify whether gross section yielding ($\sigma_N > \sigma_Y$) occurred. The latter will show whether failure was associated with contained ($\sigma_n < \sigma_Y$) or net section yielding ($\sigma_n > \sigma_Y$, and $\sigma_N < \sigma_Y$).

It should be noted that the overall strain is usually expressed as the percentage of the original gage length. Furthermore, in reporting values of overall strain, it is a minimum requirement to state the gage length employed.

Upon completion of the test, enlarged photographs of the fracture face should be taken. If no photographs are taken, enough dimensional measurements should be provided so that the crack front contour and the extent of any ductile tearing can be reconstructed.

In order to quantify the microstructures actually sampled by the crack tip, it is now common practice to perform posttest fracture macrographic and micrographic examinations. The actual sectioning procedure for doing this is outlined in the next paper.

Performance Requirements: Assessment of Wide-Plate Test Results

There is some disagreement among experts on the ultimate application of wide-plate test results. Some experts prefer to employ wide-plate test results to quantify the degree of safety implied in the predictions [e.g., the CTOD design curve, Central Electricity Generating Board (CEGB) R6, and so forth] based on small-scale fracture mechanics tests [*1,5,37*]. In other words, wide-plate test results are used to substantiate conclusions drawn from small-scale tests and analyses. Others consider wide-plate test results to be a suitable means of assessing the structural implications of low fracture toughness properties, measured in small-scale Charpy V-notch impact or CTOD testing [*3,14*]. In this way, the wide-plate test results may assist in defining the fitness-for-purpose of specific weldments when a preset acceptance level of overall strain for the particular application can be achieved [*27–32*]. In this context, there is some difference of opinion on the required failure stress/strain acceptance level of wide-plate test performance [*3,5,22*].

From an engineering point of view, both types of assessment merit consideration and may be complementary; however, the preference for one or the other conception depends on the specified performance requirements, the objectives of the test, and the response of the particular material to the test.

Validation of the Design Curve Approach

Where wide-plate test results are used to quantify the safety factor implied in the CTOD design curve approach, it should be noted that such an assessment is not permitted when net or gross section yielding is obtained in the wide-plate test specimen [*1*]; i.e., the net section stress at specimen failure should be less than the material's yield strength (Figs. 15 and 16).

The safety factor included in such a fracture mechanics analysis is obtained by comparing the crack dimension that produced wide-plate specimen failure with the maximum allowable crack size calculated from the critical CTOD in the bend test using the design curve. The CTOD analysis utilizes the CTOD toughness value and the wide-plate specimen stress (or strain) at failure (contained yielding only) to determine the tolerable crack size [*1,36–38*]. To this end, it is also necessary to make realistic estimates/assumptions with regard to the following:

(*a*) the CTOD value to be used (the mean, minimum, or statistically based estimate),
(*b*) selection of the appropriate material property for HAZ regions,

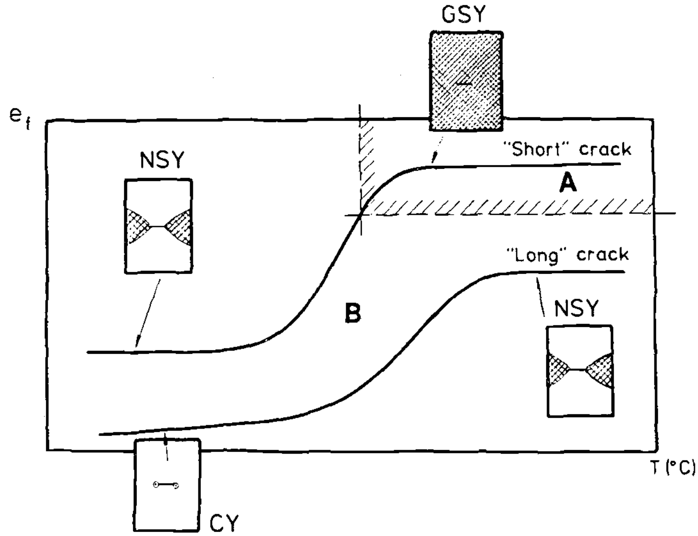

FIG. 15—*Schematic showing the relationship between fracture strain and test temperature in wide-plate test performance for short and long cracks (CY = contained yielding; NSY = net section yielding; GSY = gross section yielding). GSY gives safe operating conditions irrespective of the design condition (Area A), while the safety operating conditions for Area B depend on the notch/fracture toughness of the defective material.*

(*c*) allowance for residual stress, and
(*d*) the method of converting through-thickness to surface crack geometries.

In this context, the assessment also requires consideration of the differences between CTOD and wide-plate specimens in the location and orientation of the notch tip, as well as the effect of ligament size in the CTOD specimen ($B \times B$ versus $B \times 2B$) on the CTOD value.

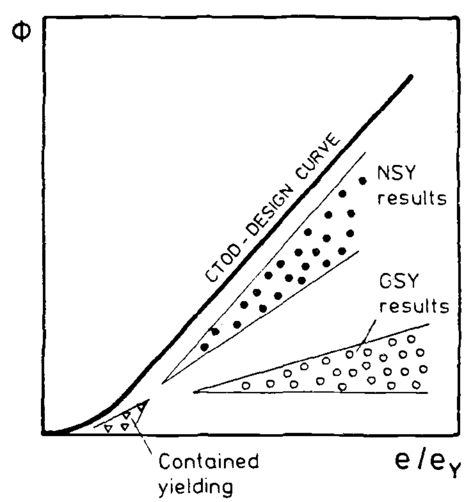

FIG. 16—*Schematic representation of the CTOD design curve, compared with measured results obtained from wide-plate tests (see also Fig. 15).*

As previously mentioned, where wide-plate specimen failure of a welded specimen occurs at stress levels beyond the plate yield strength, the CTOD approach is not applicable when the actual overall strain (plastic) at fracture is used in the analysis. In these instances, however, it is still useful to make the comparison between the crack size, which causes wide-plate failure, and the CTOD-based tolerable crack size, which is calculated by using a design-related (local) applied crack tip strain. This comparison will then permit appreciation of the limitations inherent in the CTOD analysis for notch ductile materials (Fig. 16).

Furthermore, it is also important to consider the effect of the weld metal and HAZ yield strength when the CTOD assessment is applied to weldments. Bearing in mind that the net section stress at fracture should be less than the yield strength of the base metal, weld HAZ, and weld metal, it is mandatory to ensure that the yield strength of the defective region overmatches that of the base metal [*13*]. This requirement makes it necessary to use engineering judgment when dealing with transversely loaded weldments. For the situations in which the weld metal is highly overmatching, the overall strain in the wide-plate test may be plastic, while the plastic deformation at the crack tip is confined to that area. In other words, the overall strain may not, in general, be taken to represent the strain at the crack tip. For the situation of weld metal undermatching, the applied remote deformation will occur within the width of the weld, and the overall strain will be small and may well give a completely misleading indication of the real strains in the (defective) weld region. Therefore, evaluation of wide-plate test results on the basis of CTOD design curve procedures must be related to the structural detail being assessed. Thus, for cracks in stress concentration regions, a different approach must be used for regions stressed only to normal design stresses, based on the tensile properties of the base metal.

From an application viewpoint, a one-parameter (CTOD, J, or other parameter) fracture criterion for assessment of both weldments and low-constraint situations may present considerable analytical difficulties. To solve such problems, it appears that a second parameter characterizing the degree of weld metal matching will be required, while the low-constraint problem requires consideration of the strain-hardening behavior of the material in the crack tip zone. The issue here is that at least two material property parameters are needed to solve the problem. As the extent to which strain hardening occurs depends upon both the material properties and the degree of crack tip constraint (Fig. 17), and since, where extensive yielding occurs, both the crack tip geometry and the material properties change with deformation, it is clear that development of an analytical/semiempirical treatment becomes indeed very difficult. The previous considerations illustrate that, until the interpretational difficulties associated with the CTOD analysis have been clarified, it would be inappropriate to put reliance on CTOD toughness requirements alone without giving consideration to the performance requirements of the final structure.

Gross Strain Acceptance Criterion

The overall strain acceptance criterion is used to fill the need for a measure of toughness that can be used quantitatively in design against fracture when the objective is to ensure yielding before fracture in the presence of the largest expected crack [*26–28, 31,32*].

This approach was first used in the 1960s. At that time, wide-plate test results were compared with a semiarbitrary pass/fail gross strain level of 0.5%, measured over a considerable gage length. This level corresponds to about four times the yield strain of the steels tested at that time and was derived from experimental observations that the plastic strain, with a safety factor of about 2.5, at a nozzle with an SCF of about 2.5, loaded to 1.3 (hydraulic pressure test) × ⅔ yield pressure test conditions is about that value (this criterion was also chosen as a safe measure for drawing up Charpy impact test requirement for pressure vessels and storage tanks (e.g., British Standard BS 5500 Appendix D) [*6*]. It

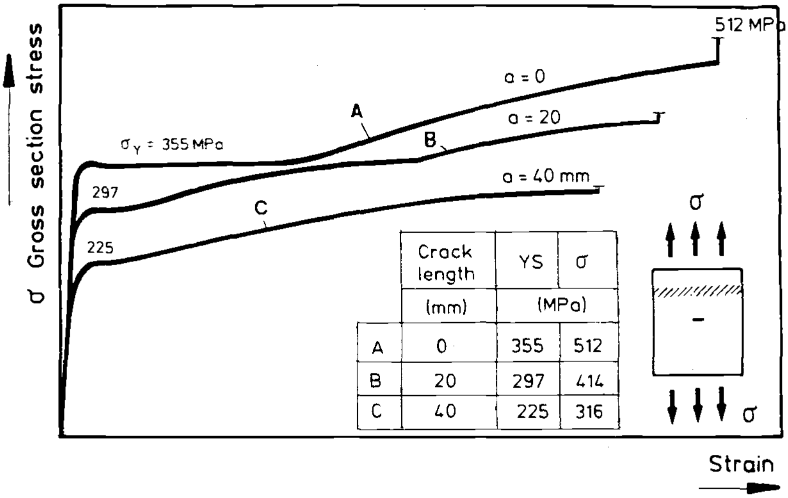

FIG. 17—*Stress-strain curves for centrally notched wide-plate test specimens, illustrating the effect of crack length on the extent of yield point elongation and strain hardening rate (the values of the yield strength and σ reflect the "gross section" stresses).*

should be noted that this criterion was developed to provide an answer for a particular problem. This implies that for other applications, as well as for higher strength steels, a four × yield criterion could be an insufficient or too severe requirement.

The necessity for a consistent but simple and practical engineering means for assessing wide-plate performance of either elastic-plastic or plastic material, or both, led in the early 1970s to the development of the gross section yielding (GSY) concept [27]. The concept rests on the idea that when the material at the crack tip can strain harden enough to compensate for the missing cross-sectional area in the plane of the crack, the applied plastic strain can be (uniformly) distributed all along the specimen length prior to specimen failure (Fig. 18).

It should be noted that the GSY approach is conceptually different from a fracture-mechanics-based assessment of brittle fracture safe design. Defining allowable or maximum tolerable crack sizes is not the main purpose. Imposing the GSY requirement is intended rather to check whether a representative crack can be safely left (fail/pass) in a structure. Note that this requirement incorporates subcritical crack growth during testing. On the other hand, the GSY requirement may be effective in defining a crack size, a_{gy}, marking the maximum crack size for which wide-plate specimen failure is associated with GSY (Fig. 19). It should be emphasized, however, that the GSY concept is rarely used to define the maximum acceptable crack size, a_{gy}.

The practical application of the GSY concept is simple and is a less sophisticated approach than any fracture mechanics defect assessment procedure. The GSY concept is almost completely empirical, and it is not required that certain assumption be made concerning the weld residual stresses, crack shape, and other factors. A direct comparison between the uniaxial yield strength of the base metal at the minimum operating temperature and the gross section stress at failure (i.e., the load at fracture divided by the gross section) determines whether or not GSY is achieved after testing (Fig. 20). When the definition of GSY is applied to transverse weldments, it must be obvious that GSY is achieved as soon as the gross section stress exceeds the yield strength of the base metal.

The question of how much total (elastic and plastic) strain should be required in the wide-

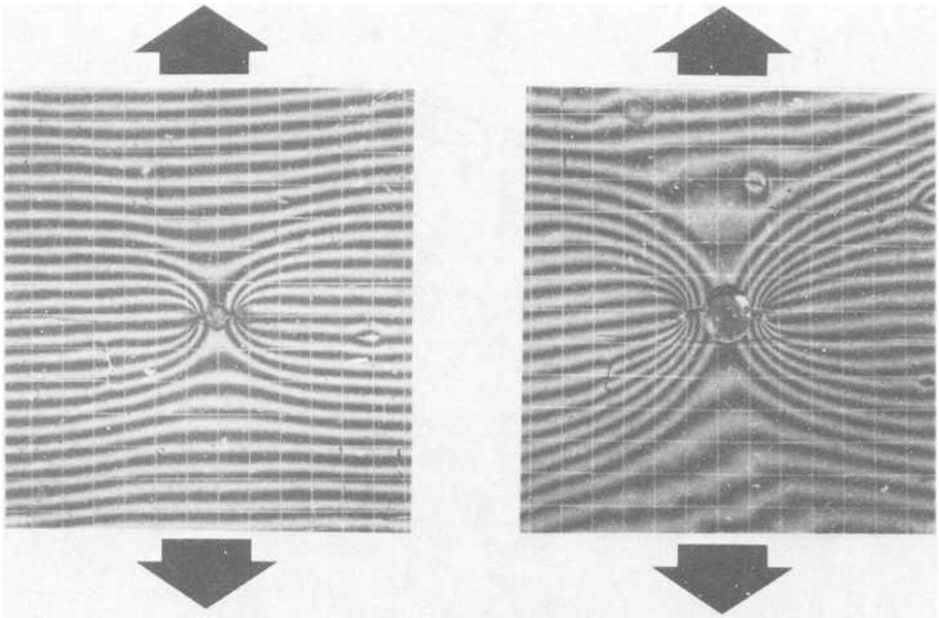

FIG. 18—*Typical moiré pictures illustrating the occurrence of gross section yielding.*

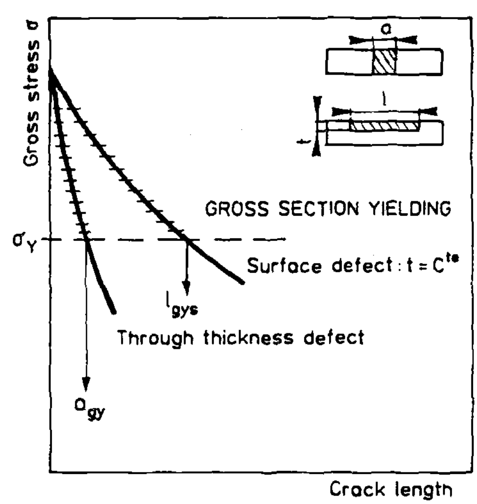

FIG. 19—*Schematic presentation of an acceptable gross section yielding defect with* a_{gy} = *the maximum length of through-thickness defect for GSY, and* l_{gys} = *the maximum length of surface defect for GSY (depth,* t = cte).

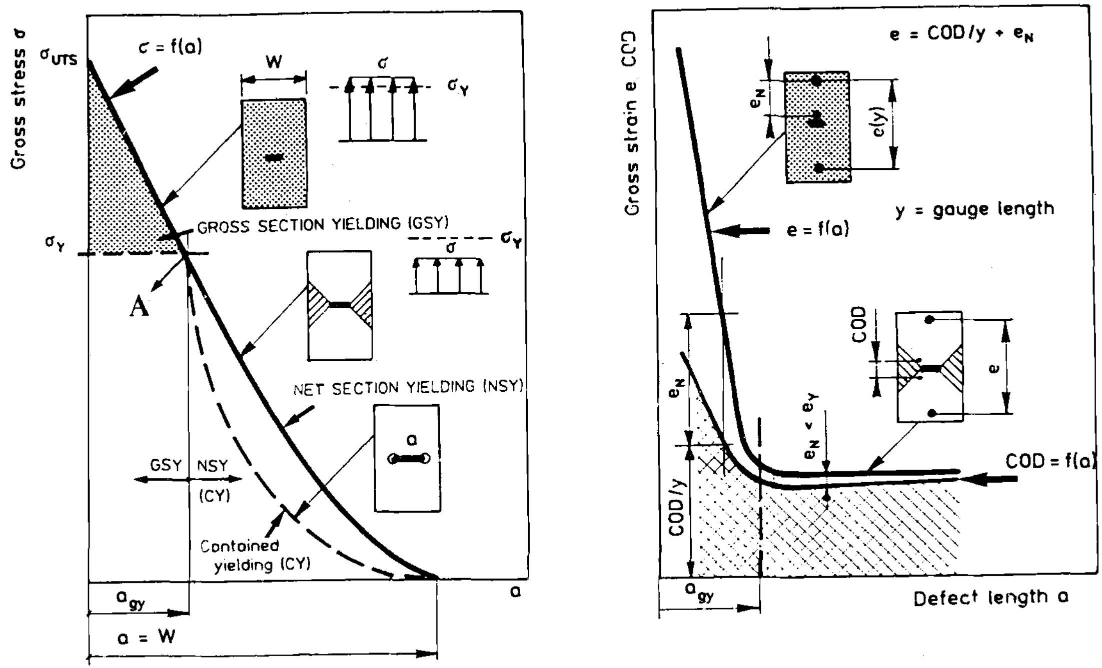

FIG. 20—*Gross stress,* σ, *overall strain,* e, *and crack-mouth opening displacement* (*COD*)/*crack length relationship for a through-thickness cracked tension-loaded specimen with indication of the corresponding plastic deformation patterns. Point A* ($a = a_{gy}$) *demarcates the transition from gross to net section yielding* (a). *Note that* (a) *has a connection with* (b), *which gives the overall strain and the strain due to the COD* (*COD*/y) *as a function of crack length.*

plate test has still to be resolved. The level of gross strain at fracture is a function of the crack size, as well as the temperature, crack shape, and, thus, the extent of relief of crack tip constraint (Fig. 15). The required overall strain depends on the ultimate purpose of the test. In this context, two situation can be considered. Where the intention is to assess wide-plate test results in pass/fail terms, there is a consensus requirement that the crack under test should be able to withstand between 1 and 2% strain. For situations where stress concentrations need to be taken into account, the requirement of GSY alone would be nonconservative. In this case, and as indicated in Fig. 21, the gross strain at fracture should exceed the $\sigma_{design} \times$ SCF/E strain level. On the other hand, some experts propose that, for HAZ tests, a demonstration of adequate ductility would be 0.5% strain measured in the (overmatching) weld metal, in which case, the base metal would also be subjected to plastic strain [5].

Failure to meet the GSY requirement could imply that the weld joint has an unacceptable fracture initiation resistance and that a smaller crack must be tested to qualify for acceptance. This opinion is not shared by those experts who base their acceptance on 0.5% strain. Instead, these experts then allow the significance of the result obtained to be established on the basis of a (CTOD) specific analysis (fitness for purpose) [5,22].

Finally, it should be emphasized that GSY may not be identified with plastic collapse; i.e., GSY provides exclusive information when the structure is expected to withstand conditions (such as an incidental overloading) involving general deformation. Since plastic collapse should be identified with net section yielding [39], it can be assumed that the occurrence of GSY in wide-plate test specimen permits the degree of conservatism implied to be quantified by the plastic collapse assessment methods actually used.

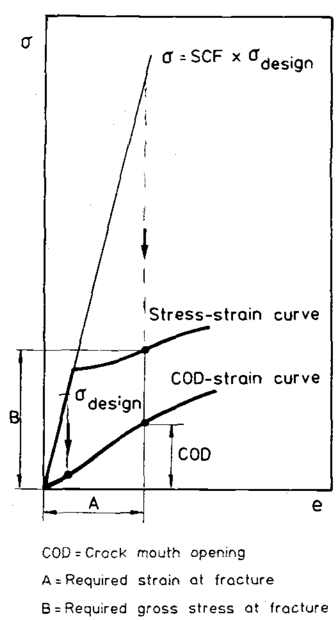

FIG. 21—*Procedure for determining the required "flat" wide-plate performance level in the case of local geometric related stress concentrations (SCF = elastic stress concentration factor; solid lines = stress/COD-strain curves of the notched wide-plate test).*

Concluding Remarks

This paper, which is Part II in this series on wide-plate testing of weldments, has dealt with various aspects related to (*a*) the selection of a wide-plate test specimen, (*b*) the preparation of the test specimen, (*c*) the wide-plate test procedure, and (*d*) the interpretation of the test results. The author has reached the following conclusions:

1. The answer to the question of whether a small or large-scale test specimen is best suited for evaluating a cracked weldment must ultimately be resolved by giving consideration to both the costs and the capability of the test to discriminate between good and poor welds. This means that every care should be taken to avoid having the chosen test specimen disqualify weldments that perform satisfactorily in service—which is to say that it is not easy to select an "ideal" test specimen for distinguishing between suitable and unsuitable service performance.
2. This paper, however, has illustrated that the wide-plate test specimen can model many structural details of interest in assessing fracture resistance of the base metal and its weldments.
3. In testing the correct wide-plate specimen design, it is important to recognize that a wide range of "external" factors may affect the results of the test. These factors include crack design, the weld bevel preparation, the difference between the weld metal/base metal properties, and other factors. The importance of this observation should not be underestimated. For instance, nowadays it is normal practice in fracture testing, and more particularly in CTOD and wide-plate testing, to modify or adjust the welding procedure, the weld bevel preparation (K- or single-V-weld preparation), the crack size, and the crack design to simulate worst-case service conditions. However, weld bevel preparations in real welds are seldom oriented perpendicular to the maximum principal stress. Similarly, real cracks are often irregularly shaped and thus not necessarily planar. In other words, the results of such tests may not be relevant to specific service configurations.
4. The discussion on the interpretation of the test data has shown that wide-plate test results can be used (*a*) to quantify the degree of safety implied in the predictions based on small-scale fracture mechanics tests and (*b*) to assess the structural implications of low fracture toughness properties measured in small-scale testing. From an engineering point of view, both assessments merit consideration and may be complementary; however, the preference for one or the other concept depends on the specified performance requirements, the objectives of the test, and the response of the particular material to the test.
5. With the foregoing in mind, it must be admitted that there is some difference of opinion regarding the required failure stress/strain acceptance level of wide-plate test performance. In this context, the differences between the yield strength properties of the various regions of the weld (i.e., the weld metal, HAZ, plate material) can produce anomalies in test performance. That is, steels with similar yield/tensile strength characteristics may show different sensitivities to fracture because of the differing yield/tensile strength characteristics of the parts composing the weld. In particular, this effect will be observed for those test geometries in which interaction between the weld metal, HAZ, and base metal is possible.

References

[*1*] Dawes, M. G., "The CTOD Design Curve Approach: Limitations, Finite Size and Application," Research Report 278/1985, The Welding Institute, Cambridge, England, July 1985.

[2] Denys, R. M., "A Study of the Effect of Yield Point Elongation and Strain Hardening Rate on the Fracture Behaviour of (Welded) Low Carbon Steels," *Proceedings*, Seventh International Conference on Offshore Mechanics and Artic Engineering, Vol. III, Houston, TX, 1988, pp. 404–413.

[3] Denys, R. M., "Toughness Requirements in Transversely Load Welded Joints—An Evaluation Based on Wide Plate Testing," *The Fracture Mechanics of Welds*, EGF Publication No. 2, J. G. Blauel and K.-H. Schwalbe, Eds., Mechanical Engineering Publications, London, 1987, pp. 155–189.

[4] Akita, Y. and Ikeda, K., "On Brittle Fracture Initiation: First Report—Deep Notch Test," *Journal of the Society of Naval Architects of Japan*, Vol. 116, December 1964.

[5] Pisarski, H. G. and Walker, E. F. "Wide-Plate Testing as a Backup to the CTOD Approach." TWI Report for the Department of Energy 3915/4/86, The Welding Institute, Cambridge, England, 1986.

[6] Woodley, C. C., Burdekin, F. M., and Well, A. A. "Mild Steel for Pressure Equipment at Sub-Zero Temperatures," British Welding Journal, Vol. 11, No. 3, 1964, pp. 123–136.

[7] Banks, E. E., "Lab Notes—Is the Wells Wide Plate Test Realistic?" *Metal Construction and British Welding Journal*, March 1973, pp. 102–103.

[8] Hall, W. J., Kihara, H., Soete, W., and Wells, A. A., *Brittle Fracture of Welded Plate, International Series in Theoretical and Applied Mechanics*, Prentice Hall, Englewood Cliffs, NJ, 1967, pp. 11–125.

[9] Degenkolbe, J., "Korrelation der Kennwerte aus den herkommlichen Verfahren der Sprodbruch-Prufung mit denen der Bruchmechanik," *Angewandte Bruchmechanik*, TUV Essen 19, Cologne, Germany, 1978, pp. 89–109.

[10] Kihara, H., Kanazawa, T., Machida, S., "Some Brittle Fracture Experiences in Japan," *Journal of the West Scotland Iron and Steel Institute*, Vol. 76, 1968–69, pp. 21–56.

[11] Ikeda, K., Akita, Y., and Kihara, H., "The Deep Notch Test and Brittle Fracture Initiation," *Welding Journal, Research Supplement*, March 1967, pp. 133–143.

[12] Burdekin, F. M., "The Properties and Testing of Welding Metal in Relation to Structural Failure from Brittle Fracture," *Colloquium*, IIW Annual Assembly, Kyoto, Japan, July 1969.

[13] Denys, R. M., "The Relevance of CTOD in Cross Welded Joints with Weld Metal Overmatching in Strength," *Proceedings*, Conference on Welding for Challenging Environments, Toronto, Canada, 1985, Pergamon Press, New York, pp. 157–166.

[14] Denys, R., "The Effect of Defect Size on Wide Plate Test Performance of Multipass Welds with Local Brittle Zones," *Proceedings*, Conference on Welding Metallurgy of Structural Steels, J. Koo, Ed., Denver, CO, February 1987, pp. 319–334.

[15] Dawes, M. G., "Testing for Fracture on Low-Alloy Q and T Steel Weldment," *Metal Construction and British Welding Journal*, December 1970, pp. 533–538.

[16] Baker, R. G., Barr, R. R., Gulvin, T. F., and Terry, P., "The Use of Wide-Plate Test Data for Design Against Brittle Fracture." Ref. II.75, *Proceedings*, Pressure Vessel Technology International Conference, San Antonio, TX, 1–4 Oct. 1973, p. 1049.

[17] Egan, G. R., "The Application of Fracture Toughness Data to the Assessment of Pressure Vessel Integrity," Ref. II.74, *Proceedings*, Pressure Vessel Technology International Conference, San Antonio, TX, 1–4 Oct. 1973, p. 1037.

[18] Ikeda, K., Akita, Y., and Kihara, H., "Brittle Fracture Strength of Pressure Vessel Steels," Paper C26/71, *Proceedings*, Conference on Practical Application of Fracture Mechanics to Pressure Vessel Technology, Institution of Mechanical Engineers, London, pp. 103–108.

[19] Masubuchi, K., *Analysis of Welded Structures, International Series on Material Science and Technology*, Vol. 33, Pergamon Press, New York, 1980.

[20] Dawes, M. G., "Fracture Control in High Yield Strength Weldments," *Welding Journal, Research Supplement*, Vol. 53, No. 9, September 1974, pp. 369–379.

[21] Gulvin, T. F., "Brittle Fracture Resistance of Welded Joints of Some High Strength Steels of Medium Thickness," *Proceedings*, C.E.C. Symposium on Production and Use of Heavy Plate, Luxembourg, Belgium, 20–21 Feb. 1979, pp. 413–466.

[22] Pisarski, H., "Philosophy of Welded Wide Plate Testing for Brittle Fracture Assessment," *The Fracture Mechanics of Welds*, EGF Publication No. 2, Mechanical Engineering Publications, London, 1987, pp. 191–208.

[23] Webster, S. E., "The Structural Significance of Low Toughness HAZ Regions in a Modern Low Carbon Structural Steel." *The Fracture Mechanics of Welds*, EGF Publication No. 2, Mechanical Engineering Publications, London, 1987, pp. 59–75.

[24] Tenge, P., Karlson, A., and Pisarski, H. G., "Assessment of the Influence of Loading Mode on Wide Plate Test Fracture Results in Relation to Code Requirements," *Proceedings*, International Conference on Steel in Marine Structures, Paris, France, 5–8 October 1981.
[25] Berge, S., Ebrahimi, F., and Read, D. T., "Wide Plates in Bending," *Proceedings*, Eighteenth National Symposium on Fracture Mechanics, Boulder, CO, June 1985.
[26] Lian, B., Denys, R., and Van de Walle, L., "An Experimental Assessment on the Effect of Weld Metal Yield Strength Overmatching in Pipeline Girth Welds," *Proceedings*, Third Conference on Welding and Performance of Pipeline, TWI, London, England, November 1986.
[27] Soete, W. and Denys, R., "Fracture Toughness Testing of Welds," *Proceedings*, Conference on Welding of HSLA (Microalloyed) Structural Steels, ASM, Rome, Italy, November 1976, pp. 63–84.
[28] Denys, R. M., "Interpretation of the Wide Plate Tension Test at Full and General Yield," IIW-DOC X-922-79, International Institute of Welding, Bratislava, Czechoslovakia, 1979.
[29] Randall, P. N., "Effects of Strain Gradients on the Gross Strain Crack Tolerance of A533-B Steel," HSSTP-TR-19, Heavy Section Steel Technology Program, Oak Ridge, TN, 15 June 1972.
[30] Randall, P. N., "Gross Strain Crack Tolerance of A533-B Steel," HSSTP-TR-14, Heavy Section Steel Technology Program, Oak Ridge, TN, 1 May 1971.
[31] Denys, R. M., "The Wide Plate Test and Its Application to Acceptable Defects," *Proceedings*, Conference on Fracture Toughness Testing—Methods, Interpretation and Application, London, England, 9–10 June 1982.
[32] Cheng, Y. W., King, R. B., Read, D. T., and McHenry, H. I., "Postyield Crack-Opening Displacement of Surface Cracks in Steel Weldments," *Fracture Mechanics: Fifteenth Symposium, ASTM STP 833*, R. J. Sanford, Ed., 1984, pp. 666–681.
[33] "Fracture Testing with Surface-Crack Tension Specimens," ASTM E740-80, *Annual Book of ASTM Standards*, American Society for Testing and Materials, Philadelphia.
[34] Dechaene, R. and Vinckier, A., "Use of the Moire Effect to Measure Plastic Strain," *Transactions of the ASME*, June 1960.
[35] Orange, T. W., "Fracture Testing with Surface Crack Specimens," *Journal of Testing and Evaluation*, Vol. 3, No. 5, September 1975, pp. 335–342.
[36] Burdekin, F. M. and Dawes, M. G., "Practical Use of Linear Elastic and Yielding Fracture Mechanics with Particular Reference to Pressure Vessels," Paper C5/71, *Proceedings*, I. Mech. E. Conference on Practical Application of Fracture Mechanics to Pressure Vessel Technology, London, England, May 1971.
[37] Kamath, M. S., "The COD Design Curve: An Assessment of Validity Using Wide Plate Tests," Research Report 71/1978/E, The Welding Institute, Cambridge, England, September 1978; or "The COD Design Curve: An Assessment of Validity Using Wide Plate Tests," *International Journal of Pressure Vessels and Piping*, Vol. 9, No. 2, 1982, pp. 79–105.
[38] Harrison, J. D., "The "State of the Art" in Crack-Tip Opening Displacement (CTOD) Testing and Analysis," W.I. 7302.10/80/210.2, The Welding Institute, Cambridge, England, 1980.
[39] Willoughby, A. A., "A Survey of Plastic Collapse Solutions Used in the Failure Assessment of Part Wall Defects," Research Report 191/1982, The Welding Institute, Cambridge, England, September 1982.

Rudi M. Denys[1]

Wide-Plate Testing of Weldments: Part III—Heat-Affected Zone Wide-Plate Studies

REFERENCE: Denys, R. M., **"Wide-Plate Testing of Weldments: Part III—Heat-Affected Zone Wide-Plate Studies,"** *Fatigue and Fracture Testing of Weldments, ASTM STP 1058*, H. I. McHenry and J. M. Potter, Eds., American Society for Testing and Materials, Philadelphia, 1990, pp. 204–228.

ABSTRACT: This paper, Part III in this series on wide-plate testing of weldments, reviews the latest developments in wide-plate test procedures used for evaluation of the heat-affected zone (HAZ) toughness in steel weldments. In particular, emphasis is placed on the transversely loaded wide-plate test specimen in which the orientation of both the crack and the weld is transverse to the loading direction. This wide-plate test configuration is often conducted to evaluate the structural significance of low HAZ CTOD values. To this end, fatigue-precracked surface-notched wide-plate specimen tests are employed to assess this specific local brittle zone (LBZ) problem. The need for sectioning the wide-plate specimen after testing to identify whether the intended microstructures have been sampled is discussed, and examples are given to illustrate the type of information which is currently produced.

KEY WORDS: weldments, wide-plate testing, heat-affected zone (HAZ), crack-tip opening displacement (CTOD), brittle fracture, cracks, toughness requirements, high-strength steels, local brittle zones, coarse-grain microstructure

In the early 1980s, heat-affected zone (HAZ) crack-tip opening displacement (CTOD) fracture toughness measurements of modern low-carbon microalloyed structural steels revealed that very low CTOD results could occur when the crack tip was located in the coarse-grained HAZ. These regions were defined as local brittle zones (LBZs) when they produced CTOD value lower than 0.1 mm.

To evaluate the engineering significance of such LBZs, extensive use is now being made of surface fatigue-precracked wide-plate specimen tests. In particular, emphasis is placed on the transversely loaded wide-plate test specimen in which the orientation of both the crack and the weld is transverse to the loading direction [*1–8*]. If any comparison between the CTOD test and the wide-plate test results is to be valid, it is essential that the same care be exercised to ensure that the fatigue crack tip is located in the same microstructure that produced low CTOD values.

As the wide-plate test specimen is to be notched after welding, defect designs representative of the types of cracks that are seen in a real structure can be tested. In this connection, one should note that, since the size of the potential low-toughness LBZ/HAZ regions is rather small, the placement of the crack tip in these regions necessitates the use of specific notching procedures. Also, it is essential to verify that the fatigue crack tip has effectively sampled the desired microstructure.

[1] Professor and manager, Laboratorium Soete Rijksuniversiteit Gent, B 9000 Gent, Belgium.

Such posttest metallographic examination procedures have already been developed and appear to be an integral part of HAZ CTOD testing. Those procedures have recently been included in offshore steel (purchase) specifications [*9–11*]. Comparable procedures have been applied in a few European laboratories for HAZ-notched wide-plate test specimens.

On the basis of the preceding observations, it can be deduced that detailed testing procedures have to be followed in current wide-plate testing. The main aspects of these procedures are reviewed and, where appropriate, illustrated with detailed sketches and photographs.

Local Brittle Zones

What a Local Brittle Zone Is

Metallographic examination of the weld HAZ of carbon-manganese structural steel plates allows identification of significant differences in HAZ microstructures [*12–32*] (Fig. 1).

The HAZ of a *single-pass* weld can be subdivided into four characteristic regions, depending on the peak temperature that the region was exposed to during the weld thermal cycle: the coarse-grained HAZ (CGHAZ), the fine-grained HAZ (FGHAZ), the intercritical HAZ (ICHAZ), and the subcritical HAZ (SCHAZ) (Fig. 1). In general, the CGHAZ region exhibits the lowest toughness in fracture testing. On the other hand, the FGHAZ normally does have acceptable fracture toughness properties, while the ICHAZ and SCHAZ may also produce reduced fracture toughness properties.

In a *multipass weld*, part of the CGHAZ connected with a single-weld bead is refined by the subsequent weld passes, whereas the other part is substantially modified in lower temperature reheated CGHAZ regions (Figs. 1 through 4). The modified CGHAZ regions which retain the coarse-grained structure are defined as (*a*) the intercritically reheated CGHAZ (ICCGHAZ) and (*b*) the subcritical reheated CGHAZ (SCCGHAZ). Adjacent to both the grain-refined CGHAZ and the low-temperature CGHAZ regions, one can also identify regions of unmodified CGHAZ. In fracture toughness testing, the unaltered CGHAZ, the ICCGHAZ, and the SCCGHAZ regions are normally responsible for low HAZ toughness properties and are called local brittle zones (LBZs). It should be added here that the presence of these low-toughness regions can be readily detected using standard CTOD tests.

The LBZ regions in the HAZ of a multipass weld are small; they occur discontinuously and are predominantly bounded by ductile material. The size of a LBZ is normally less than 0.5 mm wide and a few millimetres deep. Both the width (distance from the fusion boundary) and the depth (through-thickness direction) of a LBZ region depend upon the welding procedure, the weld heat input, the cooling rate, the weld bead geometry, the microalloy design of the steel, the steel manufacturing route, and the amount of weld bead overlap [*26,32*]. For example, Fig. 3 shows the extent of the various HAZ regions observed in weldments made with increasing heat input.

Location of LBZs in Real Welds

There is a close interaction between the geometry of the weld preparation and the position of the LBZ regions. The distribution of the LBZs along a (square) straight weld edge will differ from that at the inclined weld edge. The angle included between both plate edges of the weld also has a strong effect on the amount of weld bead overlap and thus on the LBZ size (Fig. 5).

The situation is further complicated when the locations of the LBZs are compared at various positions within the same weld. The fact that it is not feasible to deposit a weld bead with a consistent cross section over larger lengths implies that variations in the location

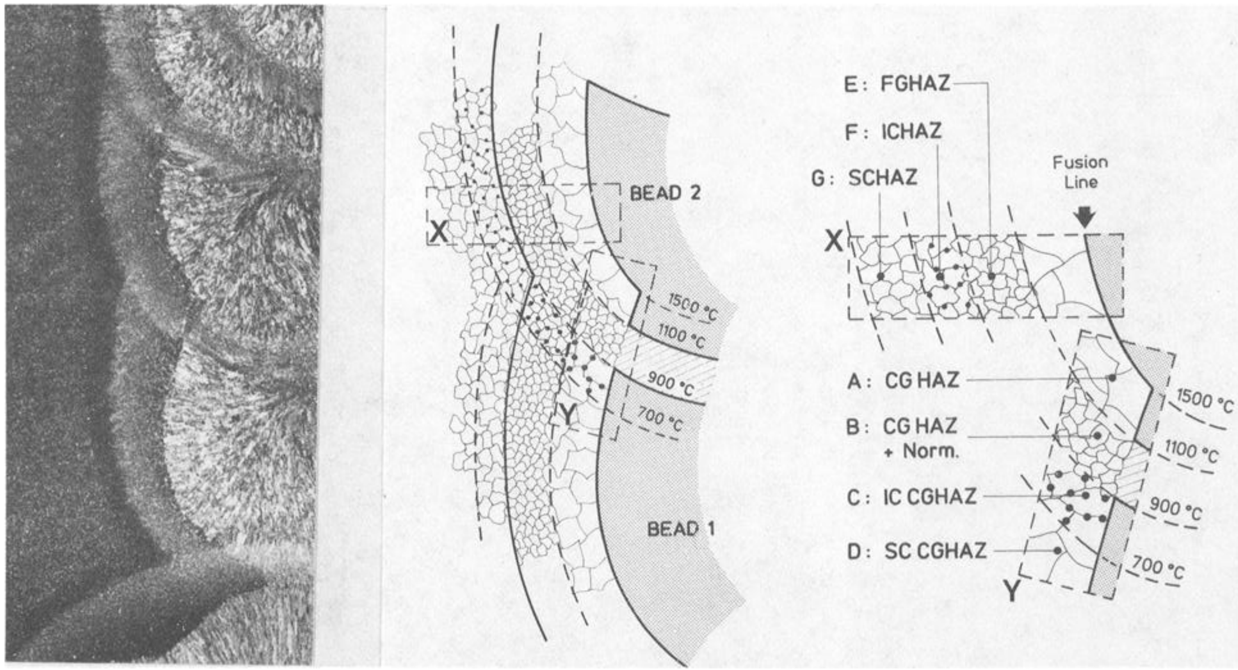

FIG. 1—*Part of the straight-edge HAZ in a multipass weld, with identification of the various HAZ microstructures.*

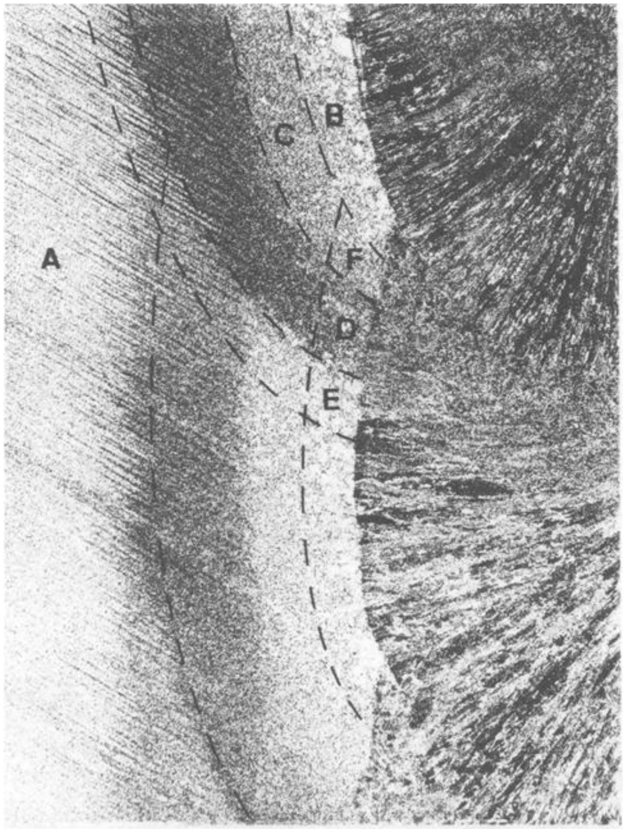

FIG. 2—*Photomicrograph of two weld beads in a multipass weld (magnification,* ×*10) (see also Fig. 3).*

of the LBZ regions occur in three different directions: i.e., along the length of the weld, in the through-thickness direction, and in the transverse (perpendicular to the weld) direction. Deviations of the fusion boundary profile over relatively short distances of more than 1 mm are not unusual (Fig. 6) [*33–34*].

LBZ and Wide-Plate Testing Aspects

Specimen Design

Strictly speaking, the design of the wide-plate test specimen cannot be standardized in the same way that, for example, a CTOD test specimen can because the test may also be used to represent some structural detail, and this may vary, as has been discussed in the previous paper, Part II of this series on wide-plate testing.

For the purpose of LBZ/HAZ fracture evaluation, the simplest and the most effective way to investigate the effect of LBZs on weldment performance is to place the test crack wholly in the transformed HAZ of a welded flat wide-plate specimen in which the orientations of both the crack and the weld are transverse to the loading direction. In this context, one should note that, since the yield strength is a measure of the driving force for plastic

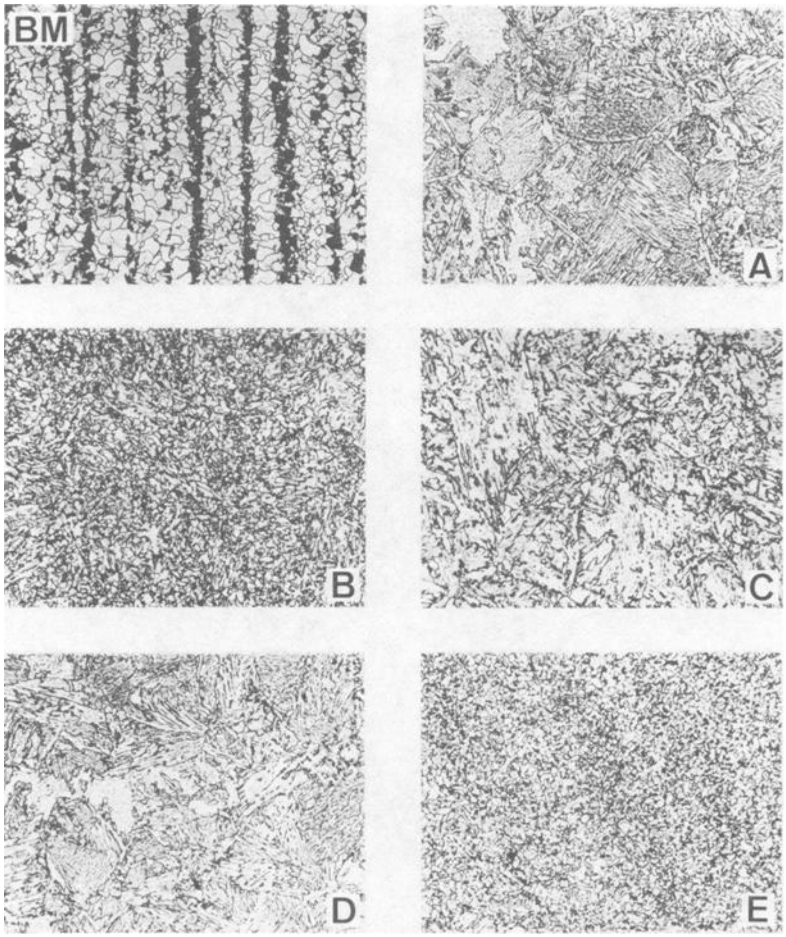

FIG. 3—*Photomicrographs of the various HAZ regions in a multipass weld (magnification, ×250):* (a) *base material;* (b) *grain-coarsened HAZ, as deposited;* (c) *fine-grained HAZ, as deposited;* (d) *intercritically reheated grain-coarsened HAZ;* (e) *subcritically reheated grain-coarsened HAZ; and* (f) *fine-grained HAZ, which was previously grain-coarsened HAZ.*

deformation and fracture, the fracture behavior of a HAZ-cracked transversely loaded specimen will be affected by the differences in yield strength of the parts composing the weldment. In other words, due consideration should be given to selection of the welding consumable, since the interaction between the differing stress-strain characteristics of the weld metal, the HAZ, and the base plate is directly incorporated into the test specimen. Note also that the longitudinally welded specimen in which the crack is transverse to the weld is unsuitable for the simple reason that the crack front can only intercept a very small proportion of LBZ regions.

The testing conditions can be made more structure-specific when it is of interest to examine the effect of either the yield magnitude residual stresses or the geometric discontinuities, or both, on weldment performance. The former can be modeled by use of an (expensive) test specimen containing a longitudinal and a transverse weld; the latter can be simulated

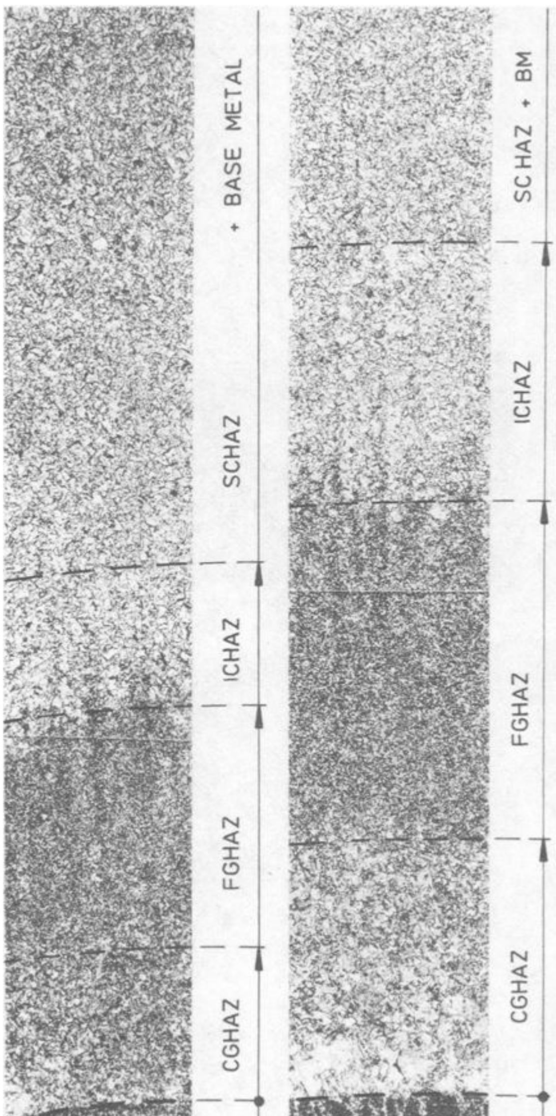

FIG. 4—*HAZ microstructures produced in straight bevel welds for steels of different composition welded with different welding processes:* (a) *SAW weld, 4-kJ/mm heat input, low C-Mn steel;* (b) *SAW weld, 5.6-kJ/mm heat input, C-Mn steel (magnification,* $\times 33$).

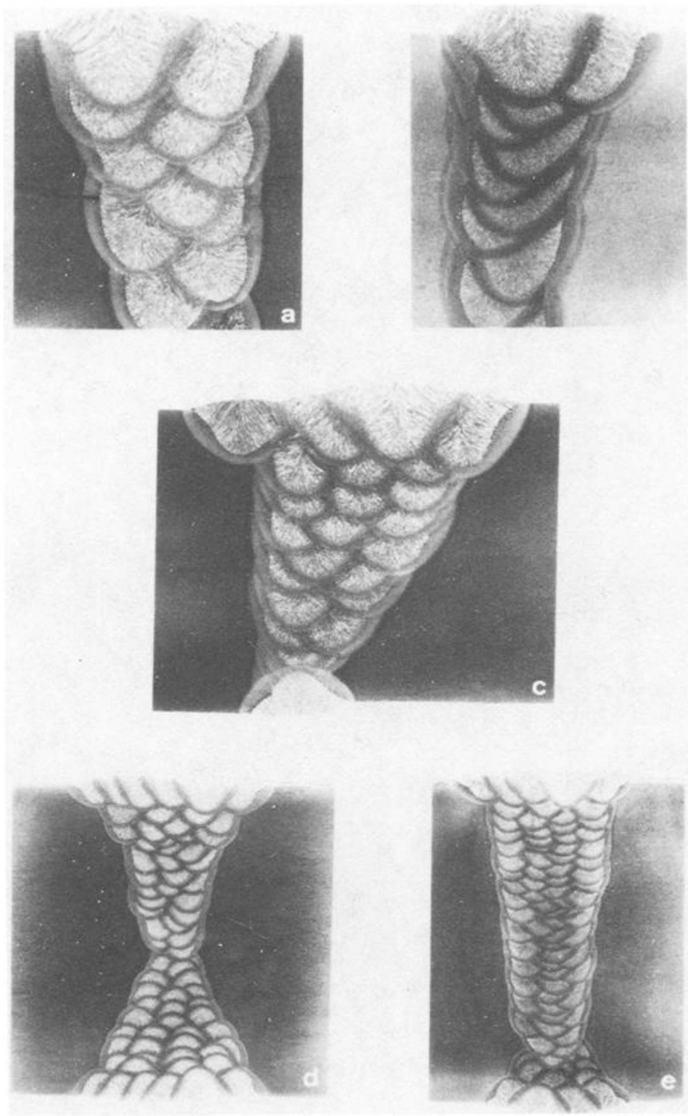

FIG. 5—*Photomacrographs of weld preparations for prequalification testing:* (a), (b), *and* (c) *straight-edge welds;* (d) *and* (e) *production welds.*

by incorporating a structure-specific angular distortion, weld misalignment/mismatch, or transverse stiffener into the specimen design. Note that the crack in the transversely loaded specimen is only affected by the transverse residual stresses, which are of the order of 20 to 50% of the plate material yield strength [*35*].

Selection of Weld Preparation

To facilitate an easy placement of the fatigue crack tip in the desired LBZ regions of a wide-plate test panel it is advantageous to use a straight and perpendicular fusion boundary,

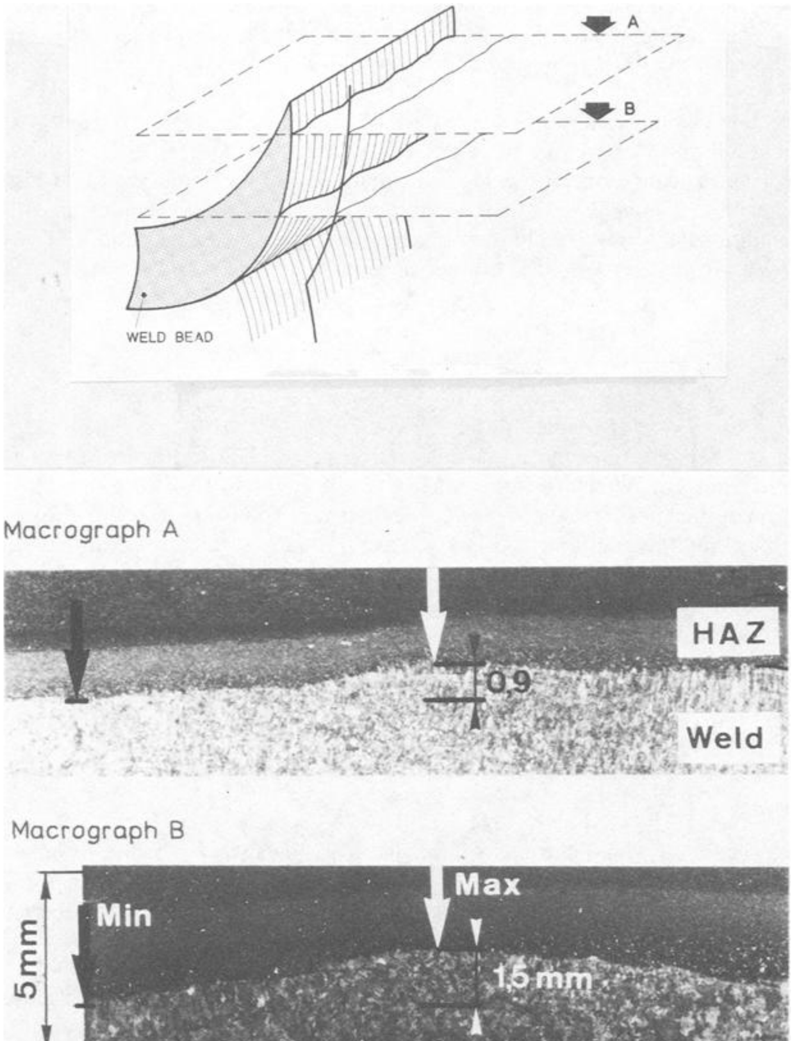

FIG. 6—*Variation in the fusion boundary along the length of the weld. The plane of sectioning is parallel to the plate surface.*

i.e., a single-V- or a K-weld preparation. This requirement has also resulted in specially designed welding procedures which involve a high weld bead depth to width ratio. In certain instances use is made of a narrow-angled single-V-weld preparation so as to produce some isolated but long regions of LBZ microstructures (Fig. 5). Furthermore, the same weld preparation and plate orientation should be used for both the CTOD and wide-plate tests. It would also be desirable, when account is taken of the type of crack used in the wide-plate test specimen, to employ surface-notched CTOD specimens ($B \times B$) [*2,3,8*].

The geometry effects associated with the use of a straight (square) weld preparation instead of the real weld preparation (e.g., single or double preparations) can be minimized when the test weld is made with the same degree of weld bead overlap, and thus the same degree of CGHAZ refinement, along the straight (test) edge as in the real weld. As is recognized in Refs *2, 3,* and *8,* and because the weld bead shape and positioning cannot be kept constant along the length of the weld, the implementation of such welding procedures is experimentally very complicated and requires a high degree of expertise to produce a representative test weld.

Although the implementation of a "special" weld geometry and a strictly controlled welding procedure (*a*) increases the likelihood of sampling larger LBZ portions and (*b*) tests a worse-case condition for a given heat input, it is to be emphasized that testing such LBZ regions may ignore the fact that the test results might not be relevant at all when no similar conditions in terms of weld joint preparation, bead placement, and heat input occur in real welds. In that respect, it is of interest to compare the photomacrographs shown in Figs. 5 and 6.

Defect Shape

It is mandatory that (part of) the fatigue crack front in a HAZ-notched wide-plate test specimen will sample the same microstructure as the CTOD test specimen in which the LBZs were detected. When account is taken of the location of LBZ regions, the possibility that a through-thickness crack will sample significant portions of LBZs is nearly excluded. On the other hand, actual cracks in service are normally surface breaking and are of an irregular shape. Therefore, the fatigue-precracked surface-partial wall crack is the most commonly used crack configuration. The disadvantage of this crack design, although unavoidable, is that the tip of the crack will sample material of varying properties.

When it is clear that the dominant dimension of a surface crack is its depth, it is clear that complications will arise in locating and simulating a practical crack in the desired HAZ region, and this is discussed in more detail below.

Fatigue Crack Propagation

In thick-sectioned wide-plate test specimens, it is not always possible to maximize the depth of the machined starter notch so as to prevent fatigue crack path deviation from the selected LBZ regions. Experience to date and the experimental information reported in Refs *33* and *34* illustrate the following:

(*a*) the plane of fatigue crack growth can give rise to a pronounced deflection at the junction between the weld bead and the HAZ;
(*b*) the plane of fatigue crack extension in HAZ regions can take any direction with respect to the fusion boundary; and
(*c*) provided that the yield properties of the base metal are lower than those of the cracked HAZ, there is a tendency of fatigue cracks to curve away from the LBZ regions towards the base plate side of the weld.

The practical implication of these data is that, when the combined effects of crack path wandering and weld bead contour/fusion boundary variation (in the direction perpendicular to the fusion boundary, along the length of the weld, and in the through-thickness direction) are taken into account, it is virtually impossible, unless the coarse-grained regions are both very long and very wide, for a straight fatigue crack to occur consistently in the CGHAZ. Provided that the yield properties of the various HAZ structures are greater than those of the parent plate, it is quite possible that the desired LBZ regions can be completely missed. As a consequence, special notching procedures are needed ensure an adequate sampling of the LBZ regions.

Defect Design

In order to make sure that the leading edge of a surface crack samples representative portions of LBZs (this region is not exclusive with regard to the proposed notching procedure), it is necessary to modify the design of the mechanical starter notch. A choice can be made between a multiple-step or a zigzag (sawtooth)-shaped crack (Fig. 7). The multiple-step notch (Fig. 8) consists of a series of individual notches with the distance between their longest axes varied in proportion to the width of the coarse-grained region (staggered or echelon notch). Examples of those alternative notch designs are shown in Figs. 7 and 8. One can observe from Fig. 7 that the extent of zigzagging or staggering is less than 1.5 mm.

The step or zigzag starter notch geometries are preferred over a straight notch because the chance of successfully sampling the desired LBZs in the through-thickness or crack depth direction can be enhanced. In addition, an irregular fatigue crack front can be produced because of the overlapping of each individual starter notch during fatigue precracking (Fig. 9). The photographs in Fig. 9, taken after wide-plate testing, illustrate the nonuniform shape of the fatigue crack front. It can further be observed from Fig. 9 that, by adding a shallow starter notch to the crack ends, it is quite easy to sample the CGHAZ regions of the cap layer, which makes it possible to sample larger lengths of the CGHAZ. On the other hand, it can be argued that the step or zigzag crack may model real fatigue cracks as well, because fatigue cracks can take any shape in a fatigue-loaded structure.

The varying crack depth may, provided the yield properties of the various microstructures at the crack front are the same, result in different stress intensities along the leading edge of the crack. These variations are not considered significant because cleavage is a weak-link fracture process that depends on the stress/strain conditions local to the weak link, that is, the LBZ [7].

Notch Positioning in a Wide-Plate Specimen

It should be recalled that in the wide-plate specimen the fusion line contour varies over the specimen width. Thus, locating the crack tip in the desired microstructure is a major

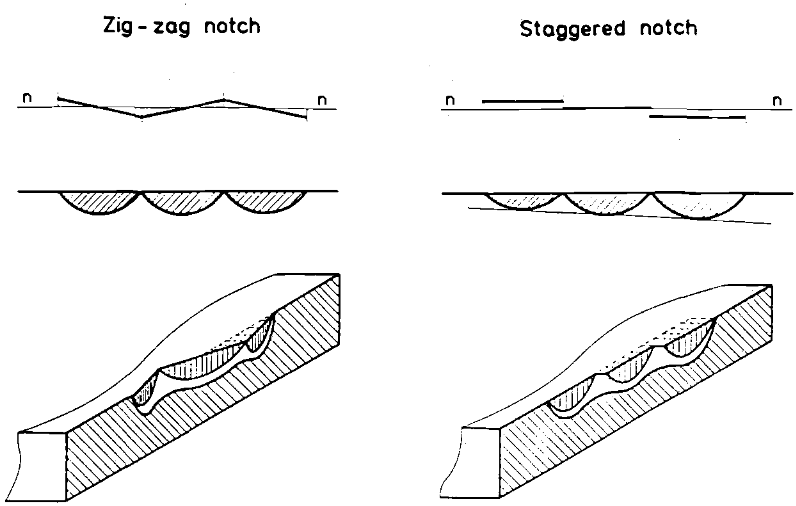

FIG. 7—*Alternative starter notch configurations used for sampling local brittle zones in HAZ-notched wide-plate specimens.*

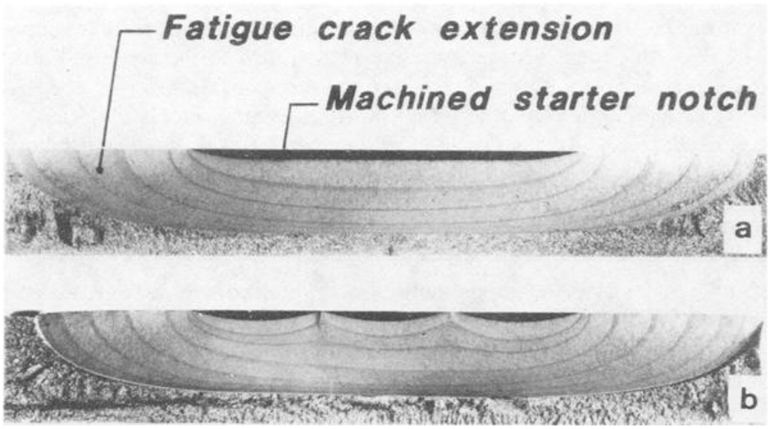

FIG. 8—*Fatigue crack extension profiles:* (a) *for a single starter notch;* (b) *for multiple starter notches (the depth of the machined starter notches was 2 mm).*

experimental problem (similar problems, though less pronounced, are faced in notching CTOD specimens). It is quite possible that an area of grain coarsening aimed for on the basis of 1-m-spaced outer macrospecimens may not exist in the area of the central portion of a 1-m-wide test specimen.

The experimental problems which arise in placing the fatigue crack tip in the CGHAZ,

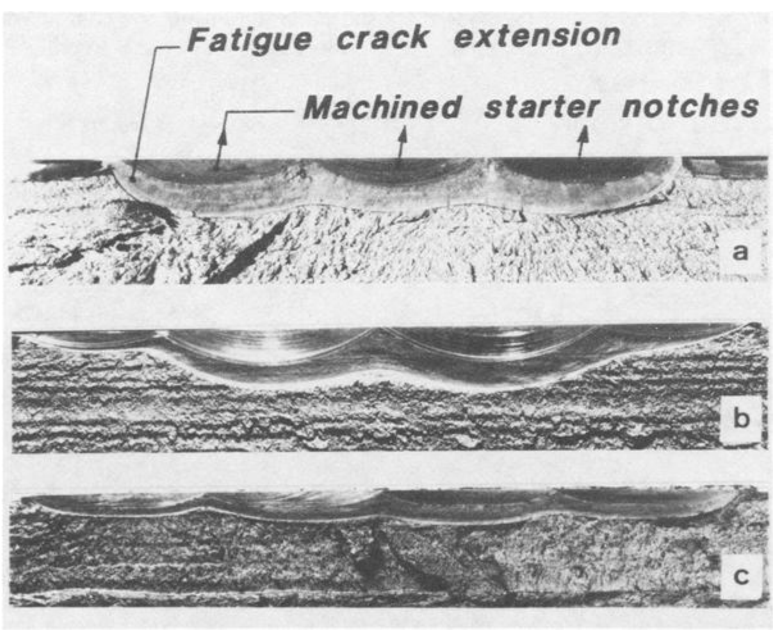

FIG. 9—*Examples of fatigue crack fronts tested in HAZ-notched wide-plate specimens.*

whose length and depth would be fairly close to the predetermined target values, may be overcome by following a careful experimental procedure.

Since the regions of low toughness in the through-thickness direction are not known in advance, a detailed metallographic examination will be needed before the test specimen can be notched. For that purpose, two cut-off macrospecimens (polished to a 1-μm finish and etched in 2% nital) are to be taken to identify the position of the LBZ regions along the straight edge of the weld on each macrograph (Fig. 10). As previously mentioned, one should note, however, that the end macrospecimens are to be extracted several hundreds millimetres away from the future notch position in the center of the wide-plate specimen.

The information extracted from these examinations is usually presented in the form of a bar chart describing the fusion boundary microstructure. Whenever possible, a sketch of the weld bead contours and the adjacent regions of CGHAZ should be made in order to facilitate the selection of the final notch tip location. The macrospecimens and the schematic presentation of the LBZ regions are further used for reference. As indicated in Fig. 10, the examinations are generally directed toward that side of the weld which contains the most prominent regions of grain coarsening. In general, the HAZ of the straight-sided weld edge

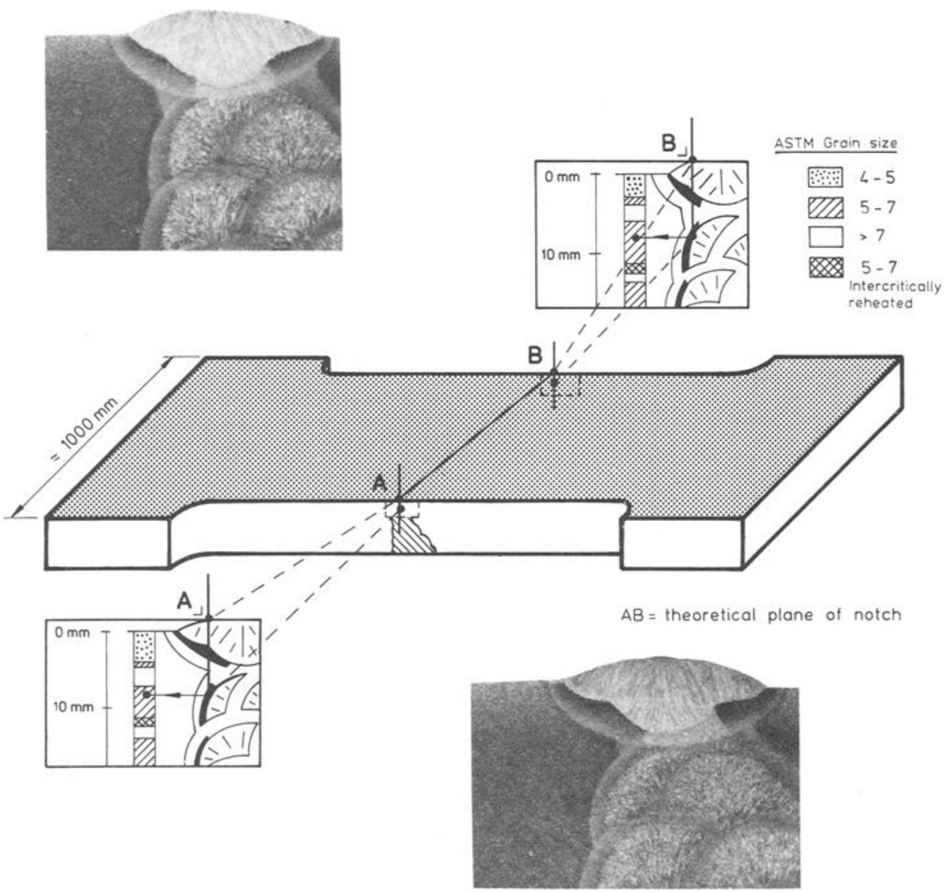

FIG. 10—*Schematic showing the procedure for marking out the theoretical fusion boundary in a wide-plate specimen.*

at the root side contains the largest portions of LBZ. These regions are located within the outer 15 to 20% of the specimen thickness. On the other hand, the areas of grain coarsening along the straight edge and towards the cap have normally smaller ligament depths.

The position of the fatigue crack tip at both ends of the wide plate specimen is then marked on the fusion line (Fig. 10). The relevant distances from the weld metal root (or cap pass) edge to the selected LBZ region are subsequently defined. This action is to be taken at both transverse ends of the wide-plate specimen. The position of Points A and B are referenced to the plate surface, and a reference line AB is drawn on the plate surface, which joins the two transferred position marks. Having checked that this line is truly parallel to the weld bead, the position of the assumed plane of the notch is scribed on the plate surface in preparation for machining.

Machining of the mechanical starter notch is to be performed by means of a sharp cutting wheel (0.15 mm in width) in order to facilitate fatigue crack initiation/propagation in the selected LBZ region. The mechanical starter notches are then fatigue precracked in three- or four-point bending.

Wide-Plate Test Performance

Performance Acceptance Criteria

Provided the size of the test crack represents either the worst case that could be encountered in the actual structure (which would be difficult to define) or a particular crack size that would be structurally tolerable, the performance acceptance criteria for the test then remain to be considered. Acceptability is to be based on the following criteria:

(*a*) the performance of the test in terms of straining capacity,
(*b*) the validation of the crack tip location, and
(*c*) the assessment of the microstructures of the neighboring region to the crack tip.

Test Performance

The wide-plate panel is principally to be loaded up to fracture; however, in some instances testing is to be interrupted when the applied elongation reaches the maximum stroke of the testing machine. This corresponds normally to an overall strain in excess of approximately 2%. Since strains beyond this level have no direct engineering significance, it is normal practice to interrupt the HAZ test and not to apply a second straining/loading cycle.

The acceptability of the wide-plate test result depends on the ultimate purpose of the test. As discussed in the previous paper, two situations can be considered. The test results can be used to substantiate conclusions drawn from small-scale tests and analysis [*2,3*], or alternatively, the test results can be employed to assess fitness for purpose directly when a preset acceptance level of overall strain for the particular application can be achieved [*1*].

Where the intention is to assess the wide-plate test results in pass/fail terms, there is a consensus that the crack under test should be required to withstand significant plastic strain. However, no specific pass/fail criterion is generally accepted. Some researchers propose that, for LBZ/HAZ tests, a demonstration of adequate ductility would be 0.5% strain measured in the (overmatching) weld metal, which would cause the parent plate to be also subjected to plastic strain [2]. Others call for gross section yielding as the criterion; that is, the strain in the parent plate must be above its yield strain [*35,36*]. The occurrence of GSY involves relaxation of crack tip constraint and, thus, demonstration of crack tip deformation capacity. This implies that, when the GSY requirement is satisfied, the possibility of a low-stress brittle fracture is remote for the HAZ region tested. Thus, if a wide-plate specimen exhibits GSY toughness, the structural component is expected to do likewise. Failure to meet the gross section yielding requirement means that the weld joint has an unacceptable fracture resistance and that a smaller crack must be tested to qualify the joint's validity. This opinion is not shared by those experts who base their acceptance on 0.5% strain. Instead, the significance of the result obtained is then established on the basis of a (CTOD) specific analysis (fitness for purpose) [*2,3*].

Crack Tip Validation

Upon completion of the test, the HAZ-notched wide-plate test specimen is sectioned and subjected to detailed macrographic and micrographic examination in order to establish the success rate of the fatigue crack-tip sampling position or positions. In addition, to permit a realistic comparison between wide-plate and CTOD test results, it is imperative that a substantial part of the fatigue crack front in a wide-plate test specimen sample the same microstructural features as in a CTOD specimen. It should be noted, however, that the wide-plate crack-tip location validation procedure requires a high number of micrographic sections since (*a*) the locations of the regions of low toughness sampled are not known in advance, and (*b*) the leading edge of the crack tip in the wide-plate specimen is generally much longer than that in a CTOD specimen.

The aspects of the sectioning technique are presented in detail in the next section of this paper.

Wide-Plate Specimen Sectioning

Before valid conclusions on the significance of a wide-plate test performance can be drawn, it is essential to demonstrate that the fatigue crack tip has intercepted the intended LBZ regions [*2,3,6–8*]. For this purpose, each HAZ surface precracked wide-plate specimen test must be supplemented with additional macrographical and micrographical examinations (posttest validation) (Figs. 11 through 15). The extent of the examinations depends upon the behavior of the test specimen at the end of the test. Generally, distinction is made between unfractured and fractured specimens in examination.

Unfractured Specimen

When no complete separation of the test specimen has been achieved, a coupon encompassing the whole crack is extracted from the test specimen by saw cutting. From both ends of the crack, a full-thickness macrosection is prepared to provide a local record, at the outer end of the crack, of the weld shape and to reveal the position of the coarse-grained region which was to be sampled. As before, the macrospecimens are analyzed in terms of fusion line microstructures, and the results of this examination are compared with those obtained from the end macrospecimens used for marking out the fatigue crack position.

The subsequent analysis is then conducted in accordance with one of the following sectioning techniques:

1. Access to the fatigue crack profile can be achieved by breaking the cracked coupon at liquid nitrogen temperature. This method provides a direct picture of the crack shape, while the sectioning technique is analogous to the technique used for fractured specimens (discussed further on).

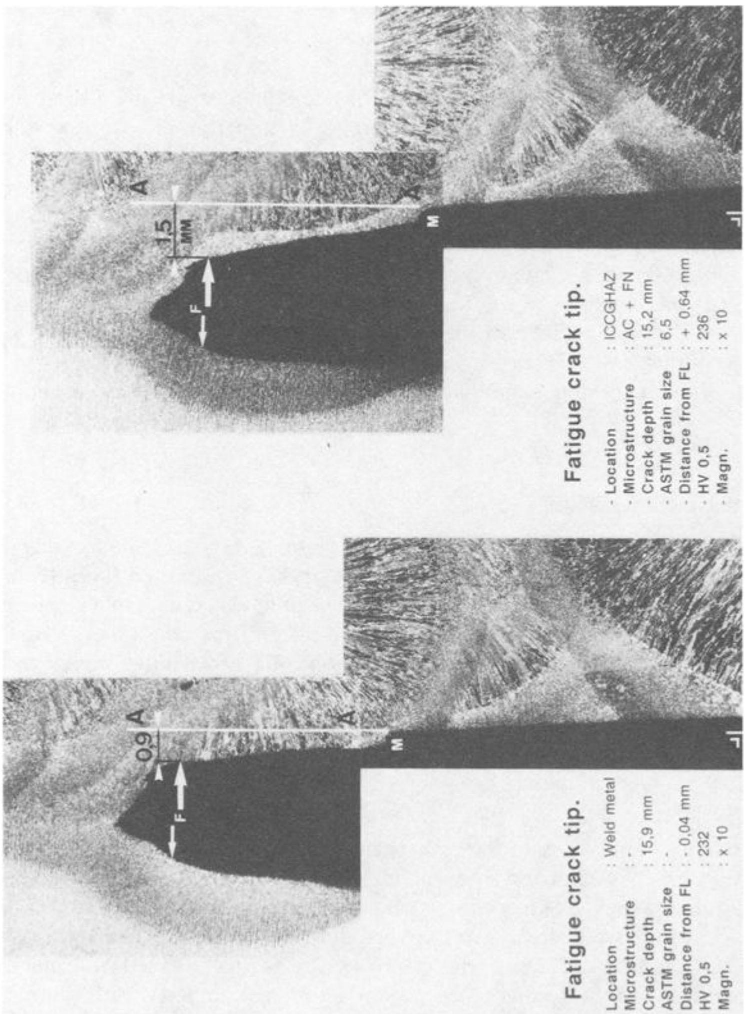

FIG. 11—*Photomicrographs illustrating the extent of crack path deviation after fatigue precracking and wide-plate testing: Line AA = the plane of crack growth normal to the axis of loading; M = the tip of the mechanical starter notch; F = the fatigue crack tip (spacing between macrosections = 20 mm) (magnification, ×10).*

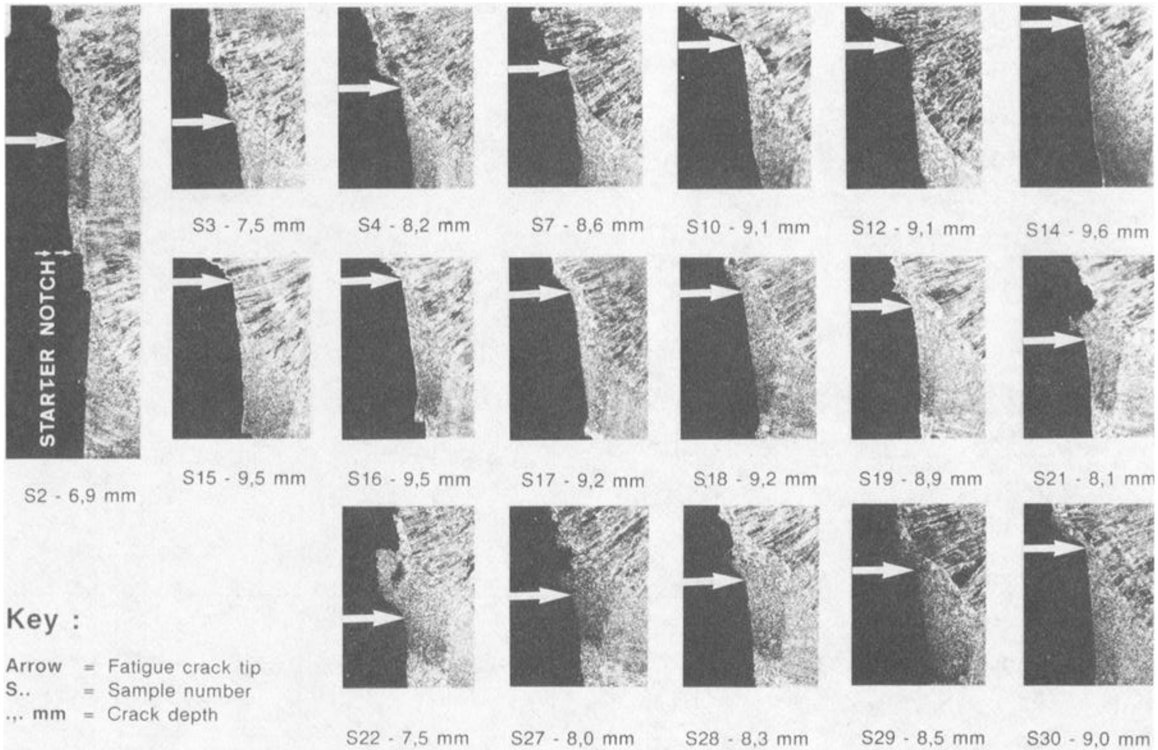

FIG. 12—*Photomicrographs showing the position of the fatigue crack tip versus the weld bead contour (magnification, ×10). The sampling positions are indicated in Fig. 13.*

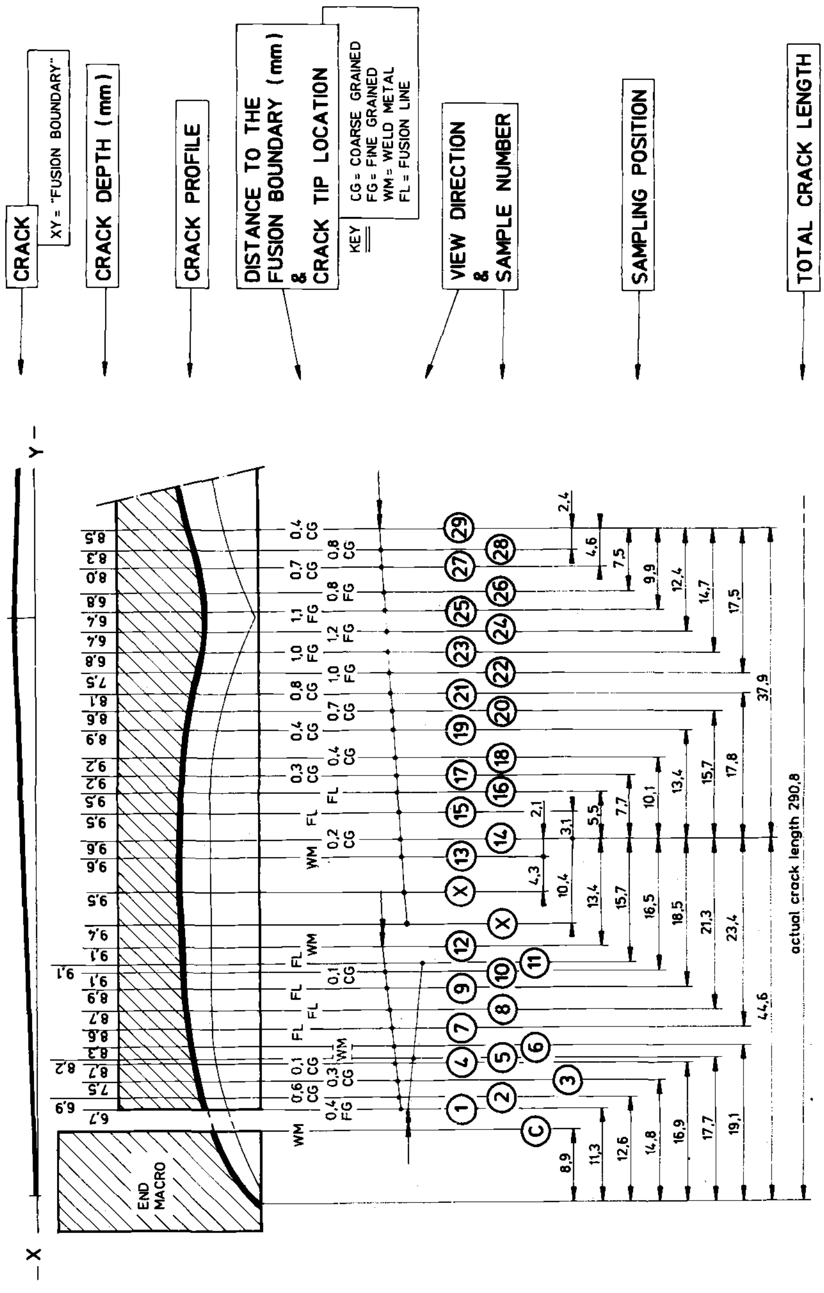

FIG. 13—*Typical example of wide-plate specimen sectioning, with indications of* (a) *the crack depth,* (b) *the microstructure sampled by the fatigue crack tip,* (c) *the distance from the fusion boundary, and* (d) *the location of the metallographic samples (see also Fig. 12).*

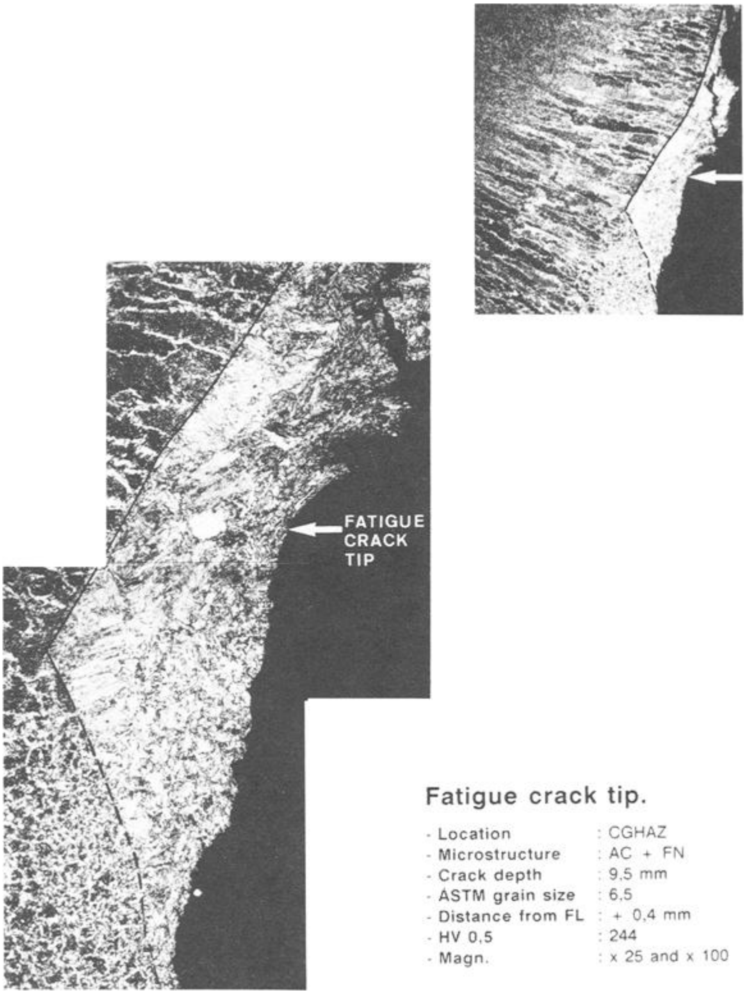

FIG. 14—*Enlarged photomicrograph showing the position of the fatigue crack tip in the grain-coarsened HAZ.*

2. Alternatively, as the breaking process may damage the crack tip profile, it may be advantageous to conduct the metallographic examinations on the unfractured coupon. In this way, the microstructures at the original crack tip can be seen, together with the microstructure associated with the ductile crack advance. Details of this procedure are discussed here.

The unbroken specimen coupon which contains the test crack is properly sectioned into 10-mm-wide samples and at the deepest point of each starter notch. The sections thus obtained are prepared for macroetching or microetching so that photographs will reveal the position of the fatigue crack tip with reference to both the fusion line and the coarse-grained HAZ at the end of test, as well as the amount of crack tip opening. Those photomicrographs

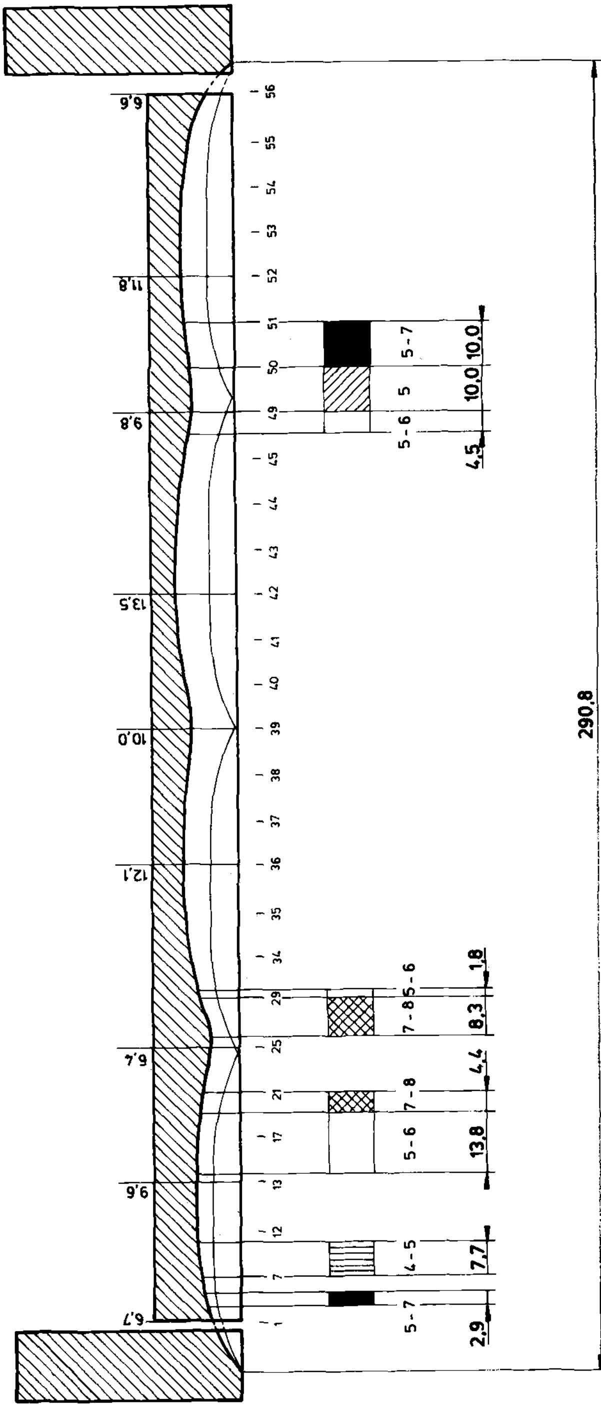

FIG. 15—*Typical example of sectioning results with indication of the crack depth and the grain size of the HAZ regions (the ASTM grain size number was below 7) sampled by the fatigue crack tip. The open, black, and hatched regions provide information on the areas of HAZ microstructures sampled and their locations within the length of the crack.*

are further used to assist in the selection of the subsequent microsections to be taken. In this context, account should be taken of both the crack path deviation and the original positions of the crack starter notches.

The photomicrographs of Fig. 11, which show a typical example of crack path deviation, illustrate that the extent of this deviation can be quite large. (The distance between these sections was 15 mm.)

When required, access to the crack profile is achieved by breaking the reduced sections at liquid nitrogen temperature. At that stage, detailed dimensional measurements of the crack front contour are performed in order to reconstruct the fatigue crack profile. That part of the various sections containing the weld is subsequently sliced perpendicular to the fracture face at several locations to trace the coarse-grained HAZ material. Further details of this procedure, which is very similar to that used for a fractured specimen, are given in the next section.

Fractured Specimen

In the event of fracture (or when access to the fatigue crack profile has been achieved for unfractured specimens), enlarged photographs (magnified one to four times) of the fracture face are taken on which the fracture initiation point, when identifiable, is indicated. The identification of that point may involve an examination by scanning electron microscope (SEM). In addition, low-magnification (50 to 100 times) SEM fractographs of the area between the prefatigue crack tip and the area of final crack extension by cleavage or fibrous tearing are taken to identify the micromechanism of the crack initiation process. In general, distinction is made between (*a*) blunting of the crack tip, which can be identified on the fracture surface as a stretch zone, (*b*) initiation by ductile shear, and (*c*) initiation by cleavage.

The weld metal side of the fracture face is then sectioned at right angles to the original plate surface through the initiation point and at several other locations. As the fatigue crack front is irregularly shaped, the author recommends that the crack front be sliced at least every 10 mm. When the subsequent micrographic examinations suggest the presence of the desired microstructures in the central portion of such a 10-mm-wide section, additional sections are taken in order to obtain a detailed picture of the desired microstructures sampled.

All sections selected for the macrospecimen and microspecimen examinations are polished to 1-μm finish and etched in 2% nital. During the investigations, emphasis is laid on a quantitative determination of the microstructures present along the length of the fatigue crack, the grain size at the very tip of the fatigue crack, and the linear extent to which the position of the fatigue crack tip differs from the fusion line (Fig. 11). As before, at every step during the said examinations, photographs at ten or twenty times magnification of typical sampling positions are taken to document the sectioning results. In that respect, such photomicrographs are very instructive in that they illustrate (*a*) that the fatigue crack tip may sample the plate material as well as the weld metal and (*b*) that even a special notching technique does not always cause a fatigue crack to propagate into the coarse-grained HAZ. The importance of this information is illustrated in Fig. 12.

An example of sectioning applied to a fractured specimen is shown in Figs. 12 and 13. The microphotographs shown in Fig. 12 are obtained from the sampling positions indicated in Fig. 13. The samples were extracted over a length of about 74 mm. These microphotographs in Fig. 12 illustrate clearly the variation in the weld bead profile and the amount of fatigue crack deviation towards the base material. This example emphasizes also the need to perform a rather detailed sectioning to obtain a complete picture of the microstructures sampled.

When the desired microstructure is sampled, it is essential that a picture be taken of the crack tip area at higher magnification (e.g., 100 to 200 times) in order to determine the precise microstructural constituents sampled and to illustrate the amount of crack tip blunting/ductile tearing which occurred prior to fracture initiation. A similar action is taken at the point of fracture initiation. The example in Fig. 14 shows the amount of plastic deformation and illustrates that the crack tip tore towards the base material side.

Finally, the relative proportions of each LBZ and its location along the fatigue crack tip are reported. This is conveniently done in the form of a bar chart on which the intercepted CGHAZ regions are indicated (Figs. 15 and 16). Figure 15 presents the results of the example given in Fig. 13. Figure 16 illustrates a slightly different way of presentation; in this figure, the microstructures sampled by the fatigue crack tip before and after testing are indicated. This figure illustrates also that the fatigue crack tip as well as the "blunted" crack tip sampled major coarse-grained HAZ regions during testing. It is not clear whether both regions may be accumulated in the validation process.

Concluding Remarks

The results of this study, which are principally concerned with notching and sectioning of HAZ cracked wide-plate test specimens, lead to the following conclusions:

1. Since the weld bead contour and, consequently, the positions of the coarse-grained HAZ regions vary considerably along the length of the weld, a careful notching procedure is needed to locate the test notch in the regions of suspected low notch toughness.
2. Since the likelihood of sampling a representative amount of LBZ region by using a straight crack-starter notch is small, it is believed that the rate of success of sampling these regions can be enhanced by using a multiple starter notch. The zigzag notch is to be preferred to the straight notch because it is possible with the former to sample a reasonable amount of LBZ region in a wide-plate test specimen, and because of its special shape, the measured toughness characteristics can be directly related to the practical situation of real fatigue cracks.
3. When the aim is to produce realistic wide-plate test data, it has been shown that, because of apparent variations in the weld bead/fusion boundary profile or profiles, the crack tip location of a HAZ crack in a wide-plate test specimen should be identified upon testing.

Overall Conclusions

The purpose of this paper is to give an overall picture of the meaning and usefulness of wide-plate test data. The previous two papers of this series, on wide-plate testing of weldments, summarize the background development and describe the role of the various wide-plate test specimen designs as well as the use of wide-plate test data in fracture research. This paper deals with the current testing requirements for HAZ testing. Various aspects of wide-plate testing, the role of the wide-plate test, and some outstanding problems with respect to weldment performance have been discussed. The following conclusions have been made:

1. Realistically sized test specimens must be used when weldment performance is evaluated. In order to apply to service behavior, the test should preferably be carried out on full-thickness specimens, while the test variables must be representative of service conditions. In other words, the purpose of the test, the specimen design, the specimen

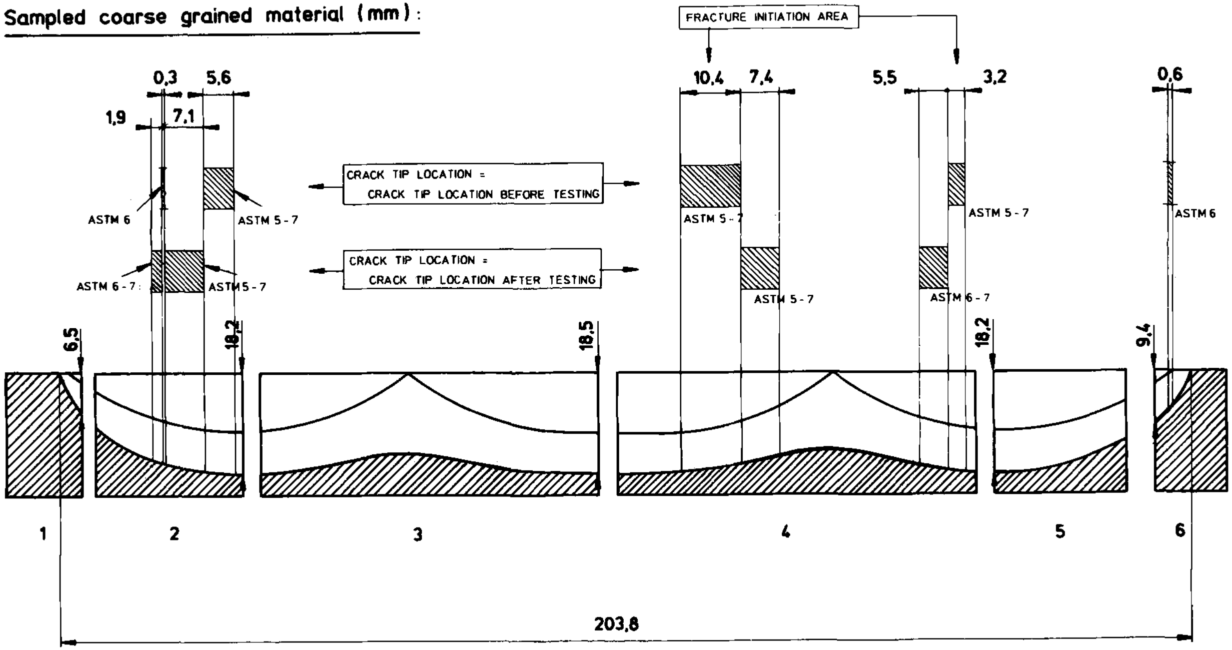

FIG. 16—*Typical example of sectioning results with indication of the crack depth and the grain size of the HAZ regions (the ASTM grain size number was below 7) sampled by the fatigue crack tip before and after testing. The hatched regions provide information on the areas of HAZ microstructures sampled and their locations within the length of the crack.*

extraction details from the test weld, the material condition, the loading conditions, the crack size to be qualified, and so forth, should be clearly stated. In view of these observations, one can expect that wide-plate testing will be retained for the assessment of "new steels" until standard test configurations allow an adequate assessment of the engineering significance of low-toughness regions contained in the weldment. Although wide-plate testing has many desirable features, its cost precludes its widespread adoption; therefore, it must be clear that the wide-plate test cannot be used as a primary investigative test and that it will never reach the status of a routine test.
2. In spite of the fact that most testing methods are able to identify the zones of low toughness in a weldment, all attempts to relate the measured toughness properties obtained from small-scale tests to those of, for example, wide-plate tests are not always successful. It appears unlikely, as can be appreciated from previous considerations, that such a solution will become available in the near future, and it may be expected that the difference in opinion on the significance of low-toughness properties measured in small-scale testing will remain for some time. One approach to clarify the controversy is to combine the small-scale and large-scale types of tests and examine data correlations. This would probably produce more convincing information than detailed theoretical considerations.

Acknowledgments

The author wishes to thank A. Vinckier, professor and director of the Laboratory Soete for Strength of Materials and Welding Technology, Gent University, Belgium, for permission to publish this paper. The financial support of IWONL and NFWO is also acknowledged.

References

[*1*] Denys, R., "The Effect of Defect Size on Wide Plate Test Performance of Multipass Welds with Local Brittle Zones," *Proceedings*, TMS Conference on Welding Metallurgy of Structural Steels, J. Koo, Ed., Denver, CO, February 1987, pp. 319–334.

[*2*] Pisarski, H. G. and Walker, E. F., "Wide Plate Testing as a Backup to the CTOD Approach," Report for the Department of Energy 3915/4/86, The Welding Institute, Cambridge, England, 1986.

[*3*] Pisarski, H. G., "Philosophy of Welded Wide Plate Testing for Brittle Fracture Assessment," *The Fracture Mechanics of Welds*, EGF Publication No. 2, Mechanical Engineering Publications, London, 1987, pp. 191–208.

[*4*] Walker, F. E., "Steel Quality, Weldability and Toughness," *Steel in Marine Structures*, Elsevier Science Publishers, Amsterdam, 1987, pp. 49–70.

[*5*] Royer, C., "A User's Perspective on Heat-Affected Zone Toughness," *Proceedings*, TMS Conference on Welding Metallurgy of Structural Steels, J. Koo, Ed., Denver, CO, February 1987, pp. 255–262.

[*6*] Denys, R. M., "Wide Plate Fracture Toughness Evaluation of the Weld HAZ of Low Carbon Micro-Alloyed Structural Steel Weldments," *Proceedings*, CIM/CSFM Symposium, Winnipeg, Canada, August 1987.

[*7*] Watanabe, I., Kagawa, H., and Matsuda, Y., "Evaluation of Coarse-Grained HAZ Toughness by Wide-Plate Testing," *Proceedings*, Seventh International Conference on Offshore Mechanics and Arctic Engineering, February 1988, pp. 387–394.

[*8*] Webster, S. E. and Walker, E. F., "The Significance of Local Brittle Zones to the Integrity of Large Welded Structures," *Proceedings*, Seventh International Conference on Offshore Mechanics and Arctic Engineering, February 1988, pp. 395–404.

[*9*] American Petroleum Institute, "Specification for Carbon Manganese Steel Plate for Offshore Platform Tubular Joints," API Specification 2H, March 1983; "Specification for Steel Plates for Offshore Structures, Produced by Thermomechanical Control Processing (TMCP)," API Specification 2W, May 1987; and "Specification for Steel Plates Quenched and Tempered for Offshore Structures," API Specification 2Y, May 1987.

[10] "Steel Specification for Fixed Offshore Structures," (1987). EEMUA Publication No. 150, Engineering Equipment and Materials Users Association, London, England, 1987.
[11] Squirrell, S. J., Pisarski, H. G., and Dawes, M. G., "Recommended Procedures for Crack-Tip Opening Displacement (CTOD) Testing of Weldments," Doc. 7807.02/86/485.2, The Welding Institute, Cambridge, England, 1986.
[12] Dolby, R. E. and Saunders, G. G., "Subcritical HAZ Fracture Toughness of C-Mn Steels," *Metal Construction and British Welding Journal*, Vol. 4, No. 5, 1972.
[13] Dolby, R. E., "The Influence of Defect Orientation and Heat Affected Zone Fracture Toughness Measurements," Research Report E/51/72, The Welding Institute, Cambridge, England, February 1973.
[14] Archer, G. L., "Fracture Toughness in the Heat-Affected Zones of a Carbon-Manganese Steel and a Low Alloy Steel," *Metal Construction and British Welding Journal*, December 1974, pp. 369–374.
[15] Dolby, R. E., "HAZ Toughness of Structural and Pressure Vessel Steels—Improvements and Prediction," *Welding Research Supplement, AWS*, August 1979, p. 225.
[16] Dawes, M. G., Pisarski, H. G., Towers, O. L., and Williams, S., "Fracture Toughness in Welded Joints," *Proceedings*, International Conference on Fracture Toughness Testing—Methods, Interpretation, and Application, The Welding Institute, London, England, June 1982.
[17] Pisarski, H. G. and Pargeter, R. J., "Fracture Toughness of Weld HAZ's in Steels Used in Constructing Offshore Platforms," *Proceedings*, Conference on Welding in Energy Related Products, Toronto, Canada, September 1983, pp. 415–428.
[18] Walker, F. E., "Fracture Toughness Testing: Present Status of Charpy V-Notch Impact and CTOD Testing," *Proceedings*, Conference on the State of the Art in Materials Testing, Gent, Belgium, November 1986.
[19] de Koning, A. C., "Modern Steels in Today's Oil Industry," *Proceedings*, Conference on the State of the Art in Materials Testing," Gent, Belgium, November 1986.
[20] Fairchild, D. P., "Local Brittle Zones in Structural Welds," *Proceedings*, TMS Conference on Welding Metallurgy of Structural Steels, J. Koo, Ed., Denver, CO, February 1978, pp. 303–318.
[21] Dolby, R. E., "Steels for Offshore Construction," *Proceedings*, Paper 6, Conference Towards Rational and Economical Fabrication of Offshore Structures—Overcoming the Obstacles, The Welding Institute, London, England, 22–23 Nov. 1984.
[22] Pisarski, H. G., "How to Measure Heat-Affected Zone (HAZ) Toughness," *Proceedings*, Conference Towards Rational and Economic Fabrication of Offshore Structures—Overcoming the Obstacles, London, England, 22–23 Nov. 1984.
[23] Thaulow, C., Paauw, A. J., Gunleiksrud, A., and Naess, O. J., "Heat-Affected Zone Toughness of a Low Carbon Microalloyed Steel," *Metal Construction*, February 1985, pp. 94–99.
[24] Haze, T. and Aihara, S., "Metallurgical Factors Controlling HAZ Toughness In HT50 Steels," IIW Doc. IX-1423-86, International Institute of Welding, Strassbourg, Germany, May 1986.
[25] Koo, J. Y. and Ozekzin, A., "Local Brittle Zone Microstructure and Toughness in Structural Steel Weldments," *Proceedings*, TMS Conference on Welding Metallurgy of Structural Steels, J. Koo, Ed., Denver, CO, February 1987, pp. 119–136.
[26] Pisarski, H. G., "Measurement of Heat-Affected Zone Fracture Toughness," *Proceedings*, Third International ECSC Offshore Conference on Steel in Marine Structures (SIMS '87), Delft, The Netherlands, 15–18 June 1987, pp. 647–656.
[27] De Koning, A. C., Harston, J. D., Nayler, K. D., and Ohm, R. K., "Feeling Free Despite LBZ," *Proceedings*, Seventh International Conference on Offshore Mechanics and Arctic Engineering, February 1988, pp. 161–180.
[28] Denys, R. and McHenry, H. I., "Local Brittle Zones in Steel Weldments: An Assessment of Test Methods," *Proceedings*, Seventh International Conference on Offshore Mechanics and Arctic Engineering, February 1988, pp. 379–386.
[29] Fairchild, D. P., Theisen, J. D., and Royer, C. P., "Philosophy and Technique for Assessing HAZ Toughness of Structural Steels Prior to Steel Production," *Proceedings*, Seventh International Conference on Offshore Mechanics and Artic Engineering, February 1988, pp. 247–256.
[30] Bateson, P. H., Webster, S. E., and Walker, E. F., "Assessment of HAZ Toughness Using Small-Scale Tests," *Proceedings*, Seventh International Conference on Offshore Mechanics and Arctic Engineering, February 1988, pp. 257–266.
[31] Satoh, K. and Toyoda, M., "Evaluation of LBZ: HAZ Fracture Toughness Testing and Utilization of Toughness Testing and Utilization of Toughness Data to Structural Integrity," *Proceedings*, Seventh International Conference on Offshore Mechanics and Arctic Engineering, February 1988, pp. 495–502.

[32] Webster, S. E., "The Structural Significance of Low-Toughness HAZ Regions in a Modern Low-Carbon Structural Steel," *The Fracture Mechanics of Welds*, EGF Publication No. 2, Mechanical Engineering Publications, London, 1987, pp. 59–75.
[33] Denys, R. M., Dhooge, A., and Lefevre, A. A., "HAZ Fatigue Precracking of Welded Plate Specimens," *Proceedings*, Conference on the State of the Art in Materials Testing, Gent, Belgium, November 1986.
[34] Denys, R. M., "The Deviation of Fatigue Crack Path in Fracture Toughness Testing," *Proceedings*, Third International ECSC Offshore Conference on Steel in Marine Structures (SIMS '87), Delft, The Netherlands, 15–18 June 1987, pp. 913–926.
[35] Masubuchi, K., *Analysis of Welded Structures, International Series on Material Science and Technology*, Vol. 33, Pergamon Press, New York, 1980.
[36] Denys, R. M., "Toughness Requirements in Transversely Load Welded Joints—An Evaluation Based on Wide Plate Testing," *The Fracture Mechanics of Welds*, EGF Publication No. 2, J. G. Blauel and K.-H. Schwalbe, Eds., Mechanical Engineering Publications, London, 1987, pp. 155–189.

Jae-Kyoo Lim[1] *and Se-Hi Chung*[2]

Stress Effect on Post-Weld Heat Treatment Embrittlement

REFERENCE: Lim, J.-K. and Chung, S.-H., **"Stress Effect on Post-Weld Heat Treatment Embrittlement,"** *Fatigue and Fracture Testing of Weldments, ASTM STP 1058,* H. I. McHenry and J. M. Potter, Eds., American Society for Testing and Materials, Philadelphia, 1990, pp. 229–255.

ABSTRACT: Post-weld heat treatment (PWHT) is carried out to improve fracture toughness and to remove residual stress in the heat-affected zone (HAZ). There are some problems, such as a toughness decrease and stress-relief cracking (SRC) in the coarse-grained HAZ subject to the effect of the tempering treatment. Therefore, in this paper, the effect of the heating rate and heat input on PWHT embrittlement under applied stresses of 0, 98, 196, and 294 MPa (0, 10, 20, and 30 kg/mm^2), applied to simulate residual stress in the welded HAZ of chromium-molybdenum (Cr-Mo) steel was evaluated using the crack-opening displacement (COD) fracture toughness test and observation of the fracture surfaces. The fracture toughness of welded HAZ decreased with an increase in the heating rate under no stress, but it improved with an increase in the heating rate under stress. Applied stress in welded HAZ during PWHT assisted precipitation of oversaturated alloying elements in the structure, so grain boundary failure from the welding heat input was barely evident at a heat input of 10 kJ/cm and a heating rate of 600°C/h, but it appeared at an applied stress of 294 MPa at 30 kJ/cm and 220°C/h and of 196 MPa at 40 kJ/cm and 60°C/h.

KEY WORDS: weldments, post-weld heat treatment, PWHT embrittlement, residual stress, heating rate, heat input, COD fracture toughness test, welded HAZ, grain boundary failure

A weldment, especially in the heat-affected zone (HAZ), is a very complicated and variable structure formed from different thermal and environmental conditions [*1,2*]. This complexity involves the inherent mechanical behavior of the weld, including its strength, hardness, and fracture toughness. In addition, three-dimensional residual stress and deformation due to welding result in a significant decrease of fracture toughness in the HAZ [*3–5*]. Therefore, in welding low-alloy steels such as chromium-molybdenum (Cr-Mo) steel, post-weld heat treatment (PWHT) is a common practice for removing undesirable residual stresses, along with welding and hydrogen existing in the weldment [*6,7*]. PWHT of these steels at very high temperatures, over 600°C, however, can cause a coarse-grained region to form near the fusion line of the HAZ, resulting not only in embrittlement but also in stress-relief cracking (SRC) [*8–10*].

It is said that the cause of PWHT embrittlement is the residual stress existing in the weld HAZ [*11,12*] or the precipitation of inclusions at the grain boundary [*13,14*]. In particular, embrittlement of a structure directly relates to its mode of fracture and appears as a difference in the fracture surface, such as grain boundary failure.

[1] Associate professor, Mechanical Design Department, Chonbuk National University, Chonju 560-756, Korea.
[2] Professor, Precision Mechanical Engineering Department, Chonbuk National University, Chonju 560-756, Korea.

Therefore, in this paper, the effect of the stress level and heating rate during PWHT and the effect of the structure of the welded HAZ on PWHT embrittlement were evaluated by the crack-opening displacement (COD) fracture toughness test [*15*], the microhardness test, and observation of the fracture surface by scanning electron microscope (SEM).

Material and Experimental Procedure

The material used in this study was Cr-Mo steel plate 16 mm thick. Tables 1*a* and 1*b* indicate its chemical composition and mechanical properties. The specimens, as shown in Fig. 1, were cut from small blanks 150 by 300 mm. After being cut, they were welded by automatic submerged-arc welding in a direction transverse to the rolling direction and were V-grooved. The electrode used was one by EG-G and the flux was F11A6 (American Welding Society classification). The welding conditions are given in Table 2. The grain sizes at the fusion line were 70, 76, and 120 μm, respectively, after heat inputs of 10, 30, and 40 kJ/cm, respectively. The single bead on the plate was cut transverse to the welding bead for the treatment. The dimensions of the first specimen employed for PWHT under constant load at the notch tip by four-point bending were 10 by 10 by 70 mm, and the specimen was machined again to the Charpy standard specimen dimensions (10 by 10 by 55 mm) for the COD test by three-point bending after PWHT.

A notch of 2-mm depth in the direction of the thickness was machined by a cut-off wheel with a thickness of 0.3 mm according to the ASTM Test for Plane-Strain Fracture Toughness of Metallic Materials (E 399-83). The notch tip was placed at the coarse-grained structure of the fusion line at the center of the bead on the plate. The prepared specimens were subjected to PWHT under the following conditions: the stress applied at the notch tip by four-point bending during heat treatment was 0, 98, 196, or 294 MPa at 650°C (923 K); the heat input was 10, 30, or 40 kJ/cm; the heating rate was 600, 220, or 60°C/h; and the holding time was the same, ¼ h at 650°C (923 K). These heat-treated specimens were tested by the COD fracture toughness test using the experimental apparatus in Fig. 2, and the range of the testing temperature was −175 to +50°C. The fracture surfaces were observed by scanning electron microscope (SEM). In order to evaluate the relationship between the fracture toughness and the hardness of the welded HAZ, the material was measured for microhardness around the notch tip using a micro-Vickers hardness tester.

Experimental Results and Analysis

Low-Temperature Fracture Toughness in Accordance with the Change in Heat Input

Figure 3 shows the results of COD fracture toughness tests of welded HAZ at a variety of heat inputs which are related to the critical COD and testing temperatures. The temperature dependence curves of the critical COD, δ_c, on the HAZ structure of the as-welded metal shift to the side of a higher temperature than that of the parent metal. We know that the welded structure of as-welded metal is embrittled more than that of the parent metal.

TABLE 1*a*—*Chemical composition of the Cr-Mo steel plate used in this study, in weight percent.*

C	Si	Mn	P	Cu	Ni	Cr	Mo	S
0.39	0.26	0.72	0.025	0.002	0.02	0.98	0.193	0.008

TABLE 1*b*—*Mechanical properties of the Cr-Mo steel plate used in this study.*

Tensile Strength, MPa	Yield Strength, MPa	Elongation, %
1020	665	19.2

Moreover, COD curves move to the area of higher temperatures according to the increase in the heat input. These results indicate that the brittleness ratio of HAZ structure increases with the heat input. Curves relating the critical COD and testing temperature of specimens with PWHT done under no stress move into the lower temperature area, as shown in Fig. 3.

Figure 4 reports the results from the fracture surfaces of COD specimens observed with the scanning electron microscope. According to these results, the entire fracture surface is a brittle surface with cleavage at a critical COD of δ_c = 0.22, 0.235 mm, but the fracture surface is mixed with a ductile fracture surface at δ_c = 0.27, 0.3 mm. Based on these results, the transition temperature, T_{tr}, between ductility and brittleness in each curve is obtained at δ_c = 0.25 mm, and we can evaluate the degree of ductility and brittleness of the microstructure by using T_{tr}. The T_{tr} of the as-welded and PWHT metal is the temperature at Points a, b, c, e, f, and g in Fig. 3.

Figure 5 shows the relationship between T_{tr}, which is obtained from Fig. 3, and the heat input value. In this figure, the T_{tr} of the as-welded metal was changed to −44, +12, and +64°C, respectively, when the parent metal (T_{tr} = −63°C) was welded at heat inputs of 10, 30, and 40 kJ/cm; that is, the T_{tr} shifts linearly to the higher temperature with the increase in heat input; in other words, the degree of brittleness increased linearly with the heat input. After PWHT, T_{tr} became −120, −143, and −155°C respectively; the fracture toughness of the welded HAZ greatly increased and the degree of toughness increment increased linearly

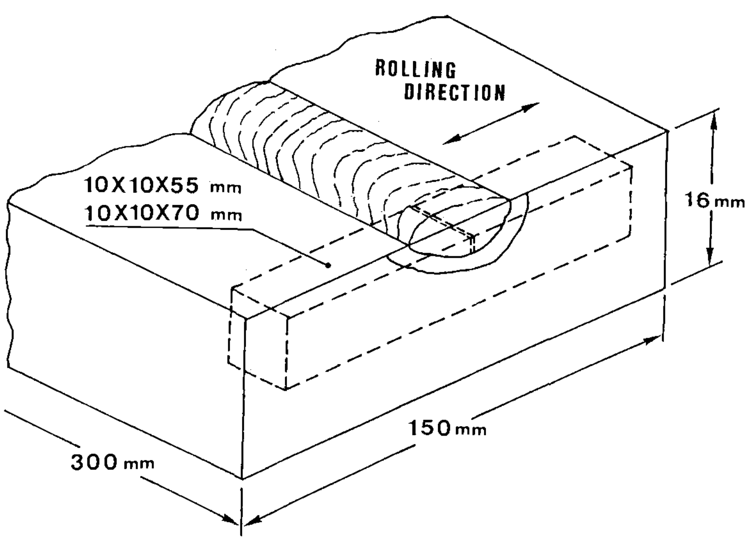

FIG. 1—*Welding plate configuration and the extraction of specimens.*

TABLE 2—*Welding conditions (submerged arc welding).*

Heat Input, kJ/cm	Preheating Temperature, °C	Current, A	Voltage, V	Welding Speed, cm/min	Wire Diameter, mm
10	200	300	20	36	3.2
30	200	500	30	30	3.2
40	200	500	40	30	3.2

with the heat input. From these results we know that the original toughness of the HAZ structure at no stress was improved greatly after PWHT, and the range of increase enlarged according to the increasing heat input. PWHT was carried out to observe the effect of stress applied to the HAZ structure on its fracture toughness under stresses of 98, 196, and 294 MPa, respectively.

Figure 6 shows the relationship between the difference in transition temperature $(\Delta T_{tr})_{\sigma=0}$ and the applied stress on the basis of specimens heat treated under the no stress (σ = 0 MPa). At the time when the heat input was 10 kJ/cm, the fracture toughness increased with the applied stress at stresses within 196 MPa, but it slowly recovered at a stress of 294 MPa. This fact shows that PWHT greatly affects the embrittlement rather than the applied stress of a small-grained structure at a low heat input (10 kJ/cm). Consequently, it appears that PWHT retards the susceptibility of embrittlement owing to the small size of the HAZ welded at low heat input. But PWHT embrittlement was observed at the welding condition of heat input of 30 kJ/cm under applied stresses over 196 MPa. That is, a fracture toughness increase results from the recovery of toughness because of the increase in elasticity deformation energy. On the other hand, the toughness at a heat input of 40 kJ/cm decreases

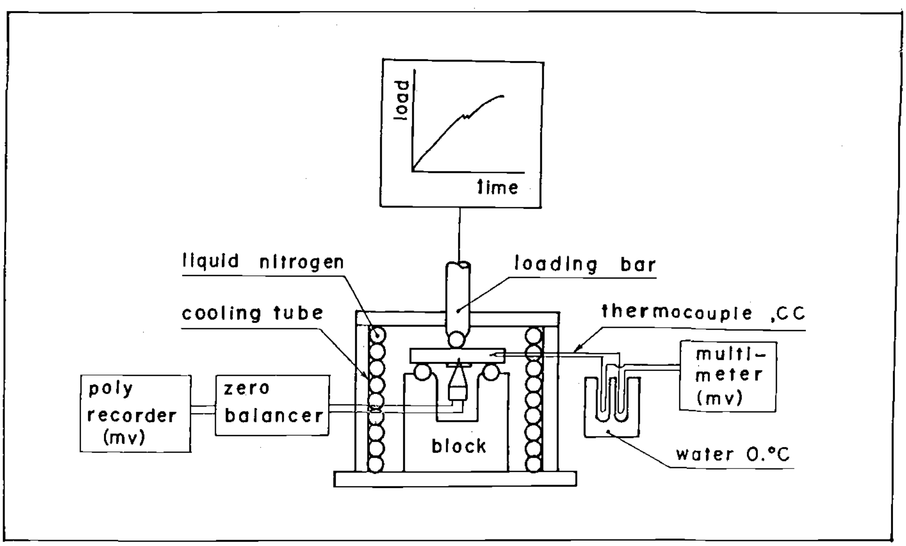

FIG. 2—*Schematic diagram of the COD test equipment.*

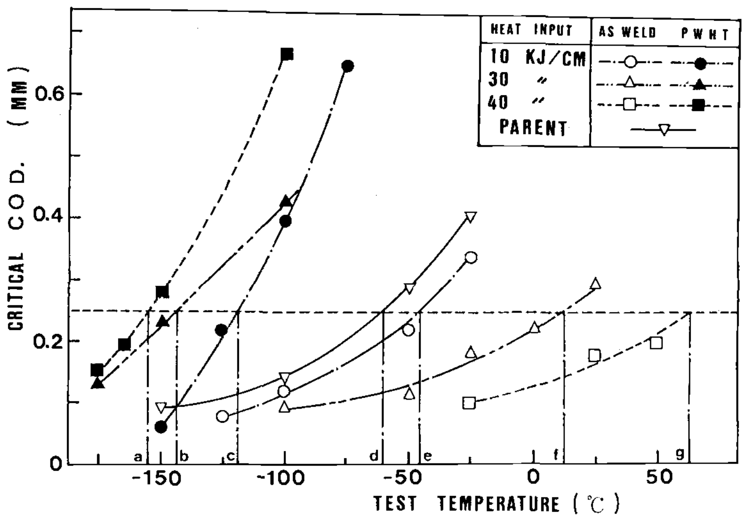

FIG. 3—*Relationship between the critical COD and the testing temperature with respect to heat input [PWHT conditions, 650°C (923 K), ¼ h, 220°C/h].*

linearly according to the magnitude of the applied stress. Consequently, PWHT embrittlement due to residual stress greatly increased in the case of high heat input.

Figure 7 shows the relationship between the difference in the transition temperature, $(\Delta T_{tr})_{\sigma=0}$, and the hardness ratio based on σ = 0 MPa, $HV/(HV)_{\sigma=0}$, according to the change in heat input. The $(\Delta T_{tr})_{\sigma=0}$ increased with the $HV/(HV)_{\sigma=0}$ of the structure according to applied stress at heat inputs of 10 and 30 kJ/cm, but $(\Delta T_{tr})_{\sigma=0}$ decreased with the increase of $HV/(HV)_{\sigma=0}$ at 40 kJ/cm, which is opposite to the effect of the heat input at 10 and 30 kJ/cm. This shows that the fracture toughness decreased in spite of the decreased hardness of the HAZ structure because of applied stress during PWHT. This fact shows that PWHT embrittlement results in the precipitation of inclusions of carbide to the grain boundary because of the applied stress in coarse-grained HAZ.

Effect of Applied Stress and Heating Rate on Welded HAZ Fracture Toughness

Figure 8 shows the results of the COD fracture toughness test as the relationship between the critical COD and the testing temperature according to the heating rate. The related curves between δ_c and the testing temperature of the heat-treated specimen under various conditions are shown, while those the as-welded metal are on the right. This result indicates that the fracture toughness of welded HAZ is improved by PWHT and that the improvement in fracture toughness changes according to the magnitude of the heating rate and applied stress. To find the degree of change of the fracture toughness due to the heating rate under applied stress, the relationship between $(\Delta T_{tr})_{\sigma=0}$ and the heating rate can be given, as is shown in Fig. 9, which indicates that $(\Delta T_{tr})_{\sigma=0}$ at 220°C/h is higher than any other heating rate at the applied stress of 98 MPa. This result shows that the heating rate of 220°C/h is the heating rate causing PWHT embrittlement. But, $(\Delta T_{tr})_{\sigma=0}$ increases with the slower and slower heating rate at the applied stress of 196 and 294 MPa; that is, the slower the heating rate is, the greater the degree of PWHT embrittlement.

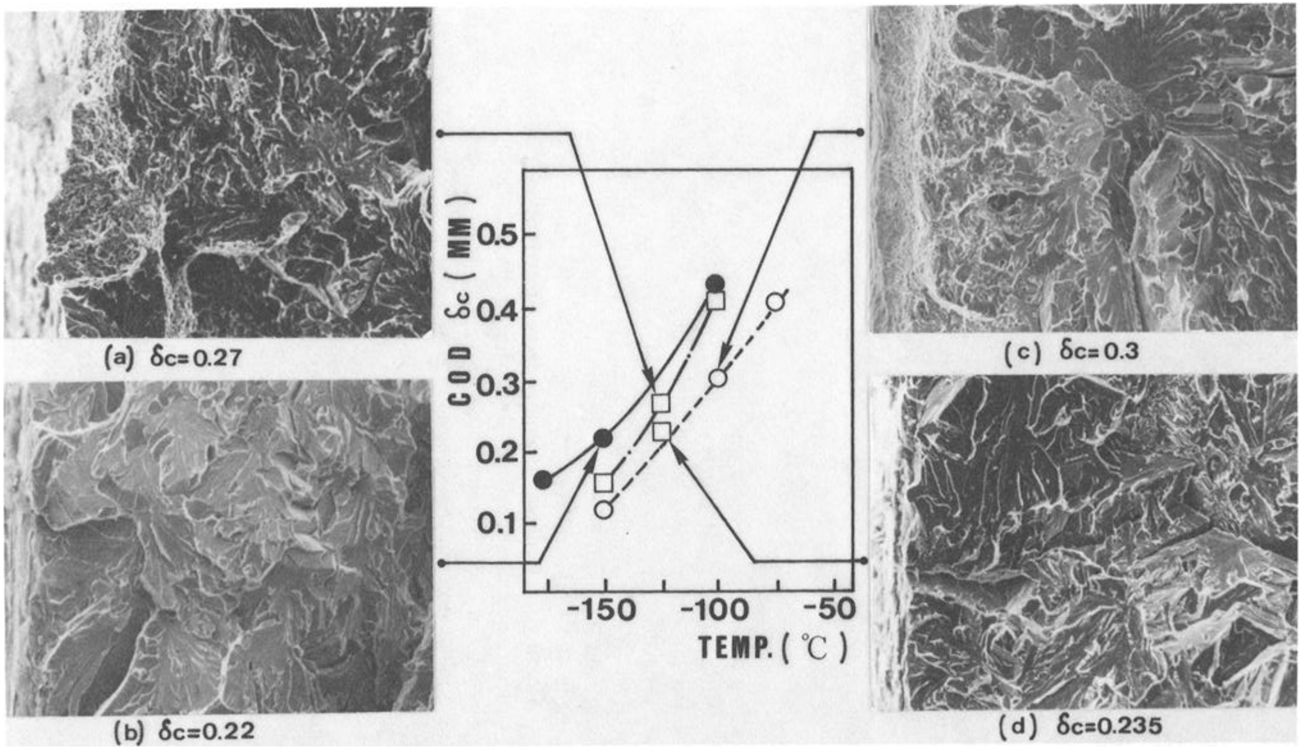

FIG. 4—*Scanning electron microscope observation of the transition temperature.*

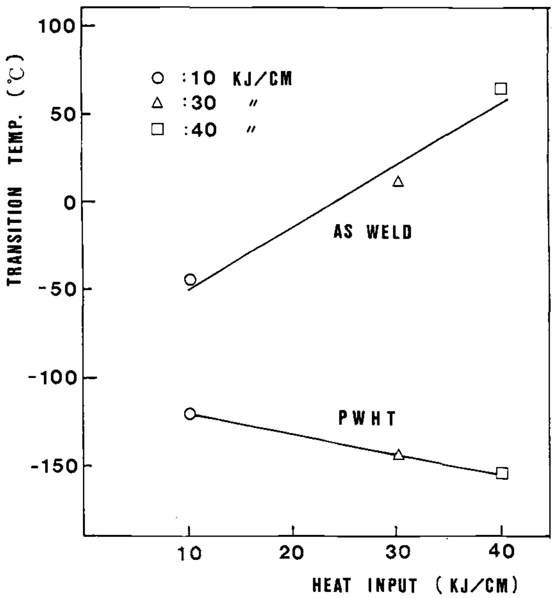

FIG. 5—*Relationship between the transition temperature,* T_{tr}, *and the heat input.*

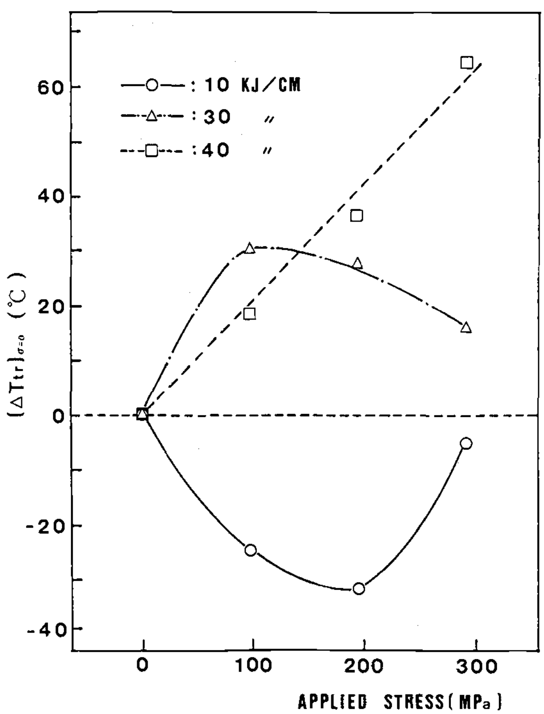

FIG. 6—*Relationship between the difference in transition temperature,* $(\Delta T_{tr})_{\sigma=0}$, *and the applied stress with respect to heat input.*

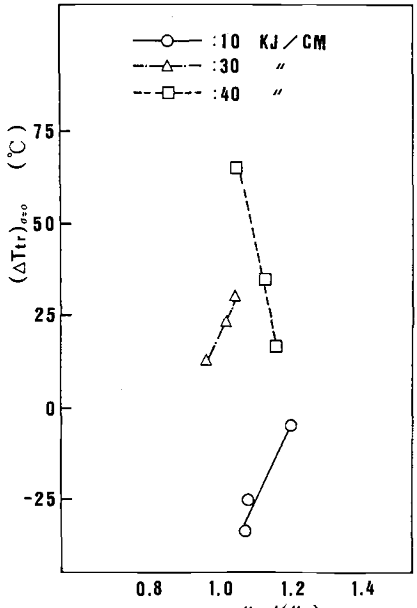

FIG. 7—*Relationship between the difference in transition temperature, $(\Delta T_{tr})_{\sigma=0}$, and the hardness ratio, $HV/(HV)_{\sigma=0}$, with respect to the heat input.*

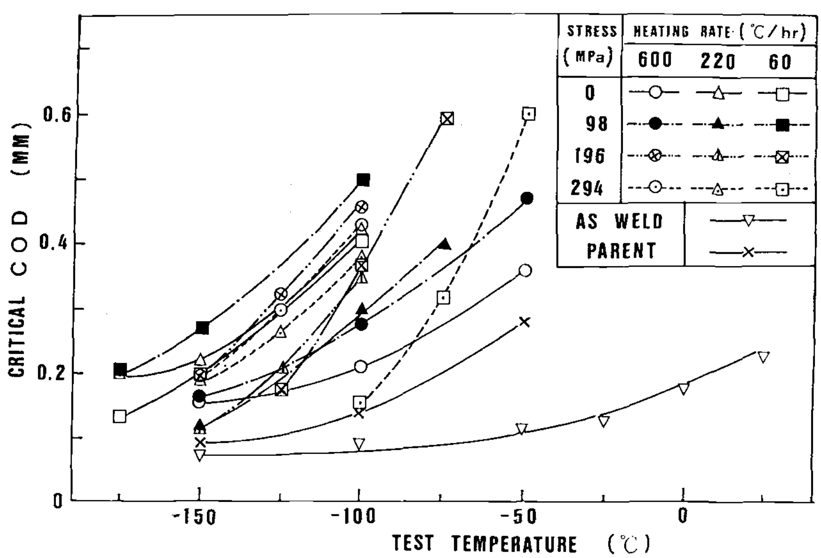

FIG. 8—*Relationship between the critical COD and the testing temperature with respect to the heating rate [heat input, 30 kJ/cm; PWHT conditions, 650°C (923 K), ¼ h].*

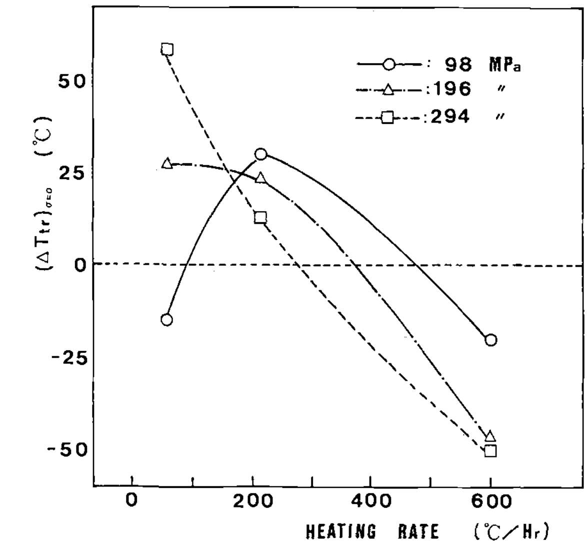

FIG. 9—*Relationship between the difference in transition temperature,* $(\Delta T_{tr})_{\sigma=0}$, *and the heating rate with respect to applied stress.*

Figure 10 shows the relationship between $(\Delta T_{tr})_{\sigma=0}$ and applied stress and indicates that $(\Delta T_{tr})_{\sigma=0}$ at the applied stress of 98, 196, and 294 MPa decreases to −20, −46, and −52°C, respectively, at the fast heating rate of 600°C/h. These results show that the applied stress of HAZ structure improves the fracture toughness at this heating rate; in particular, the stress acting on HAZ structure promotes the increase of fracture toughness. But, at the

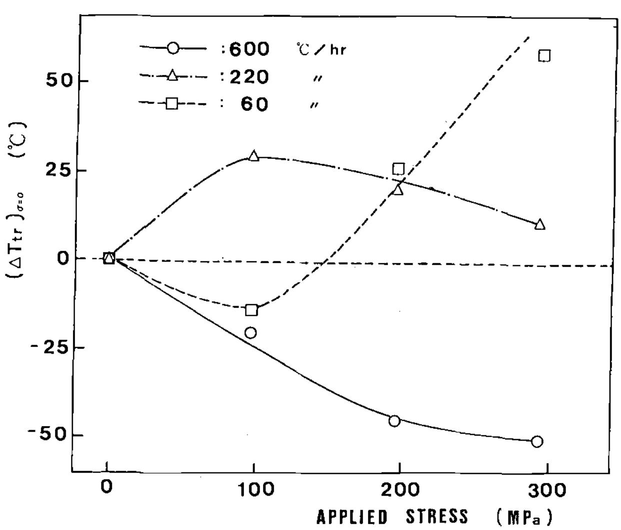

FIG. 10—*Relationship between the difference in transition temperature,* $(\Delta T_{tr})_{\sigma=0}$, *and the applied stress with respect to the heating rate.*

heating rate of 220°C/h, in spite of the promotion of fracture toughness by the structure itself, $(\Delta T_{tr})_{\sigma=0}$ stands in the high-temperature area at all applied stresses, which indicates that this heating rate is the velocity of PWHT embrittlement.

Also, at the heating rate of 60°C/h, the improvement in fracture toughness and in the ratio of brittleness of the welded HAZ are greatly affected by the applied stress, as shown in Fig. 10. That is, at σ = 98 MPa, $(\Delta T_{tr})_{\sigma=0}$ is −15°C, which indicates that the effect of full annealing appeared strongly, showing improvement in the fracture toughness, but the PWHT embrittlement of welded HAZ caused by the applied stress is greatly increased. It can be shown that $(\Delta T_{tr})_{\sigma=0}$ rises to +28 and +60°C, increasing with applied stress up to 196 and 294 MPa, which indicates that the effect of the residual stress is greater than that of the heat-treatment phenomenon on the metal structure at the heating rate of 60°C/h. These results show that PWHT embrittlement is affected not only by the cooling rate, but also by the heating rate of the PWHT and residual stress on the welding joint. Figure 11 is the relationship between $(\Delta T_{tr})_{\sigma=0}$ and the hardness ratio $HV/(HV)_{\sigma=0}$, which shows the degree of change in HAZ structure produced by the heating rate and applied stress. This diagram shows that $(\Delta T_{tr})_{\sigma=0}$ increased with the hardness ratio at the heating rates of 600 and 220°C/h; that is, PWHT embrittlement increases with the hardness ratio. But PWHT embrittlement increased significantly in spite of the decrease in $HV/(HV)_{\sigma=0}$ at the heating rate of 60°C/h. This effect is the opposite of that at 600 and 220°C/h. The decrease in fracture toughness suggests that the precipitation of secondary elements like chromium and molybdenum to grain boundaries during PWHT is the cause of embrittlement. A heating rate of 60°C/h is inadequate for PWHT because PWHT embrittlement is due to the precipitation of inclusions or carbide during PWHT.

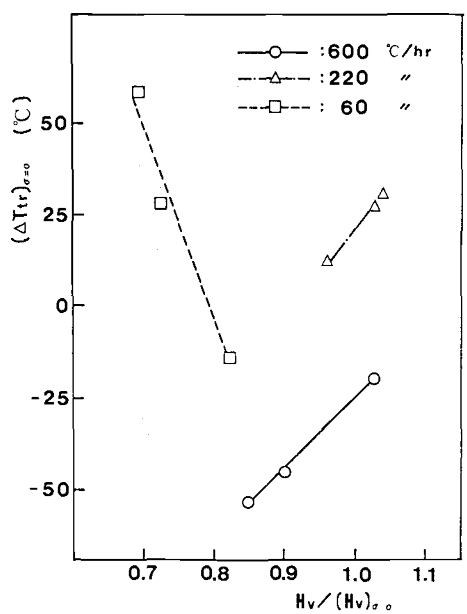

FIG. 11—*Relationship between the difference in transition temperature,* $(\Delta T_{tr})_{\sigma=0}$, *and the hardness ratio,* $HV/(HV)_{\sigma=0}$, *with respect to the heating rate.*

PWHT Embrittlement Appearance by Fractography of the Fracture Surface

The fracture surfaces of a notch tip broken at −100°C were observed to determine the effect of the PWHT parameter on fracture behavior. Figure 12 shows the fracture surface of the parent metal and as-welded metal. The surface of the parent metal at the critical COD δ_c = 0.14 mm was almost a brittle fracture surface combined with cleavage for the most part and a little quasi-cleavage, as shown in Fig. 12*a*.

The fracture surfaces of HAZ welded with heat inputs of 10 and 30 kJ/cm were perfectly brittle fracture surfaces with cleavage surfaces at δ_c = 0.12 mm and δ_c = 0.1 mm, respectively. Those showed somewhat more brittleness than the parent metal. But at a heat input of 40 kJ/cm, the fracture surface showed a perfectly brittle fracture similar to the above at a low heat input in spite of elevating the test temperature to −25°C, which indicates that a heat input of 40 kJ/cm produces as brittle an effect as raising the transition temperature. These results show that the greater the heat input at welding, the more likely the coarse-grained HAZ is to be brittle.

Figures 13, 14, and 15 show that fracture surfaces of HAZ welded with heat inputs of 10, 30, and 40 kJ/cm are changed according to the applied stress. Fracture surfaces under no stress are ductile with dimples for the most part, so fracture toughness is increased because of the softening phenomenon of PWHT. But, at an applied stress of 98 MPa, the fracture surface exhibits a mode of dimple and grain boundary failure, as is shown in Fig. 15*b* for 40 kJ/cm.

This shows that stress is one of the motive powers transferring the precipitation to the grain boundary. Grain boundary failure also appeared under an applied stress of 196 MPa at a heat input of 40 kJ/cm. The fracture surface under an applied stress of 294 MPa showed complete grain boundary failure, and precipitation was observed on the grain boundary, as is shown in Figs. 15*c* and 15*d*.

Based on these results of fractographs, the behavior of the fracture surface due to heat input and applied stress is shown in Table 3. Fracture surfaces at a low heat input of 10 kJ/cm do not show grain boundary failure because the effect due to the applied stress is small during PWHT, but at 30 kJ/cm, grain boundary failure partially starts at 196 MPa and reaches maximum at 294 MPa. At a heat input of 40 kJ/cm, grain boundary failure shows partially at 98 MPa because the degree of brittleness is greater than that of another heat,

TABLE 3—*Evaluation of the fracture surface according to changes in the heat input and applied stress.*[a]

	Heat Input, kJ/cm		
Stress, MPa	10	30	40
0	N	N	N
98	N	N	M
196	N	M	Y
294	M	Y	Y

[a] Key to abbreviations:
N = no grain boundary failure.
M = mixed grain boundary and dimple failure.
Y = complete grain boundary failure.

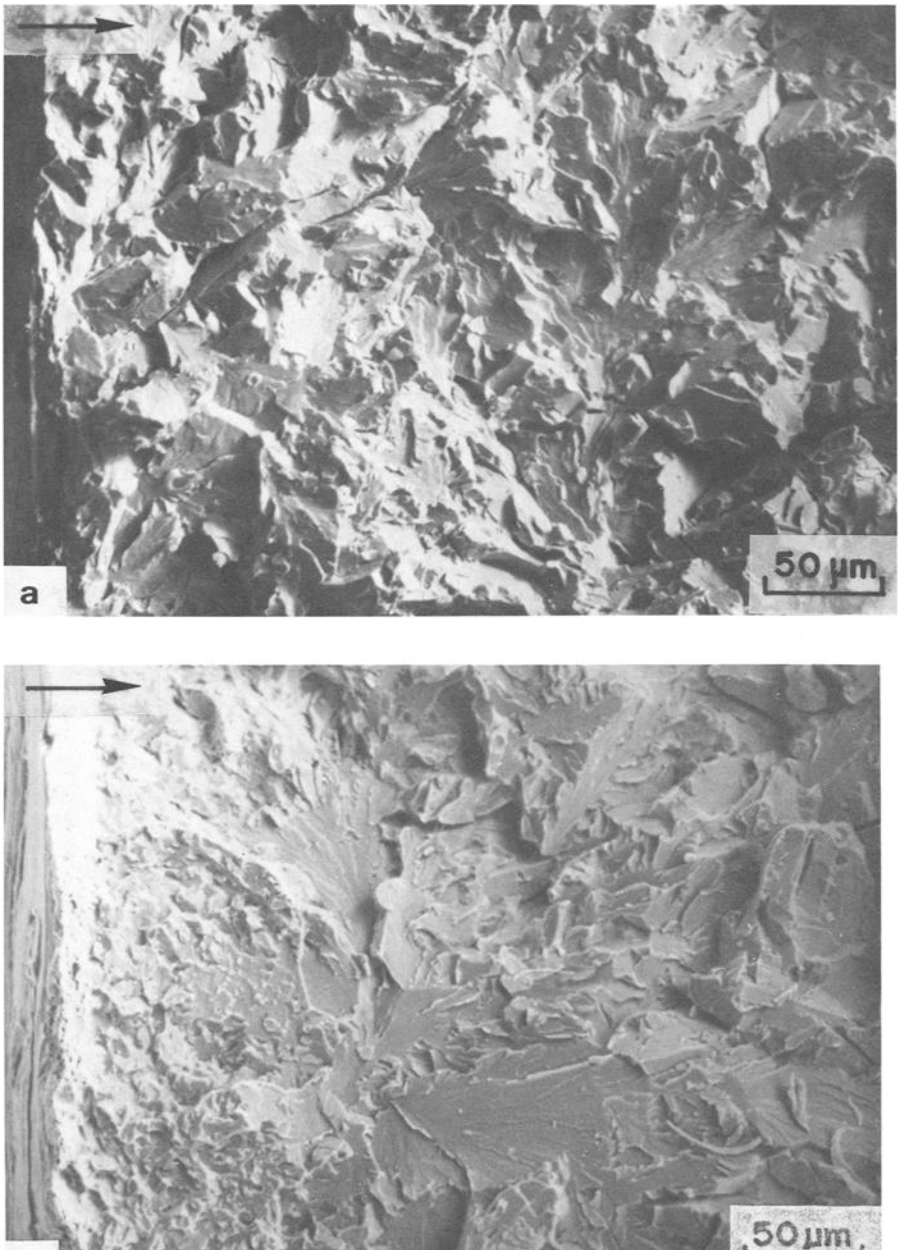

FIG. 12—*Difference between the fracture surface of the parent metal and the as-welded metal with respect to the heat input (test temperature,* $-100°C$*):* (a) *parent metal;* (b) *heat input, 10 kJ/cm.*

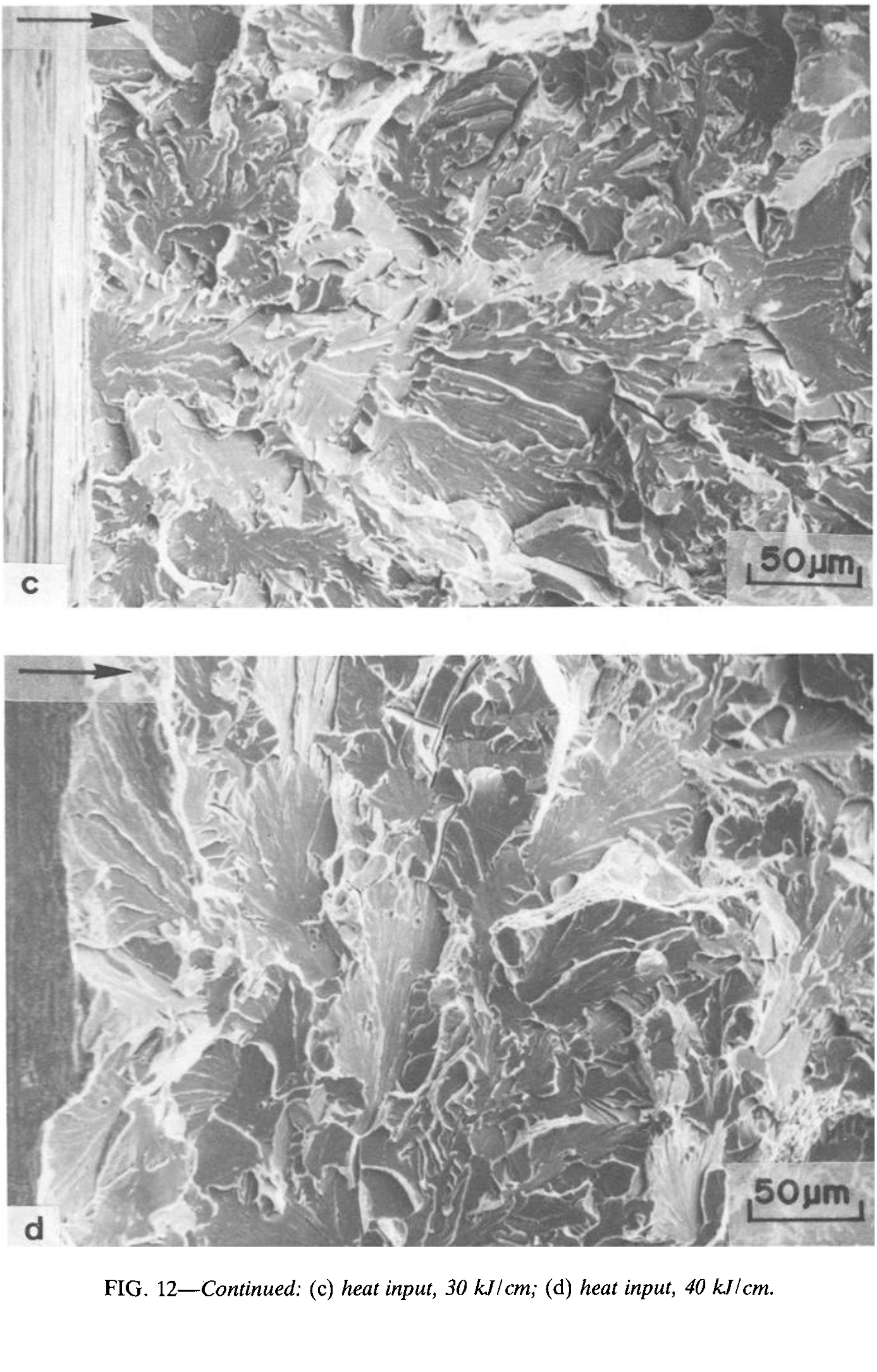

FIG. 12—*Continued:* (c) *heat input, 30 kJ/cm;* (d) *heat input, 40 kJ/cm.*

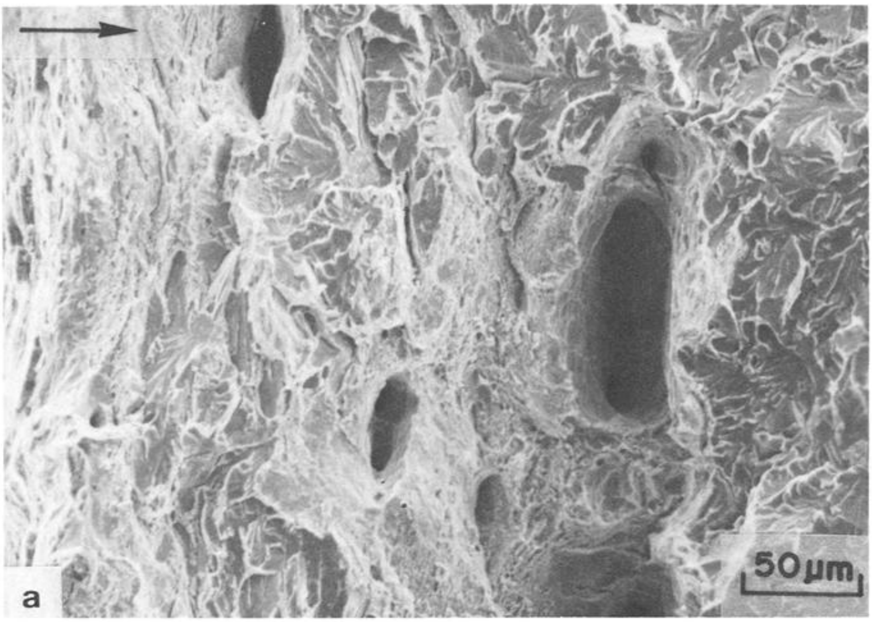

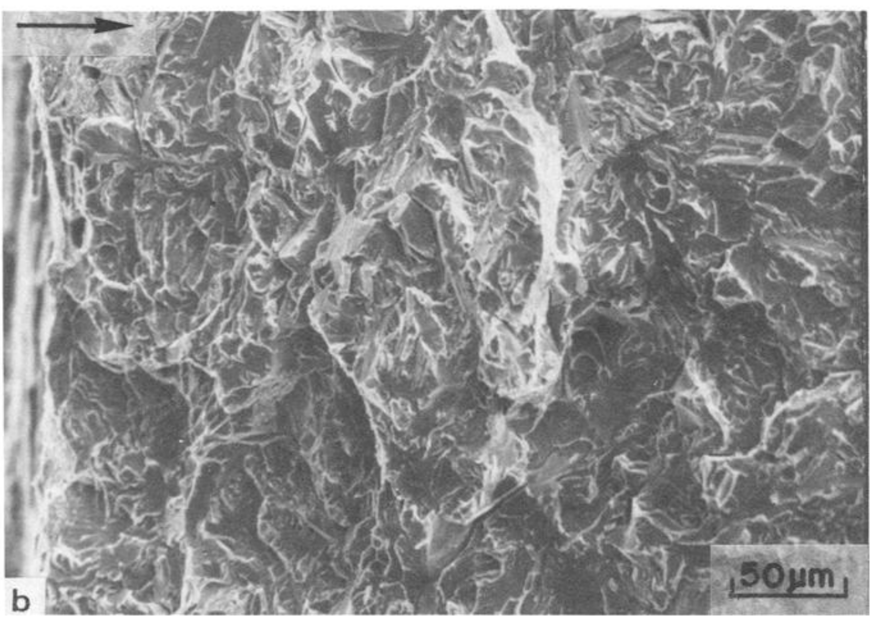

FIG. 13—*Fractographs exhibiting intergranular facets at various stages of applied stress during PWHT (heat input, 10 kJ/cm; test temperature; −100°C; PWHT conditions, 650°C (923 K), ¼ h, 220°C/h*]: (a) *stress, 0 MPa;* (b) *stress, 98 MPa.*

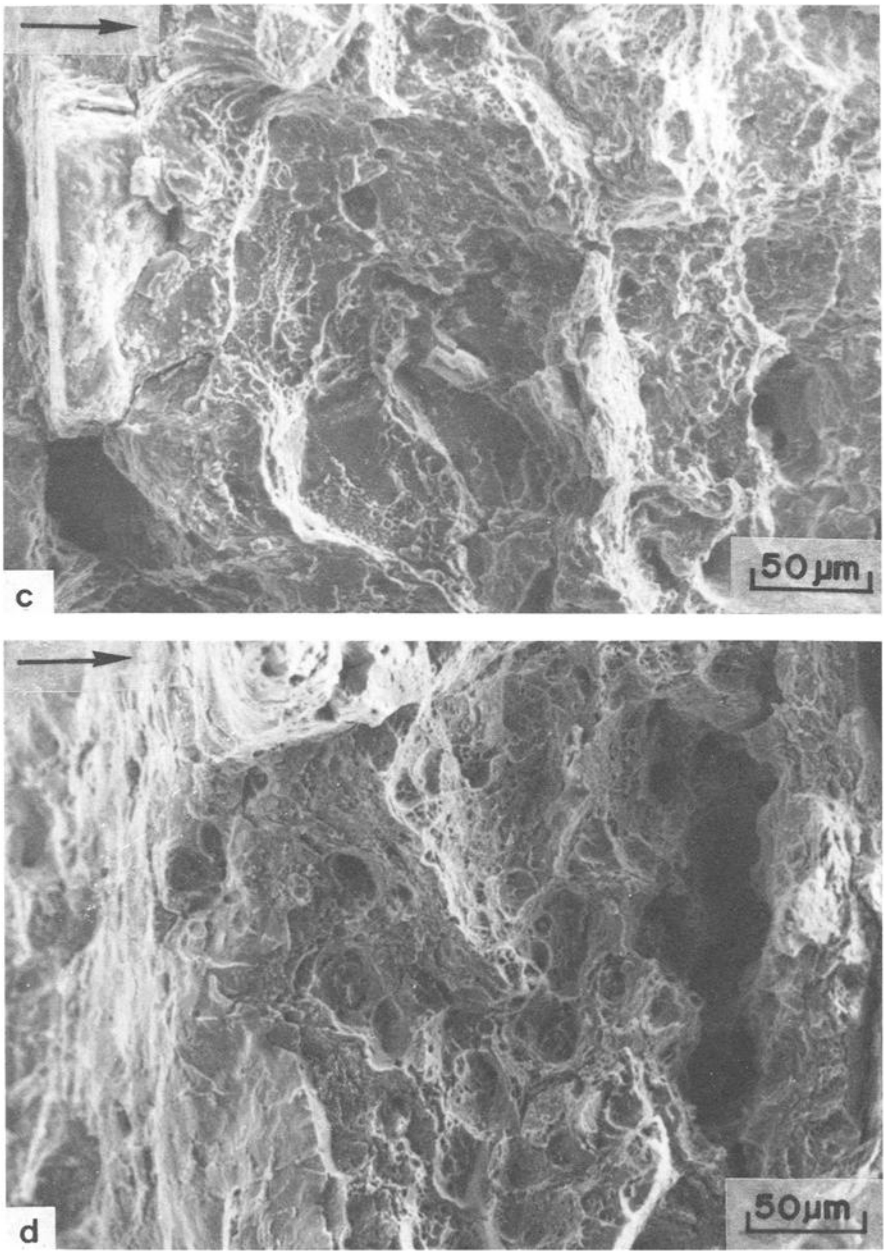

FIG. 13—*Continued:* (c) *stress, 196 MPa;* (d) *stress, 294 MPa.*

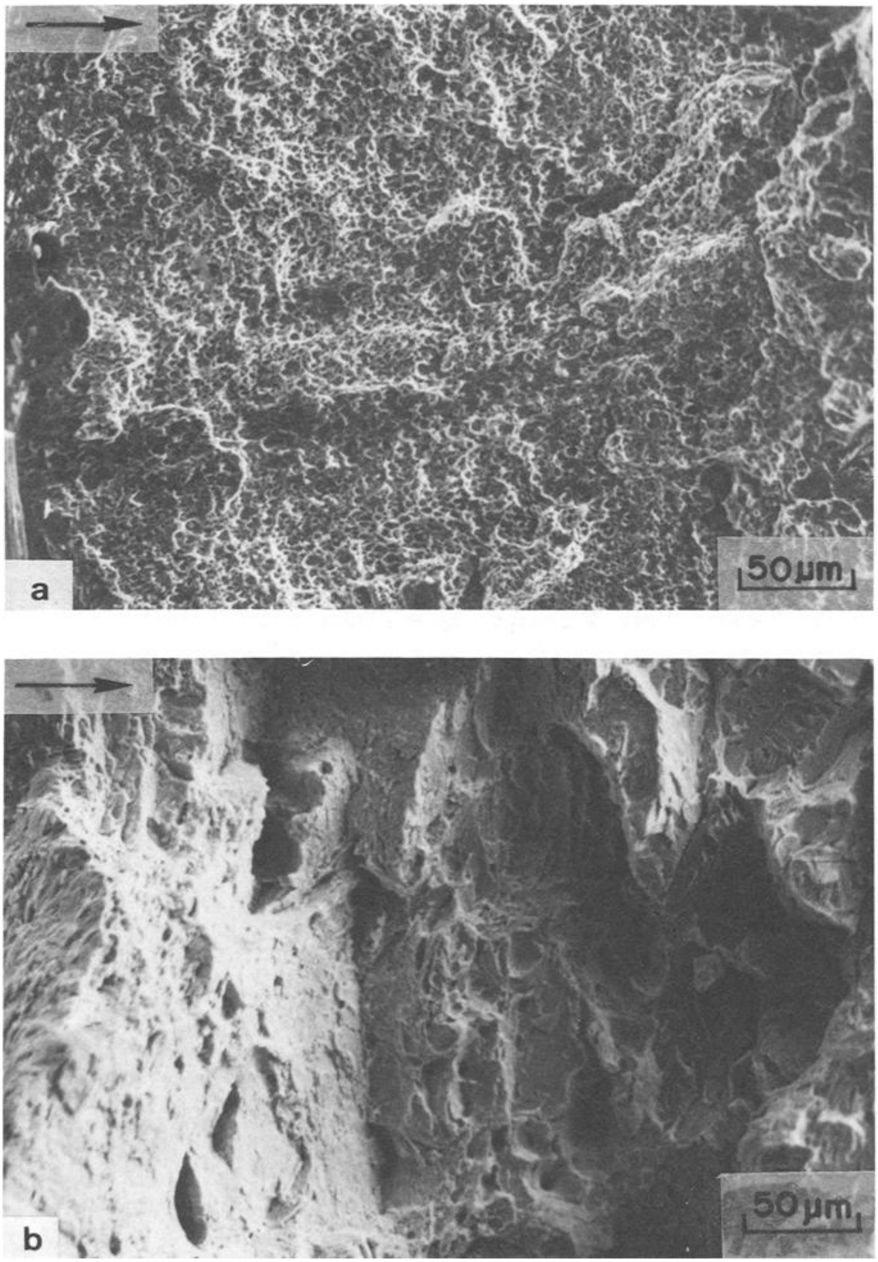

FIG. 14—*Fractographs exhibiting intergranular facets at various stages of applied stress during PWHT [heat input, 30 kJ/cm; test temperature, −100°C: PWHT conditions, 650°C (923 K), ¼ h, 220°C/h]*: (a) *stress, 0 MPa;* (b) *stress, 98 MPa.*

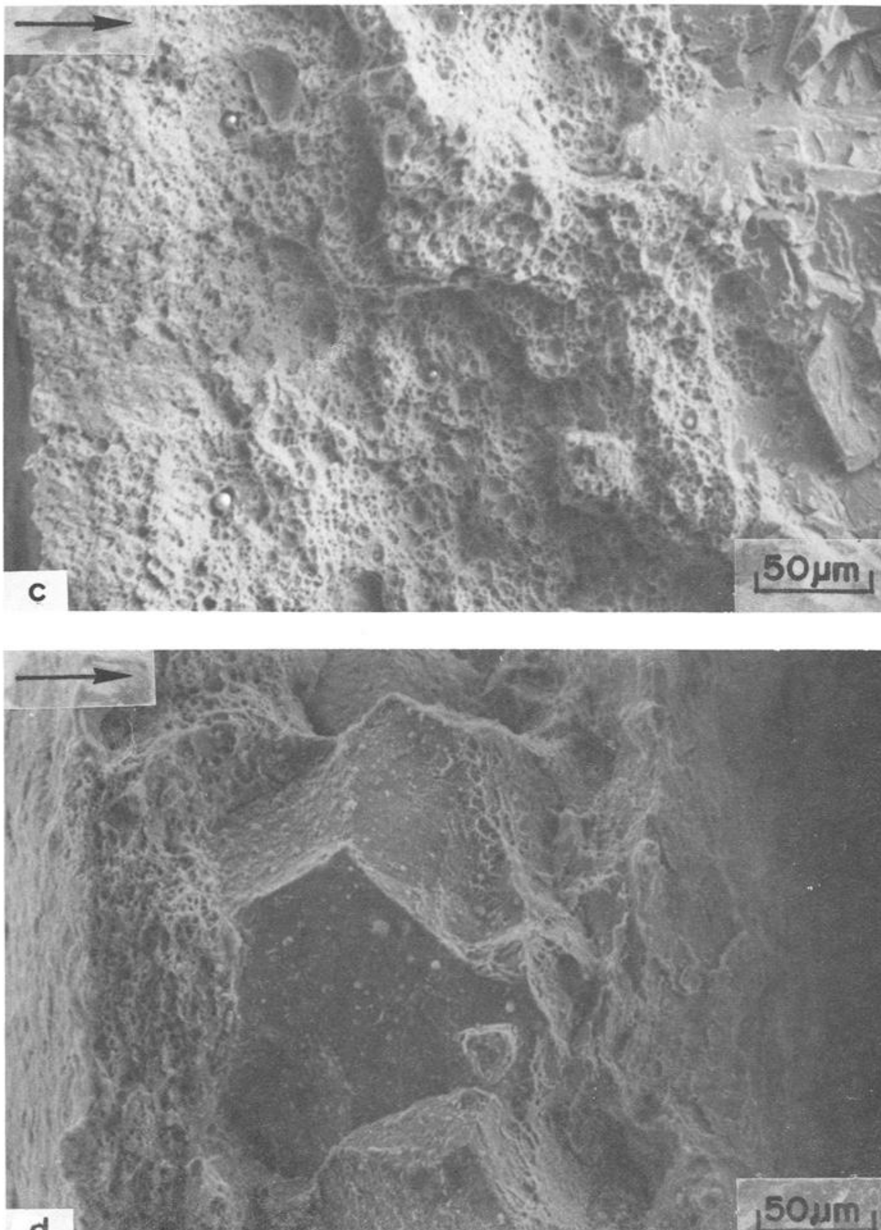

FIG. 14—*Continued:* (c) *stress, 196 MPa;* (d) *stress, 294 MPa.*

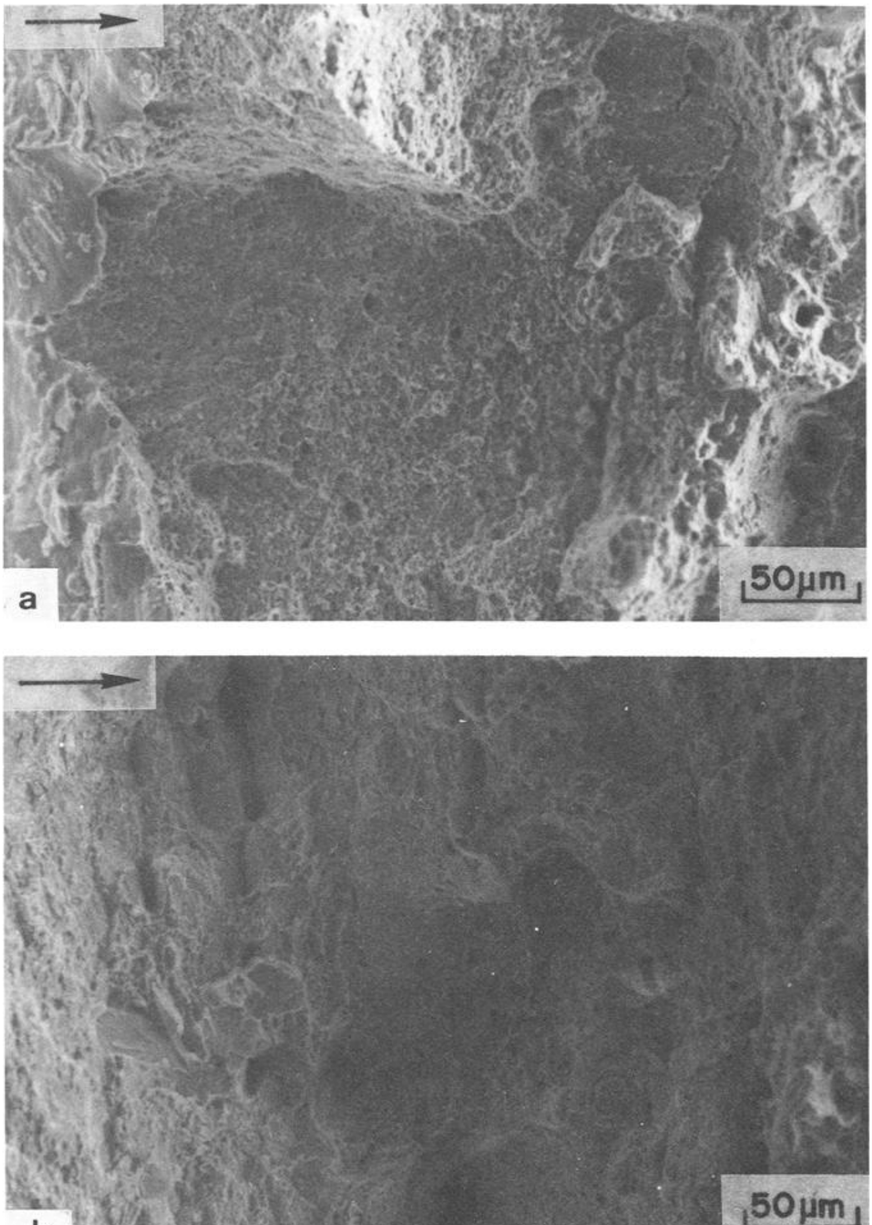

FIG. 15—*Fractographs exhibiting intergranular facets at various stages of applied stress during PWHT [heat input, 40 kJ/cm; test temperature, −100°C; PWHT conditions, 650°C (923 K), ¼ h, 220°C/h]*: (a) *stress, 0 MPa;* (b) *stress, 98 MPa.*

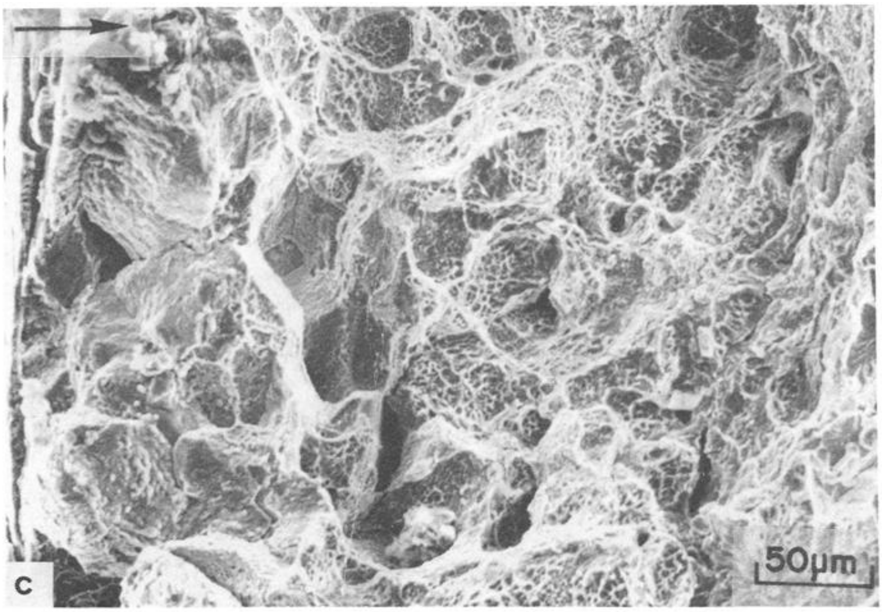

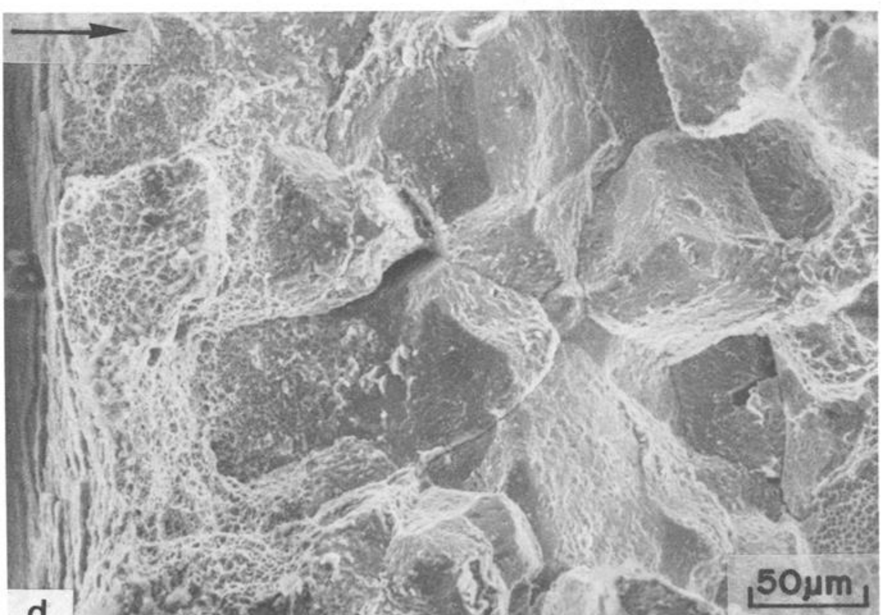

FIG. 15—*Continued:* (c) *stress, 196 MPa;* (d) *stress, 294 MPa.*

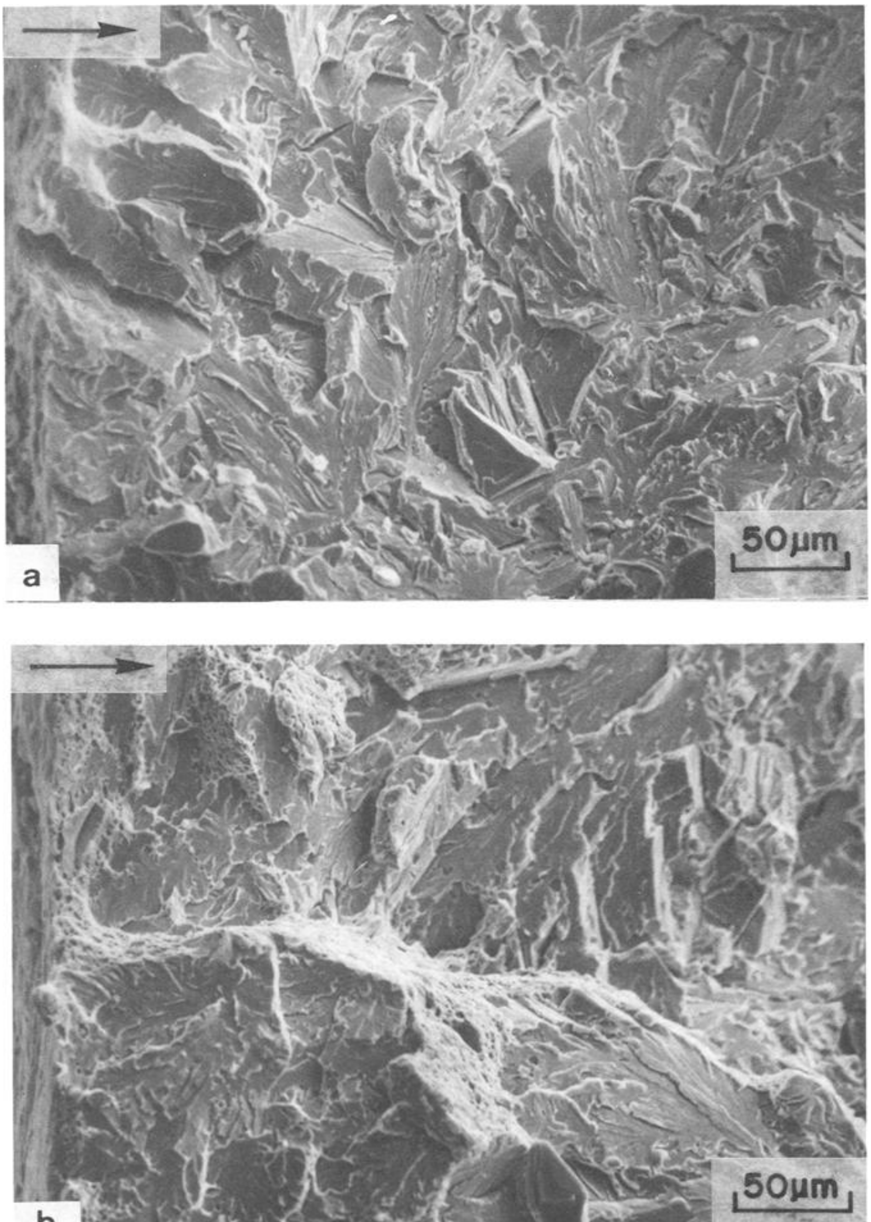

FIG. 16—*Fractographs exhibiting intergranular facets at various stages of applied stress [heating rate, 600°C/h; test temperature, −100°C; PWHT conditions, 650°C (923 K), ¼ h; heat input, 30 kJ/cm]*: (a) *stress, 0 MPa;* (b) *stress, 98 MPa.*

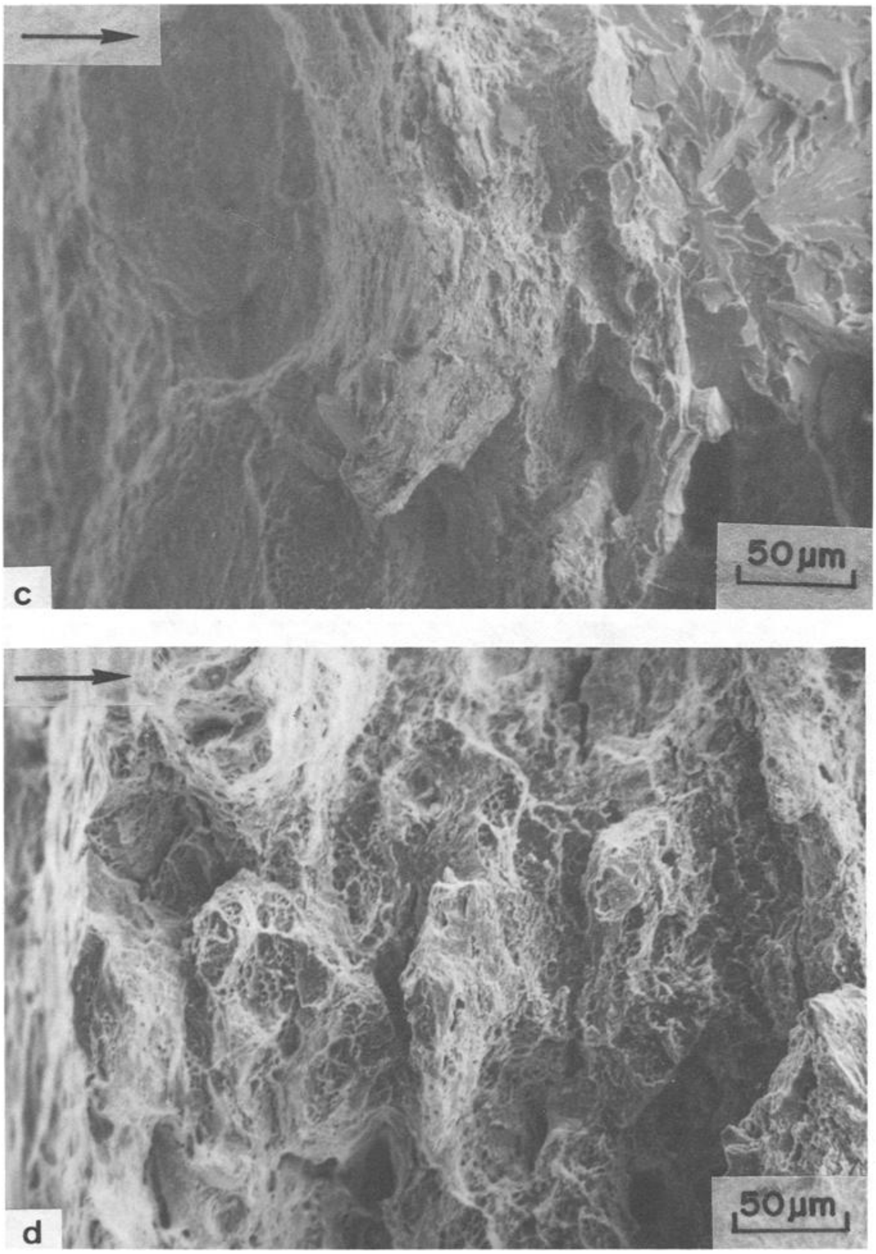

FIG. 16—*Continued:* (c) *stress, 196 MPa;* (d) *stress, 294 MPa.*

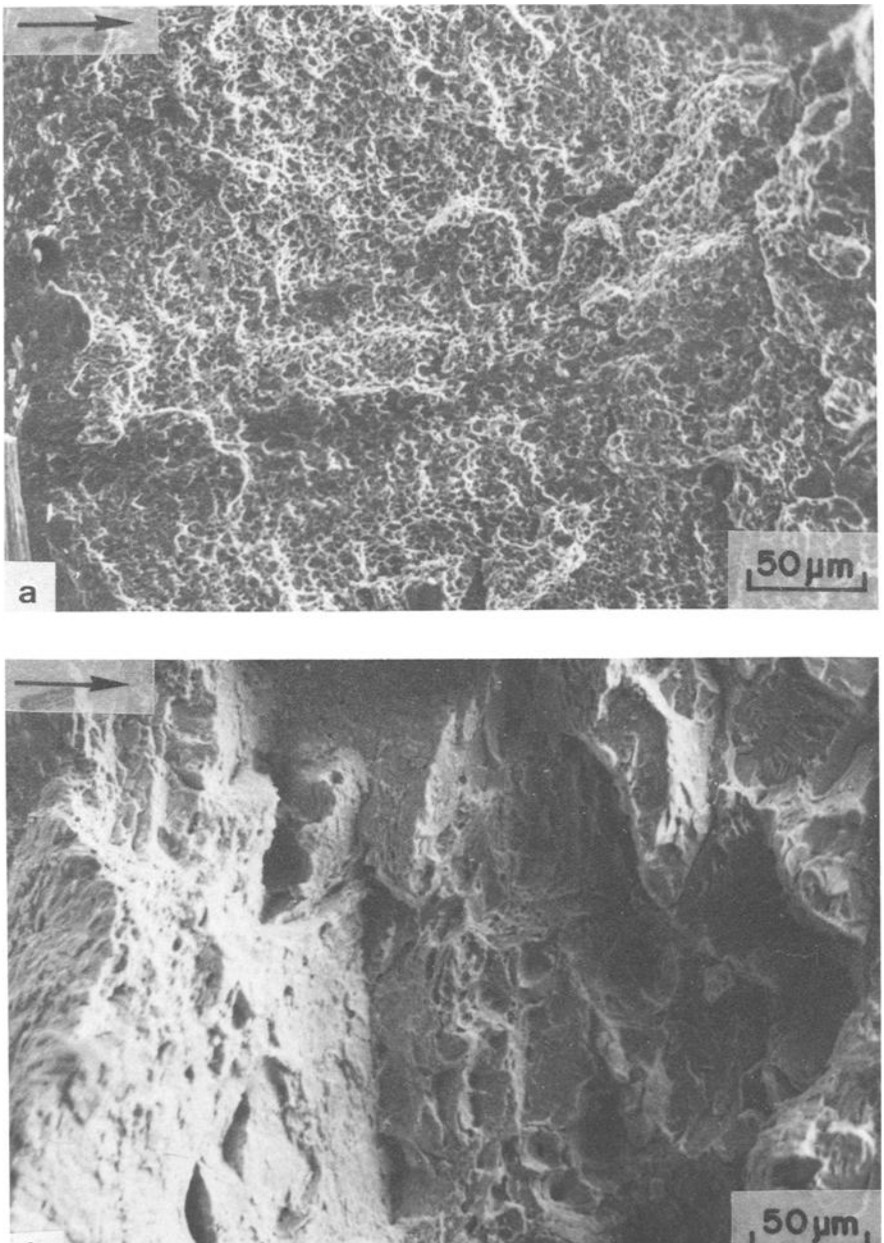

FIG. 17—*Fractographs exhibiting intergranular facets at various stages of applied stress [heating rate, 220°C/h; test temperature, −100°C; PWHT conditions, 650°C (923 K), ¼ h; heat input, 30 kJ/cm]*: (a) *stress, 0 MPa;* (b) *stress, 98 MPa.*

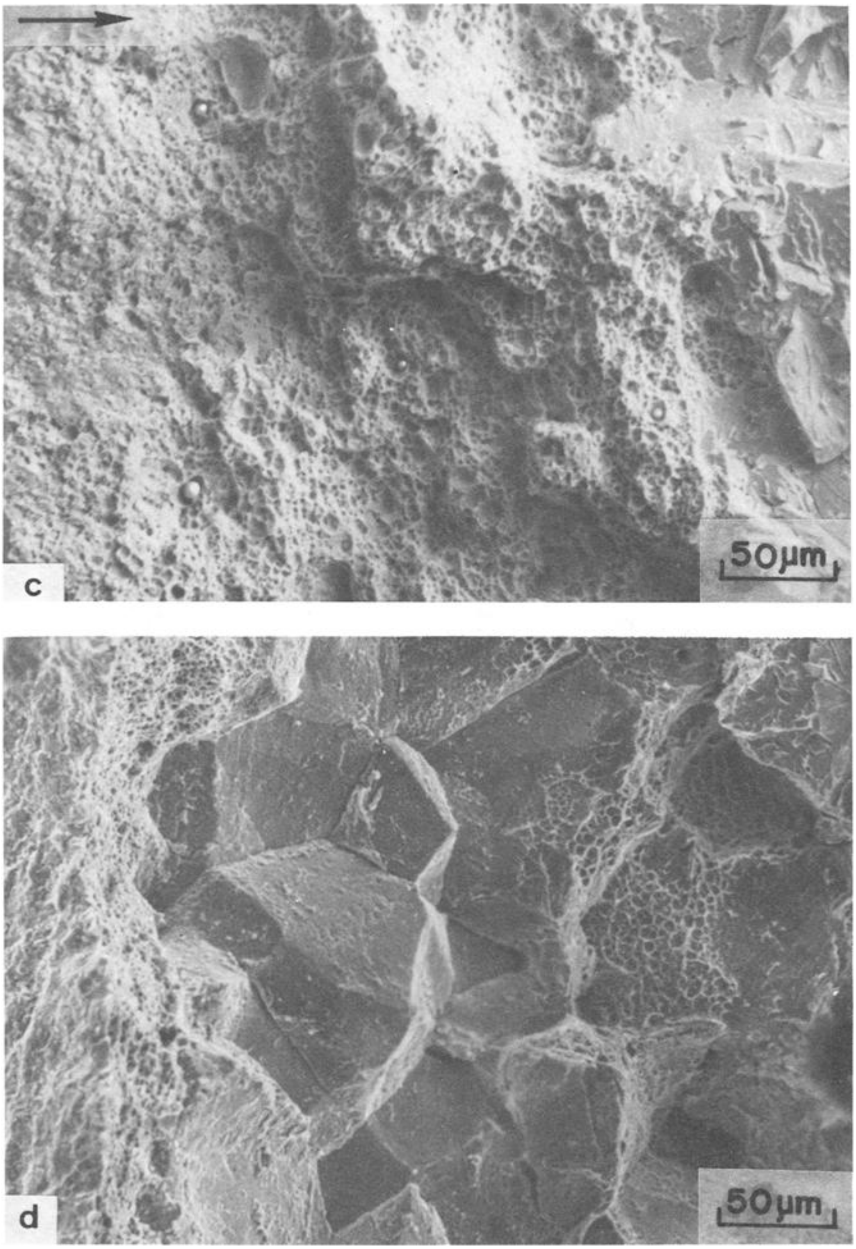

FIG. 17—*Continued:* (c) *stress, 196 MPa;* (d) *stress, 294 MPa.*

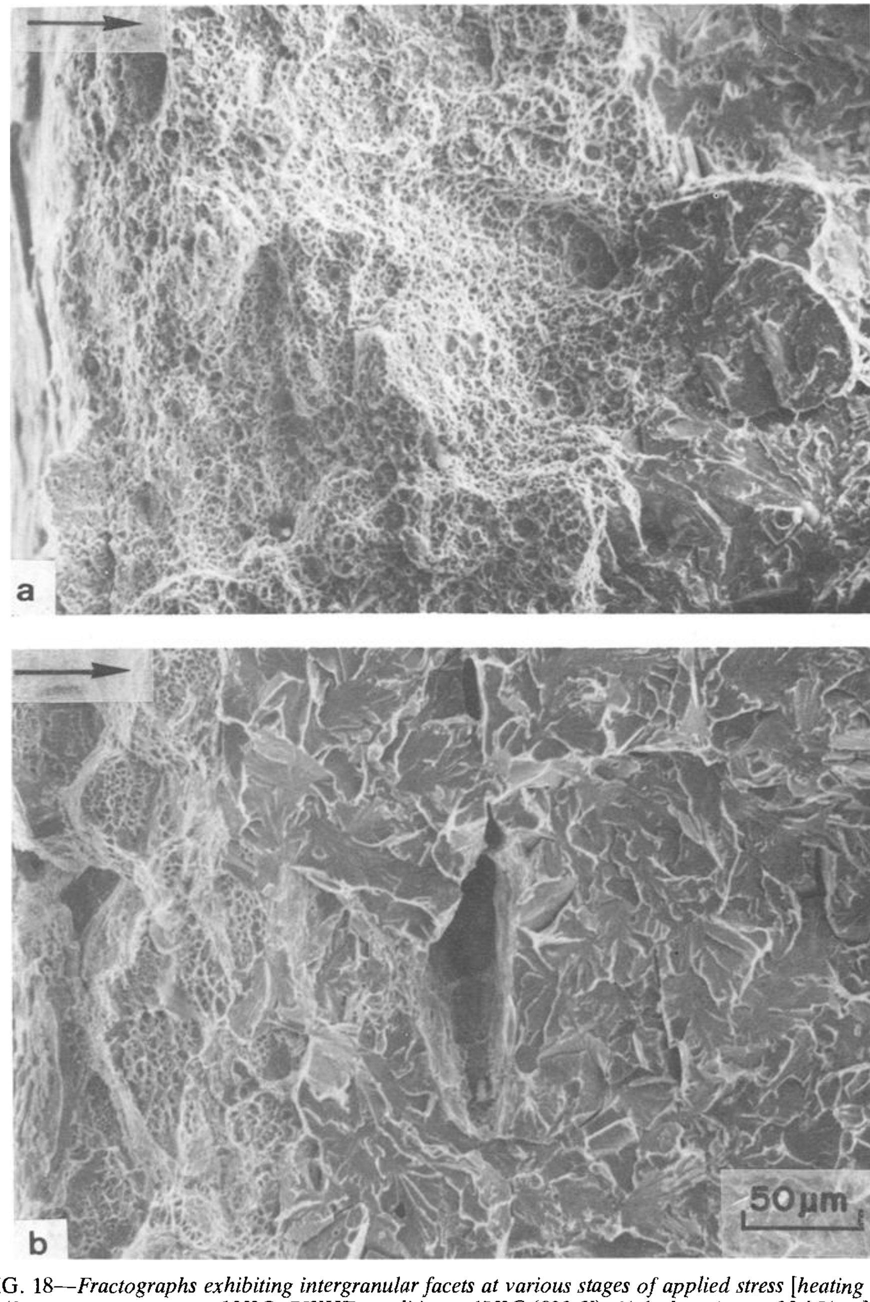

FIG. 18—*Fractographs exhibiting intergranular facets at various stages of applied stress [heating rate, 60°C/h; test temperature, −100°C; PWHT conditions, 650°C (923 K), 1/4 h; heat input, 30 kJ/cm]*: (a) *stress, 0 MPa;* (b) *stress, 98 MPa.*

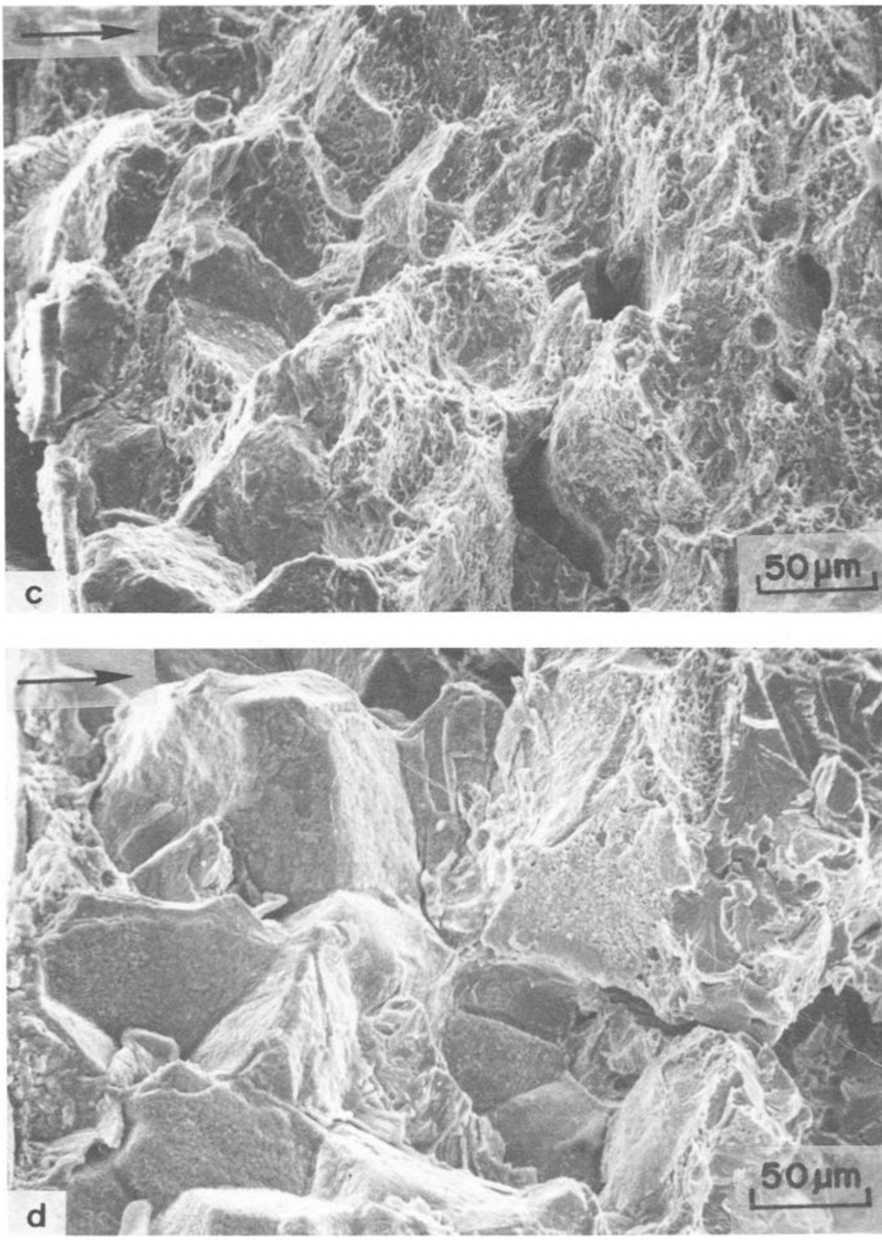

FIG. 18—*Continued:* (c) *stress, 196 MPa;* (d) *stress, 294 MPa.*

and the failure is total at 196 MPa. These results show that PWHT embrittlement is greatly affected by heat input and residual stress.

Figures 16, 17, and 18 show that fracture surfaces of HAZ welded with a heat input of 30 kJ/cm are changed according to the heating rate (600, 220, and 60°C/h) because of PWHT under the applied stress. Among these fracture surfaces at the applied stress of 196 MPa, Fig. 16*c* shows a ductile fracture surface with some cleavage surface on the notch tip at a heating rate of 600°C/h; this surface is similar to that of Fig. 17*b*, which is for 98 MPa at 220°C/h, and this fact proves that the applied stress and heating rate are directly related to the fracture toughness of the notch tip. At the heating rate of 220°C/h, most of the fracture surface was brittle; it was observed that precipitation in intergranular facets decreases the fracture toughness. At a heating rate of 60°C/h, most of the fracture surface exhibited grain boundary failure.

At a stress of 294 MPa, most of the fracture surface was a ductile fracture surface with fine dimples in grain boundaries at the heating rate of 600°C/h, which brought about an increase in fracture toughness. Also, the effect of applied stress did not appear particularly to be due to a rapid heating rate, and the forming of a void at the grain boundary was certainly observed. At a heating rate of 220°C/h, grain boundary failure was clearly observed at the tip as a result of movement into the grain boundary by precipitations. At a heating rate of 60°C/h, whole grain boundary failure was observed. In particular, there was a film of precipitation at the grain boundary, and the thickness of the film increased with an increase in the heating time and grain size, according to the magnitude of stress, which brought about a decrease in fracture toughness due to weakening of the adhesive force of the bond.

Based on the results of these fractographs, the behavior of the fracture surface due to heating rate and applied stress during PWHT is shown in Table 4. At a heating rate of 600°C/h, grain boundary failure was not apparent, because applied stress does not change the structure of welded HAZ but only increases the diffusion of defects or softening of the structure, but grain boundary failure appeared at a heating rate of 220°C/h and an applied stress of 294 MPa. And, at a heating rate of 60°C/h, grain boundary failure appeared from an applied stress of 196 MPa.

Conclusions

The effect of the applied stress and heating rate during PWHT on fracture toughness was evaluated by the COD fracture toughness test, microhardness test, and SEM of welded HAZ of chromium-molybdenum steel.

TABLE 4—*Evaluation of the fracture surface according to changes in the heating rate and applied stress.*[a]

	Heating Rate, °C/h		
Stress, MPa	600	220	60
0	N	N	N
98	N	N	M
196	N	M	Y
294	M	Y	Y

[a] Key to abbreviations:
N = no grain boundary failure.
M = mixed grain boundary and dimple failure.
Y = complete grain boundary failure.

The experimental results obtained are the following:

1. The fracture toughness of welded HAZ was dependent upon the heat cycle. It decreased with an increase in heat input and it increased linearly after PWHT.
2. Grain boundary failure from the welding heat input almost did not appear at an input of 10 kJ/cm, but it appeared from a stress of 294 MPa being applied at a heat input of 30 kJ/cm and from 196 MPa at 40 kJ/cm.
3. The fracture toughness of welded HAZ was dependent upon the heating rate and decreased with an increase in the heating rate at no stress, but it improved to increase with the heating rate under stress.
4. Grain boundary failure due to the heating rate was barely evident at a rate of 600°C/h, but it appeared at a stress of 294 MPa for a heating rate of 220°C/h and at 196 MPa for 60°C/h.
5. Applied stress in welded HAZ during PWHT assisted transgranular and intergranular precipitation of oversaturated alloying elements in the structure and decreased the fracture toughness.

References

[1] Phillip, R. H., "*In Situ* Determination of Transformation Temperature in the Weld Heat-Affected Zone," *Welding Journal*, January 1983, pp. 12s–18s.
[2] Frost, R. H., Edwards, G. R., and Rheinlander, A. D., "A Constitutive Equation for the Critical Energy Input During Electroslag Welding," *Welding Journal*, January 1981, pp. 1s–6s.
[3] Kameda, J., Takahashi, H., and Suzuki, M., "Residual Stress Relief and Local Embrittlement of Weld HAZ in Reactor Pressure Vessel Steel," IIW Doc. No. X-800-76 and Doc. No. IX-1002-76, International Institution of Welding, London, England, 1976.
[4] Dolby, R. E., "Fracture Toughness Comparison of Weld HAZ Thermally Simulated Microstructures," *British Welding Journal*, February 1972, pp. 59–63.
[5] Dawes, M. G., "Weld Metal Fracture Toughness," *Welding Journal*, December 1976, p. 1052.
[6] Suzuki, M., Takahashi, H., and Kameda, J., "Post-Weld Heat Treatment and Embrittlement of Weld HAZ in a Low Alloy Steel," *Welding Journal of the Japan Welding Society*, Vol. 45, No. 1, 1976, pp. 6–13.
[7] Bloom, J. M., "An Analytical Assessment of the Effects of Residual Stress and Fracture Properties on Service Performance of Various Weld Repair Processes," *Journal of Pressure Vessel Technology*, Vol. 103, 1981, pp. 373–379.
[8] Joshi, A. and Stein, D. F. in *Temper Embrittlement of Alloy Steels, ASTM STP 499*, American Society for Testing and Materials, Philadelphia, 1972, pp. 59–89.
[9] Hippsley, C. A., Knott, J. F., and Edwards, B. C., "A Study of Steel Relief Cracking in 2¼Cr-1Mo Steel—I: The Effect of Segregation," *Acta Metallurgica*, Vol. 28, 1980, pp. 869–885.
[10] Naiki, T. and Okabayashi, H., "Stress Relief Cracking in the Heat-Affected Zone (1–3)," *Welding Journal of the Japan Welding Society*, Vol. 33, No. 9, 1964, and Vol. 39, No. 10, 1970.
[11] Chung, S. H., doctoral thesis, Tohoku University, Sendai, Japan, 1976.
[12] Suzuki, M. and Komura, I., "Nondestructive Estimation of Weld Residual Stress by Means of Remnant Magnetization Measurement," IIW Doc. No. X-801-76, International Institution of Welding, London, England, 1976.
[13] Kameda, J. and McMahon, C. J., "The Effect of Sb, Sn, and P on the Strength of the Grain Boundary in a Ni-Cr Steel," *Metallurgical Transactions A*, Vol. 12A, 1981, p. 31.
[14] Edwards, B. C., Eyre, B. L., and Gage, G., "Temper Embrittlement of Low Alloy Ni-Cr Steels," *Acta Metallurgica*, Vol. 28, 1980, p. 335.
[15] "Method for Crack Opening Displacement (COD) Testing," British Standard 5762, British Standards Institution, London, 1979.

Robert J. Dexter[1]

Fracture Toughness of Underwater Wet Welds

REFERENCE: Dexter, R. J., **"Fracture Toughness of Underwater Wet Welds,"** *Fatigue and Fracture Testing of Weldments, ASTM STP 1058*, H. I. McHenry and J. M. Potter, Eds., American Society for Testing and Materials, Philadelphia, 1990, pp. 256–271.

ABSTRACT: The wet and wet-backed shielded metal-arc welding (SMAW) process can produce welds suitable for structural applications provided fracture control is considered in the design. Welding procedure qualification tests and fracture toughness tests [the ASTM Test for J_{Ic}, a Measure of Fracture Toughness (E 813-87)] were performed on the heat-affected zone (HAZ) and weld metal of wet, wet-backed, and dry fillet and groove welds made with (1) A36 steel and E6013 electrodes, and (2) A516 steel and nickel alloy electrodes. Despite Vickers hardness (HV) measurements exceeding 300 HV [$\times$1.0 kgf (HV 1.0)] in the HAZ of the ferritic welds and 400 HV in the HAZ of the austenitic welds, no hydrogen cracking or brittle fracture behavior was observed. Generally, the Charpy tests indicated upper-shelf fracture behavior at -2°C (28°F), and the HAZ was found to be tougher than the weld metal. Crack-tip opening displacement (CTOD) estimates were made using British Standard (BS) 5762, and the CTOD was found to be proportional to J even after large crack extension. The maximum load point values of CTOD and J are compared with the initiation values determined by the procedure of ASTM Test E 813. The fracture toughness of the welds is sufficient to be tolerant of flaws much larger than those allowed under American Welding Society (AWS) specifications.

KEY WORDS: weldments, welds, underwater welds, wet welds, fracture toughness, steels, Charpy test, crack-tip opening displacement, J_{Ic}, flaws, cracks, tolerance

The wet welding process includes the pieces to be joined, the welder/diver, and the arc surrounded by water. The wet and wet-backed shielded metal-arc welding (SMAW) process offers greater versatility, speed, and economy than underwater welding techniques involving chambers or minihabitats. However, the welds can rarely achieve the same quality as dry welds. The welds are quenched very rapidly, often resulting in a very hard weld and heat-affected zone (HAZ). Evolved gases trapped in the weld metal manifest themselves as porosity. Hydrogen (produced as water is dissociated) may cause cracking in the welds. Arc stability in water may be inferior to that in air, resulting in other discontinuities. Wet-backed welds are performed with water behind the pieces to be joined only but are subject to similar problems.

Data reported in the literature and those reported herein indicate that the wet and wet-backed SMAW process, when used to join low-carbon structural (mild) steels, can produce an intermediate quality level defined as Type-B by the American Welding Society (AWS) in its Specification for Underwater Welding. (AWS D3.6). This specification states that these Type-B welds must be evaluated for "fitness for purpose" but gives no guidelines for making this evaluation. The data herein provide a basis for performing such an evaluation.

Welding procedure qualification tests were performed on fillet and groove welds prepared

[1] Senior research engineer, Southwest Research Institute, San Antonio, TX 78248.

by the dry, wet-backed, and wet SMAW processes. These tests included visual (general and transverse macrosection) and radiographic examinations, transverse weld tension tests, bend tests, all-weld-metal tension tests, Charpy impact tests, hardness tests, fillet weld break tests, and fillet weld tension tests. In addition, the fracture toughness of the welds was characterized by the J-resistance curve and J_{Ic}. For some of these tests the crack-tip opening displacement (CTOD) was measured and related to J and the crack extension. Charpy and J_{Ic} tests were performed with the notch both in the weld metal and in the heat-affected zone. Special problems are encountered in fracture toughness testing of wet welds because of their inhomogeneous properties, very high hardness, and extreme porosity.

Two base-metal/filler-metal combinations were used in the experiments: a 0.36 carbon-equivalent (CE)[2] A36 steel with an E6013 (ferritic) electrode and a 0.46 CE A516 steel with a nickel alloy (austenitic) electrode. The experiments and subsequent statistical analysis revealed the effect and interaction of the weld type (dry, wet-backed, or wet), water depth, plate thickness, restraint, and material [1]. The scope of this paper is limited to the fracture toughness testing of wet and wet-backed welds. Other properties are briefly discussed, especially as these properties relate to fracture toughness.

Experimental Procedure and Results

Test Matrix

An experimental program was conducted as part of an effort to quantify the changes in strength, ductility, and toughness of wet and wet-backed underwater fillet and groove welds. The test matrix is shown in Fig. 1. The experiment was primarily designed to examine the effect on these properties of (1) the material, (2) the plate thickness, and (3) the depth of the weld preparation. Other plates were prepared and tested to examine the effect of restraint (restrained welds were prepared with base plates welded to strongbacks), weld preparation (double bevel versus single bevel), electrode size, fillet welds, and weld metal tensile strength.

Chemical Analysis

Chemical analysis was performed on both thicknesses of the base metals, a sample of the ferritic weld metal made at 60 m (198 ft), and a sample of the austenitic weld metal made in a wet-backed weld. At the time, it wasn't realized that the weld metal chemistry might change with depth [2]. In retrospect, it would have been better to have had samples of the weld metal from all depths, dry welds, and wet-backed welds. Table 1 shows the results of these chemical analyses. Note the particularly low manganese in the ferritic weld at 60 m (198 ft). This percentage is probably much lower than would be obtained in a dry weld and is consistent with the results of Olson and Ibarra [2].

Visual and Radiographic Examination

Wet-welded plates were generally found to have two parallel grooves along each fusion line at the weld root (inadequate joint penetration). Radiography revealed porosity in the wet welds, and slag inclusions in a few plates. Normally, a plate would be rejected on the basis of such a radiographic indication. In view of the use of these data for application in design rules, the decision was made to proceed with testing of these plates.

[2] CE = C + Mn/6 + Cr + Mo + V/5 + Ni + Cu/15 (weight %).

Weld Type	Water Depth	0.36 CE*, Ferritic Filler			0.46 CE*, Nickel Alloy Filler	
		Groove Weld 25 mm Plate	Restrained Groove 25 mm Plate	Groove Weld 13 mm Plate	Groove Weld 25 mm Plate	Groove Weld 13 mm Plate
Dry	0	X		X	X	X
Wet-Backed	10 m	X		X	X	X
Wet	10 m	X**	X	X	X	X
	20 m	X				
	30 m	X				
	35 m	X	X	X		
	60 m	X	X	X		

* CE = Carbon Equivalent

**3 test plates were prepared:
1) a standard test plate (as used for all other conditions) used a single bevel preparation and 3 mm electrode
2) a 4 mm electrode, single bevel, and
3) a 3 mm electrode, double bevel

FIG. 1—*Test matrix.*

TABLE 1—*Chemical analysis of the metals used, in weight percent.*

Plate Sample	Carbon	Manganese	Silicon	Phosphorus	Sulfur	Nickel	Chromium	Molybdenum	Copper	Vanadium	Carbon Equivalent
A36 12.7 mm (½ in.)	0.17	0.87	0.26	0.014	0.016	0.01*[a]	0.01*	0.01*	0.01	0.01*	0.32
A36 25.4 mm (1 in.)	0.14	0.86	0.23	0.033	0.023	0.09	0.02	0.01*	0.04	0.01	0.30
E6013 weld metal welded at 60 m (198 ft)	0.09	0.32	0.22	0.020	0.010	0.02	0.01*	0.01*	0.01	0.01	
A516 12.7 mm (½ in.)	0.22	1.04	0.20	0.018	0.015	0.01*	0.02	0.01*	0.01	0.01*	0.40
A516 25.4 mm (1 in.)	0.22	1.07	0.21	0.024	0.011	0.01	0.02	0.01*	0.01	0.01*	0.41
Austenitic wet backed weld metal	0.05	2.03	0.34	0.008	0.012	62.72	12.52	5.61	0.02		

[a] Asterisks indicate that the true value is less than or equal to the value given.

Side Bend Tests

Side bend tests were performed as part of the typical weld qualification tests, as outlined in AWS Specification D3.6. The test gages the ability of the weld to deform plastically as it is bent 180° at a specified radius. The austenitic wet welds did not qualify for the Type B quality level according to bend test criteria. It is interesting to note that although the austenitic wet welds exhibited poor bend test results, these welds have very good fracture toughness. These bend tests failed because pores opened up that were larger than 3.3 mm (0.12 in.), although the specimens were bent fully 180°. The present requirement of AWS Specification D3.6 is a good screening test for weld workmanship, but this test should not be regarded as indicative of the total ductile capacity to rotate or the toughness.

Transverse Weld Tension Test

Most (76%) of the specimens fractured in the base metal, with the tendency to fracture in the weld increasing with the water depth (pressure) at which the weld was made and, hence, with the porosity. Those specimens that fractured in the weld metal exhibited minimal elongation. The transverse weld tension test reveals nothing about the performance of the weld other than assuring that adequate strength and fusion are present, which can be assured by the bend test. More useful information can be obtained from an all-weld-metal tension test, e.g., the weld metal yield strength, ultimate tensile strength, and elongation.

Hardness Traverse

Small portions of the heat-affected zone (HAZ), usually found near the weld crown, had Vickers hardness (HV) values (in units of HV 1.0) of up to 334 for the wet ferritic welds and up to 460 HV for the austenitic wet welds. Nearby impressions [within 0.5 mm (0.008 in.) of the impression yielding peak hardness] were often 200 HV less hard, indicating that the high hardness was a very localized phenomenon. The dry and wet-backed welds were not nearly as hard. The statistical analysis [*1*] showed that hardness is generally independent of the water depth at which the weld was prepared and cannot be correlated with toughness or performance in the bend test. Because of the absence of cracking or brittle fracture behavior in all the wet welds, the hardness of the weld seems inconsequential.

Fillet Weld Tests

Fillet weld break-over bend tests and fillet weld tension tests were conducted. The fillet weld bend specimens failed before being bent to 45°, but failed in the throat, exhibiting good fusion and a lack of obvious defects. The failures of the fillet weld tension tests (in shear) were all remarkably ductile; i.e., the plates extended (slid apart) appreciably before breaking.

All-Weld-Metal Tension Tests

All-weld-metal tension tests were conducted on the ferritic wet welds, although these tests are not required for qualification. The results are summarized in Table 2. Note that the weld metal has a high yield strength to ultimate tensile strength ratio; i.e., it exhibits little hardening. The elongation was less than is typical for dry welds and seemed to reach a minimum at a water depth of 35 m (115 ft).

TABLE 2—*Summary of data for all-weld-metal tensile tests using 25.4-mm (1-in.)-thick A36 plate and ferritic filler.*

Length	Proportional Limit, MPa (ksi)	Yield Strength, MPa (ksi)	Tensile Strength, MPa (ksi)	Elongation, %
60 m	350 50.8	402 58.4	451 65.5	9.4
(198 ft)	350 50.8	402 58.4	451 65.5	9.4
35 m	384 55.8	437 63.5	475 69.0	6.3
(115 ft)	395 57.4	423 61.4	458 66.5	6.3
10 m	472 68.5	507 73.6	556 80.7	12.5
(33 ft)	464 67.3	493 71.6	539 78.2	9.4

Charpy Tests

Charpy impact tests are often used to estimate indirectly the fracture toughness of metals. This practice is less desirable than direct measurement of toughness with K_{Ic}, J_{Ic}, or CTOD tests. However, because of the relative difficulty and expense of these tests, the Charpy test will probably continue to be used. The correlation between the Charpy impact toughness and J_{Ic} or K_{Ic}, as well as the trends in impact energy and toughness among the variables of this experimental program, are reported in Ref *1*.

Charpy tests were conducted at −2 and 16°C (28 and 60°F) for all weldments. The impact energy for the ferritic weld metal was low [typically 20 to 47 J (15 to 35 ft · lb)] and was independent of the base plate thickness. For the 12.7-mm (0.5-in.) ferritic welds, the HAZ[3] impact energy, 54 to 76 J (40 to 56 ft · lb)], was higher than the weld metal impact energy. For the 25.4-mm (1-in.) ferritic wet welds, the HAZ impact energy, 9 to 15 J (7 to 11 ft · lb), was lower than the weld impact energy. The impact energy for the austenitic weld metal and HAZ was much higher, ranging from 45 to 155 J (33 to 114 ft · lb).

Most of the conditions tested indicate upper-shelf or full shear fracture behavior at −2°C (28°F). Specimens that did not exhibit full shear behavior included specimens of both thicknesses of the dry and wet-backed E6013 weld metal, the 25.4-mm (1-in.) ferritic HAZs, and the 25.4-mm (1-in.) dry austenitic HAZ.

If the Charpy test results exhibit upper-shelf fracture behavior at this temperature, then the more slowly loaded J_{Ic} fracture toughness, and the fracture toughness exhibited by the welds in the structure, will also be expected to show upper-shelf behavior at this temperature. Therefore, ductile tearing rather than brittle fracture would generally be anticipated in structures with underwater welds, with the following exception. As pointed out above, the HAZ of 25.4-mm (1-in.)-thick and thicker specimens is in the transition or lower-shelf region of the Charpy toughness versus temperature curve at −2°C (28°F). The fracture of structures welded with 25.4-mm (1-in.)-thick and thicker plates with the ferritic electrode cannot be generally assured to be ductile above −2°C (28°F) but may depend on the strain rate, temperature, and constraint. Ductile tearing allows load to redistribute. In a redundant structure, considerable stable tearing can be accommodated without complete separation of the component.

As the ranges above show, there was considerable scatter in the Charpy data. However, the toughness within any category of weld and in a particular location (HAZ or weld) varied in a fairly narrow range. The variance exhibited for austenitic welds is primarily due to only a few exceptionally tough specimens. The Charpy test often exhibits a great deal of scatter even for homogeneous base metals. This scatter is partly due to the fact that the Charpy

[3] The notch for these HAZ Charpy tests was located about 1 mm (0.04 in.) from the fusion line.

specimen samples only a small volume of material. This localized variation in the material properties, as was noted for the hardness test results, is more apparent in the results of a Charpy test than in a full-thickness fracture toughness test.

Fracture Toughness Tests

Tests were conducted to determine the fracture toughness of the weld and heat-affected zone. The test selected for this purpose was the ASTM Test for J_{Ic}, a Measure of Fracture Toughness (E 813-87). This test is more appropriate than the ASTM Test for Plane-Strain Fracture Toughness of Metallic Materials (E 399-83) for ductile materials. For several of the tests, the data were reduced so that the crack-tip opening displacement (CTOD) could also be determined.[4]

The tests utilized the compact specimen shown in Fig. 2, which is similar to that in ASTM Test E 813 except for the unique "knife edges" for the clip gage. Note that British Standard (BS) 5762 does not provide for a compact specimen; however, the data reduction procedure would be the same. No side grooves were used since full-thickness representative properties were desired. Precracking was performed in accord with ASTM Test E 813. The crack extension was monitored both visually and with compliance measurements. Good agreement of these techniques was obtained when the compliance data were adjusted by a factor between 1.0 and 1.1. This adjustment is often necessary to "calibrate" the compliance method against a benchmark visual measurement. The precracks sometimes would begin to lag behind on one side of the compact specimen, and a tapered loading pin was used to increase the load and hence speed up the growth on the lagging side.

Despite the lack of side grooves, the fatigue cracks in the HAZ remained within the plane of the straight side of the single-bevel welds. Both the fatigue cracks and the subsequent tearing cracks tended to zigzag within a range of a few millimetres in the HAZ and subsequent weld. Some of the tearing cracks diverged into the weld metal, but as discussed below, the weld metal is believed to be generally less tough. Thus, the cracks tended to seek the least tough material to tear. Upon inspection of the broken specimens, it was discovered that the final tearing cracks were reasonably straight fronted and conformed to the requirements of ASTM Test E 813. The angle between the cracks that diverged and the original plane was in all cases less than 30°. Chan and Cruse [*3*] have shown no significant error in the stress-intensity factor computation, treating any such cracks inclined up to 30° as if they remained on the original plane.

Figure 3 shows a typical load versus load line (clip gage) displacement trace for a J_{Ic}/CTOD test of a 25.4-mm (1-in.) ferritic weld made at 10 m (33 ft). Partial unloadings were performed to obtain the crack length by compliance. The value of J is calculated from the area under the curve, and CTOD is calculated from the clip gage displacement. Figure 4 shows the J-resistance curve. The line to the left is the blunting line. Note the clear break in slope as the initiation of tearing occurs. The J_{Ic} for this specimen was 91 kJ/m^2 (522 in. · lb/in.^{2}); the K_{Ic} derived from J_{Ic} was 135 MPa $\sqrt{\text{m}}$ (123 ksi $\sqrt{\text{in.}}$).

The bars in Fig. 5 show J_{Ic} values grouped according to the depth of the weld preparation. The J_{Ic} tests indicated great variability in toughness among the welds tested. The J_{Ic} ranged from 4.9 to 565 kJ/m^2 (28 to 3231 in. · lb/in.^{2}), and the corresponding K_{Ic} (calculated from J_{Ic}) ranged from 33 to 353 MPa $\sqrt{\text{m}}$ (30 to 321 ksi $\sqrt{\text{in.}}$). Austenitic welds were generally tougher than the ferritic welds and the minimum K_{Ic} was 45 MPa $\sqrt{\text{m}}$ (41 ksi $\sqrt{\text{in.}}$). The lowest toughness was for a ferritic weld prepared at 35 m (115 ft) from 12.7-mm (0.5-in.)

[4] In accordance with BS 5762, "Methods for Crack Opening Displacement (COD) Testing," British Standards Institution, London, England, 1979.

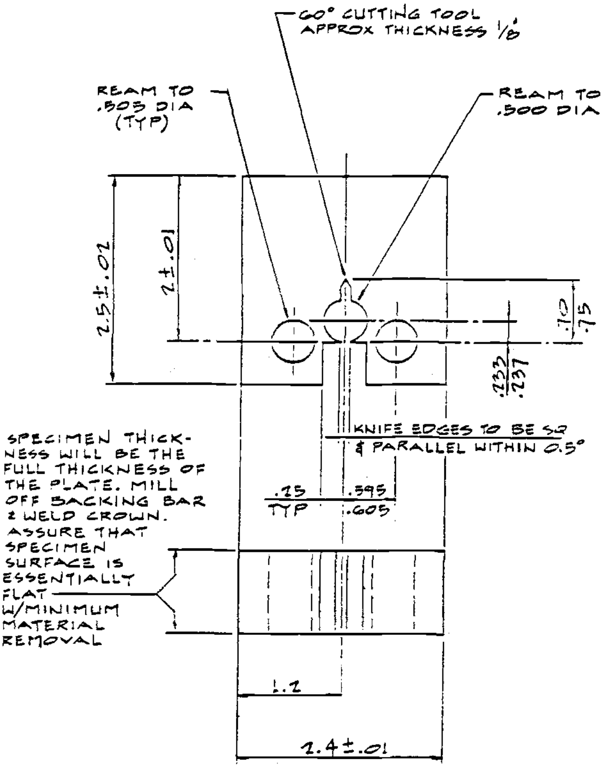

Note: Dimensions shown in inches, 1 in. = 25.4 mm

FIG. 2—J_{Ic} *compact tension specimen.*

base plate. The resistance curve for this specimen exhibited virtually no blunting. Therefore, it is believed that there may have been a defect at the initial crack tip in this specimen. The next lowest toughness (J_{Ic}) was 9.5 kJ/m^2 (54 in. · lb/in.^{2}).

Toughness seemed to decrease with the depth at which the weld was prepared, with the exception of the 12.7-mm (½-in.) ferritic HAZ specimens, in which, surprisingly but clearly, the toughness increased with depth. The toughness changes that occurred in the HAZ were probably a result of changes in the cooling rates and resulting changes in the microstructure. The decrease in toughness of the weld metal with depth was most likely due to the increase in porosity and resulting loss in net area with depth.

All fracture toughness tests failed in a ductile tearing mode. Four of 19 J_{Ic}/CTOD specimens with the crack in the HAZ exhibited a pop-in after some stable tearing. (None of the 29 test specimens of weld metal popped in.) The four plates that exhibited pop-in in the HAZ (designated in Fig. 5) were all 25.4 mm (1 in.) thick, including a *dry* ferritic weld. All of the pop-ins arrested and stable tearing was resumed as the failure mode. The maximum crack jump was about 5.1 mm (0.2 in.).

Some of the 25.4-mm (1-in.) plates were welded to strongbacks prior to the underwater welding. This restraint does not seem to influence the fracture toughness significantly, although the restrained welds consistently performed slightly worse than the unrestrained equivalent welds in both the weld metal and the heat-affected zone.

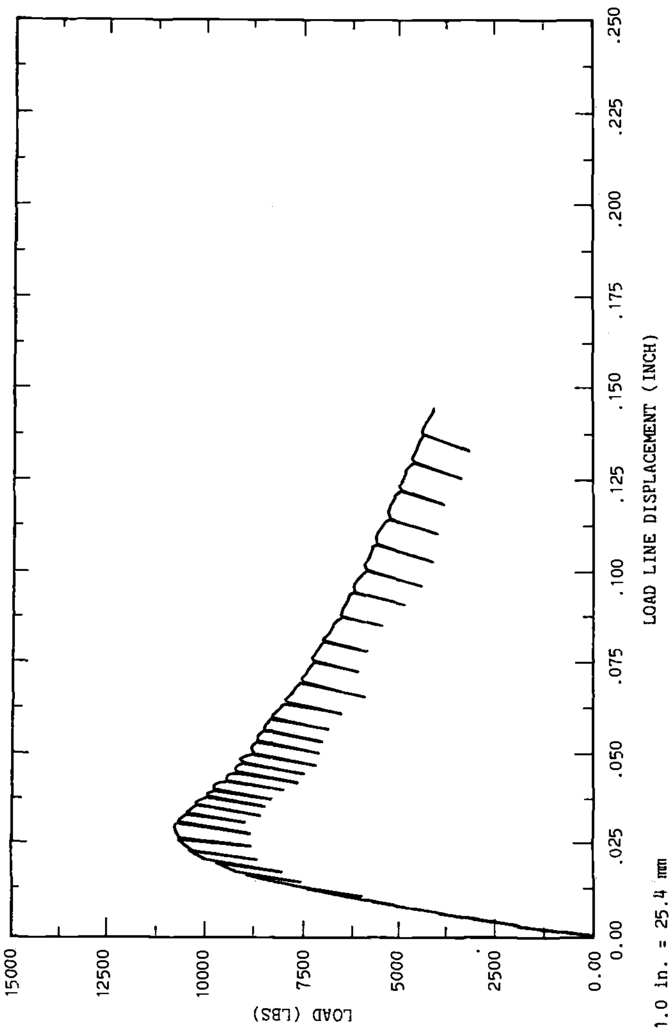

FIG. 3—*Example of load versus load line displacement for* J_{Ic}/*CTOD test 25-mm plate, wet weld prepared at a water depth of 10 m, weld metal tested.*

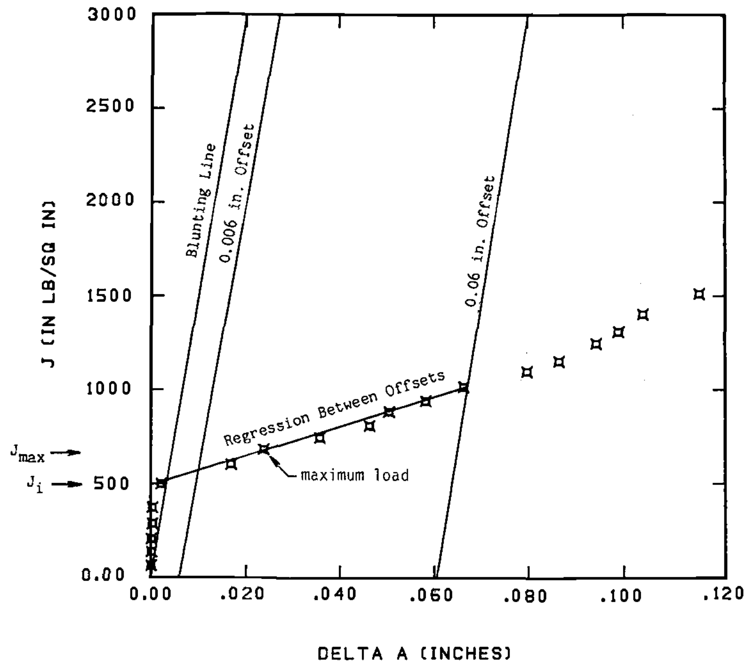

$1.0 \frac{in\ lb}{in^2} = 0.175 \frac{kJ}{m^2}$

1.0 in. = 25.4 mm

FIG. 4—*Example of the* J-*resistance curve for underwater weld 25-mm plate, wet weld prepared at a water depth of 10 m, weld metal tested.*

With two significant exceptions, a 25.4-mm (1-in.) ferritic air weld and a 25.4-mm (1-in.) austenitic wet-backed weld, the heat-affected zone toughness was generally greater than or about the same as the weld-metal toughness. This may simplify any application to design; i.e., perhaps only weld metal tests and analyses would be required to get a lower bound on weld integrity.

Discussion of CTOD and J *Methodology*

The CTOD and the J-integral methodologies each have advantages and disadvantages. A critical CTOD is a readily grasped concept that makes possible a straightforward evaluation procedure. However, it is not always easy to employ this parameter in structural integrity assessments. These assessments (see the British Standards Institution publication PD 6493)[5] usually involve empiricism and a large and often uncertain degree of conservatism. The J-integral requires a somewhat more complex and knowledgeable approach to the determination of the relevant material fracture properties. However, this is compensated for by (1) the opportunity for increased load-carrying capacity beyond crack growth initiation produced by the J-resistance curve behavior, (2) the fundamental basis that the J-integral

[5] "Guidance on Some Methods for the Derivation of Acceptance Levels for Defects in Fusion Welded Joints," PD 6493, British Standards Institution, London, England, 1980.

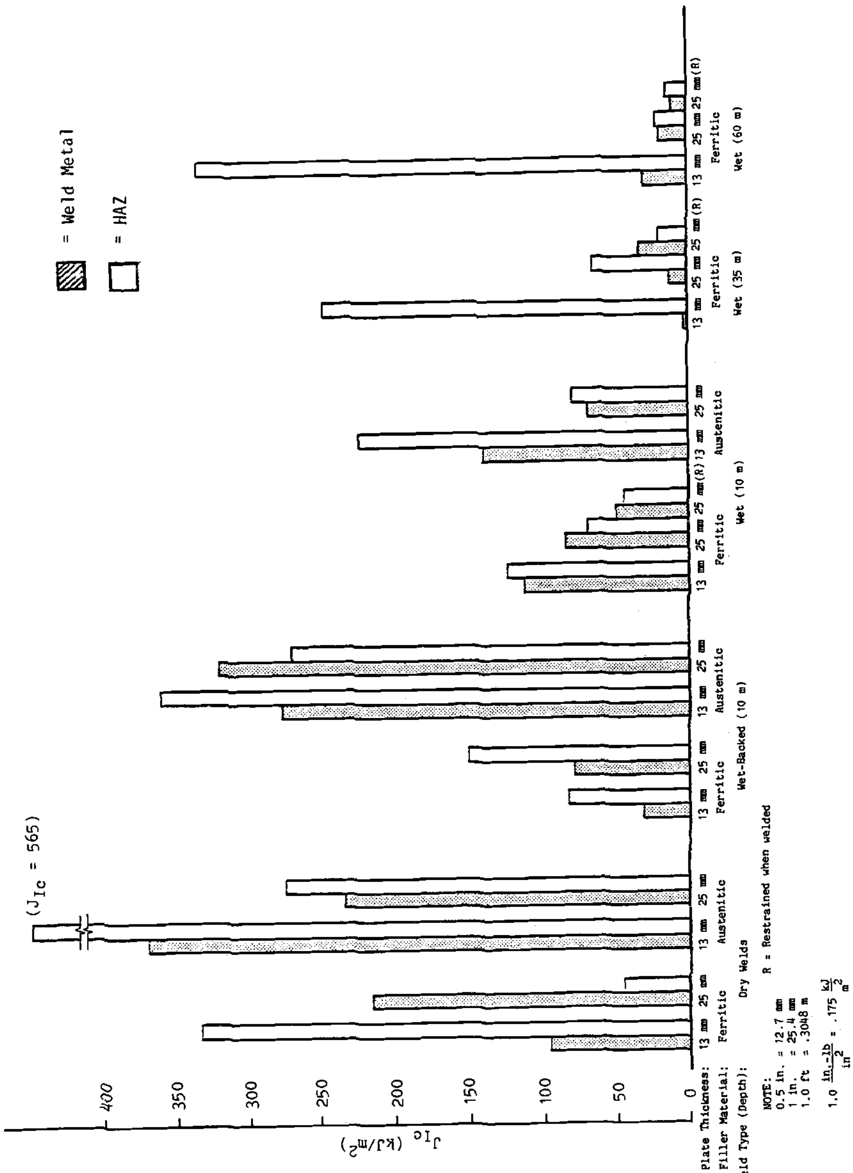

FIG. 5—J_{Ic} shown according to weld type.

possesses in those quantifiable conditions in which "J dominance" exists, and (3) its ready accommodation in structural analyses; e.g., see the tabulation of J solutions in Appendix X of Ref *4*.

The existence of these two approaches, the functional differences noted above, and the geographical distribution of proponents of the approaches may seem very baffling to the engineer planning a fitness-for-purpose evaluation. Fortunately, it can be shown that, when interpreted correctly, the measurements are equivalent and the approaches are therefore complementary.

For small-scale yielding conditions, CTOD and J can be precisely related. Thus, for a wide range of contained yielding situations, one parameter can be converted to the other, whereupon the easier small-scale specimen measurement can be used in conjunction with the more applicable structural analysis approach. What needs to be determined is how far towards large-scale yielding conditions this correspondence can be relied upon.

When the conditions of J-dominance are met, the parameter J has meaning both as the equivalent of the energy release rate, G, and as a measure of the amplitude of the stress and displacement fields at the crack tip [*5,6*]. For the special case of small-scale yielding conditions, K can be directly related to the G, J, and δ_t (CTOD) as

$$J = G = \frac{K^2}{E'} = \delta_t \sigma_y \tag{1}$$

where $E' = E$ for plane stress and $E' = E/(1 - \nu^2)$ for plain strain, while σ_y is the flow stress. A convenient definition of the flow stress is the average of the yield and ultimate stress.

Because K values are most familiar to engineers, Eq 1 is sometimes used to express values of J or δ_t in terms of K, even when small-scale yielding conditions are not met. Alternatively, whenever J dominance exists, it is possible to write the CTOD as

$$\delta_t = \frac{d_n J}{\sigma_y} \tag{2}$$

where d_n is a function of the strain-hardening exponent for power-law hardening materials (n). For typical values of n, d_n has values of approximately 0.6 and 0.8 for plane strain and plane stress, respectively. Consequently, when J reaches its critical value, the CTOD must also attain its critical value. Hence, when J dominance exits, the J-integral and the CTOD approaches to elastic-plastic fracture mechanics are equivalent.

The critical parameters K_{Ic}, J_{Ic}, and CTOD$_m$ are defined by three standards: the ASTM Test for Plane-Strain Fracture Toughness of Metallic Materials (E 399-83), ASTM Test E 813, and BS 5762, respectively. These standards characterize the critical value of the crack driving force at the initiation of crack extension, and thus allegedly represent a material property that is transferable from a test specimen to a structure. However, each procedure uses a different method to identify the point of crack initiation:

- K_{Ic} is defined at the point of intersection of a secant line (of a slope 95% of the initial slope) and the load displacement curve.
- J_{Ic} is defined by fitting a curve to the J-Δa curve and finding the intersection of this curve with the blunting line.
- CTOD$_m$ is merely defined as the CTOD at the point of maximum load.

It is only because of these differences that the critical values K_{Ic}, J_{Ic}, and $CTOD_m$ cannot be directly related.

Figure 4 shows a J-Δa curve (J-resistance curve) from a test on a 25.4-mm (1-in.)-thick underwater weld. The point corresponding to maximum load is indicated in Fig. 4. Note that the value of J at maximum load is higher than the value of J at the intersection of the blunting line. The sign and magnitude of this difference varies from material to material.

Figure 6 shows a CTOD-resistance curve constructed from the same test. Here the blunting line is given by

$$\mathrm{CTOD} = 2\ \Delta a \tag{3}$$

where Δa is the crack extension. Although the procedure for constructing such a curve is not discussed in BS 5762, this construction can be used to identify the value of CTOD at initiation ($CTOD_i$) in a procedure analogous to the procedure in ASTM Test E 813. In Fig. 6, $CTOD_i$ = 0.12 mm (0.0048 in.), while $CTOD_m$ = 0.13 mm (0.0052 in.). Note that construction of this curve does not violate BS 5762. Thus, the difference between ASTM Test E 813 and BS 5762 lies only in the interpretation of the data acquired in both test procedures.

The J-integral was derived on the basis of nonlinear elastic material behavior. Because the material is actually elastoplastic and unloading occurs in the wake of crack growth, the J-resistance curve becomes geometry dependent after significant crack extension [7,8]. Because the point of maximum load generally occurs after some crack extension, the values

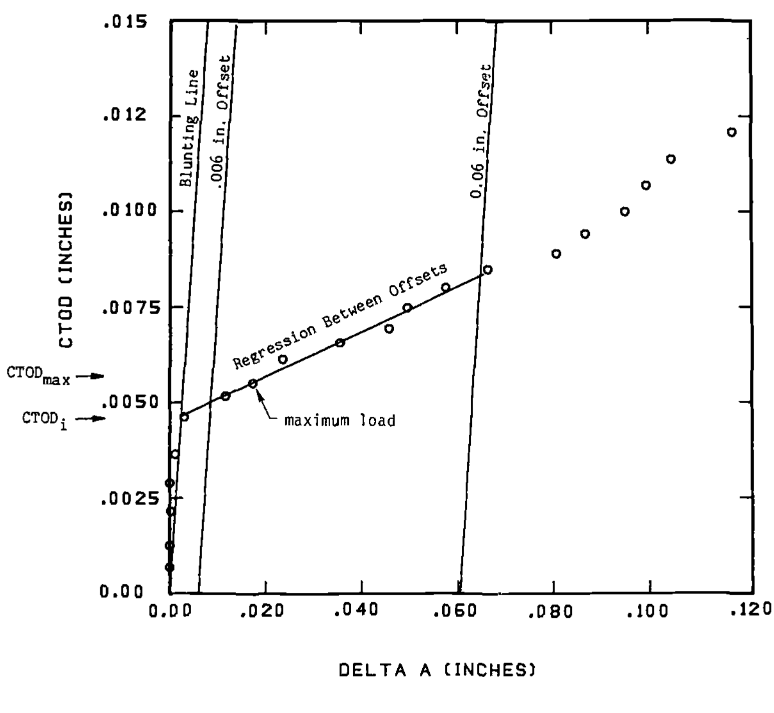

FIG. 6—*Example of the CTOD resistance curve for underwater weld 25-mm plate, wet weld prepared at a water depth of 10 m, weld metal tested.*

of J_m and $CTOD_m$ (at maximum load) may be geometry dependent, while the values of J_{Ic} and $CTOD_i$ (closer to actual crack initiation) are generally geometry independent. As shown for the ship steel ABS EH36 by Anderson and McHenry [*9*] and by Poulose et al. [*8*] for 4340 steel and various aluminum and titanium alloys, the initiation values J_{Ic} and $CTOD_i$ are independent of geometry even when the maximum load values show significant dependence on thickness and crack length.

Figure 7 shows a linear relationship between J and CTOD in the same fracture toughness test in Figs. 3, 4, and 6. Equation 2 describes this relationship for $d_n = 0.63$. Equation 2 also agrees with test results for a 12.7-mm (½-in.)-thick underwater weld if $d_n = 0.59$ [*1*]. De Castro et al. [*10*] similarly found that the CTOD and J are proportional and related by Eq 2 for Grade 50 structural steel with d_n ranging from 0.59 to 0.77 as the temperature ranged from −100°C to −10°C. Wellman and Rolfe [*11*] provided an analysis and correlation of J and CTOD test parameters on pressure vessel steel. These correlations show that Eq 2 with $d_n = 0.83$ for plane stress and $d_n = 0.63$ for plane strain is applicable for a wide range of conditions. Therefore, both J and CTOD are equivalent over the range of crack growth produced in these fracture tests.

A simple fracture mechanics analysis can be performed to show the flaw size that would be just large enough to initiate tearing as the stress approached the minimum specified ultimate tensile strength of the weld metal, i.e., 414 MPa (60 ksi). Wet-backed welds and wet welds made at 10 m (33 ft) have a fracture toughness, K_{Ic}, (derived from J_{Ic}) of greater than 102 MPa $\sqrt{m}$ (93 ksi $\sqrt{in.}$). The simple fracture mechanics analysis yields a tolerable defect size of about 25.4 mm (1 in.) for these particular welds. The fracture toughness of all weld metal and HAZ is sufficient to tolerate flaws (without initiating tearing) larger than those allowed under AWS Specification D3.6, i.e., 3.3 mm (⅛ in.).

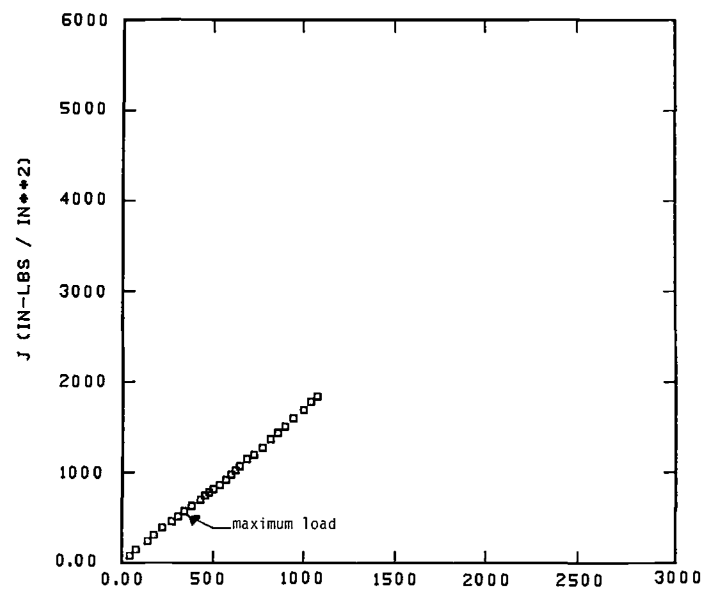

FIG. 7—*Example of the relationship between* J *and CTOD for underwater weld at a flow stress of 414 MPa (60 ksi).*

The CTOD design curve (PD 6493) procedure requires consideration of residual stress. The strain considered in a fracture assessment by the CTOD approach can be as high as twice the yield strain, and more conservative results are obtained. Considering the minimum CTOD of 0.09 mm (0.0034 in.) for wet welds prepared at 10 m (33 ft), a tolerable defect size just greater than 3.3 mm (0.012 in.) is obtained.

Conclusions

1. The data gathered from industry sources and the literature, and experimental data obtained provide a basis for the use of the wet and wet-backed SMAW process for critical structural applications, provided the limitations of the welds are considered in the design. The fracture toughness of the welds is sufficient to tolerate flaws larger than those allowed under AWS Specification D3.6.
2. All fracture toughness specimens failed in a ductile tearing mode. The HAZ is as tough as the weld metal for 25.4-mm (1-in.) welds and tougher than the weld metal for 12.7-mm (0.5-in.) welds. Austenitic welds were much tougher than ferritic welds. Toughness decreases significantly with depth, probably because of chemical and microstructural changes, as well as increasing porosity.
3. The austenitic weld and HAZ Charpy specimens exhibited fully shear, upper-shelf fracture at −2°C (28°F). The wet ferritic weld metal also exhibited upper-shelf fracture at −2°C (28°F). Dry and wet-backed ferritic welds and the HAZ of the wet ferritic welds had greater Charpy energy than the wet ferritic weld metal but did not generally show upper-shelf fracture.
4. No cracks were observed in nondestructive evaluation or in cutting out the specimens. Porosity was excessive in the wet welds and increased with the depth at which the welds were prepared. Slag inclusions and lack of penetration were found. These discontinuities were acceptable within the requirements of AWS Specification D3.6.
5. The peak hardness in the last passes of the welds, particularly in the HAZ, was high. Ferritic welds exceeded 300 HV 1.0 and austenitic welds exceeded 400 HV 1.0. Since (1) no cracking was observed in the welds, (2) no brittle behavior was exhibited, and (3) hardness could not be correlated with the bend test, toughness, or strength performance, the author concludes that the hardness is not a meaningful indicator of weld quality or performance.
6. The CTOD was shown experimentally to be linearly proportional to J for values up to 350 kJ/m^2 (2000 in. · lb/in.^{2}) and crack extensions up to 4.8 mm (0.19 in.).

Acknowledgments

The author appreciates the funding and opportunity for investigating underwater welds provided by the Ship Structures Committee and the administration provided by the U.S. Coast Guard through Contract No. DTCG-23-82-C-20017.

References

[*1*] Dexter, R. J., Norris, E. B., Schick, W. R., and Watson, P. D., "Underwater Wet and Wet-Backed Welds: Mechanical Properties and Design Guidelines," Final Report, SwRI Project No. 06-7168. Project SR-1283, Interagency Ship Structures Committee, Washington, DC, 30 Sept. 1985.

[2] Olson, D. L. and Ibarra, S., "Underwater Welding Metallurgy," paper presented at the Underwater Welding Workshop, Colorado School of Mines, Golden, CO, 13–14 Nov. 1985.
[3] Chan, K. S. and Cruse, T. A., "Stress Intensity Factors for Anisotropic Compact-Tension Specimen with Inclined Cracks," *Engineering Fracture Mechanics*, Vol. 23, No. 5, 1986, pp. 863–874.
[4] Kanninen, M. F. and Popelar, C. H., *Advanced Fracture Mechanics*, Oxford University Press, New York, 1985.
[5] Hutchinson, J. W., "Singular Behavior at the End of a Tensile Crack in a Hardening Material," *Journal of the Mechanics and Physics of Solids*, Vol. 16, 1968, pp. 13–31.
[6] Rice, J. R. and Rosengren, G. F., "Plane Strain Deformation Near a Crack Tip in a Power-Law Hardening Material," *Journal of the Mechanics and Physics of Solids*, Vol. 16, 1968, pp. 1–12.
[7] Smith, E., "Some Comments on the Geometry Dependence of the J Versus c Relation for Plane Strain Crack Growth," *International Journal of Fracture*, Vol. 22, 1983, pp. 117–124.
[8] Poulose, P. K., Jones, D. L., and Liebowitz, H., "A Comparison of the Geometry Dependence of Several Nonlinear Fracture Toughness Parameters," *Engineering Fracture Mechanics*, Vol. 17, No. 2, 1983, pp. 133–151.
[9] Anderson, T. L. and McHenry, H. I., "Fracture Toughness of Steel Weldments for Arctic Structures," Report PB83-164152, National Bureau of Standards, Gaithersburg, MD, December 1982.
[10] De Castro, P. M. S. T., Spurrier, J., and Hancock, P., "Comparison of J Testing Techniques and Correlation of J-COD Using Structural Steel Specimens," *International Journal of Fracture*, Vol. 17, 1981, pp. 83–95.
[11] Wellman, G. W. and Rolfe, S. T., "Engineering Aspects of CTOD Fracture Toughness Testing," *Welding Research Council Bulletin*, No. 299, November 1984.

Wolfgang Burget[1] *and Johann G. Blauel*[2]

Fracture Toughness of Manual Metal-Arc and Submerged-Arc Welded Joints in Normalized Carbon-Manganese Steels

REFERENCE: Burget, W. and Blauel, J. G., **"Fracture Toughness of Manual Metal-Arc and Submerged-Arc Welded Joints in Normalized Carbon-Manganese Steels,"** *Fatigue and Fracture Testing of Weldments, ASTM STP 1058,* H. I. McHenry and J. M. Potter, Eds., American Society for Testing and Materials, Philadelphia, 1990, pp. 272–299.

ABSTRACT: This paper shows that, in the temperature transition regime, scatter of weld metal and heat-affected zone toughness values is related to material heterogeneity in the welded joints. Results were obtained from impact testing of V-notched and fatigue-cracked Charpy specimens as well as from static fracture toughness tests on small-scale and full-thickness specimens. Besides material heterogeneity, mechanical heterogeneity is emphasized as having a significant influence on the fracture performance of heat-affected zone specimens.

KEY WORDS: weldments, welded joints, weld metal, heat-affected zone, heterogeneity, impact toughness, fracture toughness

Nomenclature

a Crack length
r Plastic rotational factor
r_1 Rotational factor of the lower yield-strength side
r_2 Rotational factor of the higher yield-strength side
z Distance of the crack mouth opening measurement from the specimen top surface
B Specimen thickness
W Specimen width
V_p Plastic component of the crack mouth opening
V_g Total crack mouth opening displacement
V_1 Crack mouth opening component for the lower yield-strength side
V_2 Crack mouth opening component for the higher yield-strength side
δ_1 Local crack-tip opening displacement (CTOD) for the lower yield-strength side
δ_2 Local CTOD for the higher yield-strength side
E Young's modulus
K Mode I stress-intensity factor
S_r Yield strength ratio (lower yield strength/higher yield strength) in overmatched or undermatched welded joints
α Mean orientation of columnar weld metal microstructure to the crack plane
ν Poisson ratio
σ_y Yield strength

[1] Research engineer, Fraunhofer-Institut für Werkstoffmechanik, D-7800 Freiburg, West Germany.
[2] Head of section, Materials and Component Assessment, Fraunhofer-Institut für Werkstoffmechanik, D-7800 Freiburg, West Germany.

Fracture toughness characterization of weldments in structural steel components is widely used in design and as a basis of engineering safety analysis.

In the regime of elastic-plastic material behavior, it is the crack-tip opening displacement (CTOD) concept that is preferentially applied in weld defect assessment procedures. As input data describing the material resistance to crack extension in the analysis, critical values of crack-tip opening displacement (δ) have to be determined. Since weldments are characterized by material heterogeneity of the weld metal and the heat-affected zone, depending on the composition of the materials and the weld fabrication, serious problems can arise for fracture toughness testing.

Investigations are reported here with special emphasis on the effect of weld metal (WM) and heat-affected zone (HAZ) heterogeneity on results of impact and static fracture toughness tests.

Material and Weld Fabrication

Experimental investigations were conducted on submerged-arc (SA) and manual metal-arc (MMA) welded plates. The base metals used were two different modifications of the normalized fine-grained structural steel Fe E 355 (EN 10025), with original plate thickness of 60 and 63 mm, respectively. The compositions of the steels are given in Table 1. The mechanical properties are summarized in Table 2. In the SA welds, the WM fracture toughness was determined for double-V and K joints. The HAZ toughness was evaluated on K joints. All SA welds were fabricated with a tandem wire system at a heat input of 3 kJ/mm, using a wire/flux combination of the type S3/OP121TT. The SA welds were tested in the as-welded (AW) and postweld heat-treated (PWHT) conditions (at 570°C for 2.5 h and air cooled). The MMA double-V joints were welded in the vertical-up position, whereas the welding position for the K joints was transverse. For all MMA welds, basic electrodes of Type E 7018 were used. The average heat input level for the MMA welds was 1.5 kJ/mm. The fracture toughness of MMA-WM was determined for the AW material condition.

Experimental Procedure

Tension and Charpy Impact Tests

Longitudinal (MMA-WM) and transverse (SA-WM) tension specimens were extracted as shown in Fig. 1. The WM properties were determined at −10°C and at room temperature.

Charpy impact specimens (10 by 10 by 55 mm) with through-thickness notches were extracted using two different procedures. In the first case, WM specimens were located following standard extraction recommendations, that is, at subsurface and root specimen positions (Fig. 2). The SA-WM specimens, on the other hand, were located in such a way that the V-notch sampled either the reheated or the as-deposited microstructure only. Because of the different bead geometries and the high degree of bead overlapping, this was not possible for the MMA welds. One Charpy impact specimen series with the notch position in HAZ was machined from the SA-welded K joint (Fig. 2, *bottom*).

Impact energy temperature transition curves were determined for SA-WM, MMA-WM, and SA-HAZ using Charpy V-notched specimens. The impact toughness transition behavior of reheated and as-deposited WM, as well as HAZ material, was also studied by testing fatigue-precracked Charpy-type specimens.

Fracture Mechanics Tests

Full-thickness single-edge-notched bend (SENB) specimens, prepared according to the British Standard for Crack Opening Displacement (COD) Testing (BS 5762:1979) were

TABLE 1—*Chemical composition of the base metals, in weight percent.*

Base Metal	C	Si	Mn	P	S	Al	Cr	Cu	Mo	N	Ni	V	Nb	Nb+V	CE
T StE 355	0.11	0.34	1.52	0.018	0.002	0.026	0.08	0.19	0.02	-	0.13	0.01	0.025	0.035	0.41

	C	Si	Mn	P	S	Al	Cr	Cu	Mo	N	Ni	V	Nb	Nb+V	CE
StE 355	0.14	0.41	1.43	0.013	0.001	0.040	0.08	0.17	0.03	0.009	0.06	0.01	0.040	0.040	0.41

TABLE 2—*Tensile and Charpy impact properties of the base metals.*

Material	Test temp. (°C)	UTS (MPa)	YS (MPa)	EL (%)	Absorbed energy (-40°C) (J)
T StE 355	+20	516	372	32	246
StE 355	+20	534	364	32	176

machined from the plate welds to determine fracture toughness properties for SA-WM, MMA-WM, and SA-HAZ in terms of critical values of crack-tip opening displacement (CTOD). Figure 3 shows the different SENB specimen geometries, used together with the various notch positions and orientations investigated. Before the through-thickness notched specimens to be tested in the AW condition were fatigue cracked, the ligaments of these specimens were subjected to a local compression treatment [*1*] to obtain acceptable fatigue crack front curvature. The SENB specimens of the preferred test piece geometry ($B \times 2B$) (see BS 5762) had a final relative fatigue crack length of $a/W \approx 0.5$. Subsidiary test pieces ($B \times B$) were fatigued to a final relative crack length of $a/W \approx 0.3$.

The fracture mechanics tests were done on a 600-kN servohydraulic testing machine under displacement control. The computer-based data acquisition and storage included the force, crack-mouth opening displacement, position of the hydraulic piston, A-C potential difference for crack growth detection, specimen temperature, and time.

From the stored data critical values of CTOD were determined at unstable fracture initiation (Index c), at the onset of stable crack growth (Index i), at instability after stable crack extension (Index u), or at the first attainment of a maximum load plateau (Index m).

CTOD values for WM and HAZ were calculated for the SENB specimens using the formula given in BS 5762.

$$\delta = \frac{K^2(1 - \nu^2)}{2\sigma_y E} + \frac{1}{1 + \dfrac{a + z}{r(W - a)}} V_p$$

with $r = 0.4$.

Local CTOD values were determined for HAZ specimens following a modified CTOD criterion (Fig. 4) suggested by Arimochi et al. [2].

$$\delta_{tot} = \delta_1 + \delta_2$$

$$\delta_{tot} = \frac{r_1(W - a)}{r_1(W - a) + a + z} V_1 + \frac{r_2(W - a)}{r_2(W - a) + a + z} V_2$$

$$V_g = V_1 + V_2$$

The crack-mouth opening components V_1 and V_2 can be calculated from measured V_g values following the procedure given in [2].

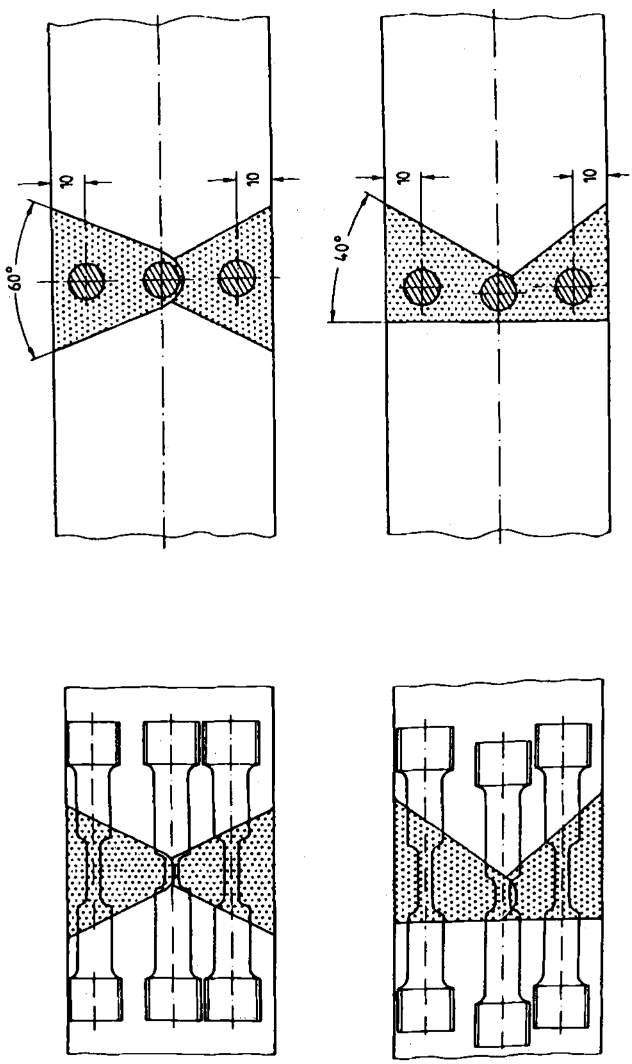

FIG. 1—*Tensile specimen extraction.*

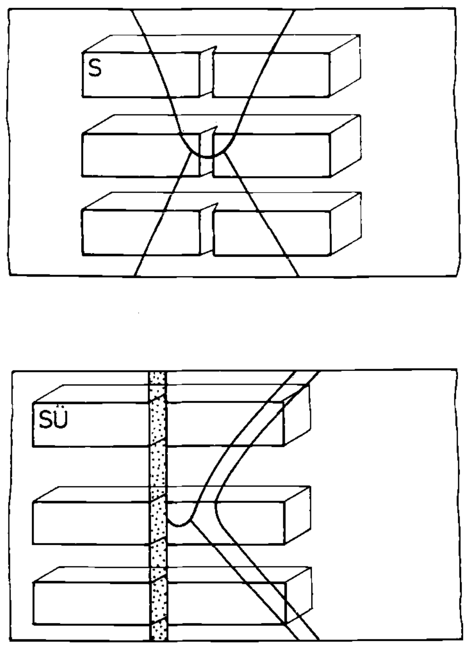

FIG. 2—*Charpy impact specimen extraction (subsurface, weld root).*

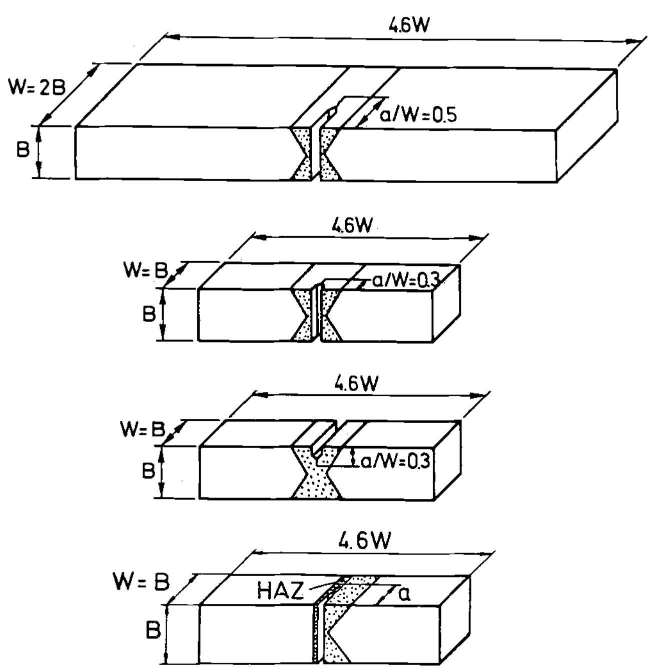

FIG. 3—*SENB specimens for weld metal and heat-affected zone testing.*

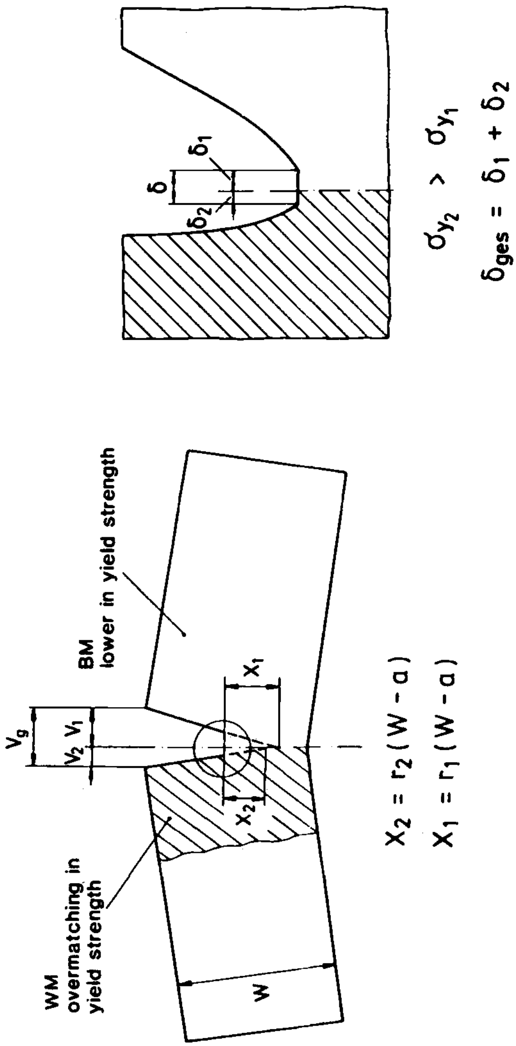

FIG. 4—*Local CTOD* [2].

Results and Discussion

Tensile Properties of Weld Metal

The tensile properties obtained for MMA-WM (longitudinal specimen orientation) are summarized in Table 3. The results for SA-WM (transverse specimen orientation) tested in the AW and PWHT conditions are given in Table 4.

In comparing the individual values of yield strength (YS) and ultimate tensile strength (UTS), as well as the results for elongation and reduction of area, a common tendency is evident, with the highest strength and lowest deformation characteristics for the specimens being taken from the root run areas of the double side welded joints.

Differences in metallurgical composition between the subsurface and root run specimens, caused by the higher dilution in the root runs and possibly by strain-aging effects, are a reason that may explain the differences in tensile behavior.

Looking at a representative macrosection (Fig. 5), it is obvious that longitudinal or transverse root run specimens sample high portions of as-deposited WM, whereas subsurface specimens can be dominated by reheated weld metal microstructure. The individual influence of each of these parameters was not quantified.

Charpy Impact Tests

In the transition temperature regime, Charpy impact energy curves determined for WM following the standard specimen extraction procedures are characterized by a wide scatter band. The difference in transition temperature between the lower and upper bound of the scatter band can be as high as 30 to 60°C (the transition temperature at 50% of upper shelf energy). This is demonstrated for MMA-WM and SA-WM transition curves in Fig. 6.

TABLE 3—*Tensile properties of MMA-WM at −10°C (longitudinal), as welded.*

Groove/ Weldg. Position	Specimen location	YS (MPa)	UTS (MPa)	El. (%)	RA (%)
Electrode A					
	1st side	542	630	29	73
K	2nd side	543	629	27	74
2G	Root	662	713	19	66
Electrode A					
	1st side	547	633	29	71
X	2nd side	523	620	28	74
3G	Root	590	662	21	67
Electrode B					
	1st side	541	623	-	-
X	2nd side	594	660	23	61
3G	Root	621	678	19	64
Electrode B					
	1st side	429	522	30	72
X	2nd side	462	535	33	70
3G	Root	587	670	23	72

TABLE 4—*Tensile properties of SA-WM at* $-10°C$ (*transverse*).

Weld/ condition	Specimen location	Ys (MPa)	UTS (MPa)	El. (%)	RA) (%)
	1st side	348	479	31	78
X	2nd side	461	570	30	74
p.w.h.t.	Root	511	612	-	73
	1st side	417	539	20	79
X	2nd side	-	-	-	-
a.w.	Root	578	646	12	73
	1st side	496	587	30	75
K	2nd side	496	587	29	75
p.w.h.t.	Root	501	685	-	70
	1st side	464	566	31	77
*K	2nd side	435	562	36	81
a.w.	Root	591	689	16	62

* tested at room temperature

Fractographic and metallographic examinations of specimens representing the lower bound of the transition scatter band revealed that most specimens consist of high portions of as-deposited WM microstructure. Since the SA weld bead geometry allowed microstructure-related specimen positioning, transition curves were determined for reheated and as-deposited WM specimens separately (Fig. 7). The upper curve, with a lower transition temperature, was obtained for specimens sampling reheated WM microstructure. The lower curve represents the transition behavior of as-deposited WM microstructure. If these curves are plotted and compared with the appropriate impact values of Fig. 6, it can be seen that the microstructure-specific WM transition curves give a good approximation for the upper and lower bounds of the scatter band obtained from conventional Charpy impact testing (Fig. 8).

Despite minimum requirements for the fracture toughness of weld metal in terms of CTOD, the optimization of the chemical composition and microstructure of WM is usually still quantified in terms of impact energy determined on Charpy V-notched specimens [*3*–*8*]. With respect to chemical and microstructural variations in WM, a sharp fatigue crack should be more sensitive than a blunt notch. Therefore, the transition behavior of reheated and as-deposited SA-WM microstructures was investigated using fatigue precracked (a/W = 0.5) Charpy-type specimens. The results in Fig. 9 show that the transition behavior of reheated and as-deposited WM is similar. Compared with the V-notched specimen results, the transition temperature shift to higher temperatures and the lowering of the upper shelf level is greater for reheated WM than for as-deposited WM (Fig. 10). Figure 11 shows that, in the case of reheated WM microstructure (*top*), the change from a blunt notch (*left*) to a fatigue crack (*right*) has an effect on the material volume but not on the type of microstructure sampled. For columnar WM microstructure it is known that deformation and fracture occur preferentially in primary grain boundary ferrite [*9,10*]. In V-notched specimens, several grain-boundary ferrite bands are sampled by a notch tip with a radius of 250 μm (Fig. 11, *bottom left*). Then deformation and fracture are concentrated at the most favorably oriented

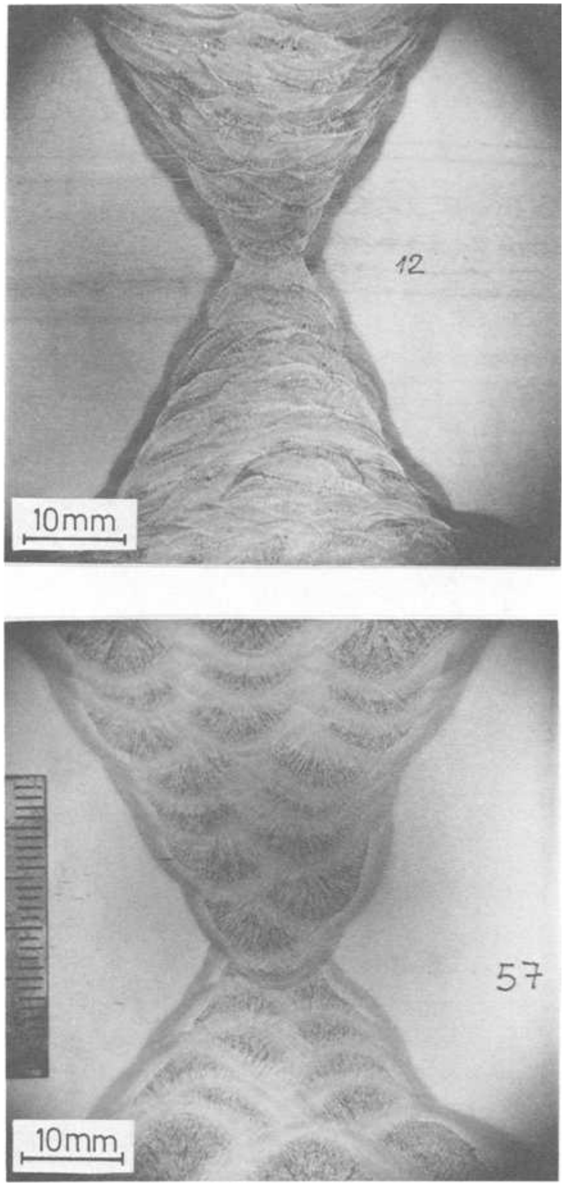

FIG. 5—*Macrosections of MMA and SA double-V joints.*

grain-boundary band. As can be seen from Fig. 11, a fatigue crack initiates at grain boundary ferrite but propagates through primary ferrite as well as acicular ferrite (Fig. 11, *bottom right*). High portions of higher toughness acicular ferrite (in comparison with primary ferrite) sampled by the fatigue crack front caused an impact toughness transition behavior for as-deposited WM similar to that found for reheated WM zones. A lower transition temperature shift for as-deposited WM is observed when using a fatigue crack instead of a blunt V notch.

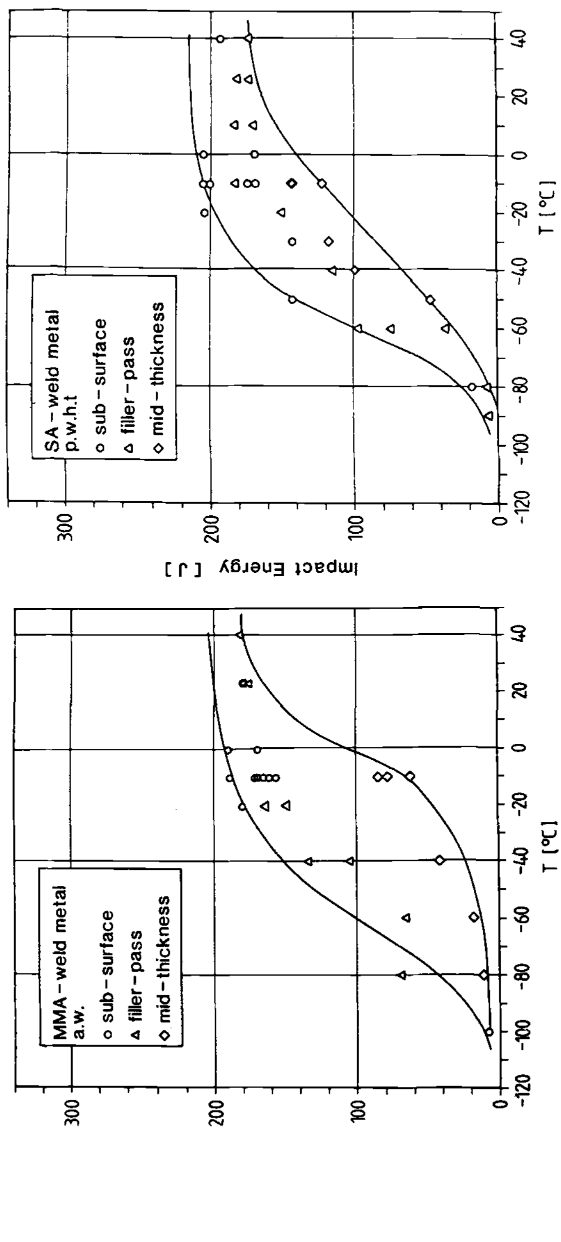

FIG. 6—*Scatter of Charpy impact energy data for weld metal in the transition regime.*

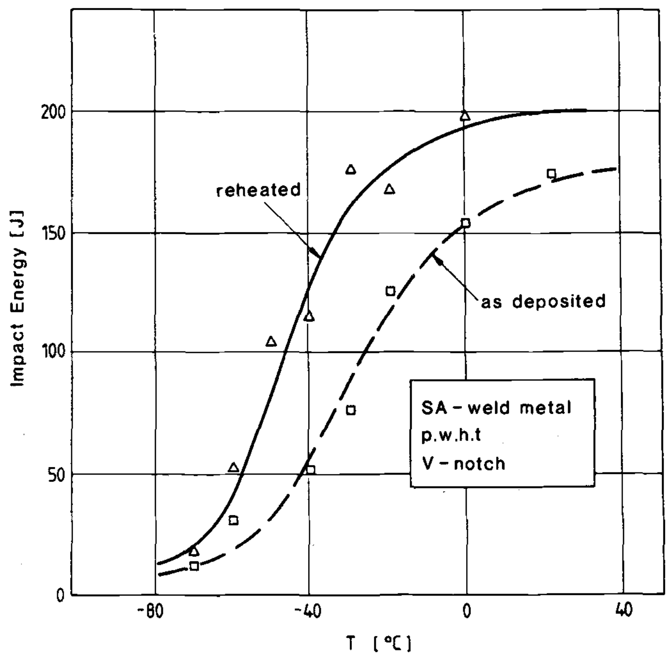

FIG. 7—*Impact energy transition behavior for reheated and as-deposited weld metal microstructures.*

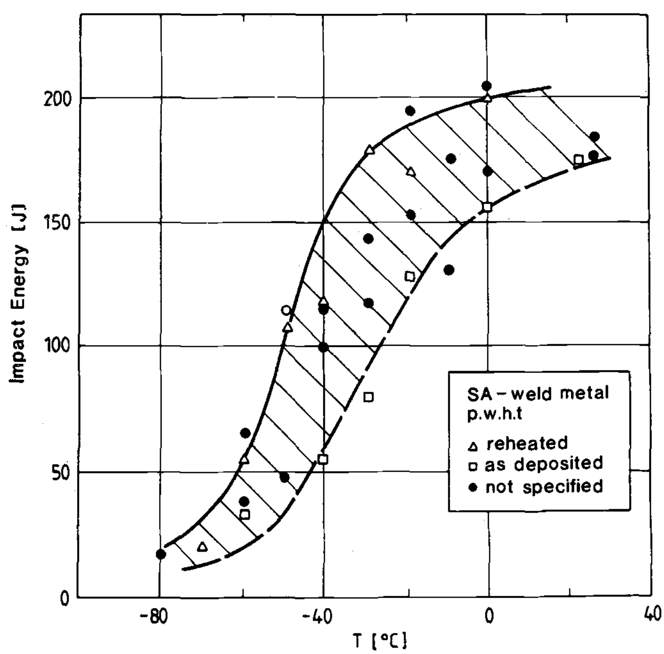

FIG. 8—*Upper and lower bound of the weld metal impact energy scatter band.*

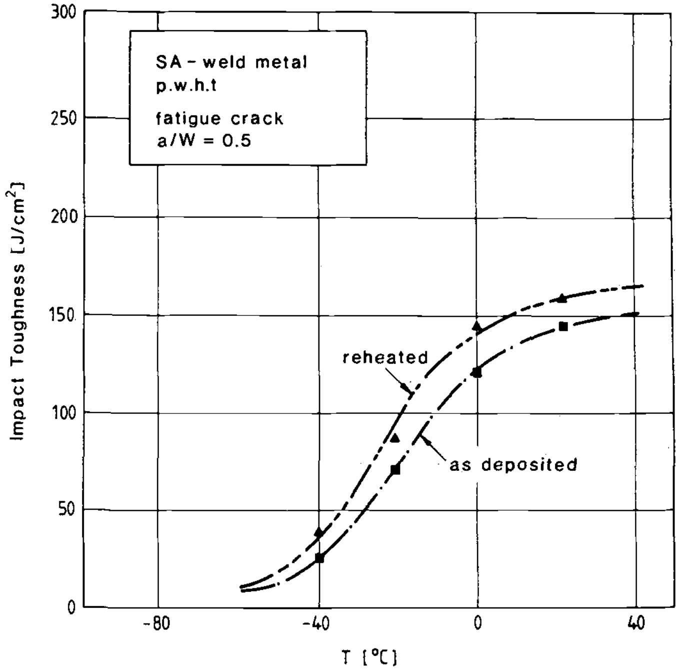

FIG. 9—*Impact toughness transition curves for reheated and as-deposited weld metal microstructures.*

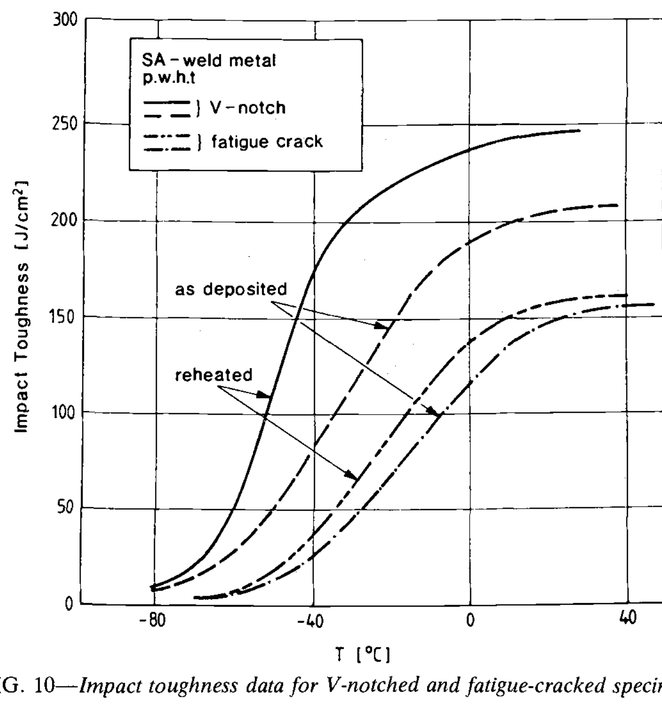

FIG. 10—*Impact toughness data for V-notched and fatigue-cracked specimens.*

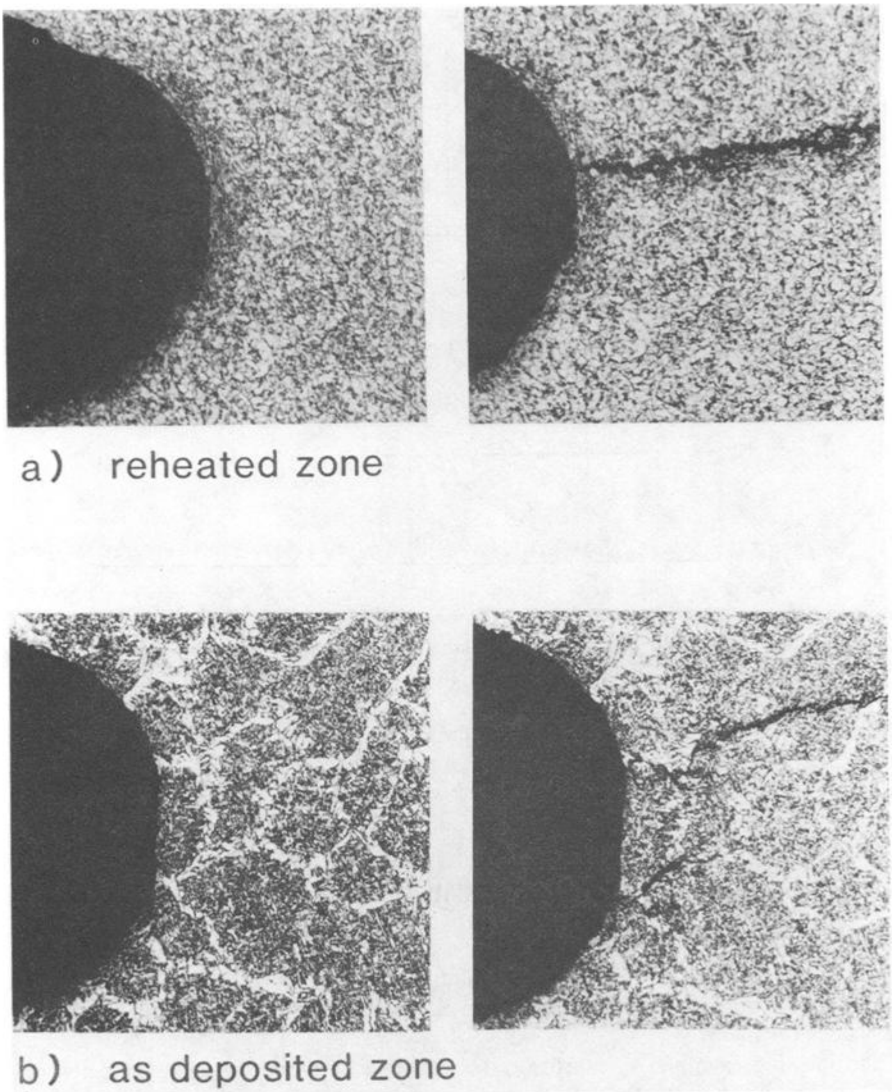

FIG. 11—*Weld metal microstructure at the V-notch and fatigue crack.*

HAZ Charpy V impact testing is performed to quantify a change in the base metal properties due to welding, i.e., to evaluate the weldability of base materials. Depending on the base metal composition and weld fabrication, coarse-grained low-toughness HAZ microstructure is built up locally to various extents along the fusion boundary. In comparison with weld metal, the geometrical sizes of low-toughness zones in HAZ are much smaller and variations in toughness can be an order of magnitude larger. Wide scatter bands are the consequence for HAZ impact energy results. While the upper bound of a HAZ transition scatter band can be approximated by the transition curve of the base material, the definition of a lower bound transition curve needs posttest examination of the specimens tested. In Fig. 12, lower bound curves are given for V-notched and fatigue-cracked HAZ specimens.

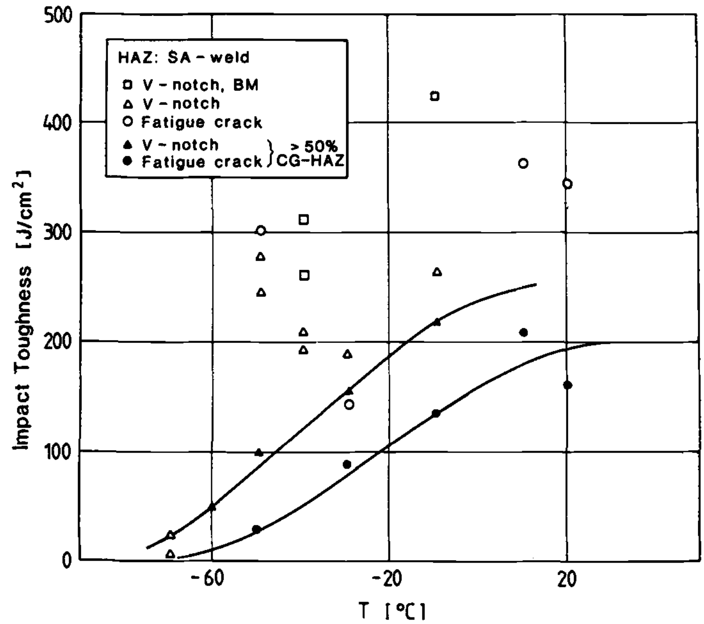

FIG. 12—*Impact toughness of V-notched and fatigue-cracked HAZ Charpy specimens (as-welded).*

As a criterion for the lower bound, it was required for V-notched specimens that the fracture initiated in coarse-grained HAZ and for fatigue-cracked specimens that the crack front sampled more than 50% coarse-grained microstructure.

Fracture Toughness of SA and MMA Weld Metal

Through-Thickness Crack Orientation

For double-sided welded symmetrical joints (double-V or K-groove joints), typical for heavy sections, through-thickness notching is used to determine lower bound fracture toughness values for the WM.

The following examples demonstrate the influence of various degrees of heterogeneity along the crack front in through-thickness notched specimens on the MMA-WM and SA-WM fracture toughness. Fracture toughness tests for MMA-WM of double-V and K joints on Steel 1, fabricated with the same electrode and approximately the same heat input (1.5 kJ/mm) but in different welding positions, gave remarkably different CTOD results (Table 5). Unstable fracture after slow stable crack growth (δ_u) was observed in WM of transverse welded K joints. WM specimens from the vertical-up welded X joint failed by unstable fracture without preceding stable crack extension (δ_c).

As a consequence of different welding positions, the weld bead orientation has changed with respect to the through-thickness crack plane (Fig. 13). In the K joint, the crack plane intersects lower toughness as-deposited WM in the midthickness region at an angle of about 30°. In the root area of vertical-up welded double-V joints, as-deposited WM microstructure has a much lower difference in orientation to the crack plane and can be more or less parallel in the first root runs, thus promoting cleavage initiation. Fractographic and metallographic

TABLE 5—*CTOD-WM results for through-thickness notched MMA welds at −10°C, as welded.*

Groove / Welding Position	Specimen type	CTOD [mm]
K 2G	SENB 2:1	0.45 (u)
		0.91 (u)
		1.21 (m)
X 3G	SENB 2:1	0.18 (c)
		0.15 (c)
		0.21 (c)

examination of fractured MMA CTOD specimens confirmed that cleavage fracture in double-V welds initiated in as-deposited root run microstructure. Using the stringer bead or weaver bead technique in MMA welding has a pronounced effect on the distribution of reheated and as-deposited WM microstructure along a through-thickness crack in multipass joints (Fig. 14). In the higher heat input weaver bead weld, the degree of weld bead overlapping results in high portions of reheated WM zones. In comparison with the stringer bead weld, lower YS, UTS, hardness values, and higher impact energy results were obtained for the WM. Average values (of three specimens) for CTOD are 0.04 mm (δ_c) in the case of the stringer bead weld, but for the weaver bead weld, the value is 0.11 mm (δ_c). Again, fractography showed that cleavage initiation originated in as-deposited root run WM microstructure. From the macrosection of the weaver bead weld it can be seen that only the first two runs of the second side of the double-V weld exhibit as-deposited WM microstructure. The degree of toughness variation along a through-thickness crack in a full-thickness specimen can be estimated qualitatively by testing small-scale SENB specimens extracted from different thickness positions and different WM microstructures. Root run specimens failed by cleavage, and subsurface specimens reached a maximum-load CTOD result (Fig. 15).

A variation of heterogeneity can also be achieved by changing the notch position within the WM. Since the width of the weld root is larger in SA double-sided welded joints than in MMA welds, the notch position was varied in a double-V SA weld.

The obtained CTOD values (Fig. 16) decreased with increasing portions of as-deposited WM microstructure along the through-thickness crack front and with a decreasing orientation difference between the notch plane and the columnar WM zones. For notch positions 2 and 3, unstable fracture initiated in as-deposited WM zones with low difference in orientation from the crack plane.

Surface Crack Orientation

The influence of different notch orientations on CTOD results is given in Table 6. The through-thickness notched specimens showed stable crack growth, resulting in critical δ values at instability (δ_u) and at maximum load (δ_m) distinctly above the surface-notched

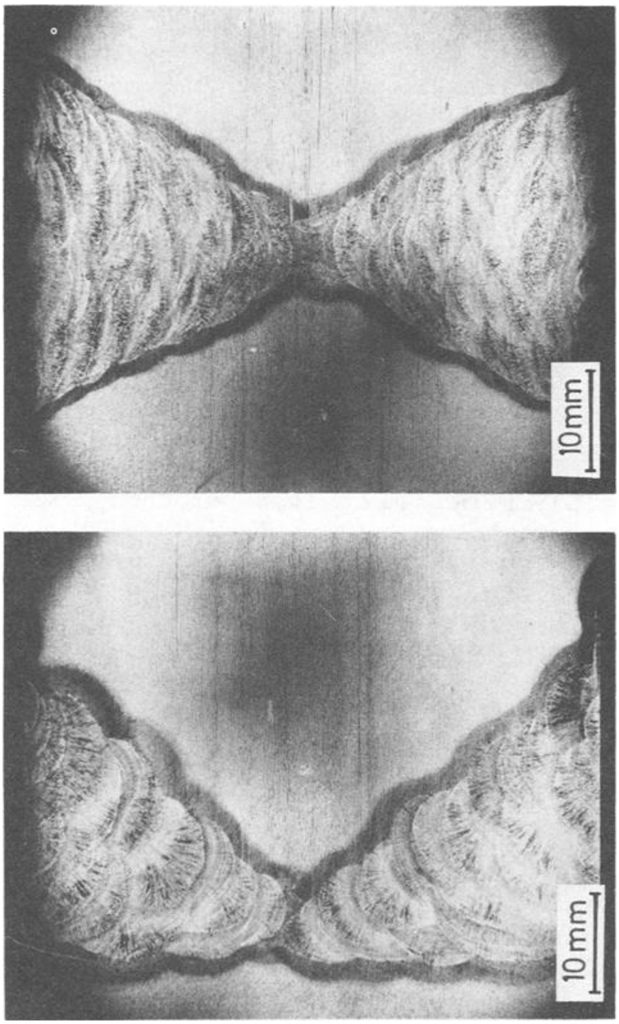

FIG. 13—*Influence of the welding position on the orientation of as-deposited weld metal microstructures (MMA weld).*

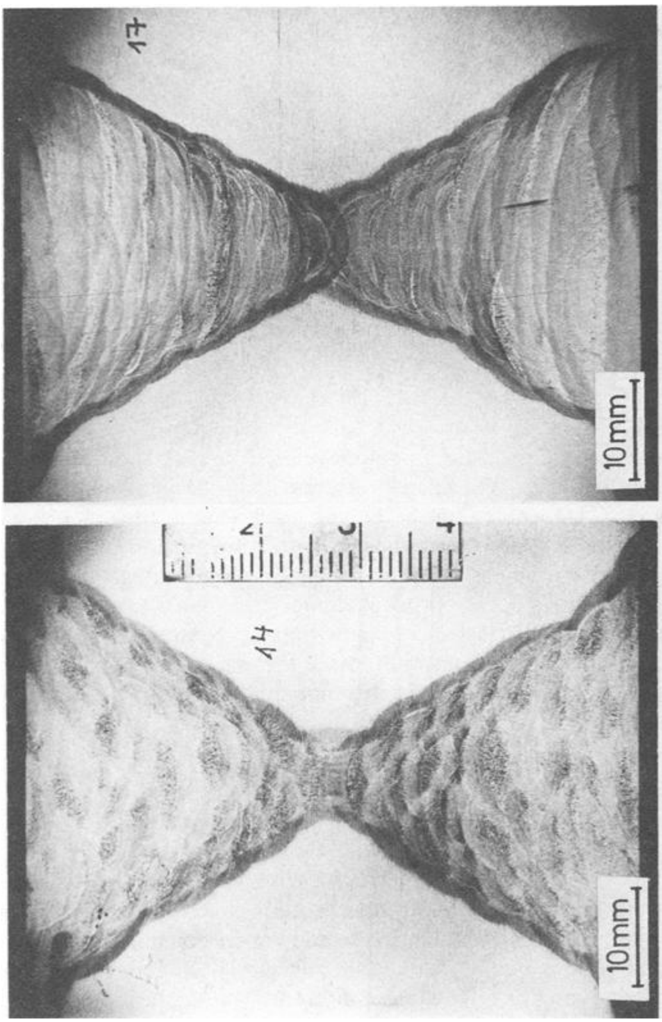

FIG. 14—*Influence of the welding technique on the distribution of reheated and as-deposited weld metal zones.*

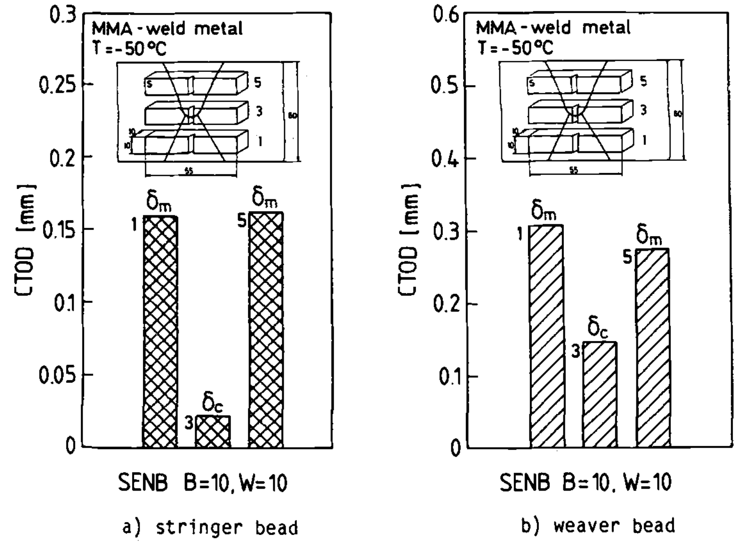

FIG. 15—*CTOD results for small-scale SENB subsurface and weld root specimens (MMA weld)*: (a) *stringer bead,* (b) *weaver bead.*

specimen results, which are derived from pop-in events (Fig. 17). These results are a consequence of extremely different WM microstructures along the individual crack fronts of each specimen (Fig. 18). Depending on the fatigue crack length, the crack front samples reheated or as-deposited WM only, which thus leads to a high scatter in test results [*11*].

Testing surface-notched specimens in the AW condition is advantageous because no additional specimen treatment is necessary to guarantee acceptable fatigue crack front geometry. On the other hand, residual stresses (approximately constant along the crack front) have an influence on local crack tip constraint. Since the crack length, WM microstructure at the crack front, residual stress state, and constraint are dependent variables, they cannot be studied separately.

HAZ Fracture Toughness

Material Inhomogeneity

Because of the weld thermal cycles, the base material microstructure adjacent to the fusion boundary is changed. In carbon-manganese and low-carbon microalloyed steels, four different metallurgical regions can be distinguished in the HAZ, reflecting different peak temperatures and cooling rates as a function of distance from the fusion line. For a single-pass weld, the HAZ is characterized by a coarse-grained, a fine-grained, a partially transformed, and a subcritical HAZ microstructure. In multipass welds, the HAZ microstructure is modified by the reheating effect of the succeeding weld beads. Therefore, HAZ microstructure varies not only as a function of distance from the fusion boundary but also in the thickness direction of the joint parallel to the fusion line. Experience has shown that the grain-coarsened HAZ often is the most critical part of the HAZ, with the lowest toughness. The size and distribution of embrittled material zones depend on the groove geometry, bead

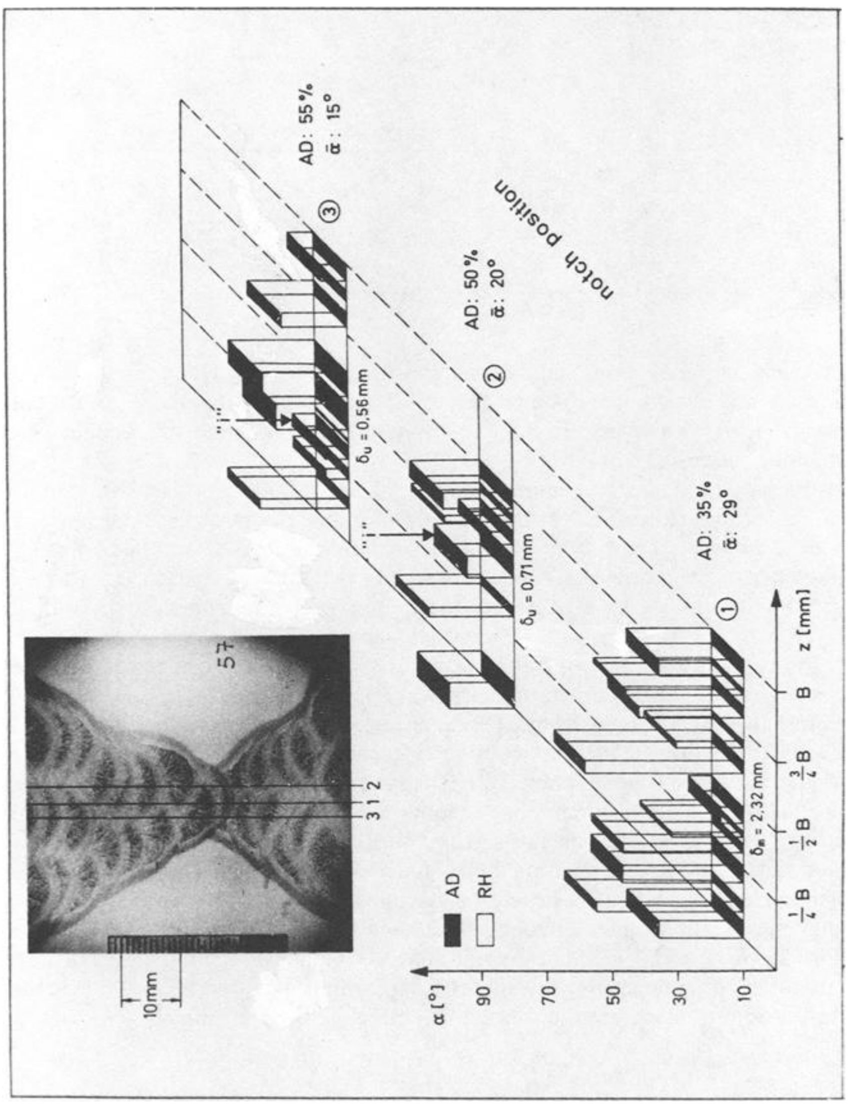

FIG. 16—*CTOD results as a function of different through-thickness notch positions.*

TABLE 6—*CTOD-WM results for the through-thickness and surface notch orientations.*

specimen	crack orientation	δ_i [mm]	δ [mm]
T1	through	0.20	0.95 (m)
T2	thickness	0.22	0.39 (u)
T3		0.23	1.20 (m)
B1	surface	-	0.01 (c)
B2		-	0.05 (c)
B3		-	0.02 (c)

sequence, welding parameters, and steel composition. To obtain HAZ fracture toughness data representative for a specific component weld, it is necessary that the test weld simulate the structural joint with respect to the total amount of low-toughness zones and their distribution along the fusion line.

Microstructural heterogeneity has a much more severe influence on HAZ fracture toughness than on WM toughness. Nevertheless, the philosophy of sampling as much low-toughness material along the crack front as possible is the same in WM and HAZ testing. For through-thickness crack orientation, HAZ mapping is used as a practical tool to achieve optimum notch position, i.e., to maximize the amount of low-toughness zones at the crack front.

Crack fronts parallel to the original plate surface (surface crack orientation) can sample either coarse-grained, fine-grained, or subcritical HAZ only.

In contrast to WM toughness characterization, posttest examination of HAZ specimens is usually performed to validate the determined fracture toughness data. Depending on the crack orientation and specimen failure type (cleavage, instability after ductile crack growth, maximum load) different sectioning procedures can be applied. Where a clear cleavage initiation site can be detected on the fracture surface, it is possible to demonstrate that initiation occurred in the coarse-grained HAZ microstructure (Fig. 19). For through-thickness notched HAZ specimens (K-bevel or single-bevel butt welds), it has to be shown that the fatigue crack front samples an adequate amount (at least 15% of B) of coarse-grained HAZ (Fig. 20 [*12*]). From a practical point of view, the above-mentioned validity criteria may be useful in determining conservative HAZ toughness data, but there is a tendency for weld fabrication not to be realistic, since it might be changed to provide optimum testing conditions.

Mechanical Heterogeneity

Assuming a crack or crack-like defect in a weld, weld metal overmatching is used to protect the weld, i.e., the crack, from macroscopic plasticity [*13*].

In HAZ fracture toughness testing, weld metal overmatching or undermatching has an

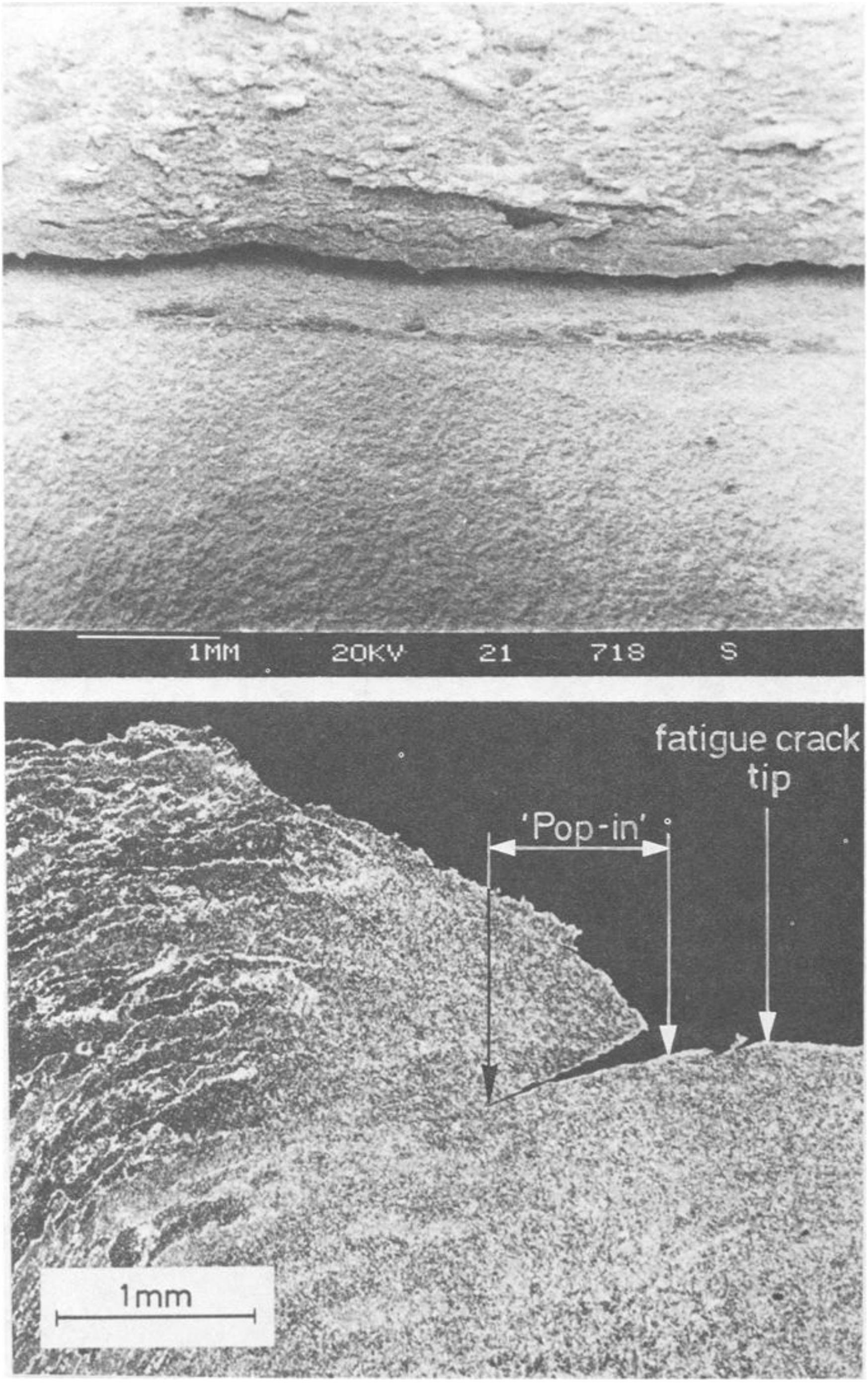

FIG. 17—*Pop-in in a surface-notched weld metal specimen.*

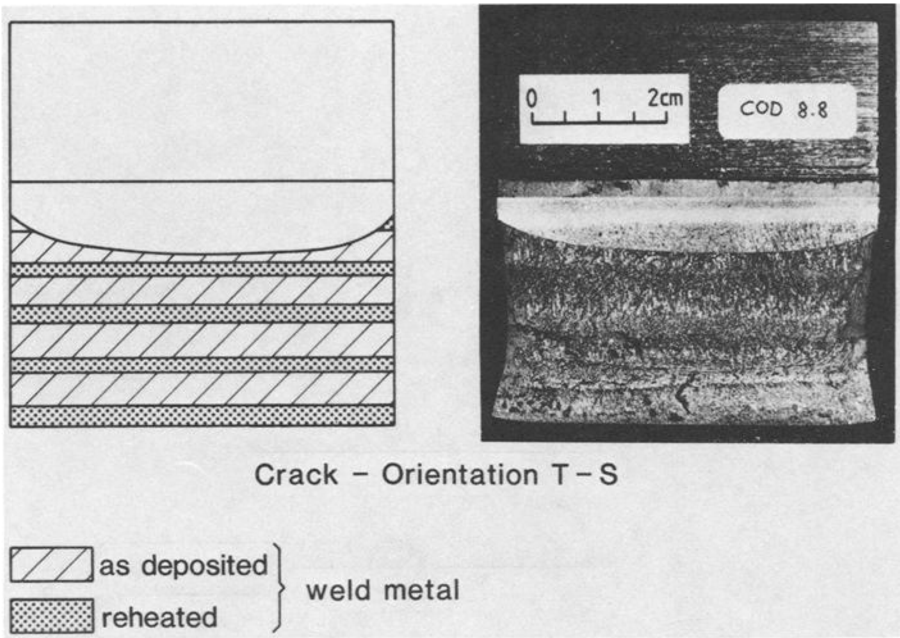

FIG. 18—*Weld metal microstructure in a surface-notched specimen—schematic and fractographic evidence.*

effect on the stress-strain state at the crack front. Depending on the degree of overmatching or undermatching, a more or less asymmetric stress state and deformation behavior can be observed at the crack tip and later on in the whole ligament. Böhme used shadow optical methods [*14*] to demonstrate this effect (Fig. 21). From Fig. 21 it is evident that CTOD cannot be determined using the BS 5762 procedure since it is based on a symmetrical hinge-type crack opening behavior.

Arimochi et al. [2] proposed the use of a local CTOD, where crack opening is described separately for the lower yield strength and the higher yield strength sides of the weld. Different rotational factors can be determined for the base metal and WM side of a specimen as a function of the yield strength ratio of base metal to weld metal (see Fig. 4). Results of a straightforward use of local CTOD are given in Fig. 22. The CTOD obtained from BS 5762 is compared with the sum of the local CTODs ($\delta_1 + \delta_2$). For a CTOD of up to 1 mm, both evaluation methods yield the same results. For higher CTOD levels, δ_{total} results are lower than δ_{BSI} results. The different yield strengths in the weld metal and base material cause unsymmetrical crack-tip opening behavior, expressed by different rotational factors used to calculate local CTOD for the higher and lower yield strength sides of the HAZ specimens. In the example shown in Fig. 23, local CTODs differ by a factor of approximately 3.

Conclusions

The scatter of WM and HAZ impact energy results and toughness data in the temperature transition regime is shown to be microstructure related. Fatigue-cracked instead of V-notched

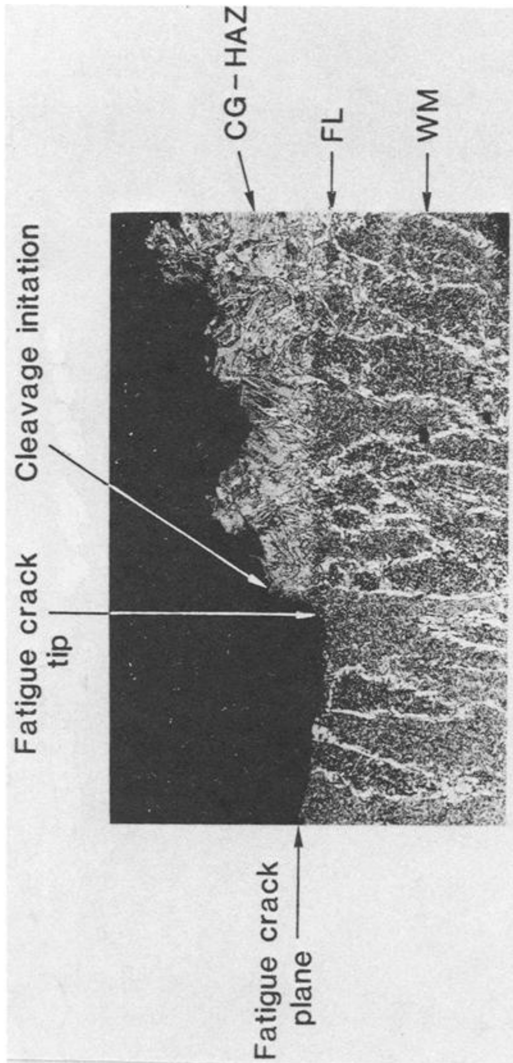

FIG. 19—*Cleavage fracture initiation in coarse-grained HAZ.*

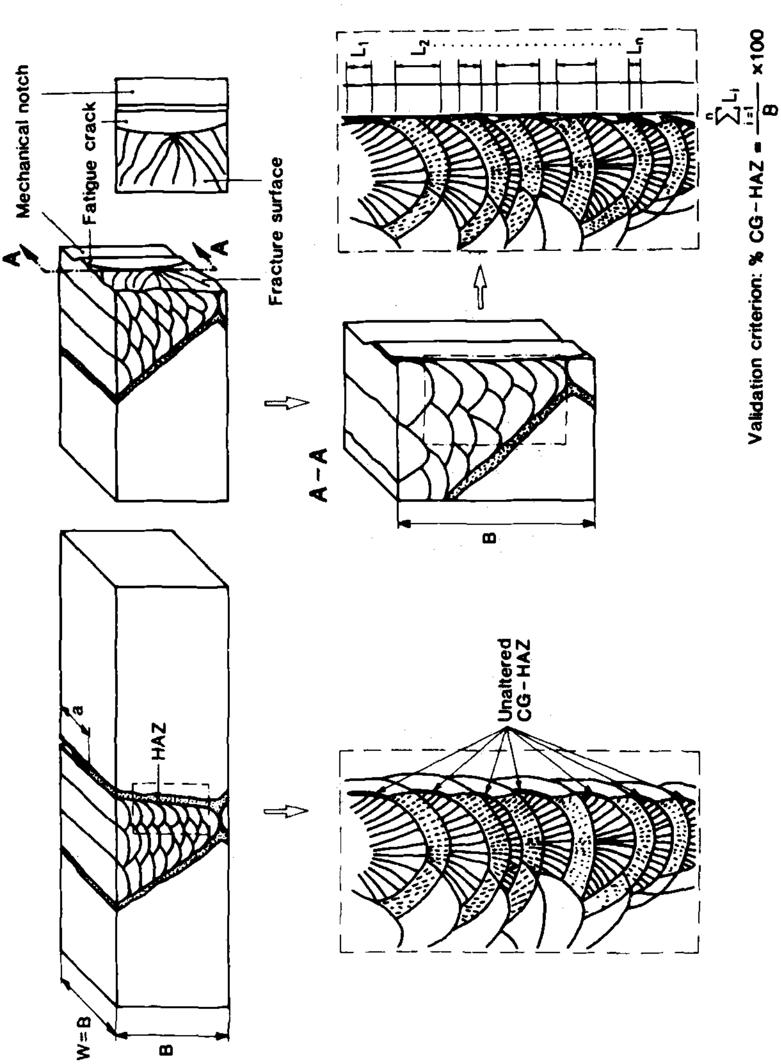

FIG. 20—*Example for validation of HAZ fracture toughness data* [12].

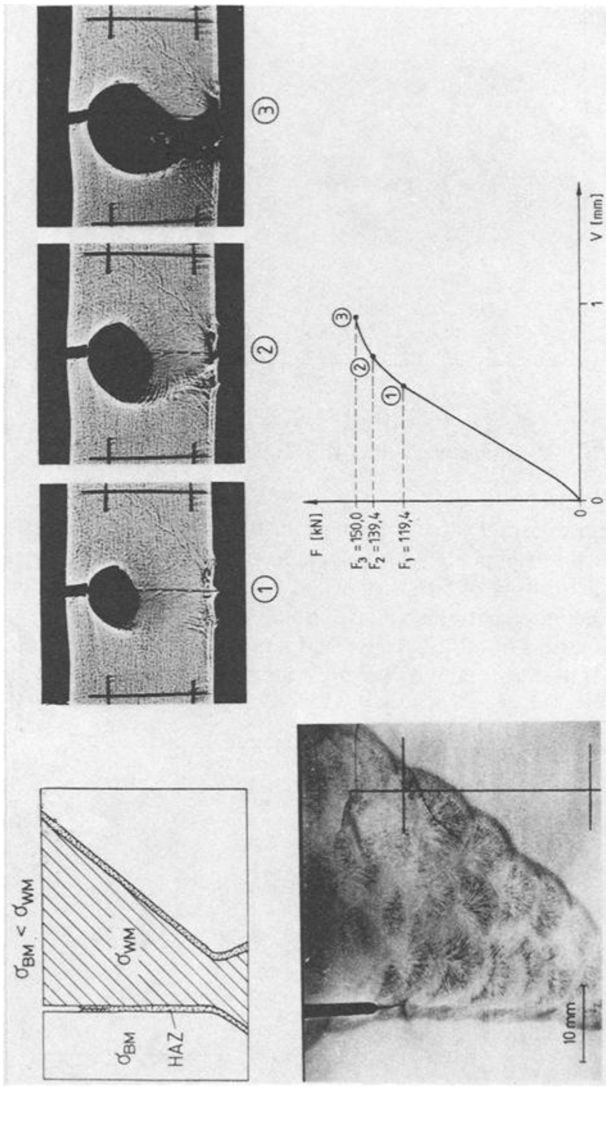

FIG. 21—*Stress-strain state at the crack tip of a HAZ SENB specimen.*

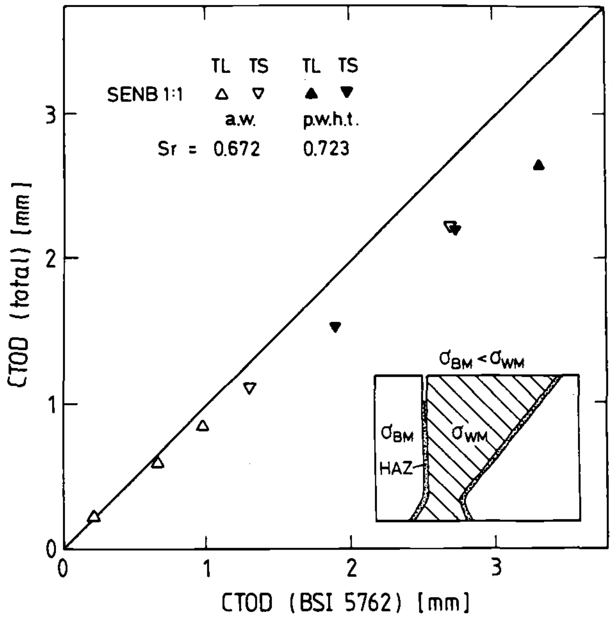

FIG. 22—*Comparison of HAZ CTOD results* (δ_{total}, δ_{BSI}).

Charpy specimens had different effects on the transition temperature shift, depending on the type of microstructure sampled. With respect to fracture toughness characterization of WM and HAZ, impact testing of fatigue-cracked Charpy specimens may be a better tool to evaluate material heterogeneity than conventional Charpy testing.

Fracture toughness testing of full-thickness WM and HAZ specimens needs more detailed testing requirements. Besides material heterogeneity, HAZ testing of overmatched and

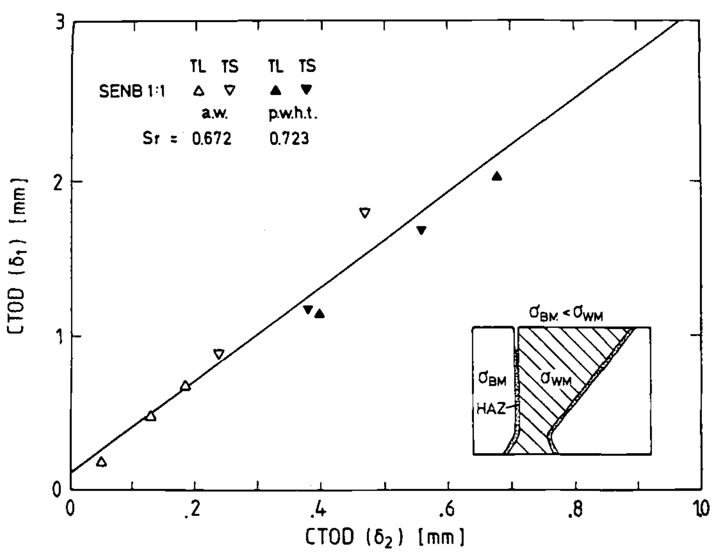

FIG. 23—*CTOD for the lower and higher yield strength sides of the joint.*

undermatched joints is dominated by a complex mechanical heterogeneity. Therefore, CTOD as defined in BS 5762 may only be an appropriate parameter to describe the global fracture behavior of HAZ specimens.

References

[*1*] Towers, O. L. and Dawes, M. G., "Welding Institute Research on the Fatigue Precracking of Fracture Toughness Specimens," *User's Experience with Elastic-Plastic Fracture Toughness Test Methods, ASTM STP 856,* American Society for Testing and Materials, Philadelphia, 1985, pp. 23–46.

[*2*] Arimochi, K., Nakanishi, M., Toyoda, M., and Satoh, K., "Local CTOD Criterion Applied to Fracture Evaluation of Weldments," Paper 2.6. *Proceedings,* Vol. II, Third German-Japanese Joint Seminar, Stuttgart, West Germany, 1985.

[*3*] Evans, G. M., "The Effect of Heat Input on the Microstructure and Properties of C-Mn All Weld Metal Deposits," *Welding Journal,* Vol. 61, No. 4, 1982, pp. 125s–132s.

[*4*] Evans, G. M., "The Effect of Carbon on the Microstructure and Properties of C-Mn All Weld Deposits," *Welding Journal,* Vol. 62, No. 11, 1983, pp. 313s–320s.

[*5*] Evans, G. M., "The Effect of Molybdenum on the Microstructure and Properties of C-Mn All Weld Metal Deposits," *Oerlikon Schweißmitteilungen,* Vol. 45, No. 115, 1987, pp. 10–27.

[*6*] Farrar, R. and Harrison, P., "Microstructural Development and Toughness of C-Mn and C-Mn-Ni Weld Metals, Part 2-Toughness," *Metal Construction,* Vol. 19, No. 8, 1987, pp. 447R–450R.

[*7*] Glover, A. G., McGrath, J. T., Tinkler, M. J., and Weatherley, G. C., "The Influence of Cooling Rate and Composition on Weld Metal Microstructures in a C-Mn and HSLA Steel," *Welding Journal,* Vol. 56, No. 7, 1977, pp. 267s–273s.

[*8*] Evans, G. M., "Factors Affecting the Microstructure and Properties of C-Mn Weld Metal Deposits," Document II-A-460-78, International Institute of Welding, Tokyo, Japan, 1978.

[*9*] Erikson, K., "On the Effect of Pro-eutectoide Ferrite upon the Fracture Toughness of Weld Metal," Fifth International Conference on Fracture, Vol. 2, Cannes, France, 1981, pp. 715–722.

[*10*] Levine, E. and Hill, D. C., "Structure-Property Relationship in Low-C Weld Metal," *Metallurgical Transactions A,* Vol. 8A, September 1977, pp. 1453–1463.

[*11*] Ruge, J., Lee, B.-Y., and Wösle, H., "Einfluß der Kerblage auf die Kerbschlagarbeit unterpulvergeschweißter Nähte," *Schweißen und Schneiden,* Vol. 36, No. 4, 1984, pp. 177–179.

[*12*] "API Specification for Preproduction Qualification for Steel Plates for Offshore Structures," API RP 2Z, American Petroleum Institute, Dallas, TX, March 1987.

[*13*] Lian, B., Denys, R., and Van de Walle, L., "An Experimental Assessment on the Effect of Weld Metal Yield Strength Overmatching in Pipeline Girth Welds," *Proceedings,* Third International Conference on Welding and Performance of Pipelines, London, England, 1986.

[*14*] Böhme, W. and Burget, W., unpublished results, Fraunhofer Institut für Werkstoffmechanik, Freiburg, West Germany, 1988.

Indexes

Author Index

Subject Index

ISBN 0-8031-1277-7